Copyright Warning & Restrictions

The copyright law of the United States (Title 17, United States Code) governs the making of photocopies or other reproductions of copyrighted material.

Under certain conditions specified in the law, libraries and archives are authorized to furnish a photocopy or other reproduction. One of these specified conditions is that the photocopy or reproduction is not to be "used for any purpose other than private study, scholarship, or research." If a, user makes a request for, or later uses, a photocopy or reproduction for purposes in excess of "fair use" that user may be liable for copyright infringement,

This institution reserves the right to refuse to accept a copying order if, in its judgment, fulfillment of the order would involve violation of copyright law.

Please Note: The author retains the copyright while the New Jersey Institute of Technology reserves the right to distribute this thesis or dissertation

Printing note: If you do not wish to print this page, then select "Pages from: first page # to: last page #" on the print dialog screen

ABSTRACT

RATIONAL DESIGN OF HYDROGEN-FREE CATALYTIC ACTIVE SITES

by
Andrei Ioan Loas

Materials that are organic-based and exhibit oxidative catalytic activity, including free-radical pathways, while being refractory to the activated oxygen species are not known. The synthesis of several classes of such materials, their electronic and structural characterizations as well as catalytic properties are reported. Their rational molecular design and biologically inspired reactivity are based on enzymatic active sites, which are reengineered into robust metal-organic fluoroalkylated scaffolds that, for the first time, exhibit structural asymmetry and tunable π–π interactions both in solution and solid state. In these complexes, labile C–H bonds are replaced with chemically and thermally resistant C–F bonds to create a "Teflon coating" of the metal active site, keeping it open for catalysis while protecting the molecule against self-decomposition.

The first part presents the synthesis, spectroscopic and X-ray structural characterization of new, mixed alkyl-perfluoroalkyl trispyrazolylborate (Tp) ligands and several of their sodium and silver derivatives. These complexes are subject to an N_3-coordinating agent bearing a −1 charge. The metal is encapsulated in a fluorine-rich environment and exhibits a high Lewis acidity, allowing additional coordination by toluene, triphenylphosphine, methyldiphenylphosphine and triphenylphosphine oxide. X-ray crystallographic analysis of the new materials allows for the development of a structural model that predicts interatomic distances and the relative stability of this class of compounds. The balancing of electronic and steric effects of substituents on the Tp and additional ligands can lead to remarkably stable compounds in solution and the solid

state, even when metals particularly prone to reduction (such as silver) are involved. Examples among the new complexes are provided.

The second part describes the design of two new classes of macrocyclic organic chromophores with enhanced N_4-coordinating ability and −2 charges, belonging to the family of fluoroalkylated phthalocyanines and produced as their zinc and cobalt complexes. The first class, bearing trifluoromethyl groups, exhibits reduced steric hindrance and solvent-dependent aggregation. A direct correlation between the degree of dimerization and the solvent's hydrogen bond donor ability is established. The second class constitutes the first asymmetric perfluorinated phthalocyanines, a property imparted by a combination of fluorine atoms and perfluoroisopropyl groups. X-ray crystal structures reveal tunable π–π stacking in the solid state for representatives of both classes.

The new compounds' ability to catalytically activate oxygen from air and consequently oxidize substrates is tested on two processes of industrial importance: the environmentally benign conversion of corrosive thiols to disulfides and the photocatalytic oxidation of (*S*)-citronellol. The extreme electronic deficiency imparted on the metal complexes supports a new strategy for broadening catalytic activity to include thiols with poor basicity, which under normal circumstances cannot be oxidized. Quantitative substrate conversion and virtual immunity of the catalysts to chemical attacks is demonstrated for the first time in a metal-organic assembly through oxygen consumption and stability studies, thus opening pathways for development of new materials.

RATIONAL DESIGN OF HYDROGEN-FREE CATALYTIC ACTIVE SITES

by
Andrei Ioan Loas

A Dissertation
Submitted to the Faculty of
New Jersey Institute of Technology
in Partial Fulfillment of the Requirements for the Degree of
Doctor of Philosophy in Materials Science and Engineering

Interdisciplinary Program in Materials Science and Engineering

May 2012

APPROVAL PAGE

RATIONAL DESIGN OF HYDROGEN-FREE CATALYTIC ACTIVE SITES

Andrei Ioan Loas

Dr. Sergiu M. Gorun, Dissertation Co-Advisor — Date
Research Associate Professor of Chemistry and Biochemistry,
Seton Hall University, South Orange, NJ

Dr. Nuggehalli M. Ravindra, Dissertation Co-Advisor — Date
Professor of Physics, NJIT

Dr. Tamara M. Gund, Committee Member — Date
Professor of Chemistry and Environmental Science, NJIT

Dr. Robert B. Barat, Committee Member — Date
Professor of Chemical, Biological and Pharmaceutical Engineering, NJIT

Dr. Roger A. Lalancette, Committee Member — Date
Professor of Chemistry, Rutgers University, Newark, NJ

BIOGRAPHICAL SKETCH

Author: Andrei Ioan Loas

Degree: Doctor of Philosophy

Date: May 2012

Undergraduate and Graduate Education:

- Doctor of Philosophy in Materials Science and Engineering
  New Jersey Institute of Technology, Newark, NJ, 2012

- Bachelor of Science in Chemical Engineering
  Polytechnic University of Bucharest, Bucharest, Romania, 2007

Major: Materials Science and Engineering

Publications:

Loas, A.; Gerdes, R.; Zhang, Y.; Gorun, S. M. Broadening the reactivity spectrum of a phthalocyanine catalyst while suppressing its nucleophilic, electrophilic and radical degradation pathways. *Dalton Trans.* **2011**, *40*, 5162-5165.

Uncuţa, C.; Bartha, E.; Gherase, D.; Loas, I. A.; Teodorescu, F.; Varga, R. A.; Vanthuyne, N.; Roussel, C.; Berg, U. Chiral bicyclo[3.3.1]-3,7-dioxanonane derivatives: Study of crystallization mode and conformational dynamics in solution. *J. Mol. Struct.* **2011**, *989*, 20-30.

Moons, H.; Łapok, Ł.; Loas, A.; Van Doorslaer, S.; Gorun, S. M. Synthesis, X-ray Structure, Magnetic Resonance, and DFT Analysis of a Soluble Copper(II) Phthalocyanine Lacking C–H bonds. *Inorg. Chem.* **2010**, *49*, 8779-8789.

Hu, Z.; Loas, A.; Gorun, S. M. Synthesis and molecular and solid state characterization of mixed CH_3–CF_3 and CH_3–C_2F_5 fluoroalkyl pyrazoles and a new, $Tp^{C_2F_5,CH_3}$ ligand. *Inorg. Chim. Acta* **2009**, *362*, 4639-4645.

Roussel, C.; Vanthuyne, N.; Jobert, J.-L.; Loas, A. I.; Tănase, A. E.; Gherase, D. HPLC on Chiral Support with Polarimetric Detection: Application to Conglomerate Discovery. *Chirality* **2007**, *19*, 497-502.

Patent applications:

Gorun, S. M.; Loas, A. I.; Griswold, K. A.; Łapok, Ł.; Patel, H. H.; Gerdes, R. System and Method for Fluoroalkylated Fluorophthalocyanines with Aggregating Properties and Catalytic Driven Pathway for Oxidizing Thiols. U.S. Pat. Appl. 13/286,393, November 1, 2011.

Presentations:

Loas, A.; Reid, N.; Patel, H.; Badiola, C. Biologically Inspired Chemistry Uncovers "Immortal" Catalyst. Presented at the 3rd Dana Knox Student Research Showcase, Newark, NJ, April 6, 2011 (Gold Medal for Graduate Research).

Loas, A.; Patel, H.; Reid, N. Abbreviated Enzymes for Electronic Materials and Green Catalysts. Presented at the VIth Annual Graduate Student Research Day, Newark, NJ, November 4, 2010.

Darkness and light. Strife and love. Are they the workings of one mind?
The features of the same face?
Oh my soul, let me be in you now.
Look out through my eyes. Look out at the things you made.
All things shining.

(Terrence Malick, *The Thin Red Line*)

Dedicated to the memory of my parents, Ioan-Remus and Florentina Loas

May the light of your spirit always guide me

ACKNOWLEDGMENTS

First and foremost, my deepest gratitude goes toward my mentor, Prof. Sergiu M. Gorun. The completion of this work was assured by his constant guidance and unconditional support. I am indebted to him for teaching me the values of independence, mutual respect and initiative in a working environment, as well as the importance of quality, reliability and hard-data backing of scientific results.

I want to express my sincere appreciation for Prof. Nuggehalli M. Ravindra. His availability and assistance with all scientific and administrative matters were instrumental for my graduation. I commend the members of my dissertation committee, Prof. Tamara M. Gund and Prof. Robert B. Barat for their input and commitment. Special thanks go to Prof. Roger A. Lalancette for agreeing to serve on my committee, collecting the raw X-ray diffraction data and introducing me to the fascinating world of crystallography.

Grant funding from the Department of Defense and the National Science Foundation, as well as financial assistance from the Departments of Physics and Chemistry and Environmental Science at NJIT are kindly acknowledged.

I greatly benefited from the hands-on assistance of Dr. Yong Pu in the instrumental analysis labs and Mr. Yogesh Gandhi in the chemicals and glassware stockrooms. A key role in the complete characterization of the new compounds, for which I extend my heartfelt thanks, was played by Drs. Lazaros Kakalis and Roman Brukh of Rutgers University, Newark, Drs. James Windak and John Lennon of the University of Michigan, Dr. Victor Young, Jr. of the University of Minnesota, Dr. Clemens Anklin of Bruker BioSpin Corporation and Drs. Maren Pink and Yu-Sheng Chen of the Advanced Photon Source at the Argonne National Laboratory.

My thanks are also due to the staff and faculty of Seton Hall University for providing full access to external research facilities. The assistance of Prof. Stephen Kelty and Mr. Patrick Dwyer of the same institution in carrying out theoretical computations on the novel complexes is greatly appreciated.

The occasionally difficult times, both personal and professional, encountered during the initial years of my degree, were relieved and brightened by my good friend and colleague, Dr. Robert Gerdes. I will always use the knowledge, skills and techniques that he passed on to me.

My best regards go to Mr. Hemantbhai Patel for the innumerable hours of shared work and excitement in the lab. I thank the past members of the Gorun research group that I was fortunate enough to meet: Dr. Łukasz Łapok, Dr. Wycliffe Graham, Dr. Olga Tsaryova, Mr. Michael Koch and Ms. Franziska Lissel for the good times and mutually rewarding conversations.

I will miss the stimulating discussions with Drs. William Skawinski, Willis Hammond and Anthony East on the mysteries and wonders of organic chemistry.

This effort would have been futile without the immense love and support of my late father and my dear stepmother, Geta, and her family. I cherish the moments that I shared with my friends in Romania, United States and elsewhere, which constantly encouraged me to pursue this quest to its successful end.

TABLE OF CONTENTS

TABLE OF CONTENTS
(Continued)

TABLE OF CONTENTS
(Continued)

Chapter **Page**

TABLE OF CONTENTS
(Continued)

Chapter **Page**

TABLE OF CONTENTS
(Continued)

TABLE OF CONTENTS
(Continued)

TABLE OF CONTENTS
(Continued)

TABLE OF CONTENTS
(Continued)

LIST OF TABLES

LIST OF TABLES
(Continued)

LIST OF TABLES
(Continued)

LIST OF TABLES
(Continued)

LIST OF TABLES
(Continued)

LIST OF TABLES
(Continued)

LIST OF TABLES
(Continued)

LIST OF FIGURES

LIST OF FIGURES
(Continued)

LIST OF FIGURES
(Continued)

LIST OF FIGURES
(Continued)

LIST OF FIGURES
(Continued)

LIST OF FIGURES
(Continued)

LIST OF FIGURES
(Continued)

LIST OF FIGURES
(Continued)

Figure **Page**

LIST OF FIGURES
(Continued)

Figure **Page**

LIST OF FIGURES
(Continued)

LIST OF FIGURES
(Continued)

LIST OF FIGURES
(Continued)

LIST OF FIGURES
(Continued)

LIST OF FIGURES
(Continued)

LIST OF FIGURES
(Continued)

LIST OF FIGURES
(Continued)

LIST OF FIGURES
(Continued)

LIST OF ABBREVIATIONS AND ACRONYMS

abbr.	abbreviated
Ac	acetyl
AcOH	acetic acid
AO	atomic orbital
APCI	atmospheric pressure chemical ionization
aq	aqueous
Ar	aryl
AU	arbitrary units(s)
avg.	average
bp	boiling point
br	broad (spectral)
Bu, *n*-Bu	normal (primary) butyl
i-Bu	*iso*-butyl
s-Bu	*sec*-butyl
t-Bu	*tert*-butyl
Bz	benzyl
i-C_3F_7	perfluoroisopropyl
ca.	*circa* (approximately, around)
calcd	calculated
COSY	correlation spectroscopy
Cp	cyclopentadienyl
CV	cyclic voltammetry

Cy	cyclohexyl
d	doublet (spectral)
DCM	dichloromethane
DFT	density functional theory
DMF	dimethylformamide
DMSO	dimethyl sulfoxide
E1	unimolecular elimination
E2	bimolecular elimination
EI	electron impact
EPR	electron paramagnetic resonance
eqn.	equation
ESI	electrospray ionization
Et	ethyl
Et_2O	diethyl ether
EtOAc	ethyl acetate
FID	free induction decay
FT	Fourier transform
GC	gas chromatography
HBA	hydrogen bond acceptor
HBD	hydrogen bond donor
HOESY	heteronuclear Overhauser effect spectroscopy
HOMO	highest occupied molecular orbital
HPLC	high-performance liquid chromatography

HRMS	high-resolution mass spectrometry
IR	infrared
lit.	literature value
LUMO	lowest unoccupied molecular orbital
m	multiplet (spectral)
$[M]^+$	parent molecular ion
Me	methyl
Mes	mesityl (2,4,6-trimethylphenyl)
MO	molecular orbital
mp	melting point
MS	mass spectrometry
MW	microwave (radiation)
NMP	*N*-methylpyrrolidone
NMR	nuclear magnetic resonance
NOESY	nuclear Overhauser effect spectroscopy
ORTEP	Oak Ridge Thermal Ellipsoid Plot
OTf	trifluoromethanesulfonate (triflate)
Pc(s)/PcM(s)	phthalocyanine(s)/metallophthalocyanine(s)
PDT	photodynamic therapy
Ph	phenyl
Pr	propyl
i-Pr	isopropyl
Py	pyridine

Pz	pyrazole
q	quartet (spectral)
R_f	perfluoroalkyl substituent
r.d.s.	rate determining step
redox	reduction–oxidation
RT	room temperature
s	singlet (spectral)
SN1	unimolecular nucleophilic substitution
SN2	bimolecular nucleophilic substitution
t	triplet (spectral)
THF	tetrahydrofuran
TLC	thin-layer chromatography
Tol	toluene
Tp(s)	trispyrazolylborate(s)
Ts	*para*-toluenesulfonyl (tosyl)
UV	ultraviolet
vis	visible
viz.	*videlicet* (namely)
vol	volume
vs.	*versus* (against)
v/v	volume per unit volume (volume-to-volume ratio)
wt	weight
w/w	weight per unit weight (weight-to-weight ratio)

LIST OF SYMBOLS

Å	angstrom(s) (10^{-10} meters)
atm	atmosphere(s)
°C	degree(s) Celsius
cm^{-1}	wavenumber(s)
δ	chemical shift in parts per million (in NMR spectroscopy)
d	density
Δ	difference
ϵ	molar extinction coefficient (in spectroscopy)
g	gram(s)
h	hour(s)
Ha	Hartree (atomic energy unit)
Hz	hertz
i	ipso carbon atom of aromatic rings (in spectral assignments)
J	joule(s)
J	coupling constant (in NMR spectroscopy)
k	Boltzmann's constant
K	kelvin(s) (absolute temperature)
λ	wavelength (in spectroscopy)
L	liter(s) (cubic decimeters)
m	meta position of aromatic ring
μM	micromolar (micromoles per liter)
m	meter(s)

M	molar (moles per liter)
min	minute(s)
mol	mole(s)
m/*z*	mass-to-charge ratio
v	frequency of vibration (in spectroscopy)
nm	nanometer(s) (10^{-9} meters)
o	ortho position of aromatic ring
$^1O_2$	singlet oxygen
$^3O_2$	triplet oxygen
p	para position of aromatic ring
ppm	part(s) per million
s	second(s)
σ_m, σ_p	Hammett constants
$\sum$	sum
T	absolute temperature
Z	number of chemical formula units per unit cell (in crystallography)

NOTE ON NUMBERING OF CHEMICAL COMPOUNDS

All compounds encountered in reaction schemes throughout this work have been numbered following the labeling format **[x-yy]**, where **x** stands for the chapter number they are first described in and **yy** stands for the compound number in that chapter. The structure number is clearly marked in bold style, both in figures and text. Context permitting, compounds were also described by systematic chemical names.

CHAPTER 1

GENERAL INTRODUCTION

1.1 Goal of the Project

This project aims at exploring new classes of aerobic oxidation catalysts which are in the same time organic based and chemically resistant to the activated oxygen species they produce. Using rational molecular design and biologically inspired activity, enzymatic active sites are reengineered into metal-binding fluoroalkylated scaffolds that, for the first time, exhibit structural asymmetry and tunable π–π interactions both in solution and the solid state. This leads to a great range of applications in areas such as:

- catalysis that enzymes are unable to perform due to inherent chemical and thermal limitations.
- singlet oxygen photocatalysis.
- semiconductors and molecular electronic devices.

Unlike the cytochrome P450 oxidases, which they model, these new complexes contain chemically and thermally robust C–F bonds that create a fluorine-rich lining of the metal active sites. This fluorinated enclosure acts as a "Teflon-coated" molecular reactor wall (Figure 1.1), while leaving the active site open for catalytic activity.

Through fine tuning of the fluoroalkyl groups, a variable degree of aggregation is imparted on the complexes. This ensures stacking and electric conductivity in the solid state, concomitantly maintaining an appropriate amount of monomeric sites available for catalysis in solution. Molecular asymmetry displayed by most of the new compounds leads to exploratory research in chiral and stereospecific processes.

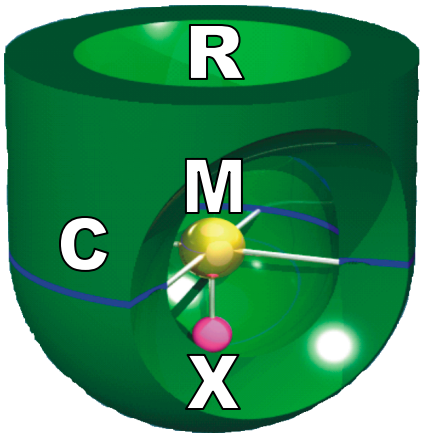

Figure 1.1 Schematic representation of a molecular reactor. R – reactive cavity; C – tunable "Teflon-coated" wall; M – catalytic metal; X – tuning group (perfluorinated substituent, axial ligand or covalently linked tether to a solid-state support).

Two classes of metal-organic materials are studied: trispyrazolylborates and phthalocyanines. For the former, efforts are directed towards a complete solid-state study of steric vs. electronic effects in a series of silver derivatives. Finding the optimal balance between the electronegativity and bulkiness of attached substituents can lead, as is shown herein, to exceptionally stable compounds even when metals prone to reduction, such as silver, are involved.

Research on metallophthalocyanines is focused on devising new versatile catalysts to promote, among others: (i) the beneficial aerobic autooxidation of thiols using cobalt complexes and (ii) singlet oxygen production and photocatalytic activity in solution for a series of zinc analogues.

Solid-state stacking of fluorinated phthalocyanine rings is essential for the electronic coupling of the molecules. Strong electron-withdrawing substituents lower the energy and stabilize the frontier orbitals, creating band gaps suitable for semiconductivity.

Investigations of electric properties in thin films of the new materials are to be explored in a future work. Intramolecular transfer of electrons from ground to final states offers the possibility of creating molecular electronic devices, an emerging interdisciplinary field of research, in which phthalocyanines have been proposed as promising candidates.

1.2 Introduction to Trispyrazolylborates

Since their discovery and pioneering work done by Trofimenko almost 50 years ago,[1] the poly(pyrazol-1-yl)borates have become one of the most widely used families of chelating agents in chemistry; these molecules, combining features of the cyclopentadienyl and *β*-diketonate systems, owe their utility to the extreme versatility they can provide, both by changing the number of pyrazolyl groups bound to the boron center and the substituents thereon.[2,3] Up to date, complexes of these ligands are known for over 70 elements of the periodic table; around 3000 papers were published and more than 200 different polypyrazolylborates were reported.[3] This huge scientific interest arises from the possibility of fine tuning the electronic and steric profile of the ligand in conjunction with the control of the coordination sphere of the metal.

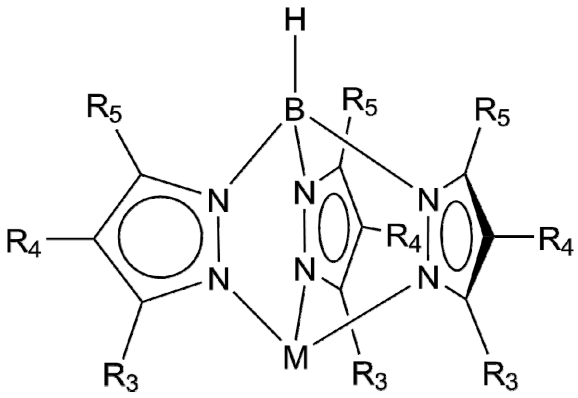

Figure 1.2 General structure of a metal trispyrazolylborate.

The vast majority of the studies on pyrazolylborates deal with the class containing three pyrazole rings attached to a boron atom, i.e., trispyrazolylborates (Tps). These chelating agents (Figure 1.2), bearing a −1 charge, have the advantage of keeping the metal ion in a tridentate, C_{3v} symmetry grip, so that chemical modifications can be performed at the remaining metal coordination sites; in this way, the Tp ligand acts as a "spectator" group, generally not interfering in the reaction processes.[3] Tps and other polypyrazolylborates can coordinate to a metal in either bidentate or tridentate fashion, like the pincers and tail of a scorpion. This versatility prompted their creator to coin them the name "scorpionates".

Owing to the ever growing expansion of the research in the field, an abbreviation system was proposed by Curtis[4,5] and later modified by Trofimenko.[6] In this system, which will be used throughout this work, the hydrotris(pyrazol-1-yl)borate ligand is abridged as "Tp". In relation to Figure 1.2, the substituents in the 3-, 4- and 5-position of the pyrazole rings are labeled R_3, R_4 and R_5 and marked as superscripts in the order: $Tp^{R_3,4\text{-}R_4,R_5}$. The hydrogen atoms are omitted unless they come in the 3-position and R_4 and/or R_5 is a substituent different than H, giving the formula $Tp^{H,4\text{-}R_4,R_5}$. To distinguish between the R_4 and R_5 groups, the R_4 substituent is labeled in all cases 4-R_4 in the superscript. If all three substituents are identical groups, R, the molecule is labeled as $Tp^{(R)_3}$. A similar formalism is used for the pyrazole precursors of Tps, *abbr.* $Pz^{R_3,4\text{-}R_4,R_5}$. If the boron atom bears a hydrogen, this is omitted from the formula; on the other hand, if the boron hydrogen is replaced with any other group, this is shown in parentheses before the Tp symbol. For example, a methyl group attached to boron is labeled as (Me)Tp. Finally, the metal coordinated to the Tp group is written directly after, with any other

adducts or ligands ("L") following in parentheses, giving the complete notation (R)TpM(L)$_n$. The atom of the "L" group directly bound to the metal appears first in the molecular formula.

Applications of trispyrazolylborates are a vast and ever expanding field. Firstly, Tps have been successfully utilized in biochemistry for enzyme modeling, due to their multidentate binding possibilities to a metal ion, which will be fixed in a protected pocket of defined shape and size. Most of the research has gone into the iron, copper and zinc complexes, which proved to be the most efficient in dioxygen and carbon dioxide binding. Examples include, but are not limited, to: Lippard's iron complex aimed at modeling hemerythrin,[7] Kitajima's model on dioxygen binding at the dicopper site of hemocyanin,[8] Tolman's work into nitric oxide adducts to mononuclear copper in nitrite reductase[9] and the extended research by Parkin on the mononuclear Tp$^{t\text{-Bu,CH}_3}$Zn(OH) complex which effectively mimics the catalytic unit of carbonic anhydrase.[10–12]

Secondly, Tps have been investigated for their promising catalytic properties in a variety of processes. Titanium Tps are useful as precatalysts for the polymerization and oligomerization of ethylene[13,14] and styrene,[15] zirconium complexes were tested as styrene, ethylene and propylene polymerization catalysts,[15,16] while rhodium tris- and bispyrazolylborates catalyze phenylacetylene polymerization in ionic liquids and DCM.[17] In the field of carbene and nitrene transfer reactions, copper complexes of the general formula Tp^{X}Cu, X = Br$_3$, Cy, Mes, have been employed as catalysts for: (i) the insertion of diethyl diazoacetate into C–H bonds of furans,[18] cycloalkanes and cyclic ethers,[19] benzene and various saturated and unsaturated alcohols;[20] (ii) aziridation of olefins[21] and (iii) cyclopropanation of alkenes and alkynes.[22,23] Last but not least, Tp complexes

containing copper, cobalt, iron and rhenium have shown oxidative catalytic activity under both homogeneous and heterogeneous conditions. For instance, $Tp^{CH_3,CH_3}Cu$ supported on silica gel acts as a heterogeneous catalyst in water for the epoxidation of styrene to styrene oxide using ozone,[24,25] while transformation of stilbenes to epoxides was performed using $Tp^{t\text{-}Bu}Fe(Cl)$.[26] In the research of Gorun and collaborators, a great interest was paid to fluorinated Tp research into homogeneous oxidation catalysts, with remarkable results: the one-pot formation of $Tp^{CF_3,CH_3}Cu$(lactate) from acetone constitutes the first example of an external substrate oxygenated aerobically with a copper complex exhibiting no C–H bonds around the metal center,[27] while oxidation of cyclohexane to a mixture of cyclohexanol and cyclohexanone was performed using a $Tp^{CF_3,CH_3}Co(NCMe)(\eta^2\text{-}NO_3)$ complex.[28] The first structural evidence for O_2 activation and conversion into a hydroperoxo species by a transition metal complex came from $Tp^{i\text{-}Pr}$Rh(1,2-bis(diphenylphosphino)ethane).[29]

Finally, trispyrazolylborates have found notable applications in the activation of arene and alkane C–H bonds, particularly rhodium and iridium complexes. $Tp^{CH_3,CH_3}Rh(NCR)$ type compounds (where NCR is an aliphatic nitrile) have been found to rearrange *i*-Pr- to *n*-Pr-hydride and *s*-Bu- to *n*-Bu-hydride derivatives through an intramolecular process.[30,31] Unsaturated, *in situ* generated $Tp^{CH_3,CH_3}Ir(Ph)_2$ causes the double α-C–H bond activation of THF and other cyclic ethers, with formation of the respective cyclic carbenes.[32]

In the vast domain of scorpionates, fluorinated complexes remain relatively unexplored; at the start of the present work, out of over 200 different Tp ligands reported, only 11 contained fluorinated substituents and about 60 derived TpM compounds were

published altogether. A complete overview of these structures will be given in Chapter 3. This lack of scientific knowledge in an area open for over 20 years (the first fluorinated scorpionate was published by Graham et al. in 1989)[33] invites to further discoveries, especially given the unique properties of perfluoroalkylated groups. Their strong electron-withdrawing nature reduces electron density at the metal center, enhancing its Lewis acid character and σ electron-accepting ability. This translates into a stronger bond of the metal to the σ-donor ligand, while increasing the metal's resistance to reduction. The stronger C–F bonds provide an oxidation-protective environment to the molecule, preventing intramolecular C–H bond activation.

Within the same field of scorpionates, structurally characterized silver compounds are scarce, owing mostly to their notorious light and sometimes air instability. This prompts for a systematic study of their fluorinated analogues. Through modification of the substituents on the pyrazole rings and variation of the σ-donor ligands on the metal side, tuning was undertaken in order to establish a connection between the overall stability of the complexes and the interplay of steric and electronic effects. Complete solid-state characterization allowed for the development of a structural model as a tool for prediction of metal–ligand interatomic distances based on a desired molecular architecture.

1.3 Introduction to Phthalocyanines

Phthalocyanines (Pcs) are one of the amazing discoveries in chemistry. Obtained accidentally in 1907 as blue solids in a pot by Braun and Tscherniac[34] while heating *o*-cyanobenzamide, they were again synthesized by chance twenty years later.[35,36] It was Reginald P. Linstead who started in 1929 the research that eventually elucidated their

structure (Figure 1.3) as a tetraazabenzoporphyrin;[37] he coined for this new class of materials the name of phthalocyanines. Early Pcs were used primarily as dyes and pigments in the paper and textile industry, as well as paints for metal and plastic surfaces, because of their high thermal, chemical and photochemical stabilities.

The extremely low solubility of phthalocyanines obtained up to the 1940s has somewhat hindered and discouraged further synthetic efforts, limiting their use to the dyes industry for a long time. Indeed, unsubstituted Pcs have a solubility of less than 10^{-5} M in any organic, polar protic or aprotic solvent.[38] The only solvent suitable for their solubilization was concentrated sulfuric acid,[39] which unfortunately cannot be used for solubilization of metal Pcs (PcMs) because of demetalation and protonation of the *meso*-nitrogens.[39,40] The outburst of Pc chemistry came in the early 1950s, when peripheral substitution methods were devised and the controlled degree of sulfonation of the Pc core resulted in enhanced solubility in organic solvents and production of water soluble phthalocyanines containing SO_3Na and SO_2XR groups.[41,42]

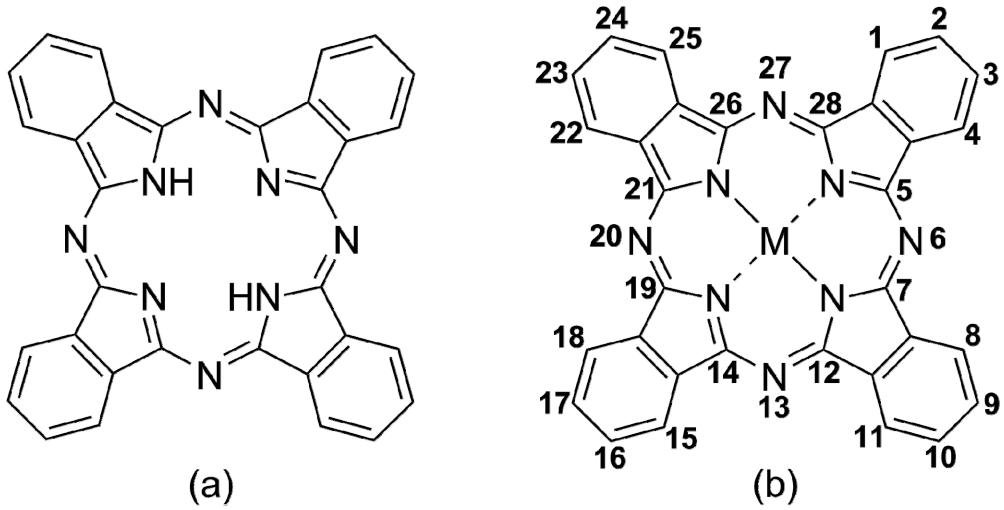

Figure 1.3 General structures of phthalocyanines. (a) Metal-free phthalocyanine, PcH_2, also named "free base" Pc. (b) Metal phthalocyanine, PcM, showing the generally adopted numbering system of the available substitution positions.

It is improbable that phthalocyanines will ever be synthesized in nature, unlike their structural analogues, porphyrins, because their precursors are not naturally present. This makes Pcs one of the pure synthetic metal-organic families. They have been obtained by tetramerization reactions of phthalic acids,[43] phthalic anhydrides,[44] phthalimides,[44] phthalonitriles[45] and diiminoisoindolines,[46] the latter two being the preferred method of choice because of the high conversions and absence of side products.

Metals of every group of the periodic table can be found at the center of the phthalocyanine ring, an N_4-coordinating ligand bearing a −2 charge. This, combined with the possibility of substitution in any or all of the sixteen aromatic sites leads to an impressive versatility and myriad of applications. Hence, since the tuning of the aromatic precursors has been made possible, phthalocyanines bearing peripheral alkyl, aryl, heteroaryl, halogens, thiols, amines, ethers and many other groups have been the subject of an enormous number of papers.[47,48]

Owing to the increased research interest in the area, applications of peripherally substituted phthalocyanines have gone beyond the traditional use as dyes and pigments[47] and include industrial catalytic systems,[49] photosensitizers for photodynamic therapy of cancer,[50–52] materials for electrophotography, inkjet printing, semiconductors, chemical sensors and electrochromic devices,[47,48,53] functional polymers and liquid crystals, nanotechnology[53] and nonlinear optics.[54] Most of these applications arise from the electronic effects and redox properties imparted on the Pc molecules by the highly conjugated system of 18 π electrons. Fine tuning, versatility and convergence of these properties can be done with the appropriate peripheral substituents,[47,48] an idea constituting the foundation of the rational approach used in this work.

Introduction of bulky groups in phthalocyanines prevents the aggregation phenomena in solution. While lack of aggregation is desired in aerobic and bioinspired catalysis,[51] it also hinders the stacking of the planar rings, which is essential for any electronic applications. The present work attempts to combine the catalytic and electronic properties in the same Pc molecules through a rational design of their structure, while keeping the fluorinated pocket which provides the robustness and chemical stability of a molecular reactor. Reducing the steric hindrance through replacement of bulky groups such as *i*-C_3F_7 with CF_3 substituents or F atoms promotes versatile aggregation in solution and controlled π–π stacking in the solid state. Several new classes of fluoroalkylated PcMs that meet this goal are produced and characterized herein; among them, the first examples of perfluorinated asymmetric PcM complexes are described. In the same time, the fluorine-rich lining of the central metal atoms preserves the catalytic capabilities of the molecules towards aerobic oxidation and single site photocatalysis.

CHAPTER 2

EXPERIMENTAL METHODS AND TECHNIQUES

Standard synthetic, separation and purification laboratory procedures were employed for production of all compounds. Standard techniques were used for the manipulation of all gas cylinders. Heating up to 200 °C was performed using a silicone oil bath, while higher temperatures were achieved with the aid of a molten Wood's metal alloy bath. Stirring was performed with magnetic Teflon-coated bars inserted in the reaction flasks. Light sensitive materials were usually obtained by covering the reaction flasks with aluminum foil. All moisture-sensitive reactions were carried out under a nitrogen or argon atmosphere in oven-dried (150 °C) glassware. Reaction mixtures were monitored, whenever possible, by TLC on precoated aluminum-backed silica gel 60 F_{254} plates.

Separation of organic materials from the reaction mixtures was most often achieved by extraction with appropriate solvents. Removal of solvents was performed with a Buchi R-3000 rotary evaporator, connected to a KNF Neuberger chemically resistant vacuum pump. Occasionally, traces of solvents were removed under air or nitrogen stream. Filtration of solids was done with the aid of fritted glass funnel filters and Buchner flasks of various sizes, connected to an in-house vacuum line.

Purification of the materials was performed by recrystallization, sublimation under vacuum, celite or silica gel filtration, flash chromatography or normal phase column chromatography, as stated under each experimental section. Silica gel was purchased from Fisher Scientific (Suwanee, GA) in 200–500 μm (35–70 mesh) and 63–200 μm (70–230 mesh) sizes; pore size was in all cases 60 Å. Elution systems used for chromatography are described separately under the appropriate sections.

Melting points were taken using capillary tubes under air in a Mel-Temp apparatus (Laboratory Devices, Cambridge, MA) and are uncorrected. TGA was performed on a TA Instruments Universal V4.5A machine.

2.1 Inert Atmosphere Techniques

2.1.1 Glove Box

Materials highly sensitive to air and/or moisture were obtained in a Vacuum Atmospheres glove box (Vacuum Atmospheres Co., Hawthorne, CA) equipped with a Vacuum Atmospheres HE-43-2 Dri-Train, under argon or nitrogen atmosphere. The necessary vacuum was maintained using a Varian SD-90 dual stage rotary vane pump. Argon was purchased from Matheson Tri-Gas (Parsippany, NJ) with 99.998% minimum purity. Zero-grade nitrogen was purchased from Airgas (Piscataway, NJ) with 99.99% purity. A circulation fan contained in the MO 40-2 inert gas purifier unit continuously passed the inert gas through the Dri-Train to remove residual air and water vapor. The Dri-Train was regenerated every three months, by heating over a nitrogen–hydrogen (85/15%) atmosphere and then evacuating the gases overnight to remove trapped water, solvents and oxygen. The Dri-Train container was replenished every two years with molecular sieves (Vacuum Atmospheres Co.) and alumina containing copper, nickel, and cobalt oxides. Oxygen concentration inside the box (in ppm) was monitored with a Vacuum Atmospheres AO 316-C electrochemical sensor.

2.1.2 Schlenk Line

Standard air and solvent removal–inert gas atmosphere techniques for air- and moisture-sensitive syntheses were achieved using a three port glass stopcock, single-manifold Schlenk line (Chemglass, Vineland, NJ). The inert gas line was connected to a zero-grade nitrogen tank. The system was closed by way of a gas bubbler to monitor the flow rate and to balance the pressure in the set-up. The vacuum line was serviced by a Precision Scientific D25 belt drive rotary vane pump. A cold trap consisting of a dewar filled with dry ice–acetone was placed between the line and the pump in order to protect it from solvent spillover.

2.2 Microwave Syntheses

Syntheses under microwave radiation were performed using a CEM Discover system (CEM Corporation, Matthews, NC) equipped with a non-contact infrared sensor for temperature control. The instrument's pressure sensing device was calibrated through the supplier using a Cecomp Electronics digital pressure gauge. The machine was interfaced to a computer using the ChemDriver v. 3.6.0 Discover Application Software. Reactions were performed using the closed vessel method in 10 mL thick walled Pyrex glass reaction vessels sealed with Teflon septa caps (CEM).

2.3 Infrared Spectroscopy

Infrared spectra were obtained by averaging 25 scans on a Perkin–Elmer Spectrum One FT-IR Spectrometer with a resolution of 2 cm^{-1}, interfaced to a computer using the Spectrum v. 3.02 software. The solid samples were prepared by grinding the compound to a fine powder in KBr pellets.

2.4 UV-Vis Spectroscopy

Electronic absorption spectra were collected in absorbance mode on a Varian Cary 50 Bio UV-vis spectrophotometer connected to a computer running Cary Win-UV software. The typical scanning range was 330–800 nm with a precision of 0.2 nm; occasionally an extended range of 330–1100 nm was used for detection of near-IR absorptions. Liquid samples were prepared as dilute solutions of the analyte in 1.0 cm and 1.0 mm quartz cells. Solutions were prepared fresh on the same day absorbances were measured; all absorbances were corrected to zero value at 800 or 500 nm. Concentrated samples (40–400 μM) were measured in 1.0 mm cells, while dilute samples (0.5–40 μM) were measured in 1.0 cm cells; three common concentrations (40, 20 and 10 μM) were measured in both cells for all solvents used for aggregation studies to confirm machine accuracy. Gradually lower concentrations for determination of molar extinction coefficients were achieved by successive volume dilutions of an initial 100.0 mL solution.

2.5 NMR Spectroscopy

FT NMR spectra were obtained at ambient temperature on a Bruker ARX 300 instrument (^{1}H, 300.15 MHz; ^{13}C, 75.5 MHz; ^{19}F, 282.4 MHz; ^{31}P, 121.5 MHz) running XWinNMR software. High resolution ^{19}F spectra were acquired with a Bruker Avance 400 instrument (^{19}F, 376.3 MHz) at Bruker BioSpin Corporation (Billerica, MA) or a Varian Inova 600 (^{19}F, 564.6 MHz) at Rutgers University (Newark, NJ). ^{13}C and ^{31}P spectra were acquired with proton decoupling, unless otherwise stated. Assignment of all chemical shifts was based on the 1D spectral data. Chemical shifts (δ) for ^{1}H spectra are reported in ppm relative to the residual proton signals from the deuterated solvents[55] ($CDCl_3$ $\delta = 7.26$; $(CD_3)_2CO$ $\delta = 2.05$). ^{19}F chemical shifts were referenced to an internal

$CFCl_3$ (δ = 0.00) standard. ^{13}C chemical shifts are reported vs. the residual carbon peak of the solvent[55] ($CDCl_3$ δ = 77.16, $(CD_3)_2CO$ δ = 29.84, $(CD_3)_2SO$ δ = 39.52). ^{31}P chemical shifts were referenced to an external 10% H_3PO_4 in D_2O (δ = 0.00) standard.

Spectral data were processed by phase optimization, baseline correction and, occasionally, resolution enhancement, using the SpinWorks 3 software.[56] The 5 mm glass NMR sample tubes and the calibration standards were purchased from Wilmad Labglass (Buena, NJ) and the deuterated solvents were acquired from Cambridge Isotope Laboratories (Andover, MA) and Sigma-Aldrich (Saint Louis, MO). Once opened, the solvents were stored over 4 Å molecular sieves.

2.6 Mass Spectrometry

Nominal (MS) and exact (HRMS) mass spectra were acquired at the University of Michigan (Ann Arbor, MI) using electron impact at 70 eV on a VG Micromass 70-250-S magnetic sector spectrometer or atmospheric pressure chemical ionization in either positive or negative mode on a Micromass LCT time-of-flight spectrometer.

2.7 X-ray Crystallography

Single crystals suitable for X-ray diffraction were grown by slow evaporation of solutions, either at room temperature or in an explosion proof refrigerator. In some cases, crystals were obtained by sublimation in a sealed vial. Crystals isolated from the supernatant liquid were mounted on a thin loop. Data collection was carried out at the Chemistry Department of Rutgers University (Newark, NJ) on a Bruker SMART APEX CCD diffractometer using Cu Kα (1.54178 Å) radiation and equipped with a variable-temperature nitrogen cold stream. In exceptional cases when crystals proved too small

for a conventional instrument, diffraction was carried out using synchrotron radiation at the Advanced Photon Source, Argonne National Laboratory (Argonne, IL). Data were collected at 100(2) K, unless otherwise stated.

Absorption corrections were applied using the program SADABS.[57] The structures were solved using direct methods and refined using full-matrix least-squares on F^2. Non-hydrogen atoms were refined anisotropically, while H atoms were placed at calculated positions and were refined using a riding model. Computations were carried out using the SHELXTL package.[58] Structures of single molecules were visualized as ORTEP representations, with the thermal ellipsoids set at 35 to 50% probability. Packing diagrams and all other structural representations were obtained with the Mercury suite.[59] Searches of the Cambridge Structural Database were performed with the aid of the ConQuest software.[60]

2.8 Catalytic Oxidations and Photooxidations

Before use, the PcZn photosensitizers and PcCo catalyst powders were dried to constant weight at 150 °C. Oxidations were performed at 25±0.2 °C under oxygen atmosphere (99.998% purity) in a closed system (Figure 2.1) with intense stirring for 3 h (photooxidations) and 5 h (all other). The temperature was kept constant with a Lauda Brinkmann Ecoline RS-106 refrigerating circulator. Oxygen was dosed with a Dosimat 665 dispenser (Metrohm, Switzerland) and its consumption was measured manometrically. Reaction solutions were placed in a 100 mL double-walled jacketed glass vessel. Catalyst stability measurements were performed by UV-vis analysis of 3 mL aliquots of the reaction mixtures, taken at various time intervals up to 48 h.

Reaction mixtures for photooxidation experiments consisted of 50 mL of a 20±2 μM PcZn catalyst solution in ethanol and 180 μL (1.0 mmol) (*S*)-(–)-citronellol. Substrate/catalyst ratio was ~1000:1. Illumination was performed using 300 W halogen lamps with a Kodak Ektagraphic III slide projector, creating a light intensity of 4.6±0.1 × 10^5 lux, measured at the outer wall of the reaction vessel with a EA33 model lightmeter (Extech Instruments, Waltham, MA).

Reaction mixtures for thiol catalytic oxidations consisted of 50 mL of a 10±1 μM PcCo catalyst solution in THF, 1 mL NaOH 0.25% (aq) and 7.1 mmol of the thiol of choice (500 μL 2-mercaptoethanol, 755 μL 4-fluorobenzenethiol or 950 μL perfluoro-benzenethiol, respectively). Volumes under 1 mL were measured with a micropipet. Substrate/catalyst ratio was ~13000:1. Thiol/NaOH ratio was ~110:1.

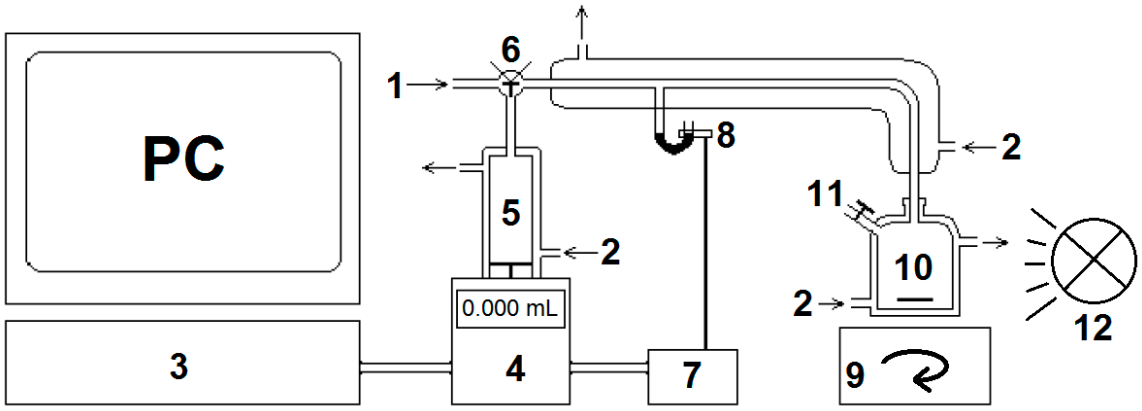

Figure 2.1 Components of the catalytic oxidation equipment. (1) Gas inlet; (2) thermostated water inlet; (3) computer-monitored oxygen consumption over time; (4) Dosimat; (5) oxygen reservoir; (6) three-way tap; (7) electrical couple for Dosimat dispenser control; (8) mercury switch; (9) magnetic stirrer; (10) 100 mL double-walled glass reaction vessel; (11) solution inlet; (12) light source.

2.9 Solvents and Reagents

All solvents and reagents used in this work were purchased from Fisher Scientific (Suwanee, GA), Sigma-Aldrich (Saint Louis, MO), TCI America (Portland, OR) and Matrix Scientific (Columbia, SC). Part of the inorganic reagents were purchased from Strem Chemicals (Newburyport, MA).

Solvents employed were ACS grade, except for chloroform (technical grade) and ethanol (reagent grade). THF, NMP and DMF were distilled from P_2O_5 prior to use. For production of perfluorinated nitrile precursors, acetonitrile was freshly distilled from CaH_2. THF used for catalytic studies (99.5% purity) was stabilized, kept under nitrogen over 4 Å molecular sieves and used fresh. All other solvents were used as received.

Sodium trifluoroacetate, cesium fluoride, copper(I) iodide, sodium borohydride, silver(I) nitrate and silver(I) trifluoromethanesulfonate were dried under vacuum for 2 days over P_2O_5 at 100 °C prior to use and then stored in a dessicator. All other reagents purchased from commercial sources were used as received.

CHAPTER 3

SYNTHESIS, CHARACTERIZATION AND SOLID-STATE STUDY OF FLUORINATED PYRAZOLES AND TRISPYRAZOLYLBORATES

3.1 Introduction

Trispyrazolylborates (Tps) are composed of two main classes: symmetrical (homoscorpionates), in which the three pyrazole (Pz) units are identical, and unsymmetrical (heteroscorpionates), in which two or even all three Pz units are different. Homoscorpionates coordinate the central metal as tripodal N_3-donors and exhibit a C_{3v} symmetry; heteroscorpionates, difficult to obtain and isolate, can act in either bidentate or tridentate manner, depending on Pz substituents' nature.[3] Unsymmetrical Tps, although they formed the object of some extended studies[61] and hold interesting properties such as molecular chirality, were obtained in low yields and most of the time as the minor component of mixtures of symmetrical Tps, rendering their industrial production unfeasible. As such, they do not constitute the object of this work. However, it is worth mentioning that a recent literature search revealed only one published unsymmetrical Tp with boron-centered chirality.[62]

The most widely employed method for production of symmetrical Tps has been established by Trofimenko.[1d] First, the pyrazole precursor, if not commercially available, is prepared through the condensation of the appropriate 1,3-diketone with hydrazine hydrate, usually in ethanol.[63–65] Then, sodium or potassium borohydride is added to an excess of pyrazole melt at 170–190 °C to form the corresponding alkaline Tp salts.[1,2] Both steps are detailed in Figure 3.1, using the general structures of intermediates bearing perfluorinated R_f groups used in this work.

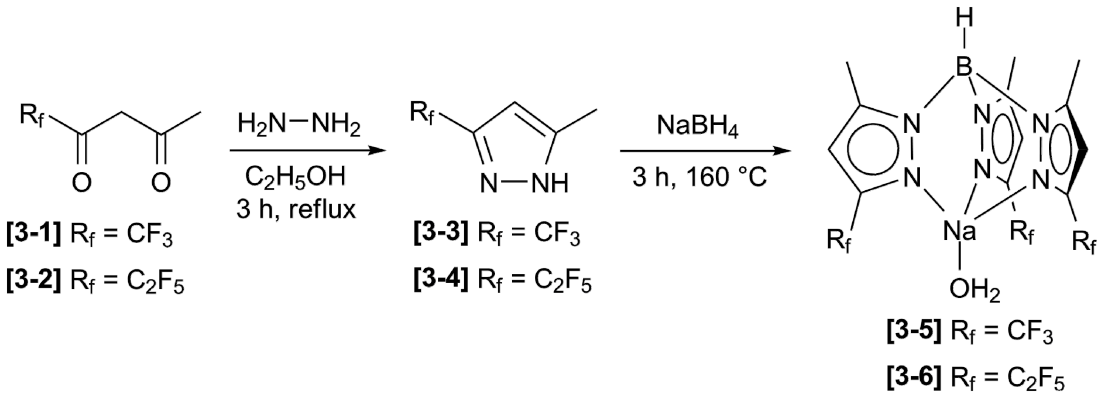

Figure 3.1 Reaction scheme for production of TpNa salts.

Table 3.1 Fluorinated Diketones, Pyrazoles and Sodium Trispyrazolylborates

R_f	Diketone	Pyrazole	Trispyrazolylborate
CF_3	1,1,1-trifluoro-2,4-pentanedione	3-trifluoromethyl-5-methylpyrazole	hydrotris(3-trifluoromethyl-5-methyl-pyrazol-1-yl)borato-sodium hydrate
		abbr. Pz^{CF_3,CH_3}	*abbr.* $Tp^{CF_3,CH_3}Na(H_2O)$
	[3-1]	**[3-3]**	**[3-5]**
C_2F_5	5,5,6,6,6-penta-fluoro-2,4-hexane-dione	3-pentafluoro-ethyl-5-methyl-pyrazole	hydrotris(3-pentafluoroethyl-5-methyl-pyrazol-1-yl)borato-sodium hydrate
		abbr. $Pz^{C_2F_5,CH_3}$	*abbr.* $Tp^{C_2F_5,CH_3}Na(H_2O)$
	[3-2]	**[3-4]**	**[3-6]**

Table 3.1 details the nomenclature, abbreviations and numbering of the compounds used herein as precursors for production of silver scorpionates. For synthetic purposes, sodium or potassium Tp salts are preferred because of their thermal stability and good solubility in organic solvents. They can be safely used in reactions at high temperature without any danger of significant ligand decomposition during the process.[2,6] In this study, NaTps **[3-5]** and **[3-6]** were produced from the corresponding fluorinated pyrazoles **[3-3]** and **[3-4]**, respectively, and further used for obtaining AgTps by the one-pot metal exchange between Na and Ag (Figure 3.2). The silver source was either

silver(I) nitrate ($AgNO_3$) or anhydrous silver(I) trifluoromethanesulfonate (also known as silver(I) triflate, *abbr.* AgOTf). The most suitable solvent for this process was found to be THF, and the σ-donor ligands used for complexation of the Ag^+ cation ranged from toluene (in η^2 coordination) to triphenylphosphine oxide. Table 3.2 presents a summary of the silver complexes produced, including systematic names, structure numbers and abbreviations used henceforth.

Table 3.2 Silver Scorpionates

L	**$R_f = CF_3$**	**$R_f = C_2F_5$**
Toluene (Tol)	hydrotris(3-trifluoromethyl-5-methylpyrazol-1-yl)borato-silver(I)-(η^2)-toluene *abbr.* $Tp^{CF_3,CH_3}Ag(Tol)$ **[3-7]**	hydrotris(3-pentafluoroethyl-5-methylpyrazol-1-yl)borato-silver(I)-(η^2)-toluene *abbr.* $Tp^{C_2F_5,CH_3}Ag(Tol)$ **[3-8]**
Methyl-diphenyl-phosphine ($PMePh_2$)	hydrotris(3-trifluoromethyl-5-methylpyrazol-1-yl)borato-silver(I)-methyldiphenylphosphine *abbr.* $Tp^{CF_3,CH_3}Ag(PMePh_2)$ **[3-9]**	hydrotris(3-pentafluoroethyl-5-methylpyrazol-1-yl)borato-silver(I)-methyldiphenylphosphine *abbr.* $Tp^{C_2F_5,CH_3}Ag(PMePh_2)$ **[3-10]**
Triphenyl-phosphine (PPh_3)	hydrotris(3-trifluoromethyl-5-methylpyrazol-1-yl)borato-silver(I)-triphenylphosphine *abbr.* $Tp^{CF_3,CH_3}Ag(PPh_3)$ **[3-11]**	Did not form*
Triphenyl-phosphine oxide ($OPPh_3$)	hydrotris(3-trifluoromethyl-5-methylpyrazol-1-yl)borato-silver(I)-triphenylphosphine oxide *abbr.* $Tp^{CF_3,CH_3}Ag(OPPh_3)$ **[3-12]**	hydrotris(3-pentafluoroethyl-5-methylpyrazol-1-yl)borato-silver(I)-triphenylphosphine oxide *abbr.* $Tp^{C_2F_5,CH_3}Ag(OPPh_3)$ **[3-13]**

* Several reaction pathways were attempted, none of which produced the desired compound. These will be discussed in Section 3.3.1.

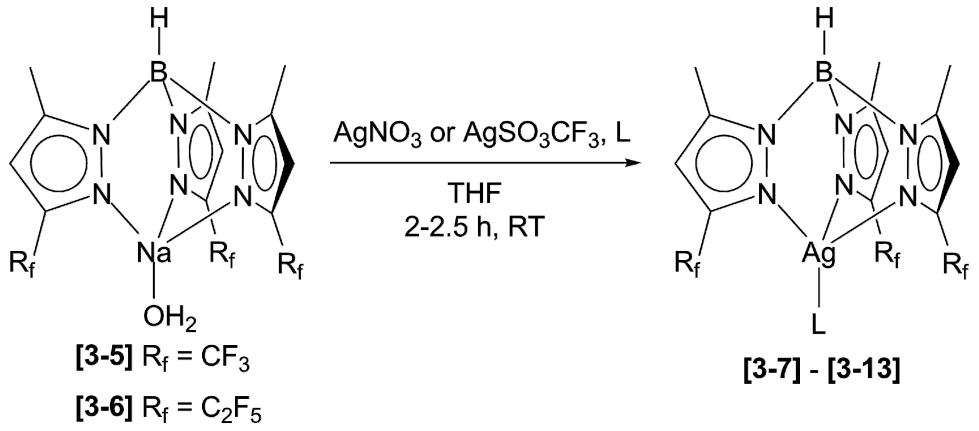

Figure 3.2 Reaction scheme for production of silver trispyrazolylborates.

3.1.1 Fluorinated Trispyrazolylborates as Chelating Agents

Most of the studies involving Tps, past and present, have been focused on conventional, non-fluorinated complexes.[2,3,6,66–68] The fluorinated analogues, either partially- or per-fluorinated, were obtained relatively late, and since the first published member of this class, $Tp^{CF_3,CH_3}Ir(CO)(\eta^2\text{-}C_2H_4)$ in 1989,[33] they remained practically unexplored. Among the only 11 fluorinated Tp ligands (and around 60 associated TpMs) known, research has revolved around the symmetrical, perfluorinated Tp^{CF_3,CF_3}, with over 40 TpM compounds published. However, it is the mixed alkyl-perfluoroalkyl substituted Tps that have shown increased stability and the most promising applications in dioxygen binding, homogeneous catalysis and intramolecular C–H activation,[27,28,33,69–73] while the perfluorinated compounds containing groups like Tp^{CF_3,CF_3} proved to be either inefficient in these processes[74] or too unstable in obtaining the desired metal adducts.[75] An overview of the majority of fluorinated Tps published to date, along with their reported properties and applications, is given in Table 3.3. Abbreviations follow the guidelines described in Section 1.2.

Table 3.3 Literature Overview of Fluorinated Trispyrazolylborates[†]

Tp	M(L)	Reported properties and literature reference
Tp^{CF_3}	$Na_2(THF)_2$ *dimer*	Characterization[64]
	$Ag(PPh_3)$	
	$Mn(CO)_3$	Characterization, comparison with nonfluorinated analogues, CV studies[76]
	Cu(CO)	
	$Ag(P(i\text{-}Bu)_3)$	Characterization[77]
$Tp^{C_2F_5}$	$Na(Pz^{C_2F_5})\bullet Pz^{C_2F_5}$	Characterization, stable copper(I) adducts with carbon monoxide[78]
	Cu(CO)	
$Tp^{C_3F_7}$	Na	Characterization, stable copper(I) adducts with carbon monoxide[78]
	Cu(CO)	
$(Me)Tp^{CF_3}$	Tl	Characterization[79]
	$Cu(\eta^2\text{-}C_2H_4)$	
	$Ag(\eta^2\text{-}C_2H_4)$	Characterization[80]
$(Me)Tp^{C_2F_5}$	Li	Characterization, first boron-protected fluorinated Tp ligand[81]
	Ag(CO)	
	$Ag(\eta^2\text{-}C_2H_4)$	
$(Ph)Tp^{CF_3}$	$Ag(\eta^2\text{-}C_2H_4)$	Characterization[80]
$Tp^{C_2F_5,CH_3}$	$Na(H_2O)$	Characterization, first publication of the mixed $Tp^{C_2F_5,CH_3}$ ligand[85]
$Tp^{CF_3,Ph}$	Na(THF)	Characterization[84]
	$Na(H_2O)$	
	Cu(CO)	
$Tp^{CF_3,Tn}$	Tl	Characterization[86]
Tp^{CF_3,CH_3}	K	First publication on the Tp^{CF_3,CH_3} ligand,[33] intramolecular C–H activation and increased stability,[33,69,70] photochemical benzene activation and ethylene insertion[70]
	$Ir(CO)(\eta^2\text{-}C_2H_4)$	
	Cu(NCMe)	Characterization, Cu–NO chemistry, kinetic and spectroscopic studies[9]
	Cu(CO)	
	$Cu(\eta^2\text{-}O_2N)$	
	Rh(COD)	Characterization and solution behaviour[82]
	$Rh(CO)_2$	Characterization, isomerism and coordination geometry studies[83]
	Rh(NBD)	
	$Na(H_2O)\bullet Pz^{CF_3,CH_3}$	Characterization[84]
	$Co(\eta^2\text{-}O_3N)(NCMe)$	Characterization, oxidation catalysis[28]
	$Mn(\eta^2\text{-}O_3N)(NCMe)$	
	Cu_2O_2 *dimer*	Characterization, exceptionally stable dinuclear copper(I)-peroxo complex[71]
	Cu_2 *dimer*	Characterization, reversible binding of oxygen[72]
	Cu(NCMe)	Characterization, spontaneous aerobic acetone oxidation in solution[27]
	Cu(lactate)	
	$Cu(PPh_3)$	Characterization, observations on stability and reactivity with various ligands[73]
	Cu(CO)	

Table 3.3 (continued) Literature Overview of Fluorinated Trispyrazolylborates†

Tp	M(L)	Reported properties and literature reference
	In	Characterization[87a]
	Ag(THF)	Characterization[87a,b]
	Cu(CN*t*-Bu)	Characterization[87c]
	K(DMA)	Characterization[64]
	$Na(H_2O)$	
	Cu(DMA)	
	$Cu(PPh_3)$	
	$Ag(PPh_3)$	
	Au(CO)	Characterization, thermal and solvent stability[87d]
	Au(CN*t*-Bu)	
	Ag(CO)	Characterization[87b,e]
	Ag(η^2-Tol)	
	Ag(η^2-C_2H_4)	Characterization[87e]
	Ag(η^2-C_2H_2)	
	Ag(η^2-C_2HPh)	
	Ag(CN*t*-Bu)	Characterization[87b,e]
	Ag(NC*t*-Bu)	Characterization[87b]
	Ga	Characterization[87f]
	Sn(OTf)•Pz^{CF_3,CF_3}	
Tp^{CF_3,CF_3}	Ag(OC_2H_4)	Characterization[87g]
	Ag(SC_3H_6)	Characterization, metathesis reaction with formation of unsupported Ag–Ge bonds[87h]
	Ag(Ge(Cl)[$(Me)_2$ATI])	
	Ag(Ge(OTf)[$(Me)_2$ATI])	
	Cu(NNN(1-Ad))	Characterization, adducts of copper and silver with adamantane-substituted azide[88]
	Ag(N(1-Ad)NN)	
	Ag($(OCOMe)_2CN_2$)	Characterization[89]
	Ag(Ge(Cl)[(nPr)$_2$ATI])	Characterization[90]
	$Al(Me)_2$	Characterization, TpAg used as ligand transfer agent[91]
	Zn(Et)	
	Ag(DMSO)	Characterization,[93] studies of antimicrobial properties of silver compounds[92,94]
	$Mn(CO)_3$	Characterization[76]
	Cu(NCMe)	
	Ag(Ge(N_3)[(n-Pr)$_2$ATI])	Characterization[95]
	Ag(Sn(N_3)[(n-Pr)$_2$ATI])	
	$Na(OEt_2)$	Characterization[84]
	$Rh(CO)_2$	Characterization, isomerism studies[83]
	Rh(NBD)	
	Rh(COD)	

† Abbreviations: Tn = 2-thienyl; NCMe = acetonitrile, NBD = norbornadiene, CN*t*-Bu = *tert*-butyl-isonitrile, NC*t*-Bu = pivalonitrile, OC_2H_4 = ethylene oxide, SC_3H_6 = propylene sulfide, $(Me)_2$ATI = *N*-methyl-2-(methylamino)troponiminate, NNN or N_3 = azide, 1-Ad = 1-adamantyl, $(OCOMe)_2CN_2$ = di-methyldiazomalonate, (n-Pr)$_2$ATI = *N*-propyl-2-(propylamino) troponiminate, COD = 1,5-cyclooctadiene.

The little amount of data on mixed alkyl-perfluoroalkyl trispyrazolylborates, as evidenced by the previous table, asks for more exploratory research in the field. This work attempts to elaborate an in-depth study on the variation of thermodynamic stability with the electronic properties of the ligands, through complete characterization of a series of silver compounds, one of the least structurally characterized families of Tps.

3.1.2 Electronic and Steric Effects in Silver Scorpionates

The first silver scorpionates of the type TpAg(L) were reported in the 1970s and contained the common Tp, (Pz)Tp and Tp^{CH_3,CH_3} ligands, while the L group was limited to P-donors and isonitrile.[96] For almost 25 years thereafter, most of the TpAg chemistry has revolved around these few complexes, until a systematic solid-state and solution study of several silver–phosphino complexes was published by Santini et al. in 1998.[67] The obvious reason for the scarce research in the field was the ease of reduction of silver(I) to metallic silver, especially under light and/or heating, which discouraged synthetic efforts and applications. The instability of these compounds is also heightened by the reducing power of the borate anion retaining one proton, which can decompose the complexes according to the following equation:[3,67,97]

$$2\ [HB(Pz)_3]Ag(PR_3) \rightarrow H_2 + 2\ Ag + [B(Pz)_3]_2 + 2\ PR_3 \qquad (3.1)$$

The transformation above occurs with highest rates in halogenated solvents, in which the complexes are nonelectrolytes, even with strict exclusion of light and air.[97] In other solvents the degree of instability varies: they have been found stable in toluene and benzene in the dark, and some decompose to a certain extent in acetone. Most of the reported silver Tps are relatively stable in the solid state under air, and more or less light-sensitive, based on the balance between electronic and steric factors in the structure.

Although limited in number compared to other TpM complexes, around 60 structurally characterized TpAg compounds were found, most of them published in the past three decades. However, a large percent of these is composed of di- and trinuclear structures of the type $[TpAg]_n$, making them irrelevant for the scope of this work. The structural search[60] was then restricted to published $TpAg(PR_3)$ complexes, as their similarity with compounds **[3-7]** to **[3-13]** provides the most meaningful data for comparison. The 16 complexes found (Table 3.4), constitute a large enough sampling pool for analyzing the influence of electronic and steric factors in the average Ag–N (<Ag–N>) and Ag–P bond lengths. Surprisingly, no structurally characterized $Tp^{R3,4\text{-}R4,R5}Ag(OPPh_3)$ complexes, nor a $Tp^{CF3,CH3}Ag(PR_3)$ representative were reported.

The structural data suggest that the Ag–P distance is mostly influenced by steric factors, namely the bulkiness of the phosphino ligand and substituents in the 3-position of the Pz rings, and not as much by electronic factors like the basicity of the PR_3 σ-donor or the overall electron-withdrawing effects of the Tp moiety. Clearly, the longest Ag–P bonds are observed when a 3-CF_3 group is present, in the case of $Tp^{CF3,CF3}Ag(PPh_3)$; intermediate values are found for $Tp^{CH3,CH3}$ compounds and $Tp^{4\text{-}Br}Ag(PPh_3)$, in which the less bulky substituents in the 3-positions, or lack thereof, allows for a shorter length (stronger Ag–P bond) to compensate for the decreased basicity of the Pz rings. $Tp^{Indazolyl}Ag(PPh_3)$ and $TpAg(PPh_3)$ complexes, having the least steric hindrance, exhibit the shortest Ag–P distances.

Analysis of the reported average lengths of the Ag–N bond suggests a mixed electronic-steric influence. Bulky and strong electron-withdrawing 3-CF_3 groups allow for the synergy of both electronic and steric factors in imposing the longest <Ag–N>

distances of 2.433 and 2.431 Å for $Tp^{CF_3,CF_3}Ag(PPh_3)$ and $Tp^{CF_3}Ag(P(i\text{-}Bu)_3)$, respectively. This is not surprising, given that an electron-withdrawing group in the 3-position is expected to decrease the basicity of the proximal, silver-bonded nitrogen atoms, resulting in a weaker bond and, consequently, longer <Ag–N> distances.

A constant increase in the bulkiness of the PR_3 group and steric crowding around the metal center provide a uniform lengthening of the Ag–N bonds, regardless of the nature of Pz substituents; this is noticed, for example, when P(*o*-tolyl)$_3$, P(*i*-Bu)$_3$ or PBz_3 are employed instead of PPh_3.

Table 3.4 Structurally Characterized $TpAg(PR_3)$ Complexes†

$TpAg(PR_3)$	**<Ag–N>** (Å)	**Ag–P** (Å)	**Reference**
$Tp^{CH_3,CH_3}Ag(PPh_3)$*	2.345	2.348	98
$TpAg(P(i\text{-}Bu)_3)$	2.363	2.347	77
$Tp^{CH_3}Ag(P(i\text{-}Bu)_3)$	2.381	2.354	77
$Tp^{CF_3}Ag(P(i\text{-}Bu)_3)$*	2.431	2.383	77
$Tp^{CH_3,4\text{-}\gamma\text{-}Py,CH_3}Ag(PPh_3)$	2.338	2.340	99
$Tp^{CH_3,\ 4\text{-}\gamma\text{-}Py\text{-}sub,CH_3}Ag(PPh_3)$	2.321	2.315	99
$Tp^{CH_3,CH_3}Ag(PMePh_2)$	2.327	2.335	66
$Tp^{CH_3,CH_3}Ag(P(o\text{-tolyl})_3)$	2.373	2.368	66
$TpAg(PPh_3)$*	2.343	2.337	67
$TpAg(P(o\text{-tolyl})_3)$	2.356	2.369	67
$TpAg(PBz_3)$	2.359	2.327	67
$Tp^{CH_3,CH_3}Ag(P(p\text{-tolyl})_3)$	2.333	2.332	67
$Tp^{4\text{-}Br}Ag(PPh_3)$	2.374	2.344	67
$(Pz^{CH_3})Tp^{CH_3}Ag(P(m\text{-tolyl})_3)$*	2.309	2.352	100
$Tp^{Indazolyl}Ag(PPh_3)$	2.337	2.332	101
$Tp^{CF_3,CF_3}Ag(PPh_3)$	2.433	2.375	64

† Abbreviations: Py-sub = functionalized pyridine,[99] $Tp^{Indazolyl}$ = trisindazolylborate.
* Compounds displaying 2 or 3 independent structures in the crystal lattice, with slightly different angles and bond lengths; average values over all independent components are presented.

3.2 Experimental Section

3.2.1 Synthesis and Characterization of Pz^{CF_3,CH_3}

Hydrazine hydrate, 4.1 mL (4.2 g, 84 mmol) was added to a stirred solution of 12.95 g (84 mmol) of **[3-1]** in 110 mL ethanol. The reaction mixture was refluxed for 3 h and cooled to 50 °C. The ethanol was removed under vacuum giving a yellow solid, which was purified *via* recrystallization from toluene to afford **[3-3]** as a white crystalline solid in 77% yield. Mp: 86–87 °C (lit.[33] 85–86 °C); ^{1}H NMR (300 MHz, $CDCl_3$): δ 2.35 (3H, s, 5-C*H*$_3$), 6.32 (1H, s, 4-C*H*), 8.91 (1H, br, N*H*); ^{19}F NMR (282 MHz, $CDCl_3$): δ −62.24 (3F, s, 3-C*F*$_3$); IR (KBr): 3194, 3120, 2890, 2814, 2562, 1587, 1504, 1254, 1159 cm^{-1}.

3.2.2 Synthesis and Characterization of $Pz^{C_2F_5,CH_3}$

Hydrazine hydrate, 25 mL (25.73 g, 0.5 mol) was added slowly to a stirred solution of 100 g (0.49 mol) of **[3-2]** in 250 mL ethanol. The mixture was refluxed for 3 h, cooled to 50 °C and the solvent removed under vacuum. The resulting oil crystallized gradually while standing at RT. Recrystallization from hexanes gave **[3-4]** as a colorless crystalline solid in 74% yield based on **[3-2]**; alternatively, the crude oil can be purified in small amounts by sublimation under vacuum at 105 °C. Mp: 85–86 °C; ^{1}H NMR (300 MHz, $CDCl_3$): δ 2.32 (3H, s, 5-C*H*$_3$), 6.31 (1H, s, 4-C*H*), 9.28 (1H, br, N*H*); ^{19}F NMR (282 MHz, $CDCl_3$): δ −85.29 (3F, s, C*F*$_3$), −113.62 (2F, s, C*F*$_2$); ^{13}C NMR (75 MHz, $CDCl_3$): δ 8.39 (q, $^{1}J_{C-H}$ = 133 Hz, 5-*C*H$_3$), 104.97 (d, $^{1}J_{C-H}$ = 184 Hz, 4-*C*H), 112.22 (tq, $^{1}J_{C-F}$ = 257.4 Hz, $^{2}J_{C-F}$ = 40.3 Hz, *C*F$_2$), 120.3 (qt, $^{1}J_{C-F}$ = 293.7 Hz, $^{2}J_{C-F}$ = 39.5 Hz, *C*F$_3$), 143.07 (td, $^{2}J_{C-F}$ = 29.2 Hz, $^{2}J_{C-H}$ = 5.2 Hz, *C*CF$_2$CF$_3$), 143.57 (q, $^{2}J_{C-H}$ = 7.1 Hz, *C*CH$_3$); IR (KBr): 3198, 3118, 2885, 2793, 2620, 1587, 1340, 1226 cm^{-1}.

3.2.3 Synthesis and Characterization of $Tp^{CF_3,CH_3}Na(H_2O)$

A mixture of 6.9 g (46 mmol) pyrazole **[3-3]** and 0.52 g (14 mmol) $NaBH_4$ was heated without stirring to 100 °C. When the entire amount of **[3-3]** has melted, stirring was started and the mixture was heated to 160 °C for 3.5 h, monitoring hydrogen evolution by an oil bubbler. The mixture was then cooled to RT, washed with hexanes (3 × 50 mL), dissolved in chloroform (50 mL), filtered and concentrated under reduced pressure, yielding pure **[3-5]** as a white solid in 67% yield (3.63 g). Spectroscopic properties matched the previously reported values: ^{1}H NMR (300 MHz, $CDCl_3$): δ 2.40 (lit.[82] 2.44) (9H, s, 5-CH_3), 6.25 (lit.[82] 6.17) (3H, s, 4-C*H*); ^{19}F NMR (282 MHz, $CDCl_3$): δ −60.71 (lit.[82] −62.2) (3F, s, CF_3).

3.2.4 Synthesis and Characterization of $Tp^{C_2F_5,CH_3}Na(H_2O)$

A mixture of 13 g (65 mmol) pyrazole **[3-4]** and 0.6 g (15 mmol) $NaBH_4$ was heated without stirring to 100 °C. When the entire amount of **[3-4]** has melted, the stirring was started and the mixture was heated to 160 °C for 3 h. Hydrogen evolution was monitored by an oil bubbler. After 3 h, the mixture was cooled to RT, dissolved in chloroform, filtered and concentrated under reduced pressure, yielding a white solid. The solid was washed with 30 mL hexanes, filtered off and dried under air. Unreacted **[3-4]** was removed via fractional sublimation at 120 °C, affording pure **[3-6]** in 62% yield based on $NaBH_4$. Mp: 147–148 °C; ^{1}H NMR (300 MHz, $CDCl_3$): δ 2.02 (2H, s, H_2O), 2.46 (9H, s, 5-CH_3), 6.18 (3H, s, 4-C*H*); ^{19}F NMR (282 MHz, $CDCl_3$): δ −85.65 (3F, s, CF_3), −113.92 (2F, s, CF_2); ^{13}C NMR (75 MHz, $CDCl_3$): δ 13.24 (q, $^1J_{C-H}$ = 128.5 Hz, 5-*C*H_3), 104.28 (d, $^1J_{C-H}$ = 178.0 Hz, 4-*C*H), 111.87 (tq, $^1J_{C-F}$ = 249.1 Hz, $^2J_{C-F}$ = 38.8 Hz, *C*F_2), 119.32 (qt, $^1J_{C-F}$ = 285.1 Hz, $^2J_{C-F}$ = 39.0 Hz, *C*F_3), 140.38 (td, $^2J_{C-F}$ = 27.1 Hz, $^2J_{C-H}$

= 5.1 Hz, *C*CF_2CF_3), 145.93 (quintet, $^2J_{C-H}$ = 6.9 Hz, *C*CH_3); IR (KBr): 3133, 2941, 2554 (B–H), 1540, 1336, 1234 cm^{-1}.

3.2.5 Synthesis and Characterization of $Tp^{CF_3,CH_3}Ag(Tol)$

A solution of **[3-5]** (0.1 g, 0.2 mmol) in THF (15 mL) was slowly added to $AgNO_3$ (0.037 g, 0.22 mmol) in THF (10 mL) at RT under inert atmosphere. After the addition, the mixture was stirred for 2 h at RT. The solvent was then removed under reduced pressure to obtain a white residue, which was dissolved in toluene, filtered, concentrated under vacuum and dried under air to obtain **[3-7]** as a white solid in 78% yield. Mp: 135–140 °C (decomposes without melting); ^{1}H NMR (300 MHz, $(CD_3)_2CO$): δ 2.31 (3H, s, Ph-C*H*$_3$), 2.45 (9H, s, 5-C*H*$_3$), 4.5–5.7 (1H, br, B*H*), 6.29 (3H, s, 4-C*H*), 7.10–7.26 (5H, m, Ar-*H*); ^{19}F NMR (282 MHz, $(CD_3)_2CO$): δ −60.81 (3F, s, C*F*$_3$); IR (KBr, selected bands): 3134, 2940, 2540 (B–H), 1352, 1190 cm^{-1}.

3.2.6 Synthesis and Characterization of $Tp^{C_2F_5,CH_3}Ag(Tol)$

Compound **[3-8]** was prepared similarly to **[3-7]**, using 0.11 g (0.2 mmol) **[3-6]** in THF (15 mL) and 0.037 g (0.22 mmol) $AgNO_3$ in THF (10 mL) at RT, and was obtained in 76% yield. Mp: 88–90 °C (liquid decomposes at 120–125 °C); ^{1}H NMR (300 MHz, $(CD_3)_2CO$): δ 2.31 (3H, s, Ph-C*H*$_3$), 2.55 (9H, s, 5-C*H*$_3$), 4.5–5.7 (1H, br, B*H*), 6.41 (3H, s, 4-C*H*), 7.10–7.26 (5H, m, Ar-*H*); ^{19}F NMR (282 MHz, $(CD_3)_2CO$): δ −84.29 (3F, s, C*F*$_3$), −112.98 (2F, s, C*F*$_2$); IR (KBr): 3128, 2917, 2529 (B–H), 1337, 1221, 1180, 1041 cm^{-1}.

3.2.7 Synthesis and Characterization of $Tp^{CF_3,CH_3}Ag(PMePh_2)$

Under argon atmosphere, 0.15 g (0.3 mmol) of **[3-5]** were dissolved in 15 mL THF and methyldiphenylphosphine (0.08 g, 0.4 mmol) was added. This mixture was then slowly dropped under stirring over a solution of AgOTf (0.075 g, 0.3 mmol) in 10 mL THF at RT and stirred for 2.5 h. The solvent was removed under reduced pressure, and the residue was extracted into benzene. The solution was further filtered through celite and the volatile materials were removed under vacuum to obtain a white powder, which was washed with hexanes and dried under air to obtain **[3-9]** in 71% yield. Mp: 248–249 °C with partial decomposition (stable until 230 °C); ^{1}H NMR (300 MHz, $CDCl_3$): δ 1.97 (3H, s, P-C*H*$_3$), 2.47 (9H, s, 5-C*H*$_3$), 4.5–5.3 (1H, br, B*H*), 6.22 (3H, s, 4-C*H*), 7.32–7.45 (6H, m, Ar-*H*), 7.55–7.75 (4H, m, Ar-*H*); ^{13}C {^{1}H} NMR (75 MHz, $CDCl_3$): δ 13.12 (s, *C*H$_3$), 13.96 (d, $^1J_{C-P}$ = 19.3 Hz, P-*C*H$_3$), 103.79 (s, 4-*C*H), 128.4 (d, $^3J_{C-P}$ = 10.2 Hz, C_m), 129.3 (q, $^1J_{C-F}$ = 123.5 Hz, *C*F$_3$), 129.94 (s, C_p), 132.74 (d, $^2J_{C-P}$ = 16.5 Hz, C_o), 134.72 (d, $^1J_{C-P}$ = 36.4 Hz, C_i), 142.48 (q, $^2J_{C-F}$ = 36.6 Hz, *C*CF$_3$), 145.16 (s, *C*CH$_3$); ^{19}F NMR (282 MHz, $CDCl_3$): δ −61.15 (3F, s, C*F*$_3$); ^{31}P {^{1}H} NMR (121.5 MHz, $CDCl_3$): δ −3.87 ($^1J_{P-^{107}Ag}$ = 648.2 Hz, $^1J_{P-^{109}Ag}$ = 748 Hz, $^5J_{P-F}$ = 8.3 Hz); IR (KBr): 3131, 2920, 2536 (B–H), 1461, 1255, 1188, 1106, 984 cm^{-1}.

3.2.8 Synthesis and Characterization of $Tp^{C_2F_5,CH_3}Ag(PMePh_2)$

Under argon atmosphere, 0.11 g (0.2 mmol) of **[3-6]** were dissolved in THF (10 mL), and methyldiphenylphosphine (0.05 g, 0.25 mmol) was added. This mixture was dropped under stirring to a solution of AgOTf (0.056 g, 0.22 mmol) in THF (10 mL) and kept for 2 h at RT. The solvent was removed under reduced pressure and the residue was extracted into toluene. Filtration through celite followed by slow evaporation of the

solvent afforded colorless crystals of **[3-10]** in 75% yield. Mp: 154–156 °C (decomposes without melting); ^{1}H NMR (300 MHz, $CDCl_3$): δ 1.93 (3H, s, P-CH_3), 2.48 (9H, s, 5-CH_3), 4.5–5.5 (1H, br, B*H*), 6.21 (3H, s, 4-C*H*), 7.30–7.43 (6H, m, Ar-*H*), 7.51–7.63 (4H, m, Ar-*H*); ^{19}F NMR (282 MHz, $CDCl_3$): δ −85.12 (3F, s, CF_3), −113.12 (2F, s, CF_2); ^{13}C {^{1}H} NMR (75 MHz, $CDCl_3$): δ 13.28 (s, *C*H_3), 13.95 (d, $^{1}J_{C-P}$ = 30.7 Hz, P-*C*H_3), 105.04 (s, 4-*C*H), 128.33 (d, $^{3}J_{C-P}$ = 16.4 Hz, C_m), 129.76 (d, $^{4}J_{C-P}$ = 3.5 Hz, C_p), 132.19 (d, $^{1}J_{C-P}$ = 22.5 Hz, C_i), 132.65 (d, $^{2}J_{C-P}$ = 25 Hz, C_o), 140.38 (t, $^{2}J_{C-F}$ = 43.6 Hz, *C*CF_2), 145.61 (s, *C*CH_3); ^{31}P {^{1}H} NMR (121.5 MHz, $CDCl_3$): δ −5.32 ($^{1}J_{P-^{107}Ag}$ = 667.1 Hz, $^{1}J_{P-^{109}Ag}$ = 732.4 Hz, $^{5}J_{P-F}$ = 16.6 Hz); IR (KBr): 3135, 2923, 2538 (B–H), 1331, 1210, 1182, 1043, 943, 506 cm^{-1}.

3.2.9 Synthesis and Characterization of $Tp^{CF_3,CH_3}Ag(PPh_3)$

Under inert atmosphere, a solution of 0.2 g (0.4 mmol) **[3-5]** and 0.105 g (0.4 mmol) triphenylphosphine in 15 mL THF was dropped over 0.07 g (0.41 mmol) $AgNO_3$ in 10 mL THF and stirred for 2 h at RT. The solvent was removed under reduced pressure, the residue was extracted into toluene, filtered through celite and concentrated, giving **[3-11]** in 76% yield. Mp: 160–220 °C (slowly decomposes over a wide temperature range, final melting point of residue 232 °C); ^{1}H NMR (300 MHz, $CDCl_3$): δ 2.48 (9H, s, 5-CH_3), 4.5–5.5 (1H, br, B*H*), 6.23 (3H, s, 4-C*H*), 7.33–7.45 (9H, m, Ar-*H*), 7.48–7.55 (6H, m, Ar-*H*); ^{19}F NMR (282 MHz, $CDCl_3$): δ −61.11 (3F, s, CF_3); ^{31}P {^{1}H} NMR (121.5 MHz, $CDCl_3$): δ 16.53 ($^{1}J_{P-^{107}Ag}$ = 631.8 Hz, $^{1}J_{P-^{109}Ag}$ = 729.0 Hz, $^{5}J_{P-F}$ = 7.2 Hz); IR (KBr): 3139, 3056, 2921, 2538 (B–H), 1353, 1257, 1188, 1130, 1070, 985, 523 cm^{-1}.

3.2.10 Synthesis and Characterization of $Tp^{CF_3,CH_3}Ag(OPPh_3)$

A solution of 0.1 g (0.2 mmol) **[3-5]** and 0.056 g (0.2 mmol) triphenylphosphine oxide in 15 mL THF was dropped over 0.052 g (0.2 mmol) AgOTf in 10 mL THF. The mixture was stirred for 2 h at RT and the solvent was removed under vacuum, yielding a white solid which was extracted with toluene, filtered and concentrated by slow evaporation to afford colorless crystals of **[3-12]** in 86% yield. Mp: 134–138 °C (decomposes without melting); ^{1}H NMR (300 MHz, $(CD_3)_2CO$): δ 2.52 (9H, s, 5-C*H*$_3$), 4.4–5.7 (1H, br, B*H*), 6.39 (3H, s, 4-C*H*), 7.51–7.76 (15H, m, Ar-*H*); ^{19}F NMR (282 MHz, $(CD_3)_2CO$): δ −60.95 (3F, s, C*F*$_3$); ^{31}P {^{1}H} NMR (121.5 MHz, $(CD_3)_2CO$): δ 26.78 (s); IR (KBr): 3135, 3064, 2934, 2567 (B–H), 1187, 1161 (P═O), 1120, 1069, 977, 793, 544 cm^{-1}.

3.2.11 Synthesis and Characterization of $Tp^{C_2F_5,CH_3}Ag(OPPh_3)$

0.22 g (0.4 mmol) **[3-6]** in 10 mL THF was added dropwise over 0.07 g (0.41 mmol) $AgNO_3$ in 25 mL THF. The mixture was stirred for 1 h at RT under inert atmosphere and the solvent was removed under vacuum. The residue was dissolved in toluene and stirred for 30 min to obtain the toluene adduct **[3-8]**. The solution was filtered, concentrated under vacuum, redissolved in 10 mL THF and finally dropped over 0.1 g (0.36 mmol) triphenylphosphine oxide in 15 mL THF. After 1 h of stirring the solvent was removed, the white residue extracted in toluene, filtered and concentrated to afford **[3-13]** as a white solid in 72% yield. Mp: 186–188 °C (decomposes without melting); ^{1}H NMR (300 MHz, $(CD_3)_2CO$): δ 2.25 & 2.50 (9H, s, 5-C*H*$_3$), 4.5–5.7 (1H, br, B*H*), 6.25 & 6.41 (3H, s, 4-C*H*), 7.51–7.73 (15H, m, Ar-*H*); ^{19}F NMR (282 MHz, $(CD_3)_2CO$): δ –84.19 (3F, s, C*F*$_3$), –111.65 (2F, br, C*F*$_2$); ^{31}P {^{1}H} NMR (121.5 MHz, $(CD_3)_2CO$): δ 24.72 (s); IR (KBr): 3061, 2957, 2554 (B–H), 1252, 1203 (P═O), 1180, 1041, 943, 542 cm^{-1}.

3.3 Results and Discussion

3.3.1 Synthesis

Production of the mixed alkyl-perfluoroalkyl pyrazoles **[3-3]** and **[3-4]** and corresponding TpNa salts **[3-5]** and **[3-6]** (Figure 3.1), followed well-established literature procedures,[1,2,63–65] previously described in Section 3.1. $NaBH_4$ was the reagent of choice for synthesis of the alkaline Tp ligands.

The seven silver scorpionates **[3-7]**–**[3-13]** (Table 3.2), of the TpAg(L) type, were synthesized under inert atmosphere by the one-pot metal exchange reaction between Na and Ag, mixing the TpNa precursor, silver source (either $AgNO_3$ or AgOTf) and ligand of choice (L) in THF at RT (Figure 3.2). A two-step process,[87] involving production of a TpAg(THF) intermediate before reacting it with the appropriate ligand, was thus avoided and the streamlined, one-pot approach afforded 70–80% yields in all cases. Attempts to produce these complexes in methanol resulted in significant lower isolated yields, mainly because of large amounts of product being decomposed according to eqn. 3.1 during the *in vacuo* evaporation of the solvent. Maintaining a low temperature (RT to 40 °C) throughout the solvent removal process becomes a key factor in minimizing the amount of product lost by thermal decomposition. In this respect, the solvent's bp value is critical, hence THF, with a lower bp than methanol, allows for evaporation at RT.

However, even in THF and under strict exclusion of air and light, minor decomposition cannot be avoided. The resulting insoluble metallic silver and $B(Pz)_3$ residues can easily be separated by extraction of the TpAg(L) product in a non-halogenated solvent such as toluene. Still, traces of the phosphino decomposition biproducts (PR_3 in eqn. 3.1) are likely to be extracted together with the TpAg complex,

and are prone for oxidation to phosphine oxides if the vials are kept under air. This accounts for OPR_3 impurities sometimes observed in the ^{31}P NMR spectra.

Attempts to synthesize $Tp^{C_2F_5,CH_3}Ag(PPh_3)$ on multiple occasions, through different approaches, have been unsuccessful. In the one-step reaction with AgOTf, the $Tp^{C_2F_5,CH_3}Na$ ligand was recovered untransformed as a mixture of H_2O and THF adducts (identified by IR and ^1H NMR), while the silver salt formed a dimer through incorporation of two PPh_3 molecules per silver atom, according to the equation below:

$$2\ CF_3SO_3Ag + 4\ PPh_3 \rightarrow [CF_3SO_3Ag(PPh_3)_2]_2 \qquad (3.2)$$

The structural identity of the above dimer was confirmed by X-ray diffraction on crystals readily formed by evaporation of an extracted toluene fraction (Figure 3.3).

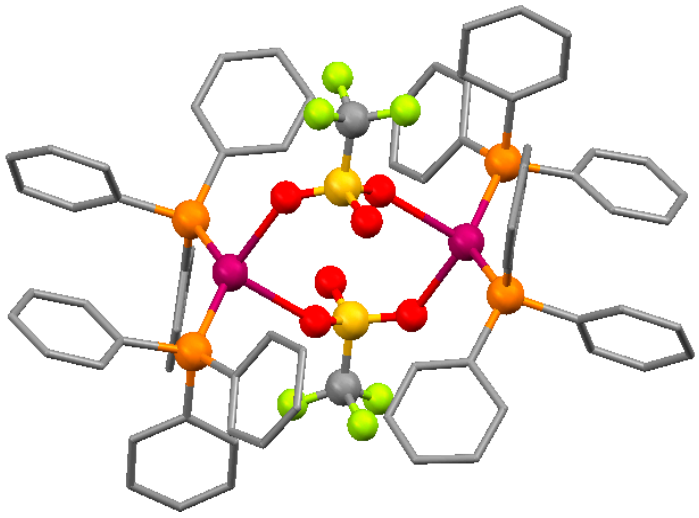

Figure 3.3 Ball-and-stick representation of the $[CF_3SO_3Ag(PPh_3)_2]_2$ dimer formed in the attempted one-pot synthesis of $Tp^{C_2F_5,CH_3}Ag(PPh_3)$. The phenyl groups are represented as capped sticks. Color code: C, gray; P, orange; O, red; F, light green; Ag, purple.

Several attempts to produce $Tp^{C_2F_5,CH_3}Ag(PPh_3)$ in two steps from the THF adduct resulted in recovery of the starting material partially decomposed; when old, unstabilized THF was used as solvent, peroxides present rapidly oxidized PPh_3 to a large enough

extent to isolate the $OPPh_3$ **[3-13]** adduct, identified by NMR and X-ray. All pieces of experimental evidence point out the fact that steric repulsion in the hypothetical $Tp^{C_2F_5,CH_3}Ag(PPh_3)$ molecule is a too high barrier to be surpassed by the basicity of PPh_3 and the electronegativity of C_2F_5 groups; consequently, the complex does not form.

3.3.2 IR Spectroscopy

IR spectra, presented in Figures B.1 to B.9, confirm the proposed structural features of the new complexes. In all cases, the *ν*(C–H) stretching vibrations of the Pz groups were found as medium to strong bands above 3100 cm^{-1}, while the "breathing" of the heterocyclic rings[67] appeared as weak to medium absorptions at *ca.* 1590–1530 cm^{-1}.

A signature of the spectra is the Tp-characteristic *ν*(B–H) stretch. The base value for this medium intensity band, recorded for the TpNa analogues, is 2538 cm^{-1} for **[3-5]** and 2536 cm^{-1} for **[3-6]**. The *ν*(B–H) band does not shift significantly upon replacement of Na with Ag, nor upon silver-coordination of various ligands except $OPPh_3$, in which case its associated wavenumber increases to 2567 and 2554 cm^{-1} in **[3-12]** and **[3-13]**, respectively.

The symmetric and antisymmetric *ν*(C–F) stretching vibrations of the CF_3 and C_2F_5 groups appear for all complexes as the strongest bands in the spectrum, in the 1170–1250 cm^{-1} region. For **[3-12]** and **[3-13]**, another strong absorption owing to the *ν*(P=O) stretch intercalates between the *ν*(C–F) bands. Its position was fixed at 1161 cm^{-1} for $Tp^{CF_3,CH_3}Ag(OPPh_3)$ and 1203 cm^{-1} for $Tp^{C_2F_5,CH_3}Ag(OPPh_3)$.

Bending *ν*(C–H) vibrations of the aromatic protons are observed at specific values between 500 and 1000 cm^{-1}, assembling the "footprint" region of each spectrum.

3.3.3 NMR Spectroscopy

All complexes described herein were characterized by ^{1}H, ^{19}F, ^{31}P (where applicable) and ^{13}C (for selected stable compounds) FT NMR spectroscopy. Heteronuclear spectra were acquired with proton decoupling, unless otherwise stated. A collection of processed spectra for compounds **[3-3]** through **[3-13]** is presented in Figures A.1 to A.31.

The NMR spectral data are particularly revealing for the unambiguous validation of the proposed structures; in all cases, they were consistent with the expected values based on literature published on similar complexes.

In the ^{1}H spectra, the methyl groups of the Pz rings consistently show at a δ value of 2.45–2.52 ppm, while the aromatic proton in the 4-position is detected as a downfield resonance at *ca.* 6.2 ppm; coordination of $OPPh_3$ in **[3-12]** and **[3-13]** slightly shifts this value to *ca.* 6.4 ppm. Resonances of the boron hydrogen appears, as expected,[67,87] as a broad signal stretched over ~1 ppm and centered around 5 ppm; most probably, the broadening is due to the interaction with the ^{11}B quadrupole ($I = 3/2$).[67]

A singular case of split ^{1}H signals was found for $Tp^{C_2F_5,CH_3}Ag(OPPh_3)$ **[3-13]** (Figure A.29). In this compound, the resonances of the 5-CH_3 and 4-*H* protons were observed as sets of two broad signals of unequal population (Figure 3.4). While the combined integration of the signals validates the proposed structure, the ratio of the integrals of the two signals in each set does not amount to an exact 2:1 split of the three Pz moieties. An $OPPh_3$ exchange in solution with the TpAg ligand was ruled out as a cause for the split, as the ^{1}H and ^{31}P resonances of the phosphine oxide ligand appeared as sharp, well-defined signals (Figures A.29 and A.31). The only reason which explains all pieces of NMR evidence is the hindered rotation of the $OPPh_3$ group around the Ag–O

bond, which, depending of the "lock" position between two bulky 3-C_2F_5 fragments, renders the adjacent Pz rings of the Tp ligand chemically and magnetically non-equivalent. A similar behavior was not noticed for the less sterically bulky CF_3 analogue **[3-12]**, which displays only sharp proton resonances. The ^{19}F signals of **[3-13]** were not effected by a similar split.

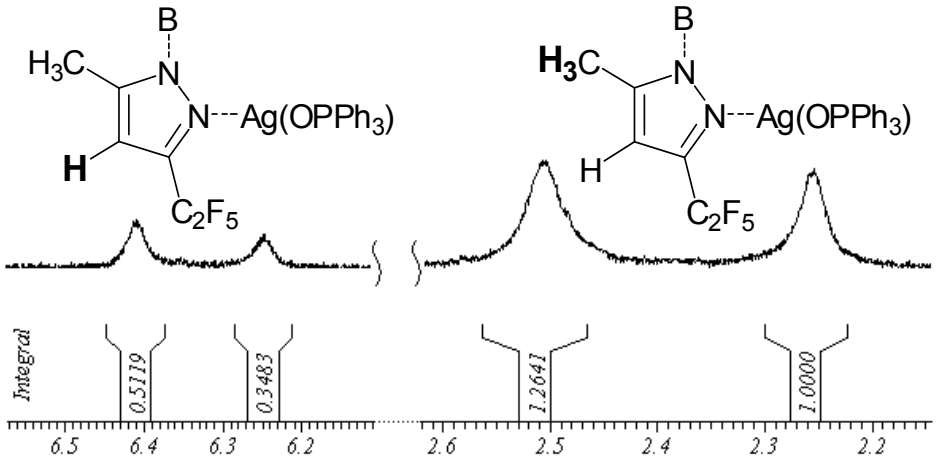

Figure 3.4 Detail of the ^1H NMR spectrum of $Tp^{C_2F_5,CH_3}Ag(OPPh_3)$, showing the two sets of broad resonances of the pyrazole protons and corresponding integration.

^{19}F chemical shifts of the CF_3 and C_2F_5 groups were consistently found at almost same positions as the base values recorded for the alkaline precursors **[3-5]** and **[3-6]**, viz. −60.7 ppm for CF_3, −85.7 (CF_2CF_3) and −113.9 (CF_2CF_3) ppm for C_2F_5, respectively. Coordination of the various ligands produced minimal shifts (< 1 ppm), if any, suggesting that the perfluoroalkyl spin system is unresponsive to electronic changes on the metal.

^{31}P NMR spectroscopy was instrumental in confirming the identity and stability of the phosphorous-containing compounds **[3-9]** to **[3-13]**. Recorded data matched previously reported observations[64,67] on signal multiplicities and Ag–P coupling constants in similar TpAg analogues. For each of the phosphino complexes **[3-9]–[3-11]**, the ^{31}P resonance showed two doublets, corresponding to the ^{107}Ag–^{31}P and ^{109}Ag–^{31}P couplings,

further split into a fine pattern by ^{31}P–^{19}F interactions (Figures A.18, A.22 and A.25). The calculated $^{1}J_{P-^{107}Ag}$ and $^{1}J_{P-^{109}Ag}$ values (e.g., 648 and 748 Hz, respectively, in **[3-9]**), are higher than the ones encountered for typical Ag(I) complexes, but not uncommon for silver scorpionates.[67] The $^{5}J_{P-F}$ coupling ranged within 7–8 Hz. A decrease of *ca.* 20 Hz of the Ag–P coupling constants when $PMePh_2$ is replaced with the less basic PPh_3 in **[3-11]** is indicative for a weaker bond. The difference in shift between the free phosphine and corresponding TpAg complexes, $\Delta\delta(^{31}P) = \delta(^{31}P_{TpAgPR_3}) - \delta(^{31}P_{PR_3})$, is on the order of 21–22 ppm (resonances for $PMePh_2$ and PPh_3 show at *ca.* −26.2 and −5.4 ppm, respectively); such a large upfield shift is characteristic of an exceptionally strong Ag–P bond. As expected, breaking the Ag–P spin coupling by intercalation of an oxygen atom, as PR_3 is replaced by $OPPh_3$ in **[3-12]** and **[3-13]**, results in drastic simplification of the ^{31}P spectra, the split signals being reduced to singlets. A comparative overview of ^{31}P spectral details for selected complexes is given in Figure 3.5.

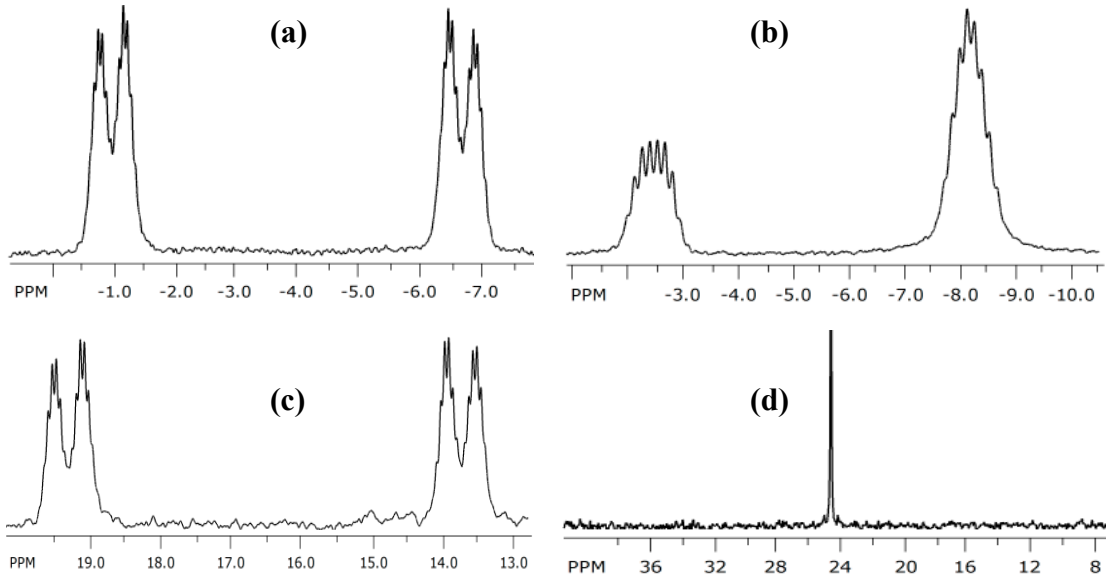

Figure 3.5 ^{31}P $\{^{1}H\}$ NMR spectra details for selected silver scorpionates. (a) $Tp^{CF_3,CH_3}Ag(PMePh_2)$. (b) $Tp^{C_2F_5,CH_3}Ag(PMePh_2)$. (c) $Tp^{CF_3,CH_3}Ag(PPh_3)$. (d) $Tp^{C_2F_5,CH_3}Ag(OPPh_3)$.

The absence of ligand exchange in solution is confirmed by sharp ^{1}H and ^{31}P resonances of all P-containing σ-donors of the new complexes. This indicates, above all else, a strong Ag–L interaction demanded by the enhanced Lewis acidity of the metal, in turn due to the extreme electronegativity of perfluoroalkyl groups (R_f) attached on the Tp moiety. Thus, it is shown that the apparent "destabilization" of the TpAg ligand by electron deficient R_f groups, through weakening of N–Ag bonds, can lead to a much more stable complex overall (with respect to regular, non-fluorinated analogues), when adequate, highly basic σ-donors are added to the metal's coordination sphere.

3.3.4 Crystal Structures

3.3.4.1 Pz^{CF_3,CH_3} and $Pz^{C_2F_5,CH_3}$. Although Pz^{CF_3,CH_3} has been known for 40 years and used extensively, its individual X-ray structure had not been reported; however, **[3-3]** was structurally characterized co-crystallized with the corresponding $Tp^{CF_3,CH_3}Na$.[84] Crystals of **[3-3]** and **[3-4]** were grown by slow evaporation of hexane solutions; they are of mediocre quality and thermally unstable, having a high vapor pressure (pungent odor). When cooled, they exhibit a marked decrease in quality, likely due to phase transitions that ultimately result in a powder pattern. X-ray data have been obtained at low temperature (100 K) from specimens that turned opaque upon cooling; the quality is not ideal and high-angle diffractions, despite the low temperature, are weak. Pz^{CF_3,CH_3} crystallizes in the tetragonal system, while crystals of $Pz^{C_2F_5,CH_3}$ are orthorhombic. In each case, four independent molecules were identified in the unit cell. The structures are shown in Figure 3.6; complete crystallographic data are provided in Appendices C and D. Both pyrazoles form "boat" type tetrameric assemblies via N–H•••N bonds (Figure 3.7); the tetramer assembly motif seems to be the norm among fluorinated pyrazoles.[102,103]

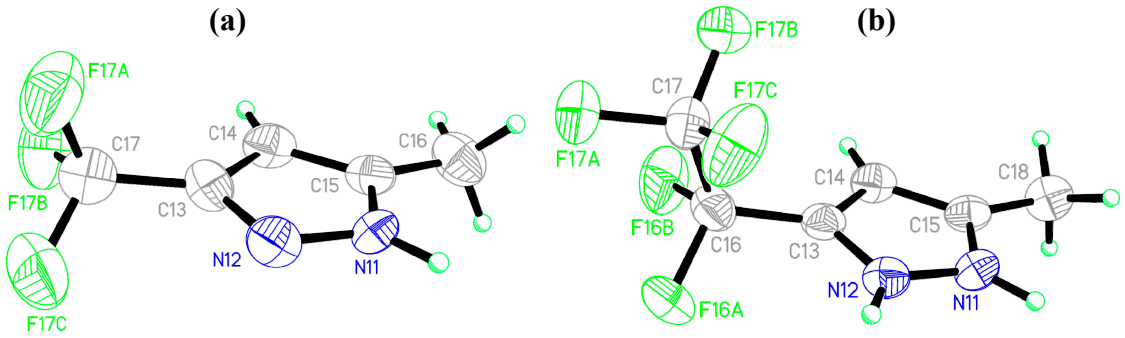

Figure 3.6 X-ray structures of Pz^{Rf,CH_3} in ORTEP representations set at 50% probability, showing in each case one of the four independent molecules. (a) Structure of **[3-3]**, R_f = CF_3. (b) Structure of **[3-4]**, R_f = C_2F_5; rotational disorder of the CH_3 group was not shown. For both, additional disorder in the fluoroalkyl groups is observed in other molecules in the unit cell (see Appendices C and D) while for **[3-4]** both N atoms appear protonated due to the disorder of the proton. Color code: C, gray; N, blue; F, green.

The compactness of the pyrazole packing within tetramers could be estimated by examining the N–H•••N distances, a 2D criterion. According to this criterion, **[3-3]** which exhibits the longer N–H•••N bond of 2.899 Å, produces the least compact tetramer, while **[3-4]**, with a N–H•••N bond of 2.872 Å, is the more compact one. However, this criterion does not account for the mutual orientation of the pyrazole planes. Therefore, a 3D criterion is proposed, namely the volume of the tetrahedron defined by the geometric centers of the four pyrazole rings.[85] Since, in general, these tetrahedra are irregular, one can approximate their volume by the volume of an idealized tetrahedron, calculated using the total surface area of the irregular tetrahedron; the latter can be easily computed considering only the lengths of the tetrahedron edges. According to this criterion, Pz^{CF_3,CF_3} (Figure 3.7(c)) produces the least compact tetramer, with a tetrahedral volume of 12.85 $Å^3$, followed by Pz^{CF_3,CH_3} and $Pz^{C_2F_5,CH_3}$, with volumes of 11.85 and 11.37 $Å^3$, respectively.[85] Note that the unit-cell volume, also a 3D criterion, is not useful in judging directly the intra-tetramers contacts since it also includes information about inter-tetramer interactions.

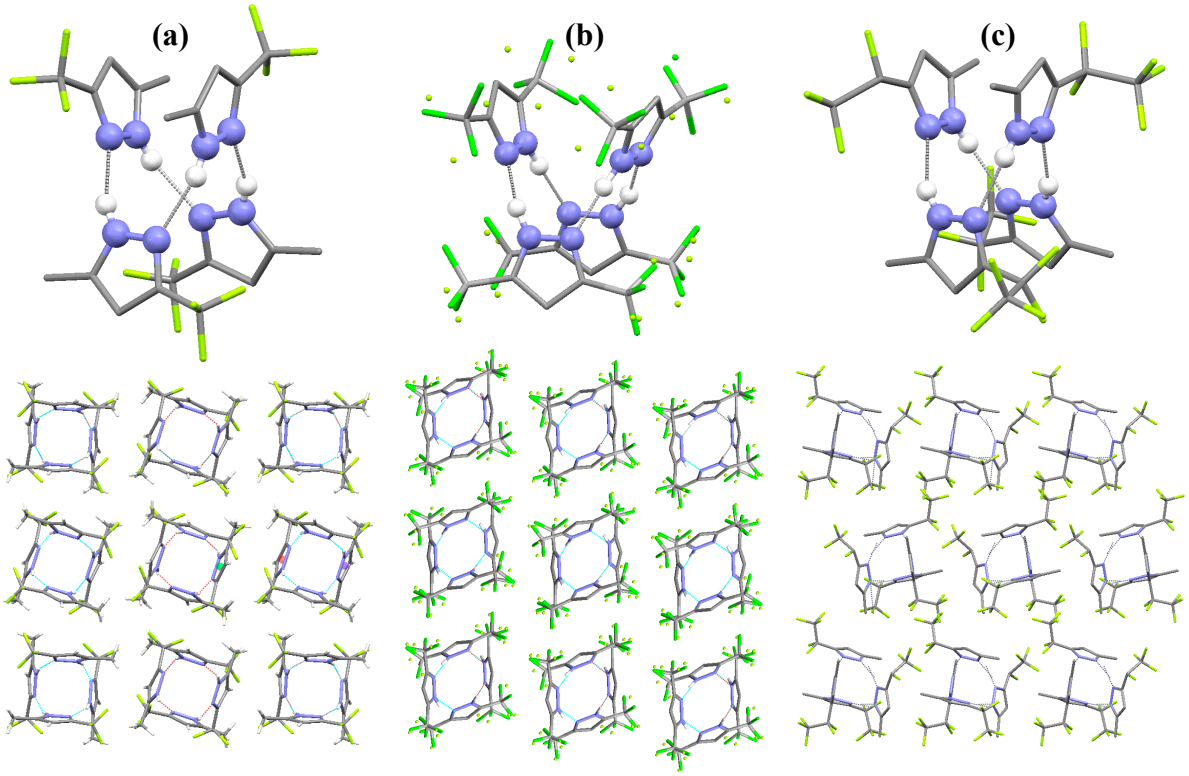

Figure 3.7 X-ray determined N–H•••N hydrogen bonded motifs present in the tetrameric assembly of $Pz^{R_f,R}$ (top row) and corresponding packing diagrams (bottom row). The atoms are colored using the scheme of Figure 3.6. The N and the H atoms bonded to them are shown as spheres; the rest of the pyrazole atoms are represented as capped sticks. C-bonded H atoms have been omitted, but rotationally disordered CF_3 groups are represented as points.[85] (a) Structure of **[3-3]**, R_f = CF_3, R = CH_3. (b) Structure of Pz^{CF_3,CF_3}, drawn using data from literature.[103] (c) Structure of **[3-4]**, $R_f = C_2F_5$, R = CH_3.

3.3.4.2 $Tp^{C_2F_5,CH_3}Na(H_2O)$. Crystals of **[3-6]** were obtained by slow evaporation from toluene in air. Their quality was mediocre, due to phase transitions occurring at the low temperatures required for X-ray data collection. The mounted crystals gradually lose transparency as the temperature is lowered beyond 191 K, resulting ultimately in the catastrophic loss of crystallinity at 177 K (Figure E.2). A compromise temperature of 192 K was, therefore, used for data collection.[85] Crystals of **[3-6]** are monoclinic; complete crystallographic parameters are given in Appendix E. An ORTEP representation is shown in Figure 3.8.

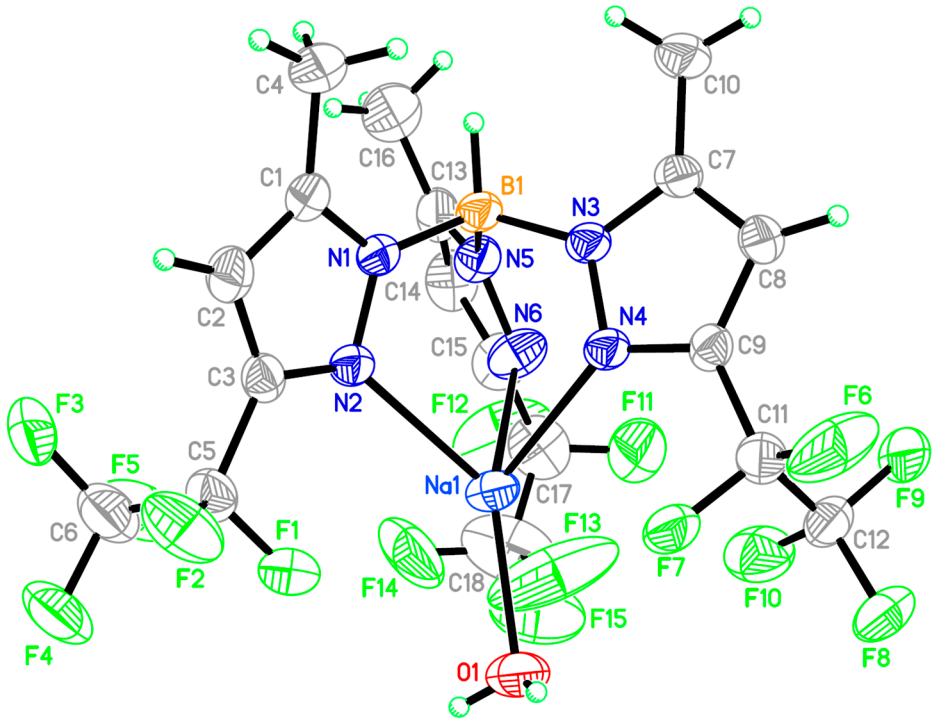

Figure 3.8 X-ray structure of $Tp^{C_2F_5,CH_3}Na(H_2O)$ in ORTEP representation at 40% probability. The disorder of the CF_3 subsets of the C_2F_5 groups is not shown for the sake of clarity. Color code: B, orange; C, gray; N, blue; F, green; Na, light blue; O, red.

The crystal packing diagram of **[3-6]** (Figure 3.9) shows weak intermolecular F•••H–O contacts (2.64, 2.53 Å) between the H atoms of coordinated water and two F atoms of the C_2F_5 groups, leading to the formation of a head-to-tail chain assembly. These distances are within the 2.70 Å value of the sum of the van der Waals radii of H and F. In contrast, **[3-5]** is a head-to-head dimer with bridging $Na(H_2O)$ units. Interestingly, a related head-to-tail chain is observed when the CH_3 group in **[3-5]** is replaced by CF_3 to give $Tp^{CF_3,CF_3}Na(H_2O)$,[64] a group whose steric demand is probably closer to CH_3 than C_2F_5. The above structures illustrate that even small differences in pyrazole substituents, while preserving the major molecular features and hydrated metal coordination, could lead to major differences in molecular isolation and crystal packing.[85]

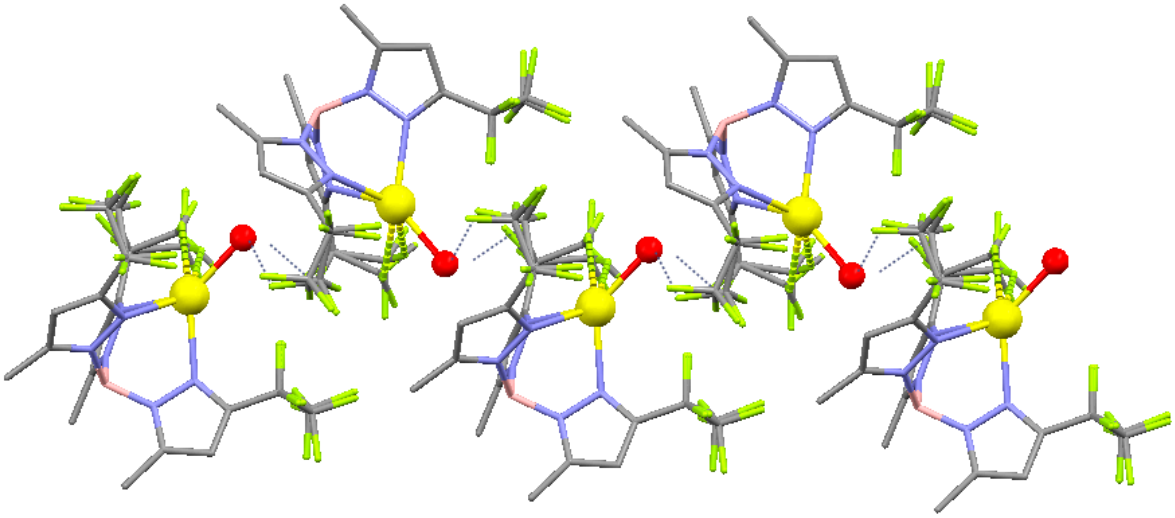

Figure 3.9 Ball and stick representation of the arrangement of $Tp^{C_2F_5,CH_3}Na(H_2O)$ molecules in the crystal lattice. H atoms have been omitted for the sake of clarity. The Na and O atoms are represented as yellow and red spheres, respectively. The F•••H–O contacts are represented as dotted lines.

3.3.4.3 $Tp^{CF_3,CH_3}Ag(Tol)$ and $Tp^{C_2F_5,CH_3}Ag(Tol)$. Suitable X-ray quality single crystals of the two toluene adducts **[3-7]** and **[3-8]** were obtained directly by slow evaporation at RT of the toluene solution used for their extraction from the reaction mixture. Inert atmosphere is not required, but exclusion of light is highly recommended in order to prevent degradation which would interfere with crystallization. Even so, darkening of some crystals was observed as soon as the solid was analyzed.

Crystals of both compounds are colorless and form in the same triclinic $P\bar{1}$ space group; four and two molecules per unit cell were identified for the CF_3 and C_2F_5 analogues, respectively. The crystal structure of **[3-7]** contained four additional toluene molecules per unit cell, highly disordered over two positions. No disorder was noticed for the perfluoroalkyl groups. Complete crystallographic data for the two complexes are provided in Appendices F and G. An ORTEP representation of **[3-7]** is shown in Figure 3.10.

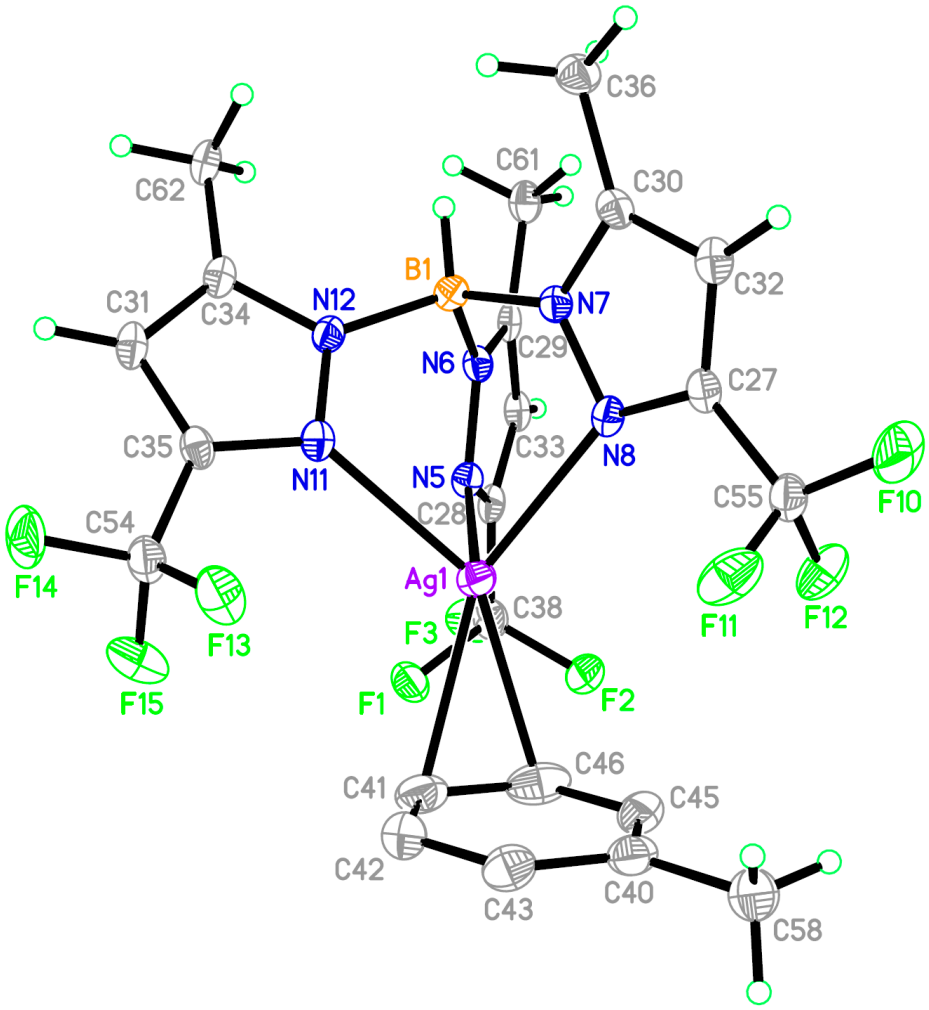

Figure 3.10 X-ray structure of $Tp^{CF_3,CH_3}Ag(Tol)$ in ORTEP representation at 40% probability. The disordered toluene molecules present in the lattice have been omitted for the sake of clarity. Color code: B, orange; C, gray; N, blue; F, green; Ag, purple.

Molecules of **[3-7]** assemble in a tridimensional structure through intermolecular F•••H interactions. Two such contacts were recognized: 2.604 Å between the 3-CH_3 group of one molecule and the 5-CF_3 moiety of the adjacent one, and 2.692 Å between Ag-coordinated toluene methyl groups and CF_3 groups of neighboring "head-to-head" oriented molecules (Figure 3.11). Both distances are typical for H-bonds of medium strength.

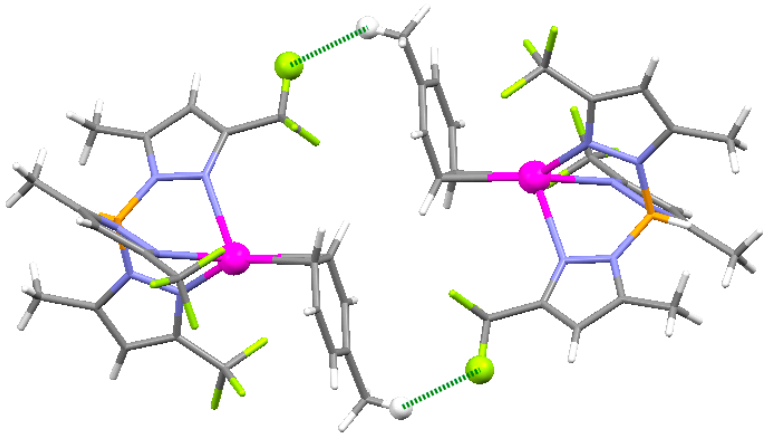

Figure 3.11 Capped sticks representation of the intermolecular contacts of two "head-to-head" $Tp^{CF_3,CH_3}Ag(Tol)$ molecules in the crystal lattice. Solvent molecules have been omitted for the sake of clarity. The Ag atoms, as well as the F and H atoms involved in the interaction, are represented as spheres, following the coloring scheme of Figure 3.10. The $F(CF_3)$•••$H(CH_3)$ contacts are shown as dotted green lines.

The crystals of **[3-8]**, mounted using paratone oil, deteriorate visibly even when kept at –10 °C. At –100 °C there is a phase transformation that cracks the crystals. In both cases powder X-ray patterns were observed. The –30 °C collection temperature was a reasonable compromise; at this temperature, the C_2F_5 groups exhibit significant motion and some degree of disorder. They were modeled initially by splitting them in two components, but there was no significant advantage over the single component model while the number of parameters increased. The coordinated toluene was refined as a rigid group with its ring geometry idealized as a hexagon. Large thermal ellipsoids are observed, but a rotationally disordered model (around the center of the phenyl ring) was unsatisfactory. Hydrogen atoms, with the exception of the boron hydrogen, which was refined, were placed in calculated positions. The largest peaks and holes, with electron densities less than 1 electron, were located near a fluorine and silver, respectively. An ORTEP representation of **[3-8]** is shown in Figure 3.12.

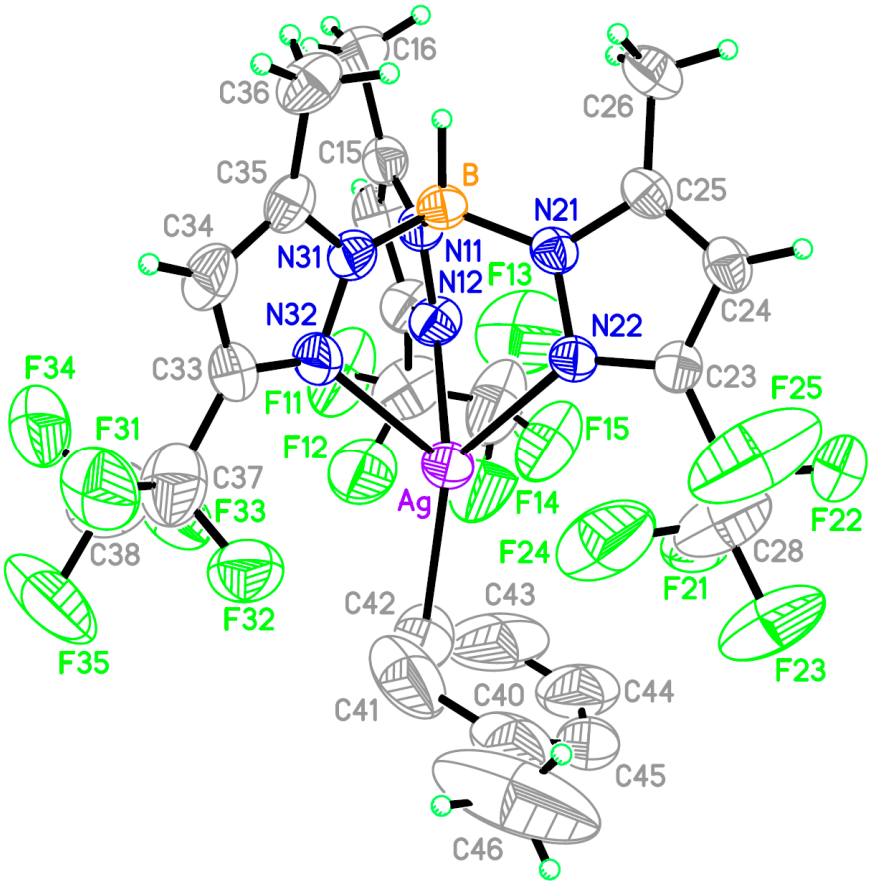

Figure 3.12 X-ray structure of $Tp^{C_2F_5,CH_3}Ag(Tol)$ in ORTEP representation at 30% probability. Color code: B, orange; C, gray; N, blue; F, green; Ag, purple.

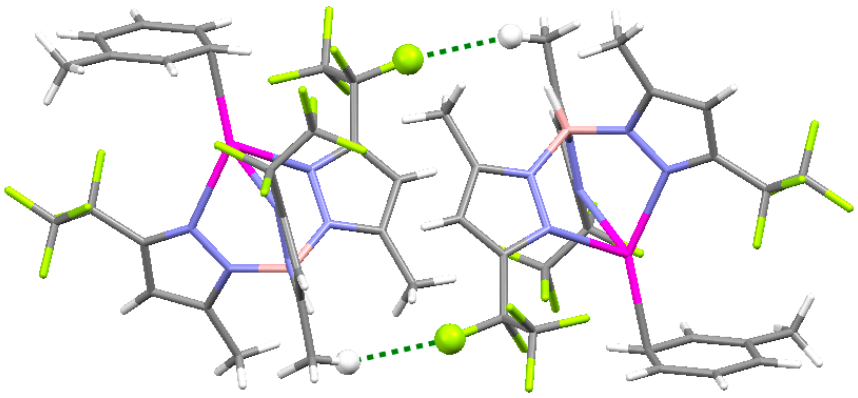

Figure 3.13 Capped sticks representation of the intermolecular $F(CF_2)\bullet\bullet\bullet H(CH_3)$ contacts between $Tp^{C_2F_5,CH_3}Ag(Tol)$ molecules in the crystal lattice. The F and H atoms involved in the interactions are represented as spheres. Atom coloring follows the scheme of Figure 3.12, with exception of B atoms colored in pink. The contacts are shown as dotted green lines.

The unit cell of **[3-8]** contains two molecules, linked by $F(CF_2)\bullet\bullet\bullet H(CH_3)$ distances of 2.518 Å in a dimer-like assembly (Figure 3.13). These "dimers" are further linked by F•••F distances of 2.856 Å with units of the neighboring cells. Both are short-contacts indicating intermolecular interactions.

3.3.4.4 $Tp^{CF_3,CH_3}Ag(PMePh_2)$ and $Tp^{C_2F_5,CH_3}Ag(PMePh_2)$. Slow recrystallization from toluene solutions at RT afforded excellent quality single crystals of **[3-9]** and **[3-10]**, exceptionally stable both under air and ambient light. Thermal ellipsoid plots of **[3-9]** and **[3-10]** are presented in Figures 3.14 and 3.15, respectively.

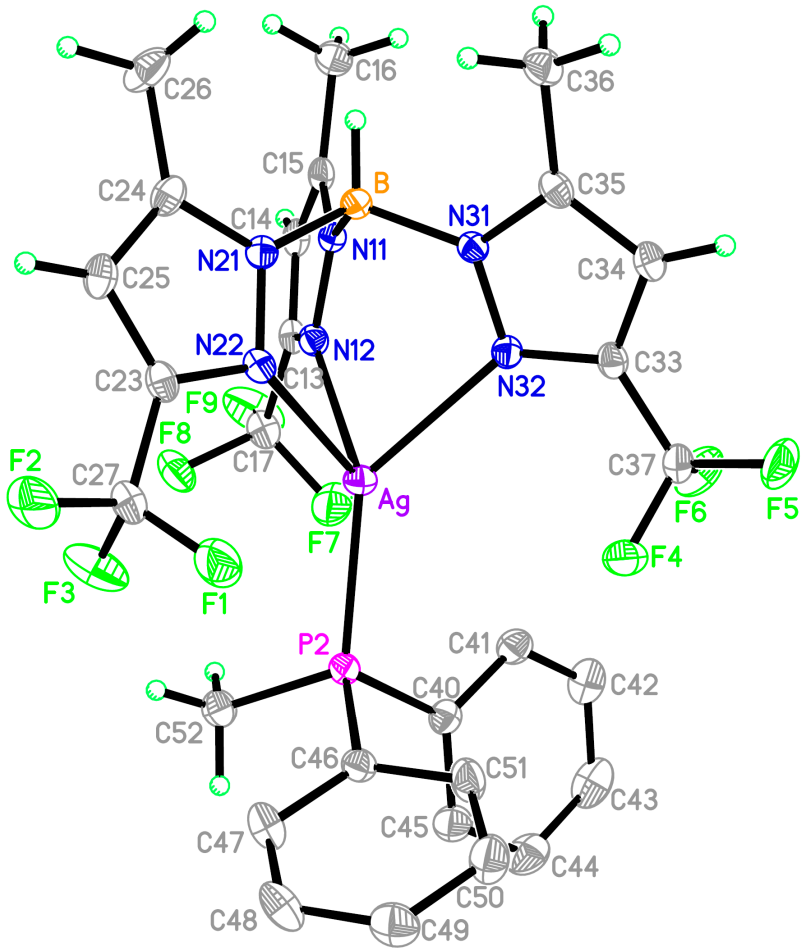

Figure 3.14 X-ray structure of $Tp^{CF_3,CH_3}Ag(PMePh_2)$ in ORTEP representation at 40% probability. Color code: B, orange; C, gray; N, blue; F, green; Ag, purple; P, magenta.

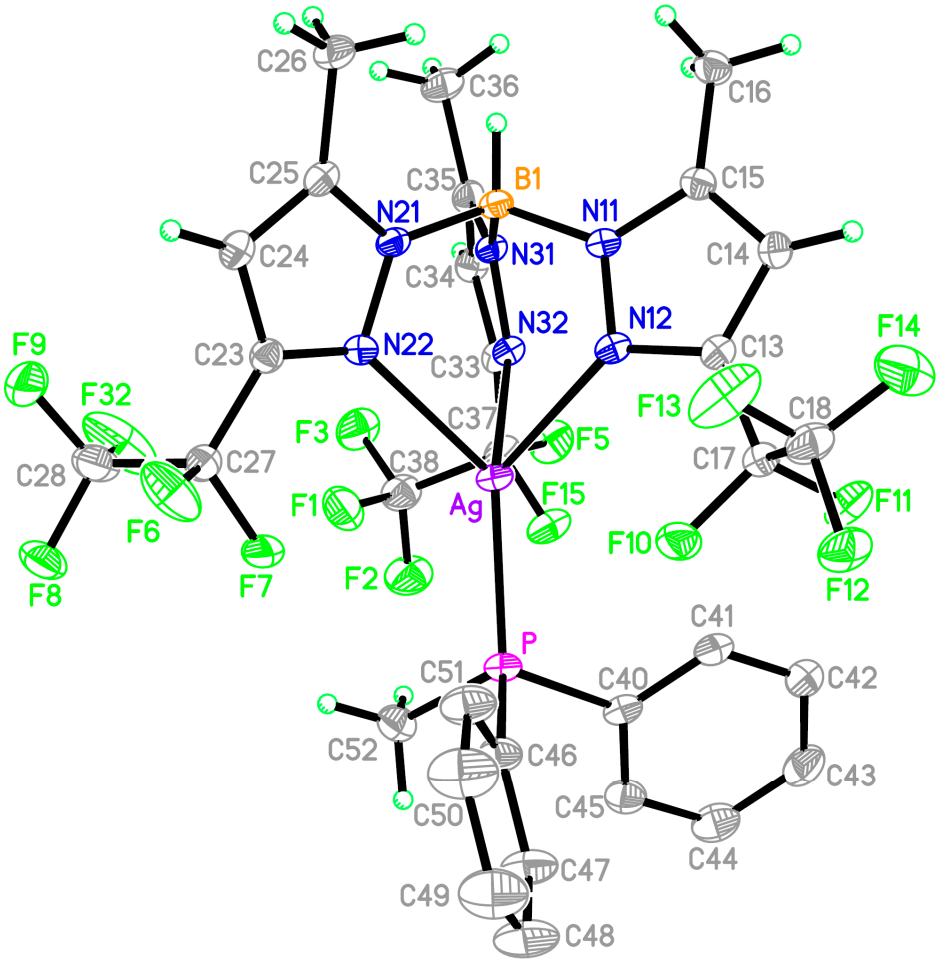

Figure 3.15 X-ray structure of $Tp^{C_2F_5,CH_3}Ag(PMePh_2)$ in ORTEP representation at 40% probability. Rotational disorder of the perfluoroethyl group at C27 was omitted for sake of clarity. Color code: B, orange; C, gray; N, blue; F, green; Ag, purple; P, magenta.

[3-9] crystallizes in the monoclinic system, space group $P2_1/n$, while crystals of **[3-10]** form in the primitive $P\bar{1}$ space group. The tightly-packed structures contain four and two molecules per unit cell, respectively. No solvent molecules were incorporated in the crystal lattices. Lack of disorder of the perfluoroalkyl groups (R_f), save for one of the three C_2F_5 units in **[3-10]**, reveals the high long-range ordering and stability exhibited by the crystals. Remarkably low R-factors (0.0274 for **[3-9]** and 0.0244 for **[3-10]**, respectively) confirm once more the quality of the crystalline materials.

Assembly of the molecules in the crystalline structure is made through the now-usual intermolecular F•••H interactions of the type previously encountered for the **[3-7]** and **[3-8]** complexes, as well as weak F•••F contacts. H-bonding occurs between the R_f groups of one molecule and methyl groups of either the phosphine or Tp ligands of its neighbors, generating an efficient 3D packing. The values of the $C(CH_3)$–P–C–C(Ph) torsion angles decrease from **[3-9]** (25° and 67°) to **[3-10]** (21° and 60°), consistent with the increase of the steric bulk of the R_f groups and rotational restraint around the Ag–P axis. Collections of refinement parameters and structural coordinates for the two complexes are provided in Appendices H and I.

3.3.4.5 $Tp^{CF_3,CH_3}Ag(PPh_3)$. Good quality single crystals of **[3-11]** were obtained by slow evaporation at RT from toluene. Data collection was carried out at −100 °C. The crystallization solvent was incorporated in the structure in a 1:1 ratio to the compound's molecules. One of the CF_3 groups is rotationally disordered over two positions. Crystals of **[3-11]** are triclinic in the $P\bar{1}$ space group; only one molecule is present per unit cell. An R-factor of 0.0257 reveals the high crystallinity of the complex. An ORTEP representation is given in Figure 3.16.

The molecular packing diagram of **[3-11]** (Figure 3.17) exhibits layers of juxtaposing phenyl rings of the solvation toluene and silver-bonded PPh_3 groups, stacked between rows of molecules. Two types of intermolecular interactions were identified: interlayer $F(CF_3)$•••$H(CH_3\text{-Ph})$ H-bonds of 2.664 Å and weak intralayer F•••F contacts of 2.918 Å. Together, they account for the majority of binding interactions in the crystal lattice. Tables of interatomic distances and crystallographic parameters are provided in Appendix J.

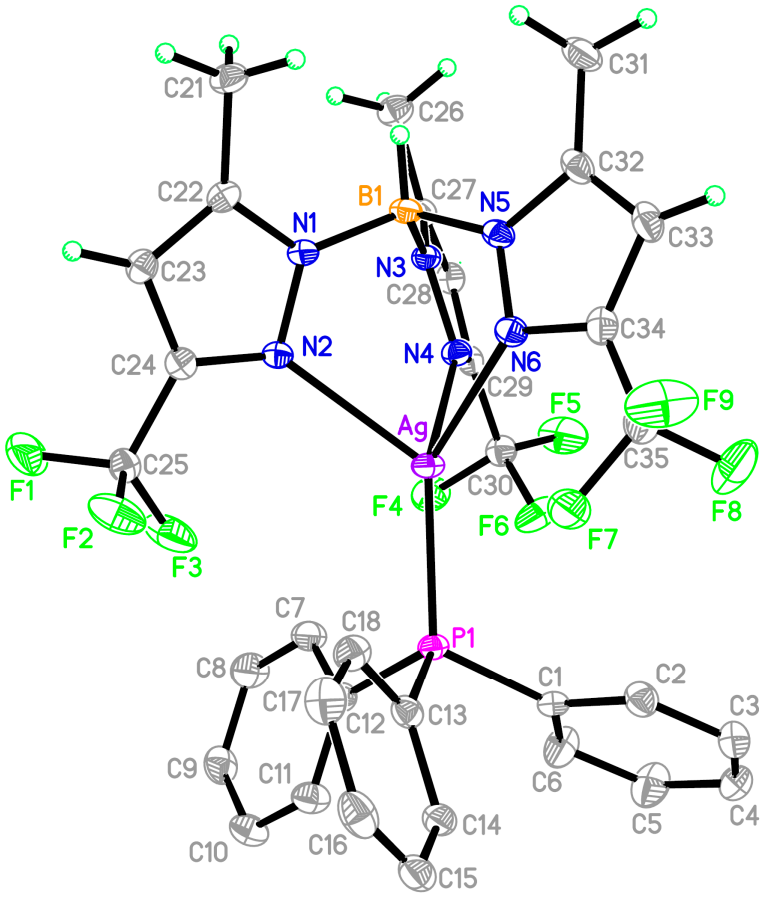

Figure 3.16 X-ray structure of $Tp^{CF_3,CH_3}Ag(PPh_3)$ in ORTEP representation at 40% probability. Rotational disorder of the CF_3 group at C35 was omitted for sake of clarity.

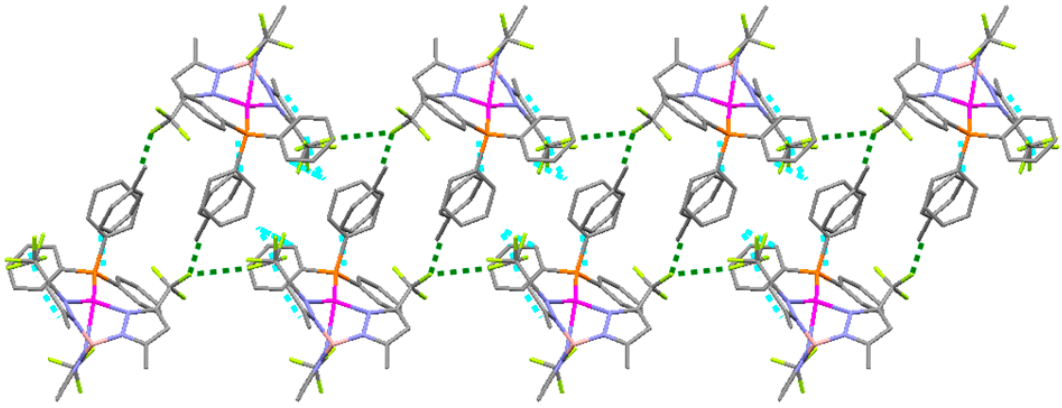

Figure 3.17 Crystal packing diagram of $Tp^{CF_3,CH_3}Ag(PPh_3)$ viewed along the *a* axis, showing the alternating rows of molecules between phenyl layers. H atoms were omitted for clarity. Color code: B, pink; C, gray; N, blue; F, green; Ag, purple; P, orange. The intermolecular F•••F and F•••H contacts are shown as dotted green lines.

3.3.4.6 $Tp^{CF_3,CH_3}Ag(OPPh_3)$ and $Tp^{C_2F_5,CH_3}Ag(OPPh_3)$. X-ray suitable single crystals of **[3-12]** and **[3-13]** were easily obtained by slow evaporation of toluene solutions. No rotational disorder of the R_f groups was noticed in either case. Complete crystallographic data are provided in Appendices K and L.

A final R-factor of 0.0204 obtained for **[3-12]** reveals the exceptional quality of the crystals. Co-crystallized solvation toluene was found in the crystal structure of **[3-12]**, belonging to the orthorhombic, *Pna*2_1 space group. A thermal ellipsoid plot of **[3-12]** is presented in Figure 3.18.

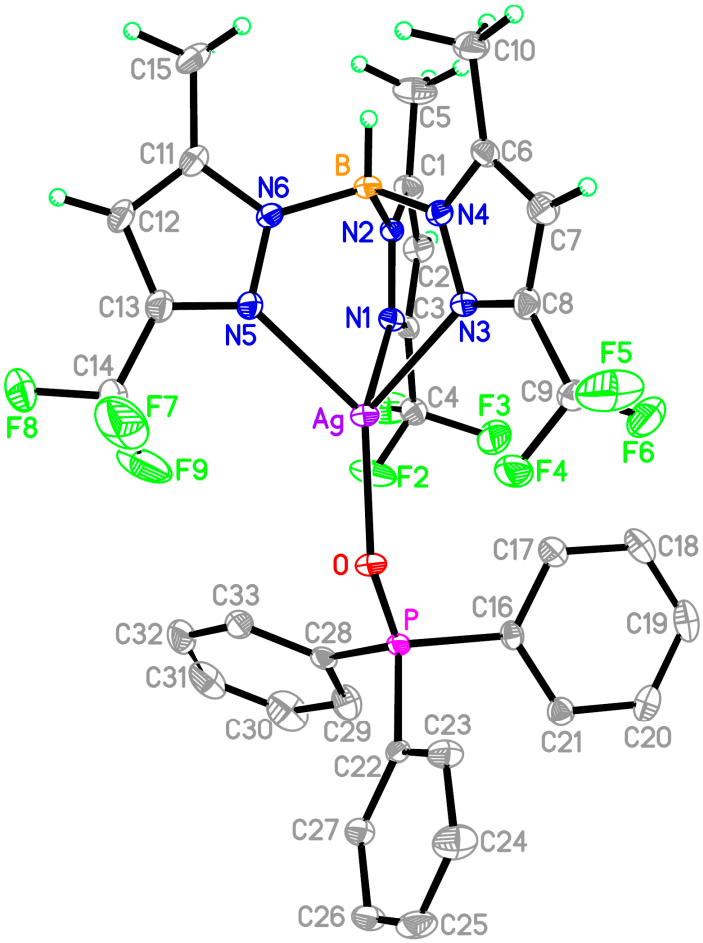

Figure 3.18 X-ray structure of $Tp^{CF_3,CH_3}Ag(OPPh_3)$ in ORTEP representation at 40% probability. Solvation toluene was omitted for sake of clarity. Color code: B, orange; C, gray; N, blue; F, green; Ag, purple; O, red; P, magenta.

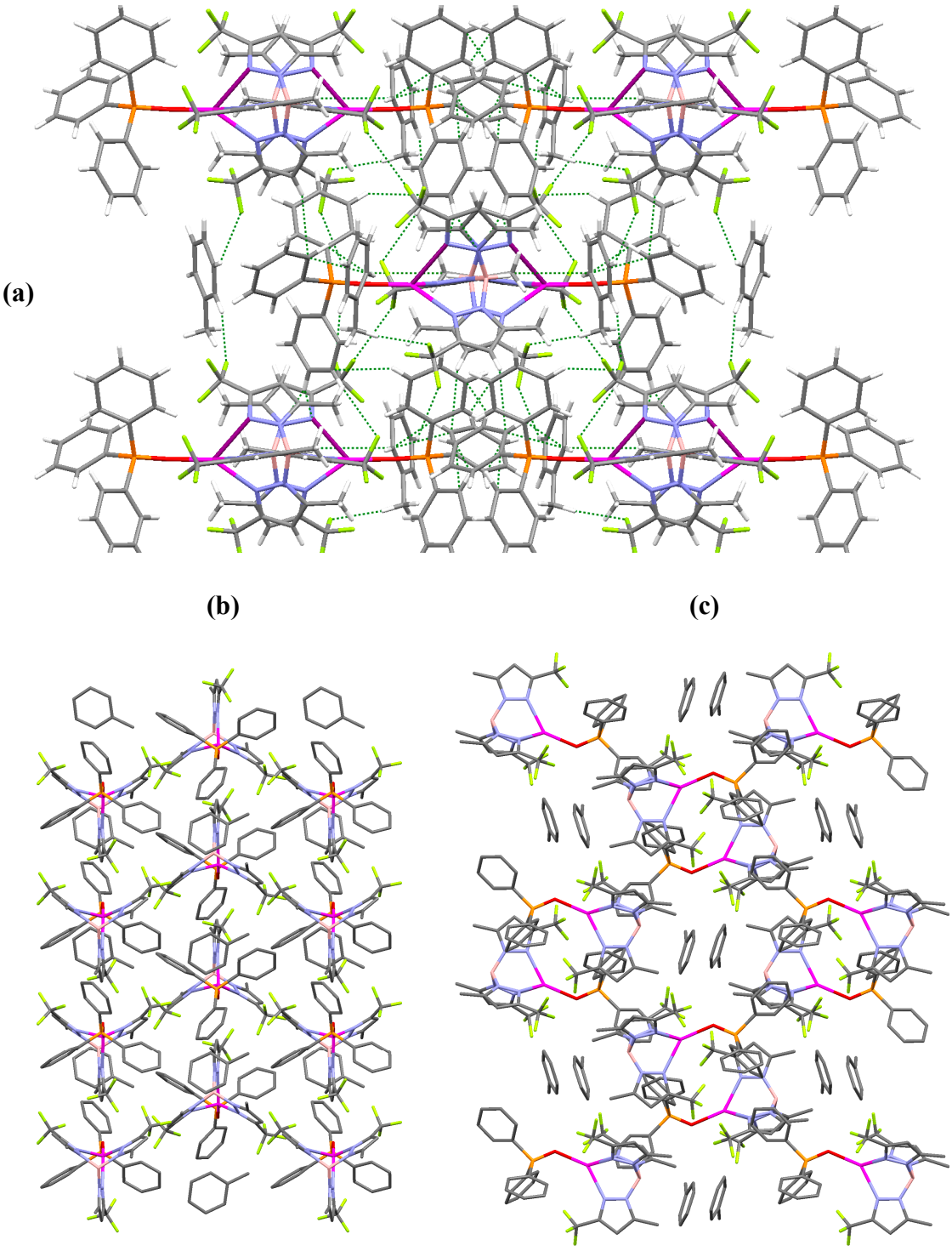

Figure 3.19 Crystal packing diagrams of $Tp^{CF_3,CH_3}Ag(OPPh_3)$ in capped sticks representation. (a) View along the *a* axis, showing the intermolecular F•••F and F•••H contacts as dotted green lines. (b) View along the *b* axis with H atoms omitted. (c) View along the *c* axis with H atoms omitted. Color code: B, pink; C, gray; N, blue; F, green; Ag, purple; P, orange; O, red.

The crystal packing diagrams of **[3-12]** (Figure 3.19) display a complex, tridimensional network of both intra- and intermolecular F•••F and F•••H interactions. The O and P atoms do not seem to be involved in any intermolecular hydrogen bonding, while the toluene molecules prove to be essential in the structural assembly of the lattice. The view along the *a* crystallographic axis (Figure 3.19(a)) reveals a highly-ordered pattern consisting of parallel molecular layers, composed of alternating rows of left- and right-oriented molecules, with respect to the central plane defined by the B, Ag, O and P atoms. Within these rows, head-to-tail molecular units of **[3-12]** are aligned in a "beads-on-a-string" fashion, yielding pillar-shaped motifs with smaller, interspersed toluene "cylinders" (view along *b* axis, Figure 3.19(b)).

The intra- and inter-layer connections are assured by H-bonds to and from the intercalating toluenes; each toluene molecule is involved in no less than three H•••F interactions with neighboring complexes: 2.554 Å and 2.629 Å bonds connect one of the methyl-H and, respectively, a *m*-H atom to two fluorine atoms of the same CF_3 group of an adjacent **[3-12]** molecule, while the third, 2.650 Å bond links an *o*-H to a CF_3 fragment of a different molecule. Relatively strong (2.542 Å) intramolecular (CF_3)F•••H(Ph) interactions explain the preferred conformation of the aromatic rings of $OPPh_3$. Additional, less intense (3-CF_3)F•••H(5-CH_3) contacts between Pz substituents on adjacent molecules were identified, with lengths of 2.876 and 2.770 Å. Weak, 2.939 Å-long intermolecular F•••F contacts, as well as T-shaped stacking interactions of solvation toluene with $OPPh_3$ fragments lower the internal lattice energy and confer added stability to the crystalline solid.

An ORTEP representation of the C_2F_5 analogue of **[3-12]**, namely $Tp^{C_2F_5,CH_3}Ag(OPPh_3)$ **[3-13]** is given in Figure 3.20.

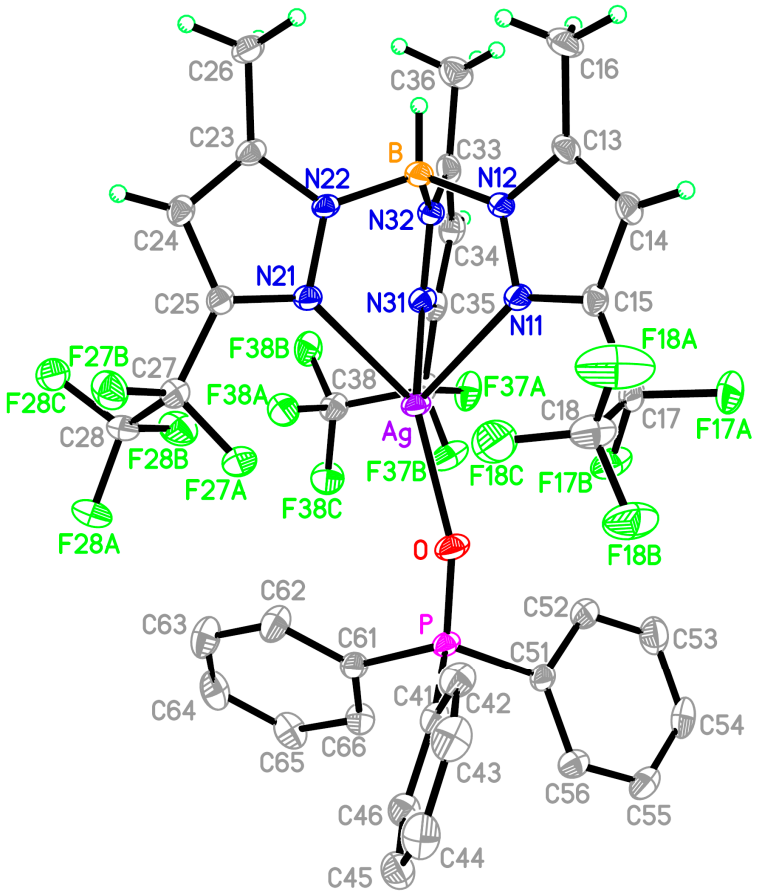

Figure 3.20 X-ray structure of $Tp^{C_2F_5,CH_3}Ag(OPPh_3)$ in ORTEP representation at 40% probability. H atoms on the phenyl rings of $OPPh_3$ were omitted for clarity. Color code: B, orange; C, gray; N, blue; F, green; Ag, purple; O, red; P, magenta.

[3-13] crystallizes in the monoclinic, *C*2/*c* space group with eight molecules per unit cell. The structure refinement R-factor of 0.0307, although reasonable, does not match the remarkable value recorded for **[3-12]**. The lack of solvent molecules in the lattice allows for fewer intermolecular interactions and a lower ordering of the solid structure in general, compared to its analogue **[3-12]**. The main structural role that

solvation toluene molecules had for **[3-12]** in creating intermolecular contacts is taken, in the case of **[3-13]**, by the aromatic rings of the $OPPh_3$ moiety.

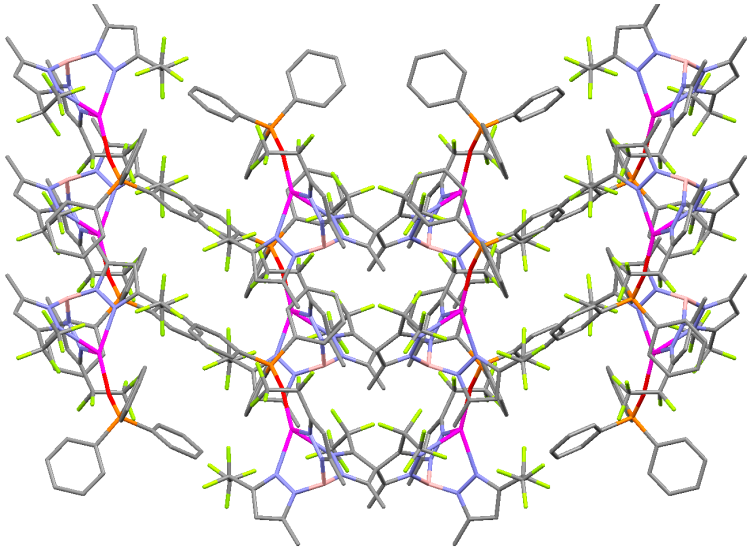

Figure 3.21 Crystal packing diagram of $Tp^{C_2F_3,CH_5}Ag(OPPh_3)$ in capped sticks representation along the *a* axis. H atoms have been omitted for clarity. Color code: B, pink; C, gray; N, blue; F, green; Ag, purple; P, orange; O, red.

The orientation of the three aromatic rings of $OPPh_3$ is dictated by intramolecular hydrogen bonds of various strength. The three *o*-H atoms form O•••H interactions of increasing length, ranging from 2.576 Å and 2.675 Å to the longest one of 2.826 Å. Two of these *o*-H atoms are also involved in internal hydrogen bonding with fluorine atoms of the R_f groups, creating $(CF_2)F$•••H and $(CF_3)F$•••H interactions across distances of 2.473 Å and 2.708 Å, respectively. The picture of intermolecular assemblies in the lattice is composed of 2.572 Å-long $(CF_3)F$•••H(3-CH_3) bonds and a multitude of weaker fluorine interactions between pairs of C_2F_5 groups belonging to adjacent molecules, viz. $(CF_2)F$•••$F(CF_3)$ and $(CF_3)F$•••$F(CF_3)$ contacts of 2.751 and 2.884 Å, respectively.

3.3.4.7 Summary of Crystallographic Data. Table 3.5 summarizes the crystal data and structure refinement parameters for the seven new silver scorpionates **[3-7]** to **[3-13]**. The information is extracted from the corresponding tables of Appendices F to L.

Table 3.5 Selected Crystallographic Data for the Novel Silver Scorpionates†

	[3-7]	**[3-8]**	**[3-9]**	**[3-10]**	**[3-11]**	**[3-12]**	**[3-13]**
System	TC	TC	M	P	TC	O	M
Space group	$P\bar{1}$	$P\bar{1}$	$P2_1/n$	$P\bar{1}$	$P\bar{1}$	$Pna2_1$	$C2/c$
T (K)	100(2)	243(2)	100(2)	100(2)	173(2)	100(2)	100(2)
a (Å)	11.5180(4)	11.5821(1)	12.0444(3)	10.9393(2)	11.0205(2)	15.7204(4)	20.4765(1)
b (Å)	11.5270(3)	12.0954(1)	19.1515(6)	11.8589(3)	11.5728(2)	17.0401(5)	11.2975(6)
c (Å)	25.0481(9)	12.5582(1)	13.4945(4)	14.7060(3)	16.5400(3)	15.1258(4)	34.8025(1)
α (°)	96.271(2)	93.548(4)	90	97.393(1)	95.635(1)	90	90
β (°)	92.511(2)	116.605(4)	94.530(1)	105.308(1)	106.430(1)	90	97.184(3)
γ (°)	119.743(1)	98.557(4)	90	91.537(1)	92.038(1)	90	90
V (Å^3)	2851.63(2)	1539.0(2)	3103.0(2)	1821.11(7)	2009.13(6)	4051.9(2)	7987.8(8)
Z	4	2	4	2	1	4	8
d_{calcd} (g/cm^3)	1.633	1.746	1.642	1.673	1.523	1.537	1.655
N_{refl}	9109	5428	5503	5905	6634	6445	7203
N_{param}	725	430	420	526	556	537	554
R_1 ($I > 2\sigma I$)	0.0551	0.0544	0.0272	0.0241	0.0256	0.0202	0.0307
R_1 (all data)	0.0582	0.0602	0.0274	0.0244	0.0257	0.0204	0.0312
wR_2 ($I > 2\sigma I$)	0.1345	0.1524	0.0695	0.0614	0.0656	0.0538	0.0764
wR_2 (all data)	0.1363	0.1606	0.0696	0.0617	0.0657	0.0540	0.0766
S	1.142	1.073	1.070	1.095	1.053	1.071	1.167

$R_1 = \sum(|F_o|-|F_c|) / \sum|F_o|$; $wR_2 = \{\sum w(|F_o|-|F_c|)^2 / \sum w|F_o|^2\}^{1/2}$; $S = \{\sum w(|F_o|-|F_c|)^2 / (N_{refl}-N_{param})^2\}^{1/2}$.
† Abbreviations used in the table and equations: T – tetragonal; O – orthorhombic; M – monoclinic; TC – triclinic; P – primitive; N_{refl} – number of observed independent reflections; N_{param} – number of parameters refined; R_1 – unweighted refinement discrepancy factor; wR_2 – weighted refinement discrepancy factor; S – goodness of fit on F^2; F_o – observed structure factors; F_c – calculated structure factors.

3.3.5 Relative Thermal and Photostabilities

All silver complexes produced were unstable in halogenated solvents such as chloroform and DCM, even at RT. This was expected and in accordance with previously reported literature data.[3,67] Slightly better photostability was noticed for some cases in $CDCl_3$, in which, for example, a solution of **[3-9]** was still clear after 5 days, whereas **[3-10]** had deposited metallic silver.

Photostability at RT under ambient light conditions greatly improved in non-halogenated solvents, in particular toluene, acetone, acetonitrile and ethyl acetate; in these solvents, some compounds (namely the PPh_3 and $PMePh_2$ adducts **[3-9]**–**[3-11]**) were stable indefinitely. The PPh_3 complex **[3-11]** exhibits a greatly reduced solubility compared to the other compounds, white solid gradually precipitating from solution with no decomposition. Heating a clear solution of any of the compounds **[3-7]**–**[3-13]** over 70 °C, under light or dark conditions, in any solvent, resulted in precipitation of dark residues.

In a photostability measurement, acetone solutions of complexes **[3-7]**–**[3-13]** (*ca.* 1 mg/mL) were exposed to visible light at 1.3×10^5 lux and monitored continuously for 30 h of illumination. Under these conditions, the two toluene adducts were mostly decomposed after as little as 3 h, while microscope-examined solutions of the $OPPh_3$ adducts had shown traces of metallic silver after 3.5 h (**[3-12]**) and 5.5 h (**[3-13]**), respectively; these complexes eventually deposited silver mirrors in the sealed vials, within several weeks of exposure at ambient light under RT. At the end of the 30 h irradiation measurement, vials containing the $PMePh_2$ and PPh_3 adducts (**[3-9]**, **[3-10]** and **[3-11]**) were still clear, and they remained clear in tightly sealed vials kept at RT, even after 2 years of exposure to ambient light, although most of **[3-11]** had precipitated as a white solid. All of the above observations are based on visual assessment of the solutions, no quantitative determination was attempted.

In the solid state, all complexes showed indefinite stability under air and light; exceptions were the toluene adducts and, to a minor extent, **[3-13]**, in which case a slight darkening of the initially white solid was noticed over time.

Under heating of the solids, in all cases except **[3-8]**, the complexes decomposed without melting, while the molten liquid of **[3-8]** turned black at 120 °C. A remarkable thermal stability was displayed by **[3-9]**, with a decomposition temperature of 230 °C. A summary of the relative stability in solution and the solid state is presented below.

Table 3.6 Relative Stability in Solution and the Solid State for TpAg Compounds

TpAg(L)	**Thermal stability (°C)**		**Photostability at ambient temperature**	
	Solid	*Solution*	*Solid*	*Solution*†
$Tp^{CF_3,CH_3}Ag(Tol)$	135	70	Partially unstable	Partially unstable
$Tp^{C_2F_5,CH_3}Ag(Tol)$	120	50	Partially unstable	Unstable
$Tp^{CF_3,CH_3}Ag(PMePh_2)$	230	70	Stable	Stable
$Tp^{C_2F_5,CH_3}Ag(PMePh_2)$	155	50	Partially unstable	Stable
$Tp^{CF_3,CH_3}Ag(PPh_3)$	180	70	Stable	Stable
$Tp^{CF_3,CH_3}Ag(OPPh_3)$	130	70	Stable	Partially unstable
$Tp^{C_2F_5,CH_3}Ag(OPPh_3)$	185	50	Partially unstable	Partially unstable

† Non-halogenated solvents only.

In general, complexes containing the $Tp^{C_2F_5,CH_3}$ ligand proved more labile in the solid state than the Tp^{CF_3,CH_3} analogues. This difference in stability can be attributed to the enhanced destabilization of the silver ion under the stronger electron-withdrawing C_2F_5 groups, combined with the increase of the overall steric strain of the complexes when moving to bulkier R_f substituents. Following all experimental observations, it appears that, given their obvious thermal and photochemical susceptibility, weak electron donors, viz. toluene in **[3-7]** and **[3-8]**, are not capable of stabilizing the complexes. Instead, the basic and sterically non-hindered $PMePh_2$ counteracts efficiently the destabilizing effect induced by the perfluoroalkyl groups, resulting in indefinite stability under ambient light at RT in non-halogenated solvents and even exceptional thermal resilience in the solid state.

3.3.6 Solid-state Study of Silver Scorpionates: A Structural Model

First, structural data obtained for **[3-6]** were analyzed. The avg. Na–N distance in $Tp^{C_2F_5,CH_3}Na(H_2O)$ **[3-6]**, 2.449 Å, is comparable with the corresponding distances observed in $Tp^{CF_3,Ph}Na(H_2O)$, 2.425 Å,[84] 2.400 Å in $Tp^{CF_3,CF_3}Na(H_2O)$,[64] and 2.485 Å in $Tp^{CF_3,CH_3}Na(H_2O)$ **[3-5]**.[84] The corresponding Na–O distances are 2.263, 2.245, 2.179 and 2.417 Å, respectively. A linear correlation of these values (Figure 3.22), although the number of data points is small, suggests that the Na–O and Na–N bonds decrease in length as the Tp substituents become better electron acceptors, translating into a higher Lewis acidity of the metal.[85] The constant Na–O/<Na–N> ratio appears to be independent of the Na coordination number and even complex nuclearity, for example in the case of **[3-5]**, which is actually formulated as a dinuclear complex with μ-H_2O groups.

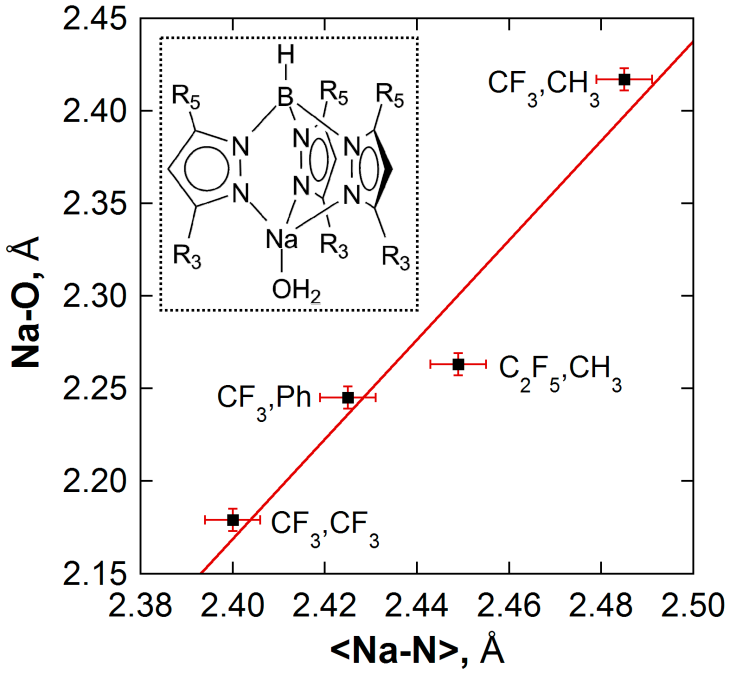

Figure 3.22 Plot of the Na–O vs. the average Na–N bond lengths in $Tp^{R_3,R_5}Na(H_2O)$ complexes. Linear correlation coefficient: 0.967. Data points are marked following the R_3, R_5 nomenclature. Error bars of ±0.006 Å are also shown.

Figure 3.22 is consistent with the notion that C_2F_5 is a better σ acceptor than CF_3, but also underscores the strong influence of the 5-substituent, as evidenced by the large difference when CF_3 replaces CH_3. The hard Na^+ ion readily replies to changes in the electronegativity of the Tp ligand by creating a stronger interaction (shorter bonds) without any appreciable detrimental effect on the compound's stability. At the same time, the small molecular volume of ligated water allows for contraction of Na–N bonds without introducing additional steric strain on the complex.

With a structural correlation established for TpNa complexes, the seven novel silver(I) complexes **[3-7]**–**[3-13]** were analyzed next. An overview of the bond lengths present within the metal coordination sphere, given as the avg. Ag–N and Ag–L distances, is presented in Table 3.7.

Table 3.7 Metal-to-ligand Bond Lengths in the New TpAg Complexes

TpAg(L)	**<Ag–N>** (Å)	**Ag–L**† (Å)
$Tp^{CF_3,CH_3}Ag(Tol)$	2.365	2.321
$Tp^{C_2F_5,CH_3}Ag(Tol)$	2.399	2.393
$Tp^{CF_3,CH_3}Ag(PMePh_2)$	2.379	2.351
$Tp^{C_2F_5,CH_3}Ag(PMePh_2)$	2.394	2.371
$Tp^{CF_3,CH_3}Ag(PPh_3)$	2.387	2.364
$Tp^{CF_3,CH_3}Ag(OPPh_3)$	2.372	2.217
$Tp^{C_2F_5,CH_3}Ag(OPPh_3)$	2.368	2.192

† Ag–L represents one of the following: (i) Ag–C or Ag–C_{cent} distance (for L = Tol), where C_{cent} is the centroid of the bond in the aromatic ring directly involved in the η^2 coordination; (ii) Ag–P bond length (for L = $PMePh_2$ and PPh_3); (iii) Ag–O bond length (for L = $OPPh_3$).

Figure 3.23 presents a visual comparison of the geometry of the $Tp^{R_f,CH_3}Ag(L)$ complexes, viewed along the virtual B–Ag axis.

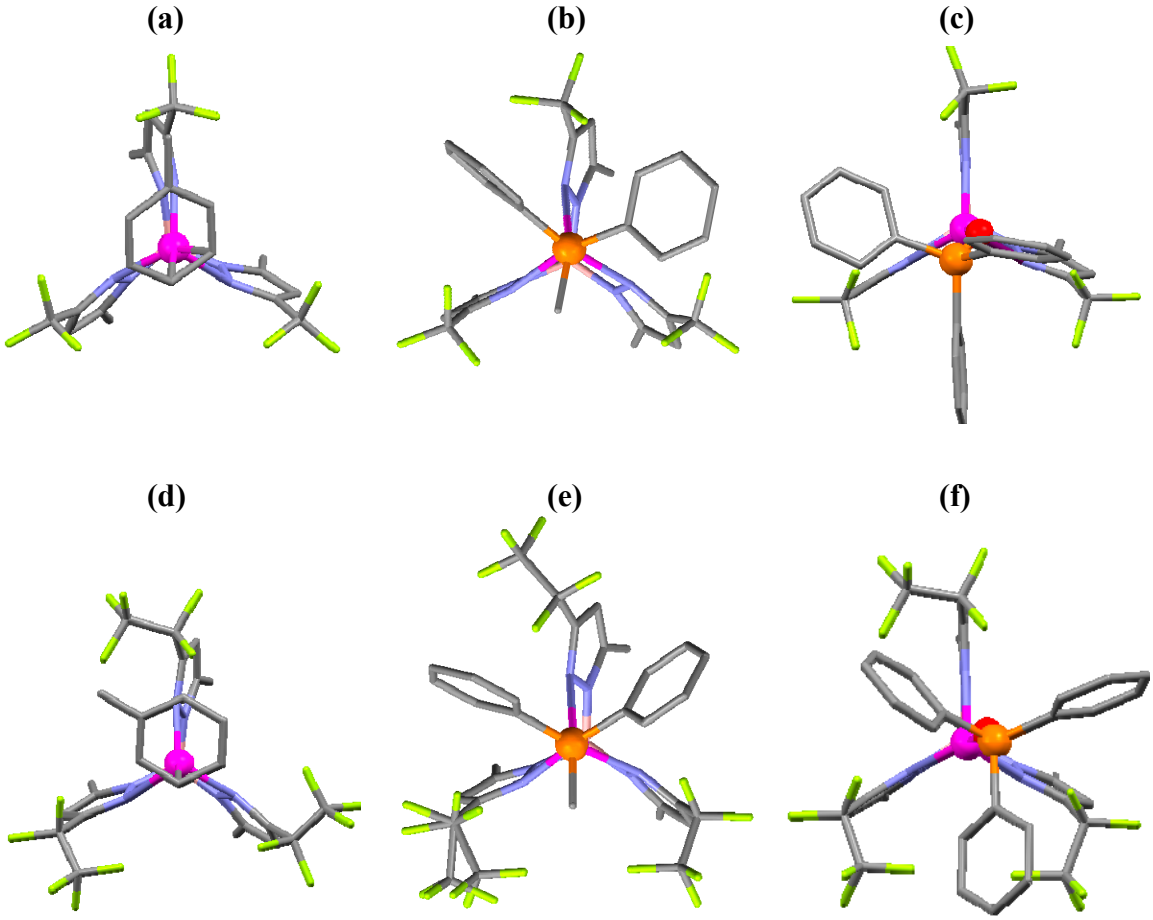

Figure 3.23 Capped sticks representations of the X-ray determined structures of $Tp^{R_f,CH_3}Ag(L)$ compounds, viewed along the B–Ag axis. (a) $Tp^{CF_3,CH_3}Ag(Tol)$ **[3-7]**. (b) $Tp^{CF_3,CH_3}Ag(PMePh_2)$ **[3-9]**. (c) $Tp^{CF_3,CH_3}Ag(OPPh_3)$ **[3-12]**. (d) $Tp^{C_2F_5,CH_3}Ag(Tol)$ **[3-8]**. (e) $Tp^{C_2F_5,CH_3}Ag(PMePh_2)$ **[3-10]**. (f) $Tp^{C_2F_5,CH_3}Ag(OPPh_3)$ **[3-13]**. The Ag, P and O atoms were highlighted as spheres. Color code: B, pink; C, gray; N, blue; F, green; Ag, purple; P, orange; O, red.

The increase in molecular steric strain as electron-donating ligands approach the Ag center is manifested in the deviation from its co-planarity with the atoms of the Pz rings, resulting in propeller-like structures of the type depicted in Figures 3.23(a)–(b) and (d)–(e) and even outward rotations of bulky Pz substituents, such as C_2F_5 in Figure 3.23(e). Such conformational changes are imposed by the tendency to achieve energy minima through avoidance of steric crowding.

When ligands that create less bulk around the metal center are used (e.g., $OPPh_3$), the TpAg scaffold can accommodate them with retention of co-planarity, as in Figures 3.23(c) and 3.23(f). This simple visual analysis already points out the foremost importance of the steric factor in the formation and stability of the complexes when large, soft metal ions are involved, an observation strongly underscored by the failure to obtain a $Tp^{C_2F_5,CH_3}Ag(PPh_3)$ complex (discussed earlier in Section 3.3.1).

The weighting of the electronic factors, namely electronegativity (electron-accepting ability) of Pz substituents and basicity (electron-donating ability) of silver-coordinating ligands can best be portrayed through a plot of the Ag–P vs. <Ag–N> distances for relevant $TpAg(PR_3)$ complexes, both previously published and first described herein. Combined data for selected compounds from Tables 3.4 and 3.7 are presented below.

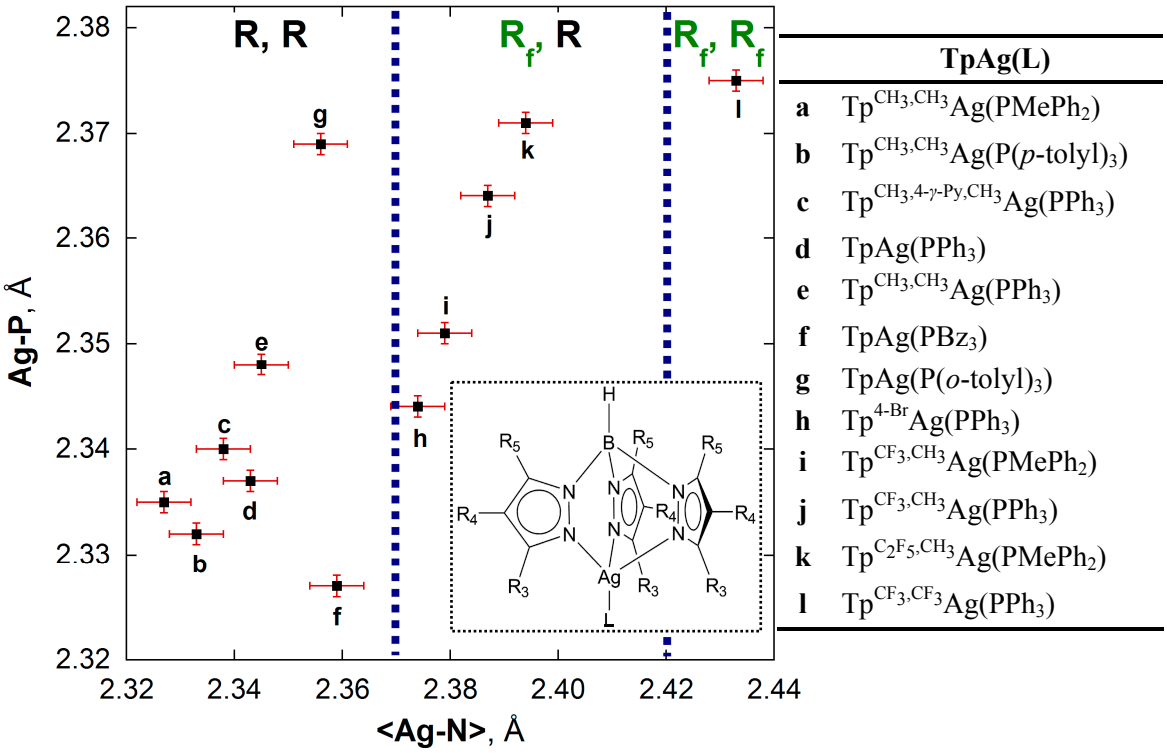

	TpAg(L)
a	$Tp^{CH_3,CH_3}Ag(PMePh_2)$
b	$Tp^{CH_3,CH_3}Ag(P(p\text{-tolyl})_3)$
c	$Tp^{CH_3,4\text{-}\gamma\text{-}Py,CH_3}Ag(PPh_3)$
d	$TpAg(PPh_3)$
e	$Tp^{CH_3,CH_3}Ag(PPh_3)$
f	$TpAg(PBz_3)$
g	$TpAg(P(o\text{-tolyl})_3)$
h	$Tp^{4\text{-}Br}Ag(PPh_3)$
i	$Tp^{CF_3,CH_3}Ag(PMePh_2)$
j	$Tp^{CF_3,CH_3}Ag(PPh_3)$
k	$Tp^{C_2F_5,CH_3}Ag(PMePh_2)$
l	$Tp^{CF_3,CF_3}Ag(PPh_3)$

Figure 3.24 Plot of the Ag–P vs. the average Ag–N bond lengths for selected $TpAg(PR_3)$ complexes. The three major domains (R = alkyl groups, R_f = halogenated or perfluorinated groups) are marked by blue vertical lines.

In the structural comparison of Figure 3.24, only silver-phosphino complexes were included. In order to obtain an accurate representation of the Ag coordination geometry's variation with the electronic properties of the Tp ligand, the same type of σ-donor had to be considered; in this respect, structurally characterized $TpAg(PR_3)$ compounds were the most abundant in the literature, hence the choice of the selection. Considering the (R_3, R_5) pair of substituents of the Pz rings, the previous figure is particularly revealing in defining three structural domains into which the average Ag–N distances fit, according to the nature of R_3 and R_5, respectively. When both groups employed are non-halogenated alkyls (R, R), the <Ag–N> lengths stop short of 2.36 Å. Mixed perfluoroalkyl-alkyl (R_f, R) Tp ligands yield <Ag–N> distances in the 2.37–2.40 Å range, while exclusively perfluorinated Tps (R_f, R_f), of which only one silver-phosphino compound, i.e., $Tp^{CF_3,CF_3}Ag(PPh_3)$, was X-ray characterized, exhibit <Ag–N> bonds exceeding 2.42 Å. The above observations suggest a reverse trend in the variation of the Ag–N bond lengths with the electronegativity of Tp substituents, in contrast to the one noticed for the Na–N bonds in Na-containing complexes.

The weakening of Ag–N bonds with the increase in electronic demand of the Tp ligand is explained by two factors: (i) a decrease in the basicity of the proximal N atom to the 3-R_f group and (ii) the soft nature and large volume of the Ag^+ ion, which cannot adapt as efficiently as Na^+ to a change in the electronic distribution of the ligand, due to its more diffuse charge density.

In contrast, the Ag–P bond lengths are dominated by steric bulk of both the R_3 and PR_3 groups; they seem to be irrespective of the P atom's basicity. In the series of $Tp^{R_3,R_5}Ag(PPh_3)$ complexes with R_3 substituents of gradually increasing size, the Ag–P

distance grows in the order: $R_3 = H < R_3 = CH_3 < R_3 = CF_3$. Within the $Tp^{H,H}Ag$ family, drastic changes are observed when, for instance, bulky P(*o*-tolyl)$_3$ replaces PPh_3 (for an 0.022 Å increase). The rule works both ways, e.g., when a more sterically relaxed phosphine such as PBz_3 is used instead of PPh_3, a 0.01 Å shortening of the Ag–P bond is noticed. To keep the concision of the present discussion, it suffices to say that Figure 3.24 and Tables 3.4 and 3.7 offer many more examples that confirm the paramount influence of the steric factor in determining the Ag–P bond length.

Figure 3.24 constitutes a structural model of the TpAg class. Based on the electronic and steric features of a given (R_3, R_5) pair of substituents and σ electron donor, the metal–ligand bond lengths can be estimated with a certain degree of confidence. Although this model is built on phosphino complexes, there is no reason why it could not be applied to ligands of similar size and basicity.

Naturally, neither electronic factors can be ruled out for determining the strength of Ag–P interactions, nor steric reasons for the formation of Ag–N bonds. However, structural data available do not allow for identification of quantitative trends in this respect, except for obvious cases where the two work together. The values measured by X-ray diffraction are an averaged result of the interplay of the two sets of factors. This study was able to identify the major influences in each case.

3.4 Conclusions

A new, mixed alkyl-perfluoroalkyl trispyrazolylborate ligand, $Tp^{C_2F_5,CH_3}$, and its corresponding pyrazole and sodium complex were reported. Syntheses of seven new silver derivatives of the type $Tp^{R_f,CH_3}Ag(L)$ were also described.

All complexes are fully characterized by spectroscopic methods in solution and solid-state, including X-ray crystallographic techniques.

The importance of the new sodium and silver complexes reported herein stems from the valuable structural information that they provide for completing the picture of relative influences of electronic and steric factors in the formation and thermodynamic stability of this class of metal-organic ligands. An inverse trend in the variation of metal–ligand distances with the electronegativity of Tp substituents is observed when sodium is replaced with silver. This behavior is attributed to the hard vs. soft nature of the two metal ions. The X-ray data allow, in conjunction with previously reported structures, the division of silver trispyrazolylborates into three domains and the assembly of a structural model of the class. Given a desired combination of ligand properties reflected in the electronic structure and steric bulk of the chosen substituents, a range of metal-to-ligand bond lengths can be estimated with the aid of this model.

Furthermore, the stability data reported herein, both thermal and photochemical, show that a larger silver coordination sphere does not necessarily imply susceptibility of the metal to reduction and subsequent ligand decomposition. Finally, it is shown that exceptional stability can be achieved if the enhanced electron-accepting nature of the perfluoroalkyl substituents (R_f) is matched by an equally-strong electron-donating ability of a basic organic molecule of appropriate size, such as $PMePh_2$. Destabilization of the silver atom due to the decrease in basicity of the nitrogen proximal to the R_f groups is efficiently counteracted by strong σ-donors of reduced steric bulk. Thus, the goals of this study are achieved.

CHAPTER 4

SYNTHESIS AND CHARACTERIZATION OF FLUOROALKYLATED PHTHALOCYANINES EXHIBITING REDUCED STERIC BULK

4.1 Introduction

In the search for a new class of phthalocyanine-type ligands exhibiting variable, but controlled aggregation, several synthetic pathways have been explored. Combining literature methods with rational molecular design approaches, three novel partially- and per-fluorinated classes were devised, along with new representatives of a known fluoroalkylated ligand. The present chapter describes partially-fluorinated PcMs exhibiting reduced steric bulk, while the following chapter presents the per-fluorinated complexes.

Through the research of Gorun and collaborators during the past decade,[104–114] production and complete investigation of tridimensional perfluorinated phthalocyanines—the structures of which are described in Chapter 5—was achieved. Amazing in their own rights for the promising catalytic properties and biological applications (e.g., PDT treatment of cancer), this class of Pcs has limited use in the field of semiconductors and electronic materials due to their bulky peripheral groups which prevent molecular stacking. Furthermore, any potential advantages gained from aggregation in solution are lost.

Fluoroalkyl substituents, through the increased energy of their C–F bonds, protect the organic ligand from accidental oxidation while greatly enhancing the solubility of corresponding PcMs in organic solvents, as opposed to their non-fluorinated counterparts. At the same time, their strong electron-withdrawing effects enhance the metal's Lewis acidity and catalytic capabilities.

With these principles in mind, a systematic approach has been undertaken in order to introduce trifluoromethyl (CF_3) groups and F atoms at the available substitution sites of the Pc macrocycle, shown in Figure 1.3. The reduced bulkiness of CF_3 as opposed to, for instance, *i*-C_3F_7, is hypothesized to allow for π–π stacking of the extended, planar aromatic cycles and endow the complexes with an entire new range of properties. All abbreviations used henceforth in the naming of PcMs take into account the number of F atoms present per molecular unit and the number of H atoms, if any.

The first step in this approach is the addition of eight CF_3 groups in the peripheral Pc positions, yielding the metallo-2,3,9,10,16,17,23,24-octakis(trifluoromethyl)-phthalocyanine class, *abbr.* $F_{24}H_8PcM$ (Figure 4.1). This ligand was initially reported by the end of the 1970s as its PcCu complex,[44] followed by the PcH_2, PcGe(Cl) and PcSn(Cl) analogues.[43] Surprisingly, no additional publications, which would investigate properties of these compounds or other representatives of the class, were found.

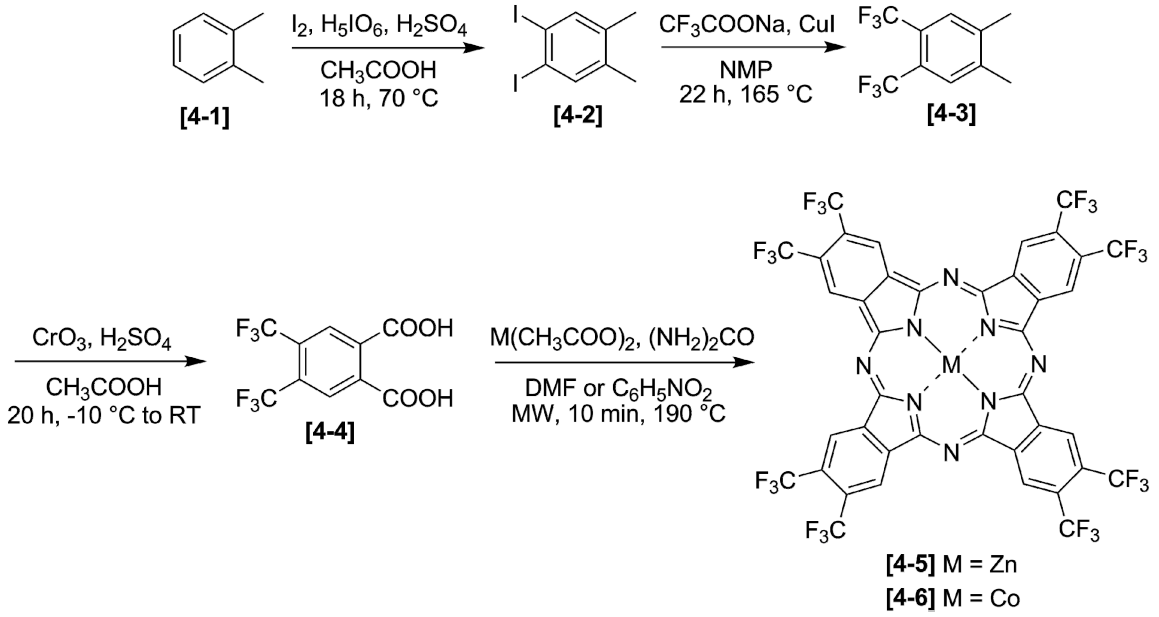

Figure 4.1 Synthetic scheme for the production of $F_{24}H_8PcM$ (M = Zn, Co).

The lack of information on the $F_{24}H_8PcM$ family prompted the synthesis of relevant analogues which could provide a standard for comparison with novel fluorine-enriched PcM classes. This study reports the production and characterization of two new metal complexes, $F_{24}H_8PcZn$ **[4-5]** and $F_{24}H_8PcCo$ **[4-6]**, through a simplified synthetic route shown in Figure 4.1. In this sequence, the common, naturally-occurring *o*-xylene **[4-1]** is iodinated through a method described by Kovalenko et al.[115] to obtain 1,2-diiodo-4,5-dimethylbenzene **[4-2]**. Next, replacement of the iodine atoms with CF_3 groups was performed with the sodium trifluoroacetate–copper(I) iodide system by adapted literature procedures.[116,117] The resulting 1,2-bis(trifluoromethyl)-4,5-dimethylbenzene **[4-3]** is then oxidized to the corresponding 4,5-bis(trifluoromethyl)-phthalic acid **[4-4]** which, under MW radiation, high temperature, addition of urea and the appropriate metal salts, readily tetramerizes to the desired PcM complexes. Noteworthy, **[4-3]** had been previously reported[43] as an intermediate in the production of the first $F_{24}H_8PcM$ analogues, but it was obtained at that time through a method which involved highly toxic and expensive perfluorinated alkynes; later,[118] **[4-3]** was reported again using a slightly different, but equally toxic procedure. This work presents an improved, cost-effective and facile procedure for synthesis of **[4-3]** by avoiding toxic gaseous mixtures.

The $F_{24}H_8Pc$ ligand still contains eight hydrogen atoms in the axial aromatic positions, susceptible to chemical attacks. A more refractory organic scaffold, suitable for catalysis, would require total or, at least, partial replacement of the aromatic protons with F atoms. Several pathways, described next, have been investigated in this respect.

A direct approach towards total fluorination—the single-step nucleophilic substitution of Ar-F atoms of the commercially available tetrafluorophthalonitrile (*abbr.* TFPN) with CF_3 groups—was explored first (Figure 4.2).

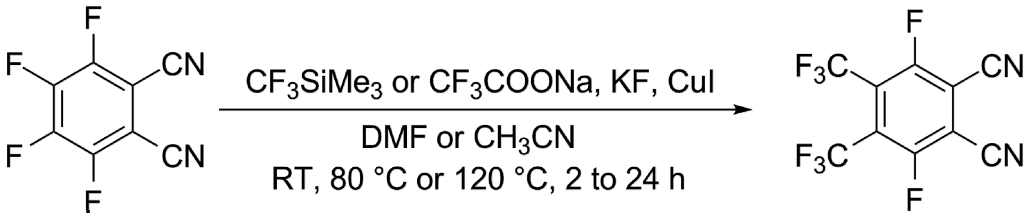

Figure 4.2 Proposed one-step synthesis of perfluoro-4,5-dimethylphthalonitrile.

An extended study* on this alternative, performed in the same laboratory prior to the start of this work, concluded that the method is unfeasible due to extremely low yields and ill-defined mixtures of products, obtained by substitution of one, two or three F atoms, one or both of the nitrile groups and a combination of F and CN groups. Literature procedures[119] were adapted, employing both (trifluoromethyl)trimethylsilane and sodium trifluoroacetate as fluorinating reagents. Trials were performed with gradually increasing TFPN/silane ratios (1:2, 1:3 and 1:5, respectively), in DMF or acetonitrile, at RT or elevated temperatures and over different time ranges (2 h, 8 h and 24 h), with or without the addition of CuI or KF and, in all cases, with strict exclusion of air and moisture. Analysis of each of the reaction mixtures was performed by TLC and GC-MS; in no case the total conversion of TFPN exceeded 20%, while no conversion was noticed when CuI and/or KF were missing. Reactions in DMF tended to yield more undesired side products than the ones performed in acetonitrile. No isolation and characterization of any product could be achieved due to *quasi*-identical physical properties and retention times.

* Gerdes, R. New Jersey Institute of Technology, Newark, NJ. Personal communication, 2008.

Since production of a perfluorinated precursor in a one-step synthesis proved discouraging, a more lengthy, but selective pathway towards aromatic fluorination was envisaged, starting from a compound already in hand, namely **[4-3]**. The design of a new fluoro-perfluoroalkylated Pc ligand, 2,3,9,10,16,17,23,24-octakis(trifluoromethyl)-tetrafluorophthalocyaninate, *abbr.* $F_{28}H_4Pc$, was achieved using a sequence of eight reactions (Figure 4.3) involving aromatic nitration and fluorination by classical methods, followed by oxidation with chromium(VI) oxide to a phthalic acid intermediate and subsequent dehydration by adapted procedures[43] to its corresponding phthalonitrile; the specifics of each step are discussed in Section 4.3.1, *vide infra*. In addition to the novel $F_{28}H_4PcZn$ **[4-14]** and $F_{28}H_4PcCo$ **[4-15]** complexes, all intermediates **[4-7]** to **[4-13]** are reported and characterized herein for the first time.

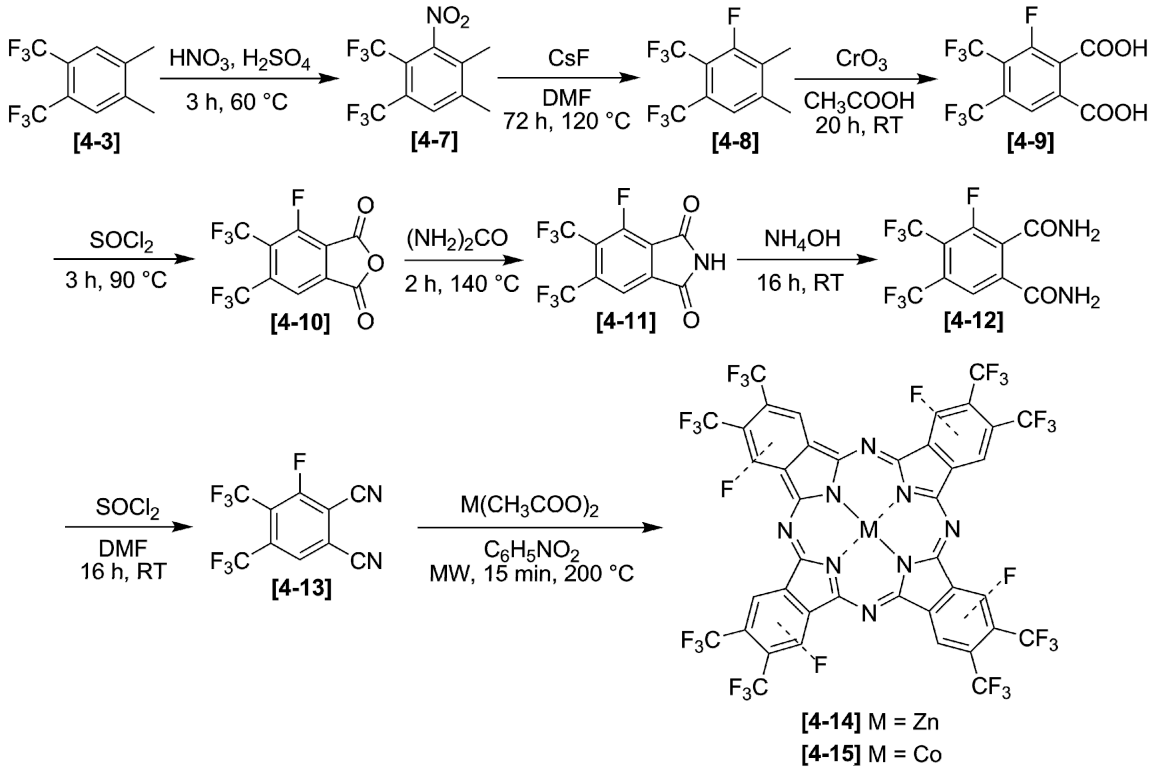

Figure 4.3 Synthetic scheme for the production of $F_{28}H_4PcM$ (M = Zn, Co).

In a parallel synthetic approach, Figure 4.4, explored in the same laboratory[†] while this work was under way, aromatic perfluorination of **[4-3]** was attempted through a secondary nitration-fluorination sequence, starting from both **[4-3]** and **[4-8]**, followed by oxidation and dehydration of the products under similar conditions to the partially fluorinated analogues of Figure 4.3.

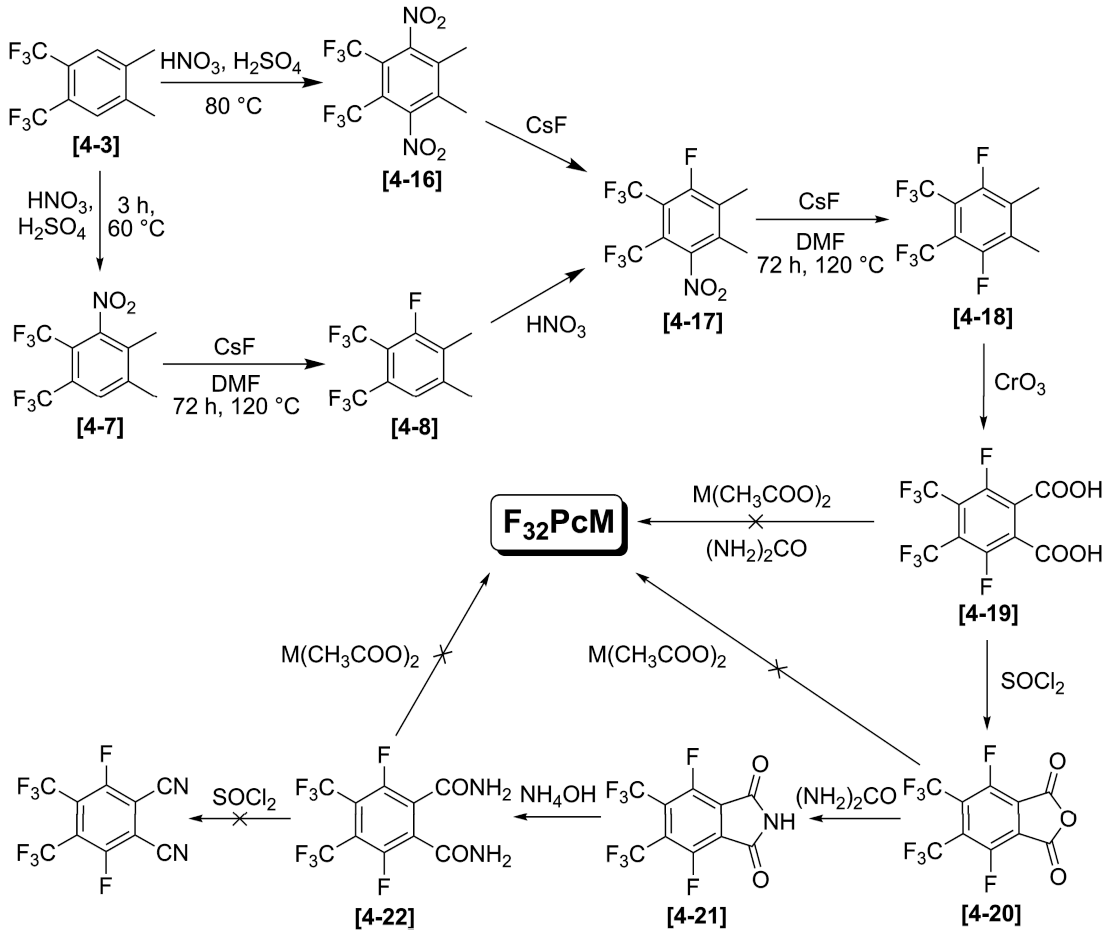

Figure 4.4 Attempted synthetic route for production of proposed F_{32}PcM.

A series of aromatic intermediates, viz. **[4-16]**–**[4-22]** in Figure 4.4, were obtained, isolated and characterized by mp, IR, ^{1}H and ^{19}F NMR.[†] However, low yields (< 40%) for each step in the synthesis of **[4-17]**, **[4-18]** and **[4-19]**, due to inherent

[†] Gerdes, R. New Jersey Institute of Technology, Newark, NJ. Personal communication, 2009.

thermodynamic equilibria, meant that very little amount of material was available for attempting production of a perfluorinated equivalent of $F_{28}H_4PcM$, hypothetically termed $F_{32}PcM$. Phthalic acid **[4-19]**, phthalic anhydride **[4-20]** and phthalamide **[4-22]** proved to be inactive towards formation of $F_{32}PcM$, under classical or MW methods, reducing all chances of obtaining the desired Pc through this synthetic route to the reactivity of the phthalonitrile which would be obtained by dehydration of **[4-22]**. Unfortunately, despite repeated efforts, no dehydrating reagent was found to be powerful enough in removing two water molecules from **[4-22]** to form the desired precursor, thus impeding any similar approaches through oxidation-dehydration of aromatic intermediates.

Metallophthalocyanines exhibit a range of characteristic properties finely tunable by appropriate modification of the number and type of substituents; these properties include color, aggregation in solution, redox and catalytic activity, high thermal stability and electric conductivity.[47] The novel $F_{28}H_4PcM$ class contains an extra F atom per aromatic quarter, but still bears four H atoms overall. While, in theory, the ligand might yet be susceptible to thermo-chemical degradations, practice has revealed a surprising improvement in stability, solubility and catalytic performance with respect to its H-richer $F_{24}H_8PcM$ counterpart, thus warranting the extended synthetic effort. Details are provided in appropriate sections described herein.

The current chapter provides the synthetic procedures and spectroscopic characterization of all aromatic intermediates and fluoroalkylated PcM complexes described in Figures 4.1 and 4.3, with an inherent emphasis on the new compounds. A complete aggregation study in solution for the $F_{28}H_4PcZn$ representative is also presented. The reactivity and catalytic properties are investigated in Chapters 6 and 7.

4.1.1 Spectral Properties, Energy Levels and Effects of Aggregation

The remarkable spectral properties of phthalocyanines are reflected in their deep green and blue colors, arising from a strong electronic absorption in the red end of the visible spectrum, with molar extinctions usually exceeding 10^5 L mol^{-1} cm^{-1}.[120,121] Such an intense absorption has attracted the interest of chemists and spectroscopists alike.[47]

Many theoretical calculations were reported on the energy levels of molecular orbitals and associated electronic transitions in PcMs.[122] In the present discussion, the widely-accepted MO diagram proposed by Gouterman et al.[123] and later expanded by Lever[124] and Stillman[47,125] is adopted (Figure 4.5). Gouterman's four orbital model, based on the highest two occupied MOs (of a_{2u} and a_{1u} symmetry) and the degenerate, lowest unoccupied orbital (e_g), accounts well for the transitions observed in the UV-vis region of the spectrum. The allowed $\pi \rightarrow \pi^*$ transitions in Pcs usually occur between 230 and 800 nm; there are five possible excitations, labeled, in increasing order of energy, Q, B, N, L and C, as shown in Figure 4.5;[125] their associated λ values are diagnostic. The strongest bands are given by the Q and B excited states, which form the signature of a Pc UV-vis spectrum. The Q band, typically the more intense of the two, is located in the 660–800 nm region and originates in the electronic transition from the HOMO, $1a_{1u}$ (π), to the LUMO, $1e_g$ (π^*) orbital. Transitions from the next two highest occupied π orbitals, $1a_{2u}$ and $1b_{2u}$, to the $1e_g$ (π^*) LUMO yield the B (also called Soret) bands, which usually appear broad and poorly defined in the blue region of the spectrum, below 350 nm. PcMs with D_{4h} or higher symmetry exhibit only one Q band, while an asymmetric PcM and a metal-free PcH_2 will display a split into two Q bands, due to several possible transitions between non-degenerate HOMO and LUMO levels.

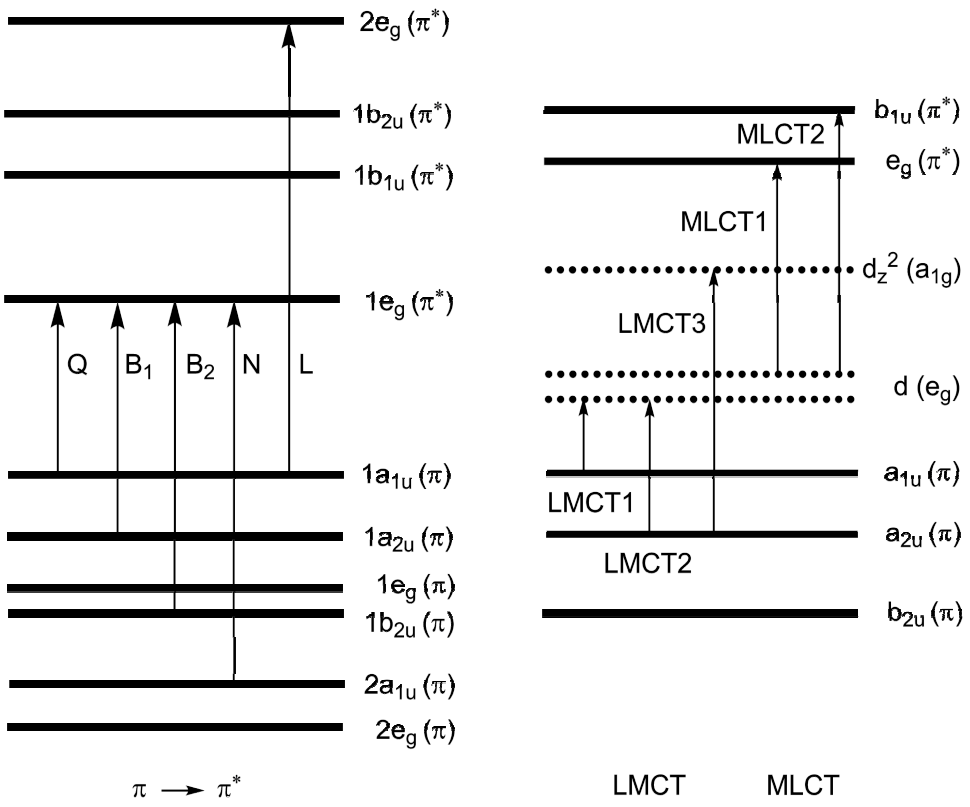

Figure 4.5 Energy levels in typical metallophthalocyanines and associated transitions.[125]

Electronic absorption spectra of transition metal phthalocyanines could contain additional bands due to metal to ligand (MLCT) or ligand to metal (LMCT) charge-transfer excitations, also shown in Figure 4.5. These bands may be observed in the visible (450 to 600 nm) or the near-IR (700 to 1500 nm) regions[123,124,126] and are missing for metals with empty (d^0) or filled (d^{10}) shells. These absorptions originate in the positioning of the metal's d orbitals between the HOMO and LUMO levels of the Pc ligand; the CT band energies are dependent on both the metal's spin and oxidation state.

An important property exhibited by most Pcs in solution is aggregation. Dimeric (or polymeric) species can form through intermolecular coupling of Pc rings if steric factors allow for an association to occur.[47] It is generally agreed upon that dimer species account for the vast majority of aggregates in solution, higher order, stable polymeric-

type structures being unlikely;[127] dimerization can be solvent- or ion-induced and has made the object of a multitude of studies, notably by Lever, Leznoff and Kobayashi.[127,128]

Spectral effects vary from band broadening to a blue shift of 30 to 80 nm of the dimer's Q and B bands, and sometimes their splitting as a result of a change in symmetry of the complexes. Aggregation between Pc molecules is generally explained through exciton coupling, a state interaction theory specifically excluding MO overlaps of each component.[129] According to this, for a D_{4h} symmetry, two pairs of doubly degenerate states will arise upon electronic coupling of two monomer Pc units, with allowed transitions only to the two higher energy, in-phase coupled states (Figure 4.6), which account for the observed blue-shift in the UV-vis absorptions.[129,130] Pcs tend to aggregate more in polar protic solvents (e.g., alcohols), and remain mostly monomeric in non-polar and halogenated solvents, such as toluene, $CHCl_3$ and DCM.[127–130] Intermediate levels of aggregation may occur in polar aprotic solvents. Aggregation becomes a concern in homogeneous catalysis, since aggregates obstruct the substrate's access to all active sites.

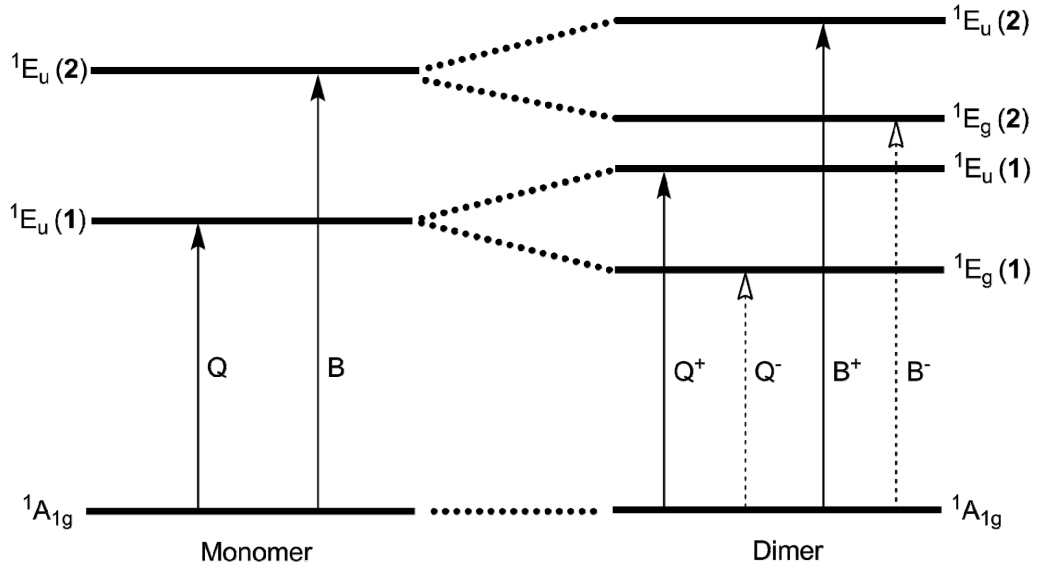

Figure 4.6 Qualitative orbital diagram for exciton coupling in a phthalocyanine dimer with D_{4h} symmetry.[129,130] Dashed lines indicate forbidden transitions.

4.2 Experimental Section

4.2.1 Synthesis and Characterization of 1,2-Diiodo-4,5-dimethylbenzene

A mixture of *o*-xylene (40.0 g, 0.377 mol), periodic acid (34.4 g, 0.151 mol) and iodine (84 g, 0.339 mol) was heated under stirring in a solution of acetic acid (200 mL), water (40 mL) and sulfuric acid 96% (6 mL) to 70 °C for 18 h. After cooling to RT, the reaction mixture was poured over a solution of 20 g $Na_2S_2O_3$ in 400 mL water and 300 mL DCM were added. Intense stirring for 5 min allowed for the reduction of iodine. The organic phase was separated and the water phase was washed with DCM (2 × 150 mL). The combined organic layers were washed with a solution of 15 g Na_2CO_3 in 450 mL water (3 × 150 mL), dried over $MgSO_4$, filtered, evaporated *in vacuo* and recrystallized from methanol (*ca.* 700 mL) to afford white crystalline plates of **[4-2]** in 69% yield (83.4 g). Mp: 88–90 °C (lit.[115] 91 °C); ^{1}H NMR (300 MHz, $(CD_3)_2CO$): δ 2.17 (6H, s, C*H*$_3$), 7.69 (2H, s, Ar-*H*); ^{13}C {^{1}H} NMR (75 MHz, $(CD_3)_2CO$): δ 18.9, 104.2, 139.9, 140.8.

4.2.2 Synthesis and Characterization of 1,2-Bis(trifluoromethyl)-4,5-dimethyl-benzene

Dry sodium trifluoroacetate (21.8 g, 0.16 mol) and copper iodide (30.5 g, 0.16 mol) were mixed in 150 mL dry NMP. To this suspension, a solution of **[4-2]** (7.2 g, 0.02 mol) in 50 mL dry NMP was added under stirring at RT. The reaction mixture was heated under nitrogen and kept at 165 °C for 22 h. Evolution of CO_2 was monitored with an oil bubbler. After cooling, the mixture was poured over 500 mL of hexanes, stirred intensively for 30 min and let to settle. The upper hexane phase was filtered over silica gel (35–70 mesh), washed with water (3 × 150 mL) and then dried over $MgSO_4$, filtered off and carefully evaporated under reduced pressure until 150 mL remained. This

solution was separated by flash chromatography with hexanes on silica gel (35–70 mesh), with the product collected as the top fraction. The solvent was removed with a rotary evaporator at 40 °C until *ca.* 20 mL remained, after which it was cooled down at −10 °C. Careful evaporation of the residual solvent under nitrogen stream resulted in a viscous liquid, which gradually crystallized by standing in the freezer for 30 min and allowed for separation of **[4-3]** as colorless crystals in 72% yield (3.5 g). Mp: 38–39 °C (lit.[43] 38–40 °C); ^{1}H NMR (300 MHz, $CDCl_3$): δ 2.37 (6H, s, C*H*$_3$), 7.58 (2H, s, Ar-*H*) (lit.[43] 2.37 (6H, s), 7.58 (2H, s)); ^{19}F NMR (282 MHz, $CDCl_3$): δ −59.58 (6F, s, C*F*$_3$).

4.2.3 Synthesis and Characterization of 4,5-Bis(trifluoromethyl)-phthalic Acid

To a solution of **[4-3]** (1.0 g, 4.12 mmol) in 100 mL acetic acid glacial, 18 mL of sulfuric acid 96% were added and the mixture was cooled to 15 °C in an ice bath, under stirring. CrO_3 (2.1 g, 21 mmol) was added stepwise within 30 min. After the addition, the ice bath was removed and the mixture was allowed to slowly warm to RT and then heated to 35 °C for 20 h. Further, the mixture was diluted with water (*ca.* 100 mL) and 15 mL methanol were carefully added to destroy the excess CrO_3. The aqueous mixture was extracted with Et_2O (3 × 100 mL), the combined organic fractions were washed with water (2 × 50 mL), dried over $MgSO_4$ and filtered. The solvent was evaporated to dryness *in vacuo* and the crude yellow solid was recrystallized from toluene (*ca.* 150 mL), separating **[4-4]** as a white crystalline solid in 59% yield (0.74 g). Mp: 220–222 °C (lit.[43] 228 °C); ^{1}H NMR (300 MHz, $(CD_3)_2SO$): δ 8.24 (2H, s, Ar-*H*); ^{19}F NMR (282 MHz, $(CD_3)_2SO$): δ −58.42 (6F, s, C*F*$_3$); ^{13}C {^{1}H} NMR (75 MHz, $(CD_3)_2SO$): δ 122.1 (q, $J_{C–F}$ = 274.4 Hz), 128.1 (q, $J_{C–F}$ = 34.3 Hz), 128.1 (s), 128.6 (s), 166.3 (s).

4.2.4 Synthesis and Characterization of $F_{24}H_8PcZn$

Solid **[4-4]** (0.06 g, 0.2 mmol), 0.018 g (0.1 mmol) zinc(II) acetate dihydrate, 0.18 g (3.0 mmol) urea and 1 mL nitrobenzene were mixed in a 10 mL reaction vessel, sealed and heated under MW radiation for 10 min at 190 °C. After cooling, the blue-green crude solid was removed from the reaction vessel, washed with water (*ca.* 50 mL), toluene (*ca.* 50 mL), dissolved in EtOAc and purified via flash chromatography on silica gel (35–70 mesh) with EtOAc. Evaporation of the solvent afforded deep blue solid **[4-5]** in 60% yield (0.035 g). Mp > 300 ºC; UV-vis ($CHCl_3$): λ_{max} (log ϵ) 667 (4.65), 639 (3.82), 604 (3.83), 367 (3.96) nm (L mol^{-1} cm^{-1}); IR (KBr): 1663, 1403, 1319, 1295, 1271, 1169, 1099, 922, 735, 614 cm^{-1}; ^1H NMR (300 MHz, $(CD_3)_2CO$): δ 9.41–9.60 (8H, br m, Ar-*H*); ^{19}F NMR (282 MHz, $(CD_3)_2CO$): δ −57.17 (24F, s, C*F*$_3$); HRMS (APCI+): calcd for $[M + H]^+$ $(C_{40}H_9F_{24}N_8Zn)^+$ 1120.9853, found 1120.9864.

4.2.5 Synthesis and Characterization of $F_{24}H_8PcCo$

Ten glass reaction vessels, each charged with magnetic stirrer, solid **[4-4]** (0.06 g, 0.2 mmol), 0.02 g (0.11 mmol) cobalt(II) acetate tetrahydrate, 0.08 g (1.3 mmol) urea and 2 mL nitrobenzene were sealed with Teflon caps and heated under MW radiation for 10 min at 190 °C. After cooling, the contents of each vessel were extracted with EtOAc (*ca.* 10 mL), using a sonicating bath, when needed, in order to break the agglomerated blue-green solid. The combined organic extracts were washed with brine (2 × 100 mL), then water (100 mL), dried over $MgSO_4$, filtered and concentrated *in vacuo*. The crude product was purified via chromatography on silica gel (70–230 mesh) using EtOAc/hexane 1:9 to remove nitrobenzene and unreacted **[4-4]**, followed by EtOAc to isolate **[4-6]** as a dark blue solid in 31% yield (0.173 g). Mp > 300 ºC; UV-vis ($CHCl_3$):

λ_{max} (log ϵ) 660 (4.51), 599 (4.05) nm (L mol^{-1} cm^{-1}); IR (KBr): 1626, 1524, 1319, 1295, 1273, 1177, 1149, 1072, 918, 755 cm^{-1}; ^{19}F NMR (282 MHz, $(CD_3)_2CO$): δ −58.38 (24F, s, CF_3); HRMS (APCI−): calcd for $[M + Cl]^-$ $(C_{40}H_8F_{24}N_8CoCl)^-$ 1149.9515, found 1149.9516.

4.2.6 Synthesis and Characterization of 1,2-Bis(trifluoromethyl)-3-nitro-4,5-dimethylbenzene

A mixture of 40 mL sulfuric acid 96% (74 g, 750 mmol) and 10 mL fuming nitric acid (15.2 g, 240 mmol) was given under stirring to **[4-3]** (4.2 g, 17.2 mmol) and heated to 60 °C for 3 h. After cooling to RT, the mixture was poured over 300 g crushed ice. The milky solution was then extracted with DCM (2 × 100 mL). The combined organic fractions were washed with an aqueous 3% Na_2CO_3 solution (2 × 150 mL) and then water (2 × 200 mL). The DCM fraction was dried over $MgSO_4$, filtered and evaporated *in vacuo*. The crude yellowish solid was purified via silica gel filtration (35–70 mesh) using hexanes to afford white crystals of **[4-7]** in 90% yield (4.45 g). Mp: 45–46 °C; IR (KBr): 3075, 2924, 1620, 1554, 1453, 1380, 1319, 1278, 1156, 1010, 952, 904, 768 cm^{-1}; ^1H NMR (300 MHz, $(CD_3)_2CO$): δ 2.32 (3H, s, 5-CH_3), 2.61 (3H, s, 4-CH_3), 8.10 (1H, s, Ar-*H*); ^{19}F NMR (282 MHz, $(CD_3)_2CO$): δ −55.25 (3F, s, 2-CF_3), −57.85 (3F, s, 1-CF_3); ^{13}C {^1H} NMR (75 MHz, $(CD_3)_2CO$): δ 14.8 (s), 20.8 (s), 118.1 (q, $J_{C–F}$ = 35.0 Hz), 122.6 (q, $J_{C–F}$ = 274.5 Hz), 123.5 (q, $J_{C–F}$ = 273.4 Hz), 127.3 (q, $J_{C–F}$ = 33.8 Hz), 131.5 (q, $J_{C–F}$ = 6.2 Hz), 135.4 (s), 147.3 (s), 151.2 (s); HRMS (EI): calcd for $[M]^+$ $(C_{10}H_7F_6NO_2)^+$ 287.0381, found 287.0389.

4.2.7 Synthesis and Characterization of 1,2-Bis(trifluoromethyl)-3-fluoro-4,5-dimethylbenzene

A solution of **[4-7]** (2.1 g, 7.7 mmol) in 25 mL dry DMF was added under stirring at RT to a suspension of cesium fluoride (3.5 g, 24 mmol) in 25 mL dry DMF. The mixture was heated under nitrogen to 120 °C for 70 h. After cooling, water (*ca.* 100 mL) was added and the mixture was extracted with Et_2O (3 × 100 mL). The ether fractions were joined, washed with water (3 × 100 mL), dried over $MgSO_4$, filtered and carefully evaporated *in vacuo*. The crude yellowish oil was purified via flash chromatography on silica gel (35–70 mesh) using hexanes. Careful evaporation under reduced pressure at 40 °C of the first eluted fraction, followed by standing for 2 h at −20 ºC allowed for the separation of **[4-8]** as colorless crystals in 34% yield (0.67 g). Mp: 22–23 °C; ^{1}H NMR (300 MHz, $(CD_3)_2CO$): δ 2.33 (3H, s, 5-CH_3), 2.49 (3H, s, 4-CH_3), 7.64 (1H, s, Ar-*H*); ^{19}F NMR (282 MHz, $(CD_3)_2CO$): δ −55.59 (3F, s, 2-CF_3), −57.85 (3F, s, 1-CF_3), −112.18 (1F, m, Ar-*F*); ^{13}C {^{1}H} NMR (75 MHz, $(CD_3)_2CO$): δ 11.2 (d, $J_{C–F}$ = 6.9 Hz), 20.0 (d, $J_{C–F}$ = 2.6 Hz), 113.7 (q, $J_{C–F}$ = 34.1 Hz), 123.2 (q, $J_{C–F}$ = 273.2 Hz), 123.7 (qd, $J_{C–F}$ = 272.6, 3.9 Hz), 125.1 (dq, $J_{C–F}$ = 3.0, 6.7 Hz), 125.7 (q, $J_{C–F}$ = 31.8 Hz), 131.7 (d, $J_{C–F}$ = 17.6 Hz), 146.3 (d, $J_{C–F}$ = 6.4 Hz), 159.9 (dq, $J_{C–F}$ = 253.6, 2.5 Hz); HRMS (EI): calcd for $[M]^+$ $(C_{10}H_7F_7)^+$ 260.0436, found 260.0441.

4.2.8 Synthesis and Characterization of 4,5-Bis(trifluoromethyl)-3-fluorophthalic Acid

Compound **[4-9]** was prepared and isolated in a similar manner to **[4-4]**, starting from 1.2 g (4.6 mmol) of **[4-8]** and using EtOAc instead of Et_2O for product extraction. Following the purification steps described in Section 4.2.3, **[4-9]** was separated as a white crystalline

solid in 53% yield (0.78 g). Mp: 195–196 °C; IR (KBr): 3600–2400, 3031, 2668, 2593, 1729, 1495, 1419, 1281, 1201, 1103, 989, 919, 737 cm^{-1}; ^{1}H NMR (300 MHz, $(CD_3)_2CO$): δ 8.36 (1H, s, Ar-*H*); ^{19}F NMR (282 MHz, $(CD_3)_2CO$): δ −56.08 (3F, s, 4-C*F*$_3$), −58.44 (3F, s, 5-C*F*$_3$), −111.36 (1F, m, Ar-*F*); ^{13}C {^{1}H} NMR (75 MHz, $(CD_3)_2SO$): δ 118.4 (qd, $J_{C–F}$ = 34.6, 14.2 Hz), 121.0 (q, $J_{C–F}$ = 275.9 Hz), 121.6 (qd, $J_{C–F}$ = 274.2, 3.5 Hz), 124.7 (octet, $J_{C–F}$ = 3.3 Hz), 127.9 (q, $J_{C–F}$ = 34.6 Hz), 130.2 (d, $J_{C–F}$ = 23.1 Hz), 134.7 (d, $J_{C–F}$ = 5.5 Hz), 156.8 (d, $J_{C–F}$ = 258.1 Hz), 163.3 (s), 163.8 (s); HRMS (EI): calcd for $[M]^+$ $(C_{10}H_3F_7O_4)^+$ 319.9920, found 319.9909.

4.2.9 Synthesis and Characterization of 4,5-Bis(trifluoromethyl)-3-fluorophthalic Acid Anhydride

0.58 g (1.8 mmol) of solid **[4-9]** were suspended in 2.5 mL (4.1 g, 34.5 mmol) thionyl chloride and heated to 90 °C under stirring for 3 h. After cooling to RT, the excess $SOCl_2$ was evaporated under an air stream. The resulting white solid was analyzed and used fresh for production of **[4-11]** in the same flask. White, solid **[4-10]** was obtained in 92% yield (0.51 g). Mp: 81–84 °C; IR (KBr): 3037, 1870, 1791, 1623, 1296, 1162, 1100, 910, 732 cm^{-1}; ^{1}H NMR (300 MHz, $(CD_3)_2CO$): δ 8.56 (1H, s, Ar-*H*); ^{19}F NMR (282 MHz, $(CD_3)_2CO$): δ −55.68 (3F, s, 4-C*F*$_3$), −58.31 (3F, s, 5-C*F*$_3$), −107.51 (1F, m, Ar-*F*). Moisture sensitivity did not allow for well-resolved ^{13}C NMR and satisfactory HRMS.

4.2.10 Synthesis and Characterization of 4,5-Bis(trifluoromethyl)-3-fluoro-phthalimide

0.5 g (1.66 mmol) of freshly obtained **[4-10]** were mixed intensively with urea (0.2 g, 3.32 mmol) and heated while stirring to 140 °C for 2 h. The white solid product was

used as received for the next step. Obtained **[4-11]** in 95% yield (0.48 g). Mp: 184–186 °C; IR (KBr): 3453, 3360, 3251, 3072, 2738, 1744, 1661, 1624, 1329, 1282, 1177, 993, 744, 654 cm^{-1}; ^{1}H NMR (300 MHz, $(CD_3)_2CO$): δ 5.39 (1H, br, N*H*), 8.21 (1H, s, Ar-*H*); ^{19}F NMR (282 MHz, $(CD_3)_2CO$): δ −55.57 (3F, s, 4-CF_3), −58.11 (3F, s, 5-CF_3), −111.33 (1F, m, Ar-*F*); HRMS (EI): calcd for $[M]^+$ $(C_{10}H_2F_7NO_2)^+$ 300.9974, found 300.9975. Low solubility hindered the acquisition of a well-resolved ^{13}C NMR spectrum.

4.2.11 Synthesis and Characterization of 4,5-Bis(trifluoromethyl)-3-fluoro-phthalamide

Solid **[4-11]** (0.48 g, 1.58 mmol) was powdered, suspended in 20 mL ammonium hydroxide 28% and stirred for 18 h. The mixture became a thick paste, which was filtered off and dried under vacuum to afford white solid **[4-12]** in 70% yield (0.35 g). Mp: 203–204 °C; IR (KBr): 3461, 3422, 3305, 3025, 1713, 1610, 1356, 1128, 766 cm^{-1}; ^{1}H NMR (300 MHz, $(CD_3)_2CO$): δ 7.27 (1H, s, 1-CONH_2), 7.48 (1H, s, 2-CONH_2), 7.62 (1H, s, 1-CONH_2), 7.74 (1H, s, 2-CONH_2), 8.06 (1H, s, Ar-*H*); ^{19}F NMR (282 MHz, $(CD_3)_2CO$): δ −55.59 (3F, s, 4-CF_3), −58.26 (3F, s, 5-CF_3), −110.59 (1F, m, Ar-*F*); HRMS (EI): calcd for $[M]^+$ $(C_{10}H_5F_7N_2O_2)^+$ 318.0239, found 318.0232. Low solubility hindered the acquisition of a well-resolved ^{13}C NMR spectrum.

4.2.12 Synthesis and Characterization of 4,5-Bis(trifluoromethyl)-3-fluoro-phthalonitrile

Solid **[4-12]** (0.1 g, 0.31 mmol) was dissolved in 2 mL dry DMF. The solution was cooled to −10 °C and 72 μL (0.12 g, 1 mmol) $SOCl_2$ in 2 mL dry DMF was dropped within 15 min. After keeping for 30 min at −10 °C, the mixture was allowed to warm to

RT and stirred overnight. The brownish solution was then given to 50 g ice and stirred for 15 min. The crude, precipitated solid was filtered off, dried under air, redissolved in acetone and filtered again from brown impurities. Evaporation of the acetone solution afforded **[4-13]** as a gray solid in 52% yield (0.045 g). Mp: 35–36 °C; IR (KBr): 3128, 3078, 2247, 1739, 1621, 1573, 1430, 1343, 1183, 1120, 1014, 930, 684 cm^{-1}; ^{1}H NMR (300 MHz, $(CD_3)_2CO$): δ 8.71 (1H, s, Ar-*H*); ^{19}F NMR (282 MHz, $(CD_3)_2CO$): δ −56.29 (3F, s, 4-C*F*$_3$), −58.69 (3F, s, 5-C*F*$_3$), −99.35 (1F, m, Ar-*F*); ^{13}C {^{1}H} NMR (75 MHz, $(CD_3)_2CO$): δ 110.5 (s), 112.7 (d, $J_{C–F}$ = 20.6 Hz), 113.9 (d, $J_{C–F}$ = 2.3 Hz), 121.4 (q, $J_{C–F}$ = 275.9 Hz), 121.8 (d, $J_{C–F}$ = 12.3 Hz), 122.0 (qd, $J_{C–F}$ = 274.9, 3.3 Hz), 122.3 (s), 129.9 (dq, $J_{C–F}$ = 4.5, 6.8 Hz), 134.3 (q, $J_{C–F}$ = 34.8 Hz), 162.6 (dq, $J_{C–F}$ = 270.0, 2.1 Hz); HRMS (EI): calcd for $[M]^+$ $(C_{10}HF_7N_2)^+$ 282.0028, found 282.0037.

4.2.13 Synthesis and Characterization of $F_{28}H_4PcZn$

0.24 g (0.85 mmol) of **[4-13]**, 0.08 g (0.43 mmol) zinc(II) acetate dihydrate and 2 mL nitrobenzene were mixed in a 10 mL glass reaction vessel, sealed and heated under MW radiation for 15 min at 200 °C. After cooling to RT, the blue-green solid was dissolved in EtOAc and purified via flash chromatography on silica gel (35–70 mesh) using first EtOAc and then acetone/hexane (1:1) as eluents. Evaporation of the solvent afforded dark blue solid **[4-14]** in 38% yield (0.096 g). Mp > 300 °C; TGA: sublimes at ~470 °C; UV-vis ($CHCl_3$): λ_{max} (log ϵ) 676 (5.25), 647 (4.42), 609 (4.44), 378 (4.56) nm (L mol^{-1} cm^{-1}); IR (KBr): 2928, 1633, 1414, 1285, 1161, 942, 720 cm^{-1}; ^{1}H NMR (300 MHz, $(CD_3)_2CO$): δ 9.11–9.46 (4H, m, Ar-*H*); ^{19}F NMR (282 MHz, $(CD_3)_2CO$): δ −53.48 (12F, br, C*F*$_3$), −56.72 (12F, br, C*F*$_3$), −109.09 (4F, br, Ar-*F*); HRMS (APCI+): calcd for $[M + H]^+$ $(C_{40}H_5F_{28}N_8Zn)^+$ 1192.9476, found 1192.9491.

4.2.14 Synthesis and Characterization of $F_{28}H_4PcCo$

Compound **[4-15]** was prepared and purified in a similar manner to **[4-14]**, using 0.035 g (0.12 mmol) of **[4-13]**, 0.012 g (0.07 mmol) cobalt(II) acetate tetrahydrate and 2 mL nitrobenzene. The crude blue-green solid obtained after evaporation of the EtOAc fraction was treated with 50 mL acetone, filtered and dried under air to afford dark purple solid **[4-15]** in 51% yield (0.018 g). Mp > 300 °C; UV-vis ($CHCl_3$): λ_{max} (log ϵ) 665 (4.56), 602 (3.92), 347 (4.24) nm (L mol^{-1} cm^{-1}); ^{19}F NMR (282 MHz, $(CD_3)_2CO$): δ −53.87 (12F, br, C*F*$_3$), −56.72 (12F, br, C*F*$_3$), −108.94 (4F, br, Ar-*F*); HRMS (APCI+): calcd for $[M + H]^+$ $(C_{40}H_5F_{28}N_8Co)^+$ 1187.9517, found 1187.9564.

4.3 Results and Discussion

4.3.1 Synthesis

The synthetic work towards the first fluoro-trifluoromethylated phthalonitrile **[4-13]** and corresponding PcMs **[4-14]** and **[4-15]** was challenging. It involved ten reaction steps, starting with the ordinary *o*-xylene and utilising known materials as well as new ones. The extensive pathway presented in Figure 4.3 emerged as a necessary compromise, owing to difficulties encountered in the use of direct, single-step substitution methods, as described in the introduction. Nevertheless, this route was equally rewarding, yielding seven new fluorinated aromatic intermediates, viz. **[4-7]** to **[4-13]**, four of which were characterized via X-ray diffraction techniques.

The yields for the various steps changed according to the specifics of each reaction. The first two transformations, following reported procedures,[115–117] occur with *ca.* 70% conversion to the desired product, but separation and purification of **[4-3]** is complicated by partial miscibility of CuI in both aqueous and organic phases, several

extractions being necessary in order to get a clear organic layer. Additional small amounts of **[4-3]** can be obtained if the residual NMP slurry is extracted repeatedly with hexanes, but the procedure is time consuming and not economically viable past the third extraction, due to large volumes of solvents involved. Then, mononitration of **[4-3]** is performed with a mixture of fuming nitric acid and sulfuric acid for 3 h at 60 °C. Care must be exercised during the reaction for strict control of both time and temperature. While traceable amounts of dinitrated side product **[4-16]** were always identified in the raw reaction mixture, they can be minimized by maintaining the optimal reaction parameters; otherwise, the transformation is close to quantitative.

The aromatic fluorination step, through an SN2 replacement of the nitro group in **[4-7]**, is the hindering process in the overall synthetic route, with its low yield of 34%. The transformation does occur, but the process is a slow, thermodynamically controlled equilibrium reached after 3 days of reaction under solvent reflux. Furthermore, the product's extreme volatility (mp 23 °C) does not help in its isolation, substantial amounts being lost during the workup of the organic phase. **[4-8]** has a sweet-pungent odor and requires storage in tightly-sealed vials in a freezer.

Next, oxidation of **[4-8]** to the phthalic acid analogue **[4-9]** proceeds with a moderate yield of 53%. Once more, the transformation is slow and the temperature must be kept below 40 °C to avoid total oxidation of the organic materials under the strong action of CrO_3. The presence of mono-oxidation side products may complicate the separation and, if their TLC-monitored ratios to the desired product prove to be too high, might require further addition of CrO_3 to the reaction flask to complete the oxidation. The high mp of **[4-9]** (196 °C) is typical of phthalic acids associated through strong H-

bonding. The final four steps in the formation of the fluorinated phthalonitrile **[4-13]** are a series of sequential one-pot operations, reproducing classical dehydration procedures.[43] The dehydrating reagent of choice was thionyl chloride. With the exception of the last step—dehydration of the phthalamide **[4-12]**—all other transformations proceed *quasi*-quantitatively. The pronounced moisture sensitivity of the acid anhydride **[4-10]** is manifested in the inability to obtain satisfactory HRMS results and the appearance of additional resonances of gradually increasing intensity over the few hours required for acquisition of a ^{13}C NMR spectrum. In contrast to **[4-10]**, the phthalimide **[4-11]** and phthalamide **[4-12]** analogues proved much more resilient towards accidental hydrolysis by atmospheric water, no degradation being noticed for months. Their exceptional thermal stability (mps of 186 and 204 °C for **[4-11]** and **[4-12]**, respectively) is indicative of strong inter- and intra-molecular (especially for the two amide groups of **[4-12]**) associations through H bonds; the increase of the mp value from **[4-11]** to **[4-12]** is consistent with the addition of one HBD (the second nitrogen) and three HBA (protons) moieties. However, a drawback of having this many H bonds is the marked insolubility of the two intermediates, in organic and aqueous solvents alike, up to the point of not producing a reasonable signal-to-noise ratio in the ^{13}C NMR spectrum. The final product, phthalonitrile **[4-13]**, is relatively volatile (mp 36 °C), but stable against air and moisture; careful isolation from the reaction mixture is recommended in order to minimize the amount lost by sublimation under air.

Revealing results, with respect to the relative electronic deficiency of the aromatic precursors, are obtained upon formation of the final Pc complexes of Figures 4.1 and 4.3. Experiments have shown that dehydration of the phthalic acid still bearing two axial

aromatic protons, **[4-4]**, to the corresponding phthalonitrile is not necessary for Pc production. **[4-4]** readily tetramerizes in the presence of urea and the chosen metal acetate, with or without solvent, affording the desired $F_{24}H_8$PcM complex as the single product. In the case of electron-poorer $F_{28}H_4$PcM, formation from the phthalic acid analogue **[4-9]**, or either of the subsequent anhydride **[4-10]**, phthalimide **[4-11]** and phthalamide **[4-12]** derivatives, did not proceed. Dehydration down to the phthalonitrile stage was required; only then, **[4-13]** templated in the presence of a metal salt to form the desired PcM. This comes to show that addition of a single aromatic F atom from **[4-4]** to **[4-9]** creates such a large electron deficit that the carboxylic acid groups are not capable of eliminating water moieties when condensation with urea is attempted, retaining their OH groups as a result of stronger, partially π-character C–O bonds. The above observation is validated through the similar behavior of the perfluorinated phthalic acid **[4-19]** and its derivatives (Figure 4.4), only that in the case of the latter the combined electronic demand of the CF_3 groups and both aromatic fluorine atoms did not even allow for dehydration to the corresponding phthalonitrile.

Formation of the two fluoroalkylated Pc ligands occurs with moderate to good isolated yields. The reaction can be performed under MW or classical heating conditions; practice, however, has shown that yields are superior when the MW method is employed, in addition to the immensely shorter time required (10–15 min vs. 4–8 h for classical). Elevated temperatures of at least 170 °C are needed for activation of precursors. For the $F_{24}H_8$Pc scaffold, the Zn complex **[4-5]** was obtained in an isolated yield almost two times higher than the Co analogue **[4-6]** (60% vs. 31%, respectively), while conversions to the $F_{28}H_4$PcZn **[4-14]** and Co **[4-15]** complexes displayed much closer values (38% vs.

51%, respectively). The significant decrease in the isolated amount of $F_{24}H_8PcCo$ **[4-6]** with respect to the Zn analogue **[4-5]** is attributed to: (i) its extremely limited solubility in all solvents, (ii) erratic mobility and solid-phase anchorage during silica gel purifications, and (iii) tendency towards rapid precipitation from solutions. A similar, but less drastic reduction in solubility was noticed for $F_{28}H_4PcCo$, but in the case of the latter the inconvenience could be resolved by adding larger solvent volumes.

The thermal stability of all solid PcM complexes is exemplary: no degradation or phase transformation could be noticed up to *ca.* 300 °C in air. Higher temperatures were not accessible due to technical limitations. A TGA performed on a sample of $F_{28}H_4PcZn$ (Figure 4.7) revealed a sublimation point of ~470 °C. This value is impressive even for particularly refractory materials such as phthalocyanines, proposing the new complexes for applications where exceptional stability under harsh conditions is required.

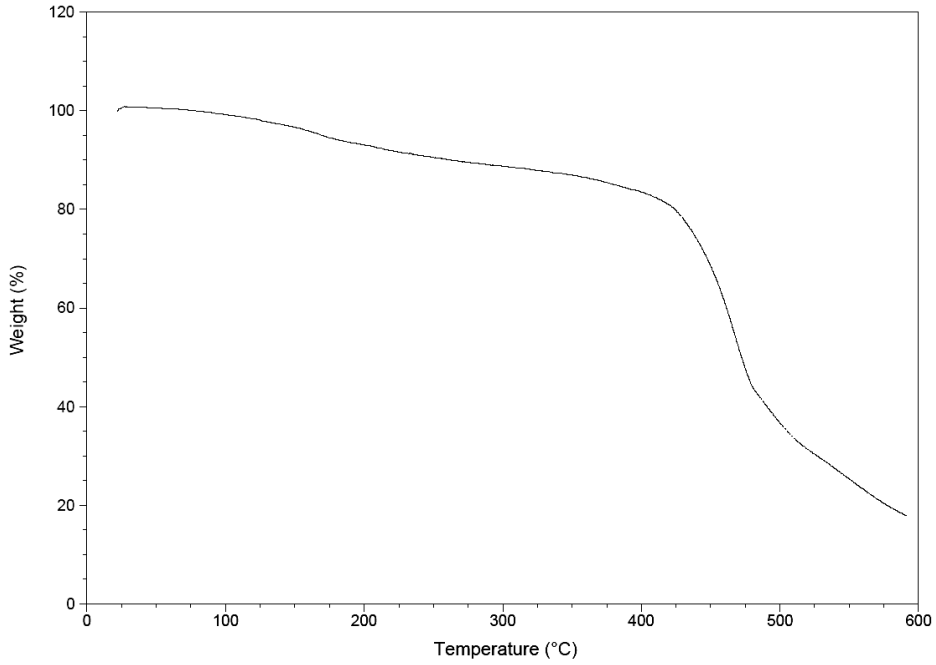

Figure 4.7 Thermogravimetric analysis of $F_{28}H_4PcZn$.

4.3.1.1 Isomers of $F_{28}H_4PcZn$. The $F_{28}H_4Pc$ ligand (Figure 4.3) can form, in theory, as a mixture of four distinct constitutional isomers, exemplified for the Zn complex in Figure 4.8 and identified as **[4-14a]**–**[4-14d]**.

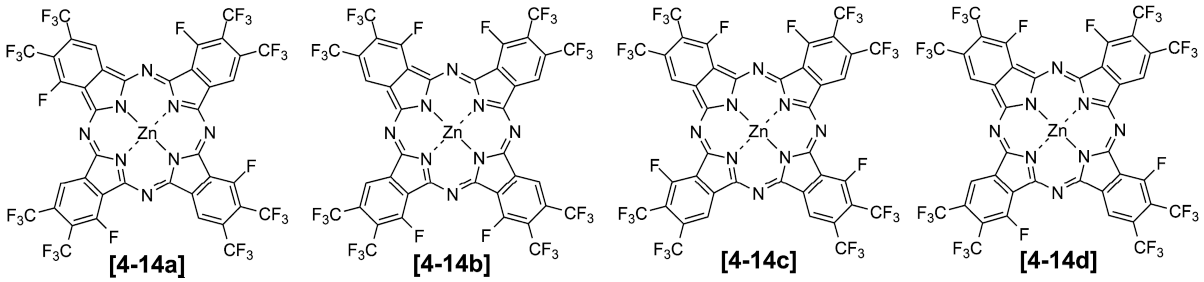

Figure 4.8 The four constitutional isomers of $F_{28}H_4PcZn$.

There is no apparent reason why any of the isomers above should be excluded *ab initio* from formation and, indeed, independent pieces of experimental evidence (NMR spectroscopy, X-ray diffractometry, DFT results), *vide infra*, strongly support the existence of an isomeric mixture. Such mixtures of constitutional Pc isomers are notoriously difficult to separate and characterize due to virtually, and, in many cases, practically identical physico-chemical properties of the constituents.[47] All chromatographic and spectroscopic data initially collected on the $F_{28}H_4PcZn$ complex (by TLC, IR, NMR and HRMS) proposed a unitary material, not allowing for any identification, and even less so for separation of individual isomers.

Preliminary DFT calculations on the four possible isomers of $F_{28}H_4PcZn$, carried out in collaboration with the group of Prof. Stephen Kelty,[‡] revealed a difference between the highest and lowest total electronic energies of the four isomers of *ca.* 0.003 Ha (8 kJ mol^{-1}). This value, obtained using the B3LYP[a] exchange-correlation functional with an RHF[b] model under the 6-31G basis set, is of no consequence in warranting a

[‡] Dwyer, P.; Kelty, S. P. Seton Hall University, South Orange, NJ. Private communication, 2012.
[a] Becke three-parameter Lee-Yang-Parr; [b] Restricted Hartree-Fock.

thermodynamic control of the reaction. A kinetic control, exclusively based on the relative nucleophilic capabilities of the two nitrile N atoms of **[4-13]** and the partial positive charges of their associated carbon atoms, arises as the most likely option, further supported by the elevated temperatures required for initiation of template tetramerization. Mulliken charges calculated for **[4-13]** revealed different electronic populations of the two *C*N carbon atoms, viz. the C2-bonded one the more deficient, with a partial charge of +0.019, while the C1-bonded carbon has a negligible negative charge of −0.010, somewhat electron-enriched through resonance effects. In light of these results, pending refinement, a mechanism for the initial step in the tetramerization of **[4-13]** to $F_{28}H_4Pc$, i.e., the formation of dimeric zwitterionic intermediates, is proposed in Figure 4.9.

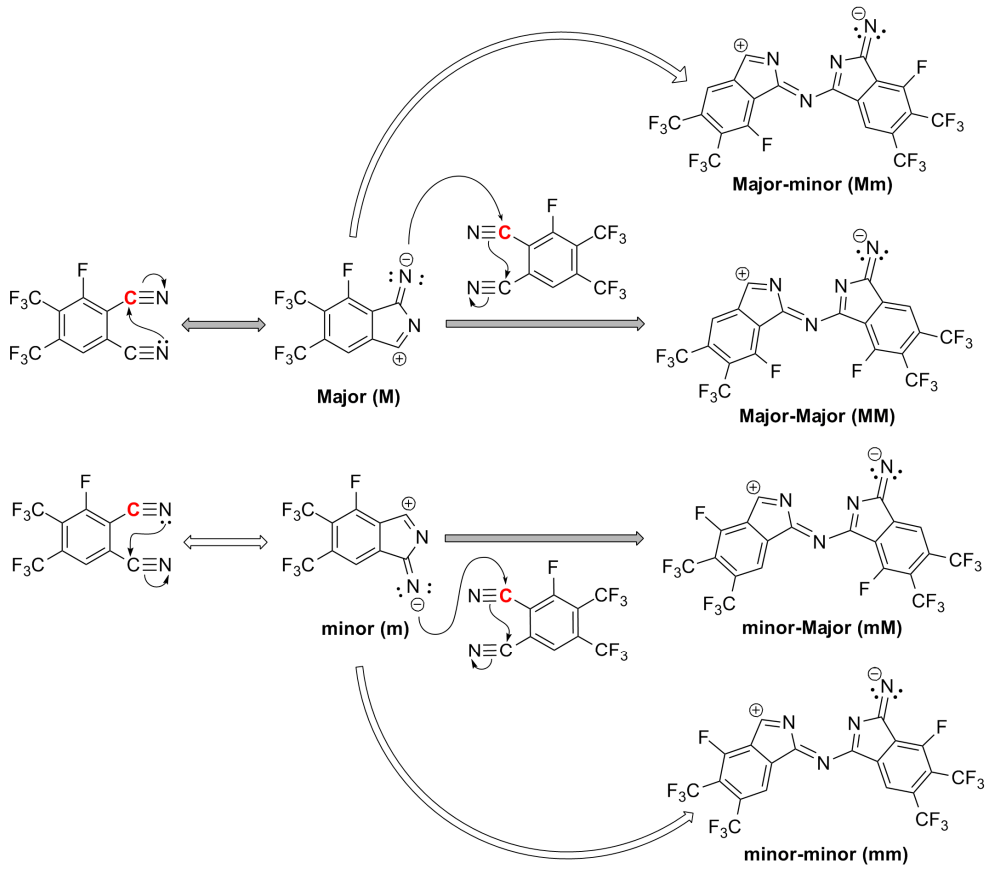

Figure 4.9 Proposed mechanism for the formation of dimeric zwitterionic intermediates of **[4-13]** through nucleophilic attacks. The electron-poorest carbon of the two CN groups is highlighted in red. The most likely routes are shown with filled arrows.

In relation to Figure 4.9, two pathways of intramolecular activation are possible, irrespective of the aid of external anions present (e.g., from the metal salt employed). The most probable route occurs via a 2-*C*N attack, yielding a monomolecular transition state with major population, termed **M**. The opposite, less likely route following a 1-*C*N attack, gives a transient intermediate with minor population, labeled **m**. Each of the two can further initiate intermolecular attacks on other neutral molecules, or combine among them to form four possible zwitterionic dimers, marked **MM**, **Mm**, **mM** and **mm** in Figure 4.9, the relative amount of which is difficult to estimate, given the complexity of the system of reactions leading to the mixture. It is a safe guess, though, to assume that the two containing an initial **M** unit (i.e., **MM** and **Mm**) are present in a vastly superior ratio to their **m**-including counterparts. Combination of either two of the zwitterionic dimers or stepwise addition of two other monomeric units of **[4-13]** eventually leads to formation of the final PcM complex, under the coordinating effect of the metal cation. For instance, isomer **[4-14a]** can only result from a combination of two **Mm** or two **mM** units, while **[4-14b]** is obtained by merging two **MM** or two **mm** fragments.

DFT computations were not yet able to determine an estimated ratio of the postulated **M** and **m** unimolecular intermediates, but the significant difference in the partial charges of the two nitrile carbon atoms suggests a significant shift towards formation of the **M** form. In-depth ^{19}F NMR and X-ray crystallographic studies, performed on the more soluble $F_{28}H_4$PcZn complex and presented herein, have confirmed the existence of at least two isomers in the uniform mixture constituted by the Pc ligand. Because of its inherent properties, previously mentioned, separation of this mixture was not attempted in this study.

4.3.2 IR Spectroscopy

Characteristic bands of the FT-IR spectra (Figures B.10 to B.17) confirm the proposed functional groups of each product. The two non-equivalent trifluoromethyl groups exhibit pairs of strong bands for all new fluoroalkylated compounds **[4-7]**–**[4-13]**. These vibrations are sometimes the predominant feature of the spectrum, and they correspond, in each pair of bands, to the antisymmetric and symmetric aliphatic *v*(C–F) stretchings of the CF_3 unit. Appearing in **[4-7]** at 1319 & 1278 cm^{-1} and 1156 & 1125 cm^{-1}, respectively, they are complemented in subsequent compounds by the lone, strong aromatic *v*(C–F) in-plane stretching band at *ca.* 1100 cm^{-1}. Slight, *ca.* 10 cm^{-1} band displacements are observed from one intermediate to the next, generally towards higher wavenumbers (stronger bonds) as the substituents of the aromatic ring become increasingly more electron withdrawing, from COOH in **[4-9]** to CN in **[4-13]**.

In particular, the symmetric and antisymmetric *v*(N–O) stretching vibrations of the nitro group in **[4-7]** are found as two strong bands at 1554 and 1380 cm^{-1}. The carboxylic acid groups of **[4-9]** show the characteristic conjugated, broad *v*(O–H) band between 3600 and 2400 cm^{-1}, coupled with the strong *v*(C=O) stretching at 1729 cm^{-1}. The broad *v*(O–H) vibration disappears upon dehydration to the anhydride **[4-10]**, concurrently with the splitting of the *v*(C=O) stretching into the antisymmetric (1791 cm^{-1}) and symmetric (1733 cm^{-1}) modes. Transformation to the phthalimide intermediate **[4-11]** results in the appearance of free (1744 cm^{-1}) and H-bonded (1661 and 1624 cm^{-1}) *v*(C=O) stretching vibrations, together with strong *v*(N–H) bands at 3453 cm^{-1} (free) and 3360 cm^{-1} (conjugated through H-bonding). The free and H-bonded *v*(C=O) stretchings are maintained during the conversion to the diamide **[4-12]** (at 1713

and 1610 cm^{-1}, respectively), along with the strong ν(N–H) bands at 3461 and 3422 cm^{-1}. Finally, dehydration to the phthalonitrile **[4-13]** brings about the weak to medium ν(C≡N) stretching band at 2247 cm^{-1}.

Formation of the Pc complexes results in an increase in the symmetry of the molecules which translates into simplified IR spectra. Once again, the vibrations of CF_3 groups are predominantly expressed as pairs of strong, antisymmetric and symmetric stretchings. Showing at 1295 and 1169 cm^{-1} in $F_{24}H_8$PcZn and 1285 and 1161 cm^{-1} in $F_{28}H_4$PcZn, respectively, the ν(C–F) bands are complemented by medium to strong ν(N=C) and ν(C=C) absorptions, slightly red-shifted due to the extended conjugation of the aromatic macrocycle. These bands appear at 1663 and 1403 cm^{-1} in $F_{24}H_8$PcZn and 1633 and 1414 cm^{-1} in $F_{28}H_4$PcZn, respectively.

4.3.3 NMR Spectroscopy

^{1}H, ^{19}F and ^{13}C spectra of all compounds **[4-2]** to **[4-15]**, presented in Appendix A, Figures A.32 to A.65, are consistent with the proposed molecular formulas.

The chemical shifts of aromatic protons—particularly the "lone" 6-H atoms in compounds **[4-7]** to **[4-13]**—are instrumental in monitoring the changes in the molecules' overall electronic deficiency, as the F content is gradually enriched from the non-fluorinated **[4-2]** to the fluoro-trifluoromethylated phthalonitrile **[4-13]**. For instance, replacing one aromatic proton of **[4-3]** with a nitro group in **[4-7]** results in a downfield displacement of $\Delta\delta$ = 0.52 ppm, while exchange of the nitro group with fluorine in **[4-8]** reverses the chemical shift trending of the only aromatic proton in an upfield difference of $\Delta\delta$ = −0.46 ppm. This is consistent with both the strong electron withdrawing effect of the NO_2 (through negative inductive, $-I$, and resonance, $-E$, effects), and the weak

donating effect of the F atom which partially cancels out its −*I* electron withdrawal. From there, the proton in the 6-position suffers gradual downfield shifts again, as the methyl groups of **[4-8]** are oxidized to the phthalic acid **[4-9]**, reaching a maximum value of 8.71 ppm in the electron-poorest dinitrile **[4-13]**.

The same tendencies are noticed in the ^{19}F spectra. While the two *o*-CF_3 groups are less sensitive to the interplay of electronic effects by other aromatic substituents ($\Delta\delta <$ 2 ppm across the entire range of compounds), the 3-F is much more responsive to its neighbors. Again, the highest δ downfield value of −99.4 ppm is recorded for **[4-13]**, the only instance when the Ar-F resonance overcomes the −100 ppm threshold (Figure A.58).

A plot of the sum of Hammett constants[131] ($\Sigma\sigma$) of non-H substituents for selected compounds **[4-1]**–**[4-13]** vs. the chemical shift of the aromatic proton in the 6-position reveals linearity with a correlation coefficient of 0.9833 (Figure 4.10). In the calculation of the sum, *ortho* substituents R_1 and R_3 (with respect to the proton) were treated as *para* groups and assigned σ_p values; although steric effects for *ortho* groups could alter the real value of the Hammett constant for these positions,[131] they cannot be omitted if an accurate description of the molecular electronic effects imparted by the substituents is desired. Ignoring the *ortho* groups altogether results in random values which neither show linearity, nor satisfy any other attempted correlation. The large iodine atoms of **[4-2]** have such a steric influence that the calculated $\Sigma\sigma$, with or without the *o*-iodines, falls well outside the linear fit; therefore, the compound was excluded from the correlation. Moreover, the cyclic structures of phthalic anhydride **[4-10]** and phthalimide **[4-11]** make the use of σ_m or σ_p constants unreliable for these analogues.

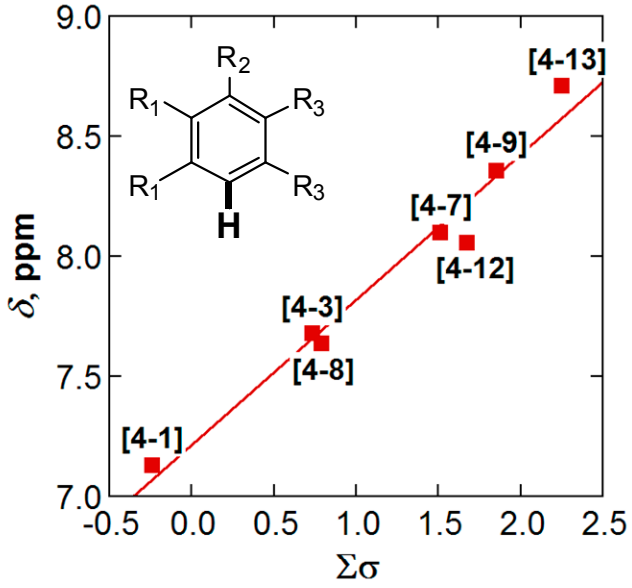

Entry	R_1	R_2	R_3
[4-1]	H	H	CH_3
[4-3]	CF_3	H	CH_3
[4-7]	CF_3	NO_2	CH_3
[4-8]	CF_3	F	CH_3
[4-9]	CF_3	F	COOH
[4-12]	CF_3	F	$CONH_2$
[4-13]	CF_3	F	CN

Figure 4.10 Plot of the sum of Hammett constants[131] calculated for selected compounds **[4-1]** to **[4-13]** vs. the chemical shift of the proton in the 6-position. Linear correlation: y = 7.216 + 0.6038x, R = 0.9833. Bicyclic analogues **[4-10]** and **[4-11]** were omitted due to unreliable Hammett parameters.

The linear fit of Figure 4.10 proves that assigning σ_p values to *ortho* substituents in the calculation of Σσ is a reasonable hypothesis for small groups, and is in accordance with the postulate that *ortho* and *para* moieties have the same type of electronic effects, provided that the reaction and substituent sites are not adjacent.[132] The direct dependence of the compounds' experimentally-determined properties with the electronic deficiency imparted by the attached substituents is thus demonstrated.

Moving to the PcM complexes, ^{1}H and especially ^{19}F spectra are revealing in the identification of major isomers and solvent-to-metal coordination equilibria in solution. Firstly, the generally low solubility of the four Zn and Co complexes, in both deuterated and non-deuterated solvents, hindered the acquisition of well-resolved ^{13}C spectra. Secondly, the two Co analogues **[4-6]** and **[4-16]** were so poorly soluble in any solvent that not even ^{1}H spectra were affordable; they were characterized solely by their ^{19}F resonances, following overnight acquisitions.

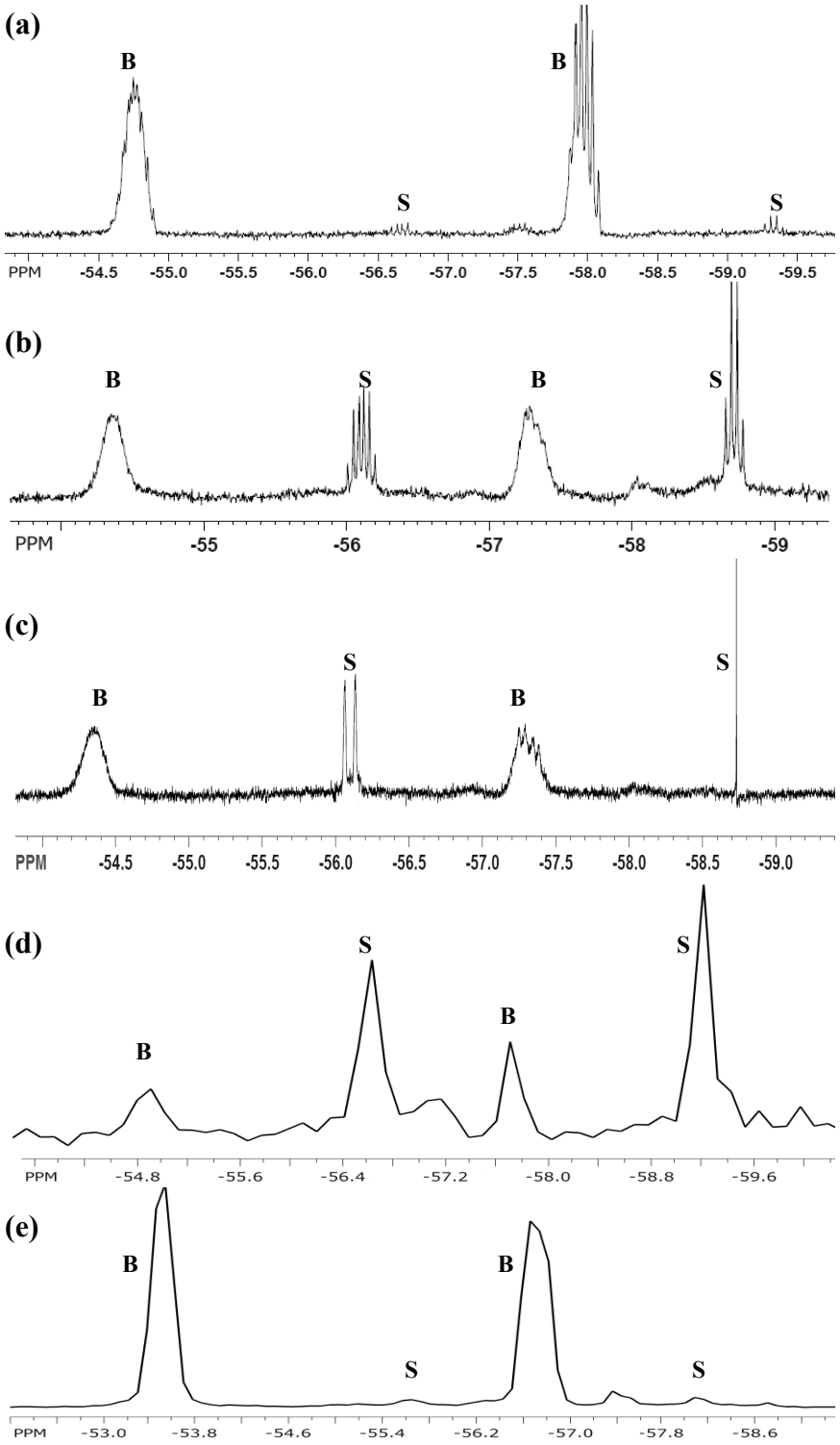

Figure 4.11 ^{19}F NMR spectra of $F_{28}H_4PcZn$, detailing the region of the CF_3 chemical shifts. (a) CD_3COOH (376 MHz, 80 °C). (b) $CDCl_3$ (376 MHz, 25 °C). (c) $CDCl_3$ (376 MHz, 25 °C) irradiated at −107 ppm. (d) $CDCl_3$ (282 MHz, 25 °C) with a drop of NH_4OH added. (e) $(CD_3)_2CO$ (282 MHz, 25 °C). **B** and **S** denote the broad and sharp sets of resonances, respectively.

^{19}F spectra of $F_{28}H_4PcZn$ recorded in $(CD_3)_2CO$ and $CDCl_3$ at 282 MHz resolution (Figures A.61 and A.62, respectively) showed a puzzling splitting of the resonances in two sets of broad (**B**) and sharp (**S**) signals. Attribution of these sets to different isomers of **[4-14]** was excluded, since the ratio between the two varied greatly from one solvent to the other; in fact, in O-coordinating solvents, the set of sharp peaks was barely distinguishable (Figure 4.11(a), (e)). This odd behavior required a more in-depth NMR study at a higher resolution and, maybe, elevated temperatures, where fine ^{19}F–^{19}F couplings could be resolved; therefore, an instrument with a 376 MHz ^{19}F resonating frequency was employed. Both the two-dimensional ^{19}F COSY spectrum of **[4-14]** in $CDCl_3$ (Figure A.63) and irradiation of the sharp resonance of Ar-F occurring at −107 ppm in $CDCl_3$ (Figure 4.11(c)), with no effect on the **B** set, state without a doubt that the two sets of signals originate from independent species. The possibility of aggregated and monomeric forms was investigated next. Heating a saturated CD_3COOH solution of **[4-14]** to 80 °C did not produce any change in the **B**/**S** ratio of the signals, but instead it caused slight sharpening of the broad set; aggregation, even if present, does not seem to lead to a chemically distinct species which would account for one of the **B** or **S** sets. Furthermore, the UV-vis spectrum of **[4-14]** in chloroform is clearly indicating *quasi*-exclusive presence of monomer, inconsistent with the balanced ratio of the two different species observed in ^{19}F NMR. The gain of negative or positive charges by the PcM complex (through axial binding and subsequent electron transfer or protonation of *meso* N atoms of the Pc core by traces of acid, respectively) was also ruled out, as the UV-vis spectra of **[4-14]** in all solvents in question (Section 4.3.6) did not show any of the characteristic bands of reduced or protonated PcMs, but only the neutral complexes.

All these pieces of evidence hint towards the most plausible explanation for the existence of broad and sharp sets of resonances: exchange equilibria in solution through metal-coordination by solvent or extraneous electron-donating species. Following the strong electronic demand of CF_3 groups, the central metal becomes highly Lewis acidic, much more readily accepting axial coordination by electron donors; in acetone and acetic acid, the donors are the solvent molecules themselves, while in solvents lacking Lewis basic atoms (e.g., chloroform) the demand is satisfied by impurities or ambient species, most probably water moieties. The new species, carrying metal-coordinated σ-electron donors, accounts for the broad resonances observed, while the sharp ones are represented by the "free" PcM complexes. The effective absence of the **S** set in acetone and acetic acid and its significant amount in $CDCl_3$ (where impurities and ambient water are in a too short supply to bind all PcM molecules), as well as the sharpening of the **B** set with temperature fully support this hypothesis. An increase in the relative amount of **S** species when a drop of NH_4OH is added to the $CDCl_3$ solution (Figure 4.11(d)) is consistent with the removal of water from the metal center following involvement in acid-base equilibria. Note that electron donors' coordination is of a pure dative nature and does not result in a transfer of electrons to the metal or Pc ligand. This enhanced affinity manifested by $F_{28}H_4PcZn$ towards binding, even in trace amounts, of water and other σ-donor ligands, is indicative of the new complexes' exacerbated electronic deficiency.

The final piece of information offered by the high resolution ^{19}F spectra of $F_{28}H_4PcZn$ is its existence as a mixture of at least two isomers. Upon closer examination at 80 °C, the broad resonances recorded in CD_3COOH (Figure 4.11(a)) show a complex multiplicity which can only be explained by an overlap of two quartets (at *ca.* −57.9 ppm)

and sextets (at *ca.* −54.8 ppm), for the *m*- and *o*-CF_3 groups relative to the Ar-F atoms, respectively. This fine multiplicity was not detectable in the lower resolution spectra.

The barely noticeable chemical differentiation of isomers is achieved only upon coordination of electron donors—probably through preferential orientations of the axially ligated moiety—since a similar splitting pattern was not encountered in the sharp resonances, which appear as a unitary compound. It remains unclear, however, if two or more isomers are presents, as either their resonances might accidentally coincide or the fine splittings are below the instrument's detection limits. Two-dimensional $^{19}F–^{19}F$ NOESY and $^{1}H–^{19}F$ HOESY experiments[§] failed to establish a structural assignment of individual isomers, owing to inadequately spaced resonances and poor signal-to-noise ratios caused by generally low solubility in the deuterated solvents used.

4.3.4 Crystal Structures

Following the synthetic route towards production of the $F_{28}H_4Pc$ ligand, no less than six crystal structures have been obtained. Five of them belong to aromatic intermediates **[4-3]**, **[4-7]**, **[4-8]**, **[4-9]** and phthalonitrile precursor **[4-13]**, while the sixth structure is represented by the Zn complex, $F_{28}H_4PcZn$ **[4-14]**.

4.3.4.1 Overview of Crystallographic Data of Aromatic Intermediates. Table 4.1 summarizes selected crystal data and structure refinement parameters for the **[4-3]**, **[4-7]**, **[4-8]**, **[4-9]** and **[4-13]** intermediates. Information is extracted from the corresponding tables of Appendices M to Q. Figure 4.12 presents thermal ellipsoid plots of the five fluorinated analogues, using data from the same appendices. The characteristic features and packing diagrams of each structure are described in subsequent, dedicated sections.

[§] Anklin, C. Bruker BioSpin Corporation, Billerica, MA. Personal communication, 2010.

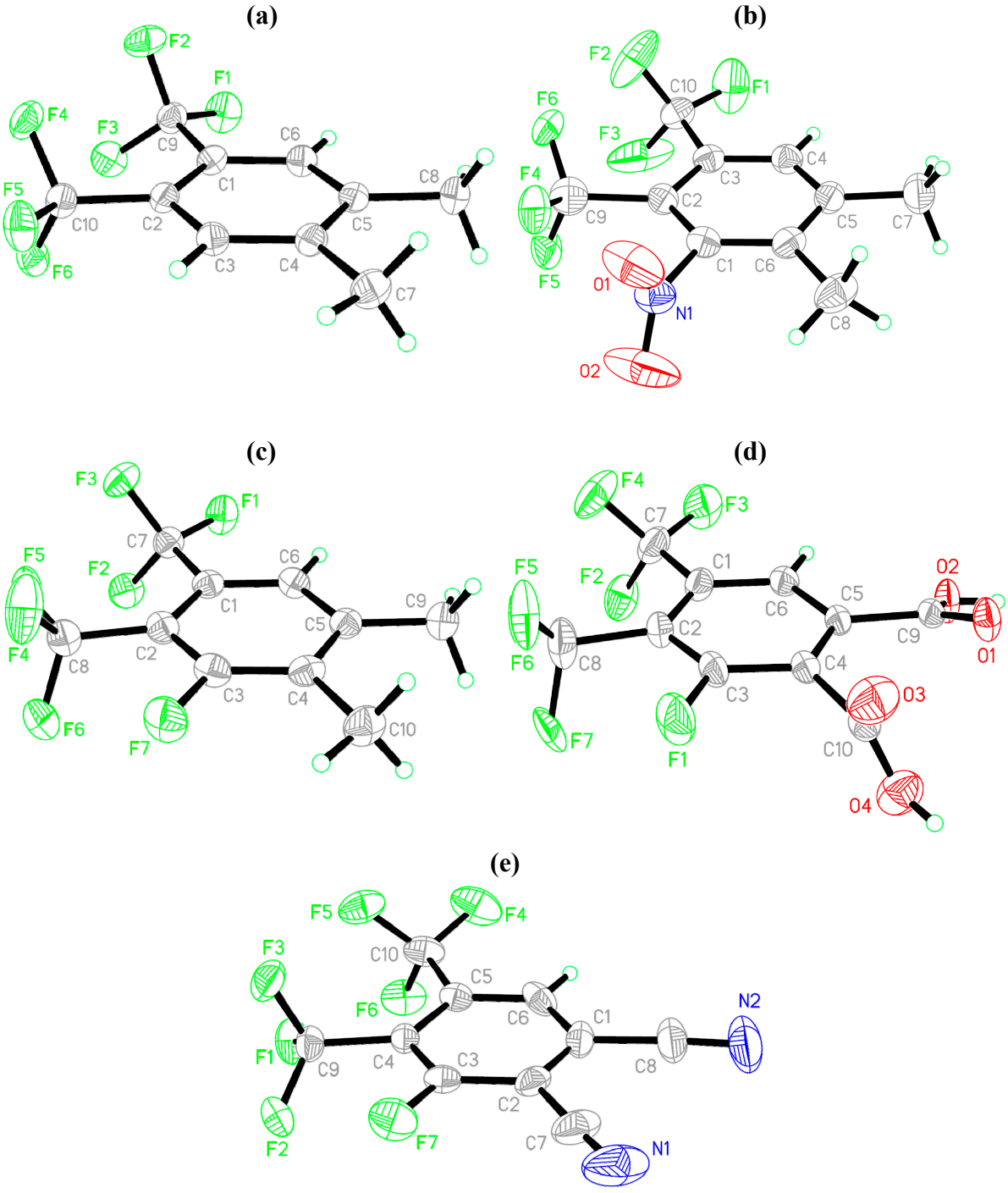

Figure 4.12 ORTEP representations of fluorinated aromatic intermediates, set at 50% probability. (a) X-ray structure of **[4-3]**. (b) X-ray structure of **[4-7]**. (c) X-ray structure of **[4-8]**. (d) X-ray structure of **[4-9]**. (e) X-ray structure of **[4-13]**. Rotational disorder of both CF_3 and NO_2 groups in **[4-7]** and of the 4-CF_3 group in **[4-9]** was omitted for the sake of clarity. Color code: C, gray; F, green; N, blue; O, red.

Table 4.1 Selected Crystallographic Data for Aromatic Intermediates†

	[4-3]	**[4-7]**	**[4-8]**	**[4-9]**	**[4-13]**
System	monoclinic	monoclinic	triclinic	monoclinic	orthorhombic
Space group	$P2_1/c$	$P2_1/n$	$P\bar{1}$	$C2/c$	$Pna2_1$
T (K)	100(2)	100(2)	100(2)	100(2)	100(2)
a (Å)	7.4166(3)	8.8699(1)	7.8599(3)	12.0233(2)	20.2206(9)
b (Å)	9.5676(4)	9.6882(1)	9.0897(3)	14.4173(3)	7.1307(3)
c (Å)	13.7504(5)	13.6311(1)	13.9740(5)	13.2233(3)	7.1706(3)
α (°)	90	90	88.231(2)	90	90
β (°)	90.908(2)	108.895(1)	85.687(2)	106.340(1)	90
γ (°)	90	90	84.709(2)	90	90
V (Å^3)	975.59(7)	1108.245(2)	991.00(6)	2199.59(8)	1033.91(8)
Z	4	4	4	8	4
d_{calcd} (g/cm^3)	1.649	1.721	1.744	1.933	1.812
N_{refl}	1661	1957	3276	1894	1718
N_{param}	147	203	312	221	174
R_1 ($I > 2\sigma I$)	0.0549	0.0506	0.0513	0.0561	0.0414
R_1 (all data)	0.0557	0.0573	0.0549	0.0575	0.0416
wR_2 ($I > 2\sigma I$)	0.1407	0.1310	0.1365	0.1635	0.1145
wR_2 (all data)	0.1414	0.1370	0.1394	0.1649	0.1147
S	1.026	1.074	1.108	1.071	1.152

$R_1 = \sum(|F_o|-|F_c|)| / \sum|F_o|$; $wR_2 = \{\sum w(|F_o|-|F_c|)^2 / \sum w|F_o|^2\}^{1/2}$; $S = \{\sum w(|F_o|-|F_c|)^2 / (N_{refl}-N_{param})^2\}^{1/2}$.
† Abbreviations used in the table and equations: N_{refl} – number of observed independent reflections; N_{param} – number of parameters refined; R_1 – unweighted refinement discrepancy factor; wR_2 – weighted refinement discrepancy factor; S – goodness of fit on F^2; F_o – observed structure factors; F_c – calculated structure factors.

4.3.4.2 1,2-Bis(trifluoromethyl)-4,5-dimethylbenzene. Single crystals of **[4-3]** suitable for X-ray diffraction were obtained by slow evaporation of a hexane solution at RT. Although the compound has been known for over 30 years,[43,44] its crystal structure had not yet been reported.[60] No disorder was observed for the trifluoromethyl groups. Crystals of **[4-3]** are monoclinic in the $P2_1/c$ space group; four molecules are present per unit cell. The value of the final R-factor, 0.0549, indicates the average quality of the crystals. These slowly deteriorate even when kept at 100 K, owing to an increased tendency towards volatilization. A thermal ellipsoid plot is presented in Figure 4.12(a).

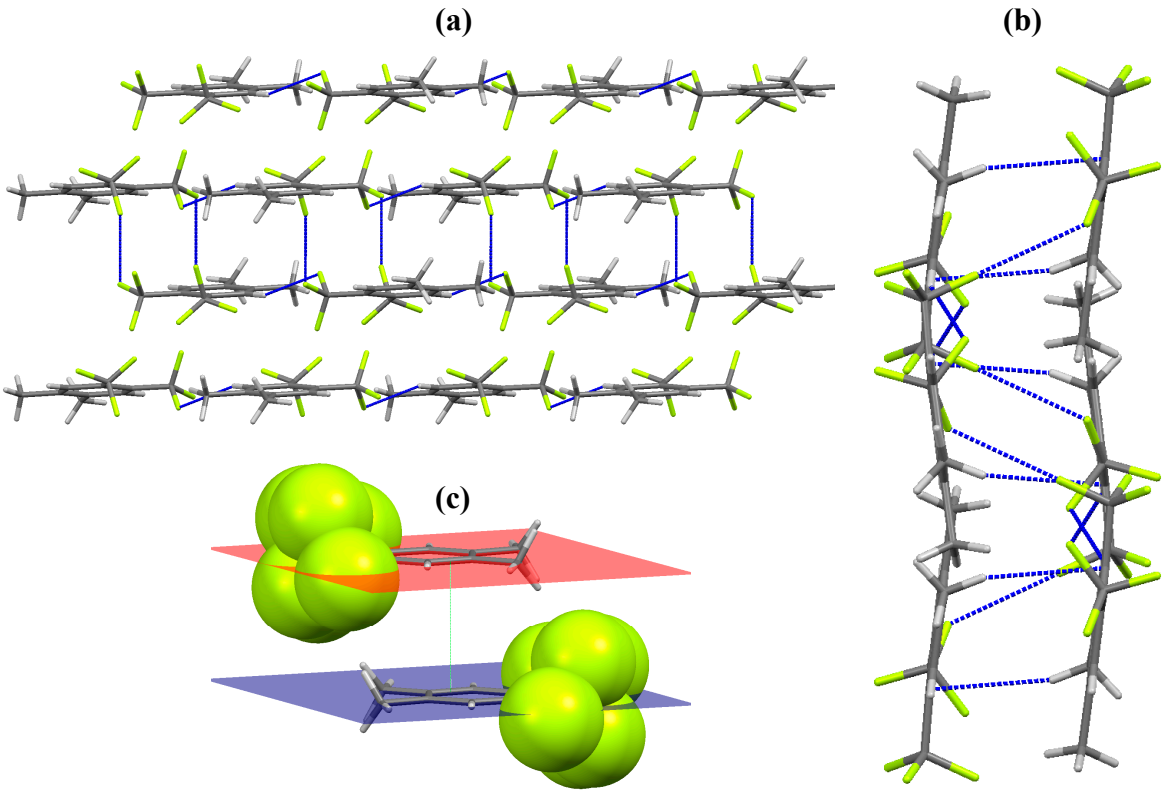

Figure 4.13 Crystal packing diagrams of **[4-3]** in capped sticks representation. (a) View along the *b* axis. (b) View along the *c* axis. (c) Stacking interaction of aromatic rings, showing the F atoms as spheres. Intermolecular F•••F and F•••H contacts are shown as dotted blue lines. Color code: C, gray; H, white; F, green.

The packing diagrams of **[4-3]** (Figure 4.13) reveal parallel, infinite layers of stacked molecules. With respect to the view along the *b* axis (Figure 4.13(a)), intermolecular interactions in the lattice are realised through weak interlayer $(CF_3)F\bullet\bullet\bullet F(CF_3)$ contacts of 2.900 Å and stronger, intralayer F•••H bonds of 2.566 Å. Stacking between the totally parallel molecular planes (Figure 4.13(c)) is achieved by aromatic π–π interactions set across a distance of 3.691 Å. The relative scantiness and overall weakness of intermolecular contacts in the solid structure of hydrophobic **[4-3]** partially accounts for its low volatility (mp 39 °C). Complete crystallographic parameters are provided in Appendix M.

4.3.4.3 1,2-Bis(trifluoromethyl)-3-nitro-4,5-dimethylbenzene. Suitable crystals of **[4-7]** were grown by slow evaporation of a hexane solution at RT. They are stable indefinitely in air and do not include any solvent molecules in the structure. **[4-7]** crystallizes in the monoclinic, $P2_1/n$ space group with four molecules per unit cell. The quality of the crystals (R-factor of 0.0506) is affected by significant rotational disorder exhibited by both CF_3 and NO_2 groups. An ORTEP representation is given in Figure 4.12(b), while complete crystallographic data are provided in Appendix N.

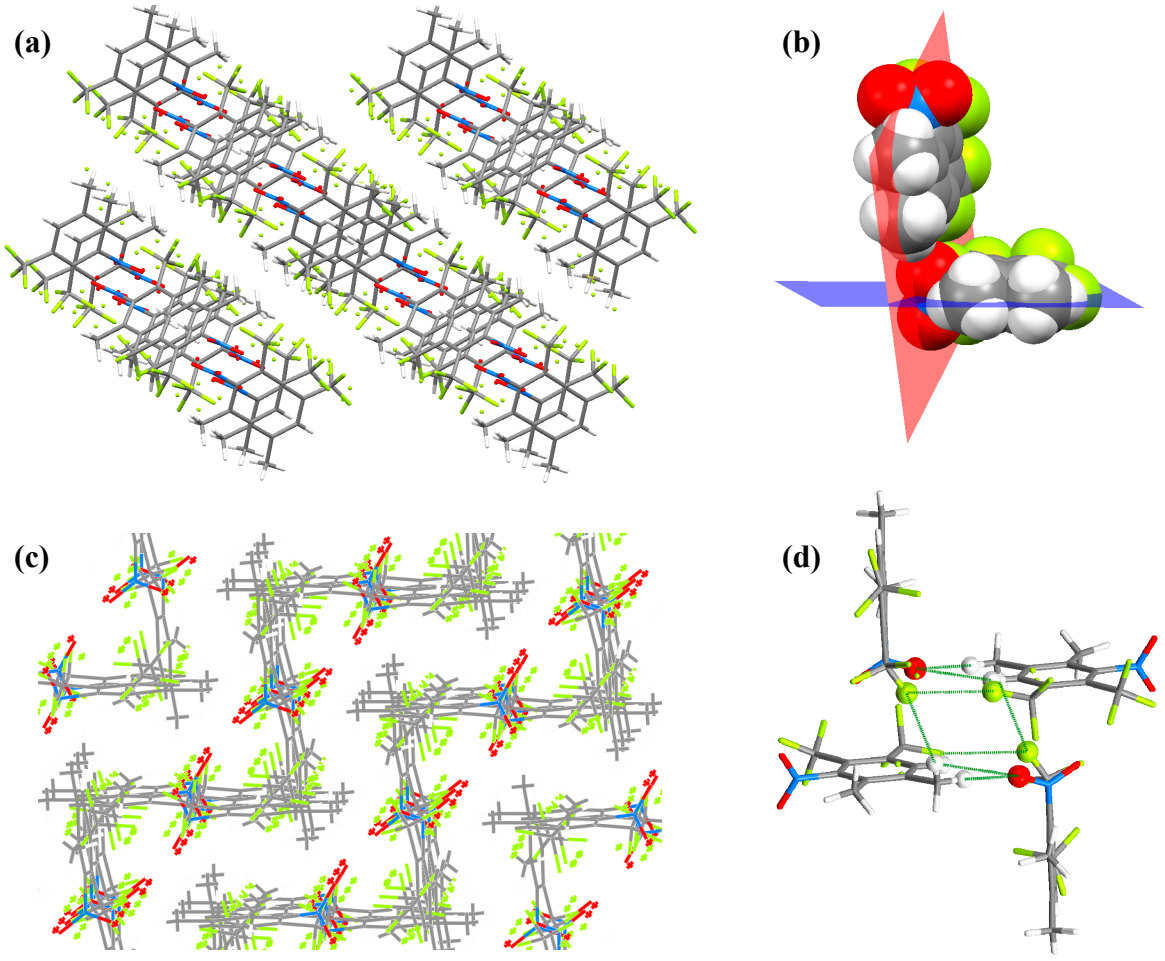

Figure 4.14 Crystal structure of **[4-7]** in capped sticks representations. (a) Packing diagram, in an offset view along the *b* axis. (b) Bimolecular repeating motif in spacefill representation, showing mutually perpendicular molecular planes. (c) Zigzag multi-layered mesh. (d) Tetrameric assembly through F•••F, O•••H and F•••H contacts, shown as dotted green lines. Color code: C, gray; H, white; O, red; N, blue; F, green.

The molecular assembly of **[4-7]** in the lattice presents several interesting features. The packing diagram along the *b* axis (Figure 4.14(a)) reveals parallel layers of molecules in alternate peripheral orientations of the CF_3 and CH_3 groups, while the NO_2 moieties are arranged on a central line, being exclusively involved in intralayer H-bonding. The structural building units are constituted by armchair-like bimolecular motifs (Figure 4.14(b)), in which mutually perpendicular molecules interact through O•••H(Ar) and O•••H(5-CH_3) bonds of 2.653 and 2.581 Å, respectively, and (2-CF_3)F•••F(1-CF_3) weak contacts of 2.940 Å. Note that orientation of the two planes defined by the aromatic rings occurs at 88.74° and is missing the required bisected geometry for a T-shaped π–π stacking. In fact, aromatic coupling interactions seem to be completely absent in the lattice, being replaced by the complex network of H-bonds. Neighboring "armchairs" further assemble into tetramers (Figure 4.14(d)) through (2-CF_3)F•••H(5-CH_3) contacts of 2.572 Å, which in turn expand into a tridimensional zigzag mesh structure, when viewed along the appropriate orientation (Figure 4.14(c)). The lattice is further stabilized by intramolecular O•••H(4-CH_3) bonds of 2.609 Å.

4.3.4.4 1,2-Bis(trifluoromethyl)-3-fluoro-4,5-dimethylbenzene. Single crystals of **[4-8]** were obtained by slow evaporation of a hexane solution at −20 °C. They were of average quality and data collection was complicated by gradual degradation of the solid over time, even at 100 K, owing to the compound's high volatility. The crystalline lattice of **[4-8]** is triclinic, space group $P\bar{1}$, containing four units per unit cell, grouped into pairs of independent molecules. The final R-factor was 0.051. An ORTEP representation of one of the independent molecules is given in Figure 4.12(c), while crystallographic data and refinement parameters are listed in Appendix O.

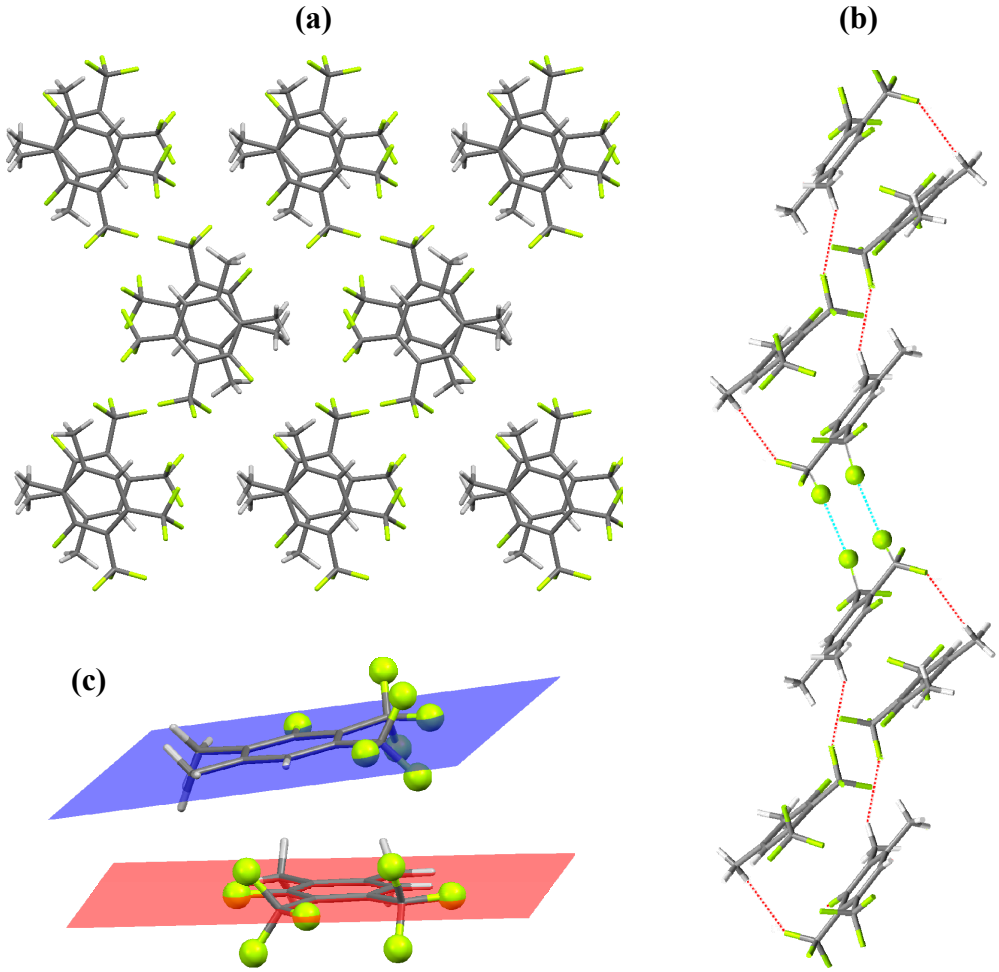

Figure 4.15 Crystal structure of **[4-8]** in capped sticks representations. (a) Packing diagram along the *a* axis. (b) Tetramer motif in the infinitely repeating molecular chain assembly, with inter-tetrameric F•••F contacts shown as dashed blue lines and the intra-tetrameric F•••H interactions as dashed red lines. (c) Tilted stacking of the two independent molecules in the unit cell, with the F atoms shown as spheres. Color code: C, gray; H, white; F, green.

The principal feature of the crystalline lattice of **[4-8]** are infinite chain assemblies between tetrameric blocks consisting of two pairs of independent molecules (Figure 4.15(b)). Within each pair, the top molecule is rotated at a *ca.* 90° angle with respect to the bottom one (Figure 4.15(a)), while the non-parallel planes defined by their aromatic rings form an 8.49° angle (Figure 4.15(c)). A network of intermolecular H-bonds was identified, extending both inside and across the pairs, and containing

(2-CF_3)F•••H(Ar), (2-CF_3)F•••H(5-CH_3), (2-CF_3)F•••H(4-CH_3) and (Ar)F•••H(5-CH_3) interactions spanning 2.522, 2.524, 2.308 and 2.650 Å, respectively. Contact between the tetramer units is made only through weak, 2.808 Å-long, reciprocal (2-CF_3)F•••F(1-CF_3) bonds. The lack of stronger interactions between the subunits of the infinite molecular chains explains the solid compound's marked volatility, accounting for an observed physical property through analysis of the solid-state structure.

4.3.4.5 4,5-Bis(trifluoromethyl)-3-fluorophthalic Acid. Single crystals of **[4-9]** were obtained by slow evaporation of an acetone solution at RT. They do not include ambient water or solvent molecules in the structure. **[4-9]** crystallizes in the monoclinic, *C*2/*c* space group with eight molecules per unit cell. The crystal quality was again average, with an R-factor of 0.0561. The 4-CF_3 group shows rotational disorder, creating a ring of electron density around its carbon. Systematic absence violations indicate the presence of non-unique crystals. An ORTEP representation is given in Figure 4.12(d), the complete crystallographic parameters being provided in Appendix P.

The packing diagrams of **[4-9]** (Figure 4.16) reveal the anticipated associations of pairs of carboxylic groups. There are no intramolecular H•••O bonds and, also, the aromatic proton does not seem to be involved in any interactions as well. In fact, with the exception of (5-CF_3)F•••F(Ar) and (5-CF_3)F•••F(5-CF_3) weak contacts of 2.821 and 2.747 Å, respectively, the rest of intermolecular interactions are exclusively achieved by carboxyl H-bonding. None of the two COOH groups of the molecule is coplanar with the aromatic ring, forming dihedral angles of 24.72° (1-COOH) and 71.03° (2-COOH), respectively. Each acid group associates with topologically equivalent moieties of two neighboring molecules in infinite undulating chains along the *a* axis (Figure 4.16(a)).

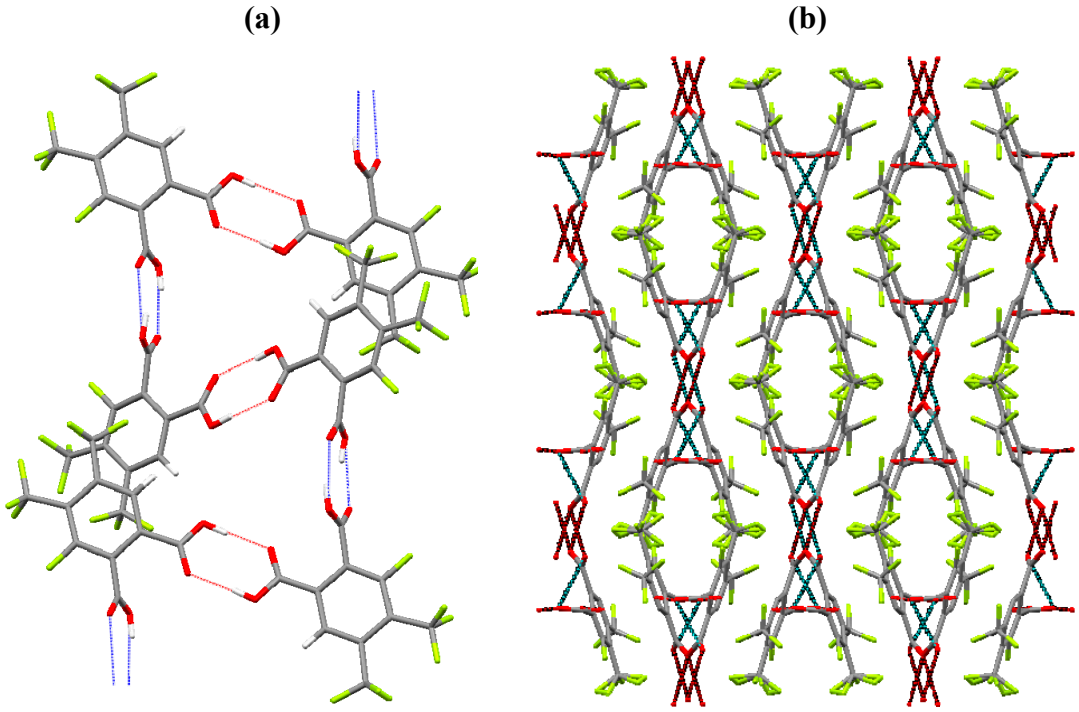

Figure 4.16 Crystal packing diagrams of **[4-9]** in capped sticks representation. (a) View along the *a* axis. (b) View along the *c* axis. Intermolecular H-bonds formed between carboxylic groups are shown as dotted lines. Color code: C, gray; F, green; O, red.

The carboxylic associations occur through exceptionally strong (1-COOH)H•••O (1-COOH) and (2-COOH)H•••O(2-COOH) bonds of 1.808 and 1.822 Å, respectively. Although these values may be subject to a certain degree of error due to placement of hydrogen atoms in calculated positions, they thoroughly account for the compound's high thermal stability (mp 196 °C), a characteristic of phthalic acid analogues. The crystal packing of **[4-9]** along the *c* axis (Figure 4.16(b)) resembles the double helix of DNA, although most of the binding interactions occur in perpendicular or oblique planes to the winding rows of molecules.

4.3.4.6 4,5-Bis(trifluoromethyl)-3-fluorophthalonitrile. The single crystal **[4-13]** used for X-ray diffraction was obtained over two months by sublimation at RT in a sealed vial. An inch-long thin needle, formed on the glass wall of the vial, was cut to yield an X-ray

quality specimen. The fluorinated phthalonitrile **[4-13]** crystallized in the orthorhombic, *Pna*2_1 space group, with four molecules per unit cell. The crystal was badly twinned. A solution could not be found the normal way using direct methods. The structure was solved in the triclinic system and then PLATON[**] was used to reveal the true symmetry. A tetragonal unit cell option was tried but did not work. The orthorhombic solution proved to be correct. Over 500 systematic absences were found (weak, but statistically significant), but were then flagged as unobserved in the true space group. No rotational disorder of the CF_3 groups was noticed. The final R-factor was 0.0414. A thermal ellipsoid plot is presented in Figure 4.12(e); complete crystallographic parameters are provided in Appendix Q.

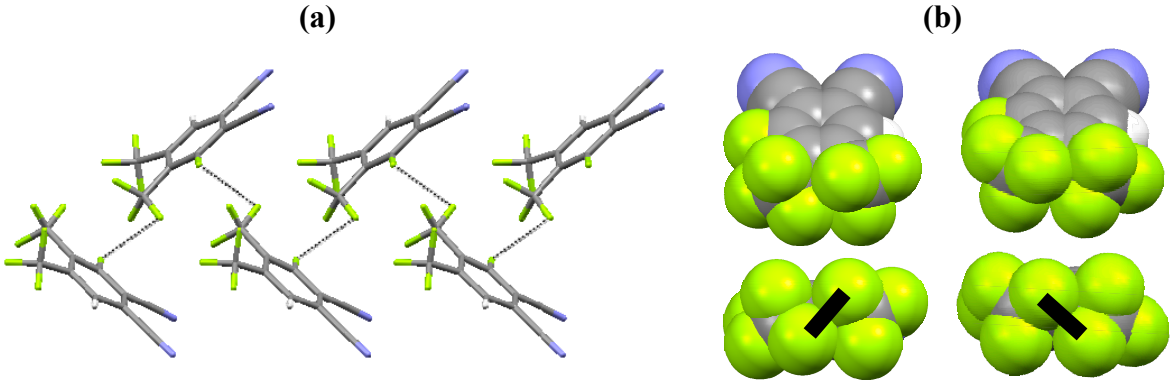

Figure 4.17 Crystal structure of **[4-13]**. (a) Packing diagram along the *b* axis in capped sticks representation, with intermolecular F•••F contacts shown as dotted lines. (b) Van der Waals surfaces representations of the two distinct enantiomers found in the unit cell.

The rotation of the CF_3 groups in solid-state is restricted, locking them in two distinct conformations with respect to the plane of the aromatic ring. This gives rise to well-defined enantiomeric pairs within the unit cell, the geometries of which are shown in Figure 4.17(b). The rotative restriction is lifted in solution, where the aliphatic F atoms are observed as single resonances in the ^{19}F NMR spectrum.

[**] Spek, A. L. PLATON, version 1.15. Utrecht University, Utrecht, The Netherlands, 1980-2011.

The only intermolecular interactions identified in the solid-state structure of **[4-13]** are weak (Ar)F•••F(2-CF_3) contacts of 2.868 Å. Surprisingly, the aromatic proton is not involved in any hydrogen bonding. With such a scarcity of lattice-stabilizing interactions, the compound's fondness for sublimation comes as no surprise.

4.3.4.7 $F_{28}H_4PcZn$. The structural work on **[4-14]** was challenging. Repeated attempts at crystallization from a multitude of solvents, both pure and mixed, protic and aprotic alike, at RT or low temperatures provided unsatisfactory results. The compound's tendency towards aggregation in all solvents, as the concentration increased with gradual solvent removal, caused a major obstacle in obtaining an X-ray suitable single crystal. The process might be complicated even more by the most-likely presence of an isomeric mixture. However, after sixth months of trials, tiny dark green rods were obtained from a 1:1 acetone/acetonitrile mixture. Too small for analysis on a regular X-ray diffractometer, a (0.12 × 0.04 × 0.01 mm) specimen was sent for data collection using synchrotron radiation at the Argonne National Laboratory. The results were eventually up to publishing standards, even if the crystal's quality still turned out to be mediocre.

Refinement of the synchrotron diffraction data was even more demanding. Solved in the monoclinic system, the structure is disordered over a mirror plane, with rings of electron densities around all peripheral CF_3 groups. An initial *Pc* solution was dropped and refined again in the higher symmetry $P2_1/c$ space group. The final unit cell dimensions are a = 7.2524(3), b = 17.3057(7), c = 17.7529(7) Å, β = 91.886(1)°, V = 2226.9(12) $Å^3$, with 2 molecules per unit cell and a borderline R-factor of 0.0755. Atomic assignments were complicated by the co-crystallization of acetonitrile and water molecules in a 1:1 ratio for each **[4-14]** molecule, but in a 1:0.5 coordination ratio to the

central Zn atom, leaving in the lattice 0.5 free water units, disordered over the same positions occupied by CH_3 groups of Zn-ligated acetonitrile. Furthermore, the Zn atom is itself disordered over two positions, above and below the plane of the N_4-ligand, at 0.289 and 0.343 Å. A thermal ellipsoid plot of $F_{28}H_4PcZn$ is presented in Figure 4.18; complete refinement parameters and interatomic angles and distances are provided in Appendix R.

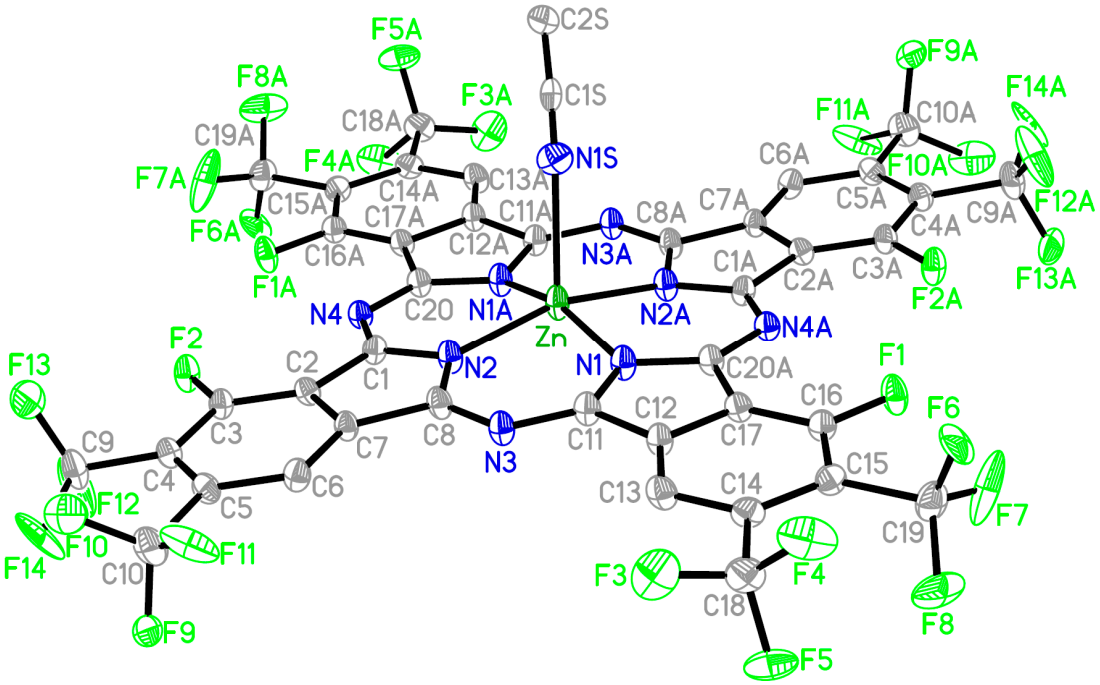

Figure 4.18 X-ray structure of $F_{28}H_4PcZn$, in ORTEP representation at 40% probability. Rotational disorder of the CF_3 groups as well as co-crystallized water and H atoms were omitted for clarity. Only the major aromatic F and Zn (with coordinated acetonitrile) populations are shown. Color code: C, gray; F, light green; N, blue; Zn, dark green.

Aromatic F atoms are found in all eight non-peripheral positions, split in two four-count sets of unequal population, in a roughly 2:1 ratio. Both sets are represented by "head-to-head" arrangements of fluorine atoms on adjacent aromatic rings, similar to the **[4-14b]** isomer in Figure 4.8; the set with major population is shown in Figure 4.18. The presence of F atoms with unequal population at all axial aromatic substitution sites, in the solid-state structure, is the strongest evidence yet of an isomeric mixture.

Still, the experimentally observed 2:1 ratio of the aromatic F populations does not help in determining the number or absolute configuration of the **[4-14]** isomers. The picture is complicated by the probable occurrence of enantiomeric pairs produced by the **[4-14a]** isomer (Figure 4.8), as right- and left-handed "propeller"-type structures become possible upon the offset of the Zn atom above and below the Pc ligand's plane. A number of scenarios could be proposed, in which various combinations of the four isomers are fitted to the 2:1 observed ratio, but, without additional, independent evidence, they remain purely speculative. Further efforts to separate and assign structures to individual isomers of **[4-14]** are beyond the scope of this report. The sufficing conclusion inferred by X-ray diffraction is that $F_{28}H_4$PcM complexes indeed come as a mixture of at least two configurational isomers.

In addition to the features described above, the X-ray structure of **[4-14]** reveals added degrees of complexity. The Zn atoms coordinate both acetonitrile (through 2.421 and 2.295 Å bonds) and water (Zn–O bonds of 2.177 and 2.299 Å) in a 1:0.5 ratio per Zn atom, with additional water molecules equally spread in the lattice on both sides of the Pc rings (Figure 4.19). The free water is associated by $(CF_3)F\bullet\bullet\bullet H$ contacts of 2.296 Å.

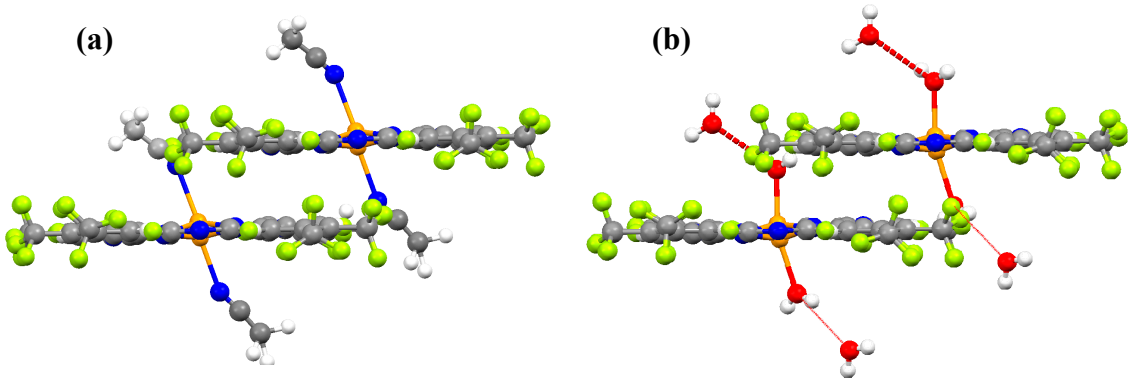

Figure 4.19 (a) Acetonitrile and (b) water coordination by Zn atoms in the X-ray structure of **[4-14]** in ball-and-stick representation. Color code: C, gray; F, green; N, blue; Zn, orange; O, red.

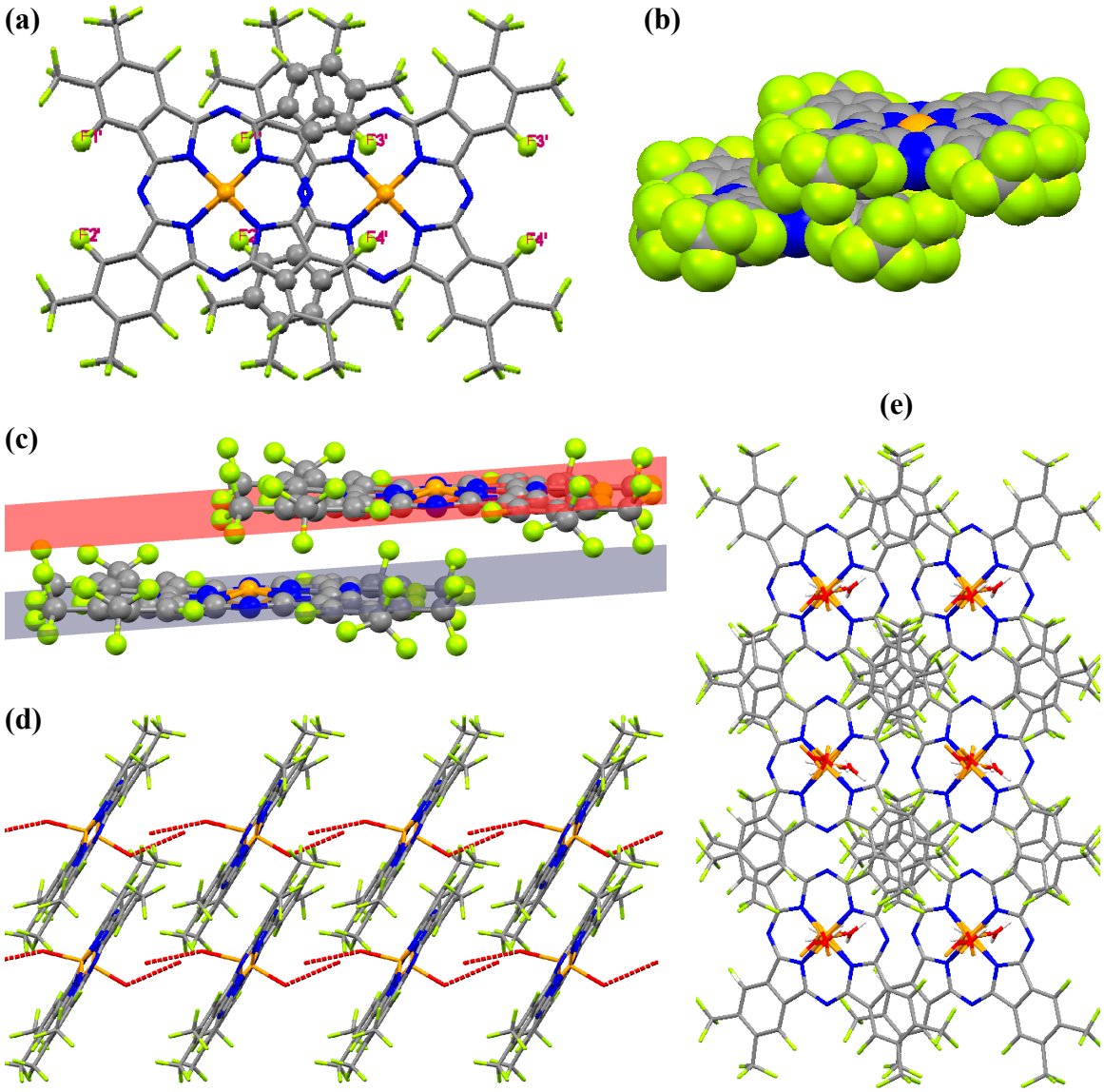

Figure 4.20 Molecular π–π stacking interactions of $F_{28}H_4PcZn$ in the solid state, in capped sticks representation. (a) Repeating dimer unit, showing the atoms of the phenyl rings directly involved in the stacking as spheres. (b) Spacefill representation. (c) Ball-and-stick representation, showing the parallel planes defined by the N_4-coordinating atoms on each stacking molecule. (d) View along the *b* axis. (e) View along the *c* axis. Colors follow the code of Figure 4.19.

A definitive information advanced by the solid-state structure of $F_{28}H_4PcZn$ is the molecular stacking attained by the new Pc ligand. A look at the packing diagrams along the *b* and *c* axes (Figure 4.20) reveal repeating dimer units, formed of partially overlapped macrocycles on *ca*. 50% of their area, slided with respect to each other across

a central N–Zn–N axis. The distance between the parallel planes defined by the N_4-coordinating atoms of the stacking molecules is 2.996 Å, well within the range of a classical π–π interaction. Thus, promotion of stacking in the solid state upon decrease of the steric hindrance of the fluoroalkylated Pc ligand was achieved, fulfilling one of the proposed goals of this work.

4.3.5 UV-vis Spectroscopy

The deep blue-green colors of the four new trifluoromethylated PcM complexes are reflected in their strong UV-vis electronic absorptions. Chloroform was chosen as a solvent for determination of molar extinction coefficients because of its ability to minimize the extent of aggregation and ensure the highest amount of monomeric species available for verification of Lambert-Beer linearity. Initial 25 μM solutions of each compound were successively diluted down to 2 μM, allowing for collection of at least six data sets. Molar extinctions were determined for each absorption maximum identified in the spectra, as the slope of the linear fit of recorded absorbances vs. total PcM concentration. Lambert-Beer plots for the representative λ_{max} Q band of the four complexes, as well as the corresponding spectra taken in chloroform are presented in Figure 4.21. Calculated log ϵ values for all maxima are shown in Table 4.2.

Table 4.2 UV-vis Absorption Maxima and Associated Molar Extinction Coefficients in Chloroform for Trifluoromethylated PcM Complexes

Compound	**λ_{max} (log ϵ)** (nm (L mol^{-1} cm^{-1}))
$F_{24}H_8PcZn$ **[4-5]**	667 (4.65), 639 (3.82), 604 (3.83), 367 (3.96)
$F_{24}H_8PcCo$ **[4-6]**	660 (4.51), 599 (4.05)
$F_{28}H_4PcZn$ **[4-14]**	676 (5.25), 647 (4.42), 609 (4.44), 378 (4.56)
$F_{28}H_4PcCo$ **[4-15]**	665 (4.56), 602 (3.92), 347 (4.24)

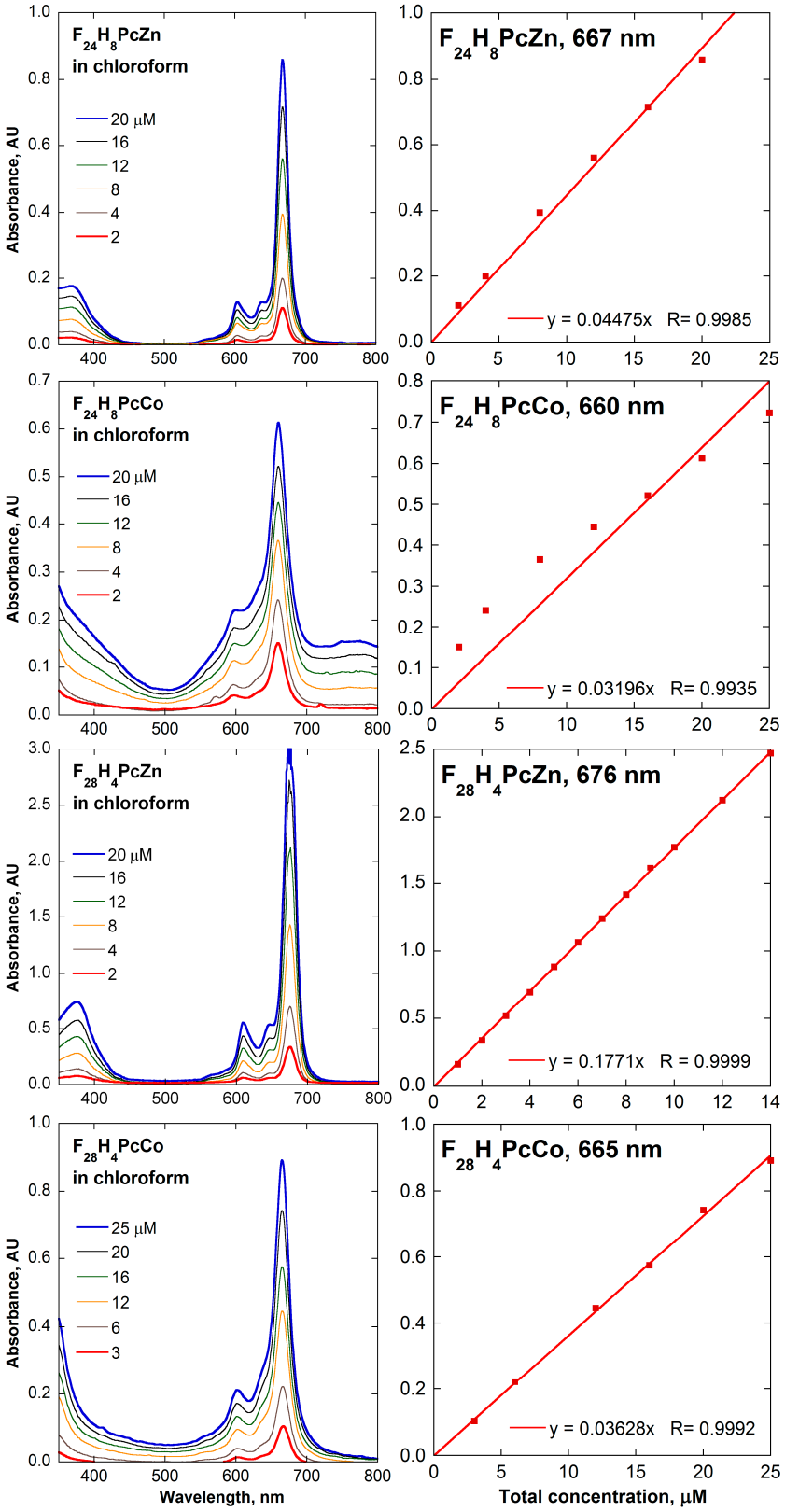

Figure 4.21 UV-vis electronic absorption spectra of $F_{24}H_8PcM$ and $F_{28}H_4PcM$ complexes (M = Zn, Co) in chloroform, showing Lambert-Beer linearity for the Q band absorption maxima. Equations for the linear fits are also provided.

By far, the most intense absorbance of all four complexes is displayed by the Q band of $F_{28}H_4PcZn$, positioned at 676 nm and yielding a molar extinction of 1.77×10^5 L mol^{-1} cm^{-1}. This remarkable electronic transition is among the strongest recorded for phthalocyanine complexes.[47] In contrast, the analogue lacking four Ar-F atoms, $F_{24}H_8PcZn$, only reaches about a quarter of the former's molar absorptivity, in its 667 nm Q band with an ϵ of 4.48×10^4 L mol^{-1} cm^{-1}. The PcCo complexes show a typical broadening of the spectral bands and decrease of the molar extinction with respect to their Zn counterparts, with ϵ values in the range of $3.1 – 3.7 \times 10^4$ L mol^{-1} cm^{-1}. A particular case of deviation from Lambert-Beer linearity is exhibited by $F_{24}H_8PcCo$ (Figure 4.21). This anomaly is ascribed to its extremely low solubility, partial precipitation still ocurring at 25 μM, and the dissapearance upon dilution of small amounts of an unknown, partially charged species producing a broad band at 750 nm.

The propensity of the complexes towards aggregation in solution is expressed through the radically different UV-vis spectra in solvents that promote aggregation extremes, such as chloroform for monomer and ethanol for dimer species. Figure 4.22 presents a series of comparative plots for the electronic absorptions of the four complexes recorded in the two solvents, expanding the 500-800 nm region representative for the dimerization equilibria. It is worth repeating, for clarification of the terms used through the end of this chapter, that aggregation of PcMs at total concentrations (C_T) below 30 μM is greatly limited to the dimer stage as a result of high dilution, a postulate confirmed and reaffirmed by multiple literature reports.[127–130,133] As such, all subsequent discussions and UV-vis studies, performed at C_T values not exceeding the agreed 30 μM limit, assume a monomer–dimer equilibrium.

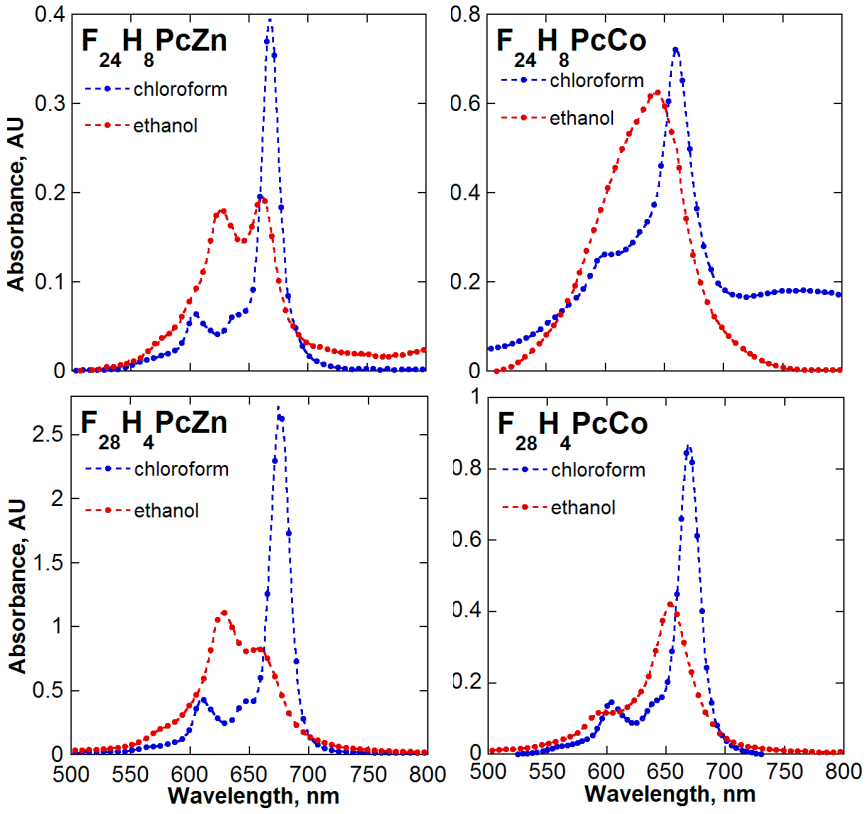

Figure 4.22 UV-vis comparison of aggregation extremes of $F_{24}H_8PcM$ and $F_{28}H_4PcM$ complexes (M = Zn, Co). Spectra are recorded in chloroform (blue, least aggregation) and ethanol (red, most aggregation).

As expected, predominance of the monomer species in chloroform is evidenced by the strong, single Q bands located at 660–675 nm, while occurence of the dimer species is observed in ethanol as strong absorbances at 620–650 nm, coupled with a slight blue-shift and broadening of the monomer's Q band, in accordance with the literature.[47,133] For the Co complexes, the Q transitions of monomer and dimer in ethanol coalesce into a broad, sometimes asymmetric band, as in the case of $F_{24}H_8PcCo$. Other polar solvents (i.e., acetone, acetonitrile, DMSO, EtOAc, AcOH) promote intermediate levels of aggregation, exemplified next for $F_{28}H_4PcZn$. Through the above findings, the solvent-dependent electronic coupling of trifluoromethylated PcMs is proved and documented for the first time, accomplishing an additional goal of this project.

4.3.6 Aggregation Study in Solution for $F_{28}H_4PcZn$

The significantly different aggregation levels exhibited by $F_{28}H_4PcZn$ in acetone, acetonitrile, EtOAc and ethanol, coupled with the great variation of the monomer/dimer ratio on narrow (1–40 μM) concentration ranges, intense molar absorptivities and, last but not least, well-defined and well-spaced (*ca*. 40 nm) dimer and monomer Q bands in all the above solvents, made the complex a promising candidate for a thorough UV-vis aggregation study. Such a study is aimed at determining, for each solvent, the concentration ranges on which a dimerization equilibrium is active, the values of the associated dimerization constants and their correlation with relevant solvent parameters.

Before any calculations can proceed, acquisition of highly accurate data sets for a significant number of concentrations in the solvents of choice is required. Great amounts of time and attention have been given to ensure accuracy and reproducibility of the results, including but not limited to fresh preparation of solutions from oven-dried solid samples of **[4-14]**, repetition of all measurements for confirmation of first-hand results and concentration corrections for solvent evaporation by cross-checking the instantaneous ϵ values with the initially determined ones. The final electronic absorption spectra of **[4-14]** used in all subsequent calculation of dimerization constants are shown in Figure 4.23. Gradually lower concentrations were obtained by volume dilutions of an initial 100 mL solution. Next, a set of assumptions and equations needs to be established for proper manipulation of the recorded UV-vis data, all of which are detailed further.

Given a general monomer–dimer equilibrium:

$$2\,A \rightleftharpoons A_2 \tag{4.1}$$

the dimer formation (dimerization) equilibrium constant is expressed as:

$$K_D = C_d / C_m^2 \quad (4.2)$$

where K_D is the dimerization constant (L mol^{-1} or, simply, M^{-1}) and C_d and C_m are the dimer and monomer concentrations, respectively (M), assuming the activity coefficients to be unity in dilute solutions.[134] Then, the total molar concentration of the complex is:

$$C_T = C_m + 2\ C_d \quad (4.3)$$

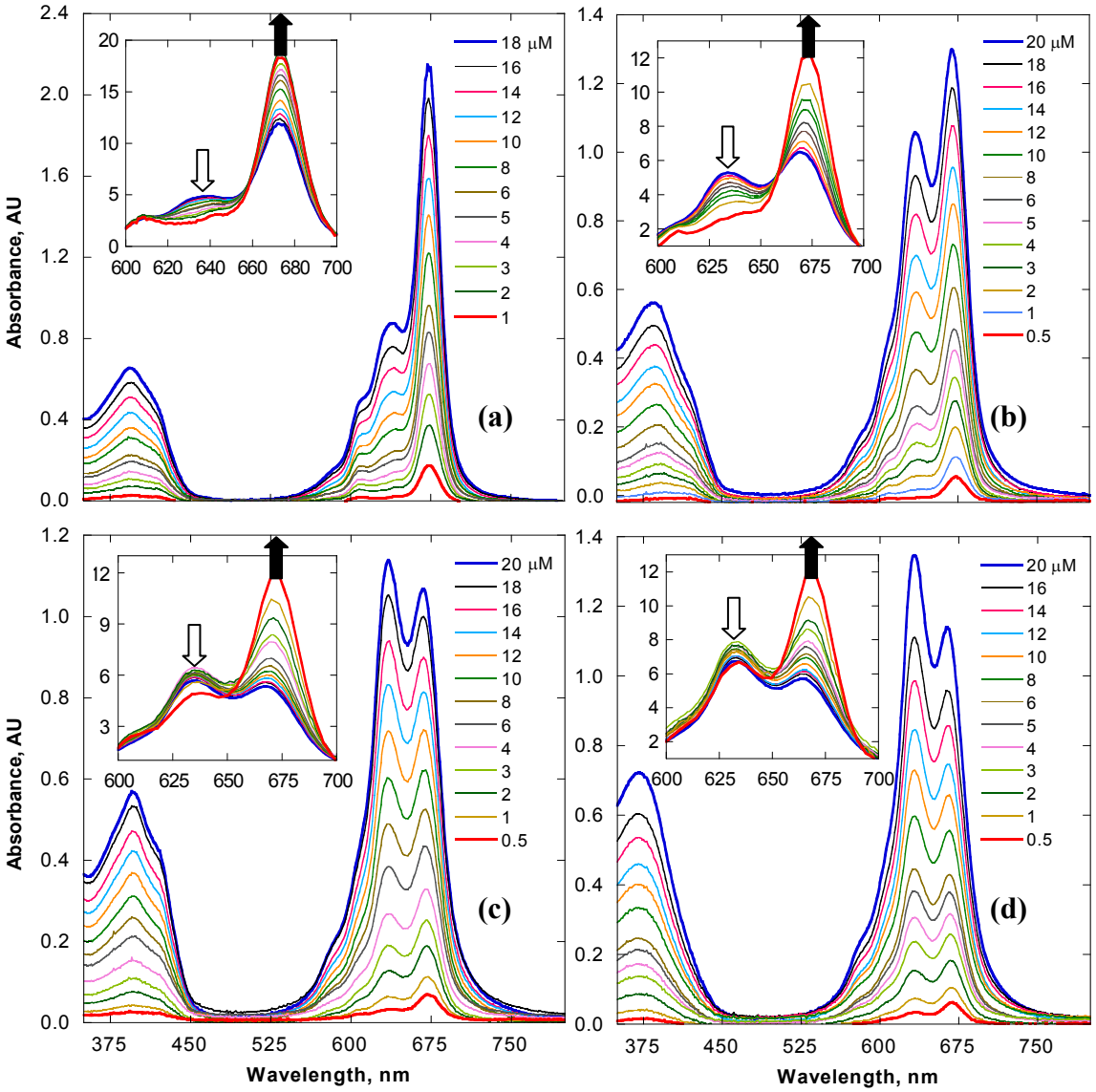

Figure 4.23 Solvent-dependent variable aggregation of $F_{28}H_4PcZn$, recorded at gradually decreasing total concentrations and arranged from (a) lesser to (d) highest extent. (a) EtOAc. (b) Acetone. (c) Acetonitrile. (d) Ethanol. Insets: molar extinction coefficients ($\epsilon \times 10^{-4}$ L mol^{-1} cm^{-1}) vs. λ (nm) in the relevant region for dimerization equilibria, showing the inverse variation of the monomer and dimer amounts.

Moving to the specific case of PcM dimerization, finding K_D requires knowledge of at least the monomer's absorbtion coefficient, ϵ_m, which is solvent-dependent and has to be determined separately in each case. This can be done in two ways: (i) solvent permitting, ϵ_m can be determined from the data set recorded at the lowest detectable total concentration (typically for C_T = 1 μM), only if visual assessment of the spectrum confirms at least a 90% predominance of the monomer; (ii) if the spectrum still shows appreciable amounts of dimer even at highest dilution, ϵ_m is determined at the point of equal absorbances of dimer and monomer Q bands, assuming the monomer concentration at that point to be ½ C_T. Among the four solvents studied, ϵ_m was determined by method (i) for EtOAc and by method (ii) for the other three, viz. acetone, acetonitrile and ethanol. Spectra of $F_{28}H_4PcZn$ in chloroform have shown no noticeable amount of dimer even at the 1 mm cell saturation limit of 400 μM, essentially proving no equilibrium is present and that the complex overwhelmingly exists in the monomer form.

Once ϵ_m for the respective solvent is known, C_m can be determined for a 1 cm cell using the recorded value of its Q band absorbance (A_m) as:

$$C_m = A_m / \epsilon_m \tag{4.4}$$

An additional assumption made is the invariance of ϵ_m over the concentration range studied for a given solvent, consistent with published procedures for calculation of K_D in PcM aggregation equilibria.[135] For the most accurate determination of K_D, finding both ϵ_m and ϵ_d is required, either through deconvolution of spectral bands or use of regression analysis.[134] However, in this specific case, a general simplification has been introduced beforehand, in order to test whether such an ellaborate procedure is needed. Thus, it was asserted, based on the avg. 40 nm spacing of the monomer and dimer Q

bands, that no significant overlap exists between the two, and, consequently, the associated absorbances are independent. Then, C_m can be calculated with eqn. 4.4 and substituted in eqn. 4.3 to find C_d at each value of the total PcM concentration. This overt simplification circumvents extensive calculations of ϵ_d and has produced meaningful results, as shown further in. While the values obtained might present a certain degree of error (say ±10%), the validity of the method was tested by the results themselves.

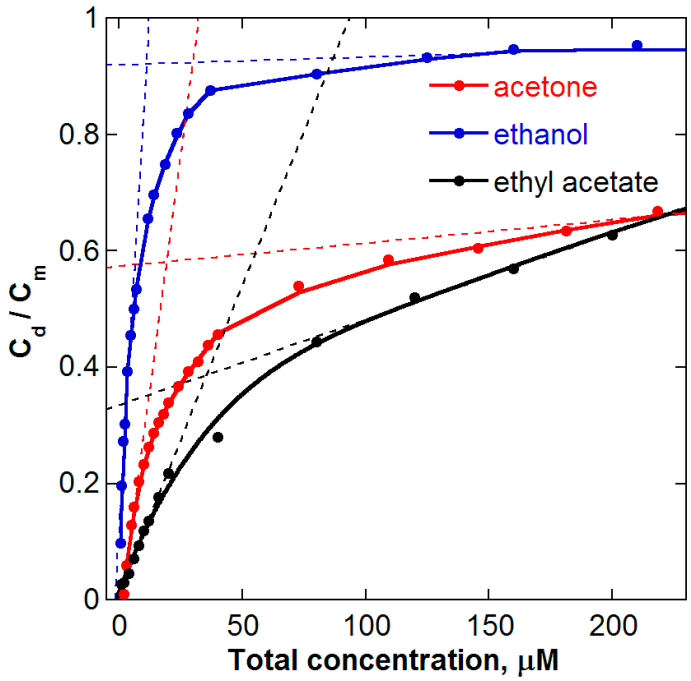

Figure 4.24 Plot of the ratio of determined dimer and monomer concentrations vs. the total PcM concentration in the 0–250 µM range. Intersection of linear fits (dashed lines) of the initial (300–150 µM) and final (1–10 µM) data provides an estimation of the range of concentration-dependent dimerization equilibrium. Data for acetonitrile are omitted for clarity.

Figure 4.24 presents the dependence of the C_d/C_m ratios vs. C_T for selected solvents, using values obtained by applying the procedure and simplifications described above. The plot reveals in all cases two specific linear regions with different slopes, connected by a transition region. The first corresponds to the higher concentrations in the

100–400 μM range, with slopes between 0.33 (EtOAc) and 0.98 (ethanol) and is descriptive for basic dilution effects and breakage of higher order aggregates (oligomers) into dimers and monomer units. The linearity cannot be tested above 400 μM because of instrument saturation. The intermediate region of rapidly decreasing C_d/C_m ratios is located at 50–100 μM and is characteristic for the transition towards a dimerization equilibrium. Below 40 μM, the second linear region can be observed, for which the monomer–dimer equilibrium sets in, obeying the rate law in eqn. 4.2 and proceeding down to the lowest detectable C_T (*ca*. 0.5 μM) or to the point when >95% of the PcM is in monomer form, after which the absorbance of the dimer Q band is hidden under the vibronic satellite of the monomer's and can no longer be detected. At that point, the dimerization equilibrium ends.

Moving on, a direct method exists to prove exclusive formation of dimers to the detriment of higher order aggregates and establish the range of concentrations for which a dimerization equilibrium is active. With respect to eqn. 4.2, taking the logarithms on both sides and subtracting the terms gives the linear dependence:

$$\log C_d = \log K_D + 2 \log C_m \tag{4.5}$$

In other words, if the plot of $\log C_d$ vs. $\log C_m$ within a certain concentration range reveals linearity with the slope of 2, this result is unequivocally indicative of a dimerization equilibrium active in that range and, furthermore, the free term of the linear fit gives the value of $\log K_D$.[134–136] If higher order aggregates were involved, their dissociation into monomer units would give a slope higher than 2. And finally, if higher aggregates were to dissociate into a mix of dimer and monomer species, the fit would not show linearity (unless due to a highly unlikely coincidence).[134]

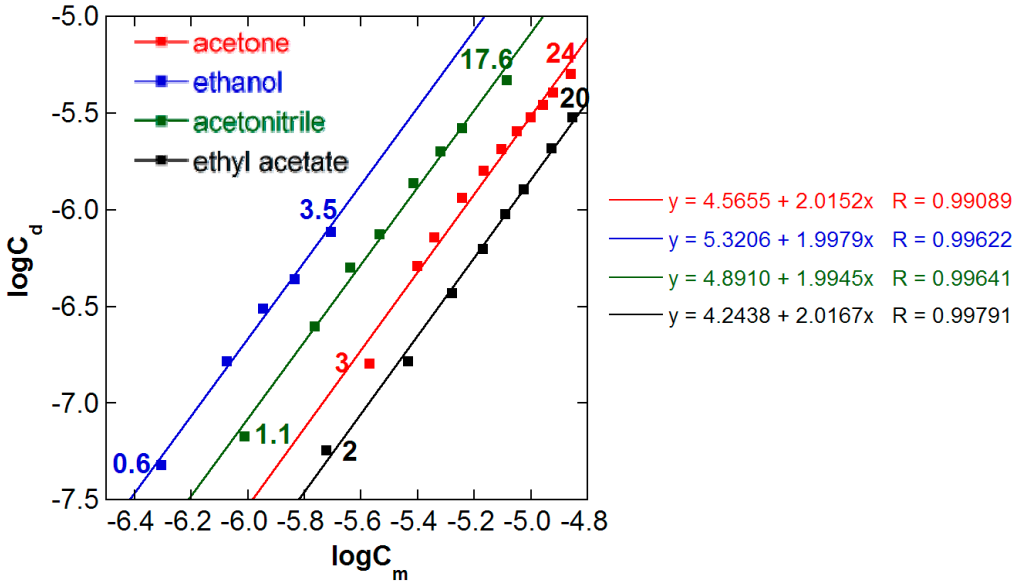

Figure 4.25 Linear fits of $\log C_d$ vs. $\log C_m$ in the range of dimerization equilibria. Numbers indicate the total concentration limits between which the equilibrium applies in each solvent. Right: linear correlations with slope 2.00±0.02, proving exclusive presence of dimeric aggregates at concentrations below 20 µM.

Figure 4.25 presents plots of $\log C_d$ vs. $\log C_m$ for $F_{28}H_4PcZn$ in the four solvents studied. As can be seen from the regression correlations, the linear fits show slopes of 2±0.02, indicative of a dimerization equilibrium within the concentration limits marked in bold figures on the graph. The values of K_D in the four solvents were directly determined from the free term of the linear correlations. One notices that in ethanol, equilibrium is strictly obeyed only for a total concentration below 4 µM, and an important amount of dimer still persists at the UV-vis detection limit of 0.5 µM. For the other solvents, concentration-dependent equilibria proceed at C_T values of 20 µM (ethyl acetate), 24 µM (acetone) and 18 µM (acetonitrile). This clear mathematical proof of dimerization equilibria based on the raw dimer and monomer Q-band absorbance data, uncorrected by deconvolution, validates the simplifications introduced in the beginning of this study; if the degree of band overlap was significant, the processed data of the non-corrected values of C_d would not have produced the linearity observed in Figure 4.25.

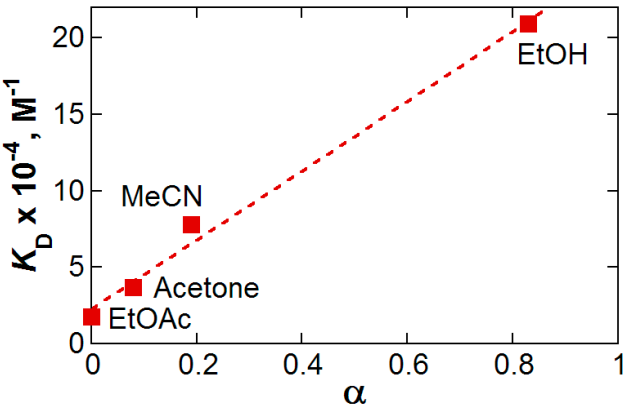

Figure 4.26 Plot of calculated K_D for various solvents ($\times 10^{-4}$ M^{-1}) vs. the Kamlet-Taft α solvatochromic parameter. Linear correlation: y = 2.2807 + 22.736x, R = 0.9957.

The significantly different K_D values obtained for $F_{28}H_4PcZn$ in various solvents prompted for a correlation of the compound's versatile aggregation behavior with specific physical solvent parameters. Even though the solvent's polarity and dielectric constant is believed to play a major role for aggregation in solution, as indicated for other PcM classes studied,[47,128,133] in this case a direct correlation of the former properties with the determined values for K_D could not be established. Instead, a uniform variation was found by taking into account the solvent's hydrogen-bond donor (HBD) ability expressed through the Kamlet-Taft α solvatochromic parameter.[137,138]

The linearity of the K_D vs. α parameter plot (Figure 4.26) reveals the true reason for the variable aggregation of **[4-14]** in the solvents of study. While this correlation might come as a surprise, a closer look at the phenomena involved in solvation of a Pc macrocycle accurately explains it. The solvent's HBD acidity is directly related to its hydrophilicity; solvents with high α values, such as alcohols, are totally miscible with water. Pc macrocycles are inherently hydrophobic as long as they contain peripheral alkyl groups, fluorinated or not; as such, they are more likely to intercalate between their molecular planes hydrophobic solvent molecules, such as chloroform, and much less so

hydrophilic ones. This explains why aggregation is hindered in non-polar, hydrophobic solvents. Hydrophilic solvents, on the other hand, are repelled by the complexes, which prefer to stack in the form of dimers and higher order aggregates, directing solvent molecules on the outside. Higher extents of aggregation should occur with the increase in solvent's hydrophilicity and associated HBD capability, a hypothesis completely validated by the presented spectroscopic data. Results of the aggregation study are summarized in Table 4.3.

Table 4.3 Kamlet-Taft Solvent Parameters, Dimerization Constants and Monomer λ_{max} for $F_{28}H_4PcZn$ in Selected Solvents

Solvent	π^*	α	β	λ_{max} (nm)	$\epsilon_m \times 10^{-5}$ (L mol^{-1} cm^{-1})	$K_D \times 10^{-4}$ (L mol^{-1})
Chloroform	0.58	0[a]	0.1[b]	676	1.770	~0[c]
Acetone	0.71	0.08	0.48	673	1.090	1.753
Acetonitrile	0.75	0.19	0.31[b]	672	1.083	3.677
Ethyl acetate	0.55	0	0.45	672	1.490	7.780
Ethanol	0.54	0.83	0.77[b]	669	1.247	20.922

[a] The α parameter for chloroform is still a subject of debate: recent sources[139] tend to agree with the initial reported value of effectively 0,[137] while at times an uncertain value of 0.44,[138] was reported.
[b] Precise values are still a subject of debate.[137–139]
[c] No detectable amount of dimer was noticed in chloroform in the concentration range allowing UV-vis characterization. In consequence, the dimerization constant is assumed to be practically zero.

4.4 Conclusions

A ten-step synthetic procedure was established for production of the novel fluoro-trifluoroalkyl $F_{28}H_4Pc$ ligand, obtained as its Zn and Co analogues. New representatives of the structurally relevant $F_{24}H_8Pc$ class were also obtained. The new metal-organic complexes and their precursors were fully characterized by NMR, IR, HRMS and, if applicable, UV-vis spectroscopic methods. Solid-state structures of five aromatic intermediates and the target $F_{28}H_4PcZn$ compound were determined by X-ray crystallography.

For the series of fluorinated aromatic intermediates, direct dependence of the overall electronic deficiency with the attached substituents is demonstrated through a linear correlation of the sum of Hammett constants with ^{1}H NMR chemical shifts. A threshold of the molecular electronic deficit's influence on reactivity is attained by the inability to dehydrate 4,5-bis(trifluoromethyl)-3,6-difluorophthalamide to its phthalonitrile.

Promotion of variable aggregation in solution and stacking in the solid state are achieved through a rational design of the ligand's architecture. Preliminary DFT calculations, high resolution ^{19}F NMR spectra and X-ray diffraction studies strongly support the formation of a unitary $F_{28}H_4Pc$ isomeric mixture, explained through a kinetic differentiation of the dinitrile precursor's reactive sites. Electronic π–π coupling interactions in the solid state are revealed for the first time for a trifluoromethylated PcM complex. All crystal structures underscore the paramount importance of hydrogen bonding for the structural integrity and thermal stability of the solids. Aggregation versatility in solution was demonstrated through UV-vis spectroscopic data acquired in appropriate solvents, favoring variable degrees of intermolecular association. Through a quantitative aggregation study, the dimerization equilibrium constants of $F_{28}H_4PcZn$ in acetone, acetonitrile, ethyl acetate and ethanol were determined, as well as the concentration limits within which the former equilibria apply. A direct proportionality between the degree of aggregation and the solvent's hydrogen bond donating ability is established.

Thus, the controlled reduction in peripheral steric hindrance results in fine tuning of molecular aggregation to the solvent of choice, fulfilling the proposed goals of this work. Aggregation variability translates into application versatility, paving the way for surface science and molecular electronics studies.

CHAPTER 5

SYNTHESIS AND CHARACTERIZATION OF THE FIRST ASYMMETRIC PERFLUORINATED PHTHALOCYANINES

5.1 Introduction

Gorun and collaborators created the first class of tridimensional perfluorinated phthalocyanines, bearing eight peripheral isopropyl groups.[104–114] The synthesis of this ligand (Figure 5.1), *abbr.* $F_{64}Pc$, was initiated by the original design of its precursor, perfluoro-4,5-diisopropylphthalonitrile **[5-3]**, through aromatic SN2 of fluorine atoms of tetrafluorophthalonitrile **[5-1]** by CsF-activated perfluoropropene **[5-2]**.[104] Next, $F_{64}PcMs$ were obtained by template tetramerization of **[5-3]** using the appropriate metal salts, under MW or classical conditions, as exemplified below for the Zn **[5-8]** and Co **[5-9]** complexes.[105,106] Similarly, **[5-1]** forms planar hexadecafluorophthalocyanines, *abbr.* $F_{16}Pc$, also shown in Figure 5.1 as the Zn **[5-6]** and Co **[5-7]** analogues.

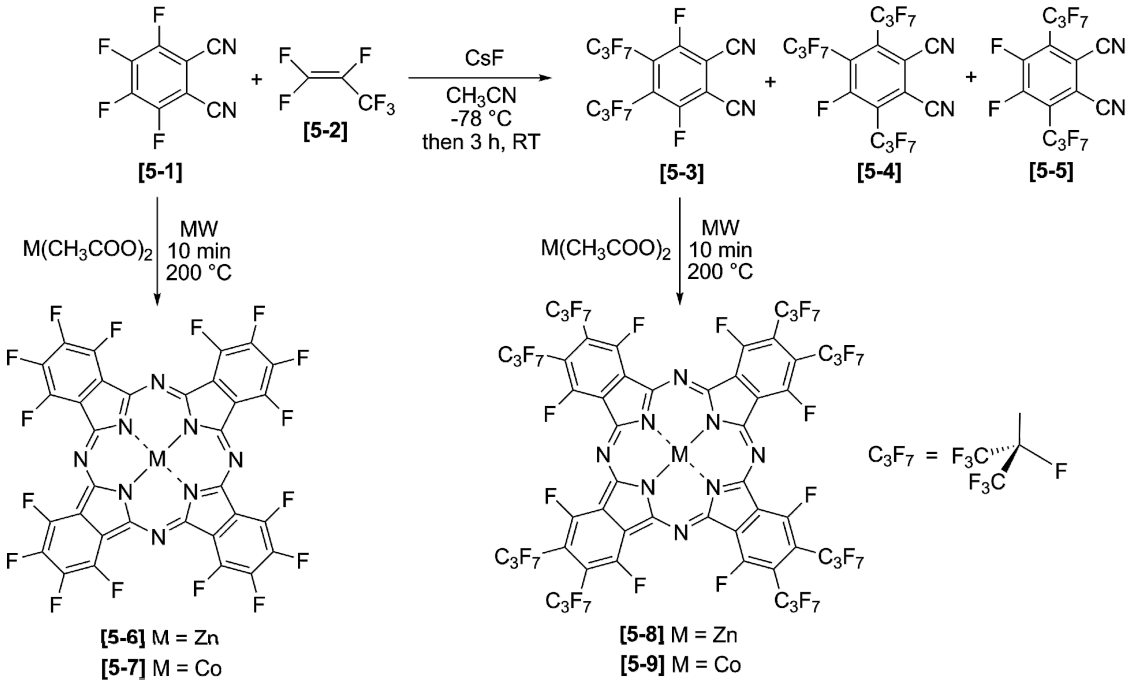

Figure 5.1 Synthetic scheme for production of perfluorinated isopropyl-substituted phthalonitriles and corresponding phthalocyanines $F_{16}PcM$ and $F_{64}PcM$ (M = Zn, Co).

The perfluorinated $F_{16}Pc$ and $F_{64}Pc$ classes hold quite opposite properties in terms of solubility, aggregation in solution and electronic coupling in the solid state. $F_{16}PcMs$ are little soluble in most solvents—although their solubility limit is generally higher than non-fluorinated Pc classes such as common, hydrogen-containing $H_{16}Pcs$—while $F_{64}PcMs$ are among the most soluble phthalocyanines known to date.[105–109] $F_{16}PcMs$ aggregate to such an extent in solution that it took decades until the first X-ray structure of one of their analogues was published;[140] on the other hand, $F_{64}PcMs$ hardly exhibit appreciable aggregation in most common organic solvents.[51] Figure 5.2 illustrates a comparison of the aggregation extremes, reproducing series of UV-vis spectra of **[5-6]** and **[5-8]** in acetone using published data,[51] along with an original example of variable aggregation achieved for the new $F_{28}H_4PcZn$ complex, described earlier in Section 4.3.6. For the solid state, electrical conduction measurements revealed a negligible extent of intermolecular electronic coupling in vapor-deposited thin films of **[5-8]**,[113] while similar studies on planar PcZn complexes of reduced steric bulk, including **[5-6]**, displayed effective conductivities two orders of magnitude higher.[141]

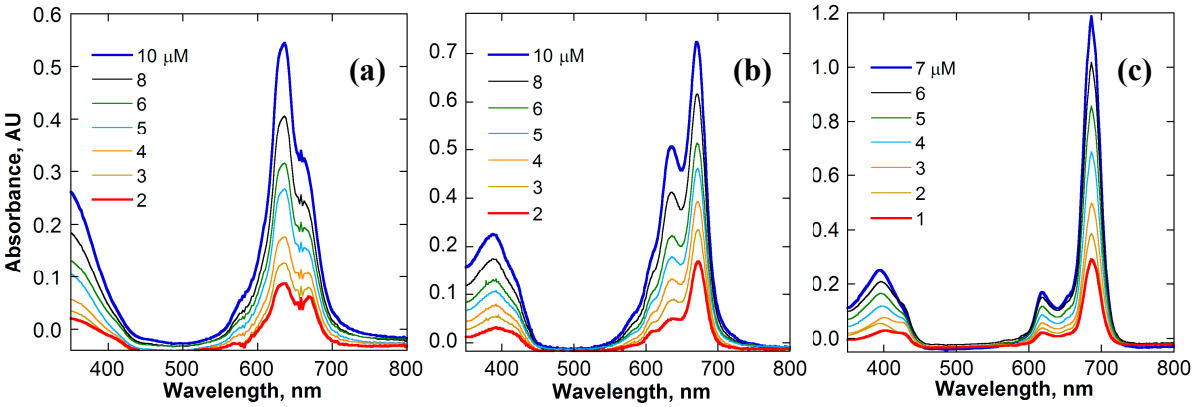

Figure 5.2 UV-vis comparison of concentration-independent aggregation extremes exhibited in acetone solutions by (a) strongly dimerized $F_{16}PcZn$ and (c) monomeric $F_{64}PcZn$, using literature data.[51] (b) Concentration-dependent aggregation of $F_{28}H_4PcZn$ in acetone.

All previous observations considered, steric factors, i.e., the bulkiness of peripheral substituents, turn out to be of crucial importance in promoting or preventing molecular aggregation. Given the indisputable advantages of the F_{64}PcM class over conventional non-fluorinated analogues in terms of stability, photophysical properties and applications,[105–114] novel classes of Pc ligands are desired, which would retain the solubility, structural integrity and remarkable features stemming from the extreme electronic demands of perfluorinated groups, while adding new properties, such as molecular asymmetry, versatile aggregation and solid-state stacking, for use in a variety of envisaged catalytic and electronic applications. These ideas led to the development of two more original classes of PcM complexes. Through a molecular design inspired by creation of the fluoroalkylated $F_{28}H_4$Pc ligand, steric bulk was reduced and, in addition, structural asymmetry was acquired by a different approach, viz. a direct one-pot mix of perfluorinated bulky and planar phthalonitrile precursors represented by perfluoro-3,4,6-trisisopropylphthalonitrile **[5-4]** and tetrafluorophthalonitrile **[5-1]**, respectively. The synthesis and structural formulas of the new asymmetric PcM classes, obtained as their Zn and Co complexes, are detailed in Figure 5.3.

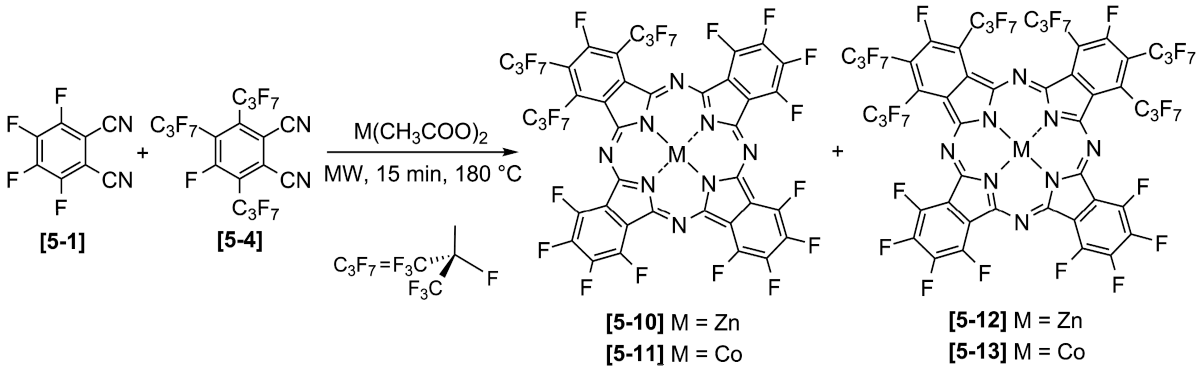

Figure 5.3 Synthetic scheme for production of asymmetric perfluorinated phthalocyanines F_{34}PcM and F_{52}PcM (M = Zn, Co).

A 3:1 combination of **[5-1]** and **[5-4]** units results in formation of metallo-perfluoro-1,2,4-trisisopropylphthalocyanine, *abbr.* F_{34}PcM, while a 2:2 arrangement affords the metallo-perfluoro-1,2,4,8,10,11-hexaisopropylphthalocyanine, *abbr.* F_{52}PcM. F_{16}PcM, formed by tetramerization of **[5-1]**, is always isolated as a side product; later on, it will be shown that its formation cannot be prevented, regardless of the variation of experimental conditions. The stereoselective, head-to-head *cis* configuration of the two units of **[5-4]** in F_{52}PcM was confirmed by TLC, HRMS, NMR and X-ray diffraction (detailed in the following pages), all of which affirmed the existence of a unique isomer.

Before further discussion on the mixed complexes of Figure 5.3, it has to be made clear that repeated attempts to produce singular PcMs by tetramerization of the **[5-4]** and **[5-5]** precursors on their own, did not yield any of the desired products, not even in trace amounts. In all cases, irrespective of the nature of the solvent or absence thereof, reaction time and temperature, choice of metal and precursor/metal molar ratio, reaction mixtures afforded brown-black residues indicative of the organic dinitrile's thermal degradation. This comes to show that the tremendous molecular steric strain induced in a hypothetic Pc containing eight axial *i*-C_3F_7 groups disallows formation of the macrocycle. Furthermore, trials for producing mixed PcM analogues by the one-pot assortment of **[5-1]** and **[5-5]** resulted, when zinc(II) acetate was used as the metal supplier, in exclusive formation of planar F_{16}PcZn, the **[5-5]** precursor being only partially recovered owing to decomposition; variations of the **[5-1]**/**[5-5]** molar ratio from 1:3 to 3:1 and the reaction temperature in the 160–210 °C range made no difference. This outcome is particularly puzzling, given that the bulkier **[5-4]** precursor easily templates with units of **[5-1]** according to the scheme of Figure 5.3. Additional investigations on this matter, both experimental and computational, could form the subject of a future study.

The reasons for choosing **[5-4]** in the design of the new complexes are straightforward. Firstly, although it was obtained and structurally characterized more than ten years ago,[104] its incorporation in a Pc scaffold has never been attempted, all research efforts being focused on its symmetric by-product **[5-3]**. Secondly, it is the only one of the three simultaneously produced *i*-C_3F_7-substituted phthalonitriles of Figure 5.1 that could confer structural asymmetry and molecular chirality to a Pc ligand. And thirdly, it is the most electron deficient and sterically strained precursor of the three, containing no less than three bulky *i*-C_3F_7 groups. All these features combined may lead to both predicted and unexpected properties, as shown herein.

Finally, a mention is due with regard to the synthesis of mixed F–*i*-C_3F_7 PcM analogues by the one-pot combination of the symmetric **[5-1]** and **[5-3]** precursors. In a parallel project initiated in the same laboratory, synthesis and isolation of the Zn and Co representatives of metallo-perfluoro-2,3,9,10-tetraisopropylphthalocyanine, *abbr.* F_{40}PcM, and metallo-perfluoro-2,3,9,10,16,17-hexaisopropylphthalocyanine, *abbr.* F_{52A}PcM, were achieved according to the scheme of Figure 5.4. The preliminary findings of this study* are the scope of a separate doctoral research and will be presented in full elsewhere.

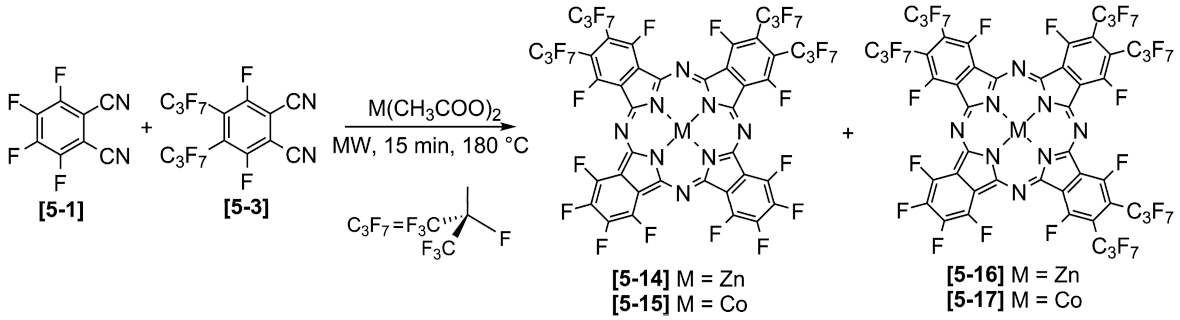

Figure 5.4 Synthetic scheme for production of mixed perfluorinated phthalocyanines F_{40}PcM and F_{52A}PcM (M = Zn, Co).

* Patel, H. H. New Jersey Institute of Technology, Newark, NJ. Personal communication, 2011.

For the sake of the present argument and additional comments in the following chapters, it suffices to say that the compositional identity of complexes **[5-14]** to **[5-17]** of Figure 5.4 was confirmed by TLC, HRMS, IR, NMR and X-ray diffraction.

The new $F_{34}Pc$ and $F_{52}Pc$ ligands obtained in this work represent the first structurally characterized classes of asymmetric perfluorinated phthalocyanines. The current chapter describes experimental procedures and complete structural and spectroscopic characterization in solution and solid-state of their Zn and Co complexes, with an emphasis on the variable aggregation in solution and X-ray determined π–π stacking interactions. Catalytic capabilities of the new compounds **[5-10]** to **[5-13]** are investigated in Chapters 6 and 7.

5.1.1 Redox Properties of Metallophthalocyanines

While spectral properties of phthalocyanines were the attraction for much of the early work done on these complexes, the diversity of species formed during oxidation and reduction of PcM complexes has led in the past decades to the development of an active field of research. Electron transfer reactions involving the Pc ring, either through charged or radical species, have made the object of in-depth studies.[142] Their demonstrated electronic coupling and photochemical excitation properties have seen PcMs being used as photosensitizers for cancer PDT,[143] one-dimensional metal[144] and semiconductor[145] applications and the development of color displays.[146]

In transition metal PcMs, both metal- and ring-oxidation/reduction can occur; the prevailing process depends on the relative order of reduction potentials, solvent and axially metal-coordinated ligands.[47] In its neutral state, the phthalocyanine ring is a dianion, Pc(−2). Ring oxidation leads to cation radical complexes, Pc(−1), and can be

achieved chemically with such agents as Br_2 and HNO_3, electrochemically in UV-transparent solvents as DMF and CH_2Cl_2, and photochemically in the presence of an appropriate electron acceptor.[142] Thin films of PcMs can also be oxidized and reduced.[146] Ring reduction results in negatively charged species, such as Pc(−3), and can also be performed chemically with sodium mirrors in THF, photochemically and electro-chemically using a mercury pool electrode in DMF.[47]

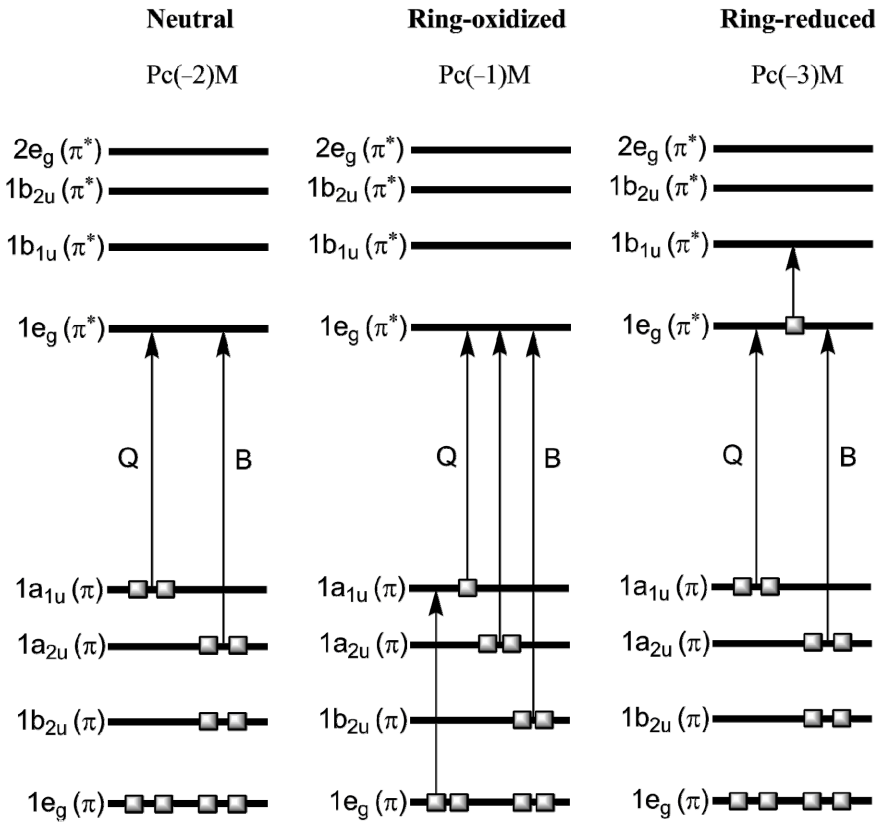

Figure 5.5 Energy levels of molecular orbitals involved in the major electronic transitions for neutral, ring-oxidized and ring-reduced PcMs.[123,147,148]

Spectral signatures of ring-oxidized and ring-reduced species are obvious in a 50 to 200 nm red-shift and a major decrease in the absorbance of the Q band due to changes in the electronic populations and energy levels of the frontier orbitals. In the same time, additional bands appear in the 400 to 550 nm region and the intensity of the B band at

300–350 nm is greatly enhanced as a result of electronic transitions from the deeper occupied levels.[47,142] Calculations of MO energy levels (Figure 5.5) have been carried out by Ohno et al.[147] and Orti et al.[148] based on the ubiquitous model proposed by Gouterman.[123]

Redox properties of PcM complexes effectively model the heme group of the cytochrome P450 class of enzymes, responsible for the oxidation of a variety of hydrocarbons in nature.[149] The overall catalytic cycle,[47,150] shown in Figure 5.6, involves the two-electron oxidation of the ferric heme group, resulting in both metal and ring oxidized species of the type $[Fe(IV)–heme(-1)]^{\bullet 2+}$.

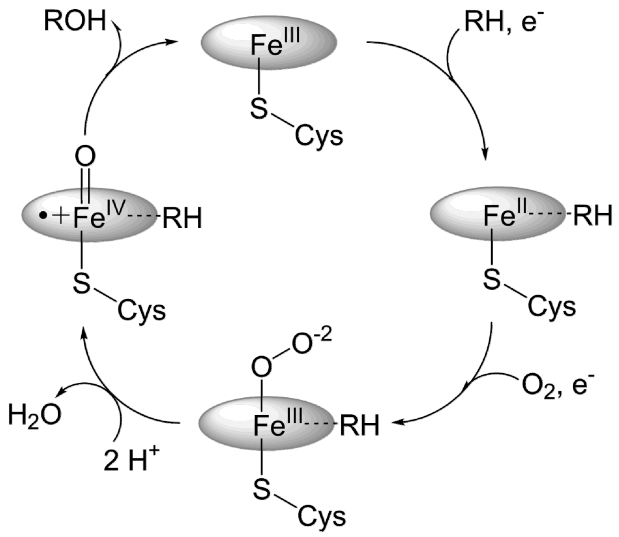

Figure 5.6 Cycle of cytochrome P450-catalyzed aerobic oxidations.[150]

5.2 Experimental Section

5.2.1 General Experimental

Tetrafluorophthalonitrile **[5-1]** and hexafluoropropene **[5-2]** were purchased from commercial sources. Perfluoro-3,4,6-trisisopropylphthalonitrile **[5-4]** was obtained and purified according to a published literature procedure.[104]

5.2.2 Synthesis and Characterization of F_{34}PcZn and F_{52}PcZn

Twenty glass reaction vessels (10 mL total volume) were each charged with 0.4 g (0.62 mmol) **[5-4]**, 0.04 g (0.2 mmol) **[5-1]**, 0.04 g (0.22 mmol) zinc(II) acetate dihydrate, 1 mL nitrobenzene and magnetic stirrers, then sealed with Teflon caps and heated with stirring under MW radiation at 180 °C for 15 min. After cooling, the crude solid of each vial was extracted with *ca*. 50 mL EtOAc, the organic fractions were combined, concentrated *in vacuo* and adsorbed to silica gel (70–230 mesh). Gel filtration using an acetone/hexane 2:98 mixture (v/v) allowed for the complete removal of nitrobenzene, unreacted **[5-4]** and most yellow impurities. Then, the blue-green solid was collected and subjected to gradient elution column chromatography. The rest of yellow impurities were removed with an acetone/hexane 2:98 mixture, followed by the separation of green F_{52}PcZn, eluted with a 10:90 mixture, royal blue F_{34}PcZn at 20:80 polarity, and finally dark blue F_{16}PcZn as a side product using a 40:60 mixture (v/v). The three colored fractions were evaporated and repurified by gel filtration on short columns, using eluent mixtures of the same compositions as for their initial separation. Solvent removal followed by oven drying allowed for isolation of **[5-12]** in 13% yield (0.42 g), **[5-10]** in 16% yield (0.26 g) and **[5-6]** in 14% yield (0.1 g), all based on starting material **[5-1]**.

F_{34}PcZn **[5-10]**: Mp > 300 °C; UV-vis ($CHCl_3$): λ_{max} (log ϵ) 689 (5.09), 672 (4.99), 632 (4.44), 614 (4.41), 365 (4.69) nm (L mol^{-1} cm^{-1}); IR (KBr): 1522, 1489, 1383, 1282, 1236, 1133, 964 cm^{-1}; ^{19}F NMR (282 MHz, $(CD_3)_2CO$): δ −69.05 (6F, br, C*F*$_3$), −72.25 (12F, s, C*F*$_3$), −97.12 (1F, s, Ar-*F*), −131.4 (1F, s, C*F*), −135.09 (1F, d, Ar-*F*), −139.18 to −141.66 (5F, m, Ar-*F*), −149.92 to −151.6 (6F, m, Ar-*F*), −161.39 (1F, d, C*F*), −165.99 to −170.18 (1F, m, C*F*); HRMS (APCI+): calcd for $[M + H]^+$ $(C_{41}HF_{34}N_8Zn)^+$ 1314.9067, found 1314.9080.

F_{52}PcZn **[5-12]**: Mp > 300 °C; UV-vis ($CHCl_3$): λ_{max} (log ϵ) 701 (5.10), 674 (4.97), 640 (4.62), 615 (4.44), 372 (4.78) nm (L mol^{-1} cm^{-1}); IR (KBr): 1523, 1489, 1375, 1287, 1236, 1166, 1127, 1050, 966, 939, 737 cm^{-1}; ^{19}F NMR (282 MHz, $(CD_3)_2CO$): δ −63.23 (3F, br, C*F*$_3$), −68.52 (3F, br, C*F*$_3$), −70.69 to −76.31 (30F, m, C*F*$_3$), −97.56 (2F, br, Ar-*F*), −130.85 (1F, d, C*F*), −137.91 to −141.55 (5F, m, Ar-*F*), −151.23 to −152.76 (4F, m, Ar-*F*), −161.49 (1F, d, C*F*), −166.47 to −170.15 (3F, m, C*F*); HRMS (APCI+): calcd for $[M + H]^+$ $(C_{50}HF_{52}N_8Zn)^+$ 1764.8780, found 1764.8804.

5.2.3 Synthesis and Characterization of F_{34}PcCo and F_{52}PcCo

Compounds **[5-11]** and **[5-13]** were prepared in a similar manner to **[5-10]** and **[5-12]**, using sixteen glass reaction vessels, each charged with 0.3 g (0.47 mmol) **[5-4]**, 0.05 g (0.25 mmol) **[5-1]** and 0.045 g (0.18 mmol) cobalt(II) acetate tetrahydrate; the MW heating was performed for 12 min at 185 °C. Initial purification of the crude solid by gel filtration was done with a toluene/hexane 1:9 mixture (v/v); the remaining work-up of the mixture was carried out as described for compounds **[5-10]** and **[5-12]** in Section 5.2.2. Evaporation of the eluted fractions and drying to constant weight allowed for isolation of green **[5-13]** in 1.5% yield (0.05 g), dark blue **[5-11]** in 11% yield (0.19 g) and **[5-7]** as a side product in 10% yield (0.084 g), based on starting material **[5-1]**. Following the purifications, 4.5 g of unreacted **[5-4]** were recovered (*ca.* 90% of initial).

F_{34}PcCo **[5-11]**: Mp > 300 °C; UV-vis ($CHCl_3$): λ_{max} (log ϵ) 680 (4.52), 667 (4.50), 611 (4.03) nm (L mol^{-1} cm^{-1}); ^{19}F NMR (282 MHz, $(CD_3)_2CO$): δ −63.58 (3F, br, C*F*$_3$), −67.36 (3F, s, C*F*$_3$), −68.75 to −76.79 (12F, m, C*F*$_3$), −100.98 (1F, br, Ar-*F*), −132.36 (1F, s, C*F*), −137.64 (1F, d, Ar-*F*), −139.44 to −142.63 (5F, m, Ar-*F*), −155.92 to −157.62 (6F, m, Ar-*F*), −165.55 (1F, d, C*F*), −169.46 (1F, br, C*F*); HRMS (APCI−): calcd for $[M]^-$ $(C_{41}F_{34}N_8Co)^-$ 1308.9040, found 1308.9032.

F_{52}PcCo **[5-13]**: Mp > 300 °C; UV-vis ($CHCl_3$): λ_{max} (log ϵ) 686 (4.62), 615 (4.18), 334 (4.58) nm (L mol^{-1} cm^{-1}); ^{19}F NMR (282 MHz, $(CD_3)_2CO$): δ −63.62 (3F, br, C*F*$_3$), −67.01 to −76.28 (33F, m, C*F*$_3$), −90.0 to −110.0 (2F, br, Ar-*F*), −137.5 to −147.5 (6F, m, Ar-*F*), −155.0 to −159.5 (4F, br, Ar-*F*), −165.82 (1F, m, C*F*), −169.76 to −171.73 (3F, m, C*F*); HRMS (APCI−): calcd for $[M]^-$ $(C_{50}F_{52}N_8Co)^-$ 1758.8753, found 1758.8763.

5.3 Results and Discussion

5.3.1 Synthesis

The perfluorinated F_{34}PcM and F_{52}PcM complexes are obtained as co-products during the mixed, one-pot template tetramerization of the **[5-1]** and **[5-4]** phthalonitrile precursors. The synthesis was exclusively performed under MW radiation in proprietary 10 mL glass reaction vessels, with the heating time set at 15 min in all cases. Highest yields of the two desired products, along with a markdown of the precursors' thermal degradation residues and of the F_{16}PcM by-product, were attained through an extensive, gradual optimization of the reaction parameters on the Zn analogues. First of all, addition of solvent greatly reduced the extent of precursor degradation—evident in the absence of black ash in the reaction vessel—and almost doubled the overall conversion into Pc products (judged by comparison of the final yields obtained), as opposed to a solid melt procedure. Second, nitrobenzene was the solvent of choice from a list which also contained DMF, NMP and pentanol, for the same reason of maximized yields. Next, the optimal ratio between the two precursors was investigated. If one employs the stoichiometric **[5-1]**/**[5-4]** ratio of 3:1 required for formation of F_{34}PcM, then F_{16}PcM is obtained as the major product, to the detriment of the desired F_{34} compound, afforded in only trace amounts. Therefore, the **[5-1]**/**[5-4]** starting ratio was inverted to a 1:3 excess of the

bulky, *i*-C_3F_7-containing phthalonitrile, resulting in an almost complete conversion of the now-limiting reagent **[5-1]**. Molar ratios of **[5-4]**/**[5-1]** higher than 3 (e.g., when a 6× excess was tried) do not favorably advance the course of the reaction; even though the F_{16}PcM by-product now only forms in traces, an excessive amount of untransformed **[5-4]** is subjected to decomposition and other side reactions with formation of unidentified brown residues, limiting its recovery and further use. Therefore, 1:2 to 1:3 molar ratios of **[5-1]**/**[5-4]** are optimal and were employed for all subsequent syntheses. Finally, a temperature survey was performed in 10 °C increments over the 140–200 °C range, keeping a 1:3 precursor ratio and $Zn(OAc)_2$ as the metal supplier. TLC plates of the reaction mixtures have shown that temperatures of 150 °C and below are too low for initiation of the tetramerization, no Pc products being formed. A 160 °C temperature produced the least amount of brown impurities and precursor degradation, but only affords traces of F_{52}PcZn with a high selectivity for F_{34}PcZn over F_{16}PcZn (13.4% vs. 6.6% yield, respectively). High temperatures of 190–200 °C are undesirable, owing to formation of F_{16}PcZn in excess of 30% yield, the F_{34}PcZn and F_{52}PcZn products not exceeding 10%. An intermediate temperature of 175–180 °C is the most appropriate, affording 13/16/14% yields of the F_{52}/F_{34}/F_{16}PcZn complexes; furthermore, at this temperature, most of the **[5-4]** excess (80 to 90%) can be recovered intact by simple gel filtration of the crude solid, with minimal thermal and side-reactions degradation, and then further re-used in a new synthetic cycle. Generally, isolated yields for the Co analogues **[5-11]** and **[5-13]** were much lower, mainly due to difficulties encountered during chromatographic separations, related to very similar retention factors and lower solubilities.

An interesting case of product stereoselectivity is encountered in the "head-to-head" adjacent positioning of the two bulky, **[5-4]**-derived units in the molecular structure of F_{52}PcM (Figure 5.3). The exclusivity of this "*cis*" arrangement (with respect to the N–M–N axis bisecting the 4- and 8-*i*-C_3F_7 groups) and the definite absence of the "*trans*" regioisomer were confirmed by multiple independent pieces of evidence, ranging from TLC, NMR and UV-vis to HRMS, HPLC and the ultimately revealing X-ray structure (to be presented in Section 5.3.4). A degree of stereoselectivity so high asks for theoretical investigations, both qualitative and quantitative, of the mechanism and factors responsible for leading the reaction on such a unique course.

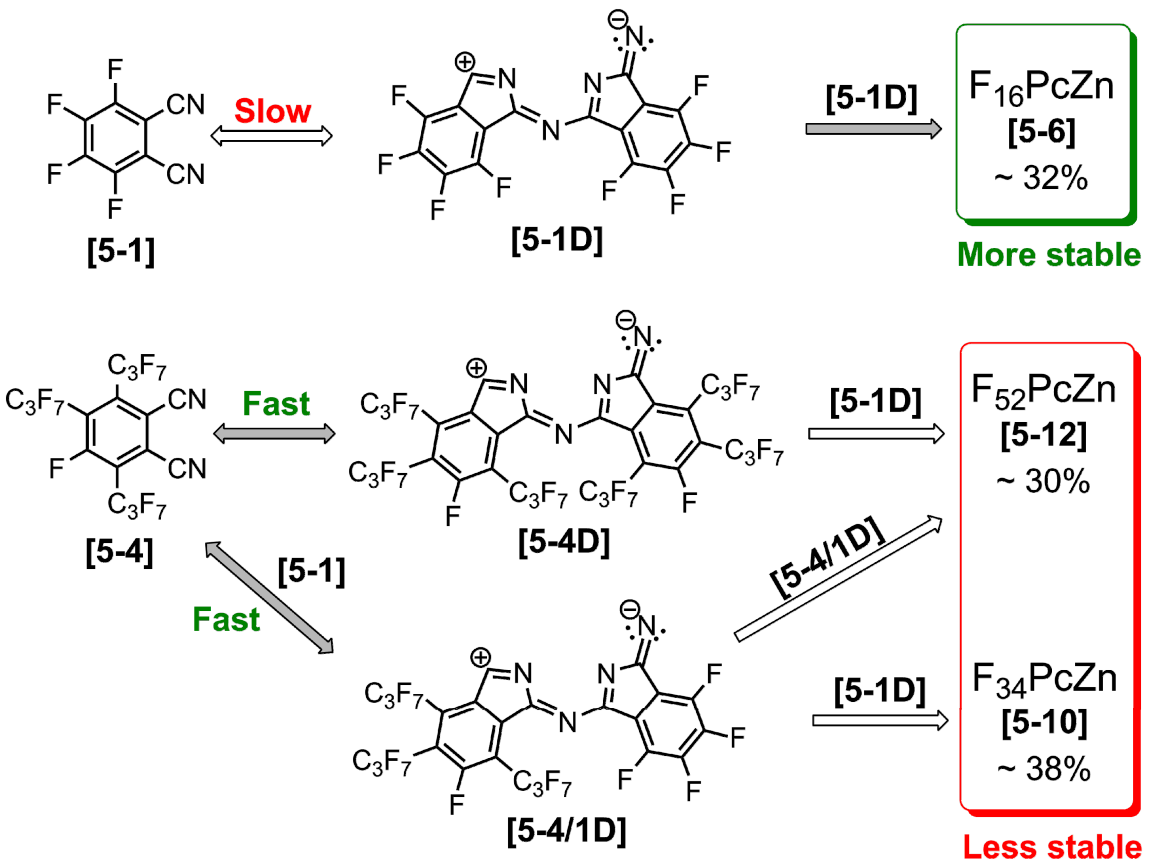

Figure 5.7 Proposed general mechanism for the formation of F_{16}PcZn, F_{34}PcZn and F_{52}PcZn co-products by the mixed one-pot template tetramerization of perfluorinated **[5-1]** and **[5-4]** phthalonitrile precursors. Relative amounts of each product in the final mixture are indicated.

Figure 5.7 proposes a general mechanism for the simultaneous formation of F_{16}PcM, F_{34}PcM and F_{52}PcM by co-tetramerization of the two precursors, indicating the relative amounts obtained in the final mixture of the three Zn complexes. The determined yields and all experimental observations concerning the increase in the F_{16}PcM amount with temperature, are best explained through a kinetically controlled first mechanistic step, yielding dimeric zwitterionic intermediates through intermolecular nucleophilic attacks of activated precursor species, of a similar type with the ones described in Figure 4.9 for the **[4-13]** phthalonitrile analogue. Since **[5-1]** is a symmetric molecule, intramolecular activation results in a single structure, bearing no preference to the electrophilicity of carbon atoms in the nitrile groups; further intermolecular attacks between molecules of **[5-1]** also lead to a unique dimer, termed **[5-1D]** in Figure 5.7. The situation is more complex regarding the thermal activation of the **[5-4]** precursor. Clearly, the 1-*C*N carbon of **[5-4]** is the electron-poorer of the two nitrile groups, with $-I$ effects induced by both *o*- and *p*-*i*-C_3F_7 substituents, as opposed to only one such effect on the 2-CN moiety. As a result, the preference for intramolecular activation is strongly shifted towards an attack on the 1-*C*N atom, further leading through a similar reasoning to formation of the **[5-4D]** dimer in Figure 5.7; actually, **[5-4D]** appears to form exclusively, since its exact configuration was determined in the X-ray structure of the final F_{52}PcZn complex. The significant difference in electron densities between the nitrile groups of **[5-1]** and **[5-4]** leads to a differentiation of their intermolecular attack rates, with activated units of **[5-1]** reacting slower than **[5-4]** analogues. The driving force of the dimerization process is directly related to the charge difference between the attacking, activated nitrogen and the electron-deficient carbon of a susceptible precursor

molecule. Under these conditions, activated **[5-4]** would also react faster with ground state **[5-1]** than an equivalent **[5-1]** unit, forming the **[5-4/1D]** structure of Figure 5.7. Finally, under the templating effect of the M^{2+} ions present in the mix, the dimeric intermediates might either electronically couple or stepwise attach two additional monomer units to form the PcM complexes; coupling is obviously the fastest option, but that does not necessarily exclude the other. In this manner, two **[5-1D]** dimers merge into the F_{16}PcM structure, one of each **[5-1D]** and **[5-4D]** afford the F_{52}PcM complex and, finally, **[5-4/1D]** and **[5-1D]** join up into the F_{34}PcM product. Note that two units of **[5-4/1D]** could not couple directly to form F_{52}PcM, but only after a rather unlikely internal charge redistribution of one of the units; an initial, unaltered combination would lead to a *trans*-F_{52}Pc structure, the likes of which were not confirmed experimentally.

On the other hand, thermodynamic driving forces govern the second half of the reaction. Formation of the planar F_{16}PcM is thermodynamically favored, given that gradual addition of bulky groups in F_{34} and F_{52}PcM results in a significant increase of molecular steric strain and associated enthalpies of formation, manifested through severe distortions of the core macrocycle, as evidenced by the X-ray structures (Section 5.3.4). At 200 °C, the rate of the slower dimerization of **[5-1]** greatly increases, with formation of much larger amounts of **[5-1D]** which then follow the thermodynamically driven coupling to F_{16}PcM, obtained then in a *ca.* 60% quota of the final product mixture.

All the mechanistic considerations discussed herein are of a purely qualitative nature, pending confirmation through DFT calculations of atomic charges and formation energies, carried in collaboration with the group of Prof. Kelty at Seton Hall University. Nevertheless, their validity is fully supported by all previous and later experimental data.

One last experimental observation warranting a detailed look is the multi-component mixture of an initial batch of F_{52}PcZn **[5-12]**. TLC of this batch, isolated through column chromatography on silica gel, detected the presence of two closely-spaced green products, unsuitable for further separation by the above method. Initially, it was thought that the two spots correspond to *cis* and *trans* regioisomers of **[5-12]**, and the mixture was analyzed and separated by analytical HPLC using 100% methanol as eluent, in an HP 1100 series instrument with UV detection at 354 nm.

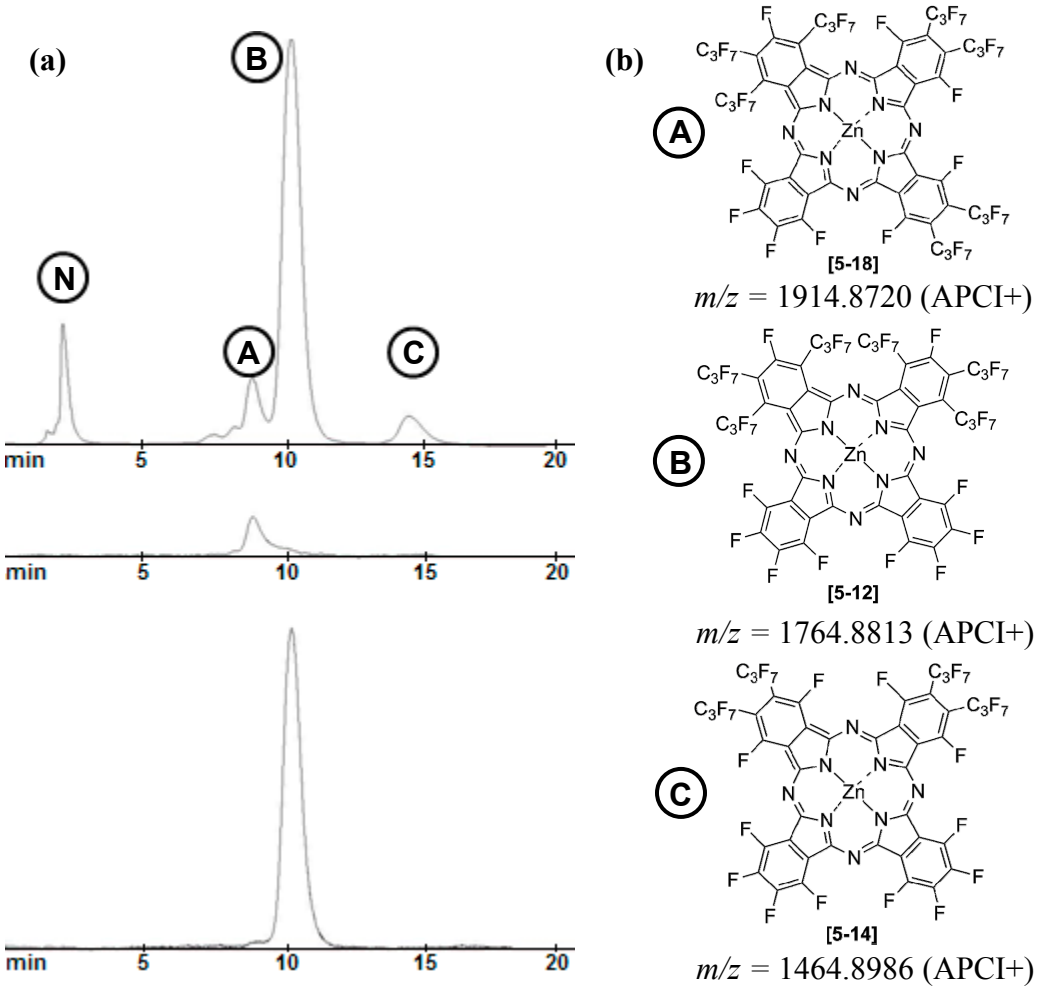

Figure 5.8 (a) Chromatograms of a raw batch of F_{52}PcZn as well as HPLC-separated component fractions. (b) Assigned structural formulas of the separated components, indicating the found *m/z* ratios of the molecular ions via APCI+. A = F_{58}PcZn, B = F_{52}PcZn, C = F_{40}PcZn, N = nitrobenzene.

Twenty injections of 50 μL each of a solution of 5 mg raw **[5-12]** in 10 mL methanol were dropwise collected into separated fractions up to 17 min total elution time, then re-analyzed and joined into unitary compound fractions, the results of the separation being shown in Figure 5.8. An initial peak was identified as residual nitrobenzene and discarded, while the structures of the three isolated components, in 0.1 mg amounts, were elucidated by HRMS using the APCI+ technique. Thus, the formerly-assumed *trans* isomer of F_{52}PcZn, fraction **A**, turned out to be a Pc side-product with 58 fluorine atoms (structure **[5-18]** in Figure 5.8) accounting for *ca.* 10% of the mixture; **[5-18]** is only obtainable by a parallel reaction involving small amounts of **[5-3]** impurifying the starting material **[5-4]**; the **[5-3]** contaminant is also responsible for the detection of F_{40}PcZn in ~5% amount, fraction **C** in Figure 5.8. Indeed, a TLC of the initially used crop of **[5-4]** confirmed the presence of **[5-3]**, owing to an incomplete chromatographic separation. The remaining 85% of the mixture, fraction **B**, is composed of pure *cis*-F_{52}PcZn, as the later-obtained crystal structure has shown. The important find of this apparently side-tracked analysis is the confirmation that a ternary mix of the **[5-1]**, **[5-3]** and **[5-4]** dinitriles does indeed produce a new asymmetric F_{58}PcM complex containing three different precursor units, in addition to the various binary combinations. Although the complexity of such a mixture considerably hinders a facile separation, further investigations of this synthetic pathway in future work should be considered.

5.3.2 IR Spectroscopy

FT-IR spectra of the F_{34}PcZn **[5-10]** and F_{52}PcZn **[5-12]** complexes (Figures B.18 and B.19, respectively) show identical features. The loss of symmetry of the Pc ligand translates into a split and overlap of ν(C–F) stretching vibrations of the CF_3 and Ar-F

groups, which remain the strongest bands in the spectrum. As such, four absorptions are recorded between 1100 and 1300 cm^{-1}, three of which, corresponding to antisymmetric and symmetric *ν*(C–F) vibrations, merge into the strongest band of the spectrum, located in both complexes at 1236 cm^{-1}. The fourth *ν*(C–F) band, of medium-strong intensity, appears at 1133 and 1127 cm^{-1} in **[5-10]** and **[5-12]**, respectively, and is attributed to the in-plane stretching vibrations of aromatic fluorine atoms. The multiple, conjugated *ν*(C=C) and *ν*(C=N) stretching modes of the Pc macrocycle are identified as medium to strong bands in the 1450–1650 cm^{-1} range.

5.3.3 NMR Spectroscopy

Since the four new PcM complexes described herein lack protons of any type, acquisition of ^{1}H NMR spectra for their characterization becomes irrelevant. Their solubility in organic deuterated solvents, although much improved over non-fluorinated analogues, still remains too low to allow for well-resolved ^{13}C spectra. The structural identity of compounds **[5-10]**–**[5-13]** was confirmed instead by ^{19}F data acquired in $(CD_3)_2CO$, shown in Figures A.66 to A.69. The resonances are broadened by partial exchange of the solvent molecules coordinated to the metal center, similar to the case detailed for $F_{28}H_4PcZn$ in Section 4.3.3, an electronic demand manifested by the acute Lewis acidity imparted on the metal by the perfluorinated ligand.

Chemical non-equivalence of the CF_3 groups contained in the *i*-C_3F_7 moieties, as a result of molecular asymmetry, is obvious in the irregular shapes and undefined multiplicities of the sets of resonances observed in each case between −60 and −80 ppm. The lone Ar-F atoms surrounded by *i*-C_3F_7 groups appear as broad singlets at *ca.* −97 ppm, with a precise integrated ratio of 1:18 to the CF_3 resonances. The Ar-F atoms of the

tetrafluorophthalonitrile fragments show as sets of sharp multiplets (for the Zn complexes) or broad doublets (for the Co ones), positioned in the −135 to −155 ppm range. Their combined integration amounts in each case to the total required for validation of the proposed molecular formulas. The excessive broadening of Ar-F resonances for the two Co complexes **[5-11]** and **[5-13]** is explained by the paramagnetic effect of Co^{2+} on the spin system of the extended aromatic cycle.

Owing to the complexity and overlap of the splitting patterns, no attempt has been made for chemical shift assignments of individual F atoms and calculation of the coupling constants, apart from singular obvious cases noted in the experimental section. High resolution ^{19}F two-dimensional COSY spectra acquired over the period of several days might help in such an endeavor, but not necessarily be successful, as any peak broadening could hinder precise assignments; research facilities permitting, these advanced spectroscopic experiments could form the scope of future work.

5.3.4 Crystal Structures

The solid-state characterization of the new asymmetric perfluorinated complexes is thorough, with three crystal structures obtained out of four compounds produced. The ease of getting suitable single crystals varied considerably, depending on the compounds' aggregation tendency, relative solubility, metal's Lewis acidity and steric bulk. Details on each structure are presented in the following sections.

5.3.4.1 Overview of Crystallographic Data. Table 5.1 summarizes crystal data and structure refinement parameters for the $F_{34}PcZn$, $F_{34}PcCo$ and $F_{52}PcZn$ complexes, combining information extracted from the corresponding tables of Appendices S to U.

Table 5.1 Selected Crystallographic Data for Asymmetric Phthalocyanines†

	$F_{34}PcZn(H_2O)$ $\bullet 2(CH_3)_2CO$	$F_{34}PcCo(CH_3CN)$ $\bullet 2Tol$	$F_{52}PcZn(OPPh_3)$ $\bullet 3Tol$
System	monoclinic	triclinic	monoclinic
Space group	$P2_1/c$	$P\bar{1}$	$P2_1/n$
T (K)	100(2)	100(2)	100(2)
a (Å)	11.0463(2)	10.540(2)	15.852(2)
b (Å)	11.4442(2)	14.554(3)	22.978(3)
c (Å)	41.9063(6)	18.695(4)	24.032(3)
α (°)	90	95.096(4)	90
β (°)	103.436(1)	94.831(4)	96.704(1)
γ (°)	90	106.229(4)	90
V (Å^3)	5152.63(15)	2724.8(10)	8694.00(19)
Z	4	2	4
d_{calcd} (g/cm^3)	1.869	1.871	1.576
N_{refl}	8939	10873	9072
N_{param}	906	866	1092
R_1 ($I > 2\sigma I$)	0.0876	0.0950	0.0922
R_1 (all data)	0.0911	0.1419	0.0978
wR_2 ($I > 2\sigma I$)	0.2343	0.2441	0.2298
wR_2 (all data)	0.2364	0.2658	0.2348
S	1.155	1.031	1.026

$R_1 = \sum|(|F_o|-|F_c|)| / \sum|F_o|$; $wR_2 = \{\sum w(|F_o|-|F_c|)^2 / \sum w|F_o|^2\}^{1/2}$; $S = \{\sum w(|F_o|-|F_c|)^2 / (N_{refl}-N_{param})^2\}^{1/2}$.
† Abbreviations used in the table and equations: N_{refl} – number of observed independent reflections; N_{param} – number of parameters refined; R_1 – unweighted refinement discrepancy factor; wR_2 – weighted refinement discrepancy factor; S – goodness of fit on F^2; F_o – observed structure factors; F_c – calculated structure factors.

5.3.4.2 $F_{34}PcZn$. Single crystals of **[5-10]** were obtained by slow evaporation at RT of an ethyl acetate/acetone 1:1 solution. The complex readily crystallizes by Zn-coordination of ambient water and incorporation of acetone molecules (2:1 ratio) in the lattice. The deep blue-colored crystals of $F_{34}PcZn(H_2O)\bullet 2(CH_3)_2CO$ are monoclinic, $P2_1/c$ space group, with 4 molecules per unit cell. An ORTEP representation is given in Figure 5.9, while the complete crystallographic parameters are listed in Appendix S.

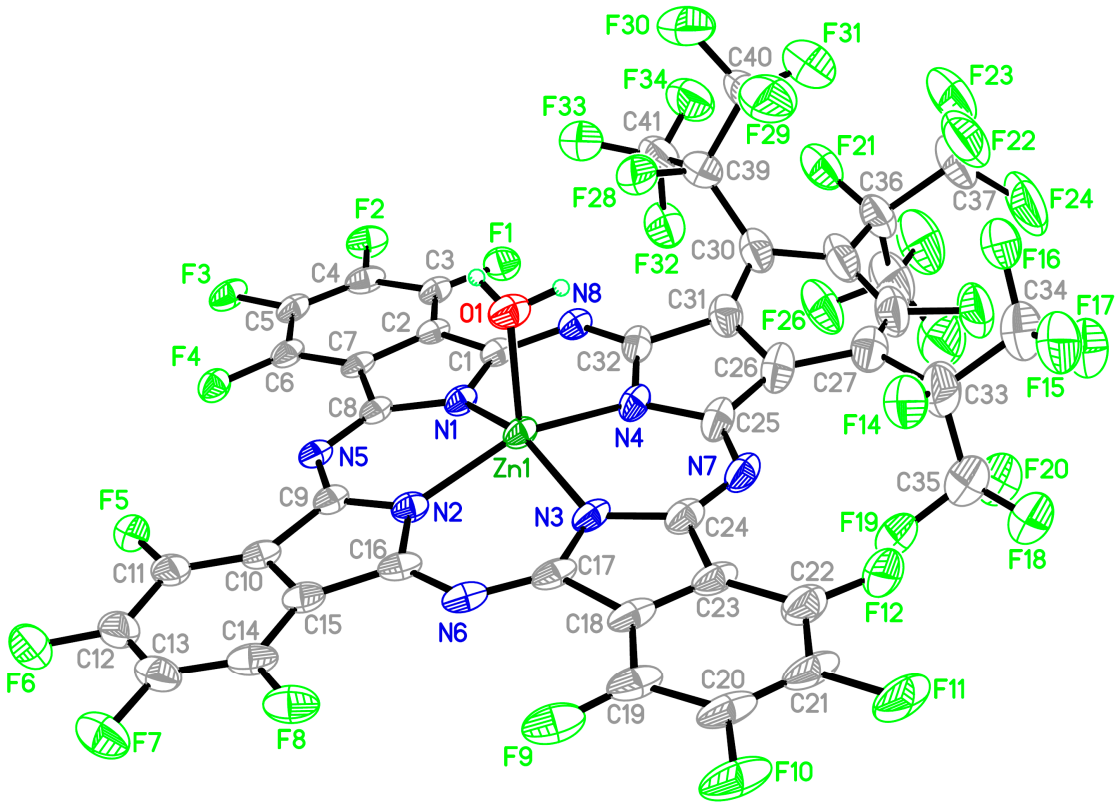

Figure 5.9 X-ray structure of $F_{34}PcZn(H_2O)$ in ORTEP representation at 40% probability. Rotational disorder of the 4-*i*-C_3F_7 group, as well as co-crystallized acetone molecules are omitted for clarity. Only one of the enantiomers is shown. Color code: C, gray; F, light green; N, blue; O, red; Zn, dark green.

The structure refinement is complicated by rotational disorder of the 4-*i*-C_3F_7 group and its adjacent atoms of the aromatic ring, yielding a final R-factor of 0.0876. In order to solve the disordered structure, SHELX[58] restraints were used to their fullest; once the disordered model converged, additional constraints were applied on all anisotropic displacements. The aromatic ring bearing the three bulky groups is distorted and lacks planarity. While this might look physically unreasonable, the combination of severe steric strain and extreme electron withdrawal of the *i*-C_3F_7 groups explains the deviations. The thermal ellipsoid plot reveals excessive libration around the disordered region. Molecular steric strain created by the disproportionate bulk of the **[5-4]**-originating

fragment brings about bending of the Pc macrocycle in the affected areas. As a result, the 5-membered pyrrole ring carrying the sterically hindering groups forms a 10.5° angle with its *trans* analogue in the cycle, while one of the adjacent, tetrafluoro-aromatic moieties tilts at 8.7°. The molecular asymmetry induced in **[5-10]** by the three *i*-C_3F_7 substituents translates, in the solid-state, into molecular chirality due to the 0.425 Å offset of the Zn atom above the plane defined by N_4-coordination. Two pairs of enantiomers are present in the unit cell, one of them being shown in Figure 5.10(c).

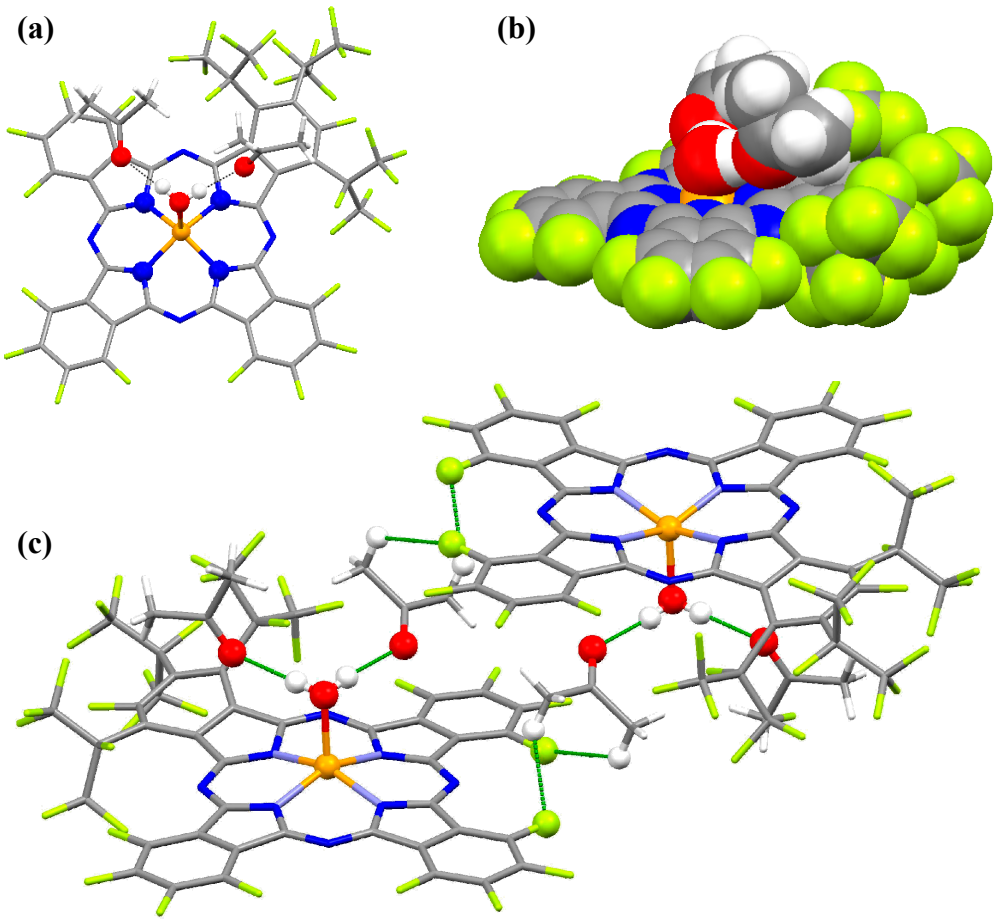

Figure 5.10 Solid-state structure of one enantiomer of $F_{34}PcZn(H_2O)$ in (a) capped sticks and (b) spacefill representations. (c) Acetone H-bonded mediation between the two enantiomers in the unit cell. The Zn, O, H and F atoms involved in bonding are shown as spheres, while the F•••H and O•••H interactions are shown as green sticks. Color code: C, gray; F, green; N, blue; O, red; Zn, orange.

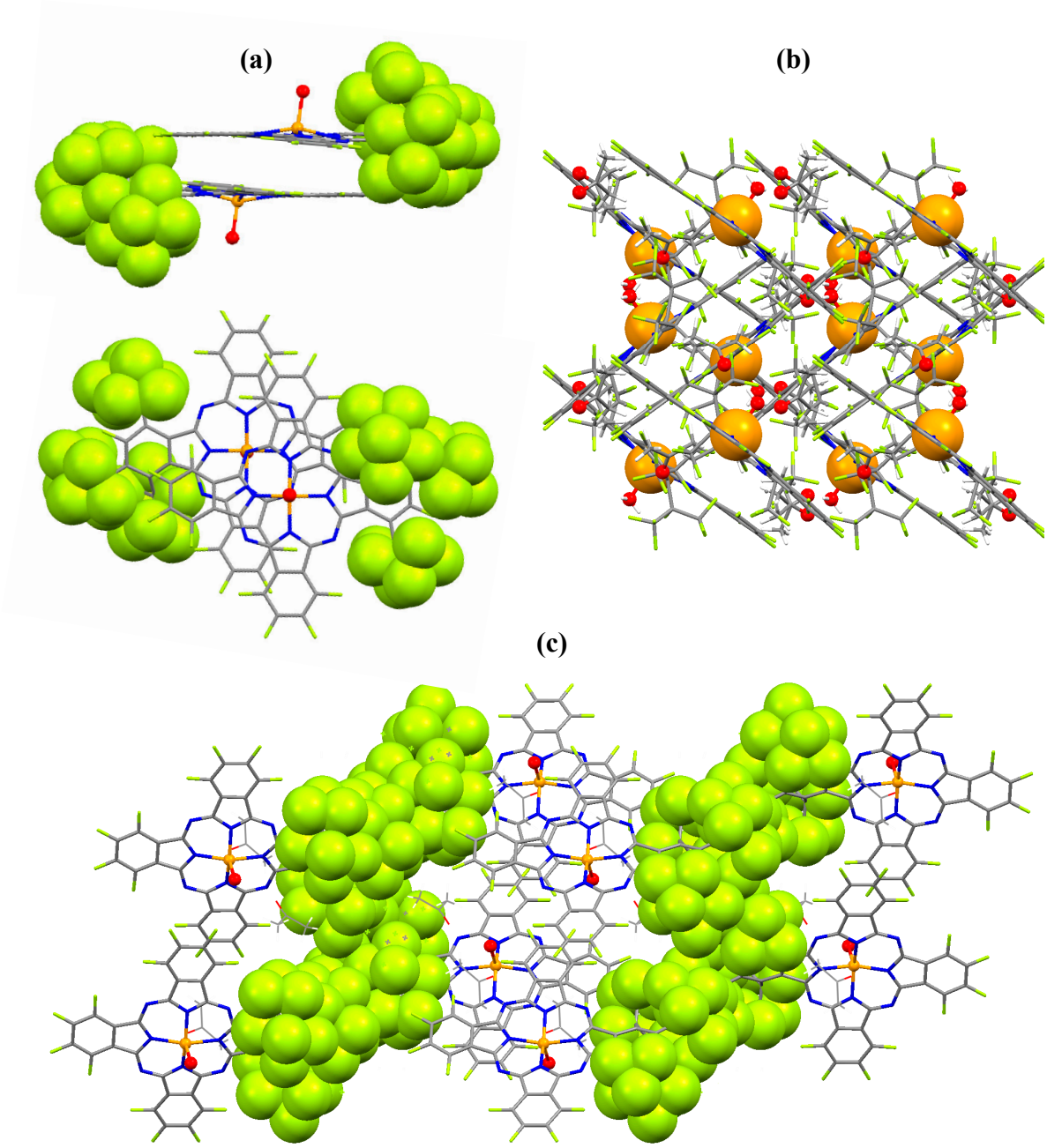

Figure 5.11 Molecular stacking of $F_{34}PcZn$ in the solid state, in capped sticks representations, with H atoms omitted. The Zn and O atoms are shown as spheres. (a) Side and top views of the dimer assemblies formed by π–π interactions, with the *i*-C_3F_7 groups depicted as van der Waals spheres. (b) View along the *c* axis. (c) View along the *b* axis. Color coding follows the scheme of Figure 5.10.

The crystal packing of $F_{34}PcZn$ (Figure 5.11) is revelatory for the existence of π–π stacking interactions, validating without a doubt the rational design approach in the synthesis of the complex, in accordance with the proposed research objective.

Pairs composed of molecules of the same enantiomer stack in a typical π–π fashion, forming dimer assemblies (Figure 5.11(a)); the distance between the parallel planes defined by the non-hindered halves of the stacking macrocycles is 3.393 Å. The monomer units stack in such a way that the molecular faces of higher bulk are oriented outwards, in a precise 180° alignment of the *i*-C_3F_7 groups, which allows for minimal steric repulsion. The inter-dimer contacts are ensured by acetone hydrogen-bonding mediation (Figure 5.10(c)). Both H atoms of Zn-coordinated water on the outer faces of the dimers are involved in 1.894 and 1.881 Å-long bonds with oxygens of two adjacent acetone molecules. In turn, H atoms of both methyl groups of an acetone moiety form H•••F(Ar) interactions of 2.447 and 2.583 Å with a PcM unit of the neighboring dimer. Thus, infinite chains are constructed of parallel, stacking dimer units, with the bulky *i*-C_3F_7 substituents arranged in between as structural "buffers", as seen in Figure 5.11(c).

5.3.4.3 F_{34}PcCo. Single crystals of **[5-11]** were obtained by slow evaporation at RT of an acetonitrile/toluene 1:1 solution. As a result, acetonitrile coordinated to the Co atoms, along with inclusion of solvation toluene in the lattice, in a 2:1 ratio to the PcM complexes. Collection of X-ray diffraction data was challenging, as only tiny dark blue rods would form on each occasion, unsuitable for analysis with a regular diffractometer. Similar to $F_{28}H_4$PcZn, data collection on **[5-11]** was performed by Dr. Yu-Sheng Chen using synchrotron radiation at the Advanced Photon Source of Argonne National Laboratory. The dimensions of the crystal used for collection were 0.035 × 0.020 × 0.005 mm. F_{34}PcCo(CH_3CN)•2Tol forms in the triclinic, $P\bar{1}$ space group. One of the toluene molecules and a CF_3 group of 1-*i*-C_3F_7 are disordered over two positions, creating difficulties in the refinement process. A final R-factor of 0.095 was obtained.

A thermal ellipsoid plot is given in Figure 5.12; complete crystallographic parameters are listed in Appendix T.

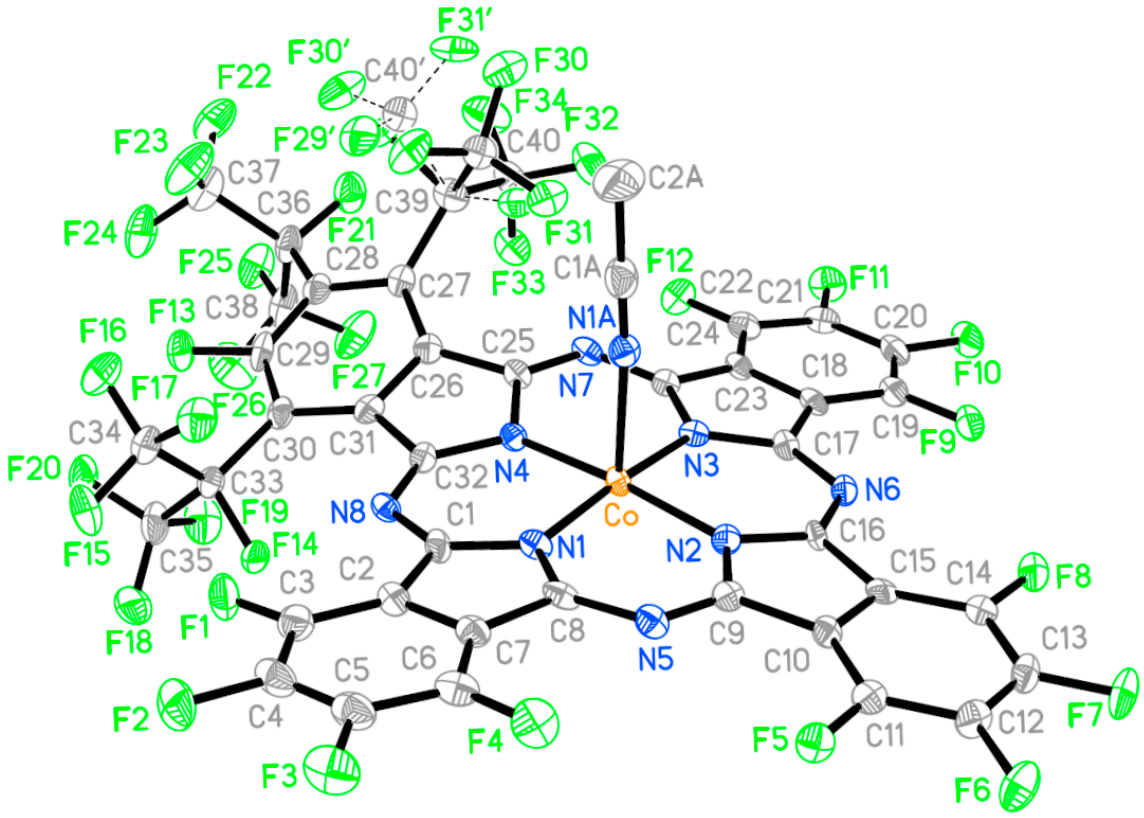

Figure 5.12 X-ray structure of $F_{34}PcCo(CH_3CN)$ in ORTEP representation at 40% probability. Rotational disorder of the 1-*i*-C_3F_7 group is shown. H atoms and solvation toluene molecules are omitted for clarity. Only one of the enantiomers is shown. Color code: C, gray; F, green; N, blue; Co, orange.

The structural features evidenced for $F_{34}PcZn$ are observed for the Co analogue as well. Thus, the unit cell is comprised of a pair of enantiomeric molecules, due to displacement of the Co atom above the N_4-coordination plane. The aromatic ring bearing the three *i*-C_3F_7 groups is similarly distorted with respect to the rest of the molecule, but this time retains its planarity while forming a 29° dihedral angle with the *trans* phenyl ring containing Ar-F. The angle between the two remaining *trans* rings is 9°.

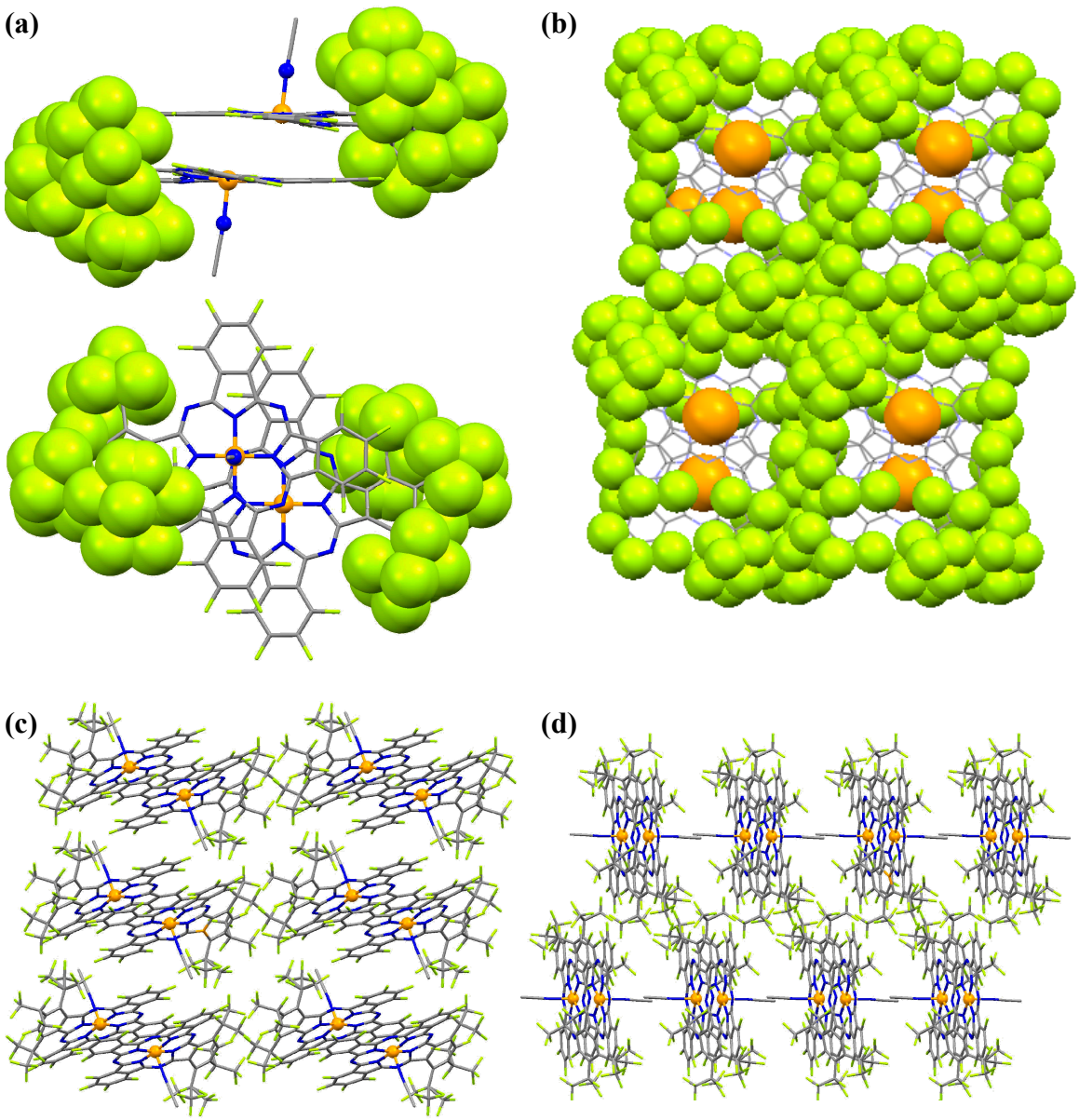

Figure 5.13 Molecular stacking of $F_{34}PcCo$ in the solid state, in capped sticks representations, with H atoms and solvation toluene omitted. (a) Side and top views of the dimer assemblies formed by π–π interactions, with the *i*-C_3F_7 groups depicted as van der Waals spheres. (b) View along the *a* axis, showing the F and Co atoms as van der Waals spheres. (c) View along the *b* axis. (d) View along the *c* axis. Color coding follows the scheme of Figure 5.12.

Dimer assemblies identical to the Zn analogue, formed through π–π stacking of molecules of the same enantiomer, constitute the repeating motif of the solid-state structure of $F_{34}PcCo$. The unequal steric hindrance of the two molecular faces favors

electronic coupling on the less hindered face and acetonitrile coordination on the opposite one. The stacking distance is 3.276 Å, measured between the parallel planes defined by the undistorted tetrafluoro-aromatic parts. The N_4-coordination planes of the two molecules are tilted at 4.2° angles to the stacking axis. The views along the three crystallographic axes, Figure 5.13(b)-(d), reveal an infinitely repeating columnar structure, with the bulky perfluoroisopropyl groups delimiting cylindrical shafts. The methyl group of acetonitrile does not seem to be involved in any bonding interactions.

5.3.4.4 F_{52}PcZn. X-ray suitable single crystals of **[5-12]** were obtained through co-crystallization with triphenylphosphine oxide (*ca.* 4× molar excess), by slow evaporation at RT of a toluene solution. Addition of an external coordinating agent was prompted by repeatedly unsuccessful attempts at getting viable crystals from single solvents or solvent mixtures. Solving the structure posed great difficulties due to inclusion of three solvation toluene moieties per molecule of **[5-12]**, disordered over five positions with unequal populations in the lattice (Figure U.1). In addition, the 4- and 8-*i*-C_3F_7 groups exhibit rotational disorder. F_{52}PcZn($OPPh_3$) crystallizes in the monoclinic, $P2_1/n$ space group, with 4 molecules per unit cell. The final value of the R-factor, 0.0922, is more than reasonable, considering the complexity of the structure and obstacles encountered during the refinement process. A thermal ellipsoid plot is provided in Figure 5.14; supporting crystallographic parameters are found in Appendix T. Presence of six *i*-C_3F_7 groups, arranged in a *cis* configuration, over two quarters of the molecule, leads to an even greater deviation in planarity of the F_{52}Pc ligand's aromatic macrocycle than the one observed for the F_{34}PcM complexes. A view along the planar tetrafluoro-aromatic part of the molecule (Figure 5.15(b)) reveals a concave, dome-distorted structure composed of

two halves featuring opposite extremes of steric bulk. According to the numbering scheme of Figure 5.14, the planes defined by the (N3, N4, N8) and (N1, N2, N6) atoms, respectively, bisect at a 25.2° angle, as shown in Figure 5.15(c).

In spite of the steric hindrance manifested by the six peripheral *i*-C_3F_7 groups, π–π stacking dominates both the intra- and intermolecular binding interactions. In addition to the usual dimers formed by stacking on the less-hindered molecular faces in clamshell-like assemblies (Figure 5.15(a),(b)), the highly symmetric coordination of $OPPh_3$ and its tight fit in the perfluorinated pocket allows for internal π–π stacking with the Pc macrocycle (Figure 5.15(d)).

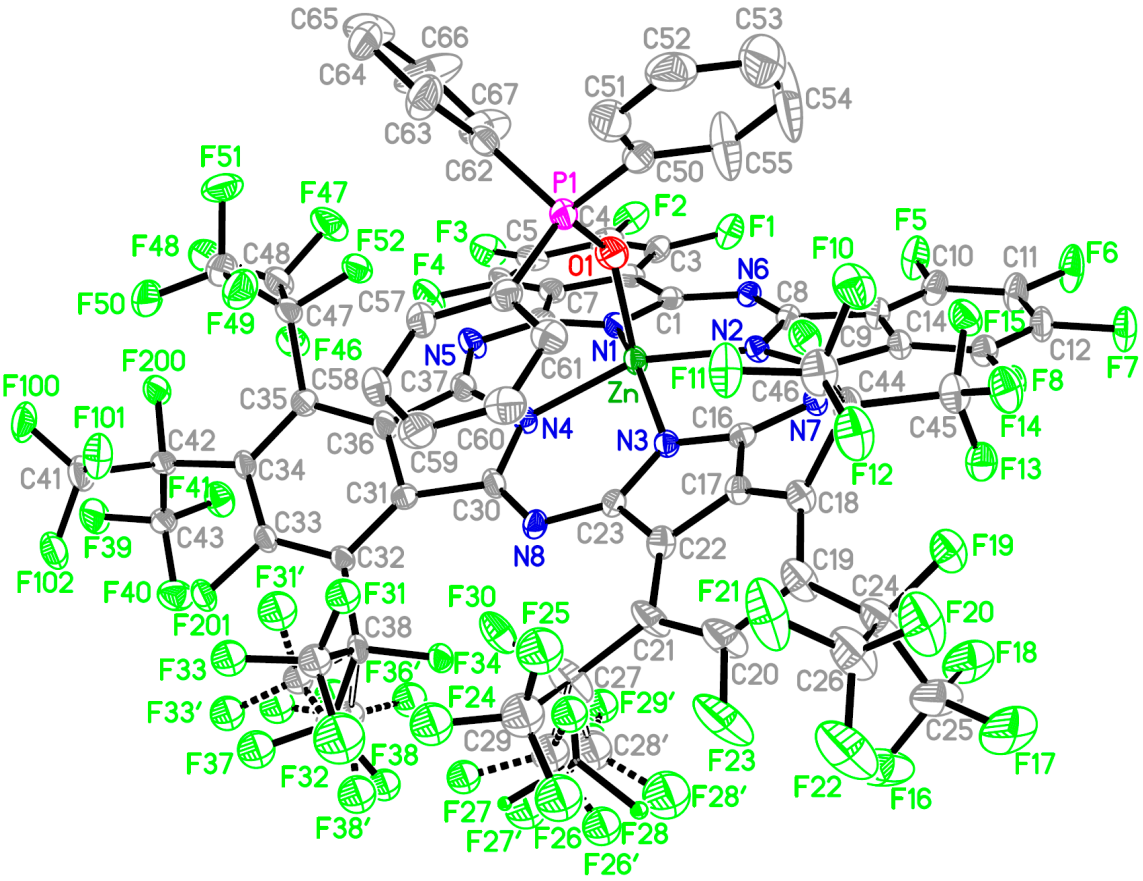

Figure 5.14 X-ray structure of $F_{52}PcZn(OPPh_3)$ in ORTEP representation at 35% probability. Rotational disorder of the 4- and 8-*i*-C_3F_7 group is shown. H atoms and solvation toluene molecules are omitted for the sake of clarity. Color code: C, gray; F, light green; N, blue; Zn, green; O, red; P, purple.

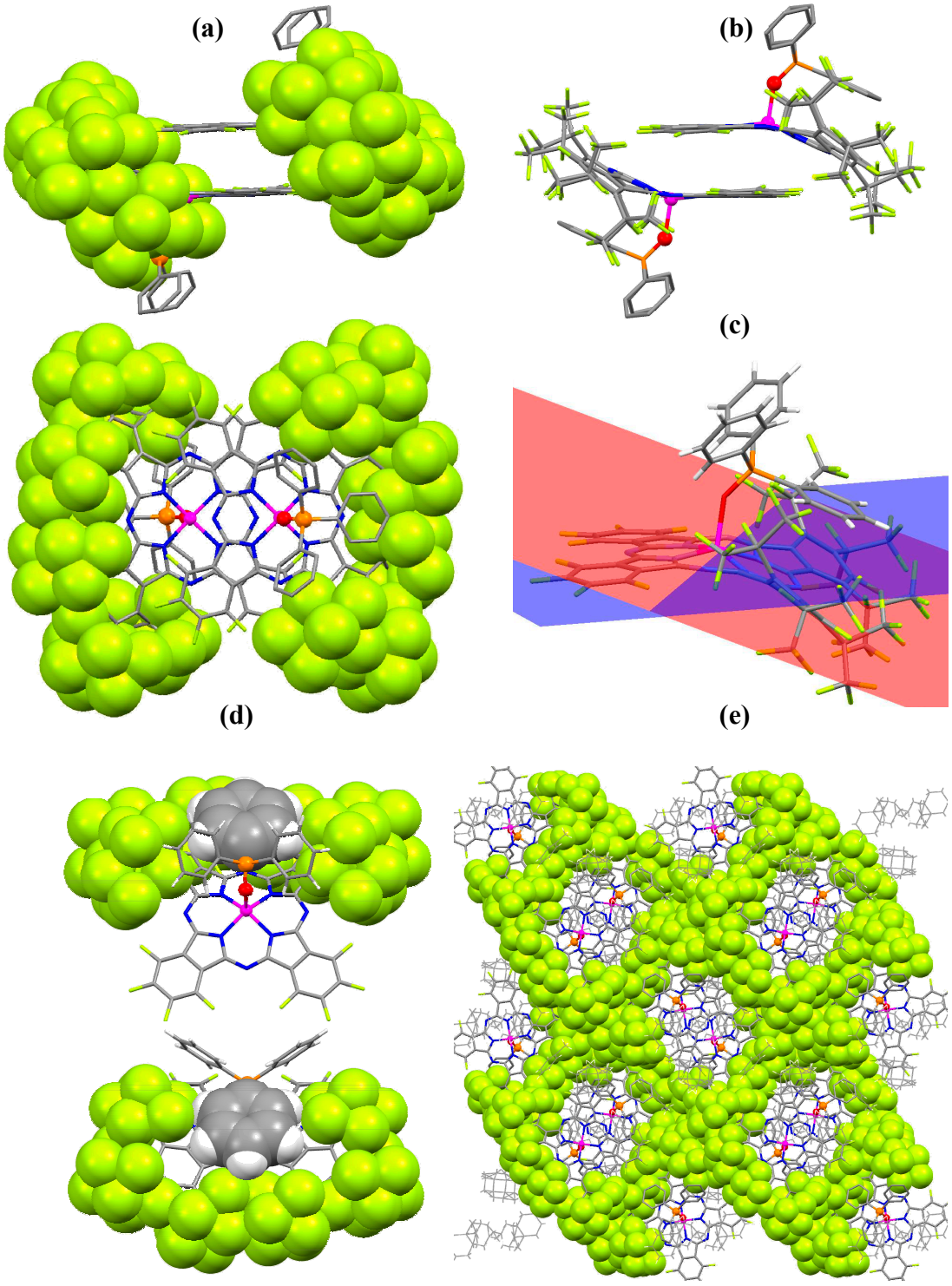

Figure 5.15 Crystal structure of $F_{52}PcZn$ in capped sticks representations. (a) Side and top views of the dimers formed by π–π stacking. (b) Dome distortion of the ligand. (c) Angle formed by the bisecting planes of planar and distorted molecular halves. (d) Front and back views of the internal stacking of one of the phenyl groups of $OPPh_3$. (e) View along the *a* axis. The *i*-C_3F_7 groups in (a), (d) and (e) are depicted as van der Waals spheres. Color code: C, gray; H, white; F, green; N, blue; Zn, purple; O, red; P, orange.

The distance between the center of the stacking phenyl ring of $OPPh_3$ and the plane of underlying Pc core atoms is 3.486 Å. The structure is further stabilized by an intramolecular H•••F(CF_3) bond of 2.576 Å involving the *p*-H of the stacked Ph ring. Although the complex is intrinsically asymmetric because of different conformations of the 4- and 8-*i*-C_3F_7 groups, coordination of $OPPh_3$ to the central Zn atom occurs in a perfectly symmetric fashion with respect to the rest of the molecule. The Zn, O, P, *meso*-N, *ipso* and *para* C atoms of the stacked phenyl ring, all lie in a pseudo-molecular mirror plane, restrained from becoming a true mirror plane only by the discrepancy in the *i*-C_3F_7 conformations. The two non-stacking Ph moieties of $OPPh_3$ align at virtually identical dihedral angles of 32.12° and 32.17° with respect to the third one.

The intermolecular π–π stacking in the dimer units is fixed at a 3.502 Å distance. A view along the *a* axis (Figure 5.15(e)) reveals a columnar crystal packing similar to the one encountered for F_{34}PcCo (Figure 5.13(b)). Toluene molecules disorderly intercalate within the channels defined by the perfluorinated scaffolds, forming weak H-bonds of variable length with F atoms of nearby *i*-C_3F_7 groups.

5.3.5 UV-vis Spectroscopy

Compared to the trifluoromethylated analogues described in Chapter 4, the asymmetric perfluorinated complexes **[5-10]**–**[5-13]** display equally strong UV-vis electronic absorptions and replicate solvent-dependent aggregation, with some key differences. Figure 5.16 presents an overview of the chloroform spectra acquired at gradually decreasing total concentrations in the 20–2 μM range, used for determination of the molar extinction coefficients through Lambert-Beer plots, exemplified for the Q-band maxima. Table 5.2 summarizes the results obtained for all absorption bands of the four complexes.

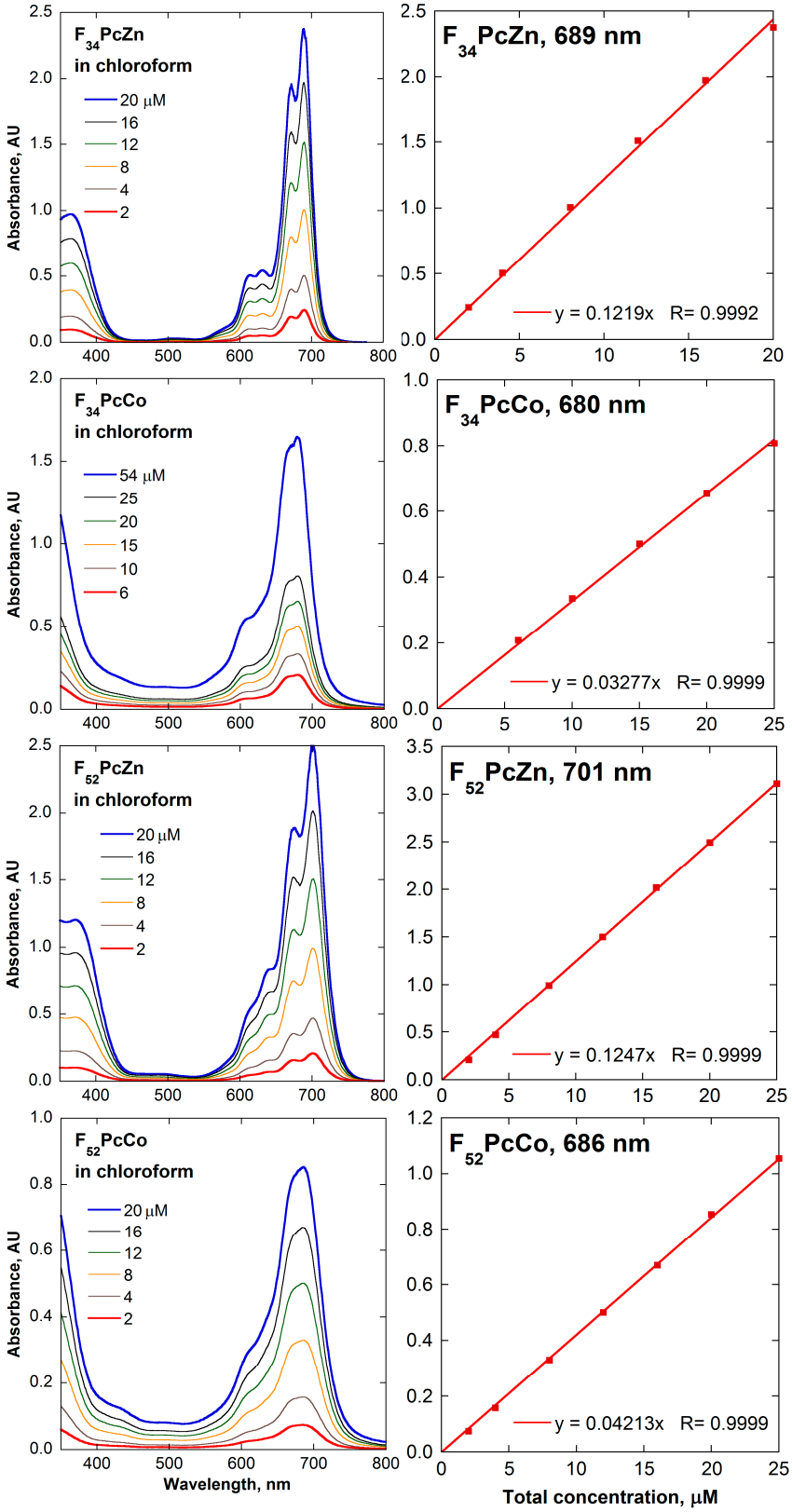

Figure 5.16 UV-vis electronic absorption spectra of F_{34}PcM and F_{52}PcM complexes (M = Zn, Co) in chloroform, showing Lambert-Beer linearity for the Q band absorption maxima. Equations for the linear fits are also provided.

Table 5.2 UV-vis Absorption Maxima and Associated Molar Extinction Coefficients in Chloroform for Perfluorinated Asymmetric PcM Complexes

Compound	λ_{max} (log ϵ) (nm (L mol^{-1} cm^{-1}))
F_{34}PcZn **[5-10]**	689 (5.09), 672 (4.99), 632 (4.44), 614 (4.41), 365 (4.69)
F_{34}PcCo **[5-11]**	680 (4.52), 667 (4.50), 611 (4.03)
F_{52}PcZn **[5-12]**	701 (5.10), 674 (4.97), 640 (4.62), 615 (4.44), 372 (4.78)
F_{52}PcCo **[5-13]**	686 (4.62), 615 (4.18), 334 (4.58)

The almost perfect linearity of the Lambert-Beer plots in chloroform solutions (Figure 5.16) confirms the absence of aggregation equilibria. Loss of D_{4h} symmetry upon inclusion of the perfluoro-trisisopropyl aromatic fragments causes the split of the major Q electronic transitions in two bands of slightly different intensities, as a result of the now non-degenerate LUMO levels (Figures 4.5 and 5.5). In the Co complexes, they broaden and coalesce into a single skewed band. Both Zn complexes **[5-10]** and **[5-12]** exhibit molar absorptivities exceeding 10^5 L mol^{-1} cm^{-1} for their Q-bands located at 689 and 701 nm, respectively. The absorption maximum of F_{52}PcZn at 701 nm is the lowest energy transition encountered among all PcM complexes studied in this work, new and published alike. This experimental outcome validates previous computational results[108,110,111] showing that perfluorination through a combination of F atoms and *i*-C_3F_7 groups further depresses the energy of the frontier orbitals with the increase in molecular F content.

The solvent-dependent aggregation of F_{34}PcM complexes follows a similar trend to the $F_{24}H_8$PcM and $F_{28}H_4$PcM analogues, showing minimal levels in halogenated and other hydrophobic solvents and variable extents in all other. As before, the highest amount of dimer species is encountered in alcohols, but this time in a much less significant ratio of the total concentration. The UV-vis spectral comparison of Figure 5.17 reveals that the monomer form of F_{34}PcZn is still present in a roughly 60% quota

even in aggregation-promoting ethanol, as shown by the strong Q-band at ~680 nm. This is a turnaround from the *ca.* 40% monomer ratio noticed for an equivalent total concentration of $F_{28}H_4PcZn$ and suggests that the considerable steric hindrance of the *i*-C_3F_7-containing moiety limits aggregation in solution through a restriction, in the random molecular motion, of the available orientations for efficient electronic coupling without steric repulsion. Moving to the more bulky $F_{52}PcZn$, the hypothesis is confirmed by its ethanol UV-vis spectrum which exhibits a barely appreciable dimerization extent, mostly resembling the tridimensional $F_{64}Pc$ regarded as the non-aggregating standard.

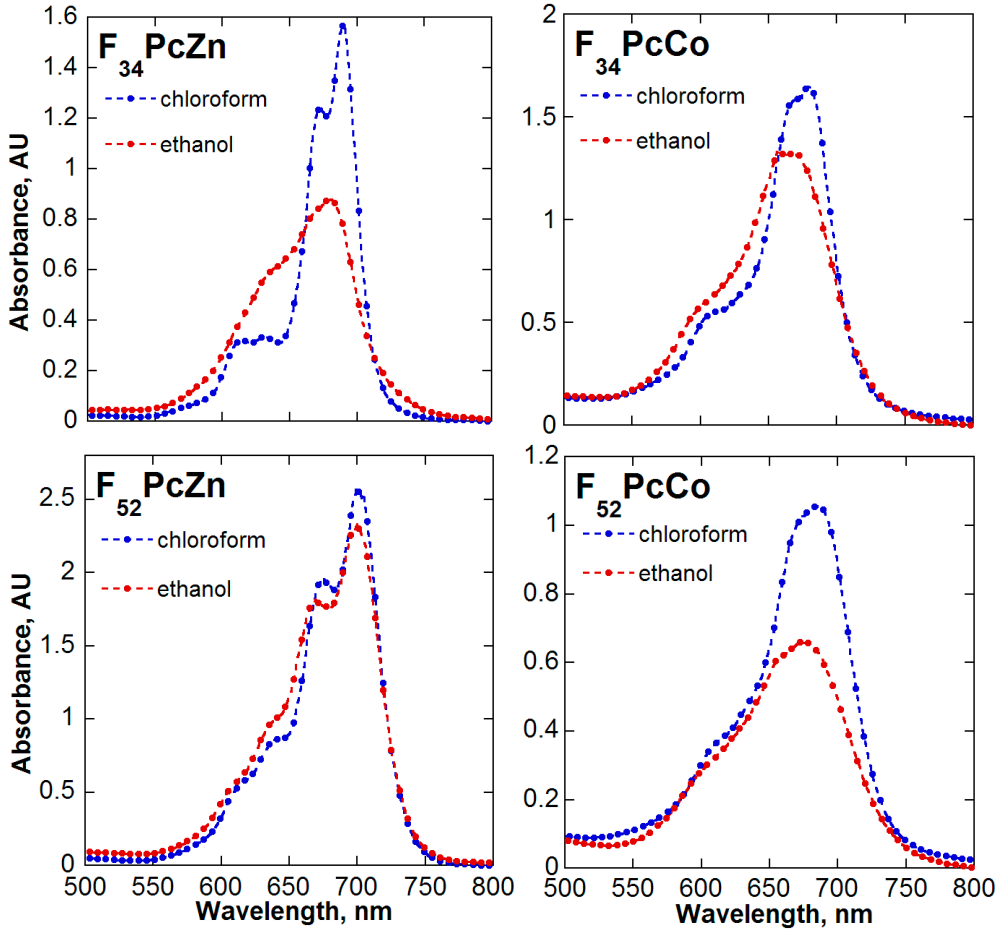

Figure 5.17 UV-vis comparison of solvent-dependent aggregation of $F_{34}PcM$ and $F_{52}PcM$ complexes (M = Zn, Co). Spectra are recorded in chloroform (blue, least aggregation) and ethanol (red, most aggregation).

5.4 Conclusions

The first asymmetric perfluorinated metallophthalocyanines were synthesized and structurally characterized by solution and solid-state methods. Owing to the rational design approach, a reduction in the overall steric hindrance of the complexes and molecular asymmetry is induced by the one-pot mix of bulky perfluoro-3,4,6-trisisopropyl- and planar tetrafluoro-phthalonitrile precursors, with formation of the two new F_{34}Pc and F_{52}Pc classes of N_4-coordinating ligands. Stereoselective formation of the *cis* configurational isomer in the case of F_{52}PcM provides insights into the relative reactivity of the two precursors and mechanism of their tetramerization, emphasizing the kinetic control in formation of the coproducts.

Rapid coordination of σ electron-donors such as water, acetone, acetonitrile and triphenylphosphine oxide, as demonstrated by the broad resonances of the ^{19}F NMR spectra and crystal structures of the complexes, attests for the enhanced Lewis acidity of the central metal. The extreme electronic demand of the perfluorinated groups is upheld by the energetic depression of the frontier molecular orbitals, as seen in the farthest red-shifted UV-vis absorption encountered yet for perfluorinated PcM complexes.

The disproportionate steric bulk of the perfluoroalkyl moieties causes severe distortions of the Pc ligand's macrocyclic architecture, while allowing for electronic stacking of all complexes in the solid state through π–π interactions. Structural asymmetry induced by the uneven combination of fluorine atoms and perfluoroisopropyl groups leads to molecular chirality in the solid state. A fine balance of the steric factors is achieved for the F_{52}Pc ligand, which retains stacking in the solid state but exhibits little aggregation in solution.

CHAPTER 6

CATALYTIC AEROBIC OXIDATION OF THIOLS IN HOMOGENEOUS SYSTEMS

6.1 Introduction

Organic-based materials which are in the same time catalytically active in aerobic oxidation processes and completely refractory to all types of activated oxygen species produced are not known. The C–H bonds of common hydrogen-containing catalysts are susceptible to radical attacks and intramolecular activation. The new fluoroalkylated phthalocyanines described in this work provide, through their stronger C–F bonds, a viable solution to the chemical stability problem, adding the characteristic thermal robustness of the Pc core structure.

This chapter investigates the ability of the new cobalt complexes to catalyze aerobic oxidations of susceptible substrates and verifies the above stated claims of chemical inertness towards decomposition, in comparison with a series of three standard representatives of gradually increasing electronic deficiency and steric bulk, i.e., H_{16}PcCo (or, simply, PcCo), F_{16}PcCo and F_{64}PcCo. The catalytic capability is tested towards a model reaction, the aerobic autooxidation of thiols (mercaptans, *abbr.* RSH) to disulfides (*abbr.* RSSR). The transformation is practiced industrially for over 20 years under the MEROX (MERcaptan OXidation) process and employs tetrasulfonated cobalt(II) phthalocyanines, with the purpose of removing corrosive and foul smelling RSH components of petroleum products.[151] It follows an overall RSH/O_2 stoichiometry of 4:1, according to eqn. 6.1, written for neutral reaction conditions.

$$4\ RSH + O_2 \rightarrow 2\ RSSR + 2\ H_2O \qquad (6.1)$$

A myriad of investigations and scientific publications starting in the 1970s have addressed the question of elucidating the mechanism of the aerobic PcCo-catalyzed thiol coupling. An exhaustive literature review is not the scope of the present study, nor is the establishment and verification of general and specific rate laws for the various mechanistic steps. Instead, this introductory section attempts at presenting a concise view of the process, with emphasis on the relevant, generally agreed-upon mechanistic steps for the compounds at hand. Following the presentation of the catalytic parameters obtained, a qualitative discussion, explaining the results based on the postulated mechanism, is offered for each substrate under dedicated sections.

One of the first well-established findings on the thiols' aerobic coupling to disulfides is that catalytic autooxidation is significantly accelerated under basic conditions,[152] attained by addition of an alkaline hydroxide which promotes formation of the thiolate anion, RS^- (eqn. 6.2). The RS^- anion is in fact the species susceptible to reaction with molecular dioxygen;[153] in neutral media, the active thiolate species are obtained by slow dissociation equilibria. In the presence of the PcCo catalyst, thiolate is oxidized to disulfide concomitantly with the stepwise two-electron reduction of oxygen to hydrogen peroxide and regeneration of hydroxide (eqn. 6.3). Finally, H_2O_2 rapidly converts two additional RSH units into disulfide and water, according to eqn. 6.4.[153–155]

$$2\ RSH + 2\ HO^- \rightarrow 2\ RS^- + 2\ H_2O \qquad (6.2)$$

$$2\ RS^- + 2\ H_2O + O_2 \overset{PcCo}{\rightarrow} RSSR + H_2O_2 + 2\ HO^- \qquad (6.3)$$

$$H_2O_2 + 2\ RSH \rightarrow RSSR + 2\ H_2O \qquad (6.4)$$

A summation of the above steps gives the overall stoichiometry of eqn. 6.1. The steps detailed by eqns. 6.2–6.4 are valid for high RSH excess to the initial HO^- amounts.

If an excess molar ratio of hydroxide to the thiol is used, RSH is totally ionized to RS^- and the overall stoichiometry can be re-written as:[155]

$$4\ RS^- + O_2 + 2\ H_2O \rightarrow 2\ RSSR + 4\ HO^- \qquad (6.5)$$

Water soluble $(SO_3H)_4PcCo$, $(SO_3Na)_4PcCo$ and $(COOH)_{2,4,8}PcCo$ complexes are the catalysts of choice for both the industrial MEROX applications and studies on the mechanistic details of the homogeneous process.[156–161] In addition, heterogenized systems were investigated, with the catalyst anchored on solid supports such as: (1) SiO_2 for PcCo,[162] $(NO_2)_4PcCo$,[162] $(COOH)_4PcCo$,[162] and $(NH_2)_4PcCo$,[155] (2) carbon for $(SO_3Na)_{1,2}PcCo$,[163] and (3) MgAl hydrotalcite for $(SO_3^-)_4PcCo$.[164] Polymer (ionene) composites have also been used.[165] Since the steps of RSH ionization and oxidation by H_2O_2 described by eqns. 6.2 and 6.4 do not involve any participation of the PcCo catalysts, they are of secondary importance to the mechanistic study of the reaction.

The focus of the overwhelming majority of published data on PcCo-catalyzed oxidation of thiols is the elucidation of the central step of O_2 reduction to H_2O_2 and concomitant generation of thyil $RS^\bullet$ radicals by the catalyst, eqn. 6.3. The literature in the field,[151–168] albeit contradictory on the exact order of the underlying reaction sequences, agrees on several important points:

1. The Co(II) central atom is involved in successive redox processes with alternation of its positive charge numbers.
2. The initial step involves formation of a binary RS–PcCo complex.
3. The RS–PcCo complex further coordinates oxygen with formation of an unstable, ternary RS–PcCo–O_2 intermediate.
4. Two-electron reduction of oxygen always occurs, with formation of peroxide and subsequent H_2O_2 identified in the reaction mixture.
5. The reaction is clean, the disulfide being the only RSH oxidation product.

Regarding the redox pathway taken by the Co(II) center, mechanisms have been proposed through both Co(II)/Co(III)[166] and Co(II)/Co(I)[155,157–162,169] pairs, involving oxidation-reduction and reduction-oxidation steps, respectively. For water soluble PcCos, the picture is confusing, with both redox pathways claimed in some cases for the same compounds. In relation to the discussion at hand on fluoroalkylated and perfluorinated complexes with a general formula $(R_f)_nPcCo$, their extreme electronic deficiency warrants the choice of the Co(II)/Co(I) pathway, justified by the inability of electron-withdrawing R_f groups to stabilize an eventual Co(III) charge and experimentally validated by: (a) the failure to electrochemically oxidize $F_{64}PcCo$ in DMF,[51] and (b) the UV-vis signature bands of metal-centered reduced species, $(R_f)_nPc(2-)Co(I)$, in the spectra of the reaction mixtures taken upon addition of RS^- (Figures V.1–V.3) and HO^- ions, (*vide infra*, Section 6.6).

Little is known about the importance of catalyst aggregation in the process. While the majority of proposed mechanisms assume intermediates formed by monomeric PcCo species, no information was found specifically alleging a detrimental influence of dimers on the reaction rates, with some studies actually suggesting that dimers are the more active form.[156,165,166] Similarly, the potential involvement of a second thiolate molecule in the ternary RS–PcCo–O_2 complex or the role of a presumable RS–PcCo–SR intermediate are poorly understood. As such, an elaboration on this topic would be purely speculative. Finally, no scientific consensus exists on whether:

- the second dioxygen reduction step from superoxide, $O_2^{\bullet-}$, to peroxide, O_2^{2-}, occurs by an electron transfer from RS^- in solution or through a new redox pathway at the Co center.
- the disulfide product forms through a disulfide radical expelled from the Co center or fast coupling of two previously Co-removed $RS^\bullet$ radicals in solution.

6.1.1 The Mercaptan Oxidation Catalytic Cycle

Taking into account all the above theoretical and experimental considerations, a comprehensive catalytic cycle for the autooxidation of mercaptans following a Co(II)/Co(I) pathway is presented in Figure 6.1, with numbering of the elementary steps. The presumed faster stages of ternary complex decomposition and radical coupling in solution are shown by simple arrows, while equilibrium arrows indicate the presumed slower steps of RS^- coordination and one electron transfer to and from the Co center.

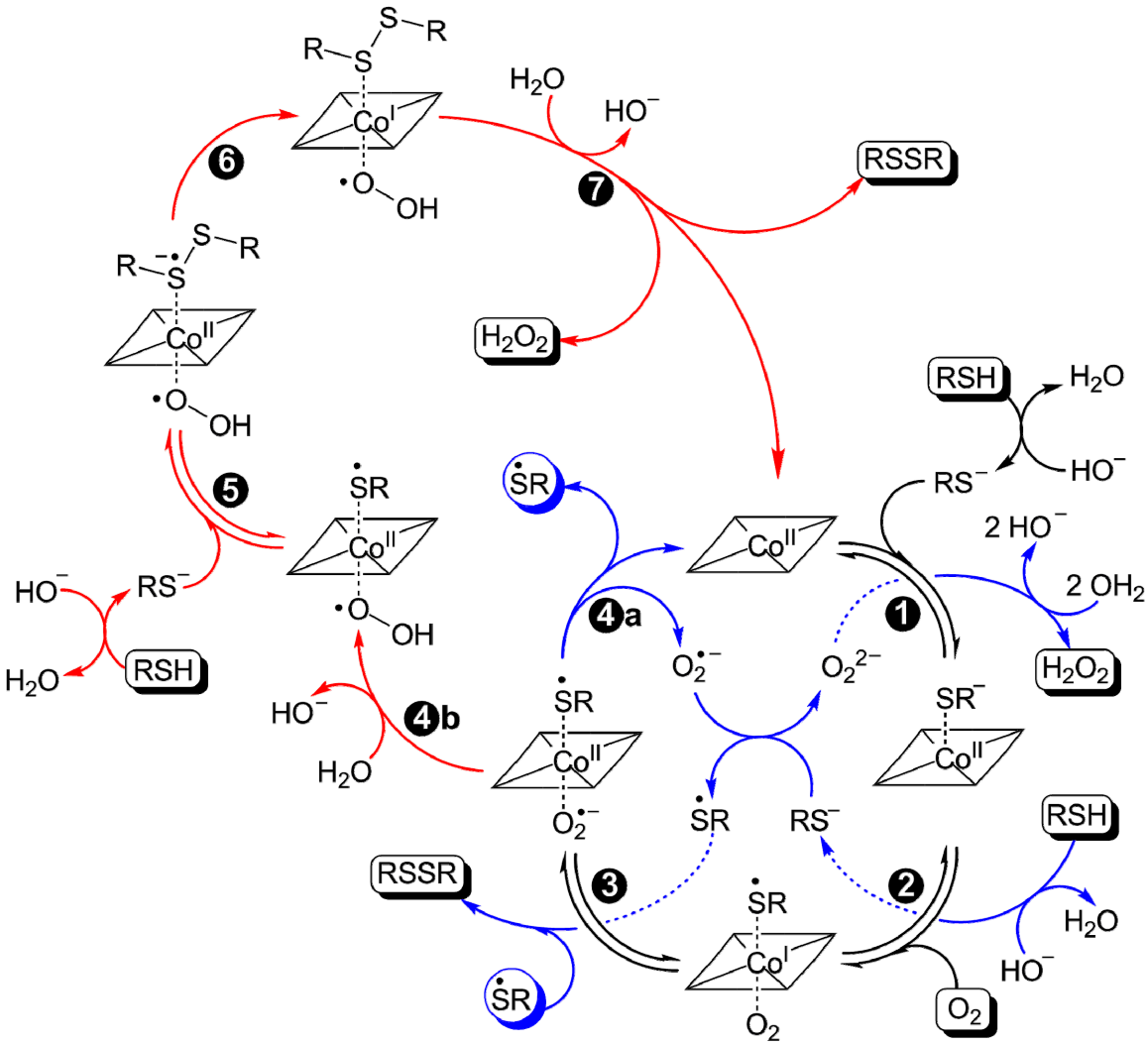

Figure 6.1 Catalytic cycle of the homogeneous aerobic mercaptan autooxidation catalyzed by cobalt(II) phthalocyanines. Dashed bonds indicate coordinative interactions. Reactant and product molecules are highlighted by shadowed boxes.

The catalytic cycle of Figure 6.1 assembles information from several literature sources[155,161,169] into a unitary picture of both possible peroxide formation routes. The blue arrows are specific for the shorter cycle of O_2^{2-} formation in solution from $O_2^{\bullet-}$ expelled from the Co center, concomitantly with a second $RS^{\bullet}$ radical. The longer cycle represented by red arrows describes a possible O_2^{2-} formation by a second electron transfer through the metal catalyst from a disulfide radical anion. The initial three steps, shown in black arrows, are common to both pathways. Alternatively, a variation of the "red" cycle is possible, in which the $RS^{\bullet}$ departs in solution, followed by coordination of a new RS^{-} with the $O_2^{\bullet-}$ superoxide still attached to the Co center. Both catalytic cycles of Figure 6.1 satisfy the prescribed stoichiometry of eqns. 6.2 and 6.3 for basic pH values. The final H_2O_2 product of each route further oxidizes two additional RSH molecules in solution, not involving the catalytic metal.

For consistency in discussing the results of this study, the shorter route described by steps 1–4a in Figure 6.1 will be considered throughout the end of this chapter, as detailed by eqns. 6.6–6.9 below. In essence, any or several of these steps could be rate determining, even the presumably fast ternary breakdown of eqn. 6.9. The weighting of each phase in the observed overall rate of transformation depends on the thiol's basicity, Lewis acidity of the Co atom and steric features of the RSH/PcCo substrate/catalyst pair.

$$RS^{-} + PcCo(II) \rightleftharpoons RS^{-}\text{–}PcCo(II) \qquad (6.6)$$

$$RS^{-}\text{–}PcCo(II) \rightleftharpoons RS^{\bullet}\text{–}PcCo(I) \qquad (6.7a)$$

$$RS^{\bullet}\text{–}PcCo(I) + O_2 \rightleftharpoons RS^{\bullet}\text{–}PcCo(I)\text{–}O_2 \qquad (6.7b)$$

$$RS^{\bullet}\text{–}PcCo(I)\text{–}O_2 \rightleftharpoons RS^{\bullet}\text{–}PcCo(II)\text{–}O_2^{\bullet-} \qquad (6.8)$$

$$RS^{\bullet}\text{–}PcCo(II)\text{–}O_2^{\bullet-} \longrightarrow RS^{\bullet} + PcCo(II) + O_2^{\bullet-} \qquad (6.9)$$

6.1.2 Thiol Substrates

Three thiols of gradually increasing acidity were chosen for testing the PcCo complexes' catalytic activity towards their aerobic oxidation, namely 2-mercaptoethanol (*abbr.* 2ME), 4-fluorobenzenethiol (*abbr.* 4FBT) and perfluorobenzenethiol (*abbr.* PFBT), with pK_a values of 9.2, 6.4 and 2.7, respectively.[170] The corresponding disulfide products following the relevant metal-catalyzed coupling steps are detailed in Figure 6.2. 2ME is an established standard for catalytic and photocatalytic thiol oxidation studies,[151–169] justifying its inclusion to the list as the representative of common, basic substrates; 4FBT delineates an intermediate step towards the million-fold acidity expressed by PFBT (with respect to 2ME). To the best of the author's knowledge, aerobic coupling of PFBT to its corresponding disulfide **[6-6]** has not been reported.

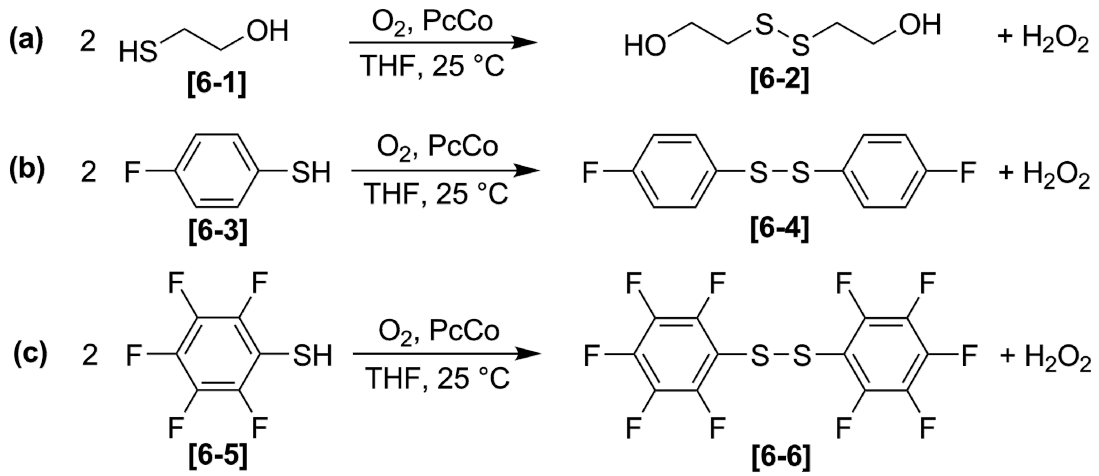

Figure 6.2 Aerobic oxidation of: (a) 2-mercaptoethanol, (b) 4-fluorobenzenethiol and (c) perfluorobenzenethiol, catalyzed by cobalt(II) phthalocyanines.

The electron-deficient fluorinated complexes of Chapters 4 and 5 may exhibit a strong thiolate binding to the Lewis-acidic Co center even when thiolates of poor basicity (obtained via highly acidic thiols) are employed. The three substrates above allow for the verification of this hypothesis.

6.2 Experimental Section

Sodium hydroxide, 2-mercaptoethanol, 2-hydroxyethyl disulfide, 4-fluorobenzenethiol, perfluorobenzenethiol, cobalt(II) phthalocyanine (H_{16}PcCo) and cobalt(II) hexadeca-fluorophthalocyanine (F_{16}PcCo **[5-7]**) were purchased from commercial sources and used as received. THF used as solvent for the catalytic oxidations was 99.5% purity, stabilized, kept extra dry under molecular sieves, sealed with a septum cap and used fresh as received. F_{64}PcCo **[5-9]** was prepared according to a published literature procedure.[106] $F_{24}H_8$PcCo **[4-6]**, $F_{28}H_4$PcCo **[4-15]**, F_{34}PcCo **[5-11]** and F_{52}PcCo **[5-13]** were prepared as described under Sections 4.2.5, 4.2.14 and 5.2.3 of this work, respectively. Milligram amounts of analytically pure F_{52A}PcCo **[5-17]** were provided by Mr. Hemantbhai Patel.* All THF solutions of the catalysts used for oxidation reactions were prepared fresh before use, using materials oven-dried (150 °C) to constant weight.

Oxidation reactions were performed in 100 mL double-walled jacketed glass vessels, using an in-house apparatus (Figure 2.1). The procedure for each reaction strictly followed the experimental conditions described in Section 2.8. In all cases, 7.1 mmol of the thiol were reacted in 50 mL of basic THF catalyst solution at 25 °C under a saturated O_2 atmosphere, achieved by 10 min purge cycles. The system was sealed and recording of oxygen consumption was started immediately after the thiol was injected to the reaction vessel and the internal pressure of the system was equalized to ambient values, as indicated by the mercury manometric switch; any initially accumulated overpressure was released by quickly purging it through a Teflon stopcock. Keeping a constant molar amount of thiol, the maximum theoretical O_2 consumption at 25 °C is limited to 43.4 mL, according to the 4:1 overall stoichiometry of eqn. 6.1.

* Patel, H. H. New Jersey Institute of Technology, Newark, NJ. Personal communication, 2011.

Table 6.1 describes several control experiments, performed in order to calibrate the equipment and test its reliability and accuracy. The lack of O_2 consumption for all catalytic experiments performed without addition of 2ME confirms the solvent's stability under the reaction conditions. No appreciable difference in the consumption rates was noticed when the PcCo-catalyzed mixtures were illuminated;‡ therefore, all reactions were performed under ambient light. To ensure reproducibility, catalytic oxidation reactions were repeated at least twice for a given substrate/catalyst pair. For results within 10% difference, the data set showing the highest oxygen consumption values was chosen for further processing. Discrepancies above 15% between data sets were investigated by equipment calibration with a standard 2ME/F_{64}PcCo trial, followed by a re-run of the initial reaction until agreement between data sets was reached.

Table 6.1 Control Experiments for the Catalytic Autooxidation of Thiols†

Entry	Thiol	Catalyst	Atmosphere	Illuminated‡	Gas Consumption
1	-	-	O_2	No	No
2	-	-	N_2	No	No
3	-	-	O_2	Yes	No
4	-	-	N_2	Yes	No
5	-	F_{64}PcCo 10 μM	O_2	No	No
6	-	F_{64}PcCo 10 μM	N_2	No	No
7	-	F_{64}PcCo 10 μM	O_2	Yes	No
8	-	F_{64}PcCo 10 μM	N_2	Yes	No
9	0.5 mL 2ME	F_{64}PcZn 10 μM	O_2	In the dark	No
10	0.5 mL 2ME	-	N_2	No	No
11	0.5 mL 2ME	-	N_2	Yes	No
12	0.5 mL 2ME	-	O_2	No	Yes*

† All experiments performed at 25 °C in basic THF solutions (50 mL THF + 1 mL NaOH 0.25% aq.) for 5 h.

‡ Illumination was achieved with a 300 W visible light halogen lamp, creating an intensity of 4.6±0.1 × 10^5 lux, measured at the outer wall of the reaction vessel. Otherwise, all reactions involving PcCo catalysts were performed under ambient light.

* Non-catalyzed aerobic autooxidations of 2ME and the other thiols employed have shown weak to appreciable oxygen consumption and are described in the results and discussion sections.

6.3 Catalyzed Autooxidation of 2-Mercaptoethanol

6.3.1 Oxygen Consumption and Process Parameters

Oxygen consumption over time data, recorded for the catalyzed autooxidation of 2ME in basic THF using the new fluoroalkylated PcCo complexes are presented in Figure 6.3. Additional data collected for the H_{16}PcCo, F_{16}PcCo and F_{64}PcCo standard catalysts, as well as for the non-catalyzed transformation, are also presented for comparison. In all cases, reactions were let to proceed in the closed system for 5 h, after which catalyst stability was analyzed by UV-vis. The process parameters are summarized in Table 6.2. The maximum turnover numbers (TON_{max}) are calculated as the actual ratio $n_{substrate}/n_{catalyst}$ (μmol/μmol) present in solution.

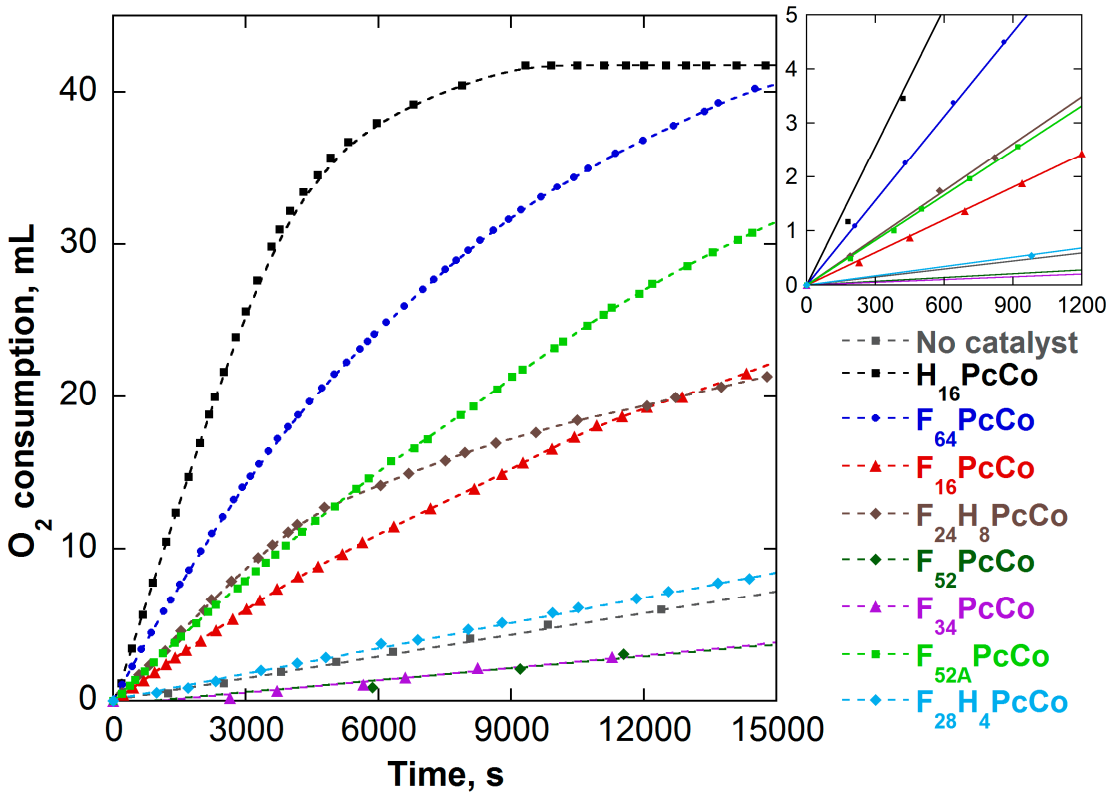

Figure 6.3 Oxygen consumption during the catalyzed autooxidation of 2-mercapto-ethanol in THF. Inset: initial reaction rates, shown as linear fits on data points recorded within the first 20 min of each reaction.

Table 6.2 Parameters of the Catalyzed Autooxidation of 2-Mercaptoethanol

Catalyst	Catalyst amount (μmol)	Stability[a] (%)	Rate[b] (μmol O_2 min^{-1})	TOF[c] (mol RSH s^{-1} mol Pc^{-1})	TON[d] (mol RSH mol Pc^{-1})	TON_{max} (mol RSH mol Pc^{-1})	$\frac{TON}{TON_{max}}$
$H_{16}PcCo$	0.53	~92	21.1	2.65	12893	13396	0.96
$F_{16}PcCo$	0.58	~90	4.9	0.56	7432	12240	0.61
$F_{24}H_8PcCo$	0.54	>99	7.1	0.88	6617	13148	0.50
$F_{28}H_4PcCo$	0.80	>99	1.5	0.12	1930	8875	0.22
$F_{34}PcCo$	0.53	>99	0.5	0.06	954	13396	0.07
$F_{52}PcCo$	0.51	>99	0.5	0.06	927	13922	0.07
$F_{52A}PcCo$	0.57	~50	6.9	0.80	9383	12456	0.75
$F_{64}PcCo$	0.49	>99	12.8	1.74	14335	14490	0.99
No catalyst	-	-	1.2	-	1165*	7100*	0.16

[a] Stability, defined as the ratio: [Q-band intensity after 5 h / Q-band initial intensity] × 100.
[b] Initial reaction rates, μmol O_2 min^{-1}, calculated as the slopes of the linear fits in the inset of Figure 6.3.
[c] Turnover frequency, mol substrate s^{-1} mol Pc^{-1}, calculated under pseudo-first order conditions with respect to RSH, using the stoichiometrically adjusted initial rate values.
[d] Turnover number after 5 h, calculated stoichiometrically as: [final O_2 volume (mL) / molar volume of O_2 at 25 °C (24.45 mL $mmol^{-1}$)] × [4000 (μmol substrate mmol O_2^{-1}) / n_{Pc} (μmol Pc)].
* For the non-catalyzed autooxidation, turnover numbers are calculated as: TON = [final recorded O_2 volume (mL) / molar volume of O_2 at 25 °C (24.45 mL $mmol^{-1}$)] × 4000 (μmol substrate mmol O_2^{-1}); $TON_{max} = n_{RSH}$ = 7100 (μmol substrate).

Figure 6.3 reveals an apparent catalytic inertness towards 2ME oxidation of the perfluorinated F_{34} and F_{52} complexes. Section 6.6 offers an interpretation of these and other catalysts' behavior in relation to the proposed mechanistic steps.

6.3.2 Reaction Products

^1H and ^{13}C NMR spectra of the reaction mixtures, the latter illustrated in Figure 6.4, prove without a doubt the exclusive formation of disulfide **[6-2]**, in accordance to the scheme of Figure 6.2. ^{13}C data are particularly informative in determining the uniqueness of the product and relative amount of untransformed 2ME, since each of the two species produce two well-spaced resonances. The direct spectral comparison of THF-evaporated mixtures following *ca*. 8 h-long transformations, with the starting material and authentic, commercially available 2-hydroxyethyl disulfide, reveals perfect matches in each case.

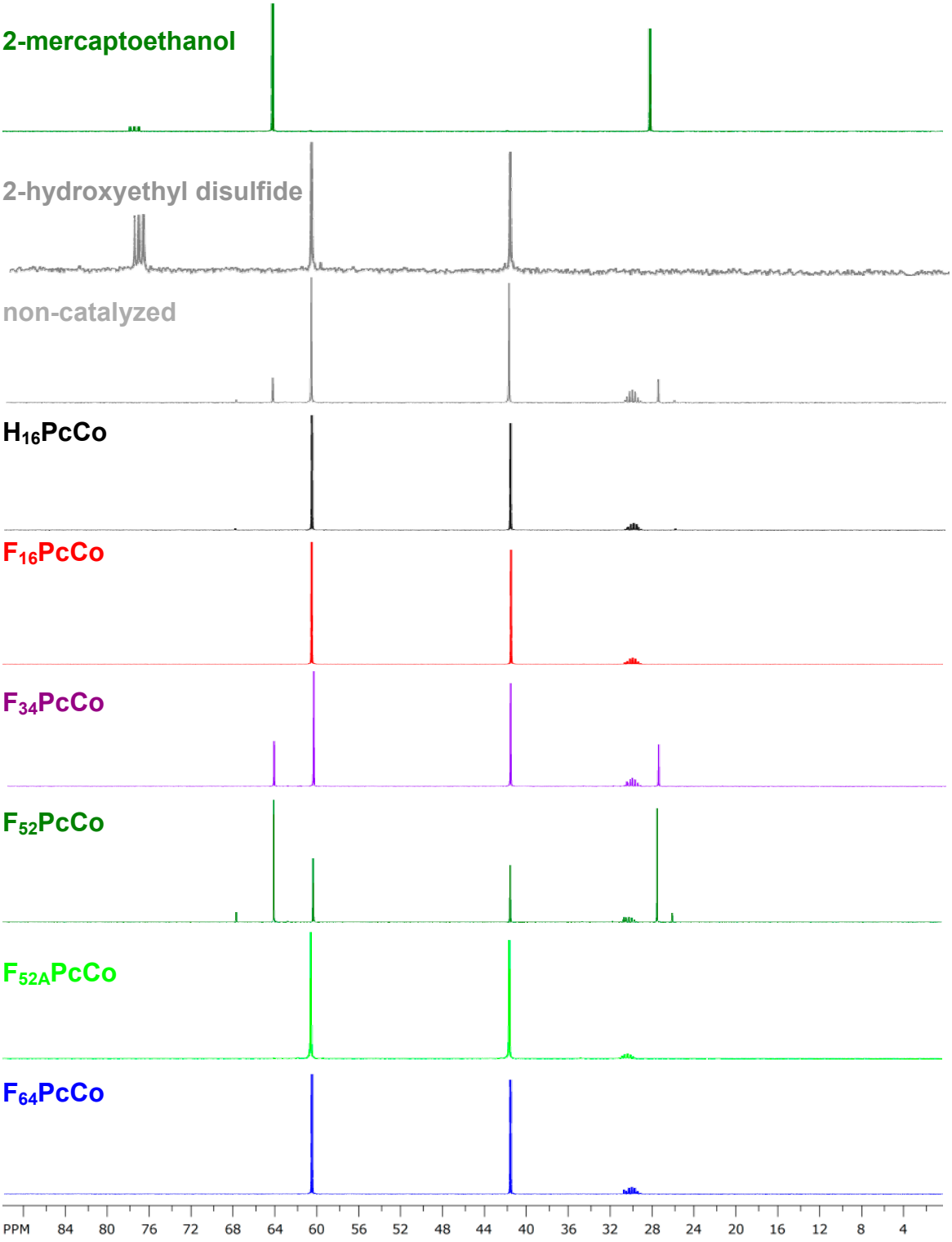

Figure 6.4 ^{13}C NMR comparison of reaction mixtures obtained in the catalyzed auto-oxidation of 2-mercaptoethanol. Spectra of 2-mercaptoethanol and 2-hydroxyethyl disulfide were recorded in $CDCl_3$, while all others were acquired in $(CD_3)_2CO$.

6.3.3 Catalyst Stability

Figure V.1 presents a UV-vis surveillance of the catalysts' stability, performed by analysis of 3 mL aliquots of the reaction mixtures. A stability vs. time plot for all complexes is shown in Figure 6.5; the dashed lines are drawn as linear or polynomial fits through the experimental points accumulated over 24 h, determined as the ratio of actual vs. initial absorbances of the main Q-bands in the spectra.

Determination of the above ratio of absorbances is complicated in some cases, viz. F_{16}PcCo and F_{34}PcCo, Figure V.1, by the constantly changing shape of the spectra over time, as a result of variable deaggregation and establishment of a concomitant PcCo(II)/PcCo(I) equilibrium in solution. In such cases, stability has been calculated using the absorbance of the most intense band identified in the spectrum at the time of the measurement.

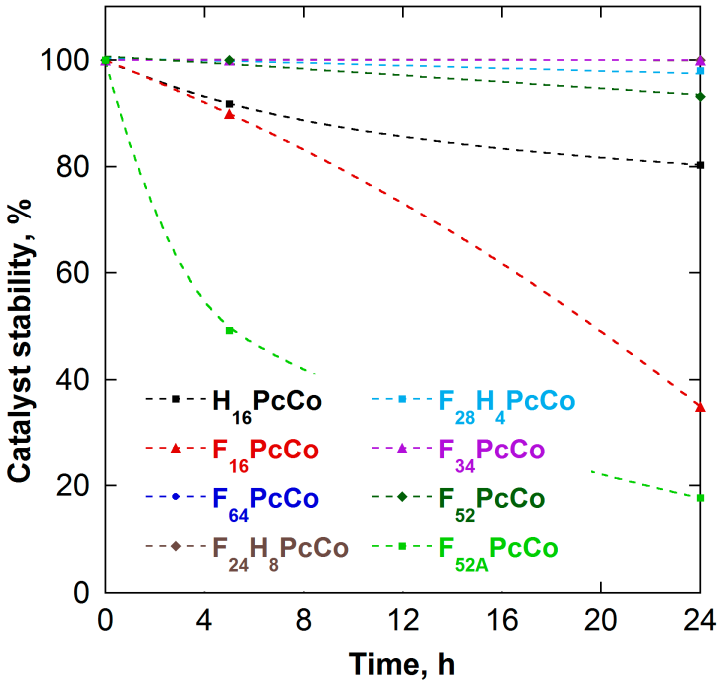

Figure 6.5 Time-dependent catalyst stability during the aerobic autooxidation of 2-mercaptoethanol in THF.

As predicted by the rational approach used in their design, stability of the new perfluoroalkylated catalysts towards chemical attacks is greatly improved with respect to the conventional H_{16} and F_{16}PcCo analogues, up to the point of complete refractoriness for the F_{64}, F_{34} and $F_{24}H_8$PcCo complexes. Negligible degradation extents of *ca.* 3 and 6% within 24 h are noticed for $F_{28}H_4$PcCo and F_{52}PcCo, respectively; values of less than 5% fall within the UV-vis method's accuracy limits and solvent evaporation effects.

The seemingly "immortal" nature of the five perfluoroalkyl-substituted catalysts under the action of highly reactive O- and S-centered radicals formed is essential for their successful application in homogeneous processes. Resistance of the scaffolds to nucleophilic and electrophilic attacks was also confirmed by the absence of degradation for at least 2 days in refluxing, basic aqueous THF, and in heated concentrated sulfuric acid, respectively. Since the aromatic F substituents and *ipso* positions of the Pc core should be more susceptible to nucleophilic attacks, as a result of the overall increased electron deficiency, the protective steric effect imparted by the *i*-C_3F_7 and CF_3 groups becomes apparent and prevalent, even more so when related to the added inertness of vulnerable aromatic protons in $F_{24}H_8$PcCo and $F_{28}H_4$PcCo.

An accelerated degradation is observed for the perfluorinated, but sterically accessible and electronically vulnerable F_{16}PcCo, which suffers a decay of *ca*. 65% over 24 h (Figure V.1), most probably due to breakdown of the Pc ring structure under the action of the strong $HOCH_2CH_2S^-$ nucleophile. The planar, non-fluorinated H_{16}PcCo is moderately stable, with roughly 80% remaining by the end of the measurements. No attempts have been made at identifying the degradation products, the focus of this study resting on the catalytic usefulness of the complexes.

One consternating result—unmistakably confirmed by five separate trials using different batches of material—is observed in the case of F_{52A}PcCo. Its degree of decomposition surpasses even the figure encountered for F_{16}PcCo, with a meager 15% left following a 24 h transformation, rendering the complex basically unusable for catalytic applications of similar composition, despite the reasonable activity it displayed during the initial reaction stage (Figure 6.3). Furthermore, the contrasting structural integrity it displayed during the coupling of the more acidic 4FBT and PFBT substrates in basic THF (effectively no decomposition up to 50 h of reaction, Figures V.2 and V.3) asks for clarifications on the reactive species responsible for its degradation.

First, a neat, 10 μM THF solution of F_{52A}PcCo is stable indefinitely—no detectable degradation was observed within two weeks by UV-vis surveillance at RT. Second, when a 100× molar excess of aqueous NaOH is added to this solution, closely reproducing the 2ME catalysis parameters, the complex is again stable (< 1% degradation over 24 h, Figure 6.6). This undoubtedly confirms that the less nucleophilic HO^- is not responsible for the extreme degradation noticed under 2ME oxidation.

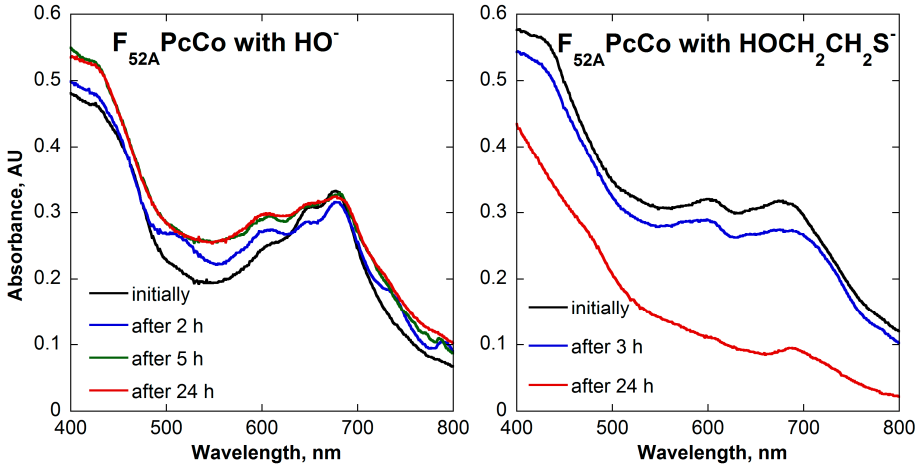

Figure 6.6 UV-vis monitored stability of F_{52A}PcCo under basic conditions. Left: 100 fold excess of HO^-. Right: 100 fold excess of 2-hydroxyethane thiolate, obtained by adding a 10^4 molar excess of 2-mercaptoethanol to the HO^- solution.

Once 2ME is added to the same NaOH solution that displayed stability up to that point, an accelerated degradation begins (Figure 6.6), reproducing the initially observed catalytic results (Figure 6.5). Thus, since all other activated oxygen species are also present in the non-degrading 4FBT and PFBT reaction mixtures, the only agent responsible for the compound's decay has to be 2-hydroxyethane thiolate, $HOCH_2CH_2S^-$, by far the strongest nucleophile of the three thiolates employed. Presumably, F_{52A}PcCo's unusual vulnerability is a result of preferential, open *ipso* attack sites of extreme electrophilicity, located on the single planar tetrafluoro-aromatic quarter of the molecule. The sterically-eased access of non-bulky $HOCH_2CH_2S^-$ nucleophilic species to these sites results in repeated, focused attacks on the unprotected part of the molecule. It is unreasonable to assume that the neutral **[6-2]** disulfide product would play any role in this decomposition. In the case of 4FBT and PFBT thiolates, their increased steric bulk and reduced nucleophilicity prevents an equally destructive attack.

6.4 Catalyzed Autooxidation of 4-Fluorobenzenethiol

6.4.1 Oxygen Consumption and Process Parameters

Plots of oxygen volumes consumed during the catalyzed autooxidation of 4FBT in basic THF for all studied PcCo complexes are presented in Figure 6.7. Reaction conditions and calculations of catalytic parameters follow the procedures described under Sections 6.2 and 6.3.1. Fast reaction rates and *quasi*-quantitative conversions of the substrate were recorded for all catalysts employed, along with a noticeably slower non-catalyzed transformation. A mechanistic interpretation of the results is given in Section 6.6.3. The process parameters are summarized in Table 6.3.

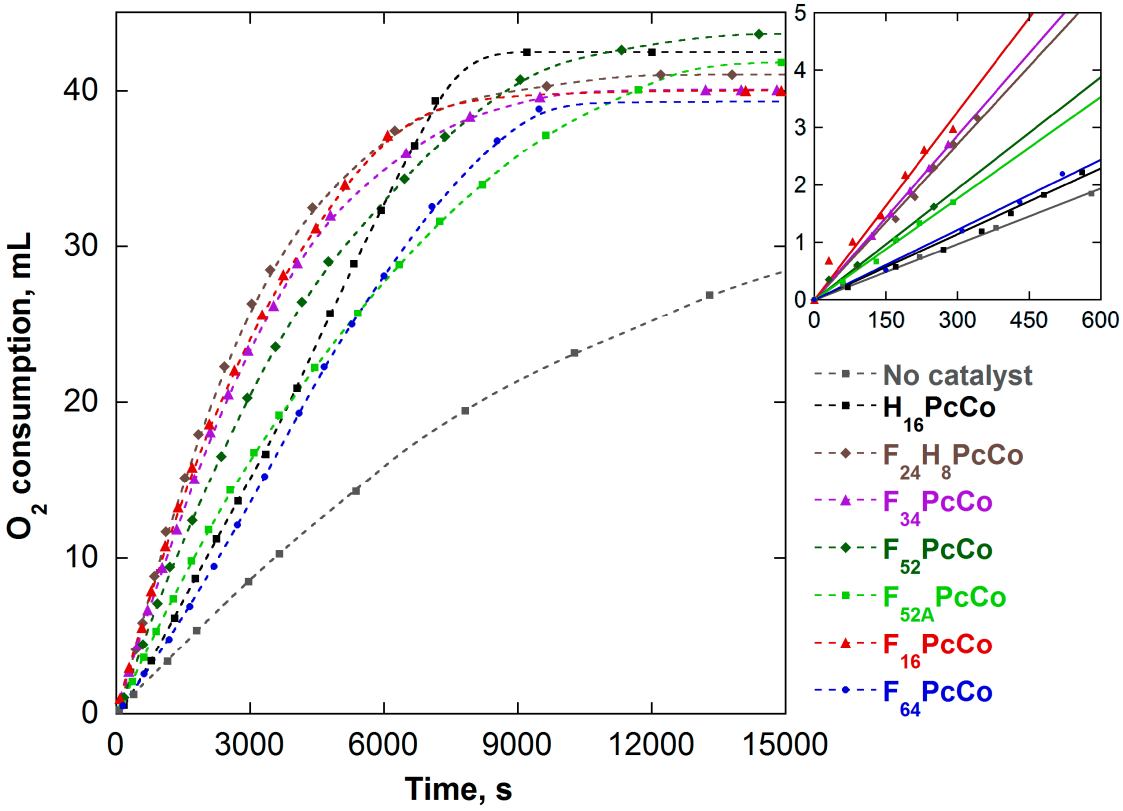

Figure 6.7 Oxygen consumption during the catalyzed autooxidation of 4-fluorobenzenethiol in THF. Inset: initial reaction rates, shown as linear fits on data points recorded within the first 10 min of each reaction.

Table 6.3 Parameters of the Catalyzed Autooxidation of 4-Fluorobenzenethiol

Catalyst	Catalyst amount (μmol)	Stability[a] (%)	Rate[b] (μmol O_2 min^{-1})	TOF[c] (mol RSH s^{-1} mol Pc^{-1})	TON[d] (mol RSH mol Pc^{-1})	TON_{max} (mol RSH mol Pc^{-1})	$\frac{TON}{TON_{max}}$
$H_{16}PcCo$	0.53	~95	9.3	1.17	13113	13396	0.98
$F_{16}PcCo$	0.58	>99	26.8	3.07	11290	12240	0.92
$F_{24}H_8PcCo$	0.54	>99	22.3	2.76	12430	13148	0.95
$F_{34}PcCo$	0.53	>99	23.6	2.96	12372	13396	0.92
$F_{52}PcCo$	0.51	>99	16.0	2.09	13996	14200	0.99
$F_{52A}PcCo$	0.51	>99	14.5	1.89	13415	13922	0.96
$F_{64}PcCo$	0.49	>99	10.1	1.37	13128	14490	0.91
No catalyst	-	-	7.9	-	4915*	7100*	0.69

[a] Stability, defined as the ratio: [Q-band intensity after 5 h / Q-band initial intensity] × 100.
[b] Initial reaction rates, μmol O_2 min^{-1}, calculated as the slopes of the linear fits in the inset of Figure 6.7.
[c] Turnover frequency, mol substrate s^{-1} mol Pc^{-1}, calculated under pseudo-first order conditions with respect to RSH, using the stoichiometrically adjusted initial rate values.
[d] Turnover number after 5 h, calculated stoichiometrically as: [final O_2 volume (mL) / molar volume of O_2 at 25 °C (24.45 mL $mmol^{-1}$)] × [4000 (μmol substrate mmol O_2^{-1}) / n_{Pc} (μmol Pc)].
* $TON_{non\text{-}catalyzed}$ = [final recorded O_2 volume (mL) / molar volume of O_2 at 25 °C (24.45 mL $mmol^{-1}$)] × 4000 (μmol substrate mmol O_2^{-1}); $TON_{max} = n_{RSH}$ = 7100 (μmol substrate).

6.4.2 Reaction Products

A comparative ^{13}C NMR examination of the reaction mixtures obtained by oxidation of 4FBT (Figure 6.8), reveals, without exception, quantitative formation of 4-fluorophenyl disulfide **[6-4]** as the only product. Its unambiguous identification is facilitated by the diagnostic C1 shift from 127.4 ppm, in 4FBT, to 132.8 ppm in the disulfide. The product's molecular symmetry is obvious in the occurrence of only five distinct resonances, the C4 signal being split in both compounds by C–F spin coupling. The complete absence of starting material in the catalyzed mixtures is entirely consistent with the maximum stoichiometric consumption of oxygen recorded for all reactions, within the experimental error of manometric detection (Figure 6.7).

6.4.3 Catalyst Stability

UV-vis surveillance of the reaction mixtures (Figure V.2) reveals imperviousness of all fluorinated catalysts employed to the attacks of radical and nucleophilic species present in the aerobically-oxidized 4FBT solutions. The non-fluorinated $H_{16}PcCo$ is decomposed in a *ca.* 28% ratio over 24 h (Figure 6.9), similar to its behavior during 2ME oxidation, probably due to a combined action of nucleophilic (HO^-) and radical (H_2O_2) degradation pathways. The highly 2ME thiolate-vulnerable $F_{52A}PcCo$ and, to a lesser extent, $F_{16}PcCo$ complexes (Figures 6.5 and 6.6) acquire complete resistance to the action of the much less nucleophilic 4FBT analogue. Although the much decreased nucleophilicity of the 4FBT thiolate should primarily account for the lack of PcCo degradation, its increased steric bulk and structural rigidity also disfavors a coordinated attack on the Pc core, coupled with an accelerated transformation rate which allows for little to no build-up of potentially destructive free radical, peroxide and thiolate species in solution.

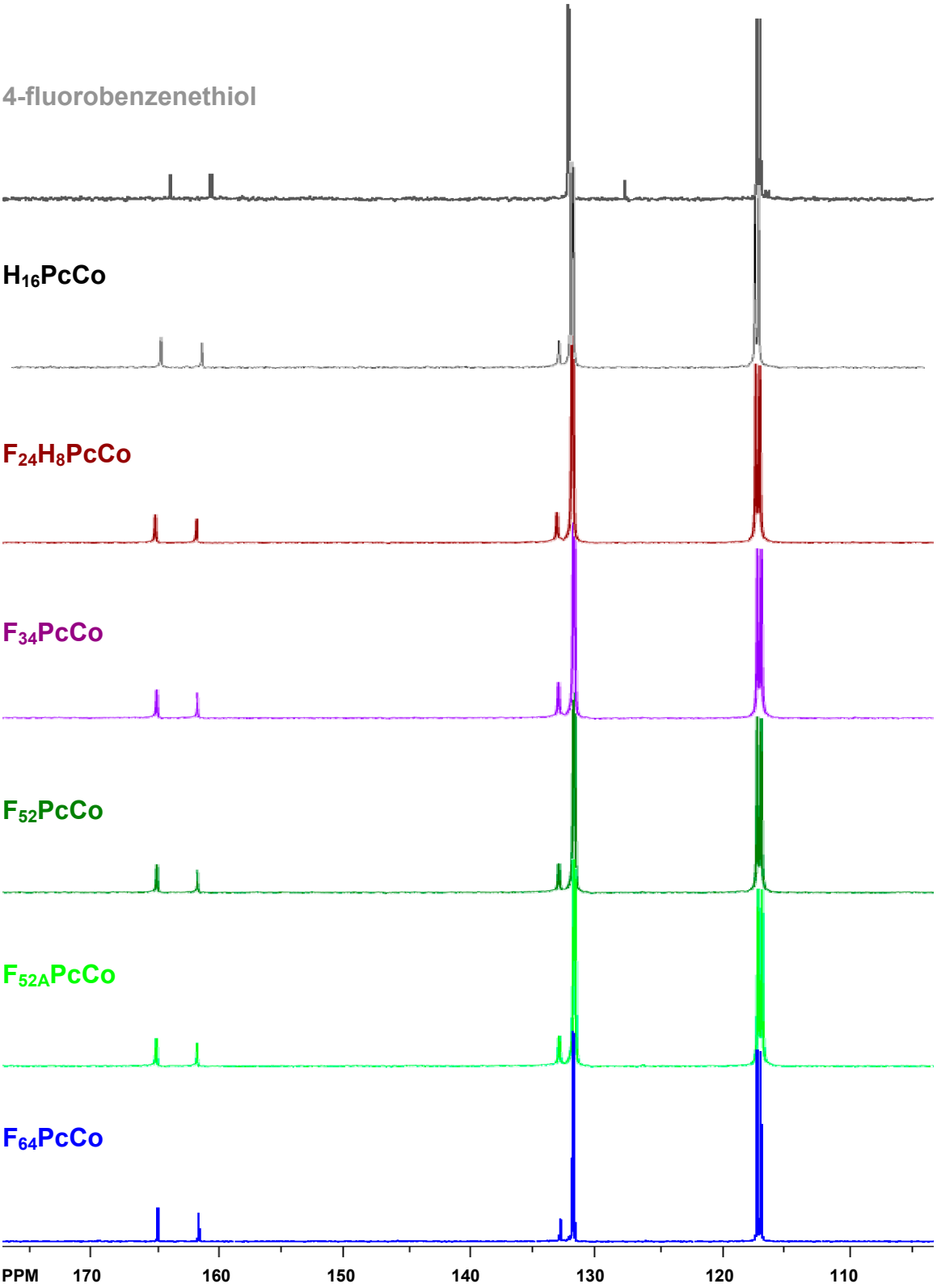

Figure 6.8 ^{13}C NMR comparison of reaction mixtures obtained in the catalyzed auto-oxidation of 4-fluorobenzenethiol, using the starting material as the reference. Spectra were acquired in $(CD_3)_2CO$.

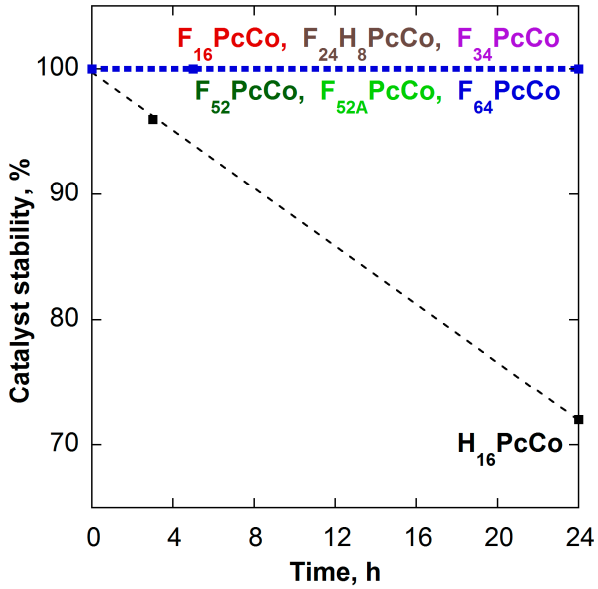

Figure 6.9 Time-dependent catalyst stability during the aerobic autooxidation of 4-fluorobenzenethiol in THF.

The plot of Figure 6.9 confirms once more the exemplary inertness of the new $(R_f)_nPcCo$ catalysts towards at least hundred-fold excess of HO^- accumulated in solution.

6.5 Catalyzed Autooxidation of Perfluorobenzenethiol

6.5.1 Oxygen Consumption and Process Parameters

Oxygen consumption curves during the catalyzed autooxidation of PFBT in basic THF for the studied PcCo complexes are presented in Figure 6.10. Table 6.4 provides a summary of the catalytic process parameters. A parallel reaction involving dimerization of the PFBT substrate through nucleophilic attacks of its thiolate, described next, complicates an accurate estimation of the catalysts' activity towards aerobic coupling and lowers the overall **[6-6]** disulfide yields observed. Basic mechanistic interpretations are discussed in Section 6.6.3.

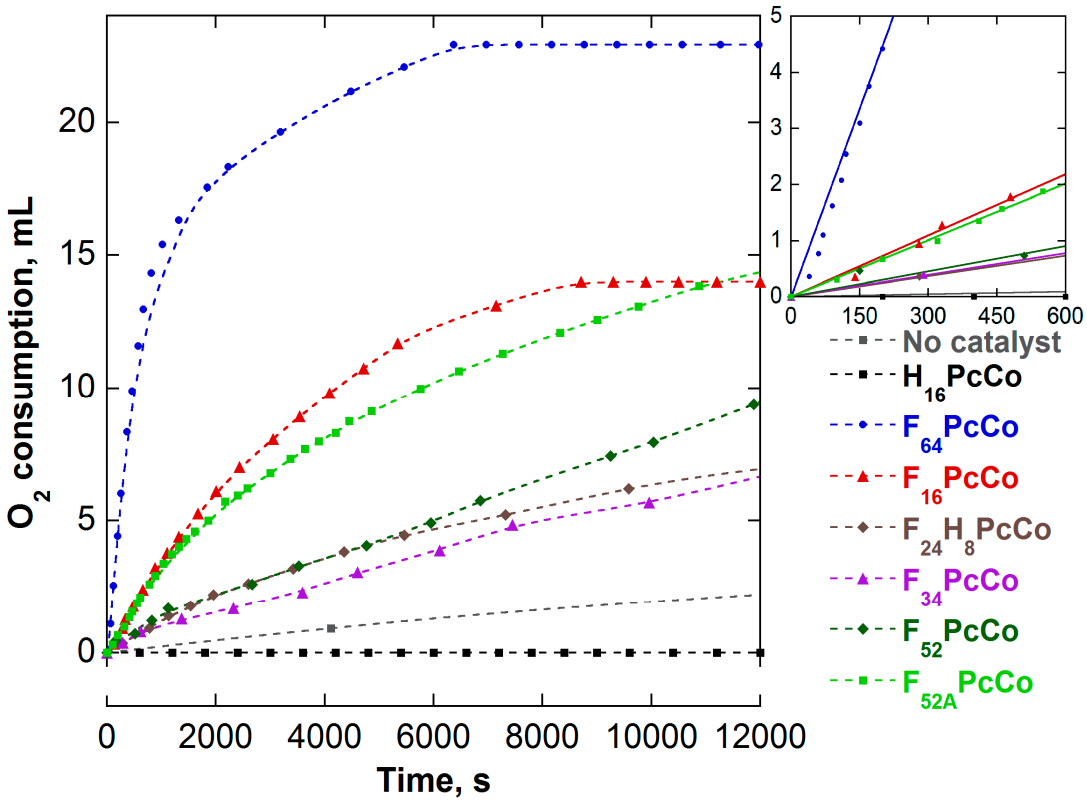

Figure 6.10 Oxygen consumption during the catalyzed autooxidation of perfluorobenzenethiol in THF. Inset: initial reaction rates, shown as linear fits on data points recorded within the first 10 min of each reaction.

Table 6.4 Parameters of the Catalyzed Autooxidation of Perfluorobenzenethiol

Catalyst	Catalyst amount (μmol)	Stability[a] (%)	Rate[b] (μmol O_2 min^{-1})	TOF[c] (mol RSH s^{-1} mol Pc^{-1})	TON[d] (mol RSH mol Pc^{-1})	TON_{max} (mol RSH mol Pc^{-1})	$\frac{TON}{TON_{max}}$
$H_{16}PcCo$	0.53	>99	0.0	0.00	0	13396	0.00
$F_{16}PcCo$	0.58	>99	8.8	1.02	3952	12240	0.32
$F_{24}H_8PcCo$	0.54	>99	2.9	0.36	2578	13150	0.20
$F_{34}PcCo$	0.53	>99	3.2	0.40	2997	13396	0.22
$F_{52}PcCo$	0.51	>99	3.7	0.48	4250	13920	0.31
$F_{52A}PcCo$	0.75	>99	8.3	0.74	3905	9470	0.41
$F_{64}PcCo$	0.49	>99	55.0	7.48	7652	14490	0.53
No catalyst	-	-	0.5	-	437*	7100*	0.06

[a] Stability, defined as the ratio: [Q-band intensity after 5 h / Q-band initial intensity] × 100.
[b] Initial reaction rates, μmol O_2 min^{-1}, calculated as the slopes of the linear fits in the inset of Figure 6.10.
[c] Turnover frequency, mol substrate s^{-1} mol Pc^{-1}, calculated under pseudo-first order conditions with respect to RSH, using the stoichiometrically adjusted initial rate values.
[d] Turnover number after 5 h, calculated stoichiometrically as: [final O_2 volume (mL) / molar volume of O_2 at 25 °C (24.45 mL $mmol^{-1}$)] × [4000 (μmol substrate mmol O_2^{-1}) / n_{Pc} (μmol Pc)].
* $TON_{non\text{-}catalyzed}$ = [final recorded O_2 volume (mL) / molar volume of O_2 at 25 °C (24.45 mL $mmol^{-1}$)] × 4000 (μmol substrate mmol O_2^{-1}); $TON_{max} = n_{RSH}$ = 7100 (μmol substrate).

6.5.2 Reaction Products

The aromatic SN2-driven dimerization of PFBT to the **[6-7]** thioether-thiol of Figure 6.11 was earlier reported under basic conditions;[171] however, its aerobic coupling to the **[6-6]** disulfide, Figure 6.2, has not been reported.

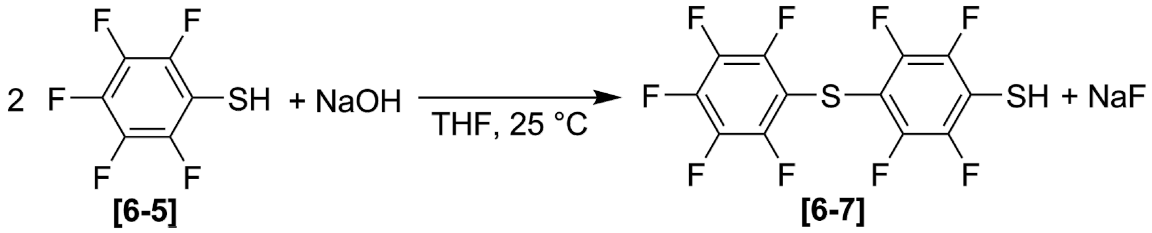

Figure 6.11 Nucleophilic dimerization of perfluorobenzenethiol in basic media.

Perfluorobenzenethiolate, $C_6F_5S^-$, although the weakest base of the three thiols studied, seems to be a good enough nucleophile to perform the intermolecular SN2 reaction of Figure 6.11, aided by the enhanced electron deficiency of the *para* substitution site as a result of combined $-I$ effects from the 5 Ar-F atoms. Large amounts of **[6-7]** thioether substitution product are identified in all ^{19}F NMR spectra of the reaction mixtures, Figure 6.12, confirming the appreciable rate of this side reaction, along with formation of higher order oligomers by subsequent *para* attacks, which show as several unassigned minor resonances. The competitive SN2 side reactions greatly limit the amount of available monomeric thiolate for aerobic coupling, as evidenced by the much lower O_2 consumption volumes recorded compared to, e.g., 4FBT. The relative ratios of the products in the final mixture are difficult to determine by integration of the ^{19}F resonances, due to major differences in solubilities of the disulfide **[6-6]** and thioether-thiol **[6-7]** formed; most of **[6-7]** precipitates as a white solid out of the initial THF solution and can only be re-dissolved in hot acetone.

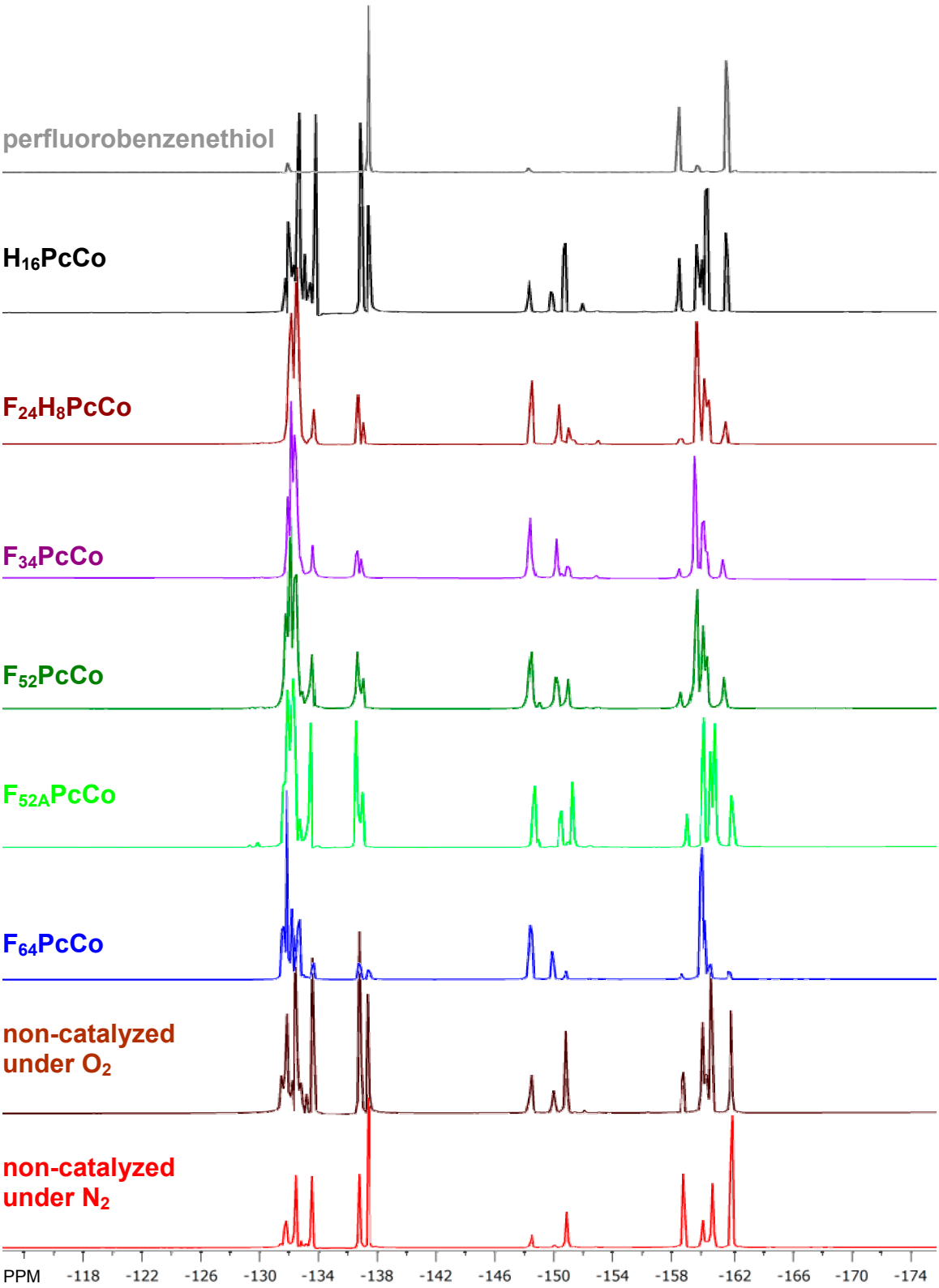

Figure 6.12 ^{19}F NMR comparison of reaction mixtures obtained in the catalyzed auto-oxidation of perfluorobenzenethiol. Spectra were acquired in $CDCl_3$ (for the reference substrate and non-catalyzed runs) and $(CD_3)_2CO$ (all others).

The assigned chemical shifts for the three major species of the ^{19}F spectra acquired in $(CD_3)_2CO$ are as follows: **[6-5]**: δ −138.7 (2F, s, *m-F*), −161.1 (1F, s, *p-F*), −164.1 (2F, s, *o-F*); **[6-6]**: δ −133.5 (4F, s, *m-F*), −150.5 (2F, s, *p-F*), −162.2 (4F, s, *o-F*); **[6-7]**: δ −133.9 (2F, s), −135.1 (2F, s), −138.3 (2F, s), −153.2 (1F, s, *p-F*), −162.9 (2F, s, *o-F*).

6.5.3 Catalyst Stability

All PcCo complexes used for catalysis of PFBT aerobic coupling, this time H_{16}PcCo including, displayed once again ideal stability towards the nucleophiles and radicals present. As the UV-vis monitored reactions show (Figure V.3), no detectable catalyst degradation was observed up to the end of the 24 h aerobic stirring of the mixtures. The apparent inertness of H_{16}PcCo is intriguing, but can be explained, as for the other catalysts, by considering the poor basicity, extreme bulkiness and structural rigidity of the substrate and SN2 products formed, which consume all available HO^- from solution without formation of disulfide (Figure 6.10). With no activated oxygen species present either, since no reduction of O_2 occurs, there are no more reactive species left in solution to attempt degradation of the H_{16}Pc ring. Thus, its catalytic inactivity actually protects it from decay by favoring the parallel substitution reaction.

6.6 Discussion

6.6.1 Steric and Electrochemical Premises

Two of the potentially rate determining steps (*abbr.* r.d.s.) of the thiol aerobic oxidation catalytic cycle using PcCos, Figure 6.1, involve changes in the metal's oxidation state, viz. a reduction from Co(II) to Co(I) (eqn. 6.7a), followed by reoxidation to the initial −2

state by one-electron reduction of coordinated O_2 (eqn. 6.8). As such, the electronic and, maybe, steric influences exerted by both fluorinated and non-fluorinated Pc ligands in stabilizing one oxidation state over the other become crucial for a complete understanding of the overall mechanism and interpretation of kinetic parameters obtained.

From an electronic point of view, stabilization of Co(I) is desired. Overstabilization, however, could hinder the reoxidation step to Co(II), eqn. 6.8, and thus the catalytic process. A Sabatier plot of the rates of electrocatalytic oxidation of 2ME vs. the PcCo(II)/Co(I) reduction potentials exhibits a negative slope,[172] indicating that the reoxidation to Co(II) is the r.d.s. In turn, the corresponding potentials, $E°'_{Co(II)/Co(I)}$, linearly correlate with the sum of PcCo substituents' Hammett constants,[131] $\Sigma\sigma$, as shown by the plot of Figure 6.13(a).[173] Previous to the determination of $E°'$ for F_{64}PcCo,[51] F_{16}PcCo was the low-rate extreme, owing to F-induced stabilization of Co(I).

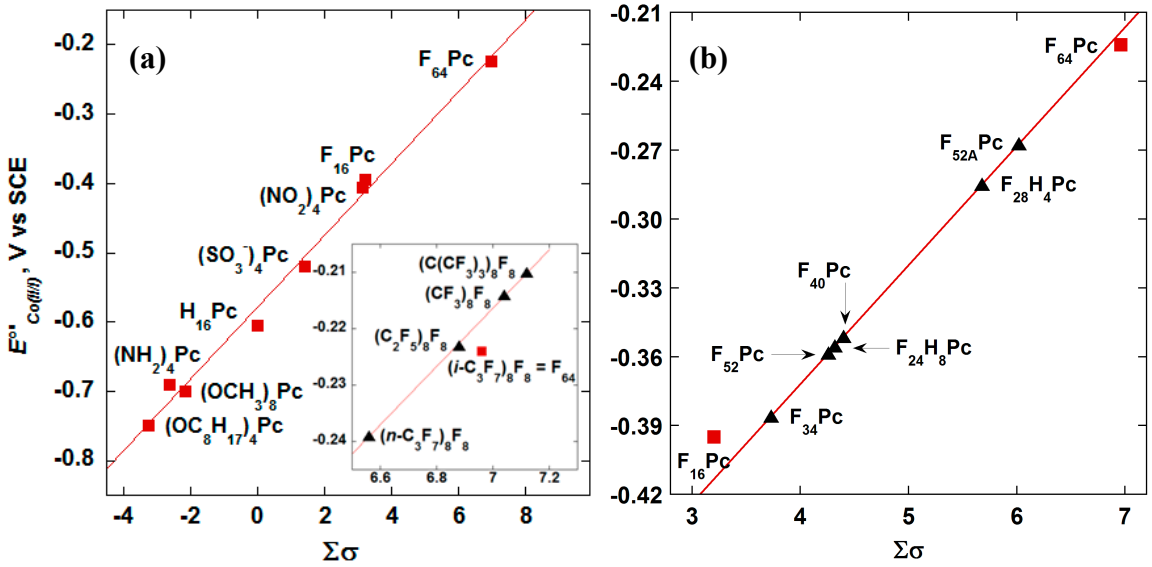

Figure 6.13 (a) Plot of selected PcCo(II)/Co(I) reduction potentials vs. the sum of substituents' Hammett constants, $\Sigma\sigma$.[173] Linear correlation: $y = -0.579 + 0.0518x$, $R = 0.9955$. Inset: calculated reduction potentials for hypothetical, symmetric $(R_f)_8F_8$PcCos with substituents of known Hammett constants.[131] (b) Plot of calculated reduction potentials for the new $(R_f)_n$PcCo complexes vs. $\Sigma\sigma$, using the correlation equation of Figure 6.13(a). The F_{16} and F_{64} experimental points are shown as red squares.

The strong experimental correlation of Figure 6.13(a) establishes $F_{64}Pc$ as the new extreme of electronic deficiency. Meanwhile, the predicted reduction potentials for the new perfluoroalkylated complexes, based on the correlation equation (Figure 6.13(b)), suggest intermediate levels of catalytic activity between the F_{16} and F_{64} standards, translating into gradually lower thiol oxidation rates down to the level of, perhaps, catalytic inhibition due to a too stable Co(I) form. In calculation of $\Sigma\sigma$ for all PcM complexes, the method proposed by Lever[174] was adopted, in which peripheral substituents are treated as *para* and assigned σ_p values, while axial ones are treated as *meta*.

The published data presented above conclude, on electronic grounds, that highly deficient ligands should stabilize lower Co oxidation states. In order to verify if steric factors induce a similar (or opposite) effect, a statistical X-ray analysis[60] was performed on all reported Co porphyrins and Pcs solid-state structures, indicating that Co deviates by less than 0.1 Å from the ligand's N_4-coordination plane, regardless of its oxidation state (I, II or III) or coordination number.[173] For Pc ligands, the mean <Co–N> distances when all Co(II) and Co(III) complexes are considered amount to a 1.927±0.003 Å avg. For the only PcCo(I) complex whose X-ray structure has been reported,[175] the <Co–N> distance is 1.896 Å. Shortening of <Co–N> upon reduction to Co(I) by 0.035 Å is identical for both porphyrins and Pcs. The mean <Co(II)–N> distance in F_{64}PcCo, 1.926 Å,[106] is typical for both Co(II) and Co(III) and, thus, Co(I) is not favored by the extreme bulk of the ligand. Taken together, the X-ray data suggest neither a structural hindrance for oxidation of Co(II) to Co(III), nor a preference for the reduction to Co(I).[173]

Consistent with the view that Ar-F replacement with R_f groups stabilizes the lower Co(I) oxidation state, chemical reduction of F_{64}PcCo occurs easily at the metal

center in the presence of HO^- ions, in a clean $F_{64}Pc(-2)Co(II) \leftrightarrow F_{64}Pc(-2)Co(I)$ process, as indicated by the presence of isosbestic points and the increase of the 710 nm Q-band of the Co(I) complex at the expense of the 670 nm Q-band of the Co(II) one, Figure 6.14(a). Addition of HCl completely reverses the reduction. In contrast, the reduction of the Zn analogue under identical conditions, Figure 6.14(b), is, as expected, a Pc ligand-centered process: $F_{64}Pc(-2)Zn(II) \leftrightarrow F_{64}Pc(-3)Zn(II)$.[173] As a side note, the ease of reducing Co(II) was later confirmed for all other perfluorinated complexes by diagnostic $(R_f)_nPc(-2)Co(I)$ electronic transitions in UV-vis spectra of the reaction mixtures acquired under the reducing action of the thiolate anions (Appendix V).

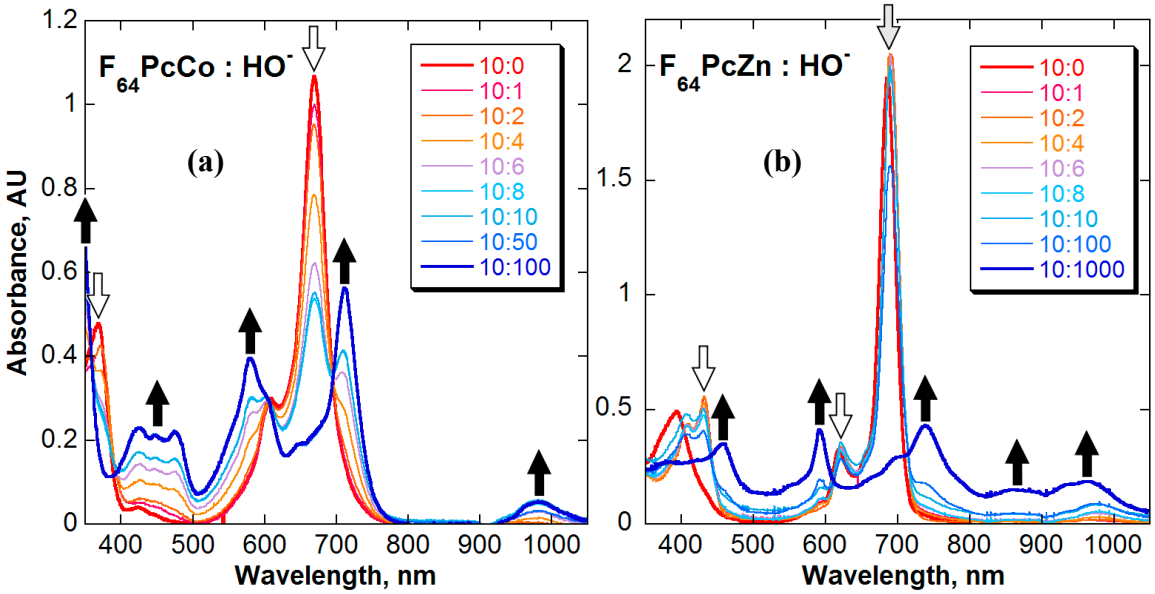

Figure 6.14 (a) Metal-centered chemical reduction of $F_{64}PcCo$ in THF by UV-vis titration with an aqueous NaOH solution. (b) Ligand-centered chemical reduction of $F_{64}PcZn$ in THF under similar conditions to (a), manifested in the broad Pc(−3) radical-specific bands between 800 and 1000 nm.

While the $(R_f)_nPcCos$ studied herein could function as redox catalysts for 2ME aerobic oxidation according to the mechanistic steps of eqns. 6.6–6.9, all factors considered through previously published observations, *vide supra*, rendered their activity

far from certain before the start of these experiments. Additional barriers to catalysis could be presented by strong S–Co thiolate bonding, eqn. 6.6, favored by the R_f-induced high Lewis acidity of the metal and the soft nature of both low-valence Co(II) and 2ME thiolate ions.[173] At least, one would have expected a much lower rate for the F_{64}PcCo-catalyzed reaction, the electron-deficient extreme, than for the F_{16} analogue.

Eventually, the entire family of fluoro-perfluoroalkyl catalysts, known and new alike, displayed catalytic ability towards aerobic coupling of all three substrates studied, with generally moderate to fast transformation rates, relieving the initial concerns about a possible lack of their reactivity. This section details a breakdown of the catalytic data previously presented—viz. oxygen consumption and process parameters, Sections 6.3.1, 6.4.1 and 6.5.1, respectively—with comments on particular results encountered for each substrate and discussion of the postulated mechanistically relevant steps leading to them.

Common features for all substrates have to be mentioned first. The initial reaction rates (*abbr.* r_0), in μmol O_2 min^{-1}, were determined in all cases as the slopes of linear fits through the O_2 consumption data points recorded within the first 20 (for 2ME) or 10 min (for 4FBT and PFBT). Time-linear dependencies of the volumes of oxygen gas consumed within the first *ca.* 60 min of each catalyzed reaction are indicative of zero-order general kinetic rate laws with respect to the thiolate concentration, as established previously for both homogeneous and heterogeneous mercaptan oxidation systems.[155]

Partial catalyst deactivation is noticed in the later stages of the transformations through deviations from linearity of the oxygen consumption plots for, e.g., 2ME (Figure 6.3). These set in at earlier times for less active catalysts and become more pronounced as the substrate concentration nears zero values. Similar curvatures appear in the

analogue plots for the 4FBT and PFBT substrates, Figures 6.7 and 6.10, respectively. Several possible deactivation pathways have been investigated, including poisoning of the catalyst by traces of sulfur oxo-acids generated by H_2O_2,[153] competitive binding of the disulfide product to the metal active site,[155] and formation of μ-peroxo-bridged PcCo dimers.[167] The latter becomes a significant problem for planar ligands favoring solution aggregation and can be overcome by site-isolation in heterogeneous catalysts or addition of bulky peripheral groups. All above considered, the deviations observed for the data sets presented herein do not constitute an exception and may be due to a combination of all deactivation pathways. Further investigations in this respect were not attempted.

6.6.2 Catalysis of the Aerobic Oxidation of 2-Mercaptoethanol

The aerobic coupling of 2ME **[6-1]** to its disulfide **[6-2]** occurs quantitatively within the first 5 h of reaction only for the H_{16} and F_{64}PcCo catalysts. The reaction rates are significantly lower for the other catalysts, down to the point of near-inhibition for F_{34} and F_{52}PcCo. A non-catalyzed transformation also occurs. The calculated r_0 values, Table 6.2, are partly incongruent with the variation of the experimental and predicted reduction potentials, Figure 6.13. For instance, the calculated F_{16}PcCo/H_{16}PcCo r_0 ratio based on reduction potentials is 0.16, not too far from the observed value of 0.24, given the radically different types of experiments. The greatest discrepancy is displayed by F_{64}PcCo, supposedly a less efficient catalyst relative to F_{16}PcCo; yet its rate is 20 times higher than expected, exceeding that of the latter by a factor of 2. Since the sum of Hammett constants for all three complexes account well for the linear correlation of the redox potentials, the reason for this inconsistency, and the additional significantly accelerated rates of $F_{24}H_8$PcCo and F_{52A}PcCo, is less likely to be purely electronic.

Possible explanations for the enhanced rates of $F_{64}Pc$,[173] $F_{24}H_8Pc$ and $F_{52A}PcCo$ catalysts include: (i) additional steric repulsion leading to an accelerated departure of the thyil radical from the active site, (ii) a supplemental decrease in the polarizability of Co^{2+} due to the R_f groups that render it "harder" and thus less likely to coordinate neutral S-radicals, (iii) hydrophobic preference for neutral ($RS^{\bullet}$) over charged (RS^{-}) species in the immediate fluorinated catalytic environment. In addition, the steric crowding around the Co active site could destabilize the ternary $RS^{\bullet}$–PcCo(I)–$O_2^{\bullet-}$ intermediate of eqn. 6.8, the sp^3 S-hybridization forcing the thiolate backbone too close to the R_f groups. This destabilization vanishes upon electron transfer and departure of the resulting thyil radical.

2ME is a basic substrate, $pK_a = 9.2$,[170] and its conjugated thiolate is an even better electron donor. Its compact aliphatic structure containing only four sp^3 atoms makes it highly flexible in approaching the catalytic site. Thus, the initial mechanistic steps of RS^{-} binding and electron transfer to the Co center, eqns. 6.6 and 6.7, should occur with no steric or electronic impediments, even for electron-rich catalysts such as $H_{16}PcCo$, as the highest 2ME oxidation rate observed for the latter suggests. The entirety of catalytic data collected in Table 6.2 propose the Co(I)/Co(II) reoxidation by coordinated O_2 (eqn. 6.8) as the r.d.s., with the above three exceptions attributed mostly to steric reasons facilitating the radical's expulsion from the active site, eqn. 6.9. As the steric bulk of the catalyst's R_f substituents decreases, so does its catalytic activity. A totally (planar) or partially (asymmetric) sterically-relaxed fluorinated ligand actually becomes detrimental for aerobic catalysis of highly basic substrates, such as 2ME, by promoting a strong Co–S binding and overstabilizing the Co(I) species and considerably slowing the reoxidation step. The overall process is thus hindered. This hypothesis is demonstrated by the apparent catalytic inactivity manifested by $F_{28}H_4$, F_{34} and $F_{52}PcCo$.

6.6.3 Catalysis of the Aerobic Oxidation of 4-Fluorobenzenethiol and Perfluorobenzenethiol

6.6.3.1 4-Fluorobenzenethiol. Efficient binding of 4FBT by all PcCo catalysts is obvious in the expedited rates and quantitative transformations observed (Figure 6.7, Table 6.3). A marked increase in catalytic activity, up to par with both F_{64} and H_{16}PcCo electronic and steric extremes, is exhibited by all the previously-trailing complexes of 2ME oxidation. F_{34} and F_{52}PcCo, notoriously inactive towards 2ME aerobic coupling, now display two of the fastest four initial rates recorded. Such a reverse catalytic behavior demands a careful analysis of the underlying electronic and steric reasons, attempted below in relation to the postulated mechanistic steps of eqns. 6.6–6.9.

The 4FBT thiolate is *ca.* thousand times less basic than the 2ME analogue, judging by the pK_a values of their conjugated acids.[170] Combined $-I$ withdrawing effects from the phenyl moiety and its *p*-F atom result in a poor electron donor. As such, the critical thiolate binding step, eqn. 6.6, might not occur for some catalysts, or could proceed at much slower rates. However, Figure 6.7 shows fast transformations and quantitative yields for all catalysts. The extreme electronic deficiency of the fluorinated materials and even the average Lewis acidity of the Co atom of H_{16}PcCo seem to be sufficient for securing an efficacious 4FBT thiolate coordination. Since binding of the substrate does occur, as additionally confirmed by the reduced PcCo(I) species evidenced in UV-vis spectra of the reaction mixtures (Figure V.2), supplementary explanations are required for the significant differentiation in the r_0 values obtained, Table 6.3. A reverse trend in the variation of initial reaction rates with the overall steric bulk of the fluorinated catalysts—approximated by the number of F atoms contained—becomes apparent, as r_0

values steadily decrease from 26.8 to 10.1 μmol O_2 min^{-1} for $F_{16}PcCo$ and $F_{64}PcCo$, respectively. Electron-richer $H_{16}PcCo$ displays the lowest catalyzed reaction rate of 9.3 μmol O_2 min^{-1}, only marginally better than the non-catalyzed transformation. While the highly Lewis acidic Co atoms of $(R_f)_nPcs$ definitely effect a stronger binding of 4-fluoro-benzenethiolate than the $H_{16}PcCo$ catalyst, this only accounts for the latter's lowest rate.

A primary reason for the above trend can be sought in the steric features of thiolate binding interactions. Despite favorable electronic factors, steric bumps between the incoming rigid aromatic molecule and the bulky perfluoroalkyl groups are still possible, hindering the coordination to some degree while the substrate is forced to search for the Co-binding orientation providing minimal repulsion. Thus, the initial thiolate binding step, eqn. 6.6, becomes the mechanistic r.d.s., facilitating in the same time the final $RS^{\bullet}$ expulsion of eqn. 6.9, which should be equally fast for all catalysts, owing to a thermodynamically driven release of steric strain from the active site. However, steric reasons alone might provide only a partial account of the observed decrease in r_0 values.

An increment in the steric bulk of the $(R_f)_nPcCo$ complexes goes along with an increasingly easier to reduce Co(II) atom and stabilization of its −1 oxidation state, as the plots of Figure 6.13 suggest. Under the strong electronic demand of the *p*-F and Ph groups, the Co-bound 4FBT radical manifests a tendency to reclaim the electron it lost during the reduction of Co(II) to Co(I), eqn. 6.7a, which acts as an electrochemical driving force for both the subsequent Co(I)/Co(II) reoxidation and release of the radical in solution. This tendency, however strong, might not overcome the Co(I) stabilization energy, which in turn slows down the intermediate reoxidation step by coordinated O_2, eqn. 6.8, offering a second r.d.s. alternative consistent with the r_0 values determined.

Still, the highly accelerated rates compared to similar parameters for 2ME oxidation, Table 6.2, propose a play down of the electronic factors in the case of 4FBT.

All of the above acknowledged, it appears that structural reasons play the more important role in the catalytic cycle of 4FBT aerobic coupling. Steric bumps created by the rigid aromatic substrate offer an unexpected solution in counteracting the catalytically retarding electronic effect of Co(I) overstabilization by the fluorinated Pc ligands. The acquired oxygen consumption data and calculated r_0 values fully support a thiolate binding r.d.s. and a decisively fast radical expulsion from the active site.

6.6.3.2 Perfluorobenzenethiol. Most, if not all, steric considerations detailed for the binding and releasing steps of the 4FBT thiolate/radical to and from the Co active site of the electron-deficient complexes should be entirely valid for the PFBT substrate as well. However, PFBT aerobic coupling is complicated, as explained in Section 6.5.2, by the parallel reaction of thiolate dimerization and oligomerization, adding more unknowns to the mix of radical and anionic species present in solution. That said, side-reactions alone cannot fully account for the radically different parameters obtained (Figure 6.10, Table 6.4) with respect to similar 4FBT oxidation experiments. The yields in the **[6-6]** PFBT disulfide, ranging from low to moderate, with a maximum value of 53% for the F_{64}PcCo-catalyzed reaction, were estimated from the final turnover numbers (Table 6.4).

The key in interpreting the results of PFBT aerobic coupling rests on the electronic factors, viz. the relative Lewis acidity of the Co catalytic site and basicity of the binding substrate. The electronic features of the metal active sites were extensively analyzed in the previous sections and remain equally relevant. Regarding the PFBT substrate, its even larger-than-4FBT steric bulk and million-fold higher acidity than 2ME

proposes it as a difficult to bind species on both electronic and steric grounds. Indeed, H_{16}PcCo-catalyzed aerobic coupling of PFBT does not occur, as evidenced by the zero-flat oxygen consumption of Figure 6.10, due to an insufficiently Lewis acidic Co atom to coordinate such a poorly basic thiolate. The extreme, by comparison, electronic deficiency of all other PcCo complexes proves beneficial in securing an efficient-enough binding in order for catalysis to occur, leading to mixed results.

With the exception of the now-inactivated H_{16}PcCo, the variation of the rest of the r_0 values seem to loosely reproduce the results of 2ME oxidation, creating an initially confusing picture. First, it is unreasonable to assume that the similarly lower-trending rates displayed by $F_{24}H_8$, F_{34} and F_{52}PcCo are the result of a too-strong PFBT thiolate binding and overstabilization of Co(I) species, since that would blatantly contradict the established facts on the thiolate's increased bulk and poor basicity. It is precisely because of the more facile access of the bulky thiolate to the active site that, for instance, F_{16}PcCo shows a higher final yield in disulfide than the F_{34} and F_{52} analogues (32% vs. 22% and 31%, respectively); and finally, it is because of the generally slower thiolate binding by the same F_{16}PcCo, owing to an electron-richer Co atom, that the final yield it displays is 10% lower than the value for the faster-binding, faster-expelling F_{52A}PcCo.

The steric and electronic factors vary congruently, as: (a) the catalysts' ability to better bind the acidic thiolate and transfer its negative charge to the metal and (b) their bulkiness, facilitating expulsion of the thyil radical, increase from F_{34} to F_{52}, F_{52A} and F_{64}PcCo, assertively paralleled by the ascending trend in the r_0 values. The catalytically-compelling steric repulsion of the PFBT thiolate by the F_{64}Pc ligand is expressed in the

disproportionately high initial rate displayed with respect to all other fluorinated complexes, eventually leading to the highest recorded disulfide yield.

In essence, the thiolate binding and electron transfer steps of eqns. 6.6 and 6.7 are r.d.s. in the PFBT oxidation cycle, owing to both steric and electronic factors; stabilization of the Co(I) ternary intermediate during the O_2 reduction step of eqn. 6.8 is hardly possible, given the thermodynamically driven fast expulsion of the $C_6F_5S^{\bullet}$ radical from the metal site once reoxidation to Co(II) has taken place. Interference of the SN2 side products with the aerobic catalytic activity might occur through competitive thioether-thiolate **[6-7]** coordination to the active Co site and stabilization of the complex by stacking interactions with the suitable planar portions of the Pc ring.

6.7 Conclusions

The first cobalt(II) representatives of a family of fluoro-perfluoroalkylated metal–organic ligands are reported, for which electrophilic, nucleophilic and radical degradation pathways have been suppressed via rational molecular design. The complexes catalytically reduce metal-coordinated dioxygen within the fluorinated pocket, with formation of O- and, when tested against the aerobic coupling of thiols to disulfides, S-centered radicals. Homogeneous oxidation of a series of aliphatic and aromatic thiols of gradually increasing acidity is studied. Owing to the broadening of catalytic capabilities of the new complexes to include acidic substrates, as a result of the extreme metal Lewis acidity imparted by perfluoroalkyl groups, the aerobic coupling of perfluorobenzenethiol is reported for the first time. A comprehensive mechanism for the mercaptan oxidation catalytic cycle is proposed and discussed in view of the obtained results.

The transformation rates for the aerobic oxidation of 2-mercaptoethanol are only partly congruent with the expected values based on the variation of electrochemical reduction potentials. Bulky and electron-deficient catalysts of the F_{52A} and F_{64}PcCo type manifest enhanced rates, presumably due to an accelerated thyil radical expulsion from the catalytic active site. The apparent catalytic inactivity of the sterically non-hindered $F_{28}H_4$, F_{34} and F_{52}PcCo complexes is explained by an overstabilization of the cobalt(I) oxidation state and strong metal–thiolate binding, proving that perfluorination can sometimes become detrimental for oxidation of highly basic substrates.

Aerobic coupling of 4-fluorobenzenethiol is dominated by rapid and quantitative transformations to disulfide for all catalysts employed, consistent with a slower binding of the less basic thiolate and its radical's thermodynamically driven rapid removal from the active site. Steric interactions created by the rigid aromatic substrate offer an unexpected solution in counteracting the retarding effects of cobalt(I) stabilization.

The electron-richest H_{16}PcCo catalyst is unable to catalyze oxidation of acidic perfluorobenzenethiol, while the extreme electronic deficiency of all other fluorinated complexes proves beneficial in securing an efficient-enough thiolate binding in order for catalysis to occur. The process is complicated by the aromatic substrate's susceptibility for intermolecular nucleophilic dimerization.

The stabilization of ligand composition while offering active sites for catalysis is a most often difficult to meet challenge.[176] The rational design strategy used in creating the new fluoro-perfluoroalkylated complexes provides an answer to this challenge within the phthalocyanine family and proposes it for testing on other frameworks. The foremost goal of this work in obtaining stable, yet reactive organic-based catalytic materials is thus achieved.

CHAPTER 7

PHOTOCATALYTIC OXYGENATION OF CITRONELLOL

7.1 Introduction

Oxidation of suitable substrates containing labile C–H bonds by light-activation of atmospheric oxygen is an attractive perspective from both a chemical and environmental point of view. Within the broad range of alternative processes available for singlet oxygen ($^1O_2$) generation from its naturally present triplet ($^3O_2$) ground-state, activation of an appropriate light-absorbing material, i.e., photosensitizer,[177] is an industrially viable option.[178,179] Singlet oxygen has been produced by photosensitization of a variety of organic and metal–organic compounds, including porphyrins,[180] ruthenium complexes[181,182] and dyes like rose bengale and methylene blue.[183] In this respect, diamagnetic phthalocyanines, structurally relevant for this work, have attracted considerable academic, medical and industrial interest[112,184] through, *inter alia*, their photocatalytic applications in the industrial wastewater treatment[178] and PDT of cancer.[50–52] However, for conventional hydrogen-containing PcMs, a problem arises in using an organic-based photocatalyst containing labile C–H bonds for aerobic oxidation of a substrate that also contains C–H bonds.[176] The new perfluoroalkyl-substituted PcZn complexes synthesized herein, assigned the general formula $(R_f)_nPcZn$, can provide an answer to this dilemma through their protective fluorine-rich ligand environment. In addition, the highest $^1O_2$ quantum yield among all PcM complexes reported for the previously obtained $F_{64}PcZn$ analogue,[112] proposes the new perfluorinated materials as equally-efficient photosensitizers in the activation of ground-state triplet dioxygen.

The photocatalytic activity of the new PcZn fluorinated complexes is tested on a model substrate of industrial significance, viz. (*S*)-(−)-3,7-dimethyl-6-octen-1-ol **[7-1]**, a naturally-occurring acyclic monoterpenoid, traditionally also named (*S*)-(−)-citronellol (henceforth, simply citronellol). Its $^1O_2$ oxidation to a mixture of two isomeric hydroperoxides, **[7-2]** and **[7-3]**, using rose bengale as the photosensitizer, is applied in the perfume industry for production of rose oxide **[7-7]**,[182,183] a component of many fragrances, according to the synthetic route described in Figure 7.1. The final product is obtained by acid-catalyzed internal cyclisation of one of the two reduced hydroperoxides.

In this work, only the catalytically-relevant initial step of hydroperoxide formation is investigated, since the focus is determining the dioxygen activation abilities of the new PcZn photosensitizers. Ethanol was the solvent of choice, as indicated by most citronellol oxidation studies,[182] while the temperature was kept constant at 25 °C. The next sections introduce basic concepts on electronic absorption–emission processes, proposed mechanisms of singlet oxygen photosensitization and its properties.

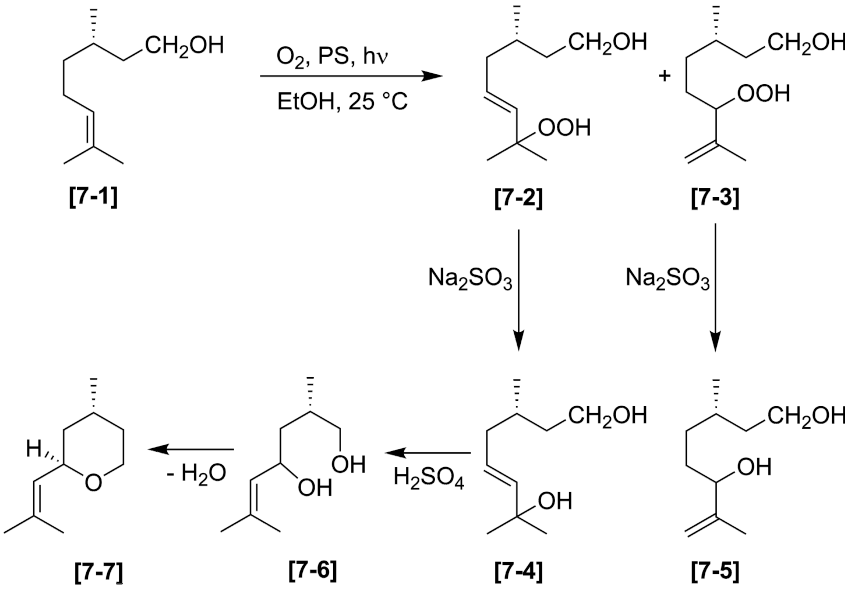

Figure 7.1 Industrial synthetic route for production of rose oxide by photooxidation of (*S*)-(−)-citronellol, using rose bengale as the photosensitizer (PS).

7.1.1 Electronic Absorption and Emission Processes

Energetically excited states of a molecule are formed by absorption of quanta of electromagnetic radiation (photons) resulting in promotion of electrons between the frontier molecular orbitals. Among these, the HOMO–LUMO electronic transition displays the lowest associated energy. The ground- and excited electronic states of a molecule and the transitions between them are best illustrated by the well-known Jablonski diagram,[185] shown in Figure 7.2 for diamagnetic PcM complexes of singlet ground-state spin multiplicity, $^1Pc_0$.

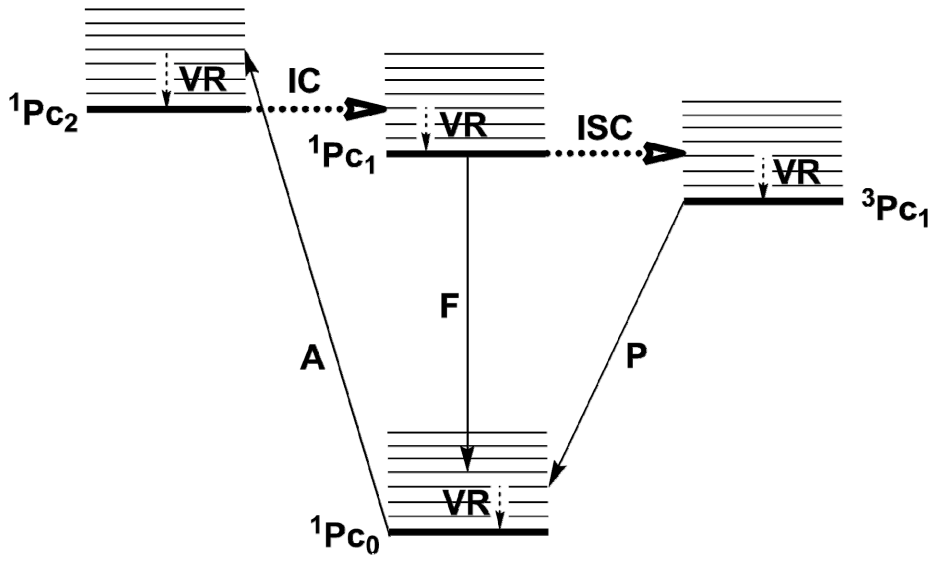

Figure 7.2 Simplified Jablonski diagram of electronically excited states for diamagnetic PcM complexes and associated transitions. Non-radiative processes are indicated by dashed arrows. Vibrational ground states of each electronic state are shown in bold lines. Notations: A, absorption; F, fluorescence; P, phosphorescence; IC, internal conversion; ISC, intersystem crossing; VR, vibrational relaxation.

In relation to Figure 7.2, absorption of light by a ground-state diamagnetic PcM molecule, $^1Pc_0$, may lead to a first ($^1Pc_1$) or second ($^1Pc_2$) excited singlet state, depending on the photon's energy. Relaxation of vibrationally excited levels occurs at very fast rates (typically 10^{-13}–10^{-12} s),[186] and results in occupation of the ground vibrational states

of $^1Pc_1$ or $^1Pc_2$, respectively. Non-radiative internal conversion occurs between two isoenergetic states of similar spin multiplicity, e.g., $^1Pc_2 \rightarrow {}^1Pc_1$, at equally fast rates to the vibrational relaxations within each electronic state. The change of multiplicity from an excited singlet ($^1Pc_1$) to an excited triplet ($^3Pc_1$) state via non-radiative intersystem crossing (ISC) is spin-forbidden, but becomes possible in paramagnetic or transition-metal containing compounds through a spin-orbit coupling process in which an electron flips its spin, leading to the $^1Pc_1 \rightarrow {}^3Pc_1$ ISC.[186] Radiative emission of energy from the first $^1Pc_1$ excited state to the ground $^1Pc_0$ level results in spin-allowed fluorescence, while a similar emission from the triplet $^3Pc_1$ excited state leads to spin-forbidden phosphorescence. Fluorescence generally occurs much faster than phosphorescence (10^{-10}–10^{-8} vs. 10^{-7}–10^{2} s, respectively),[184–187] the latter owing to significantly longer lifetimes of the excited triplet states. Emission processes almost invariably occur from the lowest excited states, $^1Pc_1$ and $^3Pc_1$, according to Kasha's rule.[186]

With respect to PcZn photosensitizers, their excited triple state lifetimes (τ) vary considerably, even within the perfluorinated family, influenced by the MO structure of each compound and solvent-induced bimolecular deactivation pathways. For instance, planar F_{16}PcZn displays a <1 μs value,[188] while the observed τ for tridimensional F_{64}PcZn was 52±3 μs.[105] The depression and stabilization of frontier orbitals energy induced by the R_f groups of F_{64}PcZn[111] must be at least partially responsible for its higher τ value,[112] proposing the new $(R_f)_n$PcZn complexes as promising photosensitizers. Promotion of longer triplet state lifetimes by the Pc ligand is essential in efficient photocatalytic production of $^1O_2$, as it insures a higher frequency of the bimolecular energy transfer processes between excited $^3Pc_1$ and ground $^3O_2$ states.

Radiative emission of energy by fluorescence and phosphorescence are unimolecular deactivation processes, in which the molecule returns to its ground-state. In addition to these, bimolecular deactivation is possible through photophysical (energy transfer) or photochemical (electron transfer) pathways in which the excited state molecule interacts with identical or different ground-state species. Relevant to the PcM complexes, a notoriously detrimental bimolecular deactivation, affecting their $^1O_2$-generating ability, is aggregation in solution through π–π stacking interactions, which effectively prevents energy transfer to a dioxygen molecule and even ISC to the triplet $^3Pc_1$ state; dimerization between an excited $^1Pc_1$ and a ground $^1Pc_0$ state leads to an excited dimer which then decays to its ground-state, as shown by eqn. 7.1.

$$^1Pc_1 + {}^1Pc_0 \rightarrow {}^1(Pc_2)_1 \rightarrow {}^1(Pc_2)_0 + h\nu \qquad (7.1)$$

The deactivation pathway above has been referred to as "quenching",[177,186] severely limiting the available population of molecules in the $^3Pc_1$ state and their lifetime. Thus, solvents minimizing the extent of Pc aggregation and/or non-aggregating PcMs are desired for conducting an efficient photocatalytic process. The versatile $(R_f)_nPcZn$ complexes obtained for this work have been proven to adapt their solvent-dependent aggregation to this requirement (Chapters 4 and 5).

7.1.2 Generation and Lifetime of Singlet Oxygen

The electronic structure of molecular oxygen can most easily be explained by MO theory. In its ground electronic state, the dioxygen molecule is a triplet ($^3O_2$, $^3\Sigma_g^-$) with two unpaired electrons distributed in the π* doubly-degenerate HOMO level, as shown by the diagram of Figure 7.3.

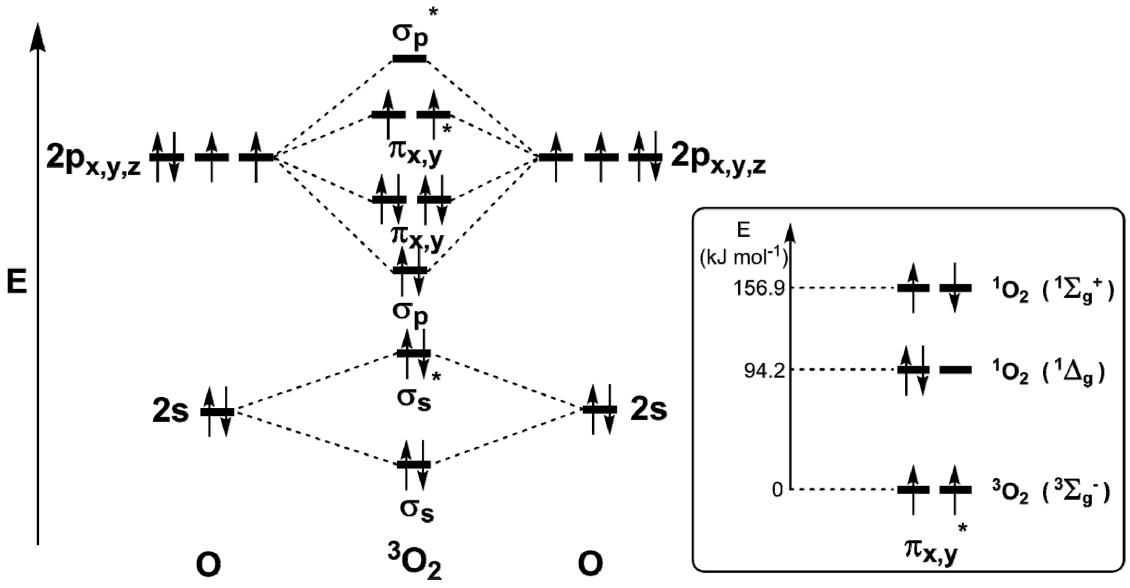

Figure 7.3 MO diagram of molecular oxygen in its triplet ($^3O_2$) and singlet ($^1O_2$) states.

The triplet multiplicity is responsible for the paramagnetic properties of molecular oxygen and its chemical inertness towards singlet ground-state organic compounds, due to the spin barrier.[179] A rearrangement of the two electrons in the degenerate HOMO π* orbitals can only occur by spin-allowed energy transfer from another triplet state of a chemically different species, in the case at hand an excited $^3Pc_1$ complex. The resulting absorption may lead to two possible diamagnetic $^1O_2$ singlet states, the single orbital electron-paired $^1\Delta_g$ state (with an energy 94.2 kJ mol^{-1} higher than $^3\Sigma_g^-$) and the $^3\Sigma_g^+$ state with the spin-pairing electrons placed in different orbitals, 156.9 kJ mol^{-1} above $^3\Sigma_g^-$ (Figure 7.3).[179] In both singlet states, the spin restriction is removed and the molecule becomes available to oxidize substrates. The $^3\Sigma_g^+$ state has a much shorter lifetime than $^1\Delta_g$, decaying to the latter before any reactions can occur; therefore, it is the lower-energy $^1\Delta_g$ species that reacts chemically as $^1O_2$, and shall henceforth be referred to as such. The lifetime of $^1O_2$ greatly depends on the solvent in which oxygenations are performed, ranging from, e.g., 3.3 μs in H_2O to 31000 μs in CCl_4.[179]

7.1.3 Reactions of Singlet Oxygen and Photosensitization Processes

The $^1O_2$ molecule is mildly electrophilic; as such, it easily undergoes specific Diels-Alder type cycloaddition reactions with electron acceptors such as *cis* dienes and aromatic hydrocarbons. Many of the other documented reactions of singlet oxygen postulate six-centered transition states typical for pericyclic transformations. Singlet oxygen reacts with a multitude of organic substrates, including dienes, alkenes, sulfides, aromatics, terpenes, fatty acids, steroids, proteins, blood pigments and synthetic polymers. An agreement on whether specific reactions occur through cycloaddition, peroxide or diradical intermediates has not been reached.[186,187]

Regarding citronellol's oxygenation to its hydroperoxide isomers, **[7-2]** and **[7-3]** of Figure 7.1, most publications[112,182] favor a classical Schenk-ene[189] mechanism of hydrogen abstraction from an activated allylic position of the alkene and concerted addition of oxygen with a migration of the double bond. This mechanism is depicted in Figure 7.4. The reaction follows a 1:1 stoichiometry and is highly regiospecific, the two hydroperoxides being the only products identified in the reaction mixture.

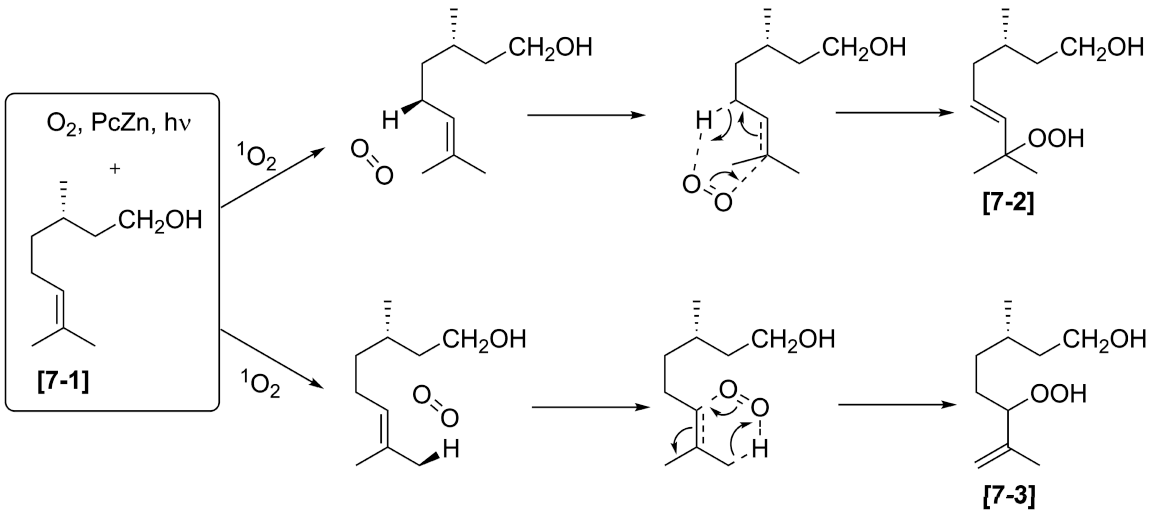

Figure 7.4 Hydroperoxide isomers formation by oxygenation of (*S*)-(−)-citronellol through a Schenk-ene mechanism.

Photosensitization[177] is a process in which a light-absorbing compound, the photosensitizer (also herein termed photocatalyst), initiates a physical, chemical or biological transformation in an otherwise non-absorbing substrate. Photooxygenation is a sub-type of photosensitization, denoting incorporation of molecular dioxygen into a different molecule through interaction with a light-activated photocatalyst. In essence, photosensitization is a desired bimolecular process between the excited triplet state of the photosensitizer and the triplet ground-state of molecular oxygen. In contrast, the bimolecular deactivation through dimerization of the photosensitizer is not desired. Several mechanisms were proposed for photooxygenation of hydrogenated substrates, RH, to hydroperoxides, ROOH; they are grouped into three main types, as follows:[177–179]

- Type I: reaction of $^3O_2$ with $R^\bullet$ radicals formed photochemically.
- Type II: reaction of RH with $^1O_2$ formed photochemically.
- Type III: reaction of superoxide $O_2^{\bullet-}$ with $R^{\bullet+}$ radical cations, both formed photochemically by electron transfer from excited states of the photosensitizer.

In Types I and III above, the excited triplet state of the photosensitizer, in this case a phthalocyanine, $^3Pc_1$, photochemically abstracts a proton from the RH substrate with formation of $R^\bullet$ radicals (Type I), or transfers an electron to and from $^3O_2$ and R molecules, respectively, forming $O_2^{\bullet-}$ and $R^{\bullet+}$ radical cations (Type III) and associated $Pc^\bullet$ (Type I) and $Pc^{\bullet+}$ / $Pc^{\bullet-}$ (Type III) species, which then further activate $^3O_2$ through a secondary electron transfer. While some studies have claimed that these two mechanisms operate for other families of sensitizers,[177–179] in the case of PcMs and, more specifically, the electron-deficient $(R_f)_nPcZn$ complexes studied herein, light-induced electron transfer with formation of oxidized species is strongly discouraged based on all previously reported experimental observations on the $F_{64}PcM$ analogues' resistance to both chemical and

electrochemical oxidation.[51,105–113,173] If, presumably, this were to happen, substrate derivatization should lead to products even in the absence of oxygen, a hypothesis definitely denied by the unchanged composition of all mixtures illuminated under N_2. Furthermore, electron transfers to and from the PcM complex, ligand- and metal-centered alike, result in immediate color changes in solution and signature UV-vis absorptions, none of which were noticed across the length of this study. Finally, under the experimental conditions of citronellol oxidation in ethanol, the absence of electron donors in solution to regenerate the photooxidized sensitizer specifically precludes any of the Types I and III mechanisms.[182] Considering all of the above, the Type II mechanism involving a classical energy transfer through a bimolecular deactivation between the excited triplet state of the photosensitizer and ground-state triplet oxygen is adopted for all photooxygenation reactions with $(R_f)_n$PcZn catalysts discussed from here on. The basic mechanistic steps are summarized as follows:

$$^1Pc_0 + h\nu \rightarrow {}^1Pc_1 \tag{7.2}$$

$$^1Pc_1 \rightarrow {}^3Pc_1 \tag{7.3}$$

$$^3Pc_1 + {}^3O_2 \rightarrow {}^1Pc_1 + {}^1O_2 \tag{7.4}$$

$$^1O_2 + RH \rightarrow ROOH \tag{7.5}$$

The next sections present the experimental setup and procedures employed for oxygenation of citronellol through photosensitization of the new materials produced for this work. A summary of the catalytic results and parameters obtained follows, along with an identification of reaction products and evaluation of the catalysts' photostability. Finally, a discussion is given on the most plausible physical and chemical phenomena which would account for the observed experimental outcome.

7.2 Experimental Section

(*S*)-(−)-Citronellol, zinc(II) phthalocyanine (H_{16}PcZn) and zinc(II) hexadecafluoro-phthalocyanine (F_{16}PcZn **[5-6]**) were purchased from commercial sources and used as received. Ethanol used as solvent for the photooxidation experiments was denatured, reagent grade and used fresh as received. F_{64}PcZn **[5-8]** was prepared according to published literature procedures.[105,112] $F_{24}H_8$PcZn **[4-5]**, $F_{28}H_4$PcZn **[4-14]**, F_{34}PcZn **[5-10]** and F_{52}PcZn **[5-12]** were prepared as described under the experimental sections of Chapters 4 and 5 of this work. Milligram amounts of analytically pure F_{40}PcZn **[5-14]** were provided by Mr. Hemantbhai Patel.* Ethanolic solutions of the catalysts were prepared fresh before use.

Photooxidation reactions were performed in 100 mL double-walled jacketed glass vessels, using the experimental setup of Figure 2.1. The procedure followed the conditions described in Section 2.8. In all cases, 1 mmol (180 μL) of the substrate were reacted in 50 mL ethanolic 20±2 μM PcZn catalyst solution at 25 °C under a saturated O_2 atmosphere, achieved by 10 min purge cycles. Illumination was performed using 300 W halogen lamps, creating a light intensity of $4.6\pm0.1 \times 10^5$ lux at the outer wall of the reaction vessel. The system was sealed and recording of oxygen consumption was started immediately after injection of citronellol to the reaction vessel and start of illumination. Any initially accumulated overpressure was released by quick purges through a Teflon stopcock. For each catalyst, illumination was maintained for 3 h, after which the system was open and the composition of the mixtures analyzed by UV-vis and ^{1}H NMR. The maximum theoretical O_2 consumption in all cases at 25 °C was limited to 24.45 mL, according to the 1:1 overall stoichiometry.

* Patel, H. H. New Jersey Institute of Technology, Newark, NJ. Personal communication, 2011.

Table 7.1 describes the control experiments performed before the start of photooxygenation reactions for instrumental calibration. The lack of O_2 consumption for all photocatalytic trials performed without addition of citronellol confirms ethanol's stability towards generated $^1O_2$. For reproducibility, photooxidations were repeated at least twice for a given catalyst, the data set showing highest oxygen consumption values being chosen for further processing. In the case of discrepancies higher than 15% between the recorded O_2 volumes, air-tightness of the system was checked and calibration runs were performed with standard F_{64}PcZn-catalyzed reactions until agreement between two successive data sets was reached.

Table 7.1 Control Experiments for the Catalytic Photooxidation of Citronellol†

Entry	Substrate	Catalyst	Atmosphere	Light Conditions	Gas Consumption
1	-	-	O_2	In the dark	No
2	-	-	N_2	In the dark	No
3	-	-	O_2	Illuminated	No
4	-	-	N_2	Illuminated	No
5	-	H_{16}PcZn 20 μM	O_2	Illuminated	No
6	0.18 mL citronellol	H_{16}PcZn 20 μM	N_2	Illuminated	No
7	0.18 mL citronellol	H_{16}PcZn 20 μM	O_2	In the dark	No
8	-	F_{16}PcZn 20 μM	O_2	Illuminated	No
9	0.18 mL citronellol	F_{16}PcZn 20 μM	N_2	Illuminated	No
10	0.18 mL citronellol	F_{16}PcZn 20 μM	O_2	In the dark	No
11	-	F_{64}PcZn 20 μM	O_2	Illuminated	No
12	0.18 mL citronellol	F_{64}PcZn 20 μM	N_2	Illuminated	No
13	0.18 mL citronellol	F_{64}PcZn 20 μM	O_2	In the dark	No
14	0.18 mL citronellol	-	O_2	In the dark	No
15	0.18 mL citronellol	-	N_2	Illuminated	No
16	0.18 mL citronellol	-	O_2	Illuminated	No*

† All experiments performed at 25 °C in 50 mL ethanolic solutions for 3 h.
*Non-catalyzed photooxidation of (*S*)-(–)-citronellol occurs with a very low rate, 1.455 mL being consumed over 3 h of irradiation (~6% transformation), a negligible value falling within the equipment's manometric detection error. Thus, no effective O_2 consumption is considered.

7.3 Photocatalyzed Oxidation of (*S*)-(−)-Citronellol

7.3.1 Oxygen Consumption and Process Parameters

Ground state $^3O_2$ consumption during the photooxidation of citronellol catalyzed by the new fluoroalkylated and perfluorinated PcZn complexes produced in this work is presented in Figure 7.5. Additional data collected for the H_{16}PcZn, F_{16}PcZn and F_{64}PcZn standards are shown for comparison and subsequent discussion. The calculated parameters of the catalytic process are provided in Table 7.2. Determination of the initial reaction rates and turnover numbers follows the procedures described in Section 6.6.1, also partly detailed in the table legend. The catalytic results are discussed in Section 7.4.

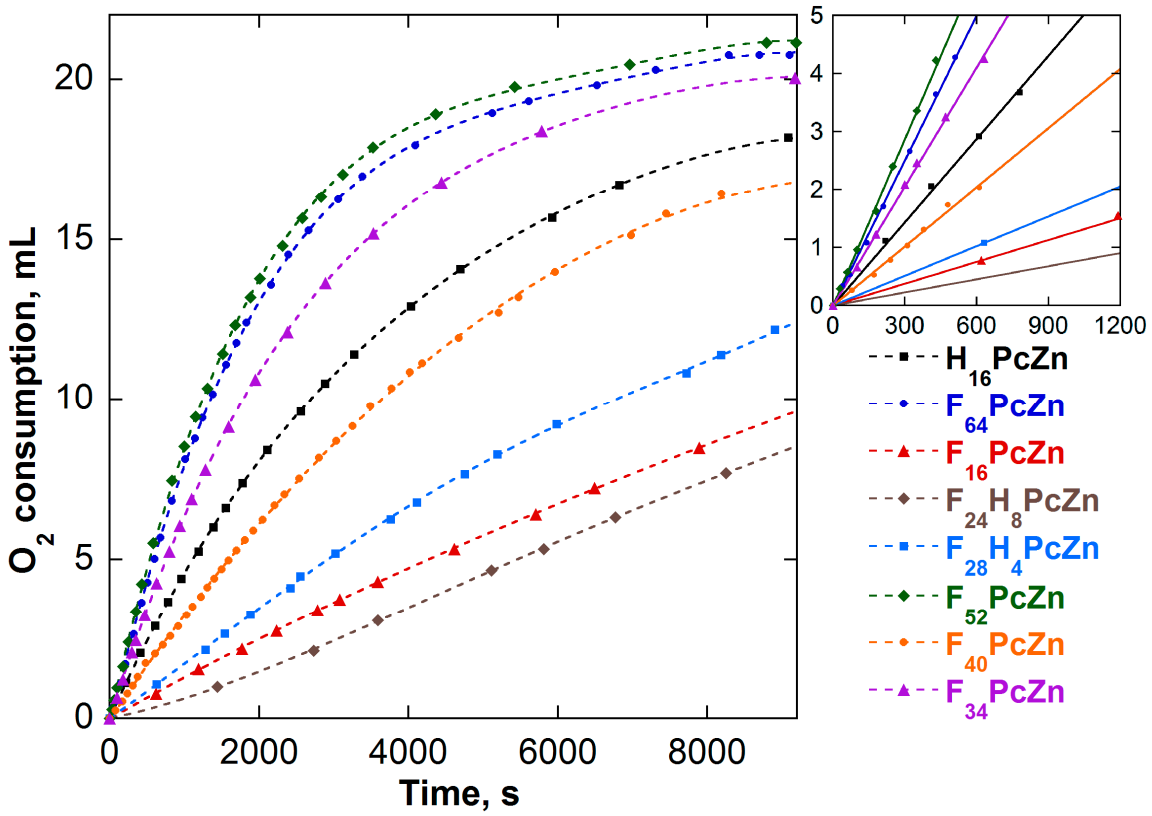

Figure 7.5 Oxygen consumption during the catalyzed photooxidation of (*S*)-(–)-citronellol in ethanol. Inset: initial reaction rates, shown as linear fits on data points recorded within the first 20 min of each reaction.

Table 7.2 Parameters of the Catalyzed Photooxidation of Citronellol

Catalyst	Catalyst amount (μmol)	Stability[a] (%)	Rate[b] (μmol O_2 min^{-1})	TOF[c] [mmol (*S*)-Cit* s^{-1} mol Pc^{-1}]	TON[d] [mol (*S*)-Cit mol Pc^{-1}]	TON_{max} [mol (*S*)-Cit mol Pc^{-1}]	$\frac{TON}{TON_{max}}$
$H_{16}PcZn$	1.10	~ 25	11.8	178	677	909	0.75
$F_{16}PcZn$	1.15	> 99	3.2	46	301	870	0.35
$F_{24}H_8PcZn$	0.98	~ 98	2.0	33	321	1020	0.32
$F_{28}H_4PcZn$	1.01	> 99	4.2	69	518	990	0.52
$F_{34}PcZn$	0.98	> 99	16.7	284	837	1020	0.82
$F_{40}PcZn$	1.19	> 99	8.3	120	581	840	0.69
$F_{52}PcZn$	1.07	> 99	23.6	370	809	935	0.87
$F_{64}PcZn$	0.92	> 99	19.9	360	923	1087	0.85

[a] Stability, defined as the ratio: [Q-band intensity after 3 h / Q-band initial intensity] × 100.
[b] Initial reaction rates, μmol O_2 min^{-1}, calculated as the slopes of the linear fits in the inset of Figure 7.5.
[c] Turnover frequency, mol substrate s^{-1} mol Pc^{-1}, calculated under pseudo-first order conditions with respect to (*S*)-(–)-citronellol, using the stoichiometrically adjusted initial rate values.
[d] Turnover number after 3 h, calculated stoichiometrically as: [final O_2 volume (mL) / molar volume of O_2 at 25 °C (24.45 mL $mmol^{-1}$)] × [1000 (μmol substrate mmol O_2^{-1}) / n_{Pc} (μmol Pc)].
* Abbreviation for (*S*)-(–)-citronellol.

7.3.2 Reaction Products

Identification of reaction products was performed by ^1H NMR analysis of ethanol-evaporated reaction mixtures after 3 h-long illumination. The ^1H data, Figure 7.6, clearly indicates the exclusive presence of the two hydroperoxides **[7-2]** and **[7-3]** of Figure 7.1. Their chemical shifts closely matched the literature reported values.[182] Citronellol was not detected, suggesting a quantitative transformation, somewhat inconsistent with the lower-than-stoichiometric volumes of O_2 recorded (Figure 7.5), especially for the less active photosensitizers. However, the substrate's disappearance from the reaction mixtures can be explained through the specifics of their workup, i.e., (1) the 70 °C temperature required for *in vacuo* removal of ethanol, possibly accelerating substrate degradation under the action of the hydroperoxide products, and (2) added time between the end of the illumination and acquisition of the spectra, allowing for the photocatalyzed reaction to continue under ambient light, with the PcZn photosensitizers still present.

The hydroperoxides were stable enough to resist the high temperature solvent removal. Minor amounts (<10%) of higher-oxidized side products, most probably aldehydes, were identified as resonances in the 9–11 ppm range. Further reduction of the **[7-2]** and **[7-3]** hydroperoxides to the corresponding diols and dehydration to rose oxide according to the scheme of Figure 7.1 was not attempted, as the focus of this study is on the photocatalytic activity exhibited by the new complexes.

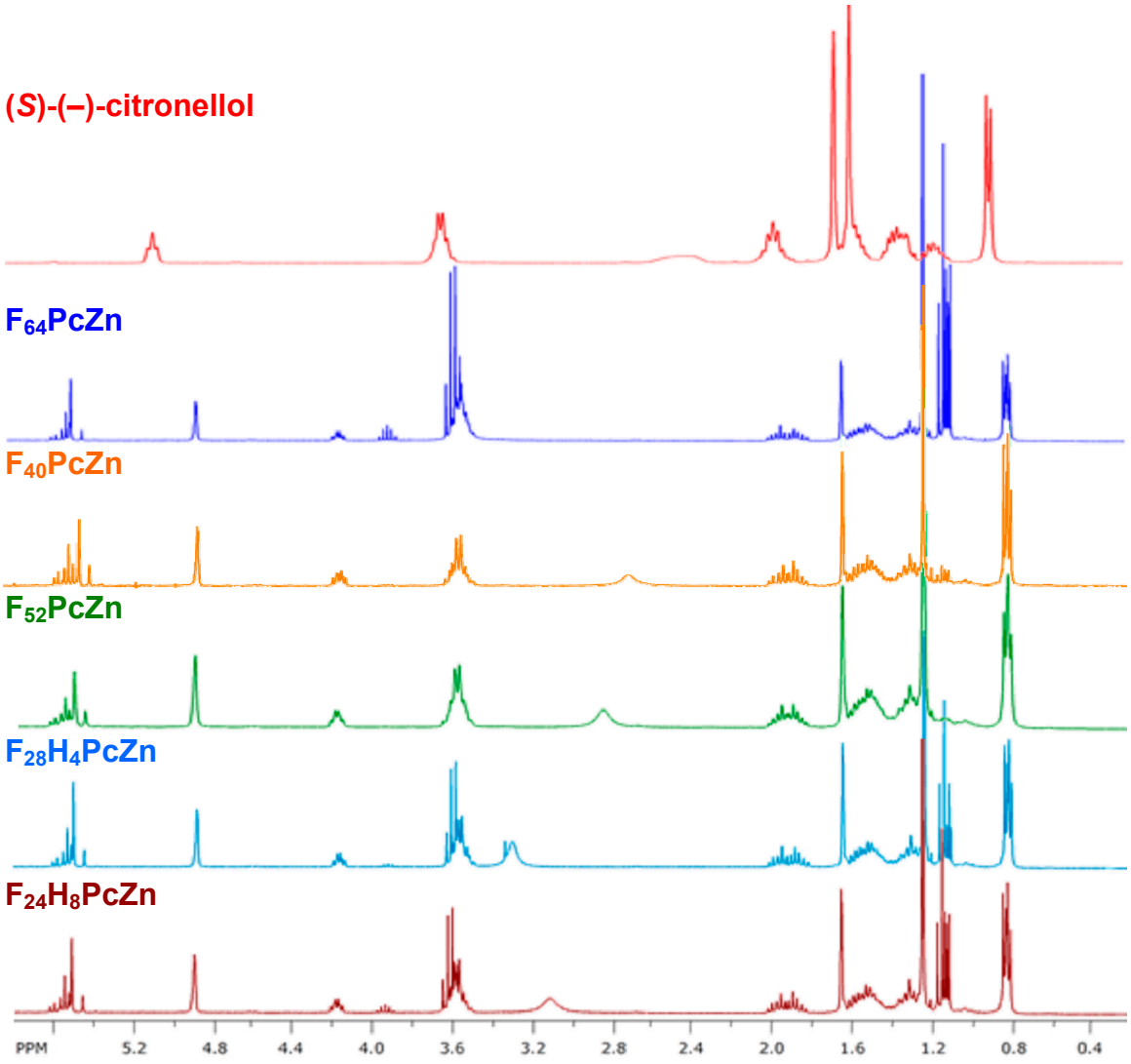

Figure 7.6 ^{1}H NMR comparison of reaction mixtures obtained for the photooxidation of (*S*)-(–)-citronellol in ethanol catalyzed by selected PcZn complexes. Residual solvent is present in the $F_{24}H_8$, $F_{28}H_4$ and F_{64}PcZn mixtures. Spectra were acquired in $CDCl_3$.

7.3.3 Catalyst Stability

As evidenced by the UV-vis spectra of the illuminated ethanolic reaction mixtures, acquired up to 48 h of stirring under air (Figure V.4), the stability of all perfluorinated complexes towards the activated $^1O_2$ as well as the **[7-2]** and **[7-3]** hydroperoxides produced is exemplary. A plot of the calculated ratios of actual and initial Q-band absorbances vs. time, Figure 7.7, shows zero or less than 3% degradation for F_{16}, F_{34}, F_{40}, F_{52} and F_{64}PcZn, respectively, over a period equivalent to sixteen 3 h-long catalytic cycles. The now-confirmed photostability of the new complexes was expected, in accordance with previously published similar observations on the F_{16}PcZn and F_{64}PcZn analogues.[112] Thus, it becomes evident that perfluorination immensely enhances the resistance of the Pc ligand to singlet oxygen attacks up to the point of near total inertness.

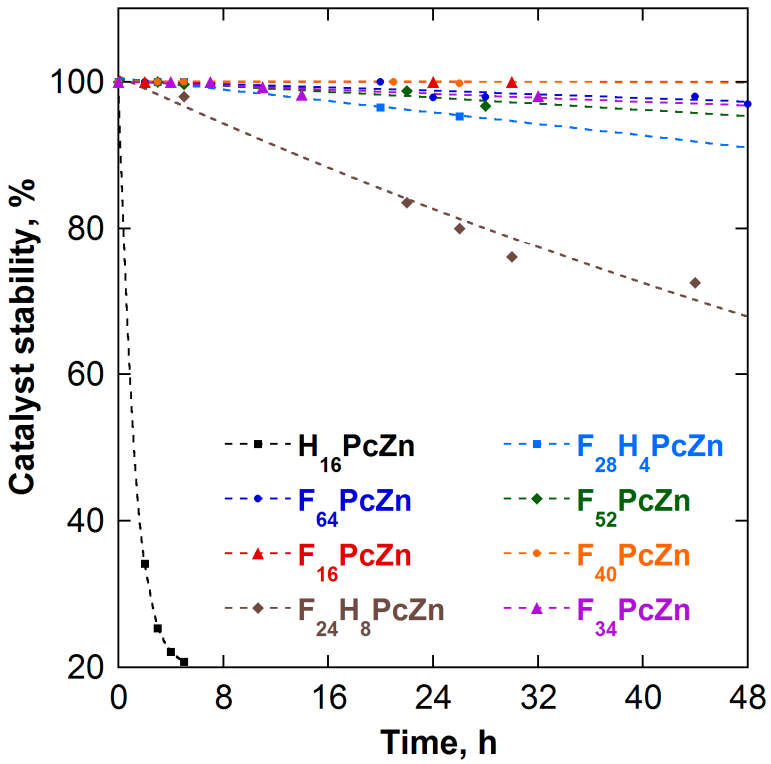

Figure 7.7 Time-dependent catalyst stability during the photooxygenation of (*S*)-(–)-citronellol in ethanol.

With respect to the initial 3 h-long transformations considered for acquisition of O_2 consumption data and calculation of process parameters, Figure 7.5, all catalysts except the non-fluorinated H_{16}PcZn show less than 2% decomposition; the latter, on the other hand, was decomposed in *ca.* 75%. After the equipment was opened to allow for UV-vis stability measurements, further illumination of the reaction solutions under air has revealed significant decomposition of the symmetrical, H-containing $F_{24}H_8$PcZn (*ca.* 30% decay after 44 h), while its four-count F richer counterpart $F_{28}H_4$PcZn displayed only a minor, ~5% degradation over 26 h. This clearly validates a much improved resilience of the fluoroalkyl Pc ligand to $^1O_2$ and OOH attacks, acquired upon inclusion of only four additional aromatic F atoms. All perfluorinated photocatalysts, as mentioned before, were stable, while the concentration of the labile H_{16}PcZn seemed to stabilize, over 24 h of illumination, at a 20–22% amount of its initial value, in a somewhat surprising observation. Such an intriguing behavior of accelerated photodegradation followed by a sudden stabilization asked for clarifications of its possible causes.

In order to check whether the pronounced instability of H_{16}PcZn was due to $^1O_2$ and hydroperoxide attacks or to a detrimental radiative decay of its excited states, an identical illumination experiment was performed under nitrogen for 20 h. Before the start of illumination and after every subsequent 3 mL UV-vis sample extraction, three vacuum-N_2 purging cycles of the reaction flask were performed with the aid of a Schlenk line. The collected electronic absorption spectra and stability plot, in comparison to the analogous results obtained under aerobic conditions, are presented in Figure 7.8 and unexpectedly show almost identical photo-decomposition rates and final stabilization; a direct comparison suggests only a minor (<5%) degradation due to action of $^1O_2$.

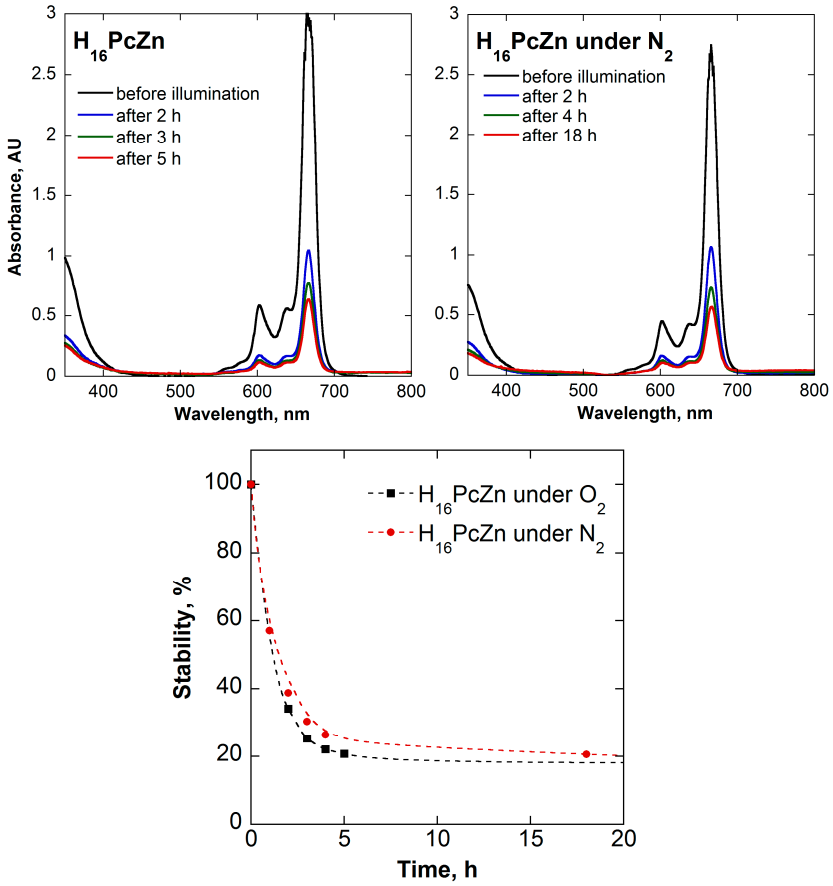

Figure 7.8 UV-vis monitored photo-decomposition of H_{16}PcZn.

Previously published reports on the photodegradation mechanism of H_{16}PcZn, Figure 7.9, indicate a singlet oxygen [4+2] cycloaddition to the *ipso* carbon atoms of pyrrole units of the Pc core, the same positions susceptible to nucleophilic attacks,[190] with formation of phthalimide, later identified in the reaction mixture. However, this might not be the only photo-activated degradation pathway, as shown by the catalyst stability determined for the anaerobically illuminated reaction mixture, Figure 7.8.

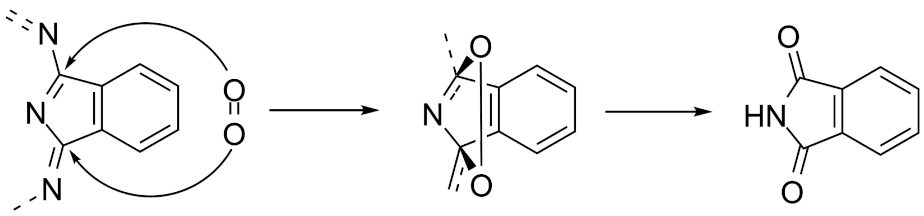

Figure 7.9 Proposed PcZn photodegradation mechanism by the action of $^1O_2$.[190]

Admittedly, traces of $^3O_2$ might still find their way into the reaction flask, despite all efforts to prevent air access to the system. The dilute, 20 μM photosensitizer solution might sanction even these insignificant amounts of residual oxygen through an appreciable photodegradation manifested in the UV-vis spectrum. But even so, the strikingly similar pictures of Figure 7.8 strongly support the existence of a parallel light-induced decay. This is best explained by radiative breakdown of the photosensitizer's singlet ($^1Pc_1$) or triplet ($^3Pc_1$) excited states, or, possibly, a combination of both. The mechanism of an anaerobic photodegradation of PcMs has been previously documented[191] by a proposed electron transfer from the excited photosensitizer to an electron-accepting substrate, as detailed by the equations below.

$$^1Pc_0 + h\nu \rightarrow {}^1Pc_1 \tag{7.6}$$

$$^1Pc_1 \rightarrow {}^3Pc_1 \tag{7.7}$$

$$^3Pc_1 + {}^3Pc_1 \rightarrow \text{photo-decomposition} \tag{7.8}$$

$$^1Pc_1 + R \rightarrow Pc^{\bullet+} + R^{\bullet-} \tag{7.9}$$

$$^1Pc_1 + {}^1Pc_0 \rightarrow Pc^{\bullet+} + Pc^{\bullet-} \tag{7.10}$$

$$Pc^{\bullet+} \rightarrow \text{photo-decomposition} \tag{7.11}$$

The mechanism above was supported by the observed inhibition of photodecomposition when reducing species were added to the reaction mixtures.[191] While formation of electronically-excited radical cation species was specifically excluded for the fluorinated $(R_f)_n$PcZn photosensitizers based on electronic and spectroscopic grounds, *vide supra*, the electron-richer H_{16}Pc ligand could allow for such a pathway to occur. The citronellol substrate and even a second Pc molecule might act, in principle, as electron acceptors. As such, the above mechanism becomes relevant.

Furthermore, it also appears that, in the case of H_{16}PcZn, the decomposition products act as inhibitors for further photodegradation, as their accumulation in the reaction flask creates a stable composition after *ca.* 4 h illumination, less than 2% extra degradation being noticed for a greater than 20 h following period. The mechanism through which these impurities act as inhibitors of the photo-decomposition process is not the scope of this report; as such, its study has not been attempted. In addition, isolation and characterization of degradation products for a compound only used here as a comparison to the catalytically relevant new fluorinated materials is of least importance.

With respect to the photodegradation mechanism proposed in Figure 7.9, the staunch resilience of the subset of $(R_f)_n$PcZn catalysts exhibiting reduced steric bulkiness is outstanding, but explainable through the specifics of their aggregation in solution. While the steric protection towards chemical attacks on the Pc core's pyrrole units imparted by the F_{64} and F_{52}Pc ligands is evident in the absence of aggregation in the ethanolic solutions employed (Figure V.4), the high (viz. F_{16}PcZn) and intermediate (viz. $F_{24}H_8$, $F_{28}H_4$, F_{34} and F_{40}PcZn) dimerization degrees exhibited by the other R_f-containing photosensitizers may actually protect them from a potentially destructive $^1O_2$ attack on the *ipso* carbon atoms through π–π interactions which block, in principle, half of the susceptible nucleophilic attack positions in the dimer units, viz. the ones located on the stacking molecular faces.

Thus, photodegradation of the new fluoroalkylated complexes is suppressed, in addition to the electrophilic, nucleophilic and radical degradation pathways documented in Chapter 6, delivering a complete solution to the dilemma of finding an "immortal" metal–organic catalyst.

7.4 Discussion

Figure 7.5 depicts a diverse view of the photocatalytic activity exhibited by PcZn complexes. However, a closer look at the calculated catalytic parameters of Table 7.2 allows the establishment of definite trends for the variation of the initial oxygen consumption rates, r_0. Since the r_0 values are invariably related to the availability of $^1O_2$ in solution, they are a direct measure of the photosensitizers' efficiency in activating ground-state triplet oxygen under illumination. Two such trends, a general and a specific one, were identified, as discussed below.

A comparative analysis of Table 7.2 and the UV-vis spectra of the ethanolic reaction mixtures, Figure V.4, immediately establishes a qualitative correlation between the photocatalytic efficiency—expressed through the r_0 values—and the amount of monomeric form in solution, roughly estimated by the percentage of its Q band absorbance relative to the sum of the monomer and dimer Q band absorbances, as read directly from the UV-vis data; Figure 7.10 provides a visual representation of the trend.

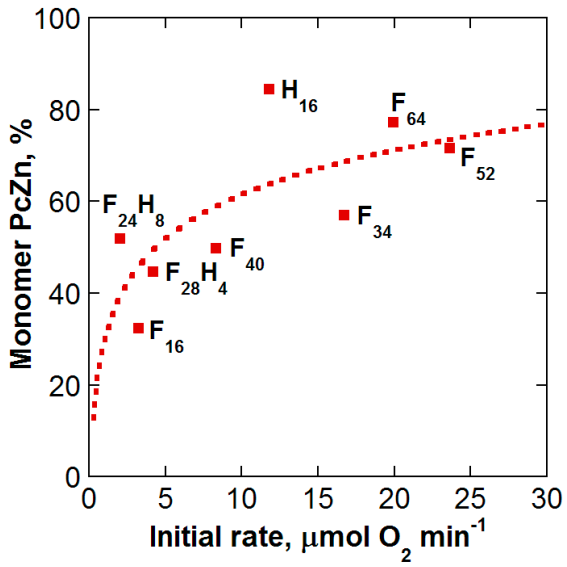

Figure 7.10 Plot of the estimated monomer PcZn percentages vs. the initial reaction rates for the photocatalytic oxidation of (*S*)-(−)-citronellol in ethanol. Logarithmic correlation: y = 29.36 + 32.09log(x), R = 0.72.

The loose (R = 0.72) logarithmic correlation of Figure 7.10, although imprecise, is qualitatively significant in confirming the detrimental effect of increased amounts of dimer species in solution for the efficient generation of $^1O_2$. The current results are completely consistent with the proposed bimolecular deactivation pathway of eqn. 7.1 and all previously published experimental observations.[112,177,186]

The specific trend in the variation of r_0 values is of a purely electronic nature, viz. the MO energy levels characteristic to each photosensitizer. In accordance with the view that R_f groups induce a drop and subsequent stabilization in the frontier orbitals' energy,[105–113] depressed energetic levels and more closely-spaced electronic bands allow for an intensification of photonic absorption and emission processes with formation of higher populations of triplet Pc excited states, as demonstrated by the highest $^1O_2$ quantum yield recorded for a PcM complex, viz. 0.81 for F_{64}PcZn.[112] Therefore, frontier orbital depression as a result of a higher F content might counterbalance a potentially detrimental aggregation level, and, inversely, higher MO energy levels of a non-fluorinated ligand may lead to lower yields in $^1O_2$ production. This valid hypothesis is illustrated by, e.g., the more active $F_{28}H_4$PcZn vs. the less dimerized $F_{24}H_8$PcZn (with r_0 values of 4.2 and 2.0 μmol O_2 min^{-1}, respectively), and the more active F_{34}, F_{52} and F_{64}PcZn vs. the monomeric extreme of H_{16}PcZn.

All steric factors aside, equally monomeric perfluorinated PcZn photosensitizers are differentiated purely by their intrinsic MO properties. In this respect, the absolute highest r_0 obtained for F_{52}PcZn, viz. 23.6 μmol O_2 min^{-1}, supported by the highest red-shift in the Q band recorded for perfluorinated PcMs (Section 5.3.5), propose it as the new efficiency standard for photocatalyzed singlet oxygen production.

7.5 Conclusions

The zinc(II) analogues of the new perfluoroalkylated Pc classes obtained in this work have been tested for their ability to photochemically activate ground-state triplet oxygen to its chemically reactive singlet form. In this manner, naturally occurring (*S*)-(−)-citronellol was selectively photooxygenated to a mixture of two hydroperoxides.

An inverse correlation is established between the fluorinated photosensitizers' dimerization degrees in the ethanolic reaction solutions and the observed rates of singlet oxygen generation. The rate for F_{52}PcZn, marginally higher than that for F_{64}PcZn, previously considered the standard in Pc-based photocatalytic production of $^1O_2$, suggests an even lower depression of frontier orbital energy levels under R_f-induced molecular asymmetry and proposes the complex as the new absolute PcM in quantum efficiency.

Through perfluorination by a mix of peripheral R_f groups and aromatic F atoms, the self-induced, light-activated degradation pathways encountered for common, hydrogen-containing Pc photosensitizers have been suppressed, along with stabilization of longer-lived triplet excited states, as proved by the clean, quantitative substrate oxygenations and efficient activation of ground-state dioxygen.

The resistance of the new fluoro-perfluoroalkyl complexes towards photo-degradation complements their already demonstrated inertness towards electrophilic, nucleophilic and radical degradation pathways, offering a viable solution to the dilemma of finding an "immortal" metal–organic catalyst and thus helping solve an important problem in catalysis. The metal-dependent bifunctionality of the new materials for redox- (electron transfer) and photo- (energy transfer) catalytic applications thoroughly validates the broad scope and utility of this project.

APPENDIX A

NMR SPECTRA

Figures A.1 to A.69 show ^{1}H, ^{19}F, ^{13}C and ^{31}P NMR spectra of all compounds described in this work, presented over the full typical scan range (in ppm) of the respective nucleus observed: −0.5 to +10.5 (^{1}H), −5 to +200 (^{13}C), −125 (or −180) to +10 (^{19}F), −40 to +40 (^{31}P). Peak labeling was done only for the signals assigned to the characterized compound. Abbreviations of systematic names used in figure captions follow the rules outlined in the corresponding chapters. Insets expanding regions of particular interest in confirming the structural identity of the compound have been inserted where appropriate. Each spectrum contains the compound structural formula and assigned number, as well as the acquisition frequency (in MHz) for the observed nuclei and the deuterated solvent of dilution.

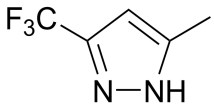

[3-3]

300 MHz, $CDCl_3$

Figure A.1 ^{1}H NMR spectrum of Pz^{CF_3,CH_3}.

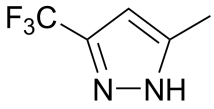

[3-3]

282 MHz, $CDCl_3$

Figure A.2 ^{19}F NMR spectrum of Pz^{CF_3,CH_3}.

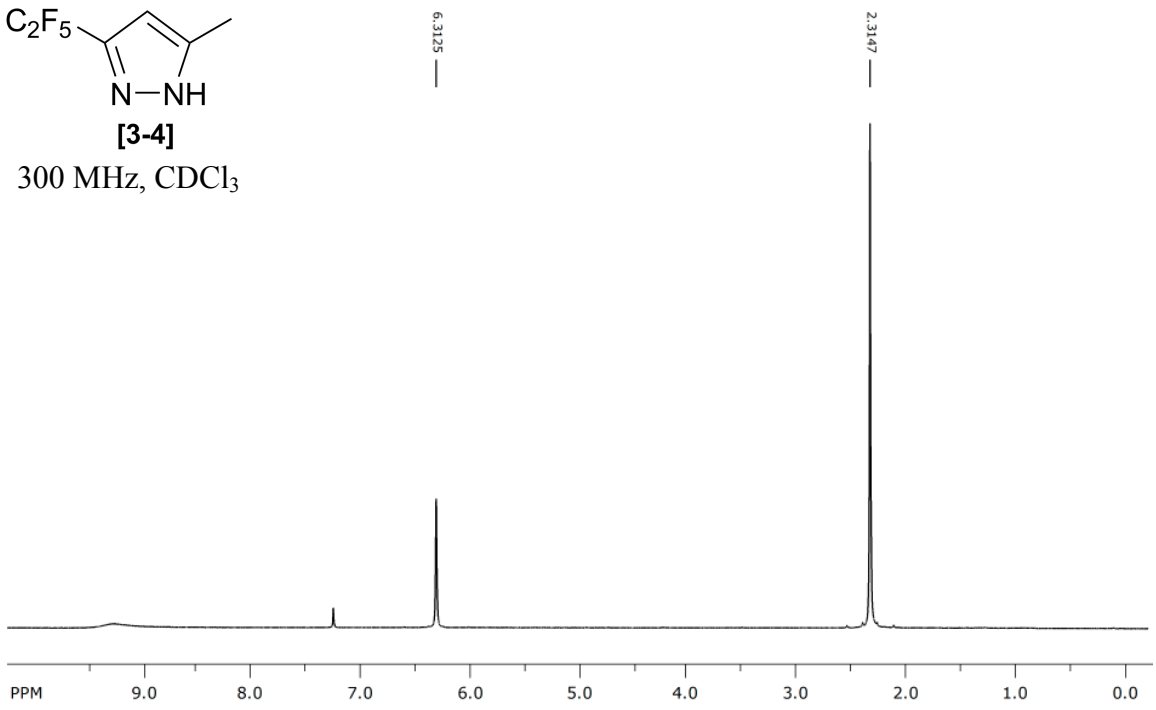

Figure A.3 ^{1}H NMR spectrum of $Pz^{C_2F_5,CH_3}$.

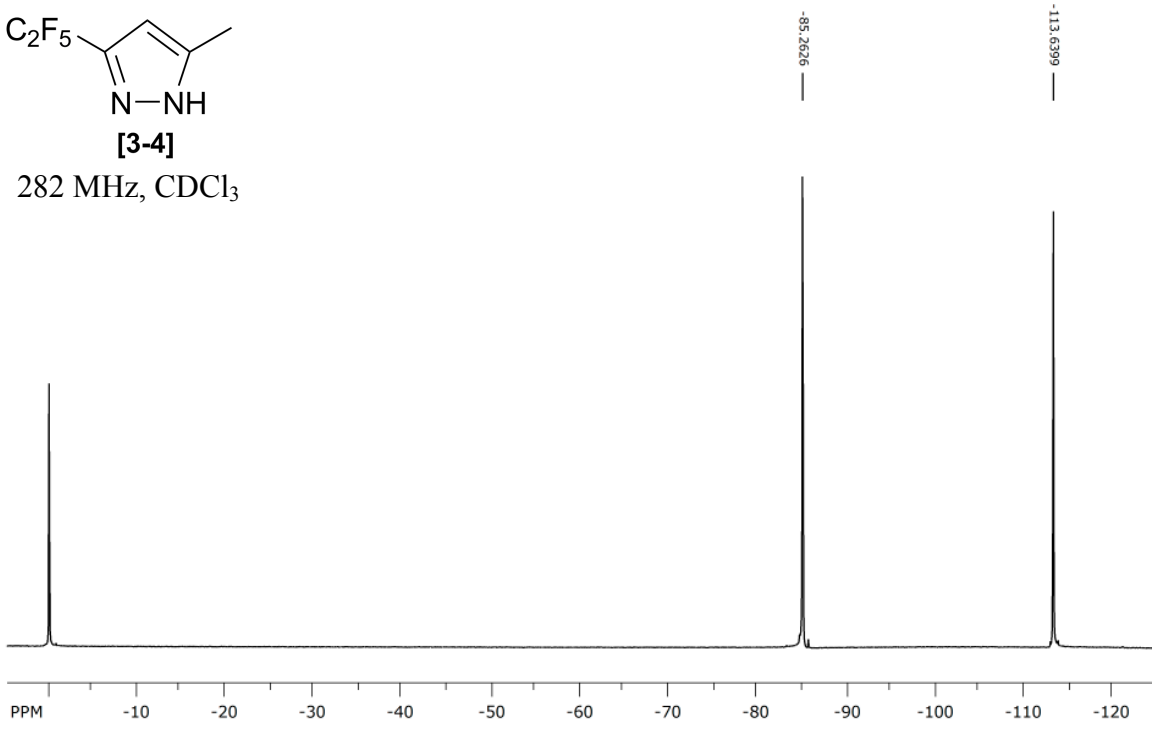

Figure A.4 ^{19}F NMR spectrum of $Pz^{C_2F_5,CH_3}$.

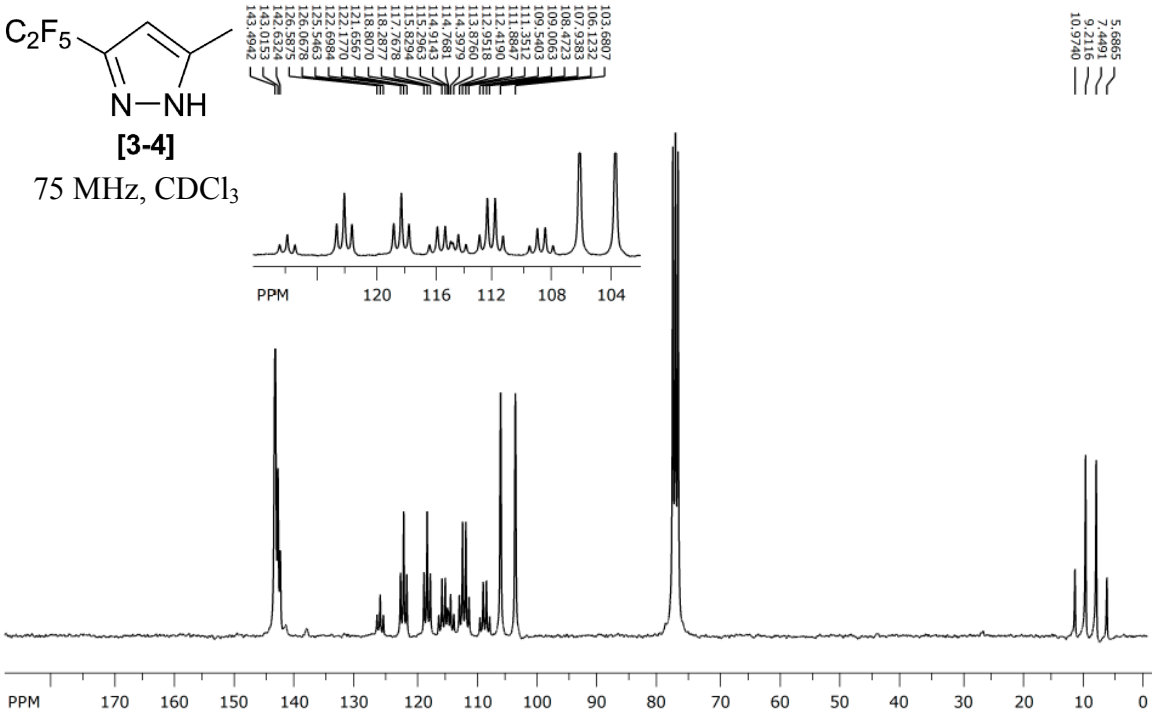

Figure A.5 ^{13}C NMR spectrum of $Pz^{C_2F_5,CH_3}$.

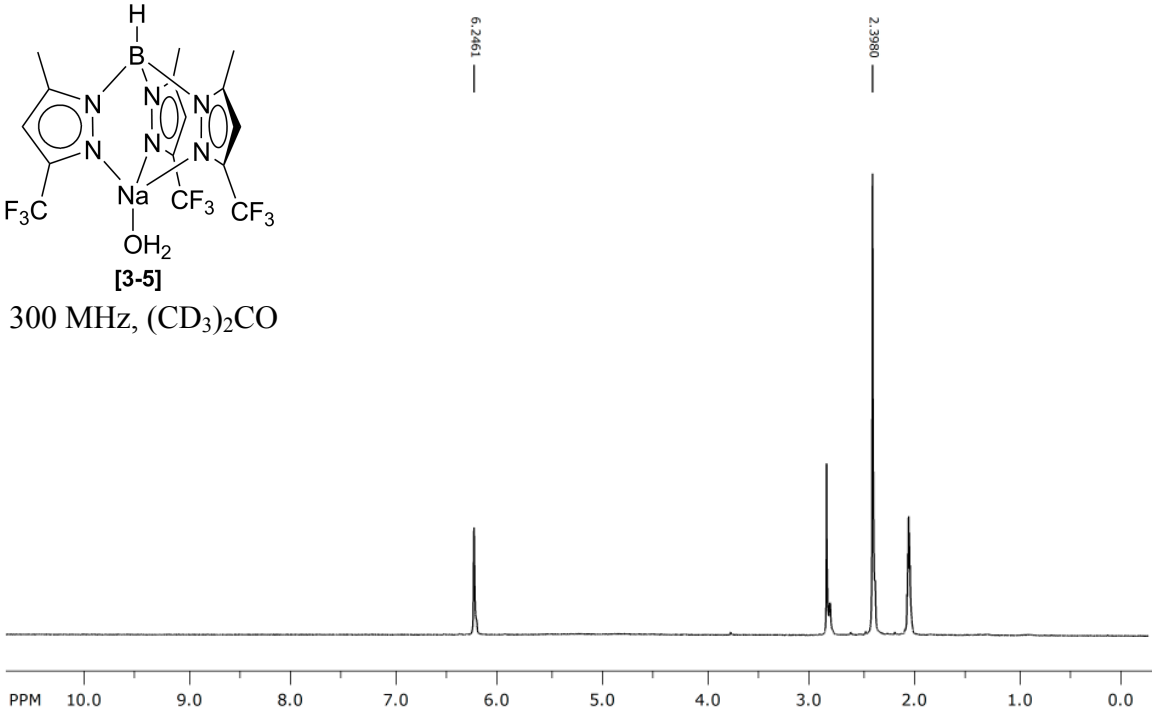

Figure A.6 ^{1}H NMR spectrum of $Tp^{CF_3,CH_3}Na(H_2O)$.

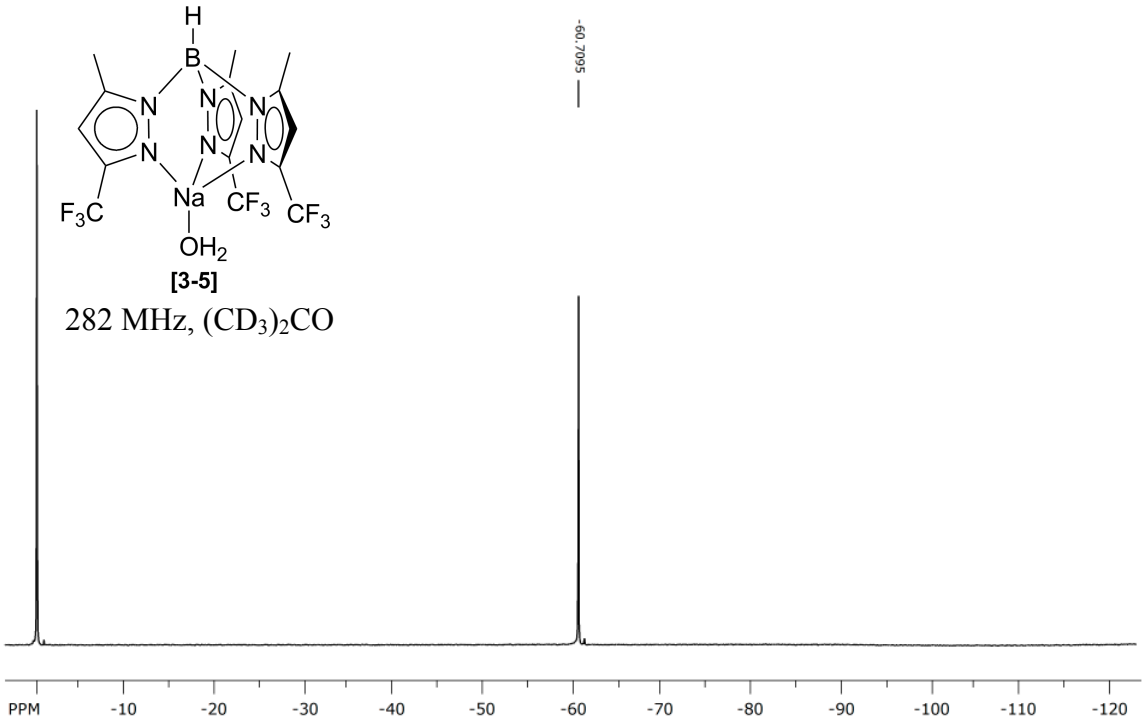

Figure A.7 ^{19}F NMR spectrum of $Tp^{CF_3,CH_3}Na(H_2O)$.

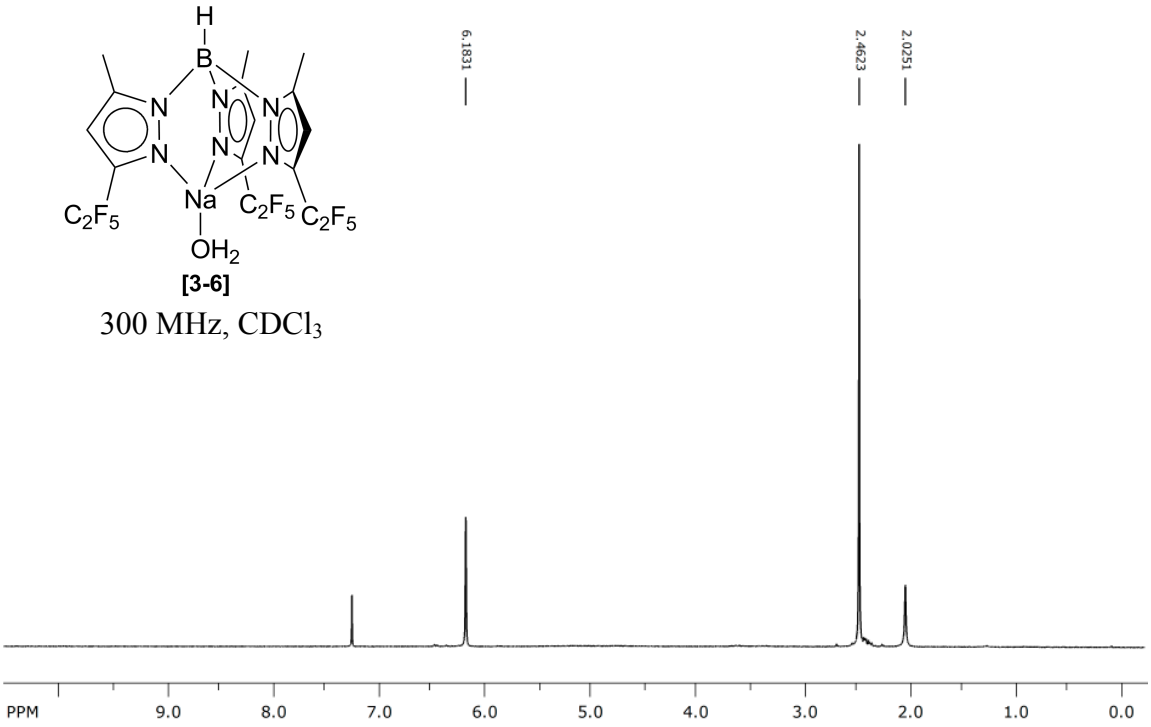

Figure A.8 ^{1}H NMR spectrum of $Tp^{C_2F_5,CH_3}Na(H_2O)$.

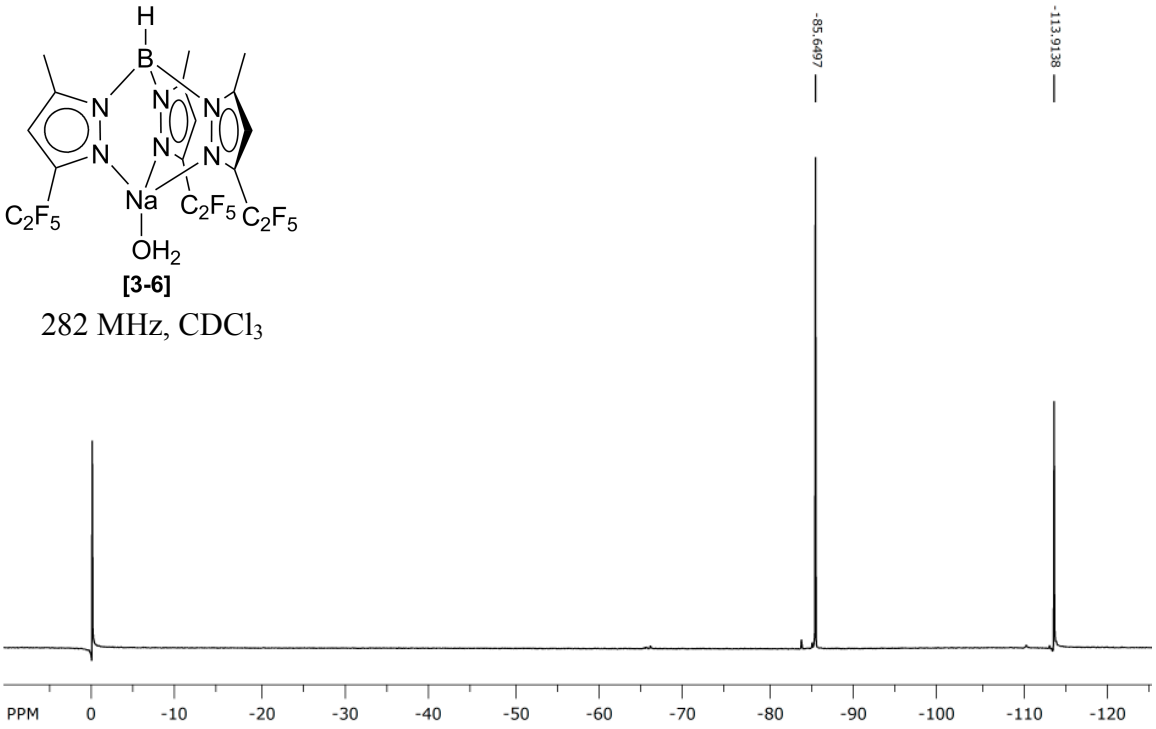

Figure A.9 ^{19}F NMR spectrum of $Tp^{C_2F_5,CH_3}Na(H_2O)$.

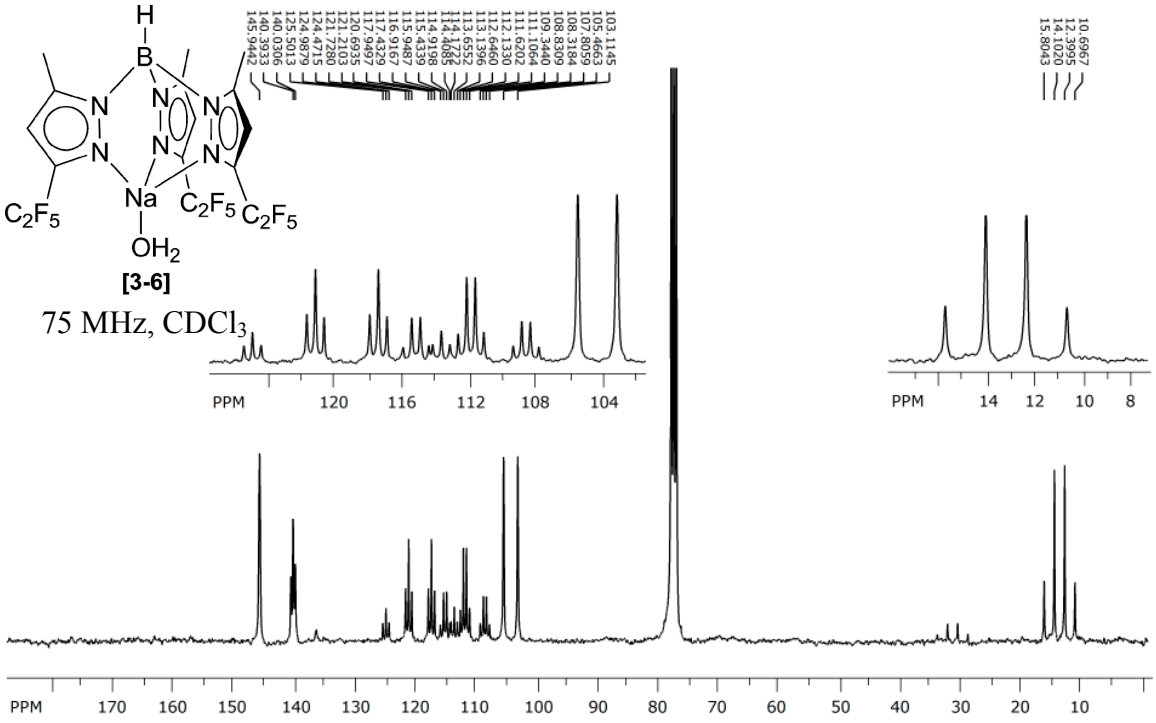

Figure A.10 ^{13}C NMR spectrum of $Tp^{C_2F_5,CH_3}Na(H_2O)$.

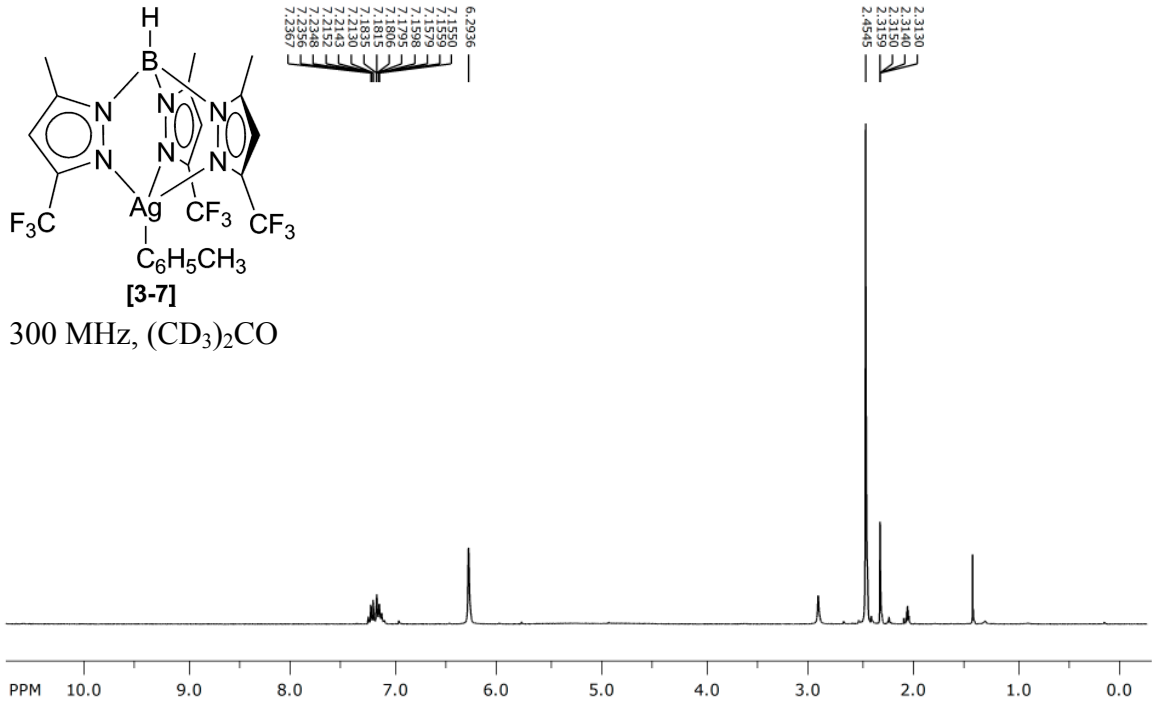

Figure A.11 ^{1}H NMR spectrum of $Tp^{CF_3,CH_3}Ag(Tol)$.

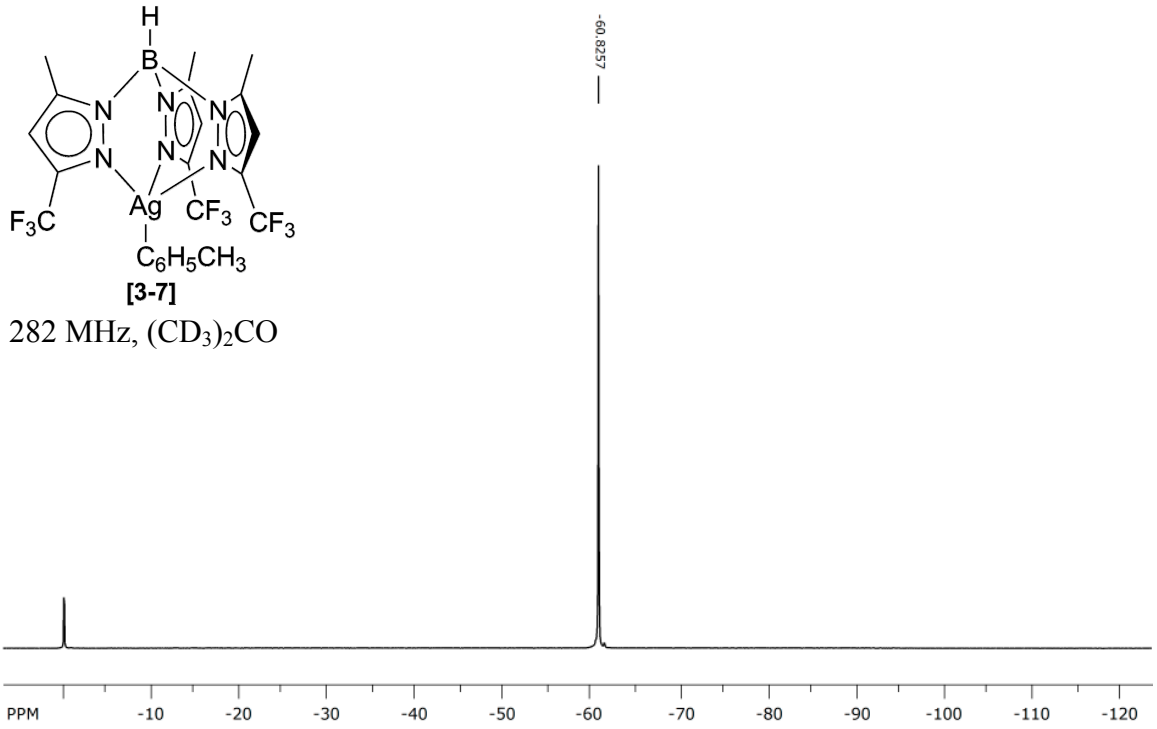

Figure A.12 ^{19}F NMR spectrum of $Tp^{CF_3,CH_3}Ag(Tol)$.

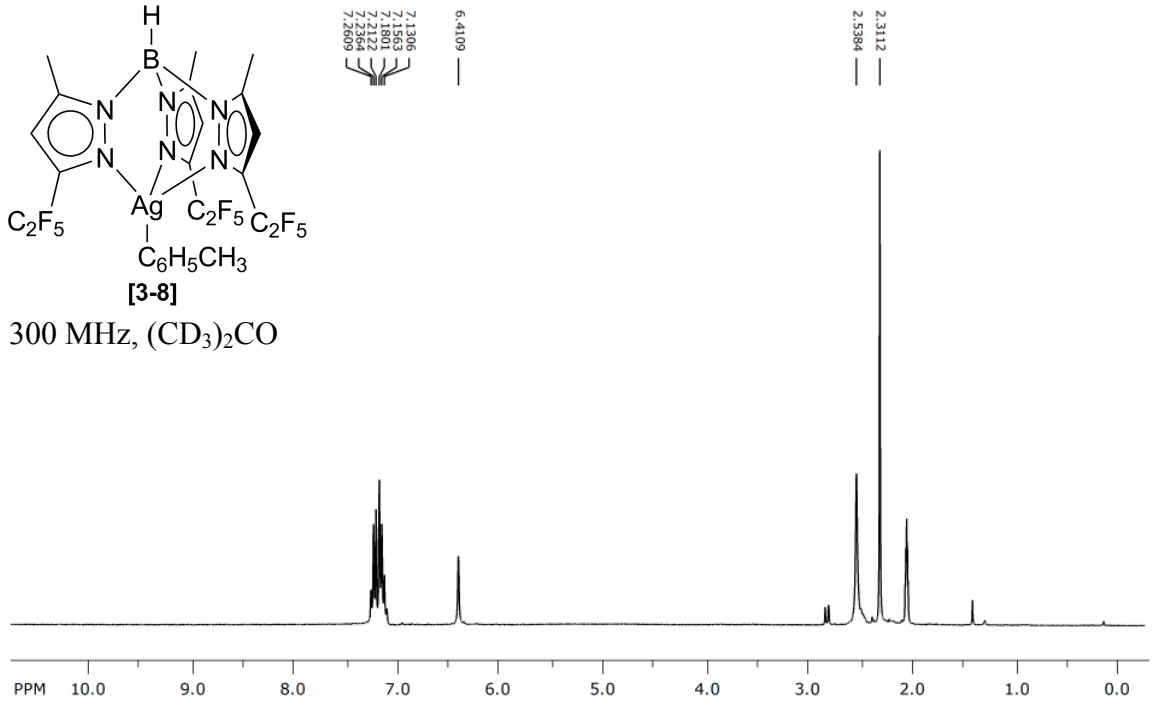

Figure A.13 ^{1}H NMR spectrum of $Tp^{C_2F_5,CH_3}Ag(Tol)$.

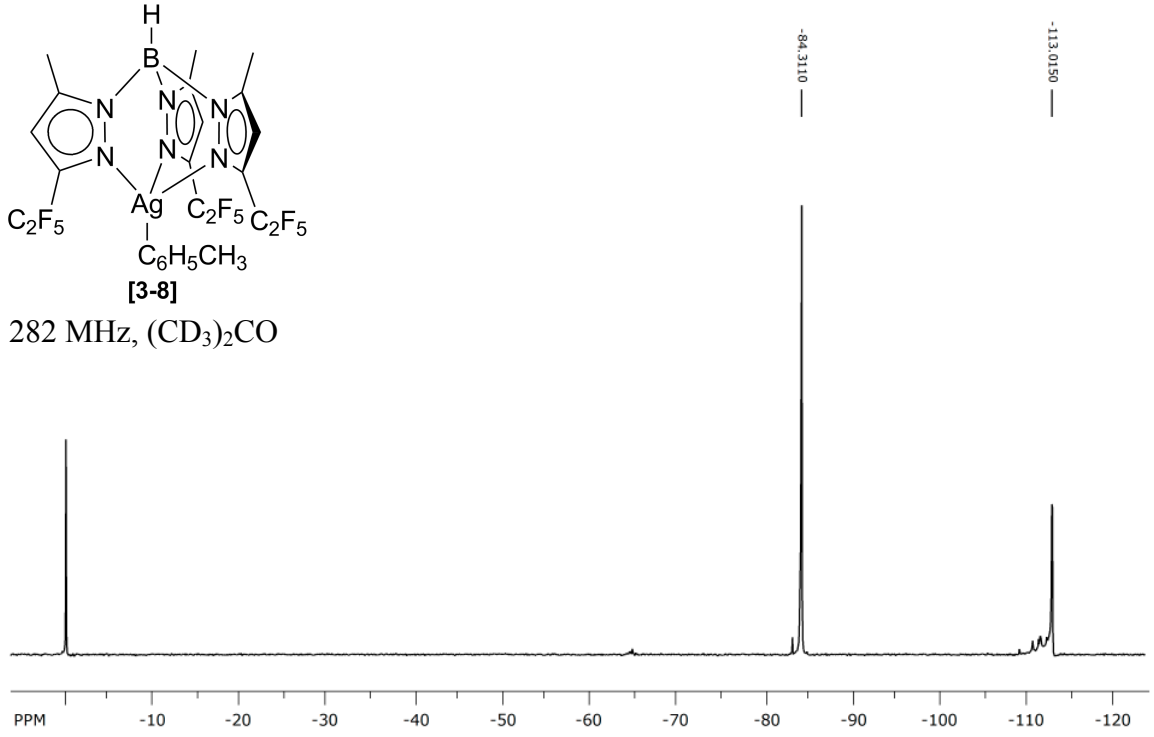

Figure A.14 ^{19}F NMR spectrum of $Tp^{C_2F_5,CH_3}Ag(Tol)$.

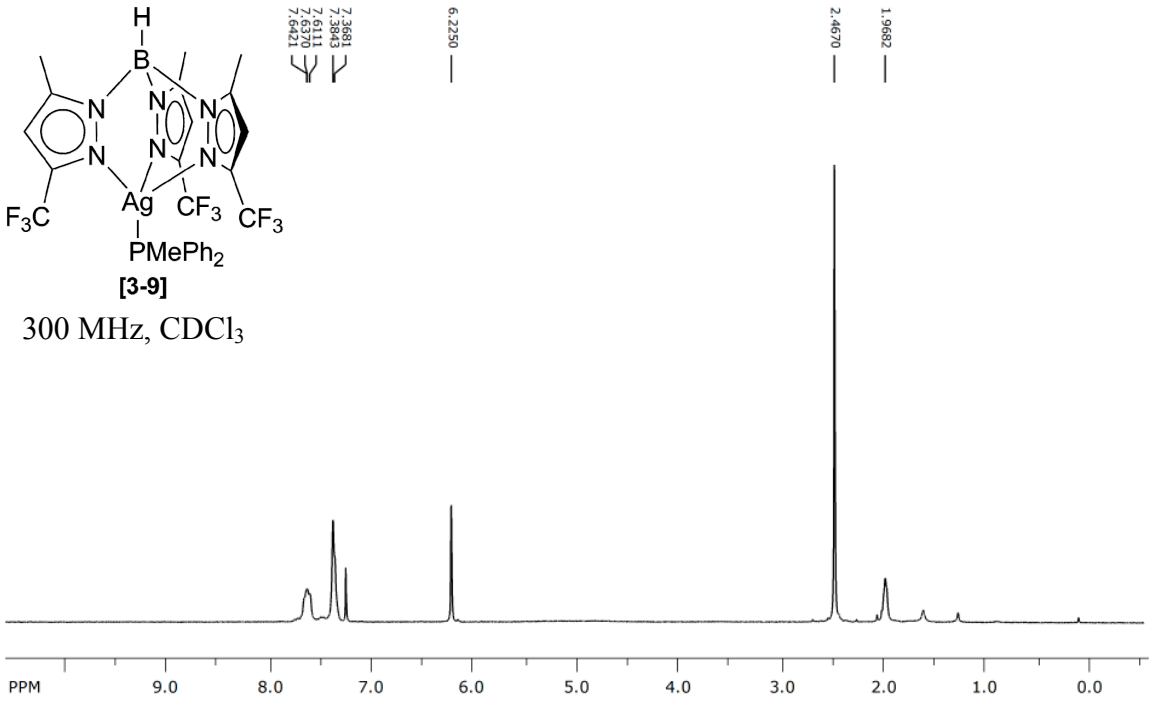

Figure A.15 ^{1}H NMR spectrum of $Tp^{CF_3,CH_3}Ag(PMePh_2)$.

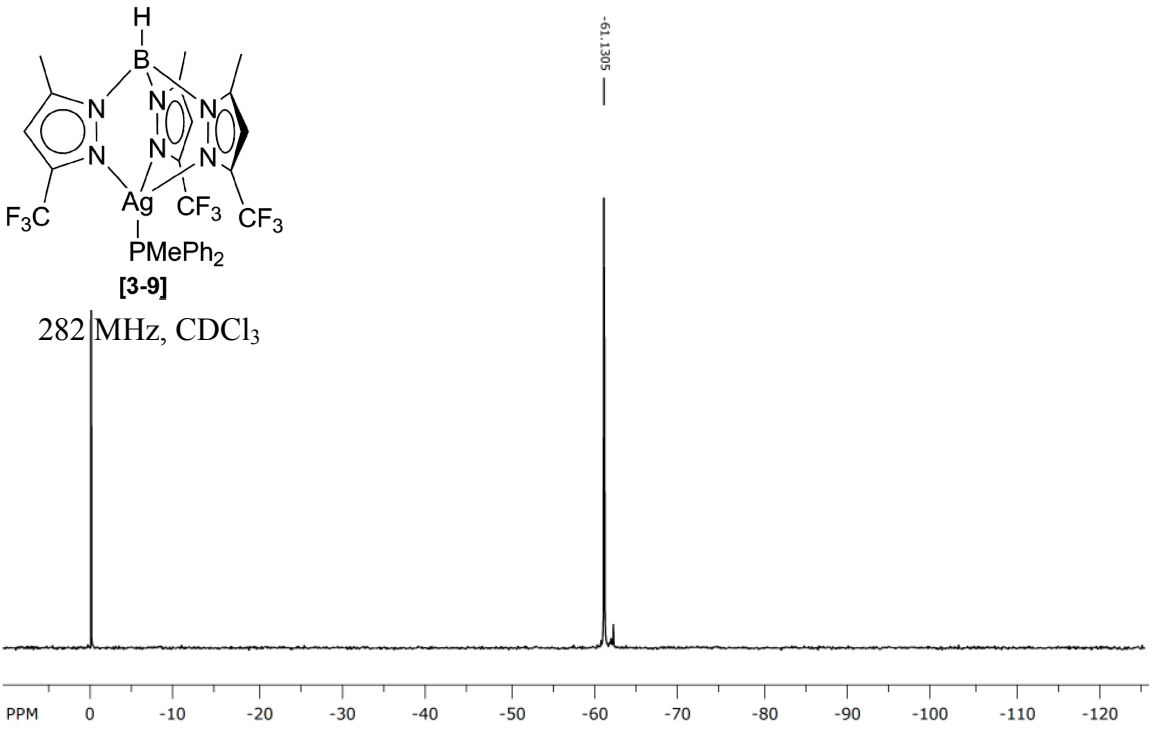

Figure A.16 ^{19}F NMR spectrum of $Tp^{CF_3,CH_3}Ag(PMePh_2)$.

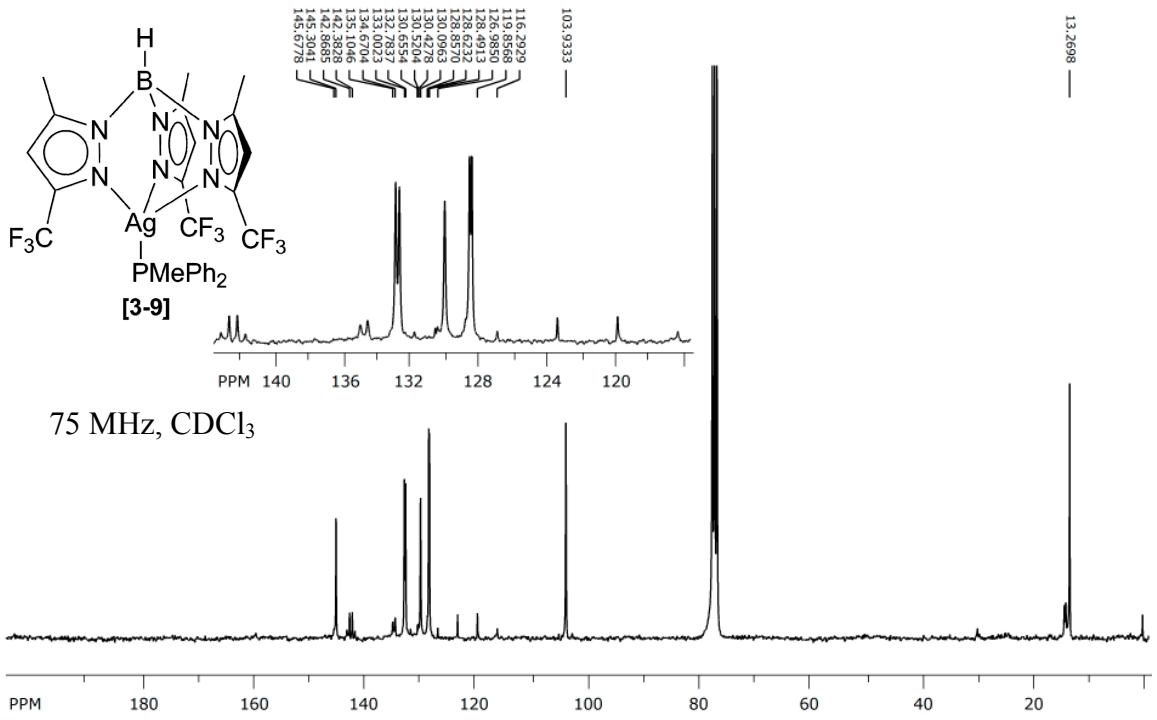

Figure A.17 ^{13}C {^{1}H} NMR spectrum of $Tp^{CF_3,CH_3}Ag(PMePh_2)$.

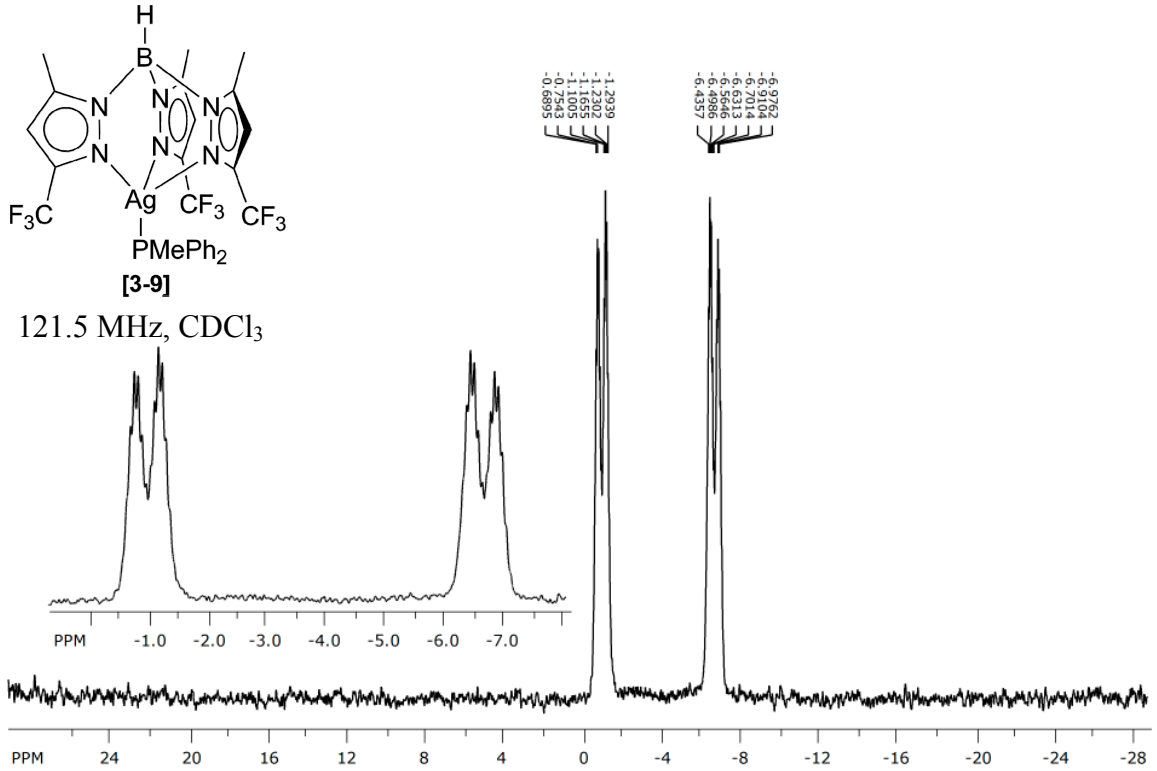

Figure A.18 ^{31}P {^{1}H} NMR spectrum of $Tp^{CF_3,CH_3}Ag(PMePh_2)$.

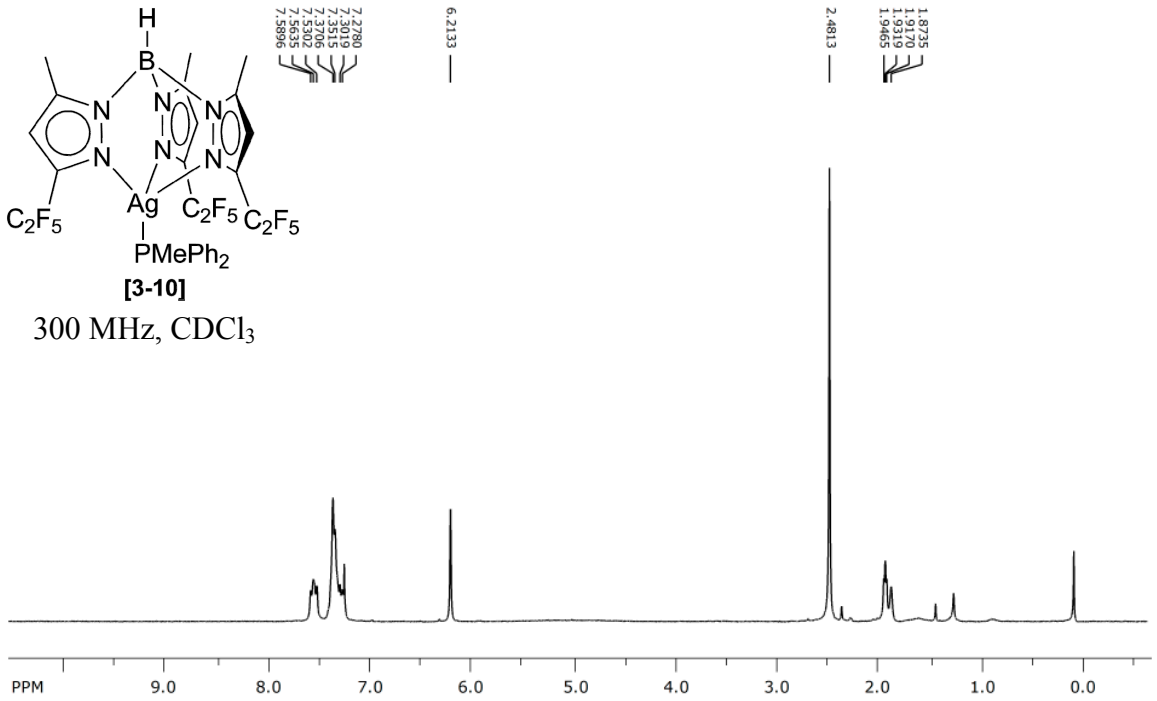

Figure A.19 ^{1}H NMR spectrum of $Tp^{C_2F_5,CH_3}Ag(PMePh_2)$.

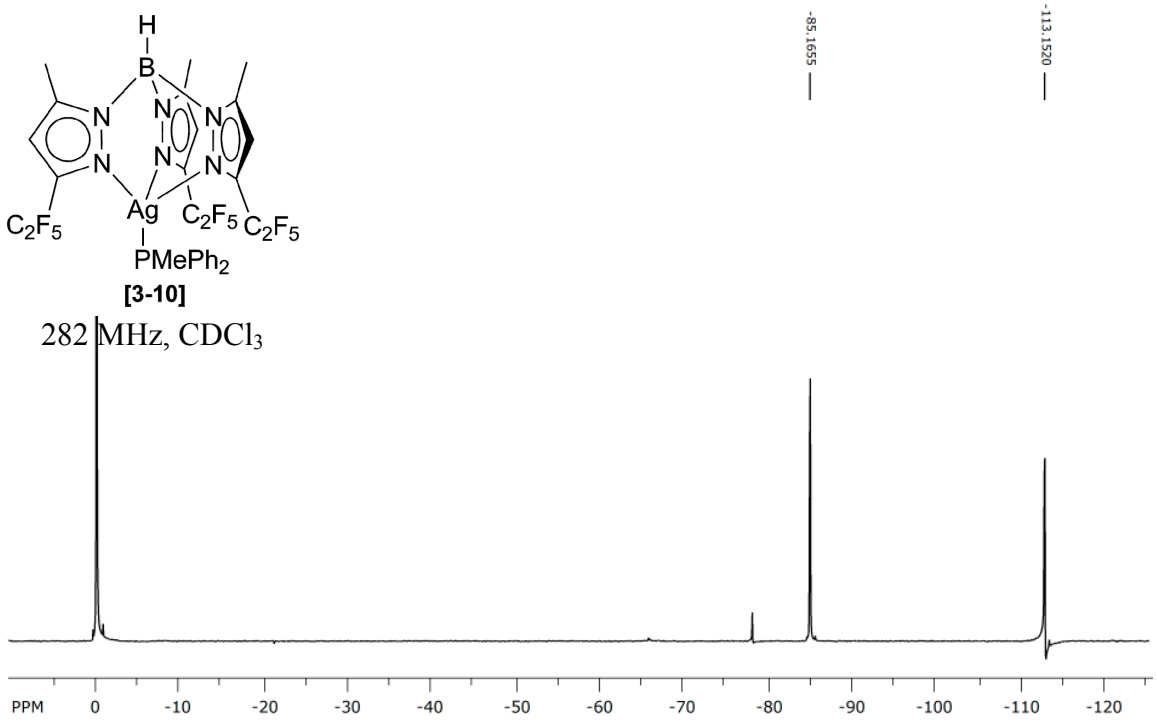

Figure A.20 ^{19}F NMR spectrum of $Tp^{C_2F_5,CH_3}Ag(PMePh_2)$.

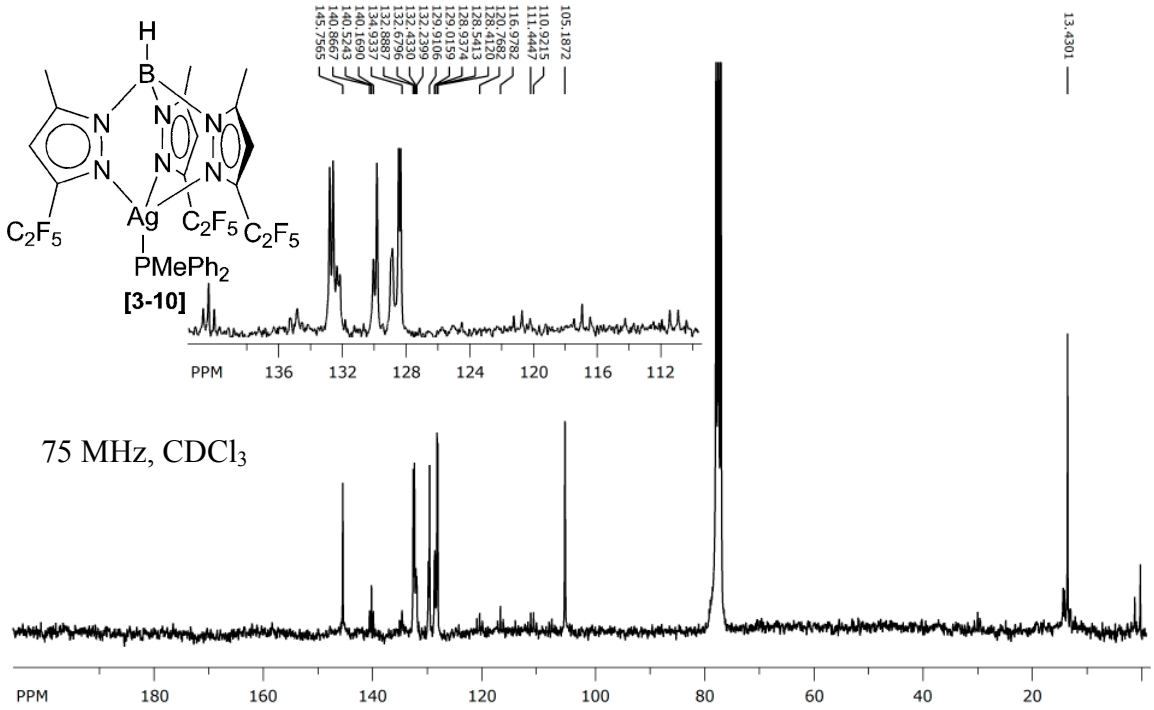

Figure A.21 ^{13}C {^{1}H} NMR spectrum of $Tp^{C_2F_5,CH_3}Ag(PMePh_2)$.

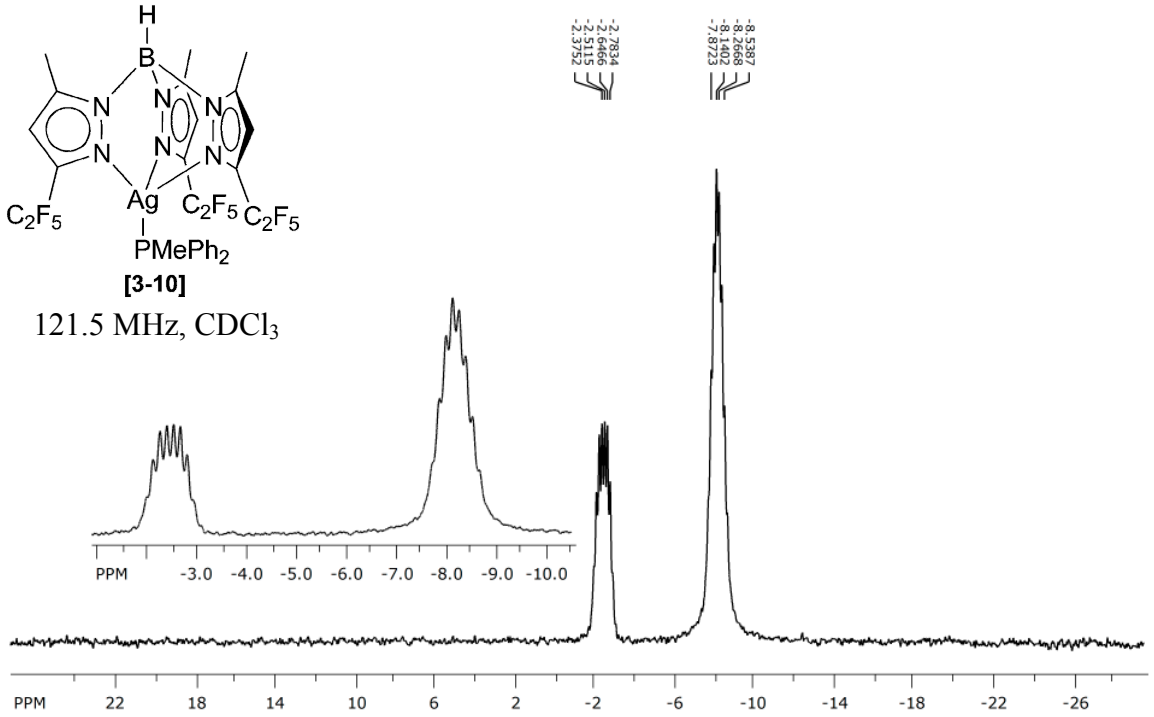

Figure A.22 ^{31}P {^{1}H} NMR spectrum of $Tp^{C_2F_5,CH_3}Ag(PMePh_2)$.

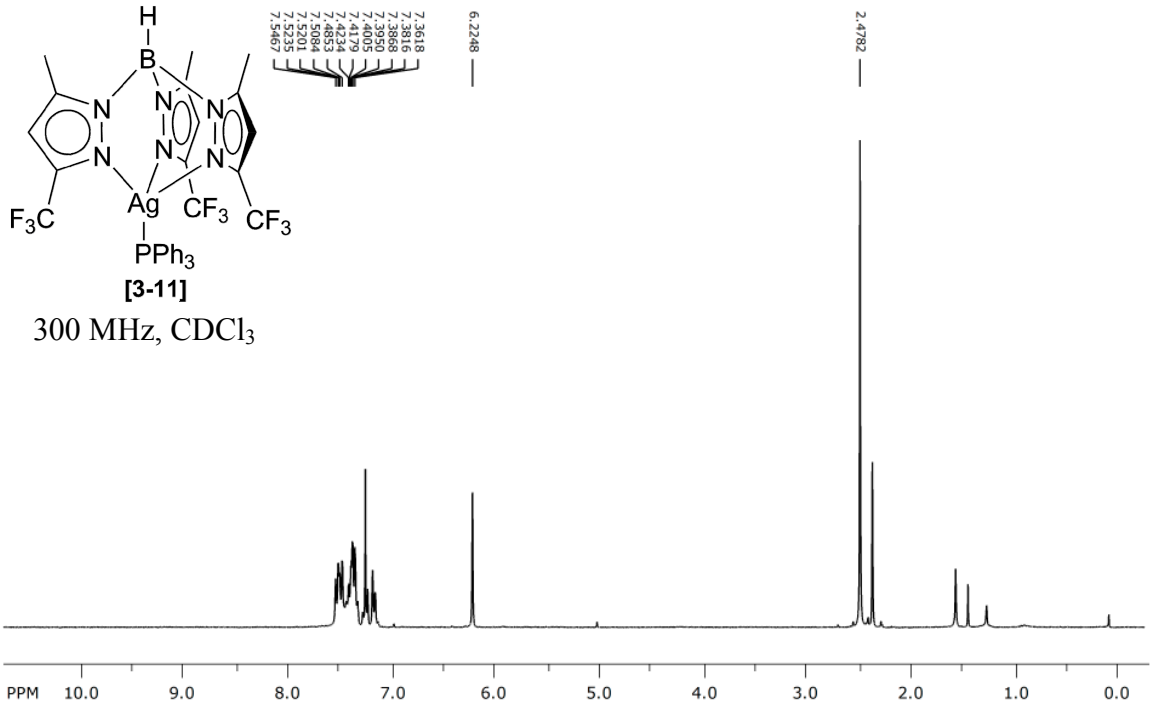

Figure A.23 ^{1}H NMR spectrum of $Tp^{CF_3,CH_3}Ag(PPh_3)$.

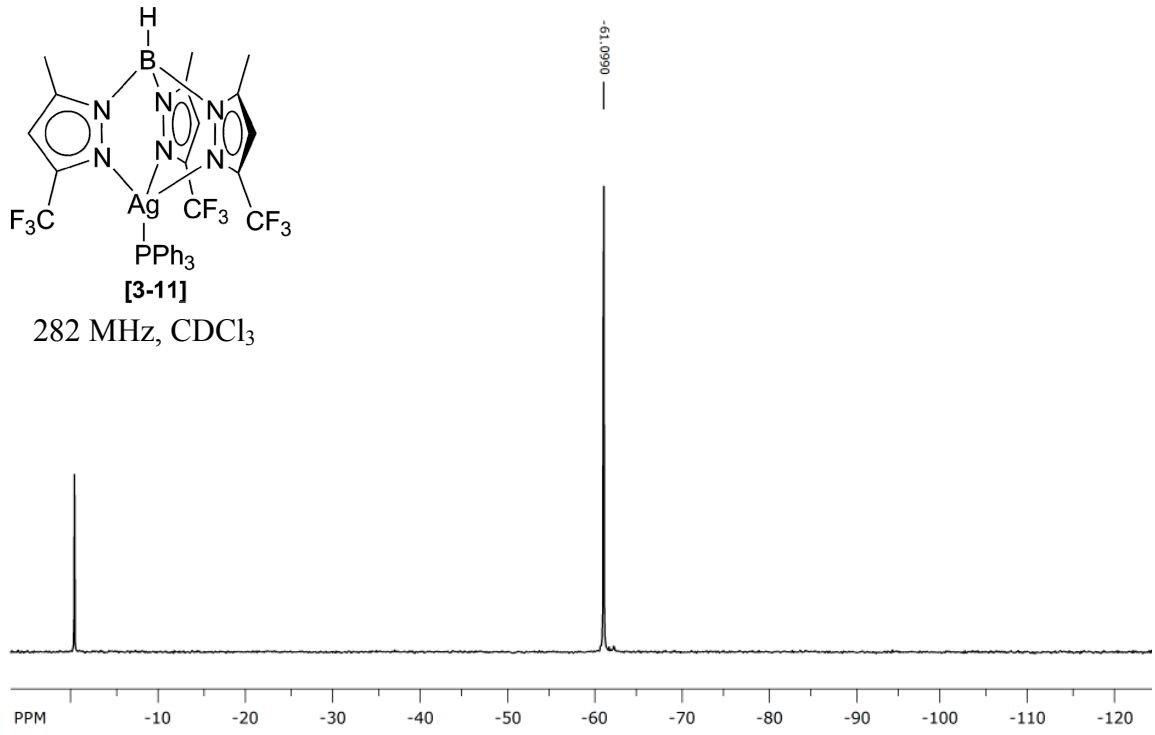

Figure A.24 ^{19}F NMR spectrum of $Tp^{CF_3,CH_3}Ag(PPh_3)$.

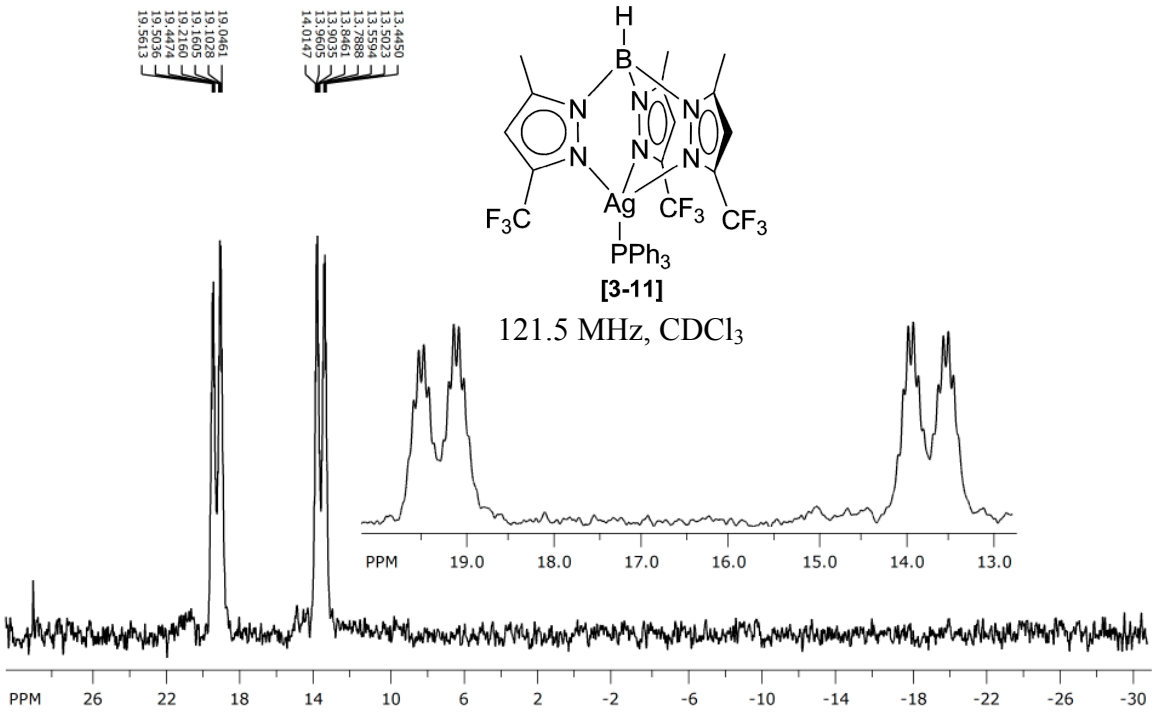

Figure A.25 ^{31}P $\{^{1}H\}$ NMR spectrum of $Tp^{CF_3,CH_3}Ag(PPh_3)$.

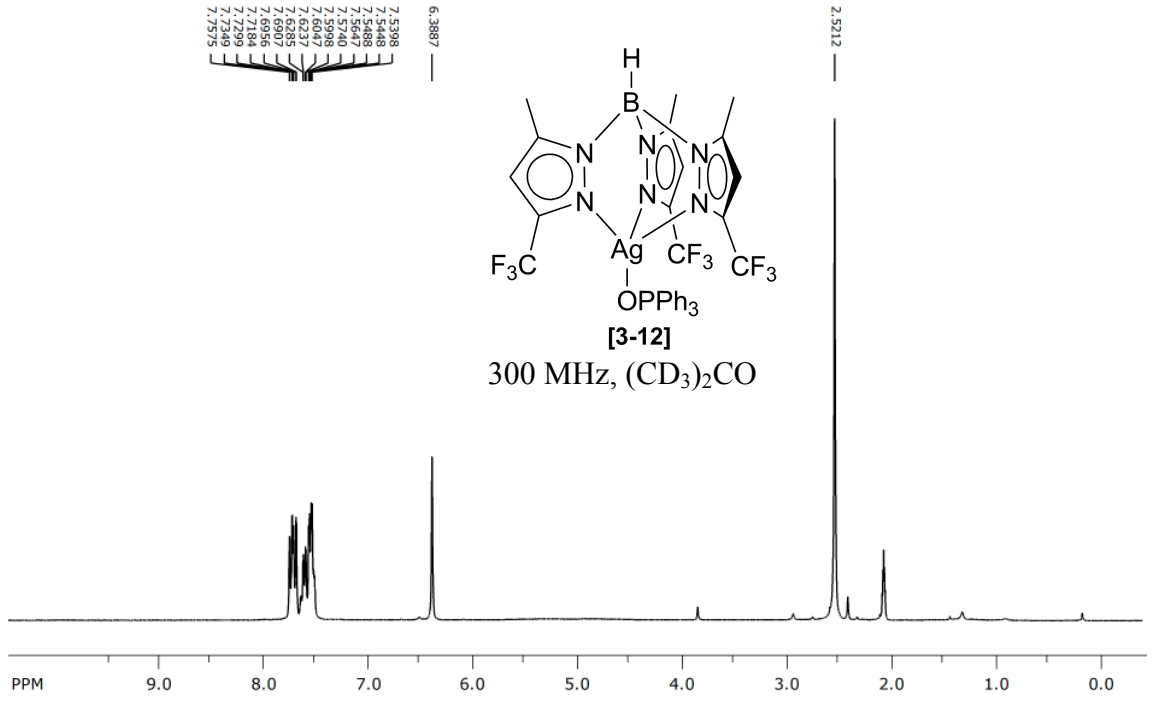

Figure A.26 ^{1}H NMR spectrum of $Tp^{CF_3,CH_3}Ag(OPPh_3)$.

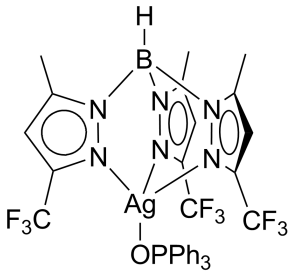

[3-12]

282 MHz, $(CD_3)_2CO$

Figure A.27 ^{19}F NMR spectrum of $Tp^{CF_3,CH_3}Ag(OPPh_3)$.

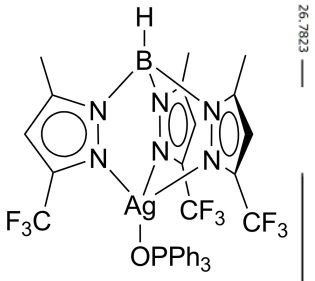

[3-12]

121.5 MHz, $(CD_3)_2CO$

Figure A.28 ^{31}P $\{^1H\}$ NMR spectrum of $Tp^{CF_3,CH_3}Ag(OPPh_3)$.

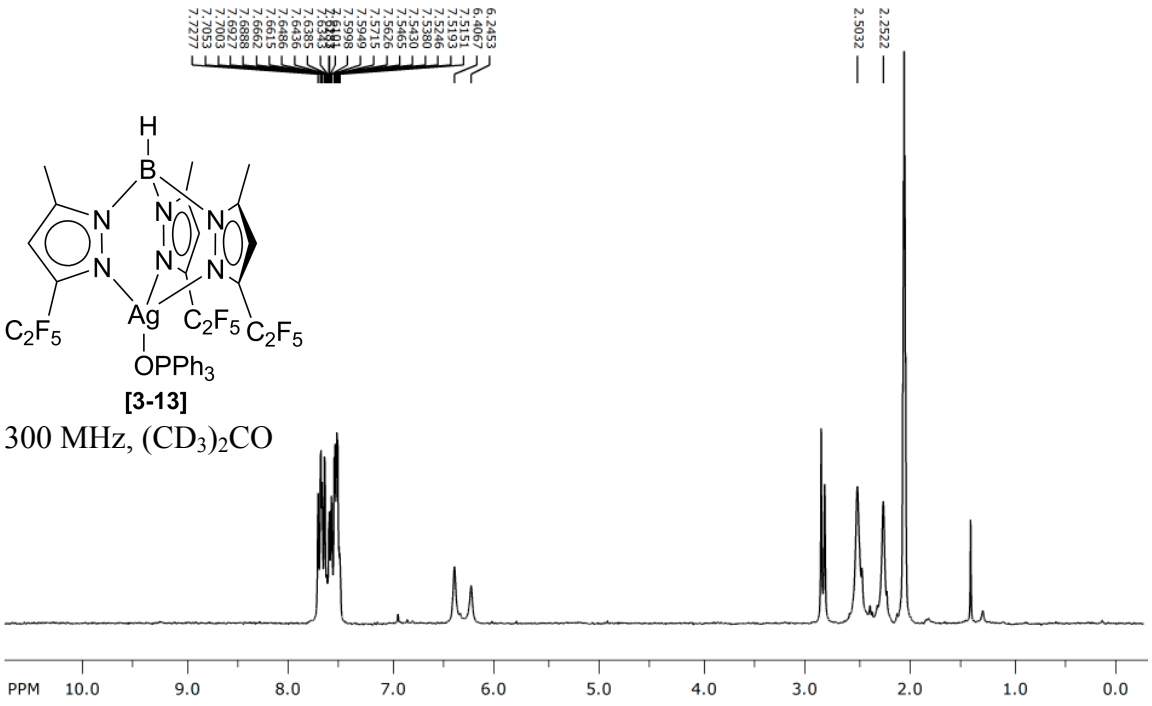

Figure A.29 ^{1}H NMR spectrum of $Tp^{C_2F_5,CH_3}Ag(OPPh_3)$.

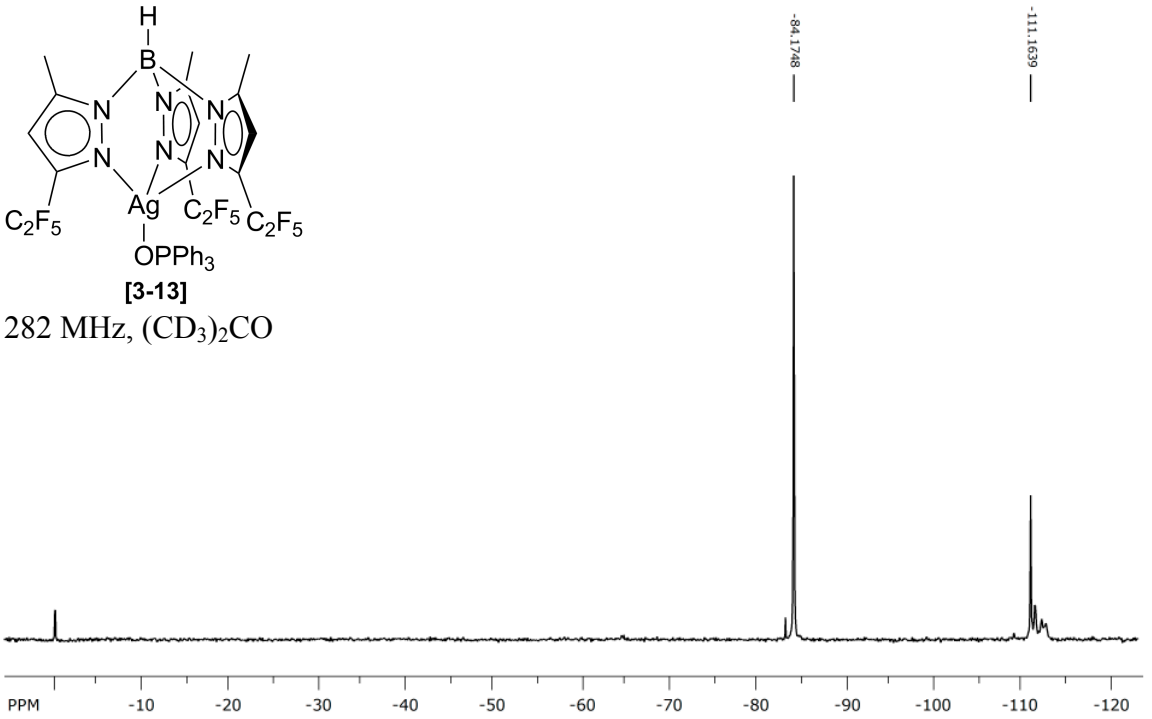

Figure A.30 ^{19}F NMR spectrum of $Tp^{C_2F_5,CH_3}Ag(OPPh_3)$.

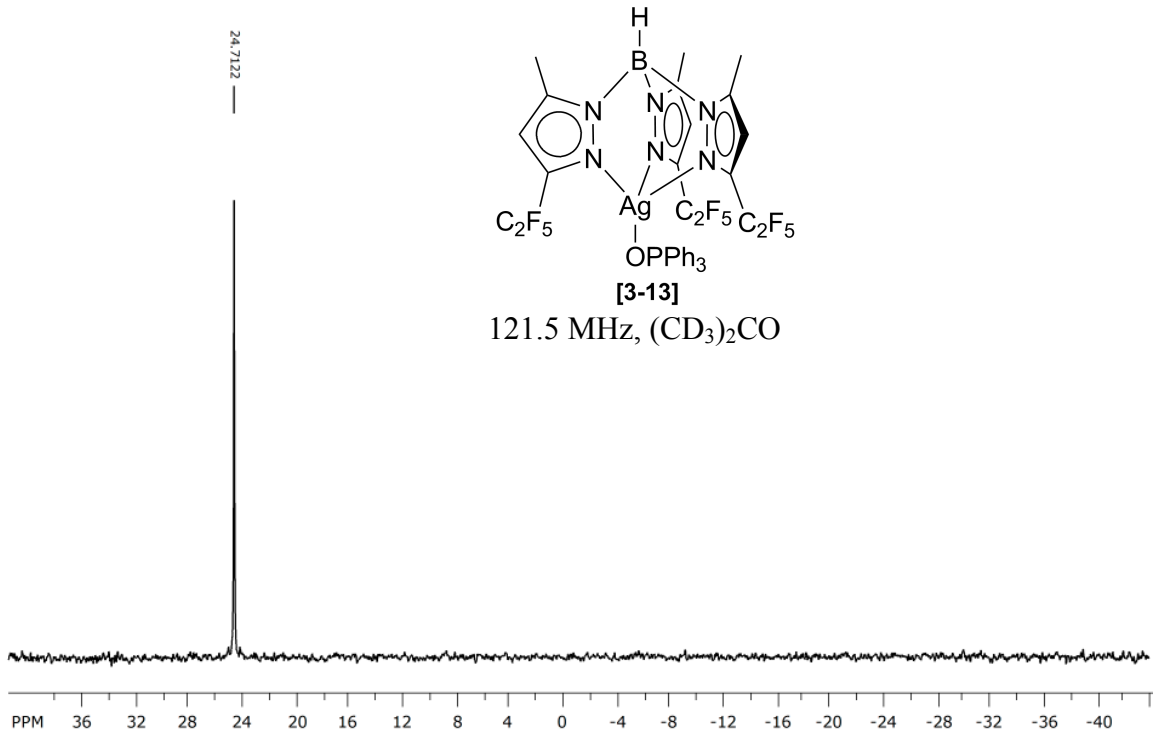

[3-13]

121.5 MHz, $(CD_3)_2CO$

Figure A.31 ^{31}P $\{^1H\}$ NMR spectrum of $Tp^{C_2F_5,CH_3}Ag(OPPh_3)$.

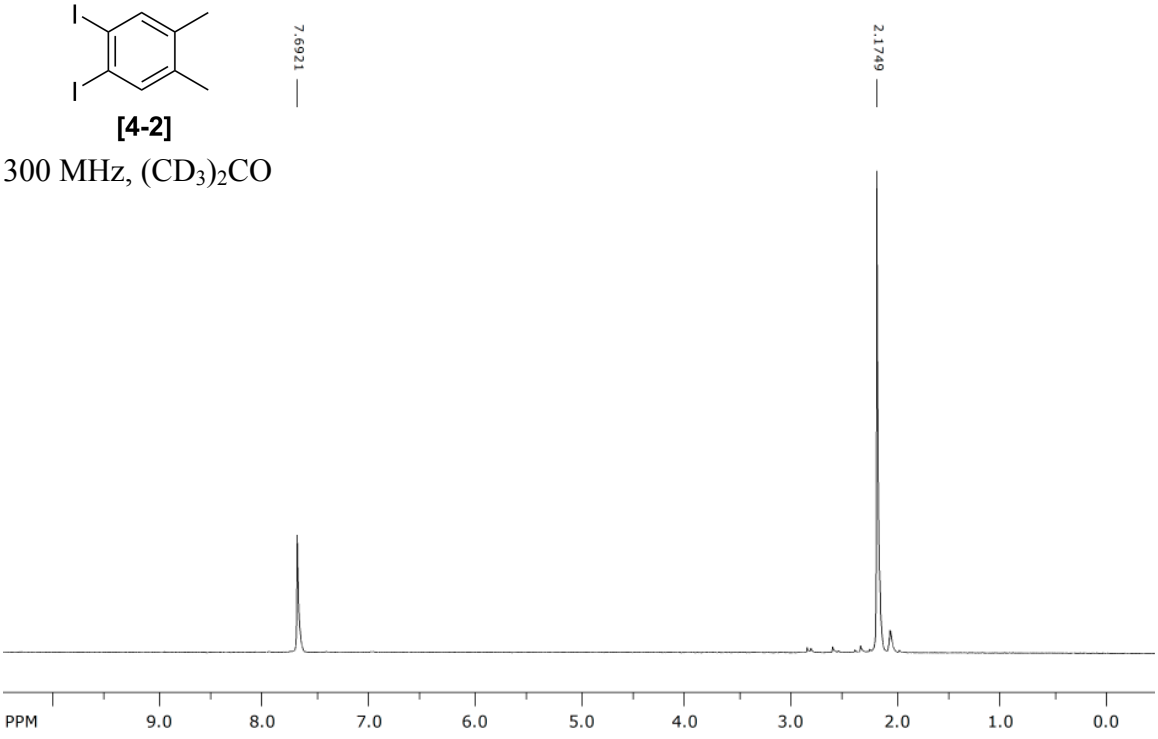

[4-2]

300 MHz, $(CD_3)_2CO$

Figure A.32 ^1H NMR spectrum of 1,2-diiodo-4,5-dimethylbenzene.

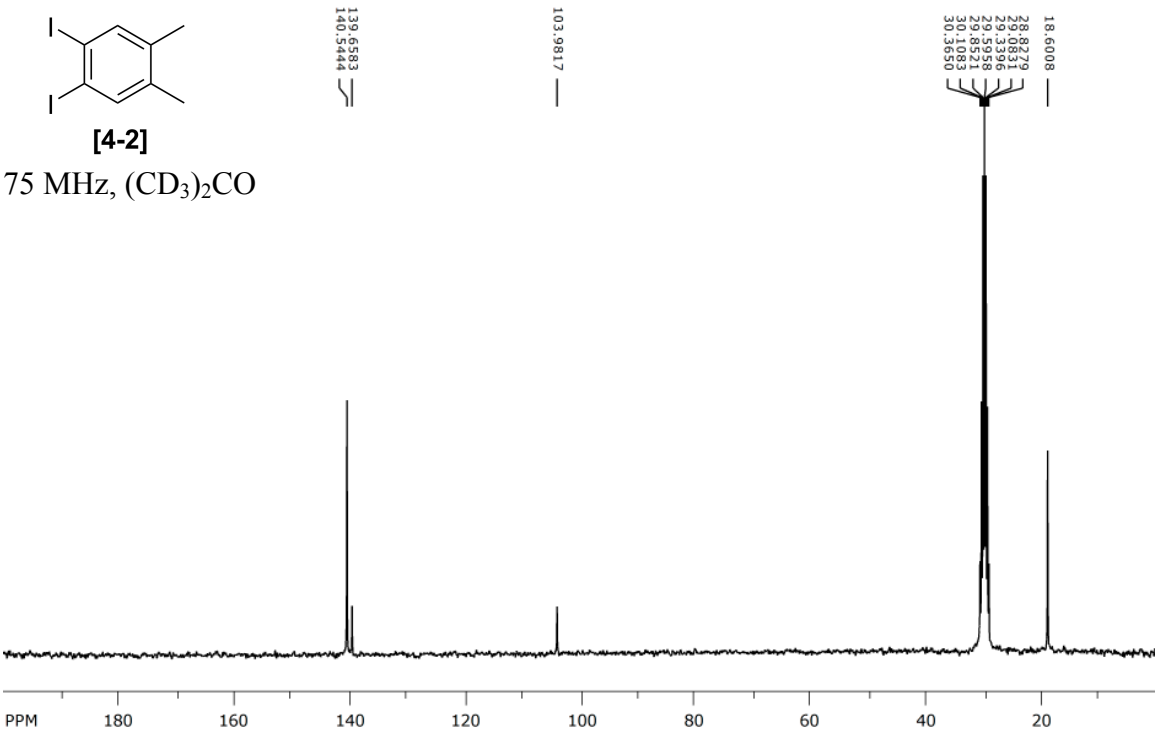

Figure A.33 ^{13}C {^{1}H} NMR spectrum of 1,2-diiodo-4,5-dimethylbenzene.

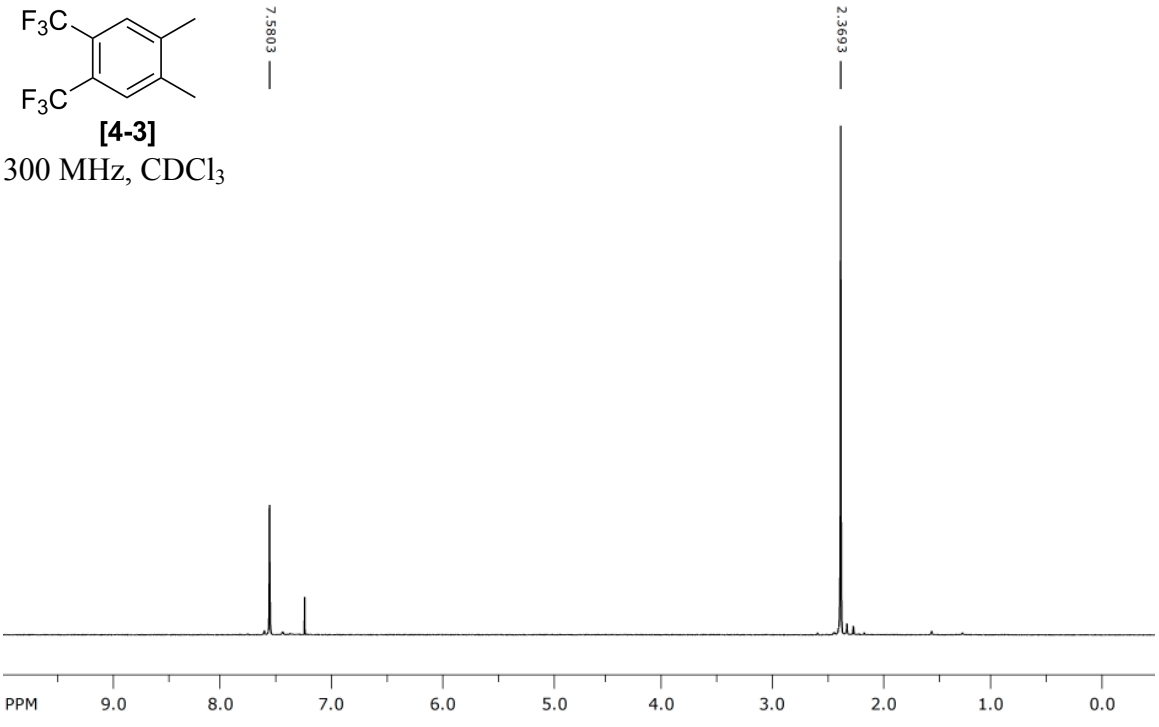

Figure A.34 ^{1}H NMR spectrum of 1,2-bis(trifluoromethyl)-4,5-dimethylbenzene.

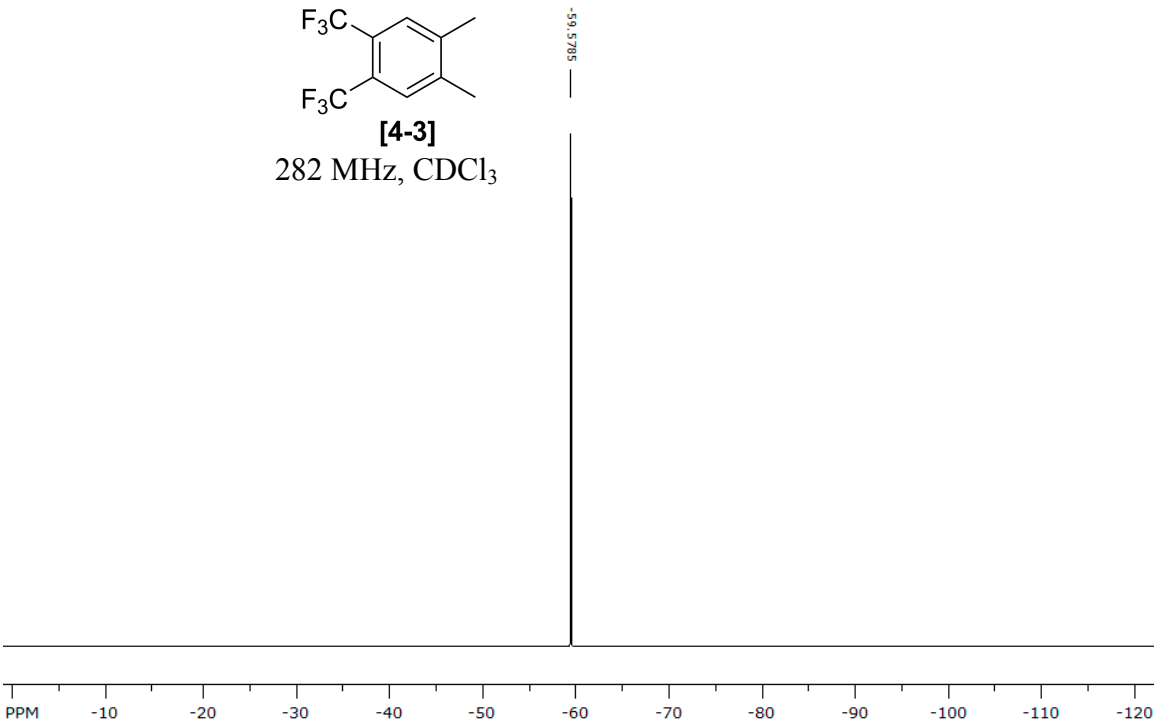

Figure A.35 ^{19}F NMR spectrum of 1,2-bis(trifluoromethyl)-4,5-dimethylbenzene.

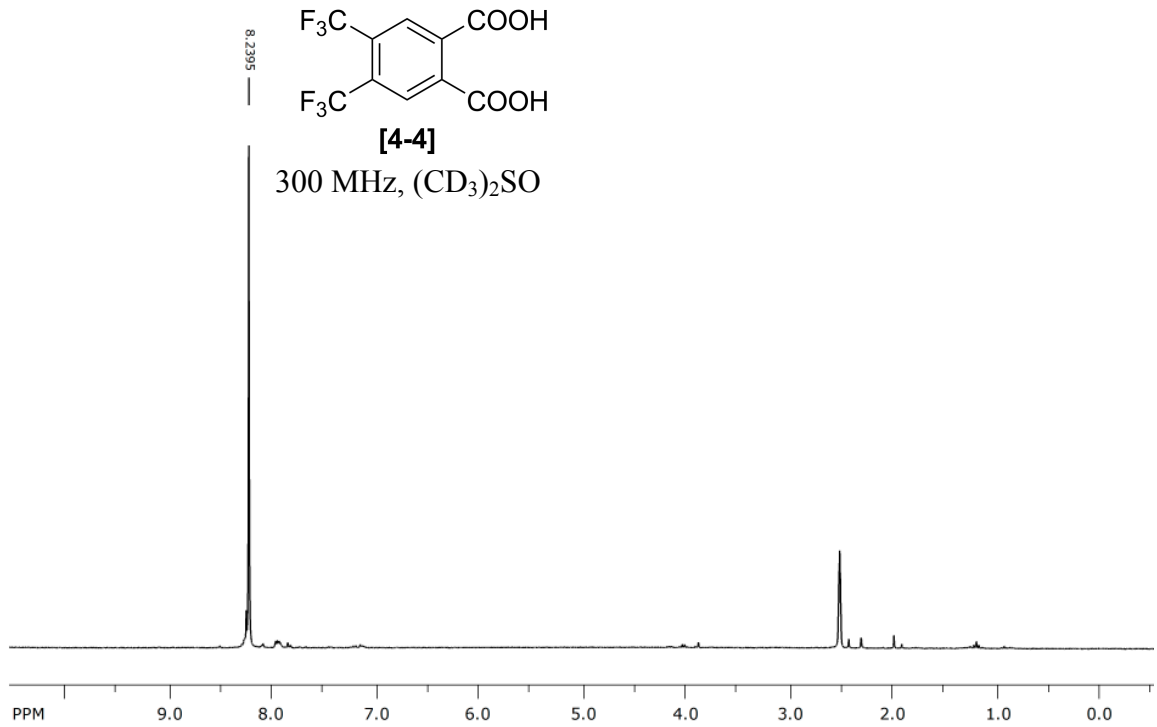

Figure A.36 ^{1}H NMR spectrum of 4,5-bis(trifluoromethyl)-phthalic acid.

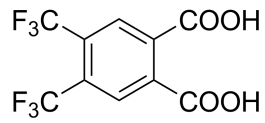

[4-4]

282 MHz, $(CD_3)_2SO$

Figure A.37 ^{19}F NMR spectrum of 4,5-bis(trifluoromethyl)-phthalic acid.

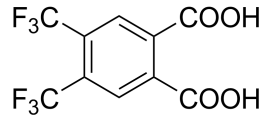

[4-4]

75 MHz, $(CD_3)_2SO$

Figure A.38 ^{13}C $\{^1H\}$ NMR spectrum of 4,5-bis(trifluoromethyl)-phthalic acid.

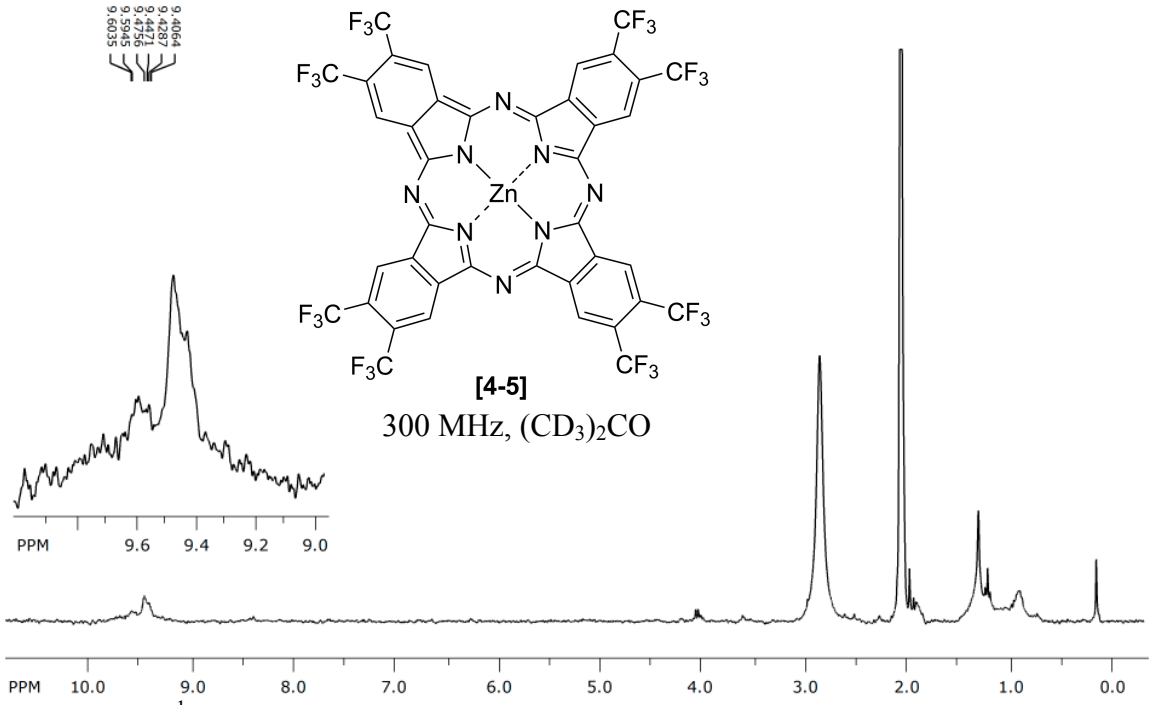

Figure A.39 ^{1}H NMR spectrum of $F_{24}H_8PcZn$.

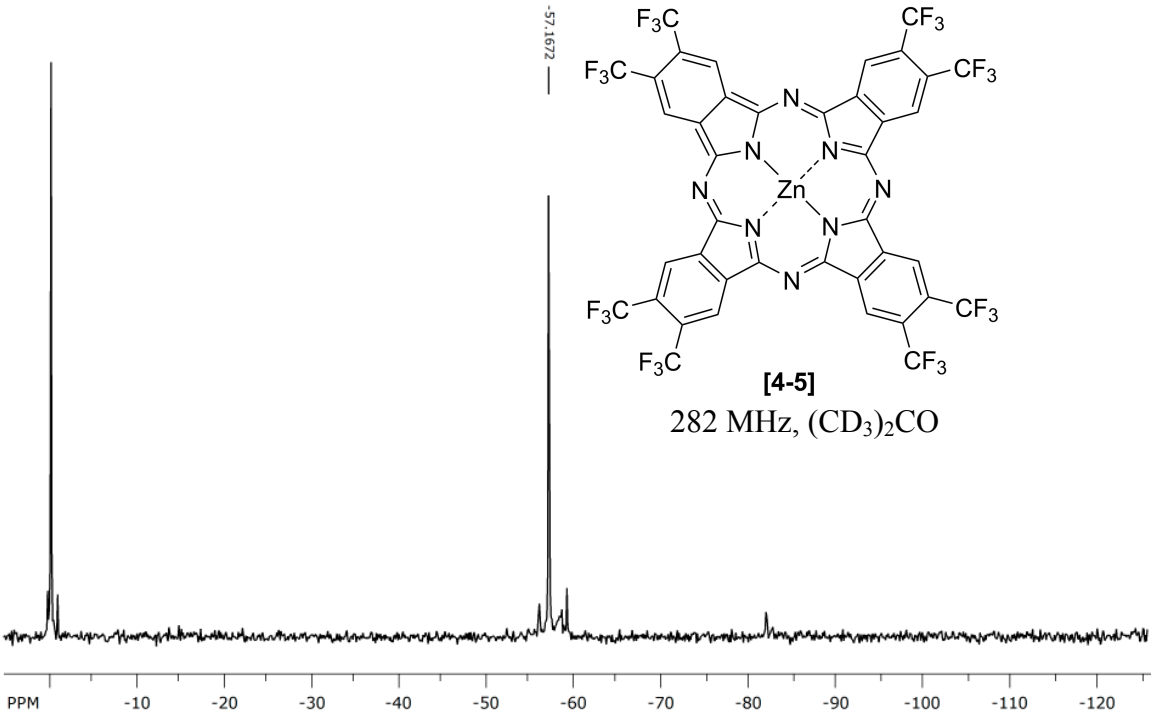

Figure A.40 ^{19}F NMR spectrum of $F_{24}H_8PcZn$.

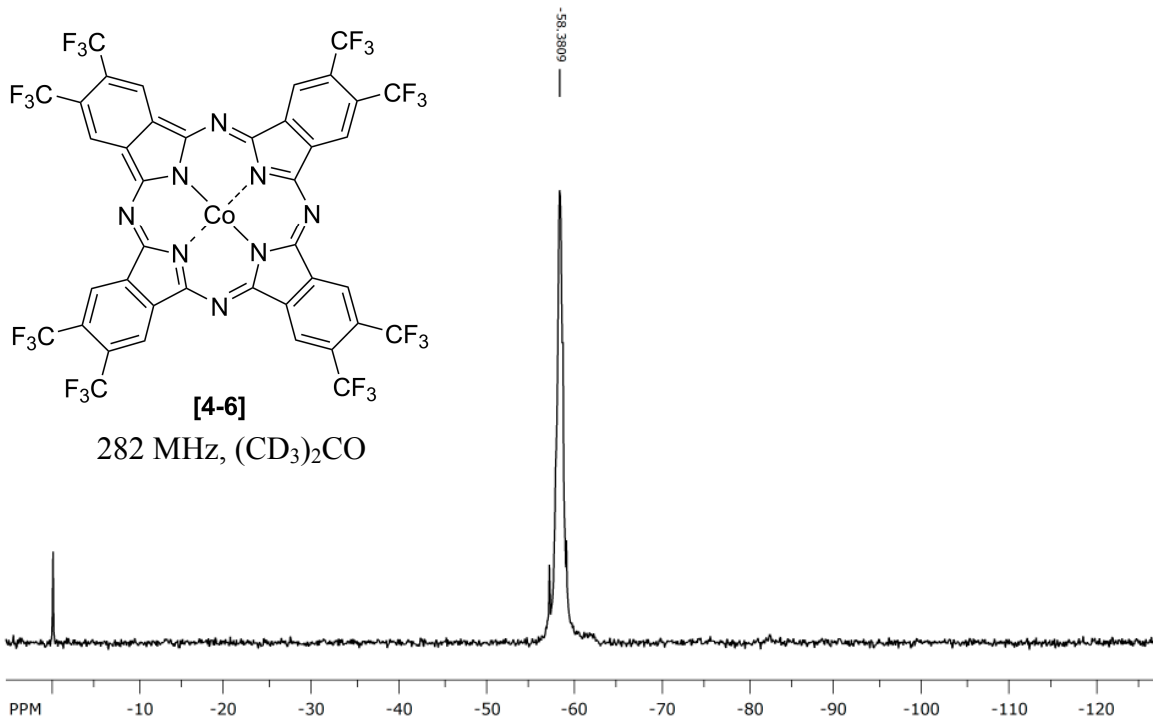

[4-6]

282 MHz, $(CD_3)_2CO$

Figure A.41 ^{19}F NMR spectrum of $F_{24}H_8PcCo$.

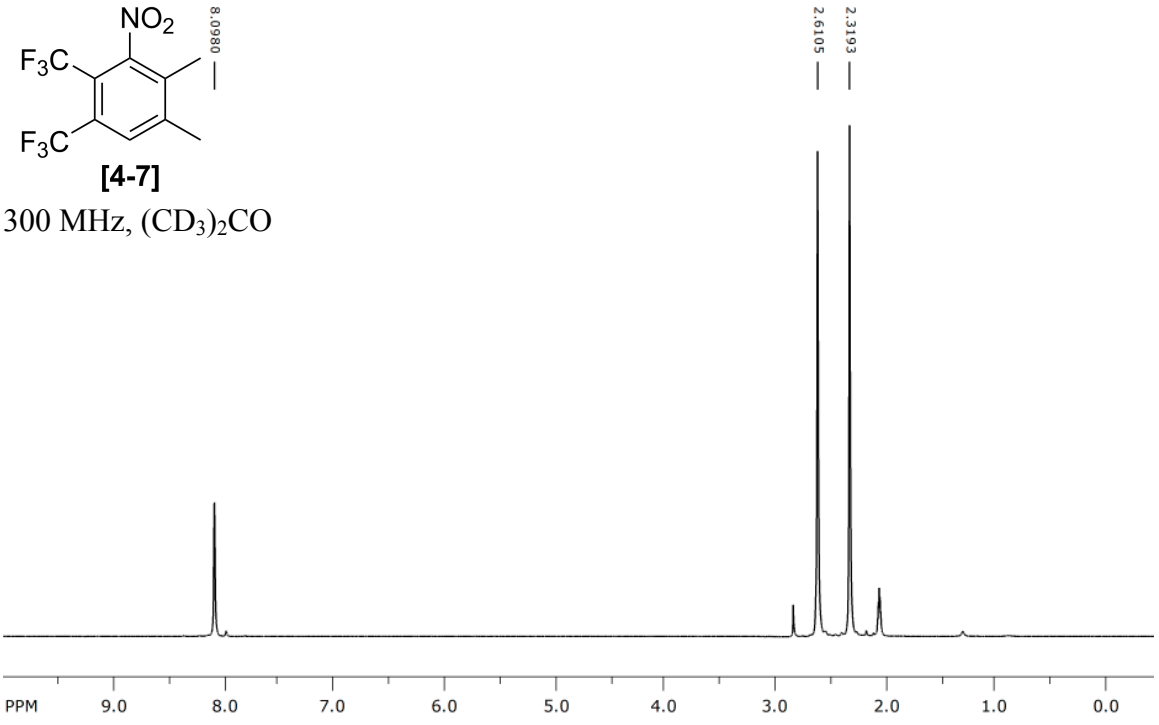

[4-7]

300 MHz, $(CD_3)_2CO$

Figure A.42 ^{1}H NMR spectrum of 1,2-bis(trifluoromethyl)-3-nitro-4,5-dimethylbenzene.

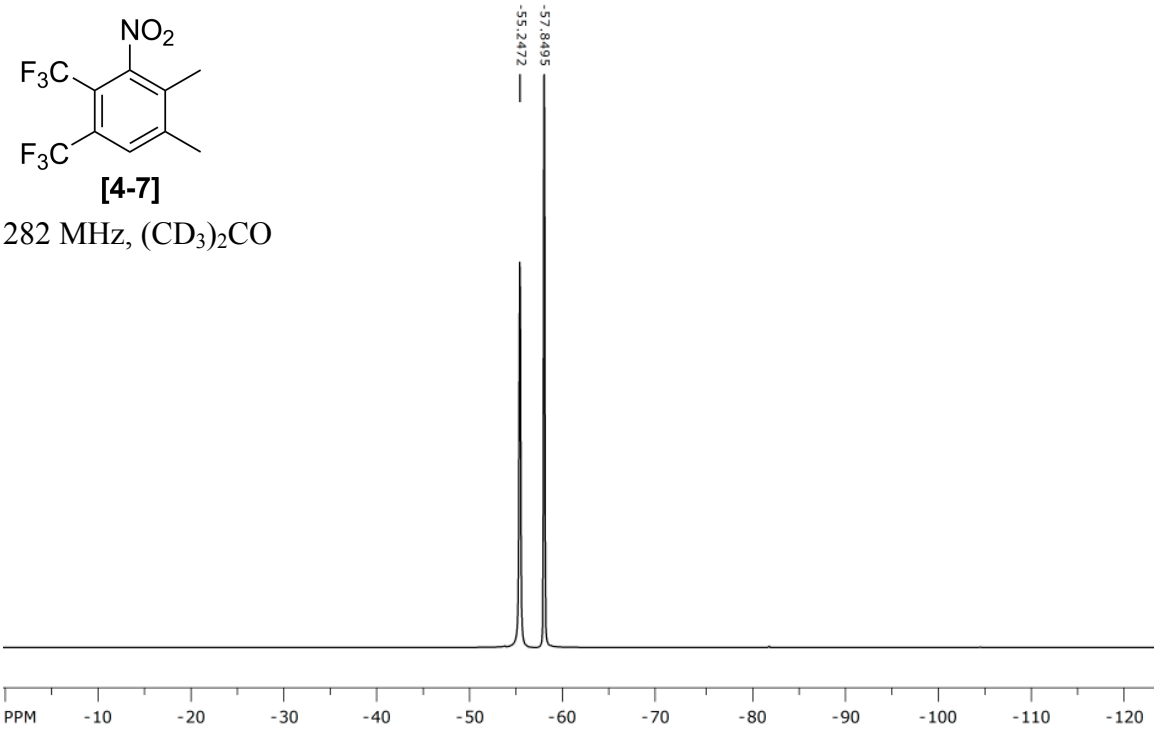

Figure A.43 ^{19}F NMR spectrum of 1,2-bis(trifluoromethyl)-3-nitro-4,5-dimethylbenzene.

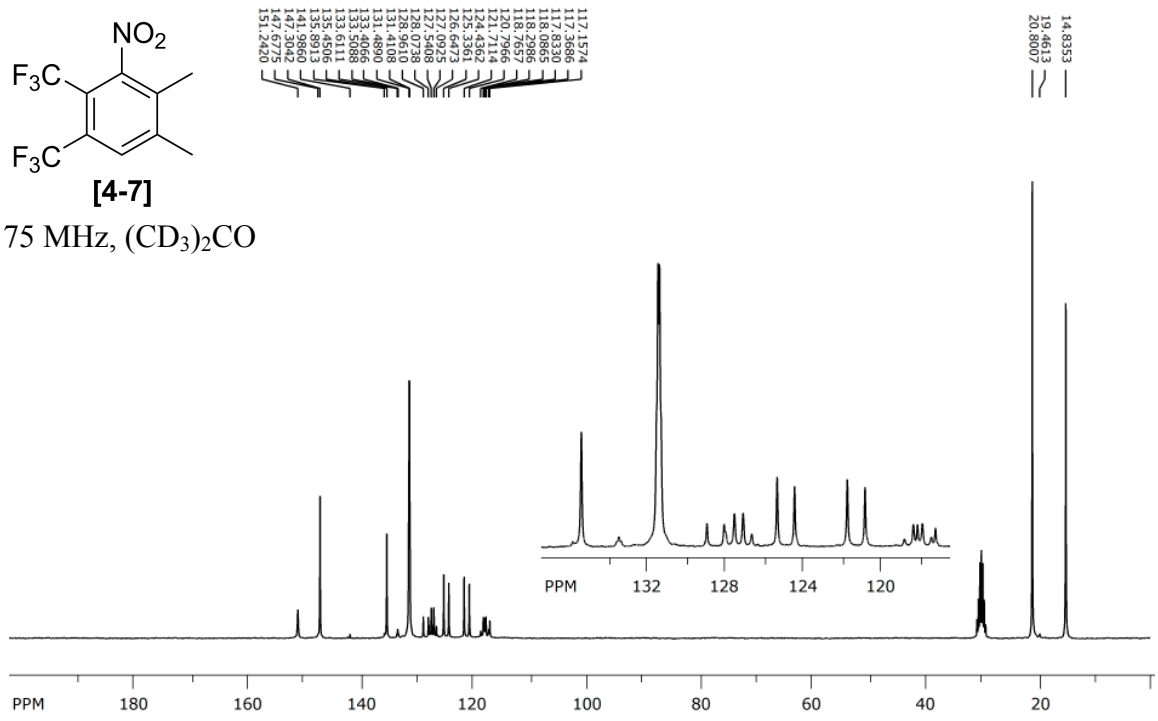

Figure A.44 ^{13}C {^{1}H} NMR spectrum of 1,2-bis(trifluoromethyl)-3-nitro-4,5-dimethyl-benzene.

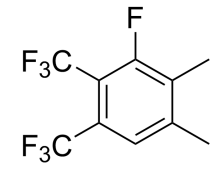

[4-8]

300 MHz, $(CD_3)_2CO$

Figure A.45 ^{1}H NMR spectrum of 1,2-bis(trifluoromethyl)-3-fluoro-4,5-dimethyl-benzene.

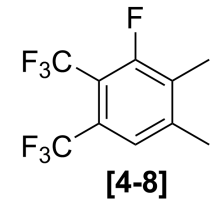

[4-8]

282 MHz, $(CD_3)_2CO$

Figure A.46 ^{19}F NMR spectrum of 1,2-bis(trifluoromethyl)-3-fluoro-4,5-dimethyl-benzene.

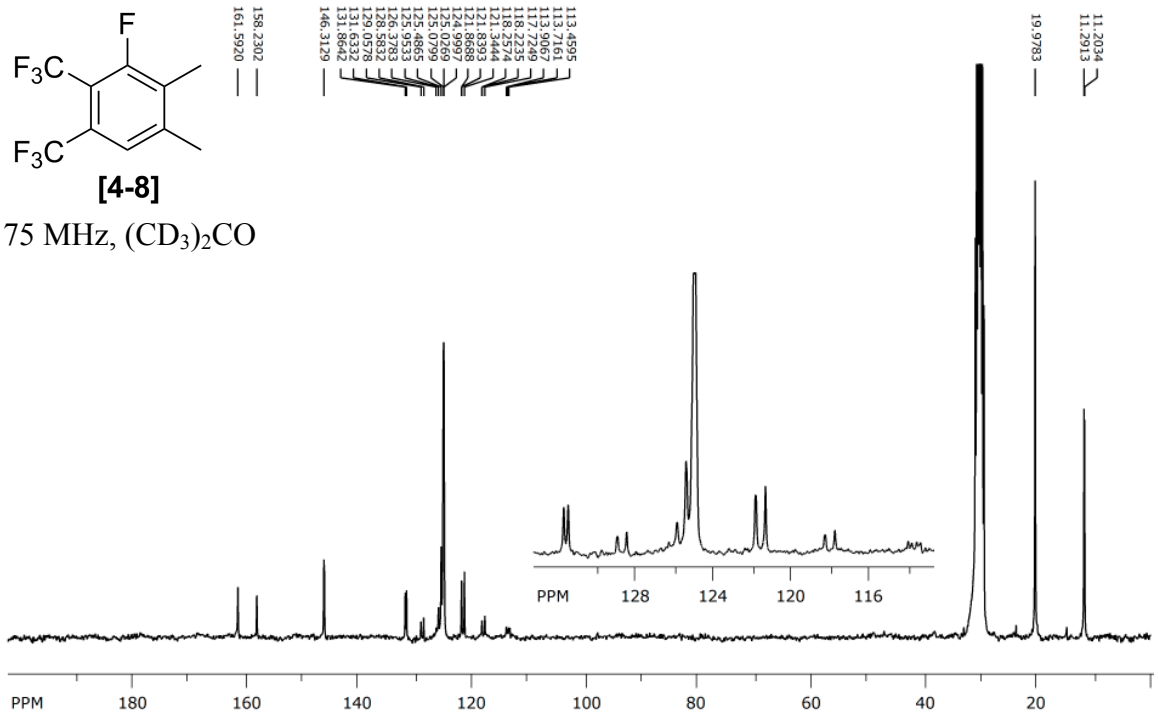

Figure A.47 ^{13}C {^{1}H} NMR spectrum of 1,2-bis(trifluoromethyl)-3-fluoro-4,5-dimethyl-benzene.

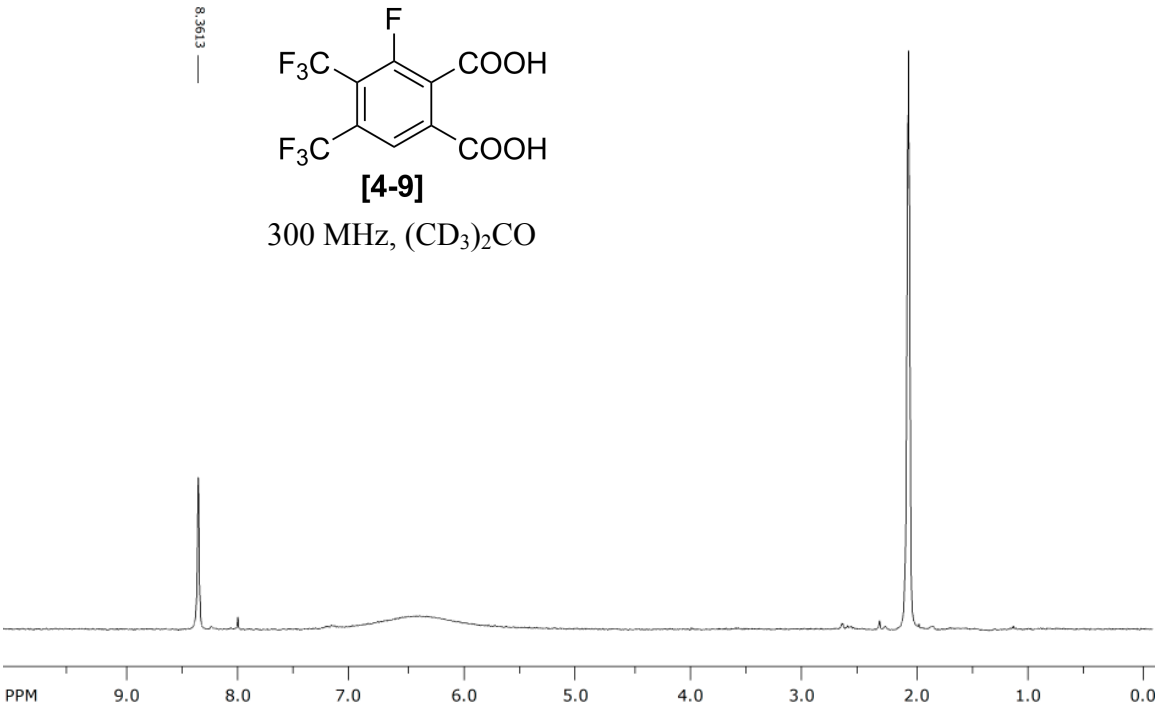

Figure A.48 ^{1}H NMR spectrum of 4,5-bis(trifluoromethyl)-3-fluorophthalic acid.

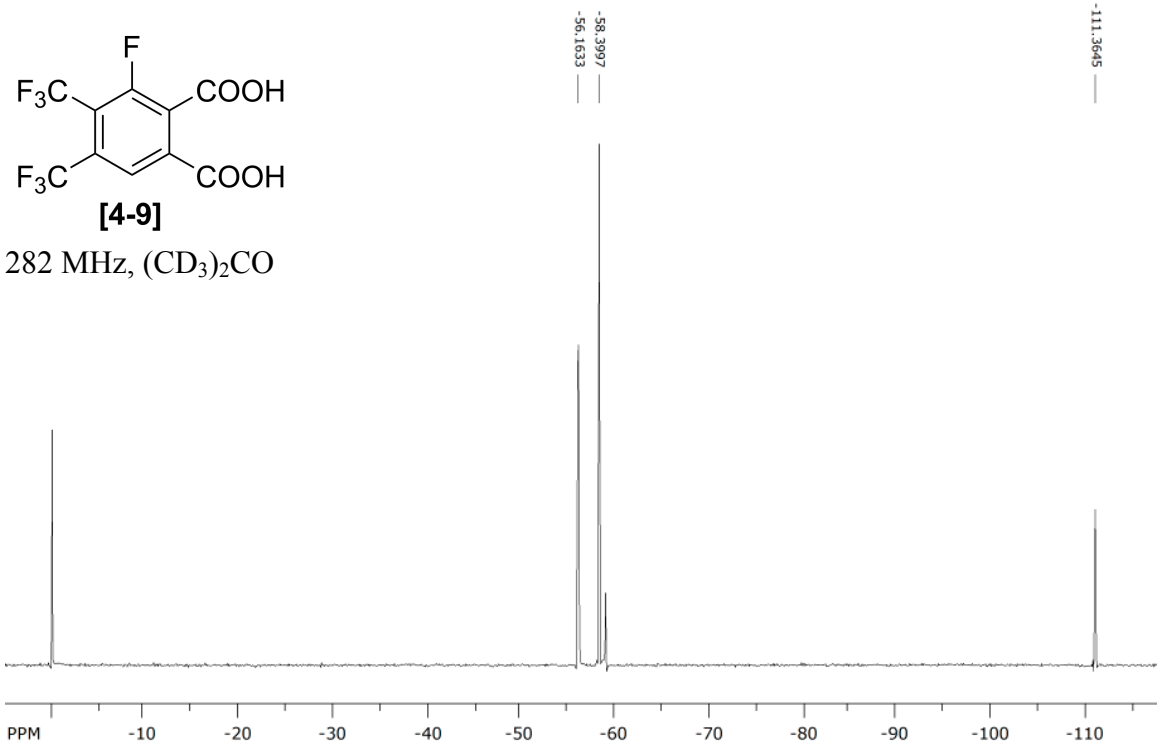

Figure A.49 ^{19}F NMR spectrum of 4,5-bis(trifluoromethyl)-3-fluorophthalic acid.

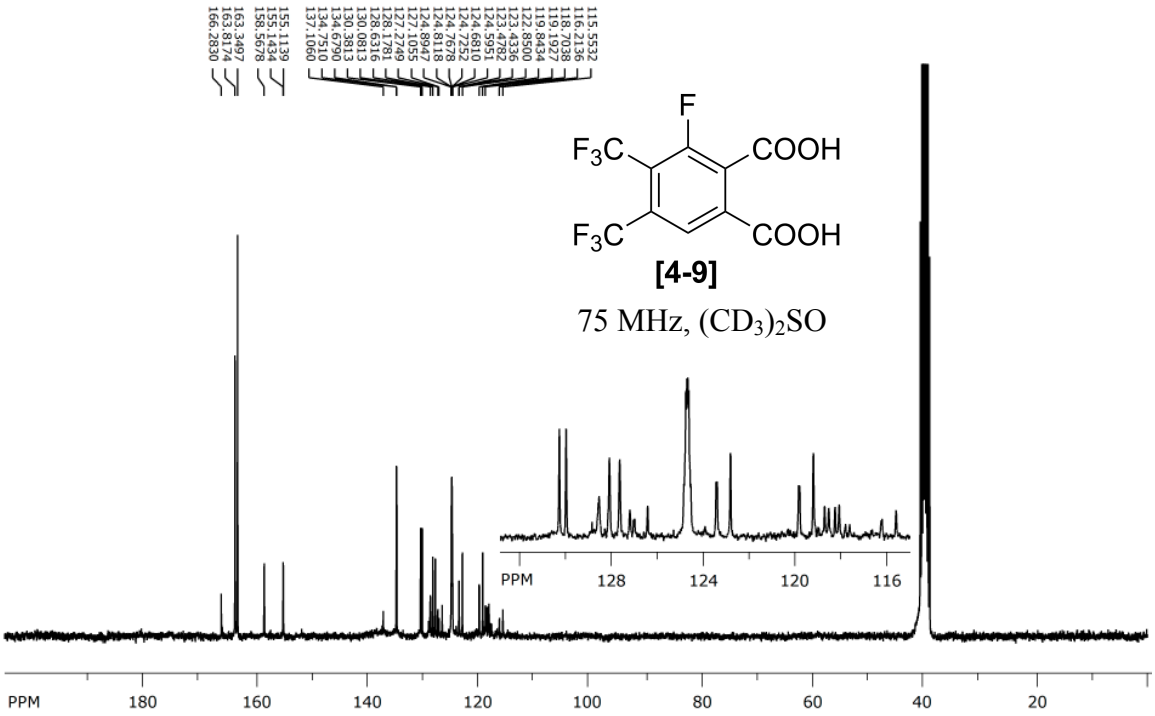

Figure A.50 ^{13}C {^{1}H} NMR spectrum of 4,5-bis(trifluoromethyl)-3-fluorophthalic acid.

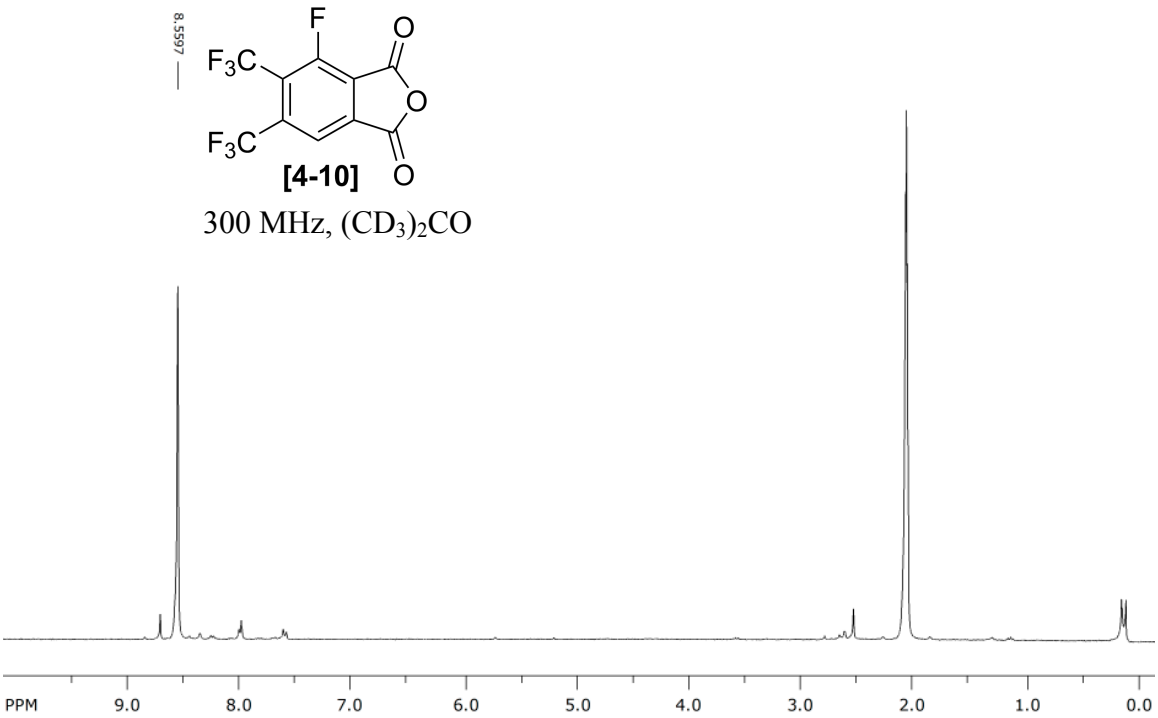

Figure A.51 ^{1}H NMR spectrum of 4,5-bis(trifluoromethyl)-3-fluorophthalic anhydride.

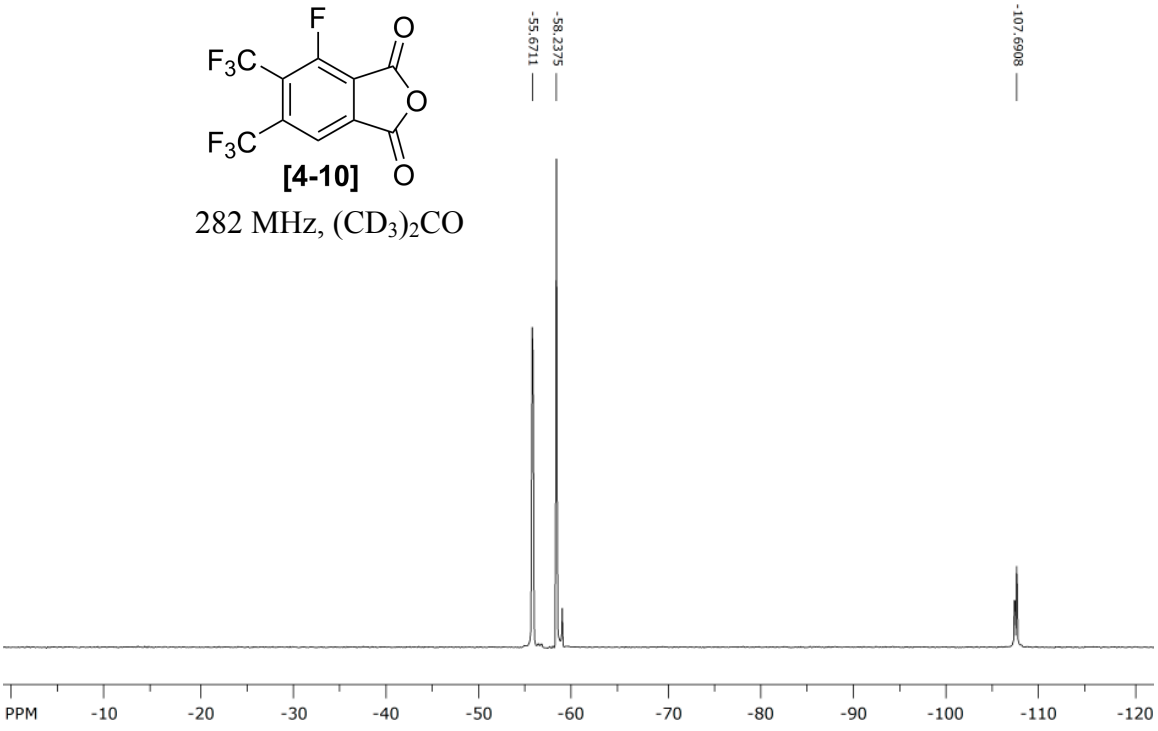

Figure A.52 ^{19}F NMR spectrum of 4,5-bis(trifluoromethyl)-3-fluorophthalic anhydride.

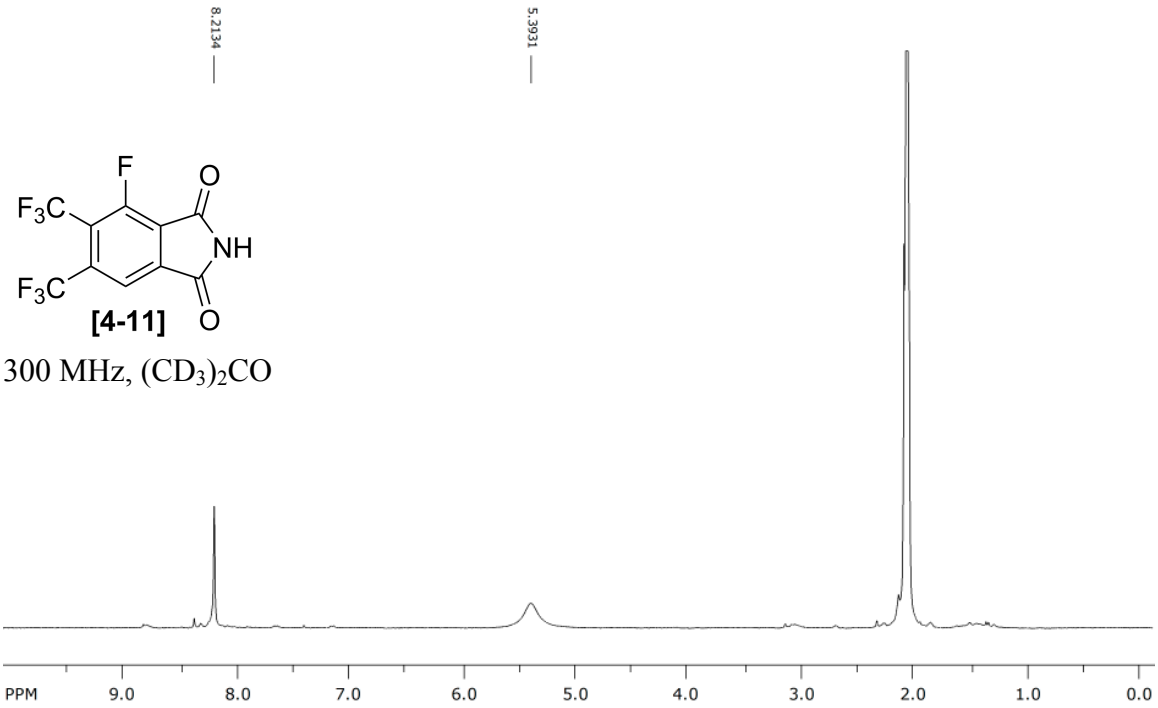

Figure A.53 ^{1}H NMR spectrum of 4,5-bis(trifluoromethyl)-3-fluorophthalimide.

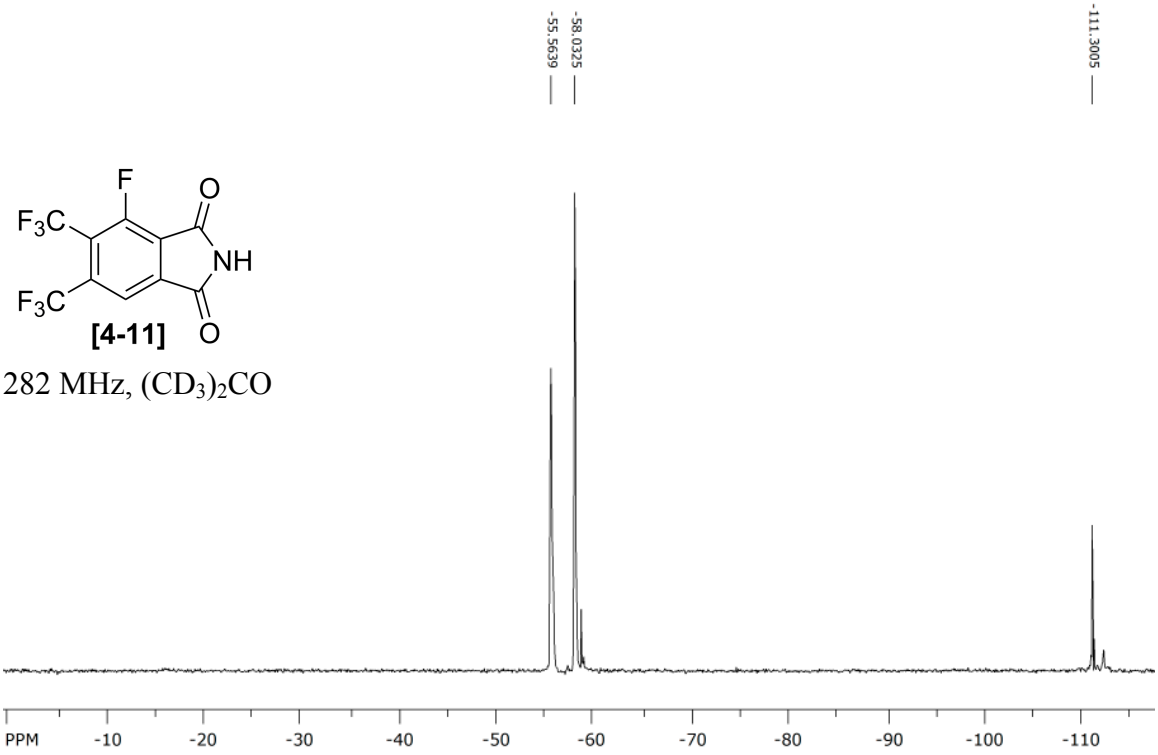

Figure A.54 ^{19}F NMR spectrum of 4,5-bis(trifluoromethyl)-3-fluorophthalimide.

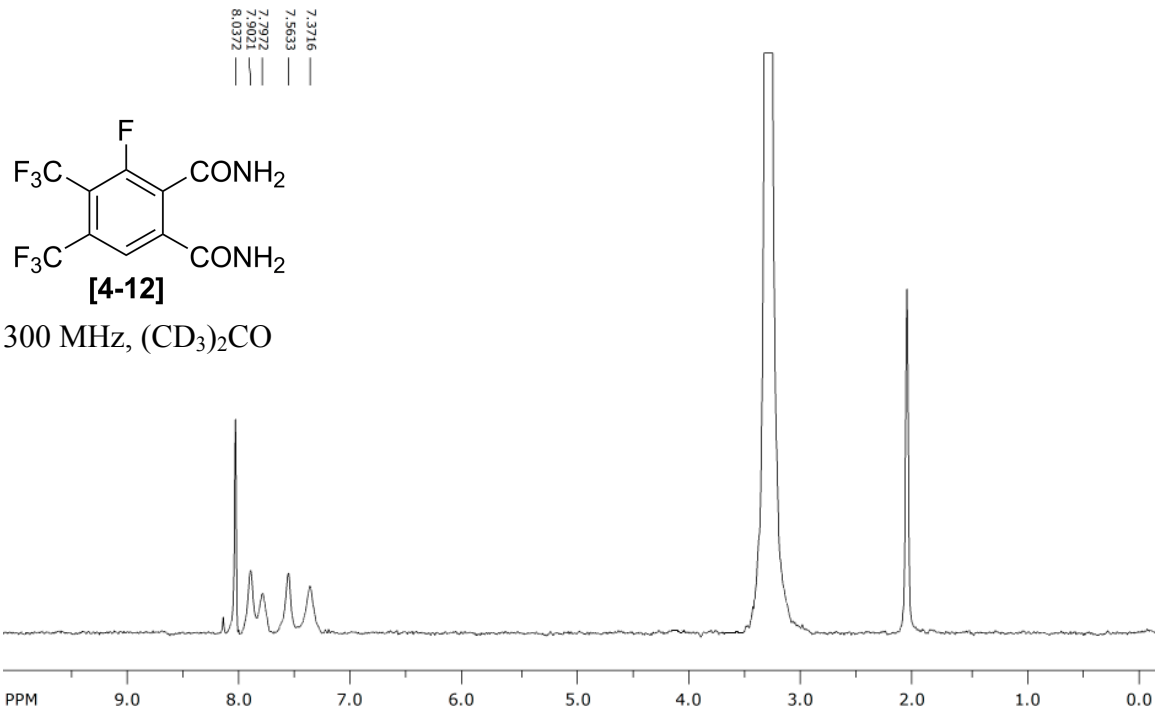

Figure A.55 ^{1}H NMR spectrum of 4,5-bis(trifluoromethyl)-3-fluorophthalamide.

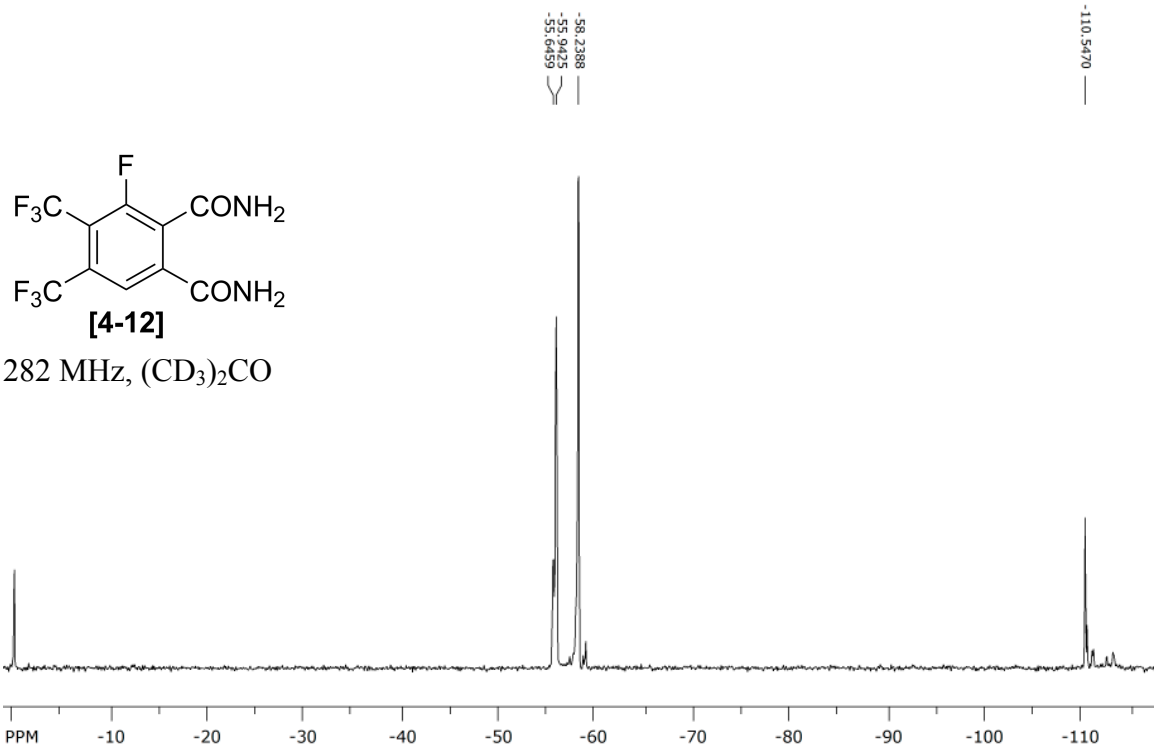

Figure A.56 ^{19}F NMR spectrum of 4,5-bis(trifluoromethyl)-3-fluorophthalamide.

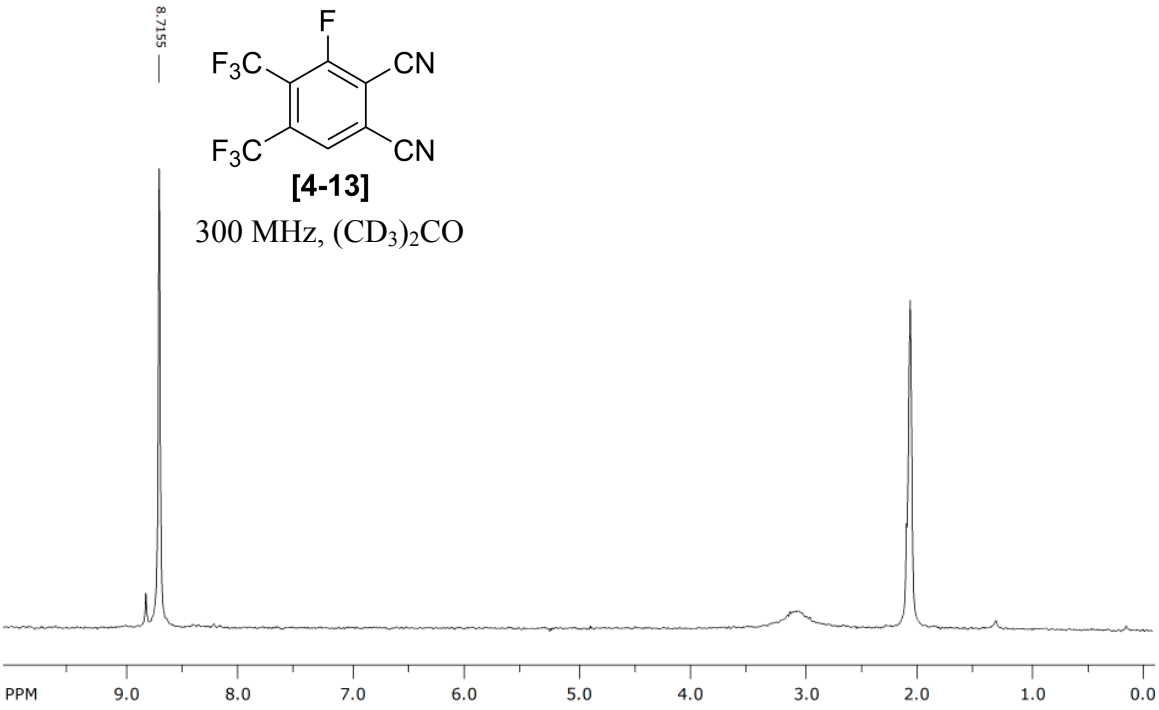

Figure A.57 ^{1}H NMR spectrum of 4,5-bis(trifluoromethyl)-3-fluorophthalonitrile.

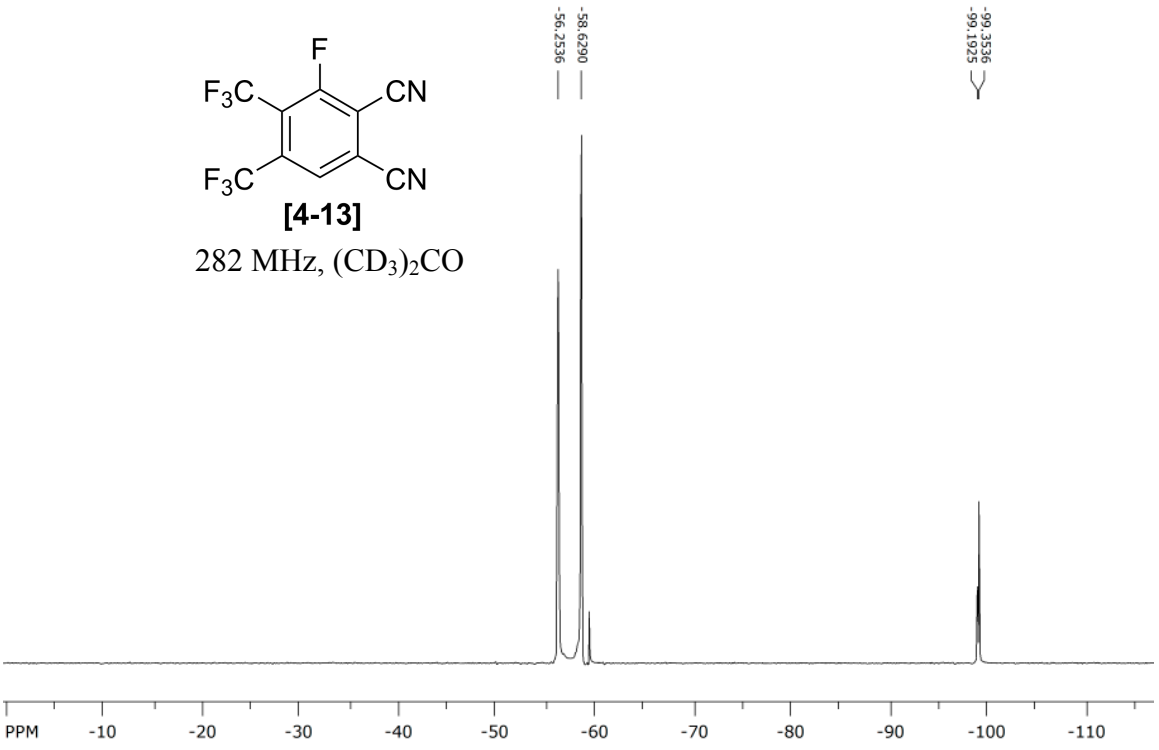

Figure A.58 ^{19}F NMR spectrum of 4,5-bis(trifluoromethyl)-3-fluorophthalonitrile.

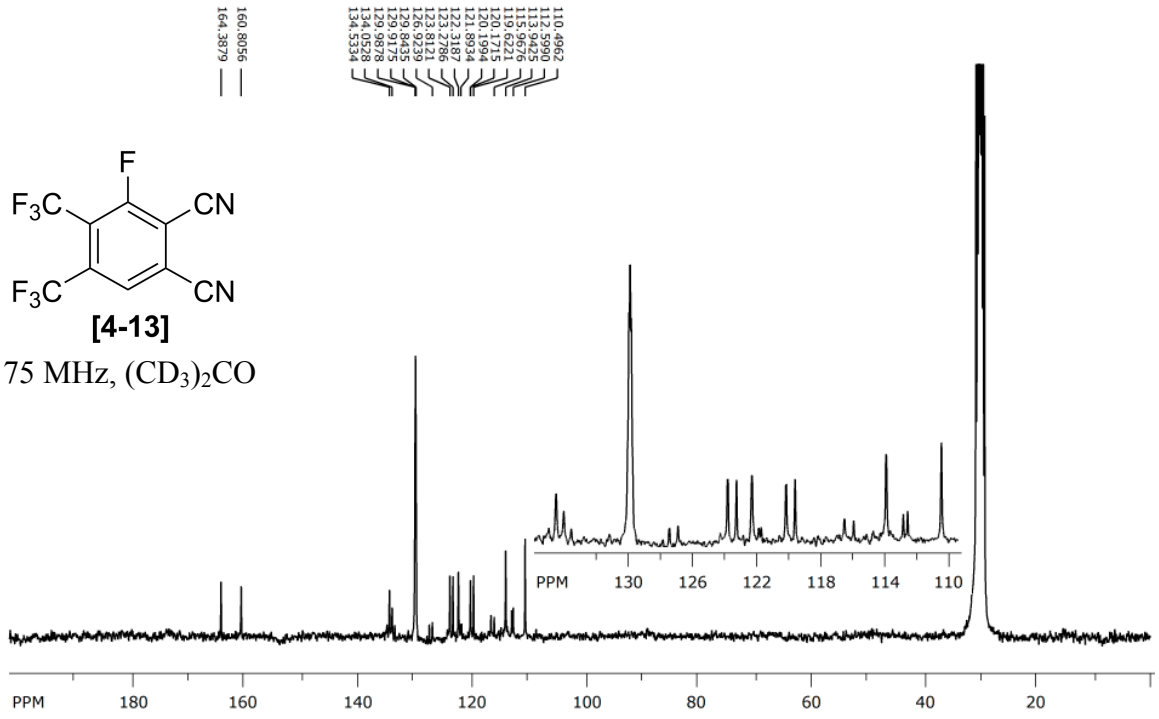

Figure A.59 ^{13}C {^{1}H} NMR spectrum of 4,5-bis(trifluoromethyl)-3-fluorophthalonitrile.

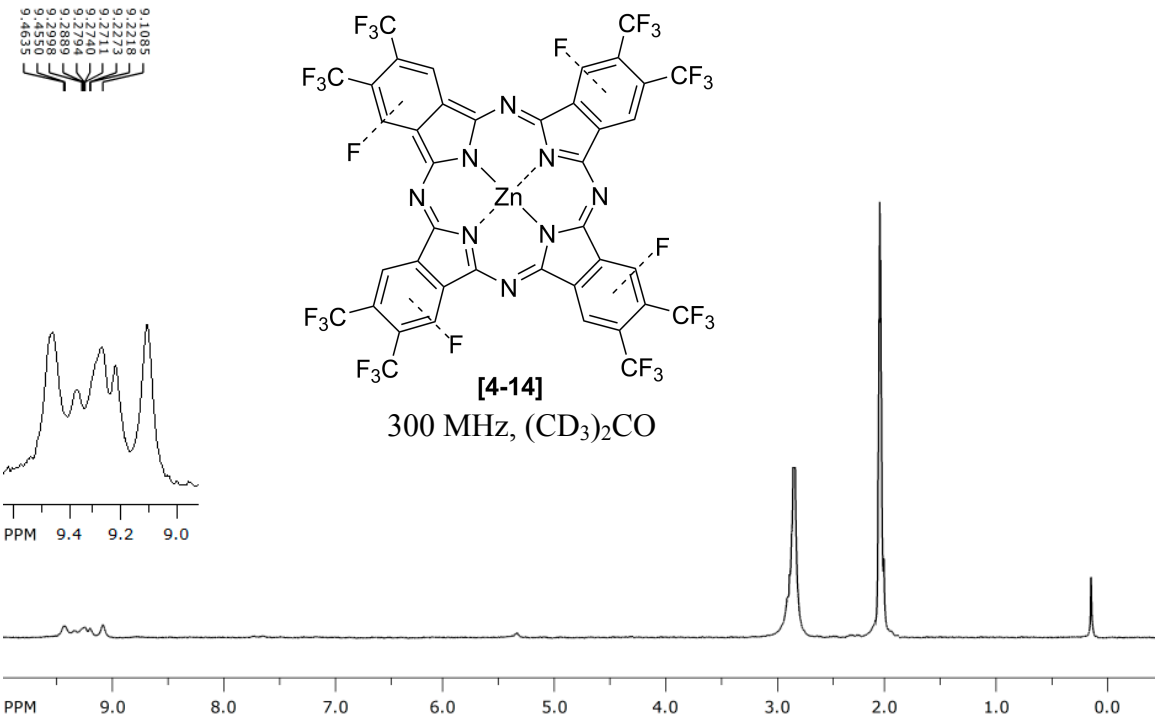

Figure A.60 ^{1}H NMR spectrum of $F_{28}H_4PcZn$ in $(CD_3)_2CO$.

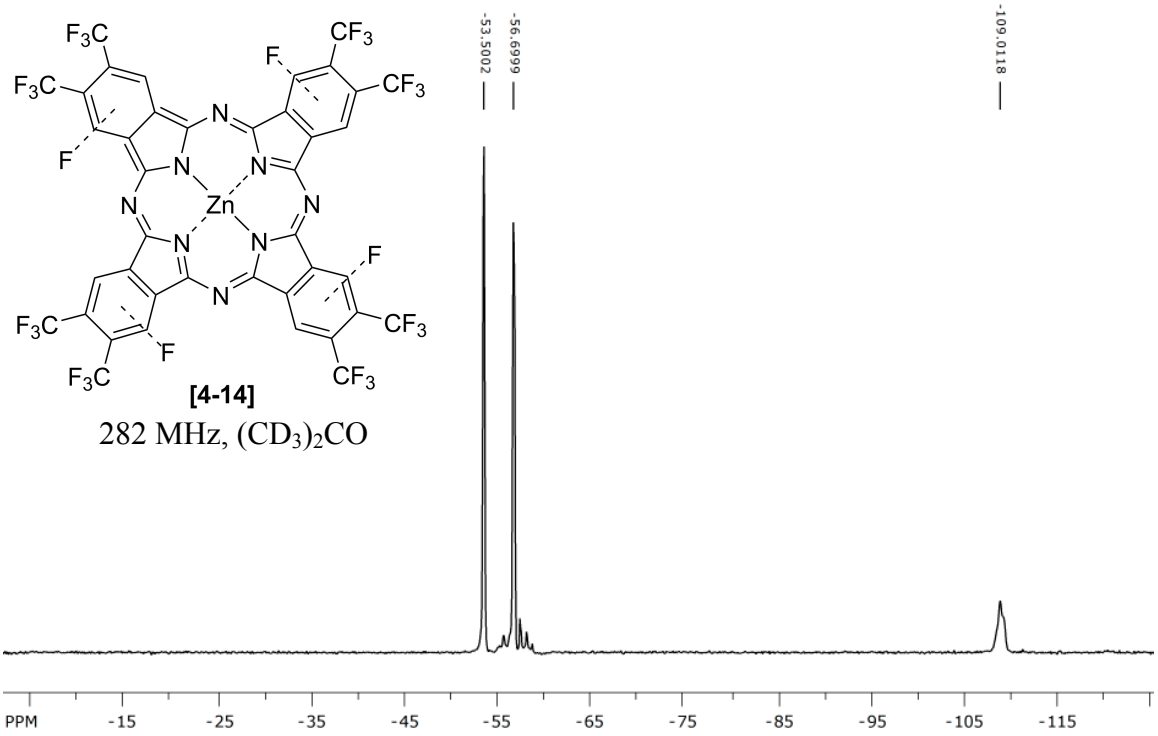

Figure A.61 ^{19}F NMR spectrum of $F_{28}H_4PcZn$ in $(CD_3)_2CO$.

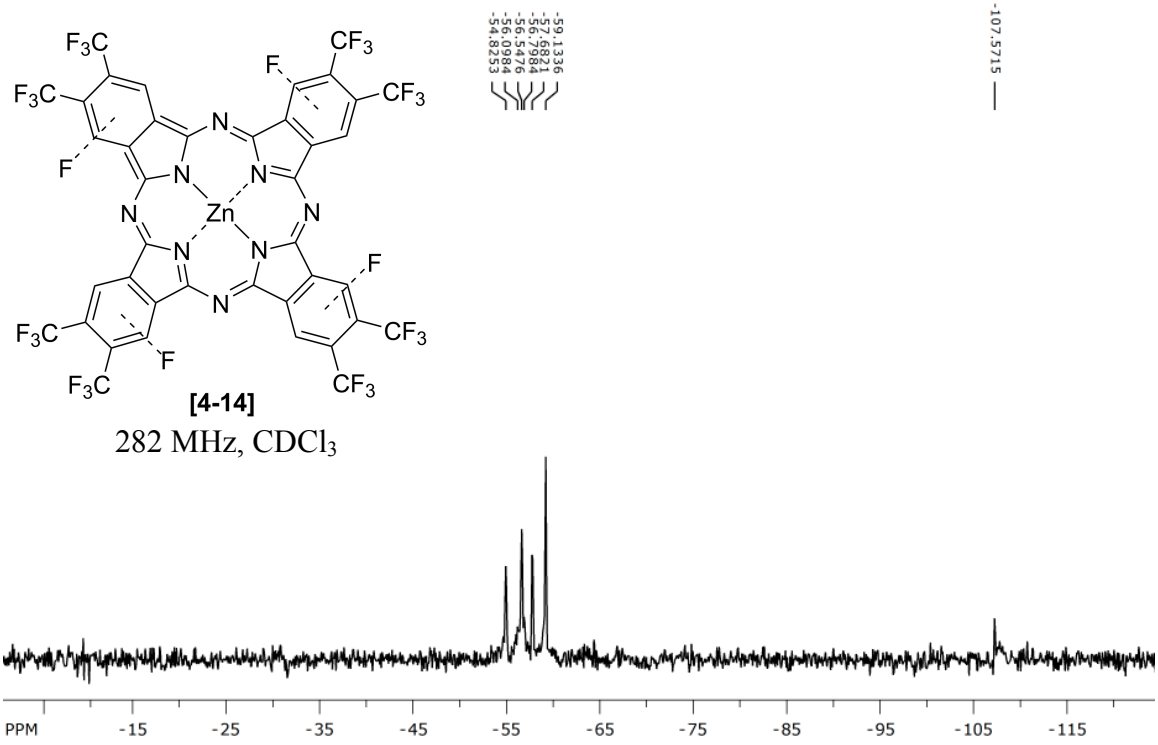

Figure A.62 ^{19}F NMR spectrum of $F_{28}H_4PcZn$ in $CDCl_3$.

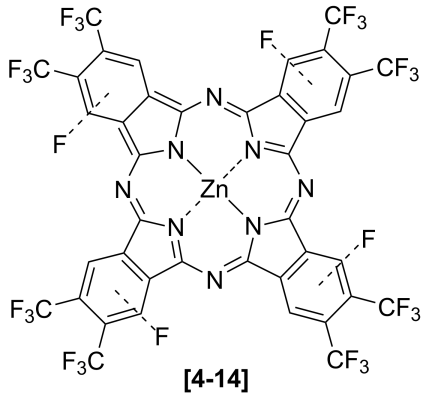

[4-14]

376 MHz, $CDCl_3$

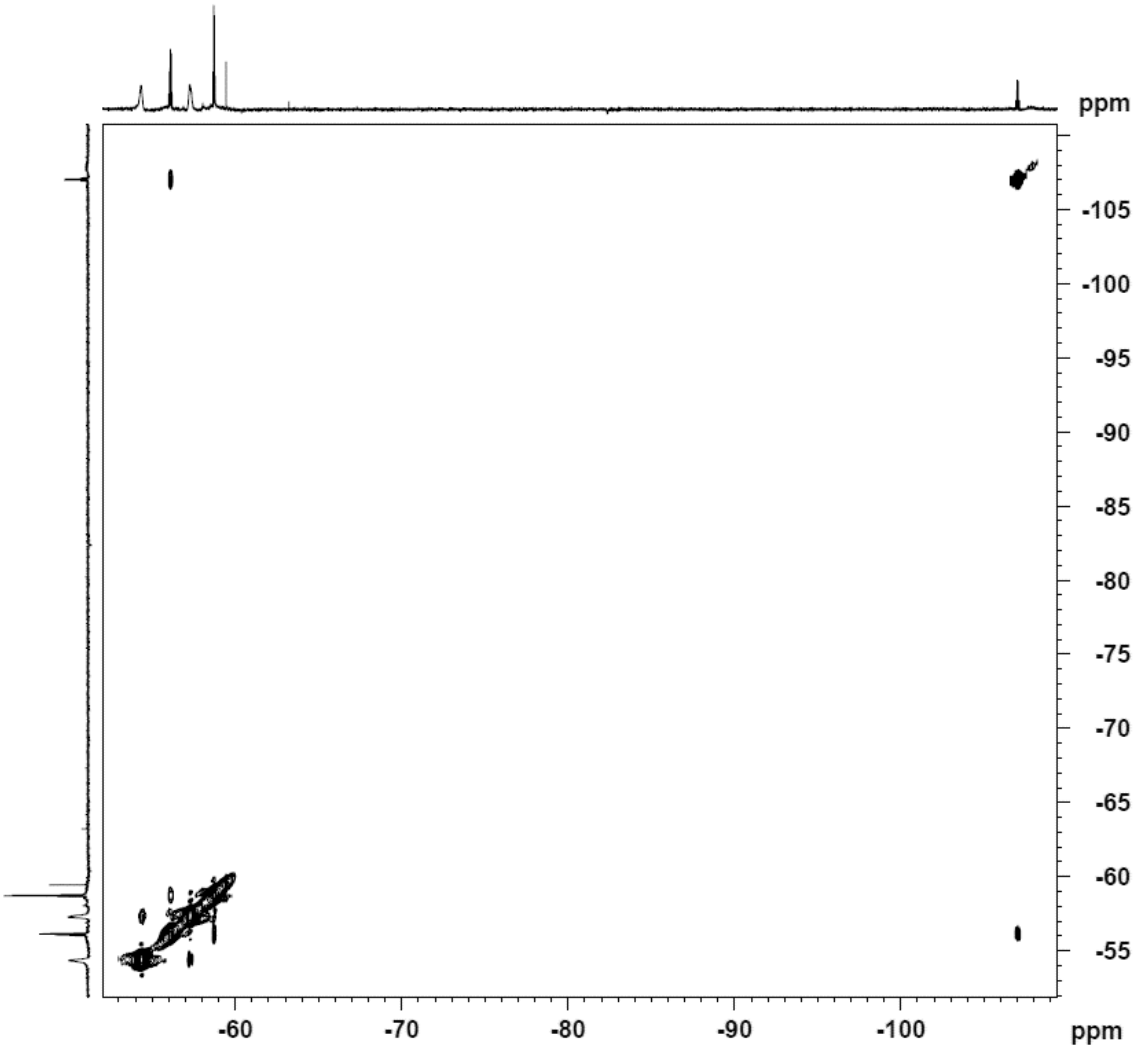

Figure A.63 ^{19}F COSY NMR spectrum of $F_{28}H_4PcZn$ in $CDCl_3$.

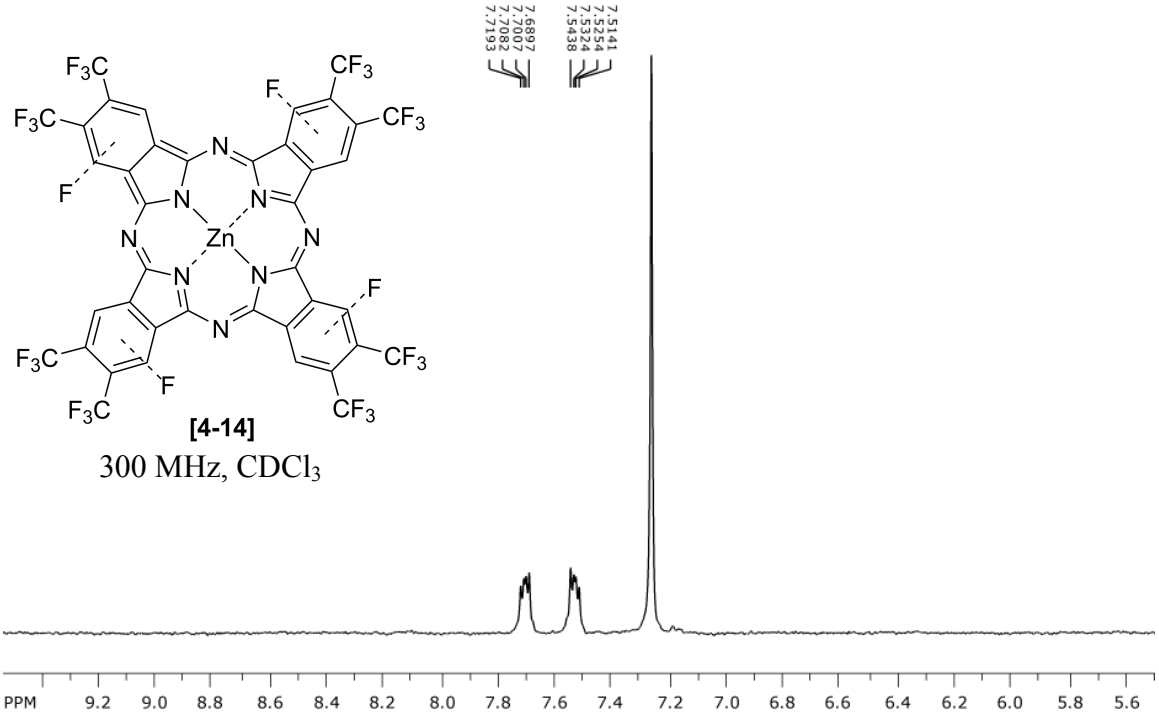

Figure A.64 ^{1}H NMR spectrum of $F_{28}H_4PcZn$ in $CDCl_3$.

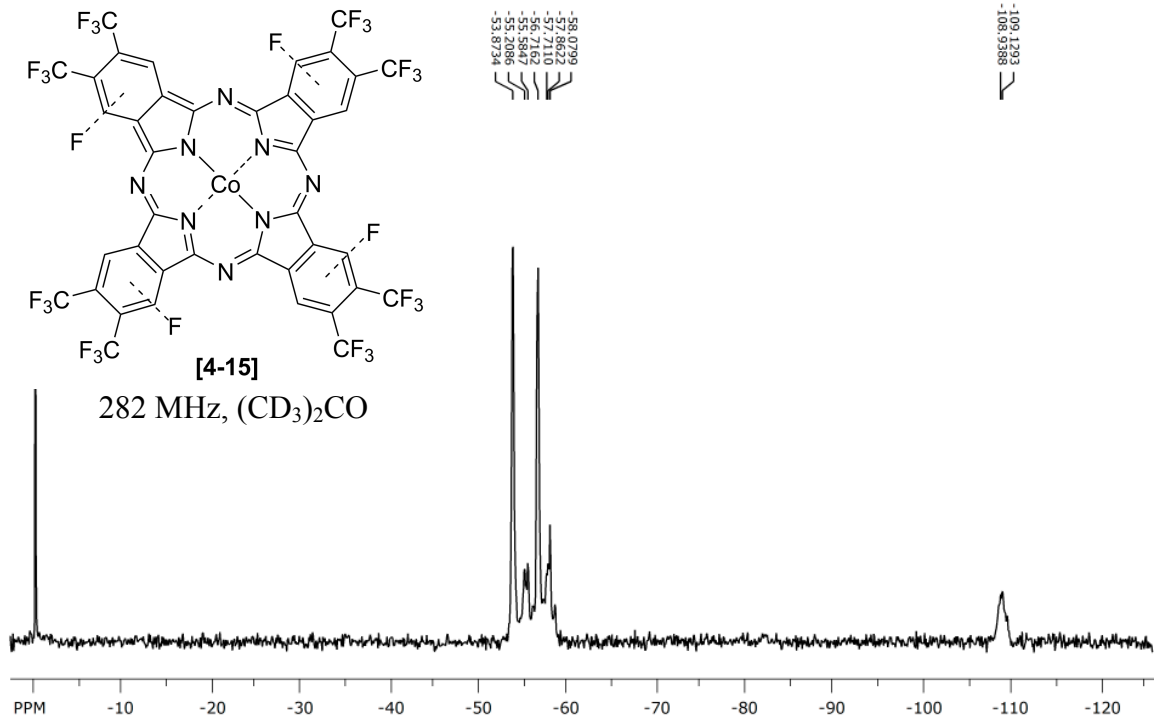

Figure A.65 ^{19}F NMR spectrum of $F_{28}H_4PcCo$.

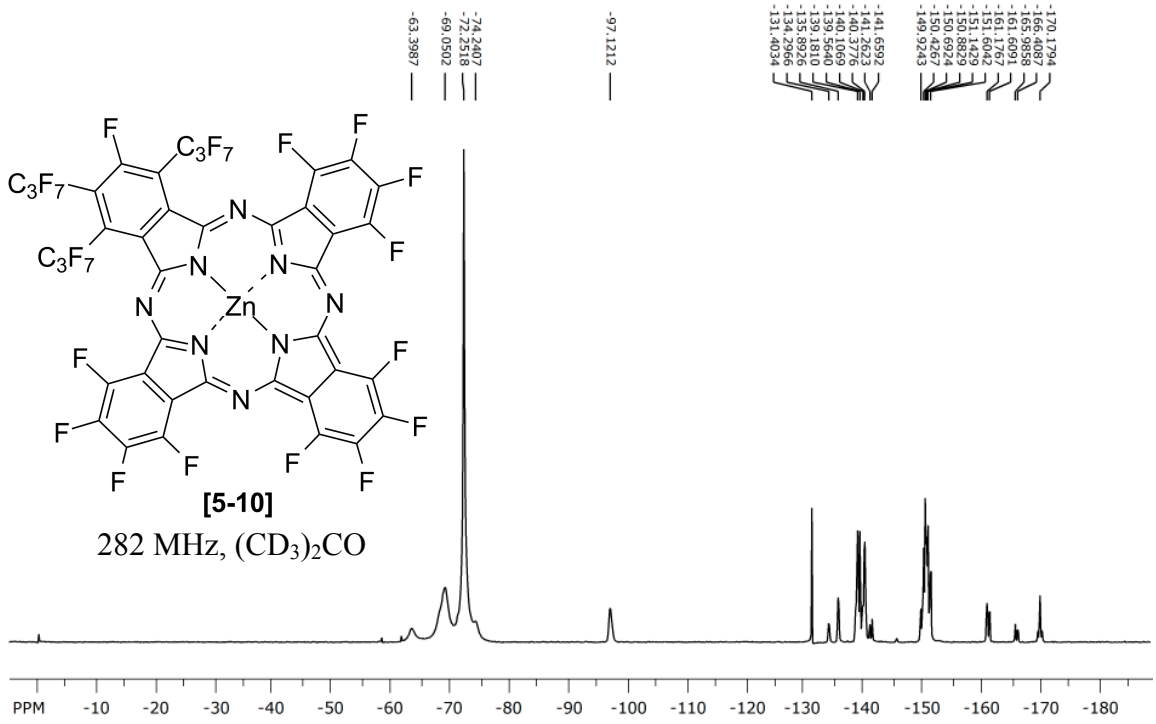

Figure A.66 ^{19}F NMR spectrum of F_{34}PcZn.

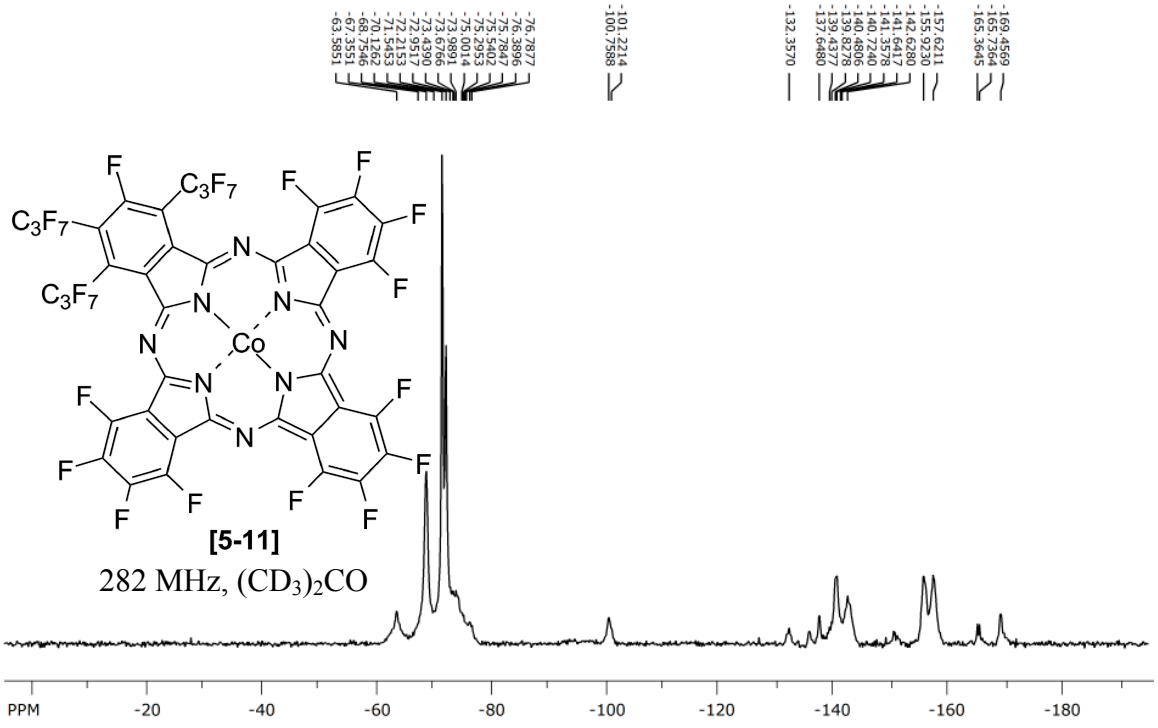

Figure A.67 ^{19}F NMR spectrum of F_{34}PcCo.

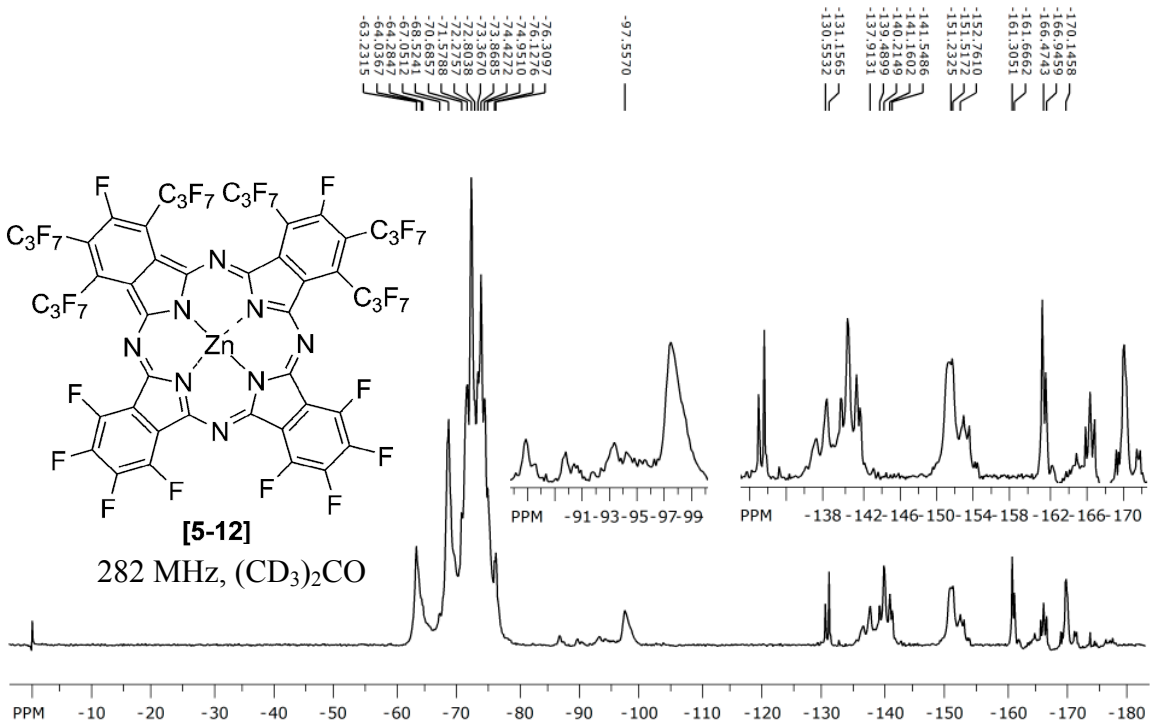

Figure A.68 ^{19}F NMR spectrum of F_{52}PcZn.

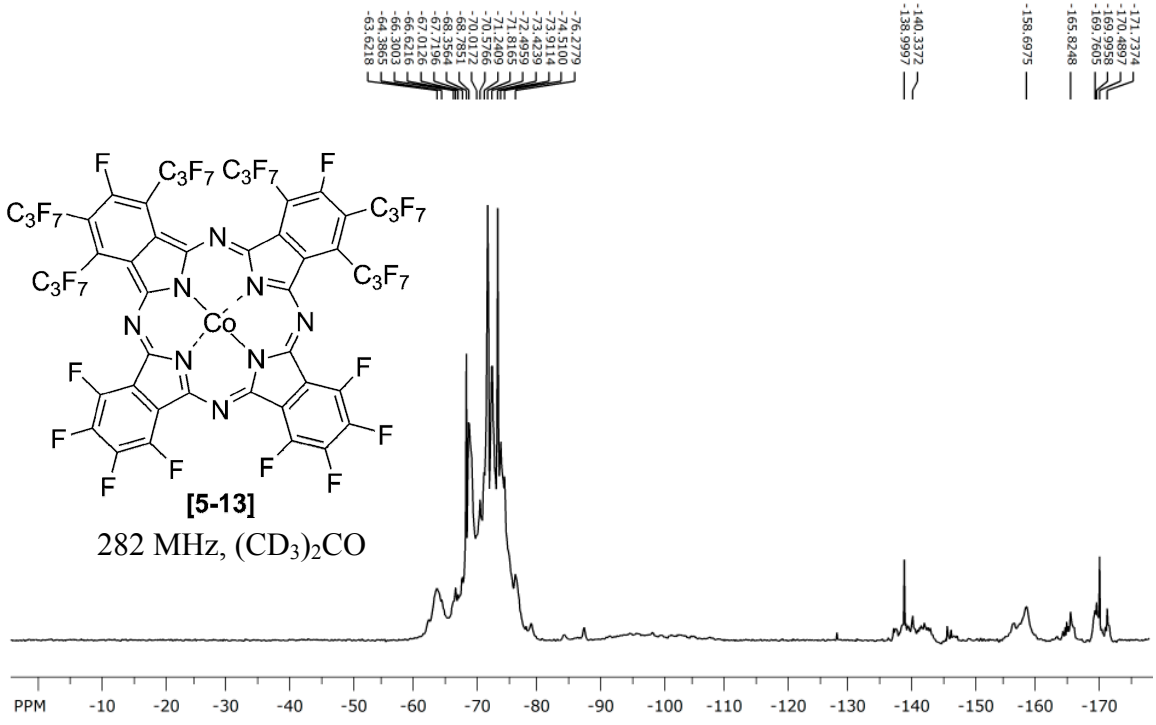

Figure A.69 ^{19}F NMR spectrum of F_{52}PcCo.

APPENDIX B

IR SPECTRA

Figures B.1 through B.19 present IR spectra of selected compounds produced in this work. All spectra were collected after grinding the compounds to a fine powder in KBr pellets. Structural formulas and assigned numbers are shown in the insets.

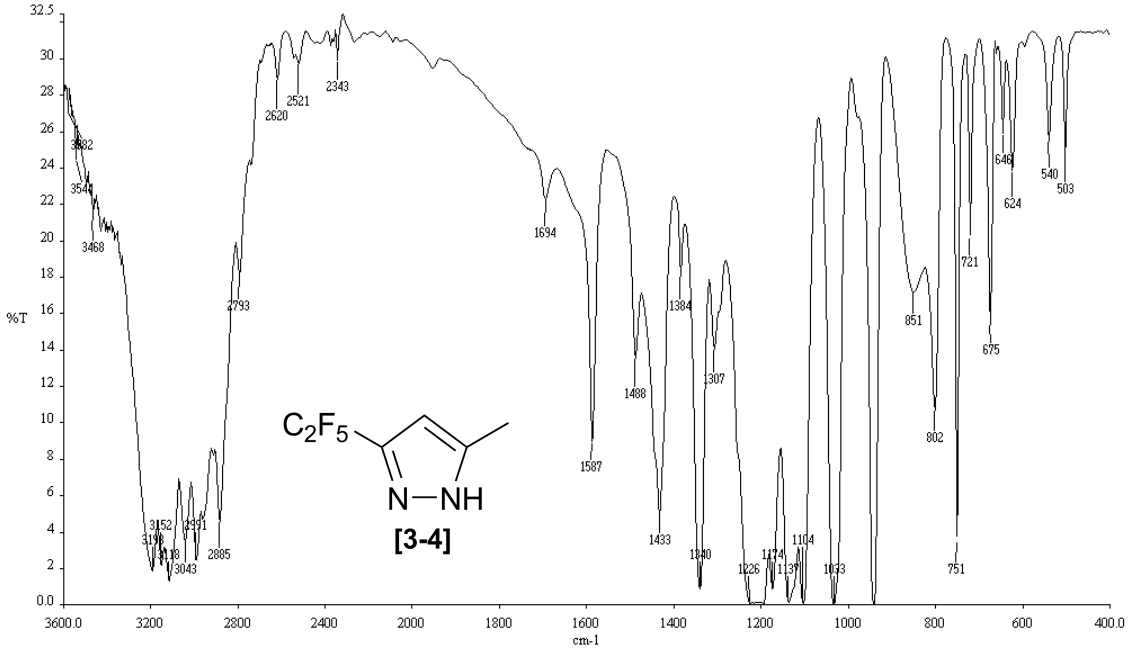

Figure B.1 IR spectrum of $Pz^{C_2F_5,CH_3}$.

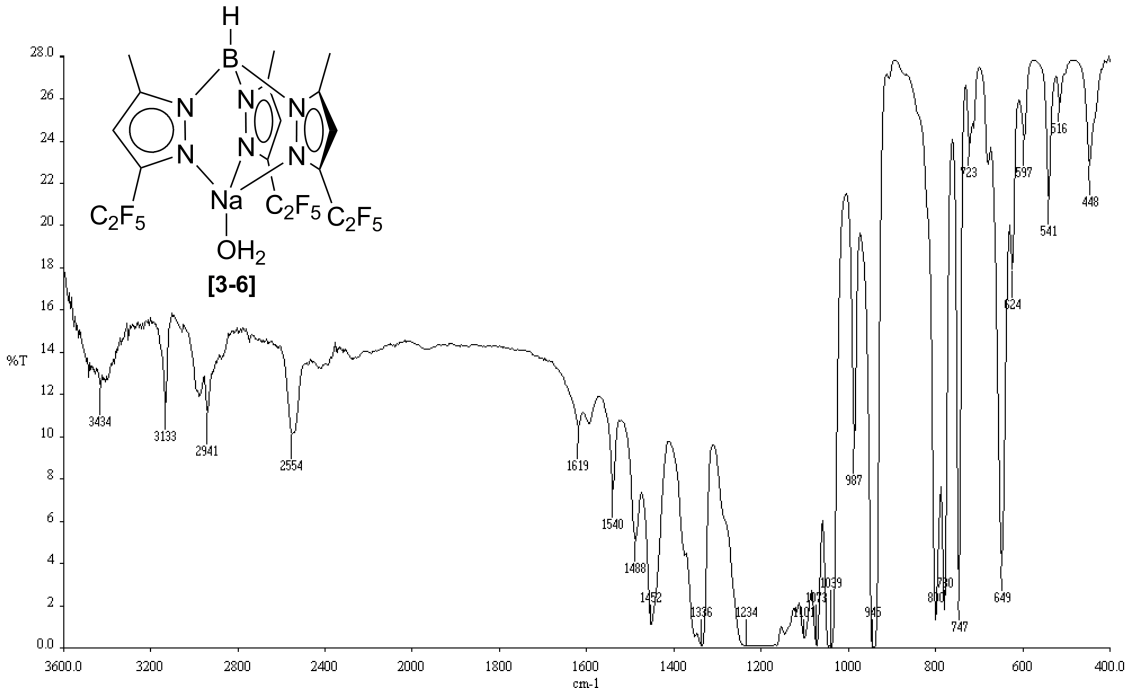

Figure B.2 IR spectrum of $Tp^{C_2F_5,CH_3}Na(H_2O)$.

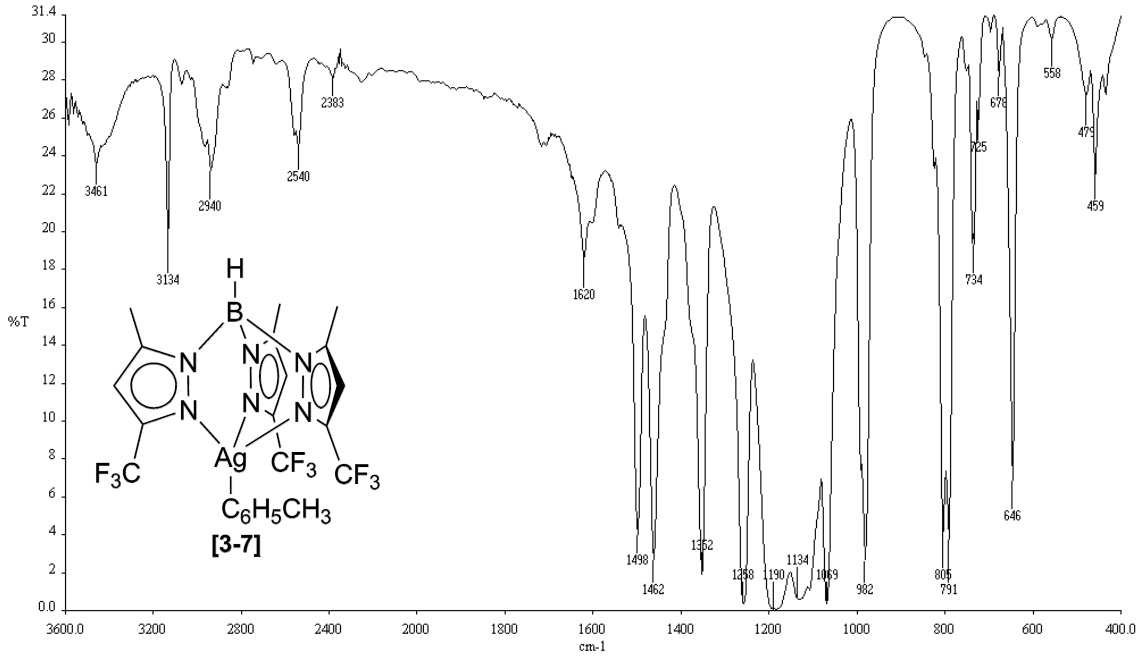

Figure B.3 IR spectrum of $Tp^{CF_3,CH_3}Ag(Tol)$.

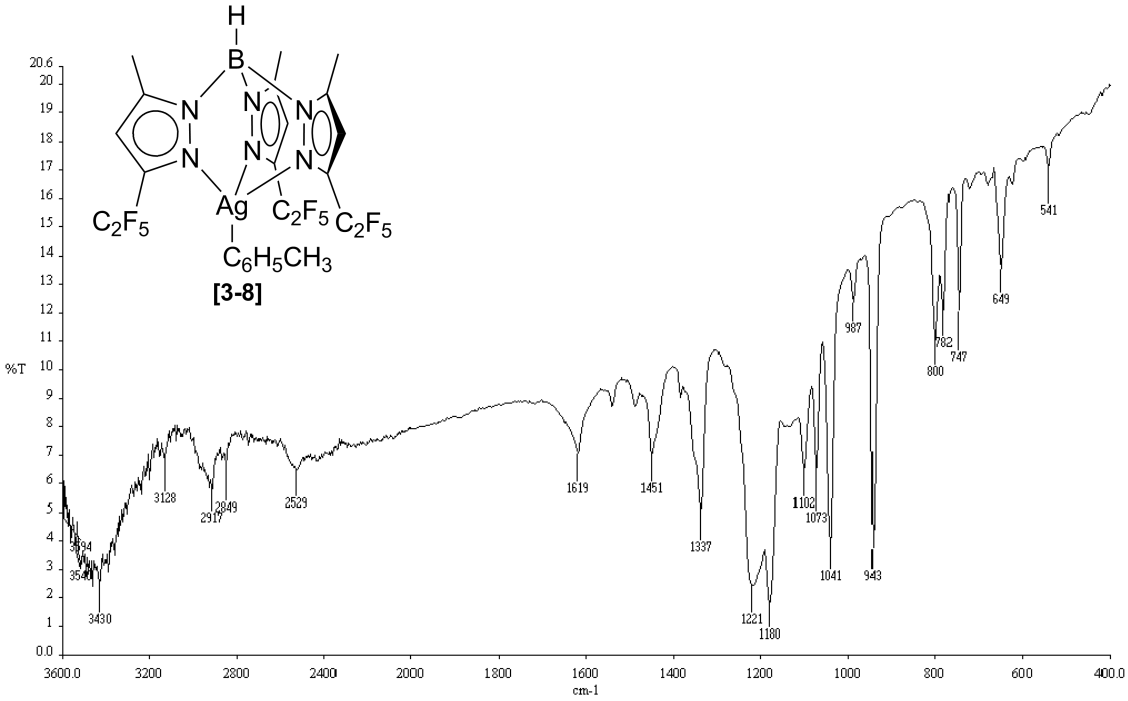

Figure B.4 IR spectrum of $Tp^{C_2F_5,CH_3}Ag(Tol)$.

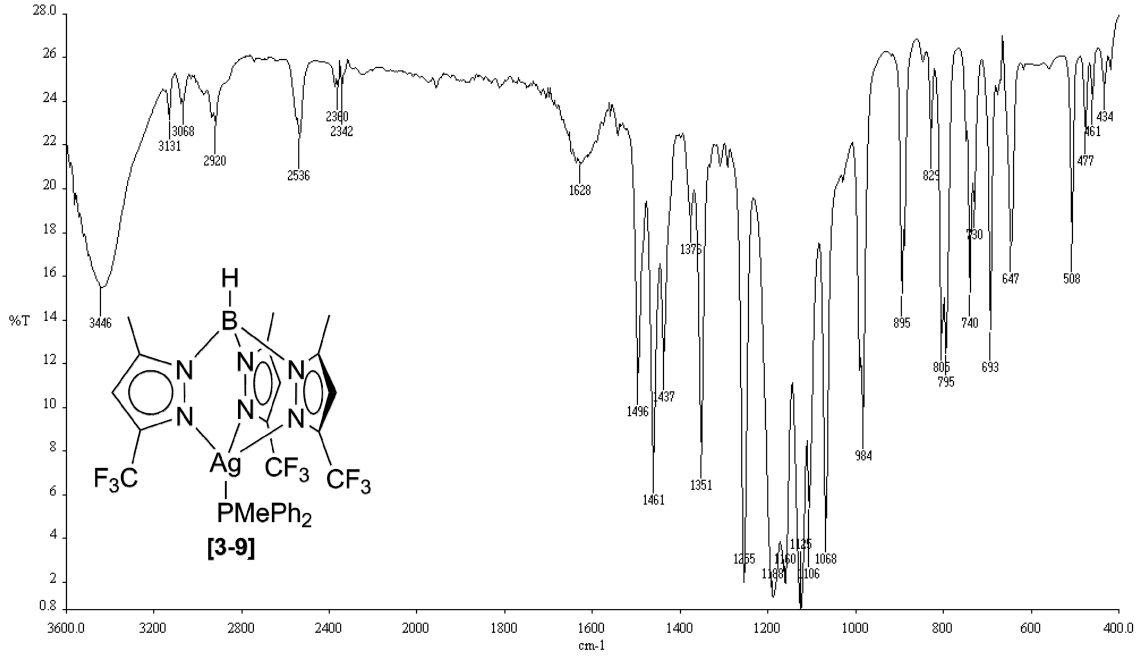

Figure B.5 IR spectrum of $Tp^{CF_3,CH_3}Ag(PMePh_2)$.

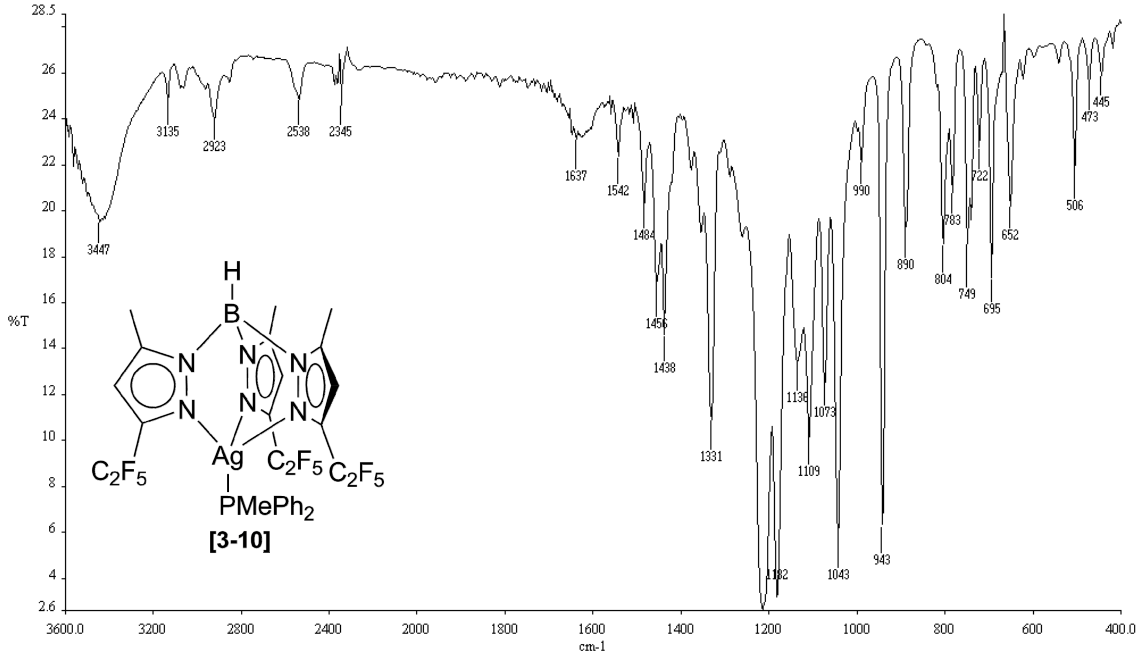

Figure B.6 IR spectrum of $Tp^{C_2F_5,CH_3}Ag(PMePh_2)$.

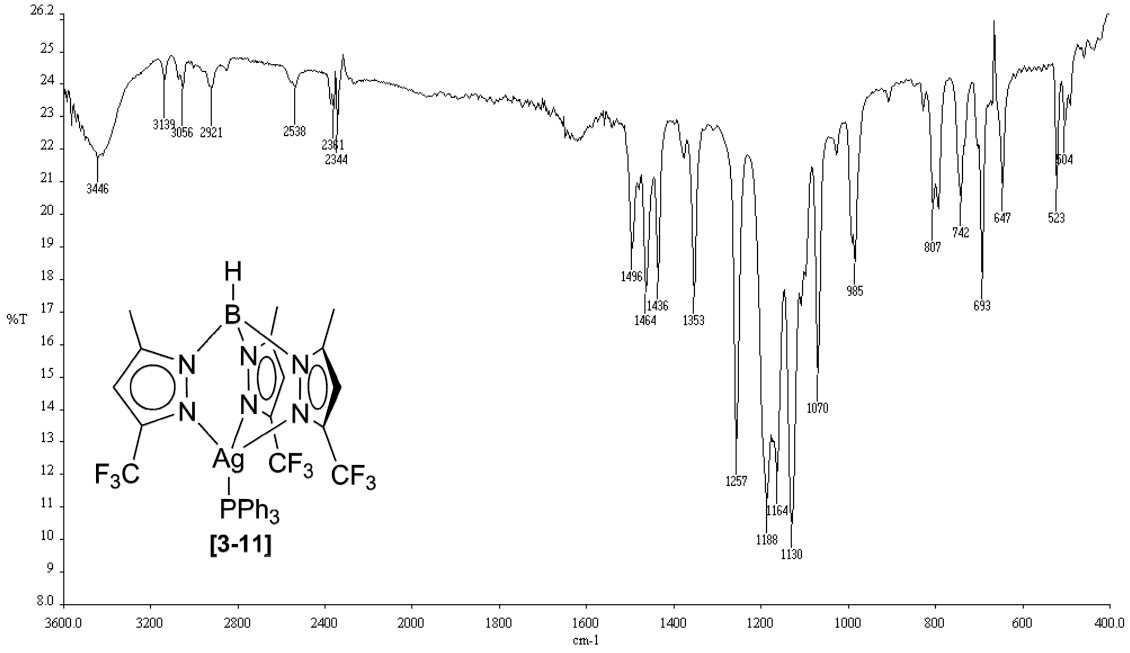

Figure B.7 IR spectrum of $Tp^{CF_3,CH_3}Ag(PPh_3)$.

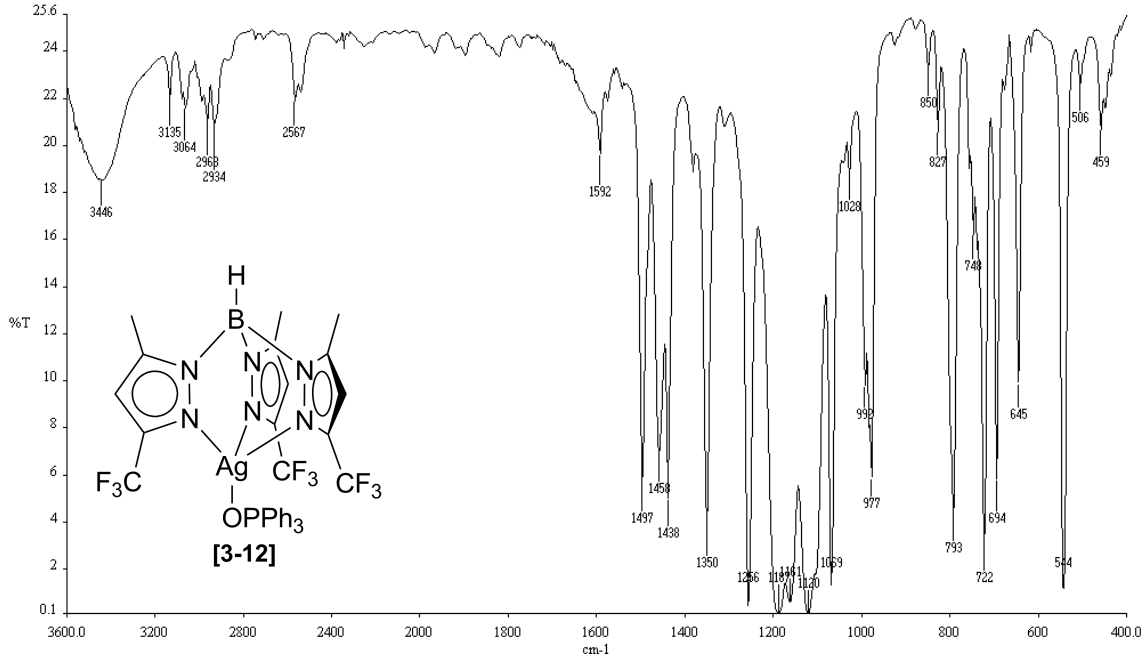

Figure B.8 IR spectrum of $Tp^{CF_3,CH_3}Ag(OPPh_3)$.

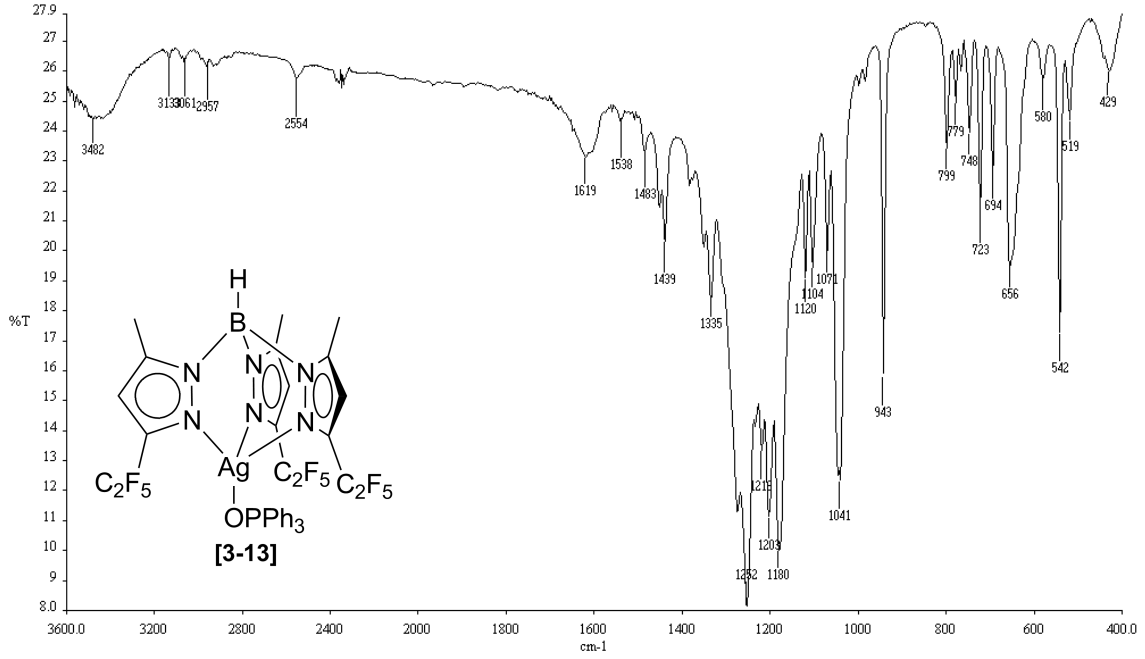

Figure B.9 IR spectrum of $Tp^{C_2F_5,CH_3}Ag(OPPh_3)$.

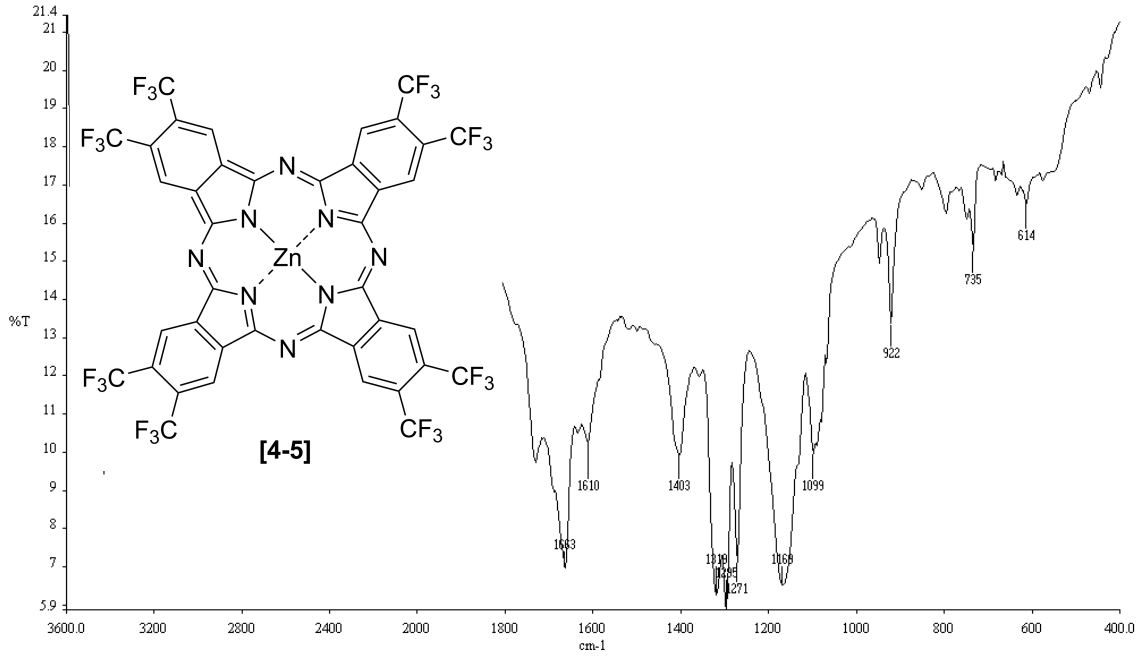

Figure B.10 IR spectrum of $F_{24}H_8PcZn$.

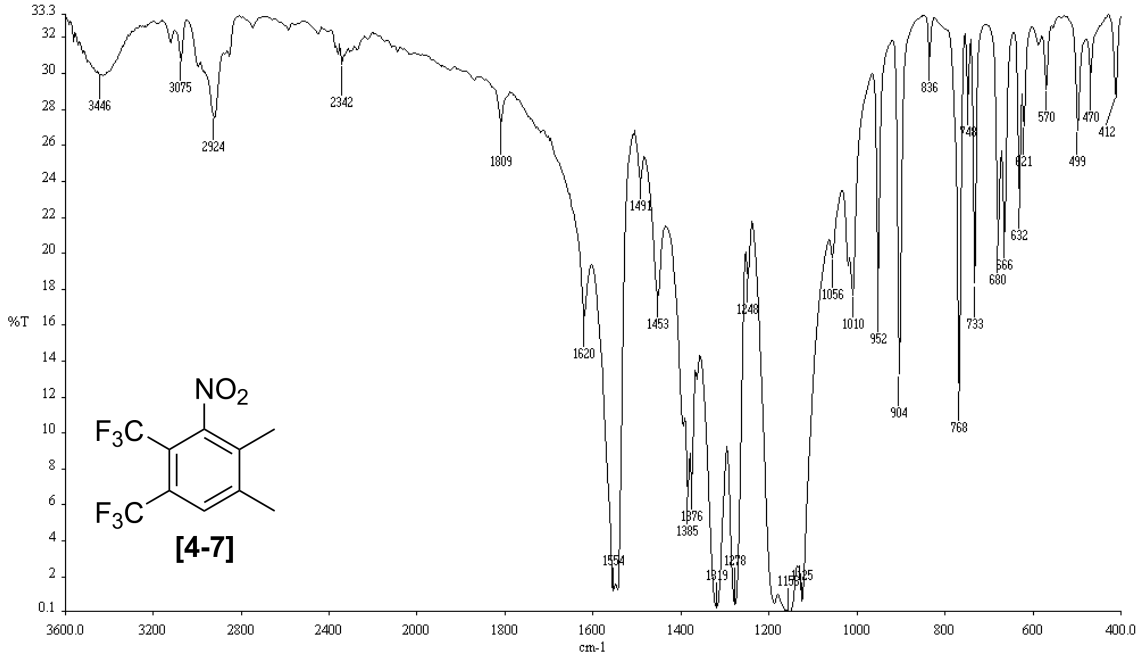

Figure B.11 IR spectrum of 1,2-bis(trifluoromethyl)-3-nitro-4,5-dimethylbenzene.

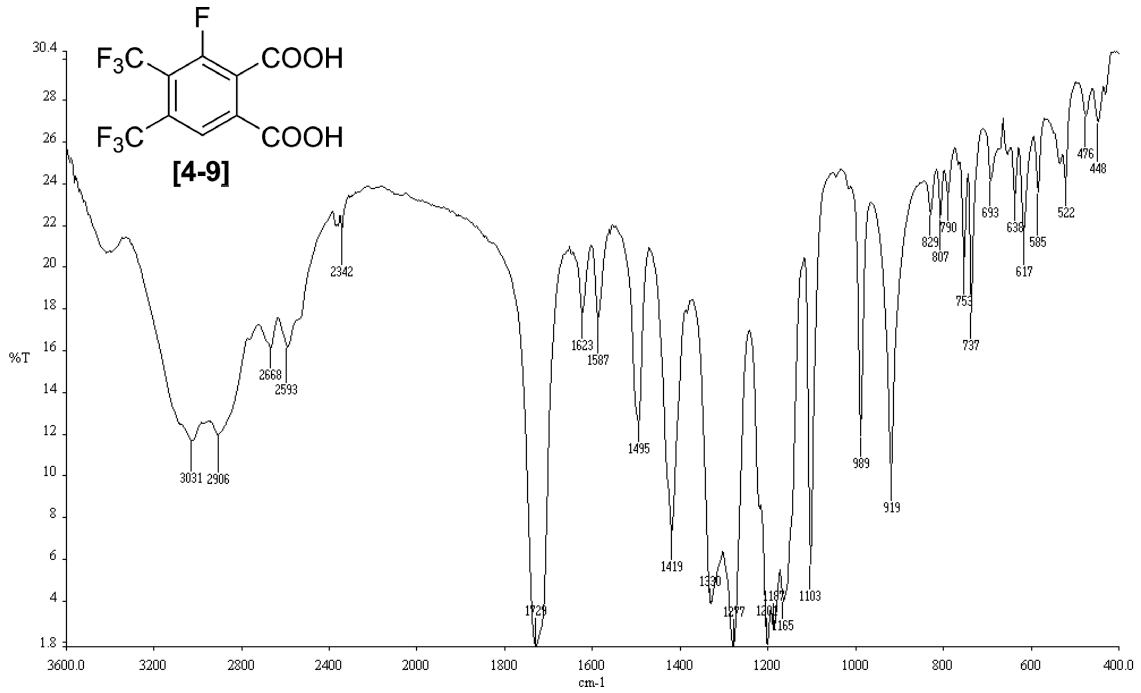

Figure B.12 IR spectrum of 4,5-bis(trifluoromethyl)-3-fluorophthalic acid.

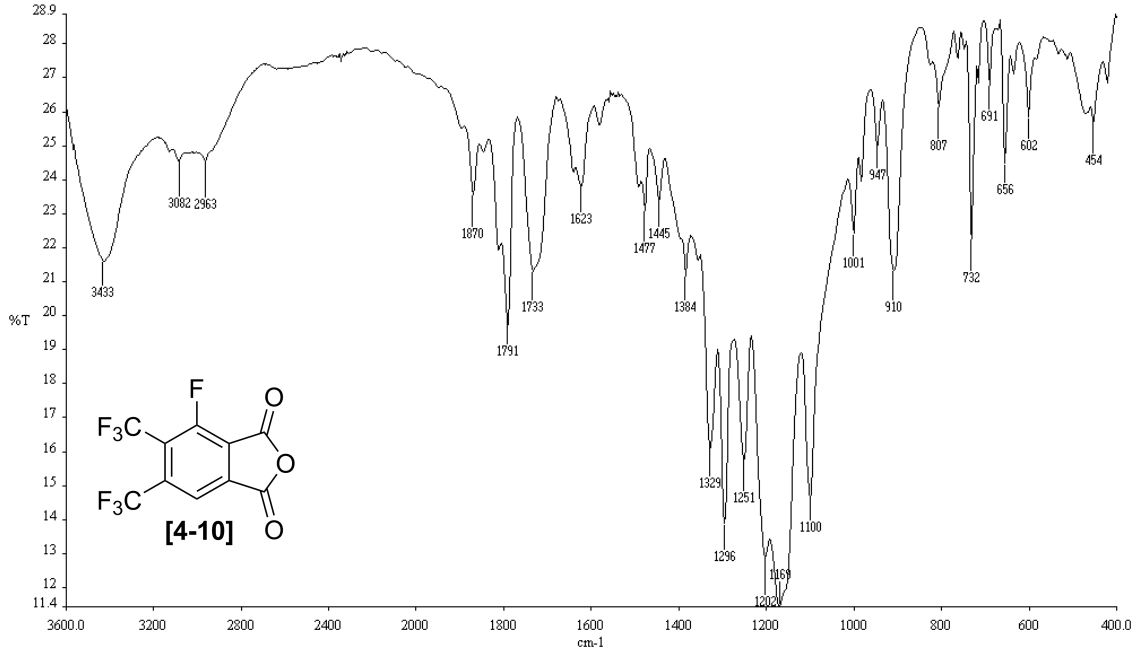

Figure B.13 IR spectrum of 4,5-bis(trifluoromethyl)-3-fluorophthalic anhydride.

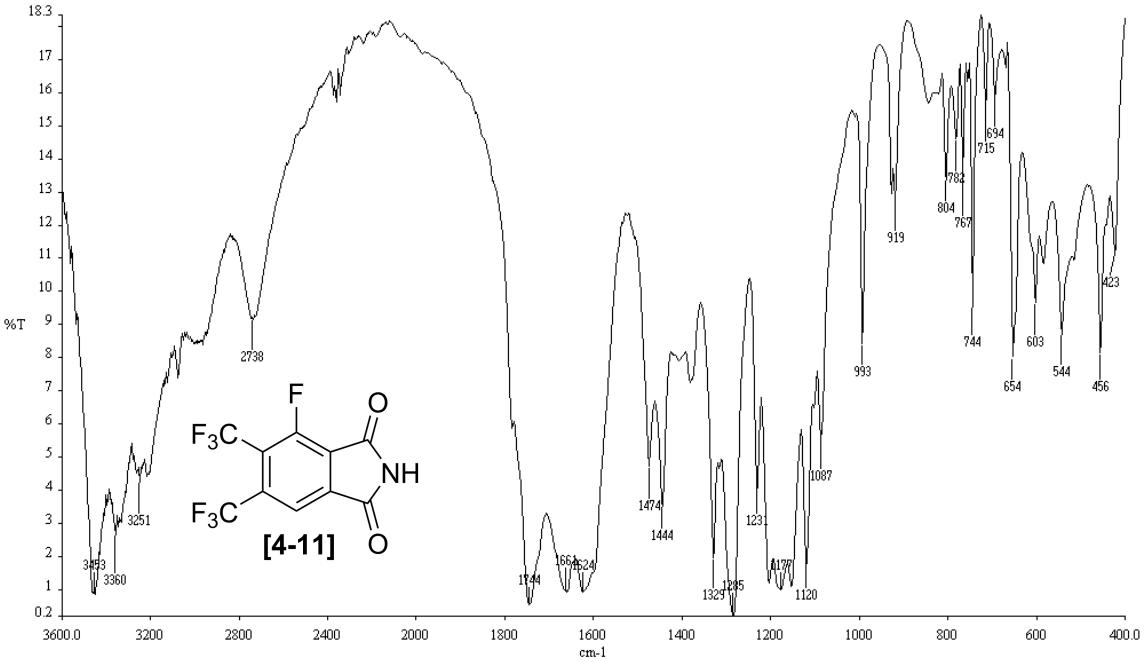

Figure B.14 IR spectrum of 4,5-bis(trifluoromethyl)-3-fluorophthalimide.

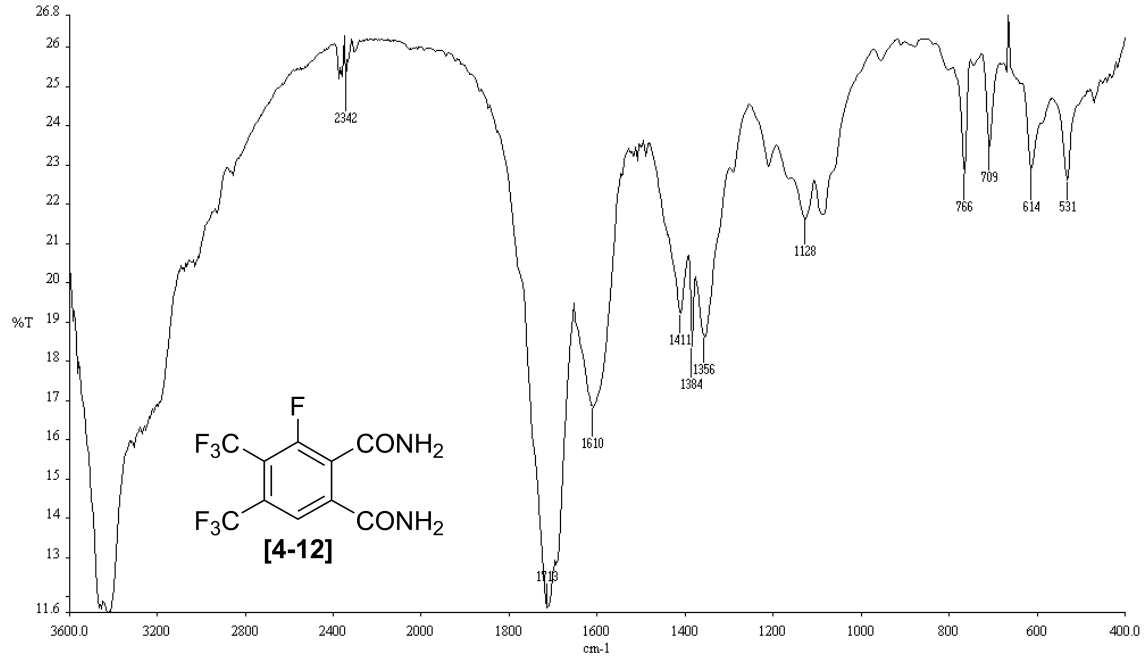

Figure B.15 IR spectrum of 4,5-bis(trifluoromethyl)-3-fluorophthalamide.

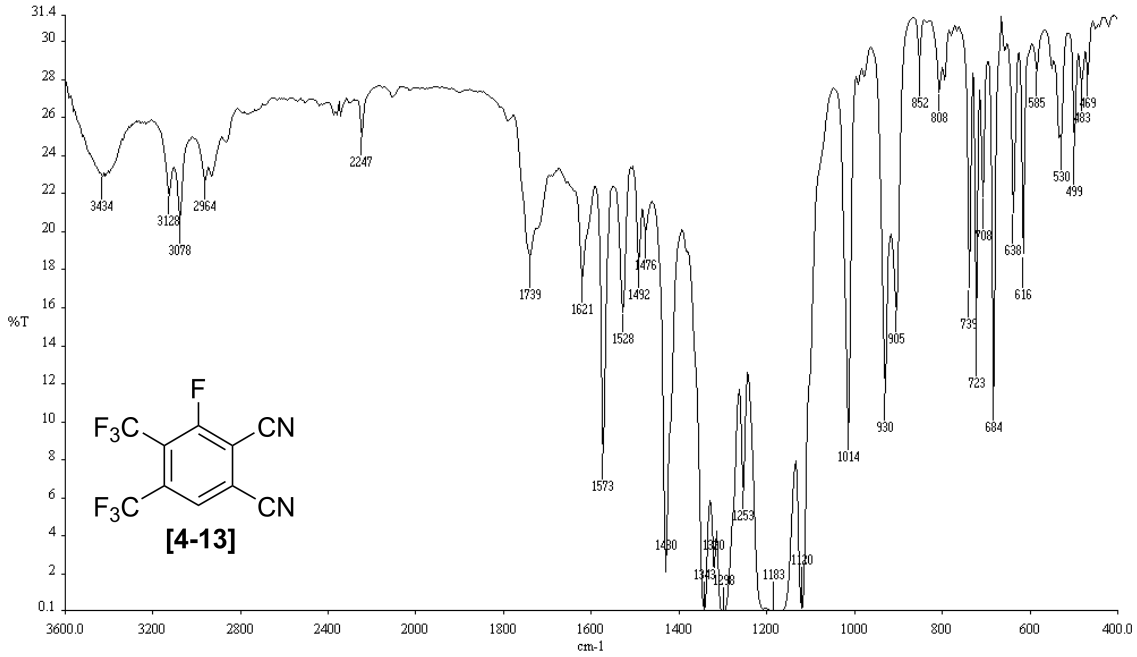

Figure B.16 IR spectrum of 4,5-bis(trifluoromethyl)-3-fluorophthalonitrile.

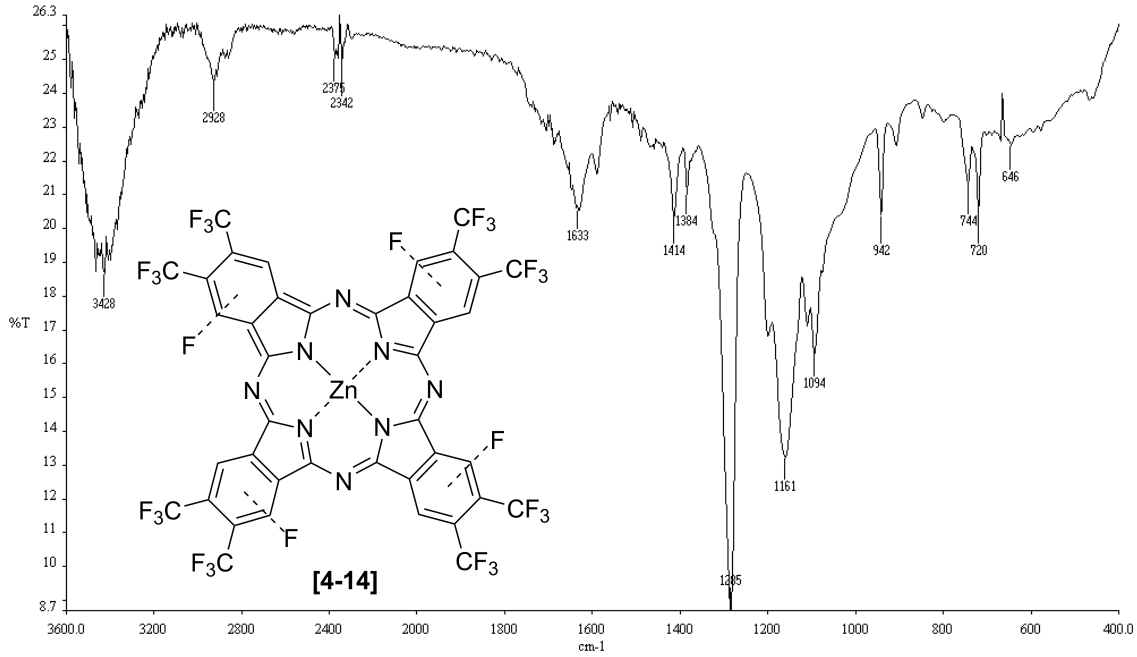

Figure B.17 IR spectrum of $F_{28}H_4PcZn$.

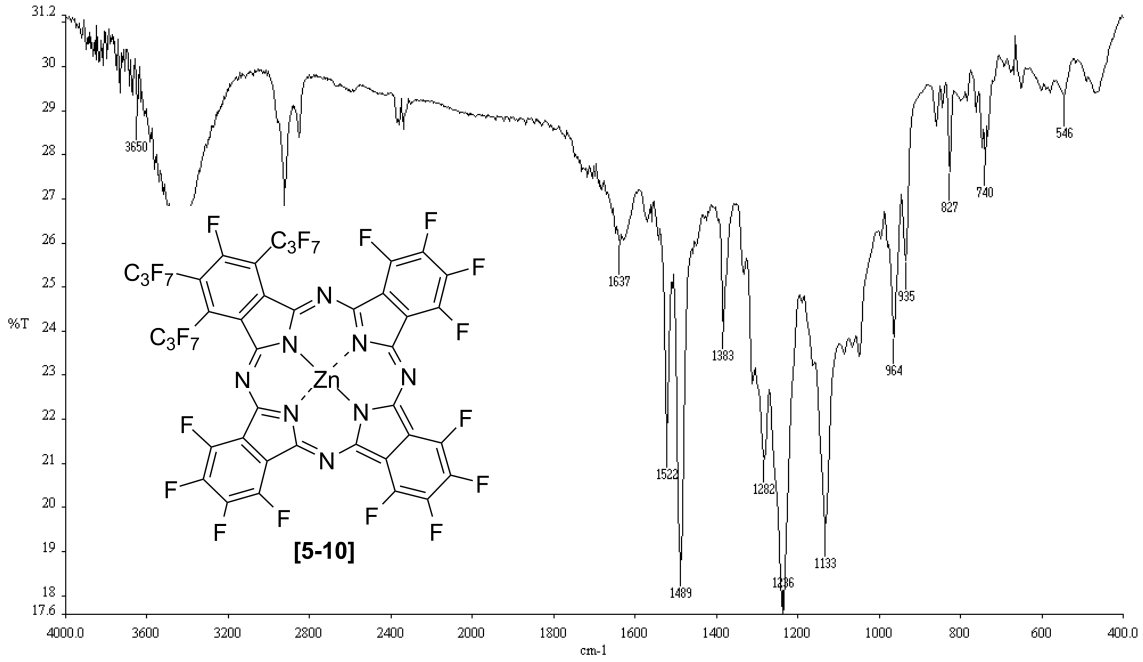

Figure B.18 IR spectrum of $F_{34}PcZn$.

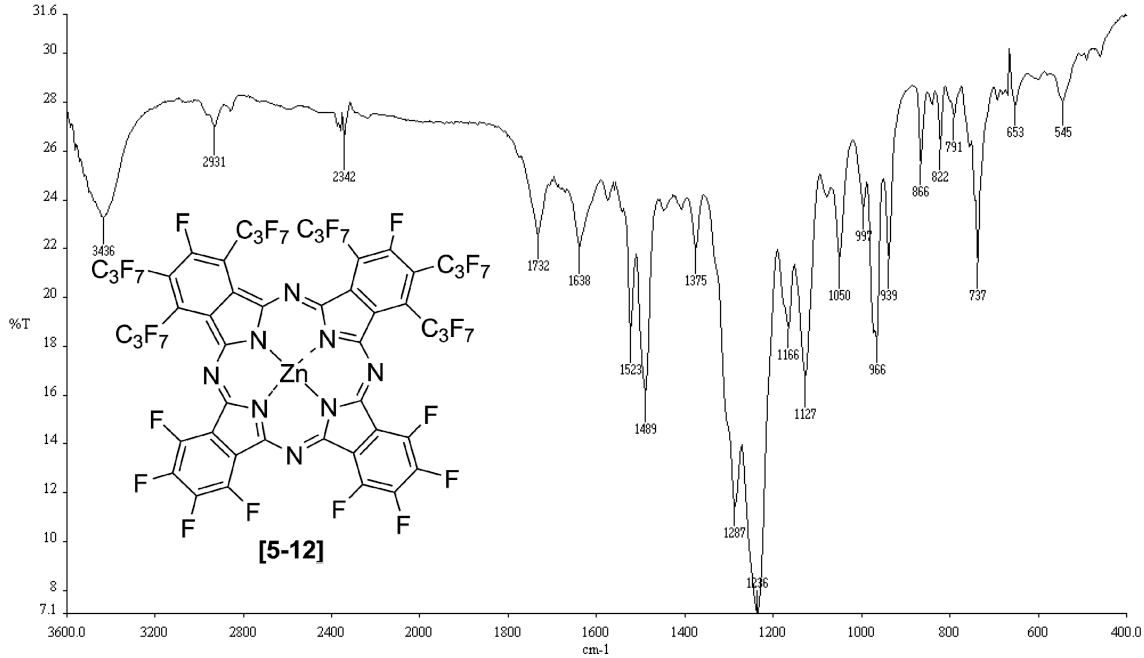

Figure B.19 IR spectrum of $F_{52}PcZn$.

APPENDIX C

CRYSTAL STRUCTURE OF 3-TRIFLUOROMETHYL-5-METHYLPYRAZOLE

Tables C.1 to C.5 list the atomic coordinates and crystallographic parameters for Pz^{CF_3,CH_3} **[3-3]** (Figure C.1).

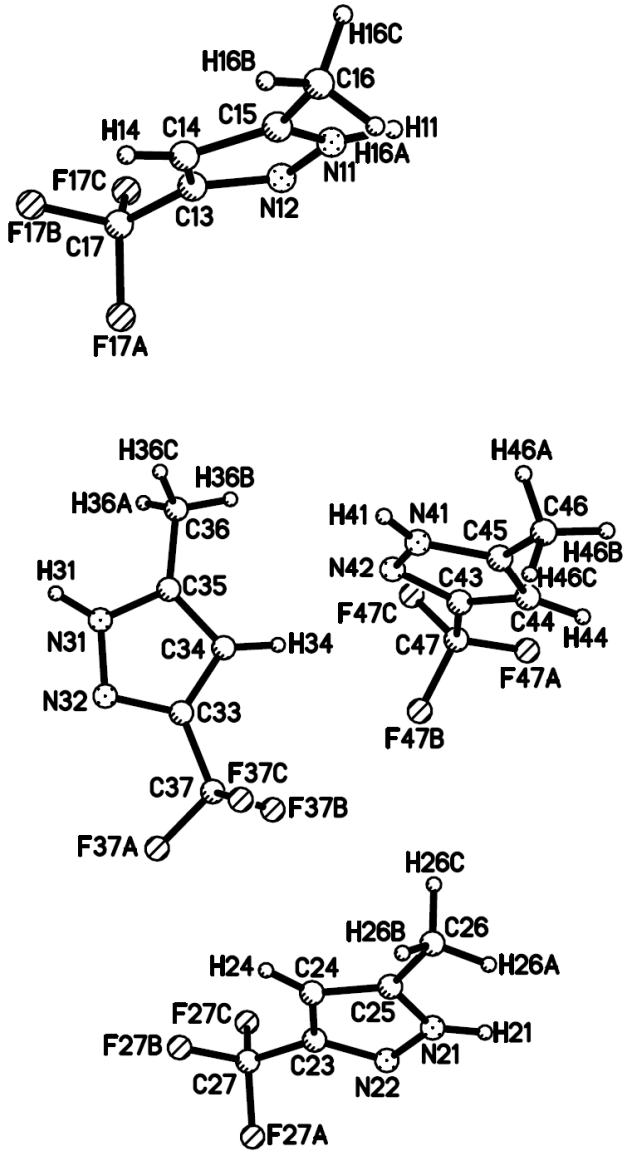

Figure C.1 Crystal structure of Pz^{CF_3,CH_3}.

Table C.1 Crystal Data and Structure Refinement for Pz^{CF_3,CH_3}

Empirical formula	$C_5 H_5 F_3 N_2$	
Formula weight	150.11	
Temperature	100(2) K	
Wavelength	1.54178 Å	
Crystal system	tetragonal	
Space group	P−4	
Unit cell dimensions	a = 15.7309(2) Å	α = 90°
	b = 15.7309(2) Å	β = 90°
	c = 10.8055(3) Å	γ = 90°
Volume	2673.94(9) $Å^3$	
Z	16	
Density (calculated)	1.492 g/cm^3	
Absorption coefficient	1.372 mm^{-1}	
F(000)	1216	
Crystal size	0.25 × 0.18 × 0.22 mm^3	
Theta range for data collection	4.97 to 54.23°	
Index ranges	$-16 \le h \le 16, -16 \le k \le 16, -11 \le l \le 11$	
Reflections collected	15747	
Independent reflections	3253 [*R*(int) = 0.0280]	
Completeness to theta = 54.23°	99.5%	
Refinement method	Full-matrix least-squares on F^2	
Data / restraints / parameters	3253 / 0 / 366	
Goodness-of-fit on F^2	1.076	
Final *R* indices [*I*>2sigma(*I*)]	*R*1 = 0.0759, *wR*2 = 0.1922	
R indices (all data)	*R*1 = 0.0783, *wR*2 = 0.1977	
Absolute structure parameter	0.4(3)	
Largest diff. peak and hole	0.680 and −0.259 e.$Å^{-3}$	

Table C.2 Atomic Coordinates (× 10^4) and Equivalent Isotropic Displacement Parameters ($Å^2$ × 10^3) for Pz^{CF_3,CH_3}*

	x	y	z	U(eq)
N(31)	1221(2)	4796(2)	3447(3)	38(1)
N(32)	952(2)	5595(2)	3605(3)	43(1)
N(12)	9405(2)	5983(2)	1185(3)	39(1)
N(11)	10205(2)	6232(2)	1343(3)	36(1)
N(41)	5172(2)	6239(2)	6030(3)	43(1)
N(42)	4368(2)	5971(2)	6210(4)	47(1)
N(22)	-295(2)	8866(2)	8775(3)	43(1)
N(21)	552(2)	8921(2)	8985(3)	39(1)
C(33)	1086(3)	5745(3)	4799(4)	42(1)
C(34)	1439(3)	5039(3)	5395(4)	44(1)
C(35)	1514(3)	4437(3)	4477(4)	39(1)
C(37)	907(4)	6580(3)	5340(5)	51(1)
F(37B)	682(4)	6521(2)	6516(4)	129(2)
F(37C)	1557(2)	7106(2)	5341(4)	79(1)
F(37A)	290(2)	6995(2)	4720(5)	88(1)

C(36)	1830(3)	3549(3)	4520(5)	56(1)
C(15)	10552(3)	6571(3)	316(4)	37(1)
C(14)	9933(3)	6541(3)	-576(4)	39(1)
C(13)	9233(3)	6169(3)	4(4)	39(1)
C(17)	8382(3)	5988(3)	-511(5)	47(1)
F(17A)	7802(2)	6559(3)	-206(4)	86(1)
F(17B)	8392(2)	6000(3)	-1753(3)	74(1)
F(17C)	8076(2)	5242(2)	-152(4)	88(1)
C(16)	11432(3)	6877(3)	269(5)	53(1)
C(43)	4229(3)	6125(3)	7393(4)	39(1)
C(44)	4935(3)	6480(3)	7958(4)	46(1)
C(45)	5534(3)	6545(3)	7053(4)	41(1)
C(47)	3398(3)	5933(3)	7959(5)	50(1)
F(47A)	3418(2)	5919(3)	9167(3)	75(1)
F(47B)	2794(2)	6488(3)	7651(4)	85(1)
F(47C)	3082(2)	5189(2)	7544(4)	98(1)
C(46)	6425(3)	6877(3)	7051(6)	59(1)
C(25)	1011(3)	8791(3)	7965(4)	44(1)
C(24)	459(3)	8648(3)	7025(4)	45(1)
C(23)	-346(3)	8705(3)	7580(4)	40(1)
C(27)	-1175(3)	8562(3)	6974(5)	51(1)
F(27B)	-1110(2)	8553(3)	5760(3)	93(1)
F(27C)	-1542(2)	7829(2)	7285(3)	71(1)
F(27A)	-1757(2)	9149(2)	7344(4)	96(1)
C(26)	1965(3)	8822(4)	8021(6)	63(2)

* U(eq) is defined as one third of the trace of the orthogonalized U^{ij} tensor.

Table C.3 Bond Lengths (Å) and Angles (°) for Pz^{CF_3,CH_3}

N(12)-N(11)	1.329(5)	C(45)-N(41)-N(42)	113.2(4)
N(12)-C(13)	1.338(6)	C(43)-N(42)-N(41)	103.7(4)
N(11)-C(15)	1.347(5)	C(23)-N(22)-N(21)	103.7(3)
N(22)-N(21)	1.355(5)	C(25)-N(21)-N(22)	112.6(3)
N(22)-C(23)	1.319(6)	N(32)-C(33)-C(34)	111.6(4)
N(21)-C(25)	1.333(6)	N(32)-C(33)-C(37)	121.1(4)
N(31)-N(32)	1.338(5)	C(34)-C(33)-C(37)	127.2(4)
N(31)-C(35)	1.331(6)	C(35)-C(34)-C(33)	104.4(4)
N(32)-C(33)	1.328(6)	N(31)-C(35)-C(34)	106.4(4)
N(41)-N(42)	1.348(5)	N(31)-C(35)-C(36)	122.8(4)
N(41)-C(45)	1.333(6)	C(34)-C(35)-C(36)	130.9(4)
N(42)-C(43)	1.320(6)	F(37C)-C(37)-F(37B)	104.5(5)
C(33)-C(34)	1.400(7)	F(37C)-C(37)-F(37A)	104.8(4)
C(33)-C(37)	1.464(7)	F(37B)-C(37)-F(37A)	108.6(5)
C(34)-C(35)	1.376(7)	F(37C)-C(37)-C(33)	114.4(4)
C(35)-C(36)	1.483(6)	F(37B)-C(37)-C(33)	111.9(5)
C(37)-F(37C)	1.317(6)	F(37A)-C(37)-C(33)	112.0(4)
C(37)-F(37B)	1.322(7)	N(11)-C(15)-C(14)	106.2(4)
C(37)-F(37A)	1.348(7)	N(11)-C(15)-C(16)	122.7(4)
C(15)-C(14)	1.370(7)	C(14)-C(15)-C(16)	131.1(4)
C(15)-C(16)	1.467(6)	C(15)-C(14)-C(13)	105.0(4)
C(14)-C(13)	1.397(6)	N(12)-C(13)-C(14)	111.1(4)
C(13)-C(17)	1.477(7)	N(12)-C(13)-C(17)	120.0(4)
C(17)-F(17A)	1.323(6)	C(14)-C(13)-C(17)	128.9(4)
C(17)-F(17C)	1.327(6)	F(17A)-C(17)-F(17C)	106.1(4)
C(17)-F(17B)	1.343(6)	F(17A)-C(17)-F(17B)	104.3(4)

C(43)-C(44)	1.385(6)	F(17C)-C(17)-F(17B)	108.0(5)
C(43)-C(47)	1.475(7)	F(17A)-C(17)-C(13)	113.6(4)
C(44)-C(45)	1.361(7)	F(17C)-C(17)-C(13)	113.0(4)
C(45)-C(46)	1.496(7)	F(17B)-C(17)-C(13)	111.3(4)
C(47)-F(47A)	1.306(6)	N(42)-C(43)-C(44)	111.7(4)
C(47)-F(47B)	1.332(6)	N(42)-C(43)-C(47)	120.7(4)
C(47)-F(47C)	1.348(6)	C(44)-C(43)-C(47)	127.6(4)
C(25)-C(24)	1.355(7)	C(45)-C(44)-C(43)	105.5(4)
C(25)-C(26)	1.503(7)	N(41)-C(45)-C(44)	105.9(4)
C(24)-C(23)	1.404(6)	N(41)-C(45)-C(46)	121.6(4)
C(23)-C(27)	1.476(7)	C(44)-C(45)-C(46)	132.5(4)
C(27)-F(27B)	1.316(6)	F(47A)-C(47)-F(47B)	106.2(4)
C(27)-F(27C)	1.333(6)	F(47A)-C(47)-F(47C)	109.0(5)
C(27)-F(27A)	1.360(6)	F(47B)-C(47)-F(47C)	102.9(4)
		F(47A)-C(47)-C(43)	113.3(4)
C(35)-N(31)-N(32)	113.6(3)	F(47B)-C(47)-C(43)	113.2(4)
C(33)-N(32)-N(31)	104.0(4)	F(47C)-C(47)-C(43)	111.6(4)
N(11)-N(12)-C(13)	104.4(3)	N(21)-C(25)-C(24)	107.4(4)
N(12)-N(11)-C(15)	113.2(3)	N(21)-C(25)-C(26)	120.1(4)
C(24)-C(25)-C(26)	132.5(4)	F(27B)-C(27)-F(27A)	110.7(5)
C(25)-C(24)-C(23)	104.3(4)	F(27C)-C(27)-F(27A)	102.8(4)
N(22)-C(23)-C(24)	112.1(4)	F(27B)-C(27)-C(23)	112.0(4)
N(22)-C(23)-C(27)	121.1(4)	F(27C)-C(27)-C(23)	113.8(4)
C(24)-C(23)-C(27)	126.7(4)	F(27A)-C(27)-C(23)	111.2(4)
F(27B)-C(27)-F(27C)	106.0(5)		

Table C.4 Anisotropic Displacement Parameters ($Å^2 \times 10^3$) for Pz^{CF_3,CH_3*}

	U^{11}	U^{22}	U^{33}	U^{23}	U^{13}	U^{12}
N(31)	39(2)	47(2)	29(2)	-7(2)	-5(2)	-6(2)
N(32)	49(2)	47(2)	32(2)	3(2)	3(2)	1(2)
N(12)	53(2)	38(2)	26(2)	1(2)	2(2)	-4(2)
N(11)	40(2)	35(2)	32(2)	7(2)	-7(2)	2(1)
N(41)	46(2)	50(2)	33(2)	-2(2)	6(2)	-1(2)
N(42)	51(2)	48(2)	41(2)	-7(2)	0(2)	-4(2)
N(22)	41(2)	41(2)	47(3)	-3(2)	6(2)	8(2)
N(21)	46(2)	39(2)	33(2)	-5(2)	-2(2)	2(2)
C(33)	45(2)	44(3)	35(3)	2(2)	5(2)	0(2)
C(34)	51(3)	53(3)	29(2)	0(2)	-10(2)	2(2)
C(35)	27(2)	50(3)	39(3)	-3(2)	-4(2)	1(2)
C(37)	63(3)	51(3)	41(3)	-3(2)	7(2)	0(3)
F(37B)	257(6)	63(2)	66(2)	2(2)	85(3)	7(3)
F(37C)	76(2)	53(2)	108(3)	-23(2)	-10(2)	-2(2)
F(37A)	76(2)	59(2)	129(3)	-11(2)	-15(2)	24(2)
C(36)	57(3)	43(3)	66(3)	-8(2)	-18(3)	15(2)
C(15)	36(2)	28(2)	45(3)	4(2)	4(2)	2(2)
C(14)	54(3)	36(2)	26(2)	4(2)	5(2)	0(2)
C(13)	40(2)	38(2)	40(3)	-5(2)	1(2)	-5(2)
C(17)	49(3)	50(3)	42(3)	-1(2)	6(2)	1(2)
F(17A)	55(2)	102(3)	100(3)	-28(2)	-19(2)	21(2)
F(17B)	68(2)	115(3)	38(2)	-15(2)	-11(1)	-9(2)
F(17C)	71(2)	84(2)	109(3)	15(2)	-15(2)	-33(2)
C(16)	47(3)	49(3)	63(3)	-4(2)	9(2)	-11(2)
C(43)	46(2)	39(2)	32(2)	-2(2)	2(2)	3(2)

C(44)	56(3)	49(3)	32(2)	-5(2)	-9(2)	-5(2)
C(45)	47(3)	39(2)	35(2)	-1(2)	-1(2)	1(2)
C(47)	56(3)	54(3)	41(3)	0(2)	3(2)	2(2)
F(47A)	73(2)	105(3)	45(2)	11(2)	14(2)	-16(2)
F(47B)	53(2)	110(3)	93(3)	30(2)	23(2)	22(2)
F(47C)	74(2)	100(3)	120(3)	-35(3)	27(2)	-37(2)
C(46)	58(3)	59(3)	60(3)	-15(3)	10(3)	-9(2)
C(25)	44(3)	38(2)	49(3)	-4(2)	0(2)	2(2)
C(24)	57(3)	46(2)	32(2)	-3(2)	4(2)	2(2)
C(23)	43(2)	45(2)	30(2)	0(2)	-3(2)	3(2)
C(27)	51(3)	60(3)	43(3)	9(2)	-4(2)	2(3)
F(27B)	86(3)	152(4)	41(2)	17(2)	-16(2)	-12(2)
F(27C)	59(2)	75(2)	80(2)	-3(2)	-7(2)	-21(2)
F(27A)	57(2)	92(2)	138(3)	4(2)	-17(2)	14(2)
C(26)	47(3)	83(4)	58(3)	-8(3)	1(2)	3(3)

* The anisotropic displacement factor exponent takes the form: $-2\pi^2 [h^2 a^{*2} U^{11} + ... + 2 h k a^* b^* U^{12}]$.

Table C.5 Hydrogen Coordinates ($\times 10^4$) and Isotropic Displacement Parameters ($Å^2 \times 10^3$) for Pz^{CF_3,CH_3}

	x	y	z	U(eq)
H(31)	1206	4532	2729	46
H(11)	10481	6181	2048	43
H(41)	5433	6216	5310	52
H(21)	776	9030	9715	47
H(34)	1593	4986	6242	53
H(36A)	1375	3161	4264	83
H(36B)	2007	3411	5366	83
H(36C)	2315	3488	3959	83
H(14)	9973	6733	-1408	47
H(16A)	11516	7312	908	79
H(16B)	11546	7124	-547	79
H(16C)	11821	6402	416	79
H(44)	4990	6644	8801	55
H(46A)	6784	6506	6544	88
H(46B)	6643	6889	7900	88
H(46C)	6431	7454	6707	88
H(24)	587	8535	6182	54
H(26A)	2143	9097	8793	94
H(26B)	2182	9147	7315	94
H(26C)	2193	8243	7992	94

APPENDIX D

CRYSTAL STRUCTURE OF 3-PENTAFLUOROETHYL-5-METHYLPYRAZOLE

Tables D.1 to D.5 list the atomic coordinates and crystallographic parameters for $Pz^{C_2F_5,CH_3}$ **[3-4]** (Figure D.1).

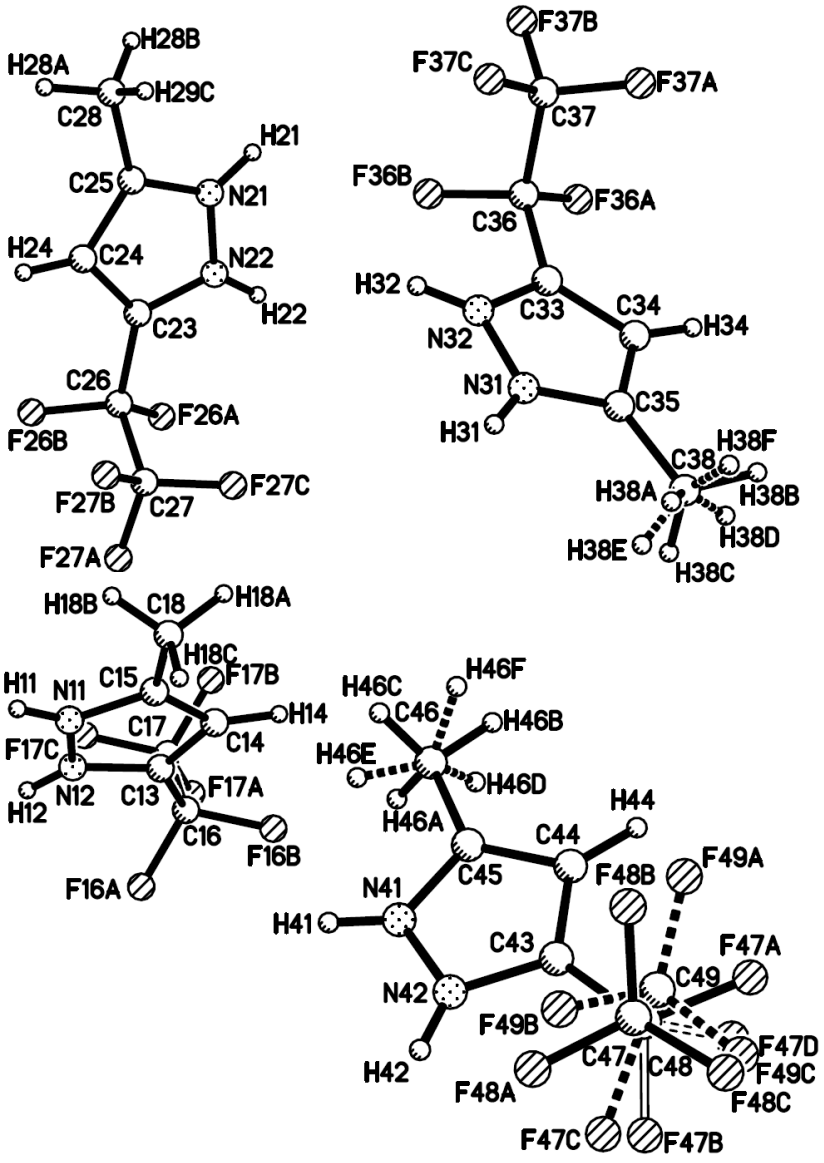

Figure D.1 Crystal structure of $Pz^{C_2F_5,CH_3}$.

Table D.1 Crystal Data and Structure Refinement for $Pz^{C_2F_5,CH_3}$

Empirical formula	$C_6 H_5 F_5 N_2$	
Formula weight	200.12	
Temperature	100(2) K	
Wavelength	1.54178 Å	
Crystal system	orthorombic	
Space group	Pbca	
Unit cell dimensions	a = 17.8156(4) Å	α = 90°
	b = 18.5880(4) Å	β = 90°
	c = 19.6774(4) Å	γ = 90°
Volume	6516.3(2) $Å^3$	
Z	32	
Density (calculated)	1.632 g/cm^3	
Absorption coefficient	1.659 mm^{-1}	
F(000)	3200	
Crystal size	0.28 × 0.27 × 0.21 mm^3	
Theta range for data collection	4.11 to 64.87°	
Index ranges	$-19 \le h \le 20, -21 \le k \le 21, -21 \le l \le 23$	
Reflections collected	31450	
Independent reflections	5465 [*R*(int) = 0.0207]	
Completeness to theta = 64.87°	99.0%	
Absorption correction	Semi-empirical from equivalents	
Max. and min. transmission	0.7220 and 0.6492	
Refinement method	Full-matrix least-squares on F^2	
Data / restraints / parameters	5465 / 57 / 507	
Goodness-of-fit on F^2	1.034	
Final *R* indices [*I*>2sigma(*I*)]	*R*1 = 0.0407, *wR*2 = 0.1045	
R indices (all data)	*R*1 = 0.0458, *wR*2 = 0.1085	
Largest diff. peak and hole	0.693 and −0.378 e.$Å^{-3}$	

Table D.2 Atomic Coordinates (× 10^4) and Equivalent Isotropic Displacement Parameters ($Å^2$ × 10^3) for $Pz^{C_2F_5,CH_3*}$

	x	y	z	U(eq)
N(11)	5868(1)	3797(1)	7595(1)	33(1)
N(12)	6570(1)	3624(1)	7402(1)	34(1)
C(13)	6521(1)	3544(1)	6730(1)	32(1)
C(14)	5791(1)	3658(1)	6498(1)	35(1)
C(15)	5382(1)	3822(1)	7069(1)	32(1)
C(16)	7201(1)	3320(1)	6348(1)	41(1)
F(16A)	7824(1)	3671(1)	6570(1)	69(1)
F(16B)	7124(1)	3462(1)	5677(1)	64(1)
C(17)	7393(1)	2523(1)	6402(1)	43(1)
F(17A)	8006(1)	2357(1)	6044(1)	60(1)
F(17B)	6838(1)	2126(1)	6168(1)	59(1)
F(17C)	7512(1)	2334(1)	7040(1)	67(1)
C(18)	4571(1)	3998(1)	7172(1)	42(1)
N(21)	3041(1)	360(1)	7033(1)	33(1)

N(22)	3742(1)	518(1)	6828(1)	30(1)
C(23)	4060(1)	813(1)	7372(1)	28(1)
C(24)	3566(1)	848(1)	7918(1)	35(1)
C(25)	2912(1)	547(1)	7684(1)	36(1)
C(26)	4852(1)	1065(1)	7340(1)	33(1)
F(26A)	5254(1)	674(1)	6883(1)	47(1)
F(26B)	5184(1)	978(1)	7952(1)	51(1)
C(27)	4961(1)	1851(1)	7150(1)	39(1)
F(27A)	5679(1)	2038(1)	7191(1)	59(1)
F(27B)	4574(1)	2274(1)	7561(1)	56(1)
F(27C)	4731(1)	1970(1)	6520(1)	55(1)
C(28)	2168(2)	427(2)	8011(2)	58(1)
N(31)	904(1)	4684(1)	5668(1)	28(1)
N(32)	797(1)	4032(1)	5948(1)	31(1)
C(33)	756(1)	3592(1)	5417(1)	32(1)
C(34)	831(1)	3956(1)	4802(1)	33(1)
C(35)	931(1)	4665(1)	4980(1)	28(1)
C(36)	603(1)	2813(1)	5541(1)	41(1)
F(36A)	853(1)	2415(1)	5017(1)	78(1)
F(36B)	940(1)	2580(1)	6116(1)	60(1)
C(37)	-229(1)	2637(1)	5631(1)	45(1)
F(37A)	-615(1)	2827(1)	5077(1)	69(1)
F(37B)	-334(1)	1935(1)	5737(1)	56(1)
F(37C)	-512(1)	2998(1)	6146(1)	57(1)
C(38)	1050(1)	5326(1)	4567(1)	35(1)
N(41)	2404(1)	8581(1)	6481(1)	34(1)
N(42)	2286(1)	9255(1)	6253(1)	32(1)
C(43)	1923(1)	9166(1)	5672(1)	37(1)
C(44)	1803(1)	8441(1)	5528(1)	45(1)
C(45)	2127(1)	8076(1)	6060(1)	39(1)
C(46)	2199(2)	7287(1)	6204(2)	56(1)
C(47)	1696(2)	9806(1)	5267(1)	51(1)
F(47A)	1369(6)	9600(3)	4669(2)	103(3)
F(47B)	2270(3)	10255(3)	5139(5)	101(2)
F(47C)	2235(8)	10318(8)	5423(10)	75(5)
F(47D)	1903(15)	9665(6)	4616(4)	83(5)
C(48)	1096(1)	10313(1)	5598(1)	40(1)
F(48A)	1386(1)	10584(1)	6157(1)	67(1)
F(48B)	492(1)	9956(1)	5777(1)	59(1)
F(48C)	889(1)	10838(1)	5181(1)	64(1)
C(49)	1031(3)	10115(3)	5445(3)	93(4)
F(49A)	502(3)	9622(3)	5380(3)	175(6)
F(49B)	1048(3)	10368(3)	6072(3)	154(6)
F(49C)	878(3)	10691(3)	5070(3)	117(3)

* U(eq) is defined as one third of the trace of the orthogonalized U^{ij} tensor.

Table D.3 Bond Lengths (Å) and Angles (°) for $Pz^{C_2F_5,CH_3}$

N(11)-N(12)	1.345(2)	N(31)-N(32)	1.344(2)
N(11)-C(15)	1.351(3)	N(31)-C(35)	1.356(2)
N(12)-C(13)	1.334(3)	N(32)-C(33)	1.330(3)
C(13)-C(14)	1.395(3)	C(33)-C(34)	1.392(3)
C(13)-C(16)	1.486(3)	C(33)-C(36)	1.494(3)
C(14)-C(15)	1.374(3)	C(34)-C(35)	1.375(3)
C(15)-C(18)	1.494(3)	C(35)-C(38)	1.489(3)

C(16)-F(16B)	1.352(3)	C(36)-F(36A)	1.344(3)
C(16)-F(16A)	1.361(3)	C(36)-F(36B)	1.353(3)
C(16)-C(17)	1.524(3)	C(36)-C(37)	1.528(2)
C(17)-F(17B)	1.318(3)	C(37)-F(37C)	1.3164
C(17)-F(17C)	1.321(3)	C(37)-F(37B)	1.3345
C(17)-F(17A)	1.336(2)	C(37)-F(37A)	1.3372
N(21)-N(22)	1.345(2)	N(41)-N(42)	1.346(2)
N(21)-C(25)	1.346(3)	N(41)-C(45)	1.346(3)
N(22)-C(23)	1.330(3)	N(42)-C(43)	1.326(3)
C(23)-C(24)	1.392(3)	C(43)-C(44)	1.393(3)
C(23)-C(26)	1.487(3)	C(43)-C(47)	1.487(3)
C(24)-C(25)	1.372(3)	C(44)-C(45)	1.375(3)
C(25)-C(28)	1.491(3)	C(45)-C(46)	1.498(3)
C(26)-F(26B)	1.352(2)	C(47)-F(47B)	1.345(4)
C(26)-F(26A)	1.360(2)	C(47)-F(47D)	1.359(6)
C(26)-C(27)	1.521(2)	C(47)-C(49)	1.362(5)
C(27)-F(27B)	1.3213	C(47)-F(47A)	1.369(4)
C(27)-F(27C)	1.3256	C(47)-F(47C)	1.386(7)
C(27)-F(27A)	1.3277	C(47)-C(48)	1.567(3)
C(48)-F(48B)	1.3128	F(27C)-C(27)-C(26)	110.47(8)
C(48)-F(48A)	1.3163	F(27A)-C(27)-C(26)	111.09(8)
C(48)-F(48C)	1.3280	N(32)-N(31)-C(35)	113.03(16)
C(49)-F(49B)	1.3203	C(33)-N(32)-N(31)	103.85(16)
C(49)-F(49A)	1.3208	N(32)-C(33)-C(34)	112.30(18)
C(49)-F(49C)	1.3275	N(32)-C(33)-C(36)	118.59(18)
		C(34)-C(33)-C(36)	129.02(19)
N(12)-N(11)-C(15)	112.82(17)	C(35)-C(34)-C(33)	104.87(17)
C(13)-N(12)-N(11)	104.28(17)	N(31)-C(35)-C(34)	105.95(17)
N(12)-C(13)-C(14)	111.60(19)	N(31)-C(35)-C(38)	121.88(18)
N(12)-C(13)-C(16)	118.73(19)	C(34)-C(35)-C(38)	132.17(18)
C(14)-C(13)-C(16)	129.59(19)	F(36A)-C(36)-F(36B)	108.62(19)
C(15)-C(14)-C(13)	105.13(18)	F(36A)-C(36)-C(33)	110.40(18)
N(11)-C(15)-C(14)	106.16(18)	F(36B)-C(36)-C(33)	111.43(19)
N(11)-C(15)-C(18)	121.58(19)	F(36A)-C(36)-C(37)	107.02(17)
C(14)-C(15)-C(18)	132.26(19)	F(36B)-C(36)-C(37)	105.30(16)
F(16B)-C(16)-F(16A)	107.61(18)	C(33)-C(36)-C(37)	113.78(16)
F(16B)-C(16)-C(13)	110.83(19)	F(37C)-C(37)-F(37B)	108.9
F(16A)-C(16)-C(13)	111.57(18)	F(37C)-C(37)-F(37A)	107.2
F(16B)-C(16)-C(17)	106.36(18)	F(37B)-C(37)-F(37A)	108.3
F(16A)-C(16)-C(17)	105.17(19)	F(37C)-C(37)-C(36)	110.66(9)
C(13)-C(16)-C(17)	114.85(17)	F(37B)-C(37)-C(36)	111.30(9)
F(17B)-C(17)-F(17C)	107.6(2)	F(37A)-C(37)-C(36)	110.34(9)
F(17B)-C(17)-F(17A)	107.51(17)	N(42)-N(41)-C(45)	112.82(18)
F(17C)-C(17)-F(17A)	108.06(19)	C(43)-N(42)-N(41)	104.27(16)
F(17B)-C(17)-C(16)	110.54(19)	N(42)-C(43)-C(44)	111.84(19)
F(17C)-C(17)-C(16)	111.19(18)	N(42)-C(43)-C(47)	119.63(19)
F(17A)-C(17)-C(16)	111.72(19)	C(44)-C(43)-C(47)	128.5(2)
N(22)-N(21)-C(25)	112.83(17)	C(45)-C(44)-C(43)	104.94(19)
C(23)-N(22)-N(21)	104.07(16)	N(41)-C(45)-C(44)	106.13(19)
N(22)-C(23)-C(24)	111.85(17)	N(41)-C(45)-C(46)	122.3(2)
N(22)-C(23)-C(26)	119.92(17)	C(44)-C(45)-C(46)	131.5(2)
C(24)-C(23)-C(26)	128.22(18)	F(47B)-C(47)-F(47D)	74.7(6)
C(25)-C(24)-C(23)	104.93(18)	F(47B)-C(47)-C(49)	116.5(4)
N(21)-C(25)-C(24)	106.32(18)	F(47D)-C(47)-C(49)	124.0(11)
N(21)-C(25)-C(28)	121.7(2)	F(47B)-C(47)-F(47A)	109.6(3)
C(24)-C(25)-C(28)	132.0(2)	F(47D)-C(47)-F(47A)	41.5(7)

F(26B)-C(26)-F(26A)	107.20(16)	C(49)-C(47)-F(47A)	88.2(5)
F(26B)-C(26)-C(23)	109.84(17)	F(47B)-C(47)-F(47C)	24.2(7)
F(26A)-C(26)-C(23)	111.13(16)	F(47D)-C(47)-F(47C)	98.8(7)
F(26B)-C(26)-C(27)	106.04(15)	C(49)-C(47)-F(47C)	104.8(9)
F(26A)-C(26)-C(27)	106.48(15)	F(47A)-C(47)-F(47C)	132.6(6)
C(23)-C(26)-C(27)	115.69(15)	F(47B)-C(47)-C(43)	113.0(3)
F(27B)-C(27)-F(27C)	108.2	F(47D)-C(47)-C(43)	106.0(7)
F(27B)-C(27)-F(27A)	108.1	C(49)-C(47)-C(43)	115.9(3)
F(27C)-C(27)-F(27A)	108.1	F(47A)-C(47)-C(43)	110.6(3)
F(27B)-C(27)-C(26)	110.77(8)	F(47C)-C(47)-C(43)	104.1(7)
F(47B)-C(47)-C(48)	102.9(3)	F(48B)-C(48)-C(47)	111.54(13)
F(47D)-C(47)-C(48)	133.8(10)	F(48A)-C(48)-C(47)	108.03(13)
C(49)-C(47)-C(48)	17.5(3)	F(48C)-C(48)-C(47)	112.03(13)
F(47A)-C(47)-C(48)	103.6(4)	F(49B)-C(49)-F(49A)	110.7
F(47C)-C(47)-C(48)	88.2(9)	F(49B)-C(49)-F(49C)	103.7
C(43)-C(47)-C(48)	116.43(19)	F(49A)-C(49)-F(49C)	111.0
F(48B)-C(48)-F(48A)	106.9	F(49B)-C(49)-C(47)	111.7(3)
F(48B)-C(48)-F(48C)	108.1	F(49A)-C(49)-C(47)	107.6(3)
F(48A)-C(48)-F(48C)	110.1	F(49C)-C(49)-C(47)	112.1(2)

Table D.4 Anisotropic Displacement Parameters ($Å^2 \times 10^3$) for $Pz^{C_2F_5,CH_3*}$

	U^{11}	U^{22}	U^{33}	U^{23}	U^{13}	U^{12}
N(11)	36(1)	32(1)	29(1)	-3(1)	-3(1)	2(1)
N(12)	34(1)	33(1)	35(1)	-3(1)	-4(1)	-2(1)
C(13)	39(1)	24(1)	33(1)	0(1)	0(1)	-5(1)
C(14)	43(1)	33(1)	29(1)	3(1)	-6(1)	-3(1)
C(15)	39(1)	24(1)	34(1)	1(1)	-7(1)	0(1)
C(16)	41(1)	42(1)	40(1)	1(1)	5(1)	-12(1)
F(16A)	45(1)	63(1)	99(1)	-26(1)	18(1)	-26(1)
F(16B)	79(1)	70(1)	42(1)	17(1)	22(1)	6(1)
C(17)	38(1)	50(1)	42(1)	-8(1)	8(1)	-2(1)
F(17A)	44(1)	69(1)	68(1)	-17(1)	20(1)	1(1)
F(17B)	51(1)	45(1)	81(1)	-19(1)	14(1)	-11(1)
F(17C)	82(1)	69(1)	49(1)	5(1)	5(1)	38(1)
C(18)	42(1)	40(1)	46(1)	2(1)	-6(1)	8(1)
N(21)	30(1)	28(1)	41(1)	-4(1)	-2(1)	-3(1)
N(22)	31(1)	29(1)	31(1)	-4(1)	1(1)	-1(1)
C(23)	30(1)	22(1)	31(1)	0(1)	0(1)	0(1)
C(24)	41(1)	33(1)	31(1)	-7(1)	6(1)	-4(1)
C(25)	36(1)	28(1)	42(1)	-4(1)	9(1)	-2(1)
C(26)	32(1)	35(1)	34(1)	-2(1)	-1(1)	3(1)
F(26A)	34(1)	43(1)	64(1)	-10(1)	12(1)	5(1)
F(26B)	44(1)	60(1)	49(1)	10(1)	-18(1)	-8(1)
C(27)	32(1)	37(1)	48(1)	0(1)	5(1)	-5(1)
F(27A)	37(1)	52(1)	89(1)	6(1)	6(1)	-15(1)
F(27B)	56(1)	32(1)	80(1)	-13(1)	20(1)	-7(1)
F(27C)	58(1)	55(1)	52(1)	20(1)	4(1)	-4(1)
C(28)	45(1)	53(2)	76(2)	-15(1)	23(1)	-15(1)
N(31)	28(1)	27(1)	29(1)	-2(1)	0(1)	2(1)
N(32)	30(1)	33(1)	30(1)	2(1)	-1(1)	2(1)
C(33)	29(1)	31(1)	36(1)	-2(1)	3(1)	2(1)
C(34)	33(1)	38(1)	30(1)	-6(1)	2(1)	0(1)
C(35)	23(1)	34(1)	28(1)	0(1)	0(1)	2(1)

C(36)	45(1)	33(1)	46(1)	0(1)	6(1)	4(1)
F(36A)	107(1)	34(1)	93(1)	-18(1)	54(1)	-6(1)
F(36B)	48(1)	43(1)	91(1)	22(1)	-20(1)	1(1)
C(37)	55(1)	33(1)	46(1)	7(1)	-12(1)	-10(1)
F(37A)	75(1)	59(1)	74(1)	19(1)	-36(1)	-28(1)
F(37B)	61(1)	38(1)	69(1)	9(1)	-4(1)	-14(1)
F(37C)	52(1)	51(1)	69(1)	0(1)	19(1)	-5(1)
C(38)	32(1)	38(1)	35(1)	4(1)	2(1)	2(1)
N(41)	30(1)	36(1)	36(1)	0(1)	-4(1)	-3(1)
N(42)	31(1)	32(1)	34(1)	-3(1)	0(1)	-6(1)
C(43)	38(1)	44(1)	30(1)	-2(1)	2(1)	-2(1)
C(44)	47(1)	50(1)	38(1)	-13(1)	-7(1)	-5(1)
C(45)	34(1)	36(1)	48(1)	-8(1)	0(1)	-6(1)
C(46)	50(2)	38(1)	81(2)	-4(1)	0(1)	-4(1)
C(47)	60(2)	60(2)	33(1)	9(1)	6(1)	5(1)
F(47A)	173(7)	99(3)	37(2)	-5(2)	-31(3)	60(3)
F(47B)	56(2)	96(3)	150(5)	89(3)	57(3)	26(2)
F(47C)	49(6)	85(6)	92(10)	55(6)	-12(6)	-33(5)
F(47D)	122(14)	105(7)	24(3)	17(4)	8(5)	0(7)
C(48)	43(3)	39(2)	40(3)	10(2)	10(2)	10(2)
F(48A)	83(3)	52(2)	67(2)	-18(2)	-8(2)	19(2)
F(48B)	32(2)	64(2)	80(2)	38(2)	13(2)	4(1)
F(48C)	66(3)	51(2)	76(3)	30(2)	24(2)	24(2)
C(49)	67(7)	100(8)	113(9)	65(7)	0(6)	5(5)
F(49A)	66(4)	166(9)	293(14)	136(9)	-74(7)	-43(5)
F(49B)	200(11)	157(7)	105(6)	80(6)	107(6)	131(8)
F(49C)	70(5)	138(6)	144(6)	106(5)	-2(4) 22(4)	

* The anisotropic displacement factor exponent takes the form: $-2\pi^2 [h^2 a^{*2} U^{11} + ... + 2 h k a^* b^* U^{12}]$.

Table D.5 Hydrogen Coordinates ($\times 10^4$) and Isotropic Displacement Parameters ($Å^2 \times 10^3$) for $Pz^{C_2F_5,CH_3}$

	x	y	z	U(eq)
H(11)	5740	3884	8019	23(8)
H(12)	6970	3576	7660	41
H(14)	5615	3629	6043	42
H(18B)	4412	3832	7622	64
H(18A)	4270	3757	6823	64
H(18C)	4499	4519	7139	64
H(21)	2703	157	6770	23(7)
H(22)	3944	444	6426	37
H(24)	3660	1039	8358	42
H(28A)	2224	451	8506	87
H(28B)	1976	-48	7882	87
H(29C)	1816	799	7861	87
H(31)	952	5082	5907	18(6)
H(32)	762	3923	6382	37
H(34)	816	3758	4357	40
H(38A)	818	5738	4797	53
H(38B)	820	5263	4119	53
H(38C)	1589	5413	4514	53
H(38D)	1327	5207	4164	53
H(38E)	1326	5672	4829	53
H(38F)	572	5526	4442	53

H(41)	2636	8482	6864	11(8)
H(42)	2421	9662	6447	39
H(44)	1552	8242	5145	54
H(46A)	2729	7166	6270	85
H(46B)	1998	7012	5821	85
H(46C)	1917	7169	6617	85
H(46D)	2522	7092	5788	85
H(46E)	2535	7205	6596	85
H(46F)	1644	7078	6172	85

APPENDIX E

CRYSTAL STRUCTURE OF HYDROTRIS(3-PENTAFLUOROETHYL-5-METHYLPYRAZOL-1-YL)-BORATO-SODIUM HYDRATE

Tables E.1 to E.5 list the atomic coordinates and crystallographic parameters for $Tp^{C_2F_5,CH_3}Na(H_2O)$ **[3-6]** (Figure E.1). Figure E.2 presents the temperature-variable phase transformations in single crystals of $Tp^{C_2F_5,CH_3}Na(H_2O)$.

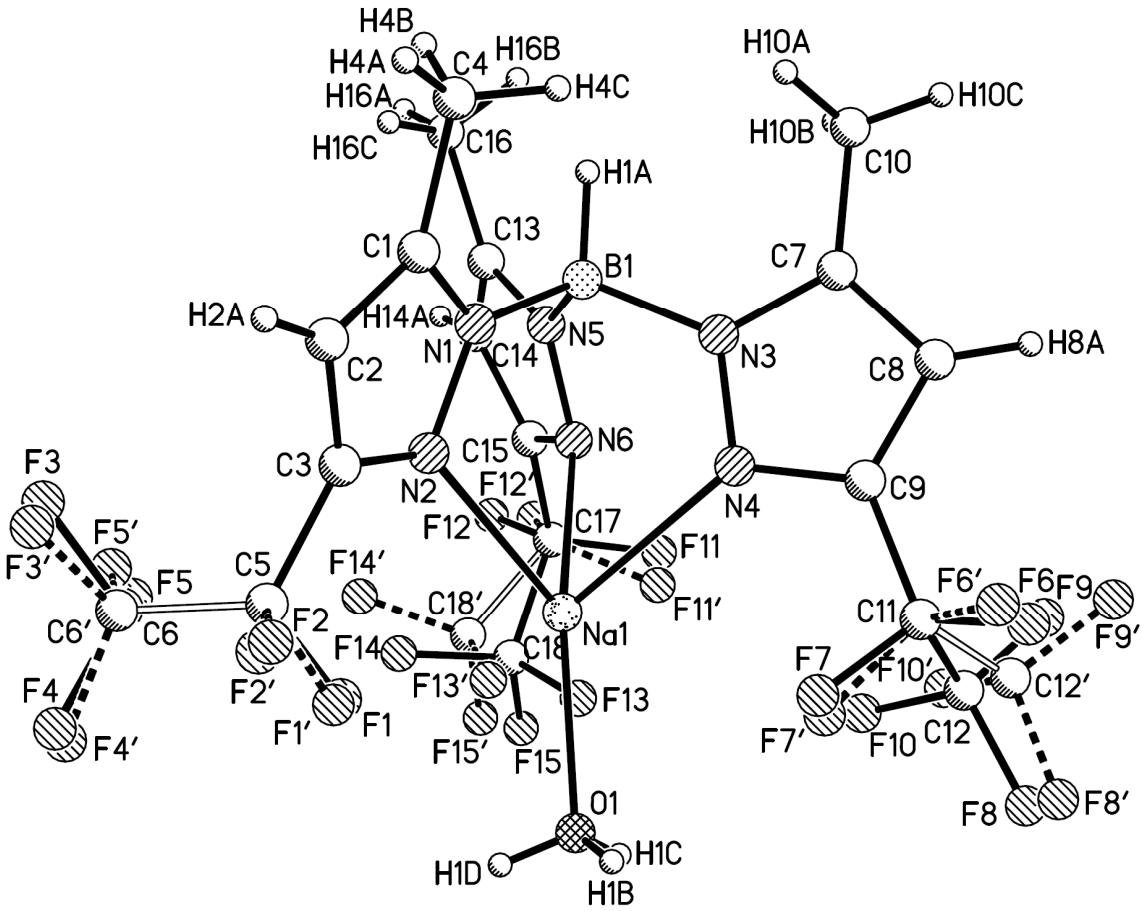

Figure E.1 Crystal structure of $Tp^{C_2F_5,CH_3}Na(H_2O)$.

Table E.1 Crystal Data and Structure Refinement for $Tp^{C_2F_5,CH_3}Na(H_2O)$

Empirical formula	$C_{18}\ H_{15}\ B\ F_{15}\ N_6\ Na\ O$	
Formula weight	650.16	
Temperature	198(2) K	
Wavelength	0.71073 Å	
Crystal system	monoclinic	
Space group	$P2_1/c$	
Unit cell dimensions	a = 11.4628(10) Å	α = 90°
	b = 21.2058(18) Å	β = 106.251(1)°
	c = 11.5152(10) Å	γ = 90°
Volume	2687.3(4) Å^3	
Z	4	
Density (calculated)	1.607 g/cm^3	
Absorption coefficient	0.188 mm^{-1}	
F(000)	1296	
Crystal size	0.45 × 0.16 × 0.12 mm^3	
Theta range for data collection	1.85 to 25.70°	
Index ranges	$-13 \le h \le 13,\ 0 \le k \le 25,\ 0 \le l \le 14$	
Reflections collected	27320	
Independent reflections	5103 [*R*(int) = 0.0329]	
Completeness to theta = 25.70°	99.9%	
Absorption correction	Multi-scan	
Max. and min. transmission	0.9778 and 0.9203	
Refinement method	Full-matrix least-squares on F^2	
Data / restraints / parameters	5103 / 645 / 461	
Goodness-of-fit on F^2	1.163	
Final *R* indices [*I*>2sigma(*I*)]	*R*1 = 0.0727, *wR*2 = 0.2237	
R indices (all data)	*R*1 = 0.0942, *wR*2 = 0.2398	
Largest diff. peak and hole	0.742 and −0.498 e.Å^{-3}	

Table E.2 Atomic Coordinates (× 10^4) and Equivalent Isotropic Displacement Parameters (Å^2 × 10^3) for $Tp^{C_2F_5,CH_3}Na(H_2O)$*

	x	y	z	U(eq)
Na1	2289(1)	1857(1)	5765(1)	48(1)
B1	2214(4)	661(2)	3743(4)	43(1)
O1	1960(3)	2635(1)	6982(3)	68(1)
N1	2137(3)	376(1)	4960(2)	39(1)
N2	2385(3)	733(1)	5982(2)	39(1)
C1	1731(3)	-204(2)	5169(3)	42(1)
C2	1725(4)	-228(2)	6357(3)	48(1)
C3	2133(3)	362(2)	6812(3)	40(1)
C4	1357(5)	-701(2)	4202(4)	64(1)
C5	2293(2)	617(1)	8061(3)	52(1)
F1	2320(40)	1251(2)	8020(50)	74(2)
F2	1361(12)	470(40)	8510(40)	87(2)
C6	3432(12)	412(9)	8977(13)	86(2)

F3	3550(20)	-210(9)	8960(20)	135(6)
F4	3430(30)	583(15)	10085(10)	104(3)
F5	4395(4)	670(14)	8740(30)	114(5)
C5'	2293(2)	617(1)	8061(3)	52(1)
F1'	2360(40)	1251(2)	8100(50)	74(2)
F2'	1289(11)	460(40)	8390(40)	87(2)
C6'	3358(13)	379(9)	9033(13)	86(2)
F3'	3250(20)	-236(9)	9190(20)	135(6)
F4'	3450(30)	668(15)	10076(11)	104(3)
F5'	4380(4)	477(14)	8730(30)	114(5)
N3	1099(3)	1089(1)	3222(2)	38(1)
N4	741(3)	1521(1)	3929(2)	39(1)
C7	329(3)	1095(2)	2085(3)	41(1)
C8	-554(3)	1539(2)	2050(3)	43(1)
C9	-255(3)	1783(2)	3217(3)	38(1)
C10	497(4)	675(2)	1091(4)	59(1)
C11	-899(2)	2282(1)	3725(2)	48(1)
F6	-2119(3)	2262(6)	3320(30)	102(2)
F7	-630(30)	2194(5)	4930(3)	78(1)
C12	-507(5)	2937(2)	3539(4)	62(2)
F8	-1191(9)	3364(2)	3880(10)	86(2)
F9	-580(8)	3037(3)	2382(5)	95(3)
F10	643(5)	3025(3)	4171(6)	81(2)
C11'	-899(2)	2282(1)	3725(2)	48(1)
F6'	-2056(4)	2077(6)	3470(30)	102(2)
F7'	-520(30)	2342(5)	4938(2)	78(1)
C12'	-929(5)	2931(2)	3212(5)	62(2)
F8'	-1557(9)	3326(2)	3699(10)	86(2)
F9'	-1435(9)	2919(4)	2024(5)	120(4)
F10'	196(7)	3149(3)	3424(10)	150(6)
N5	3404(3)	1037(1)	3924(3)	47(1)
N6	3503(3)	1646(2)	4312(4)	59(1)
C13	4467(4)	828(2)	3761(4)	56(1)
C14	5284(4)	1311(2)	4053(4)	68(1)
C15	4647(4)	1803(2)	4366(5)	66(1)
C16	4622(5)	185(3)	3327(5)	81(2)
C17	5093(3)	2470(2)	4663(3)	88(2)
F11	4611(16)	2903(6)	3806(6)	129(4)
F12	6294(4)	2465(9)	4766(9)	159(5)
C18	4969(6)	2736(3)	5826(5)	135(5)
F13	3801(7)	2818(5)	5739(10)	198(9)
F14	5454(10)	2340(5)	6722(4)	127(4)
F15	5530(11)	3289(4)	6056(8)	149(3)
C17'	5093(3)	2470(2)	4663(3)	88(2)
F11'	4267(14)	2911(6)	4139(7)	129(4)
F12'	6127(7)	2636(10)	4402(9)	159(5)
C18'	5339(6)	2557(3)	6000(4)	135(5)
F13'	4320(8)	2493(5)	6320(7)	126(4)
F14'	6134(10)	2129(5)	6580(6)	206(9)
F15'	5791(11)	3129(4)	6318(8)	149(3)

***** U(eq) is defined as one third of the trace of the orthogonalized U^{ij} tensor.

Table E.3 Bond Lengths (Å) and Angles (°) for $Tp^{C_2F_5,CH_3}Na(H_2O)$

Na(1)-O(1)	2.263(3)	Na(1)-N(6)	2.497(4)
Na(1)-N(2)	2.395(3)	Na(1)-F(1)	2.89(6)
Na(1)-N(4)	2.455(3)	Na(1)-F(1')	2.96(6)
B(1)-N(5)	1.543(6)	C(2)-H(2A)	0.9500
B(1)-N(3)	1.546(5)	C(3)-C(5)	1.499(4)
B(1)-N(1)	1.551(5)	C(4)-H(4A)	0.9800
B(1)-H(1A)	1.1000	C(4)-H(4B)	0.9800
O(1)-H(1B)	0.8400	C(4)-H(4C)	0.9800
O(1)-H(1C)	0.8400	C(5)-F(2)	1.346(3)
O(1)-H(1D)	0.8400	C(5)-F(1)	1.347(3)
N(1)-C(1)	1.360(4)	C(5)-C(6)	1.495(5)
N(1)-N(2)	1.361(4)	C(6)-F(4)	1.327(3)
N(2)-C(3)	1.332(4)	C(6)-F(3)	1.328(3)
C(1)-C(2)	1.370(5)	C(6)-F(5)	1.329(3)
C(1)-C(4)	1.506(5)	C(6')-F(3')	1.327(3)
C(2)-C(3)	1.385(5)	C(6')-F(4')	1.328(3)
C(6')-F(5')	1.329(3)	C(7)-C(10)	1.503(5)
N(3)-C(7)	1.359(5)	C(8)-C(9)	1.390(5)
N(3)-N(4)	1.363(4)	C(8)-H(8A)	0.9500
N(4)-C(9)	1.327(4)	C(9)-C(11)	1.500(4)
C(7)-C(8)	1.375(5)	N(6)-Na(1)-F(1')	130.7(11)
C(10)-H(10A)	0.9800	F(1)-Na(1)-F(1')	0.9(6)
C(10)-H(10B)	0.9800	N(5)-B(1)-N(3)	110.6(3)
C(10)-H(10C)	0.9800	N(5)-B(1)-N(1)	110.6(3)
C(11)-F(6)	1.345(3)	N(3)-B(1)-N(1)	109.2(3)
C(11)-F(7)	1.348(3)	N(5)-B(1)-H(1A)	108.8
C(11)-C(12)	1.495(5)	N(3)-B(1)-H(1A)	108.8
C(12)-F(8)	1.327(3)	N(1)-B(1)-H(1A)	108.8
C(12)-F(10)	1.328(3)	Na(1)-O(1)-H(1B)	109.5
C(12)-F(9)	1.329(3)	Na(1)-O(1)-H(1C)	109.5
C(12')-F(8')	1.326(3)	H(1B)-O(1)-H(1C)	109.5
C(12')-F(10')	1.327(3)	Na(1)-O(1)-H(1D)	109.5
C(12')-F(9')	1.328(3)	H(1B)-O(1)-H(1D)	109.5
N(5)-C(13)	1.358(5)	H(1C)-O(1)-H(1D)	109.5
N(5)-N(6)	1.360(5)	C(1)-N(1)-N(2)	110.5(3)
N(6)-C(15)	1.338(6)	C(1)-N(1)-B(1)	128.4(3)
C(13)-C(14)	1.364(7)	N(2)-N(1)-B(1)	120.9(3)
C(13)-C(16)	1.480(7)	C(3)-N(2)-N(1)	104.8(3)
C(14)-C(15)	1.379(7)	C(3)-N(2)-Na(1)	130.6(2)
C(14)-H(14A)	0.9500	N(1)-N(2)-Na(1)	118.11(19)
C(15)-C(17)	1.509(6)	N(1)-C(1)-C(2)	107.9(3)
C(16)-H(16A)	0.9800	N(1)-C(1)-C(4)	122.9(3)
C(16)-H(16B)	0.9800	C(2)-C(1)-C(4)	129.2(3)
C(16)-H(16C)	0.9800	C(1)-C(2)-C(3)	104.4(3)
C(17)-F(11)	1.348(3)	C(1)-C(2)-H(2A)	127.8
C(17)-F(12)	1.349(3)	C(3)-C(2)-H(2A)	127.8
C(17)-C(18)	1.496(5)	N(2)-C(3)-C(2)	112.4(3)
C(18)-F(14)	1.325(3)	N(2)-C(3)-C(5)	118.9(3)
C(18)-F(13)	1.326(3)	C(2)-C(3)-C(5)	128.8(3)
C(18)-F(15)	1.328(3)	C(1)-C(4)-H(4A)	109.5
C(18')-F(14')	1.326(3)	C(1)-C(4)-H(4B)	109.5
C(18')-F(13')	1.326(3)	H(4A)-C(4)-H(4B)	109.5
C(18')-F(15')	1.329(3)	C(1)-C(4)-H(4C)	109.5

		H(4A)-C(4)-H(4C)	109.5
O(1)-Na(1)-N(2)	132.14(13)	H(4B)-C(4)-H(4C)	109.5
O(1)-Na(1)-N(4)	122.60(12)	F(2)-C(5)-F(1)	105.9(4)
N(2)-Na(1)-N(4)	78.58(10)	F(2)-C(5)-C(6)	107.0(3)
O(1)-Na(1)-N(6)	140.02(13)	F(1)-C(5)-C(6)	106.7(3)
N(2)-Na(1)-N(6)	82.74(11)	F(2)-C(5)-C(3)	113(3)
N(4)-Na(1)-N(6)	77.02(12)	F(1)-C(5)-C(3)	109(3)
O(1)-Na(1)-F(1)	74.4(8)	C(6)-C(5)-C(3)	114.9(7)
N(2)-Na(1)-F(1)	58.3(7)	C(5)-F(1)-Na(1)	119(4)
N(4)-Na(1)-F(1)	118.0(4)	F(4)-C(6)-F(3)	108.4(3)
N(6)-Na(1)-F(1)	130.7(11)	F(4)-C(6)-F(5)	108.4(3)
O(1)-Na(1)-F(1')	73.8(8)	F(3)-C(6)-F(5)	108.2(4)
N(2)-Na(1)-F(1')	59.0(7)	F(4)-C(6)-C(5)	111.2(3)
N(4)-Na(1)-F(1')	119.0(4)	F(3)-C(6)-C(5)	110.4(3)
F(5)-C(6)-C(5)	110.2(3)	F(8')-C(12')-F(9')	108.4(3)
F(3')-C(6')-F(4')	108.3(3)	F(10')-C(12')-F(9')	108.5(4)
F(3')-C(6')-F(5')	108.3(4)	C(13)-N(5)-N(6)	111.1(3)
F(4')-C(6')-F(5')	108.3(3)	C(13)-N(5)-B(1)	127.3(3)
C(7)-N(3)-N(4)	110.3(3)	N(6)-N(5)-B(1)	121.6(3)
C(7)-N(3)-B(1)	128.5(3)	C(15)-N(6)-N(5)	104.0(3)
N(4)-N(3)-B(1)	121.2(3)	C(15)-N(6)-Na(1)	130.3(3)
C(9)-N(4)-N(3)	105.2(3)	N(5)-N(6)-Na(1)	112.3(2)
C(9)-N(4)-Na(1)	134.5(2)	N(5)-C(13)-C(14)	107.6(4)
N(3)-N(4)-Na(1)	116.3(2)	N(5)-C(13)-C(16)	123.0(4)
N(3)-C(7)-C(8)	107.9(3)	C(14)-C(13)-C(16)	129.4(4)
N(3)-C(7)-C(10)	122.8(3)	C(13)-C(14)-C(15)	104.8(4)
C(8)-C(7)-C(10)	129.3(3)	C(13)-C(14)-H(14A)	127.6
C(7)-C(8)-C(9)	104.3(3)	C(15)-C(14)-H(14A)	127.6
C(7)-C(8)-H(8A)	127.9	N(6)-C(15)-C(14)	112.5(4)
C(9)-C(8)-H(8A)	127.9	N(6)-C(15)-C(17)	120.6(4)
N(4)-C(9)-C(8)	112.3(3)	C(14)-C(15)-C(17)	126.7(4)
N(4)-C(9)-C(11)	119.1(3)	C(13)-C(16)-H(16A)	109.5
C(8)-C(9)-C(11)	128.6(3)	C(13)-C(16)-H(16B)	109.5
C(7)-C(10)-H(10A)	109.5	H(16A)-C(16)-H(16B)	109.5
C(7)-C(10)-H(10B)	109.5	C(13)-C(16)-H(16C)	109.5
H(10A)-C(10)-H(10B)	109.5	H(16A)-C(16)-H(16C)	109.5
C(7)-C(10)-H(10C)	109.5	H(16B)-C(16)-H(16C)	109.5
H(10A)-C(10)-H(10C)	109.5	F(11)-C(17)-F(12)	105.6(4)
H(10B)-C(10)-H(10C)	109.5	F(11)-C(17)-C(18)	106.0(4)
F(6)-C(11)-F(7)	105.6(4)	F(12)-C(17)-C(18)	105.9(4)
F(6)-C(11)-C(12)	107.8(3)	F(11)-C(17)-C(15)	115.4(8)
F(7)-C(11)-C(12)	106.5(3)	F(12)-C(17)-C(15)	106.6(8)
F(6)-C(11)-C(9)	114.7(12)	C(18)-C(17)-C(15)	116.4(4)
F(7)-C(11)-C(9)	108.0(12)	F(14)-C(18)-F(13)	109.6(4)
C(12)-C(11)-C(9)	113.6(3)	F(14)-C(18)-F(15)	109.3(4)
F(8)-C(12)-F(10)	108.7(4)	F(13)-C(18)-F(15)	108.7(4)
F(8)-C(12)-F(9)	108.1(3)	F(14)-C(18)-C(17)	109.5(3)
F(10)-C(12)-F(9)	107.5(3)	F(13)-C(18)-C(17)	109.2(3)
F(8)-C(12)-C(11)	111.5(3)	F(15)-C(18)-C(17)	110.5(3)
F(10)-C(12)-C(11)	110.1(3)	F(14')-C(18')-F(13')	108.9(4)
F(9)-C(12)-C(11)	110.8(3)	F(14')-C(18')-F(15')	109.0(4)
F(8')-C(12')-F(10')	108.5(3)	F(13')-C(18')-F(15')	108.8(4)

Table E.4 Anisotropic Displacement Parameters ($Å^2 \times 10^3$) for $Tp^{C_2F_5,CH_3}Na(H_2O)^*$

	U^{11}	U^{22}	U^{33}	U^{23}	U^{13}	U^{12}
Na1	57(1)	39(1)	52(1)	-10(1)	22(1)	0(1)
B1	60(3)	37(2)	38(2)	-1(2)	24(2)	8(2)
O1	77(2)	62(2)	64(2)	-21(1)	20(2)	8(2)
N1	48(2)	33(1)	37(1)	-1(1)	14(1)	5(1)
N2	47(2)	36(2)	37(2)	-2(1)	16(1)	5(1)
C1	47(2)	34(2)	44(2)	3(1)	10(2)	3(1)
C2	55(2)	43(2)	49(2)	10(2)	18(2)	-1(2)
C3	39(2)	45(2)	37(2)	5(1)	13(1)	9(1)
C4	85(3)	42(2)	60(2)	-6(2)	13(2)	-8(2)
C5	56(2)	62(2)	43(2)	5(2)	22(2)	10(2)
F1	105(3)	65(2)	52(5)	-13(1)	23(2)	13(1)
F2	80(2)	139(3)	55(6)	-9(6)	39(3)	-11(4)
C6	90(4)	114(5)	44(3)	-5(3)	6(3)	41(4)
F3	230(11)	107(3)	48(7)	19(3)	9(6)	84(6)
F4	118(3)	148(7)	37(1)	-11(2)	5(2)	44(4)
F5	58(2)	193(15)	80(2)	-52(9)	3(2)	30(3)
C5'	56(2)	62(2)	43(2)	5(2)	22(2)	10(2)
F1'	105(3)	65(2)	52(5)	-13(1)	23(2)	13(1)
F2'	80(2)	139(3)	55(6)	-9(6)	39(3)	-11(4)
C6'	90(4)	114(5)	44(3)	-5(3)	6(3)	41(4)
F3'	230(11)	107(3)	48(7)	19(3)	9(6)	84(6)
F4'	118(3)	148(7)	37(1)	-11(2)	5(2)	44(4)
F5'	58(2)	193(15)	80(2)	-52(9)	3(2)	30(3)
N3	53(2)	33(1)	34(1)	-1(1)	20(1)	3(1)
N4	51(2)	36(1)	36(1)	-1(1)	20(1)	7(1)
C7	60(2)	35(2)	34(2)	1(1)	21(2)	-3(2)
C8	51(2)	42(2)	35(2)	4(1)	12(2)	1(2)
C9	44(2)	36(2)	37(2)	6(1)	17(1)	5(1)
C10	85(3)	54(2)	42(2)	-7(2)	24(2)	5(2)
C11	52(2)	54(2)	42(2)	2(2)	18(2)	10(2)
F6	58(2)	77(7)	175(7)	-40(6)	40(2)	15(2)
F7	139(5)	53(5)	51(2)	5(1)	42(2)	39(5)
C12	94(7)	46(3)	51(5)	8(2)	29(5)	26(3)
F8	126(6)	55(2)	82(3)	0(2)	36(4)	41(2)
F9	193(11)	49(4)	43(3)	21(3)	32(5)	41(5)
F10	104(5)	56(4)	86(4)	-13(3)	30(4)	-16(4)
C11'	52(2)	54(2)	42(2)	2(2)	18(2)	10(2)
F6'	58(2)	77(7)	175(7)	-40(6)	40(2)	15(2)
F7'	139(5)	53(5)	51(2)	5(1)	42(2)	39(5)
C12'	94(7)	46(3)	51(5)	8(2)	29(5)	26(3)
F8'	126(6)	55(2)	82(3)	0(2)	36(4)	41(2)
F9'	213(12)	92(6)	71(5)	42(5)	67(6)	84(7)
F10'	126(8)	54(4)	320(20)	-17(9)	148(11)	-24(6)
N5	53(2)	46(2)	48(2)	4(1)	27(1)	9(1)
N6	55(2)	49(2)	84(3)	-7(2)	35(2)	0(2)
C13	58(2)	70(3)	47(2)	14(2)	27(2)	24(2)
C14	51(2)	88(3)	75(3)	14(2)	32(2)	11(2)
C15	57(3)	69(3)	81(3)	5(2)	32(2)	-6(2)
C16	75(3)	94(4)	82(3)	-5(3)	34(3)	38(3)
C17	68(3)	110(4)	88(4)	3(3)	26(3)	-7(3)
F11	167(9)	80(2)	111(5)	-1(4)	-8(5)	16(4)
F12	144(4)	127(9)	263(9)	-33(8)	148(6)	-45(5)

C18	121(10)	176(12)	123(8)	-47(8)	60(7)	-80(9)
F13	86(7)	117(8)	410(20)	-142(11)	109(10)	-47(6)
F14	199(13)	128(8)	47(4)	14(4)	25(6)	-50(8)
F15	132(6)	160(6)	149(5)	-74(5)	31(5)	-66(5)
C17'	68(3)	110(4)	88(4)	3(3)	26(3)	-7(3)
F11'	167(9)	80(2)	111(5)	-1(4)	-8(5)	16(4)
F12'	144(4)	127(9)	263(9)	-33(8)	148(6)	-45(5)
C18'	121(10)	176(12)	123(8)	-47(8)	60(7)	-80(9)
F13'	104(8)	174(11)	124(7)	-89(7)	71(6)	-55(7)
F14'	171(12)	165(11)	176(12)	-35(8)	-128(10)	32(8)
F15'	132(6)	160(6)	149(5)	-74(5)	31(5)	-66(5)

* The anisotropic displacement factor exponent takes the form: $-2\pi^2 [h^2 a^{*2} U^{11} + ... + 2 h k a^* b^* U^{12}]$.

Table E.5 Hydrogen Coordinates ($\times 10^4$) and Isotropic Displacement Parameters ($Å^2 \times 10^3$) for $Tp^{C_2F_5,CH_3}Na(H_2O)$

	x	y	z	U(eq)
H1A	2200	274	3103	64
H1B	1234	2622	7004	101
H1C	2099	2986	6710	101
H1D	2424	2585	7683	101
H2A	1494	-571	6774	58
H4A	1039	-1069	4529	96
H4B	2063	-826	3934	96
H4C	725	-531	3514	96
H8A	-1217	1653	1381	51
H10A	612	239	1380	88
H10B	1212	813	851	88
H10C	-224	701	393	88
H14A	6110	1308	4042	81
H16A	5466	128	3311	122
H16B	4078	128	2509	122
H16C	4425	-126	3872	122

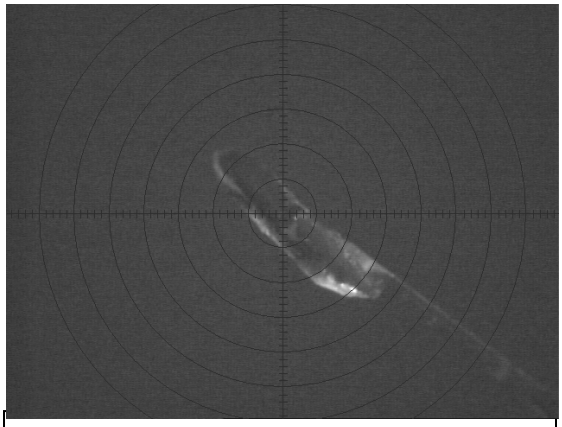

T = 191 K.
The first image, just prior to the start of a phase transition. The temperature gradient was 2°/min, starting at 293 K.

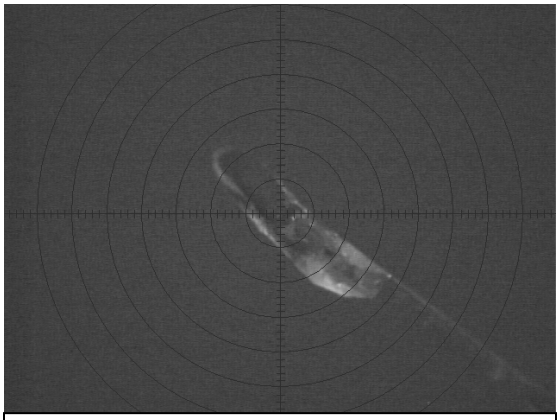

T = 188 K.
Lowest edge is beginning to transform from clear to opaque.

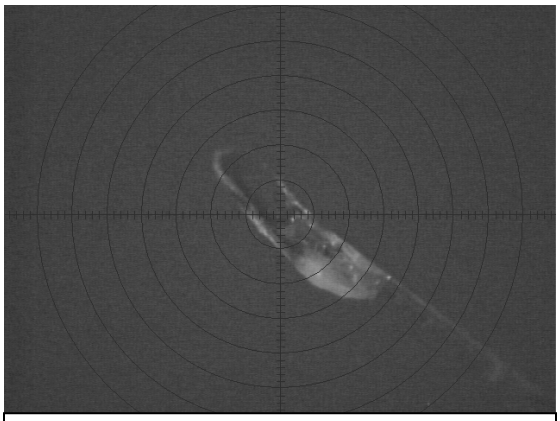

T = 178 K.
The opaque region is spreading

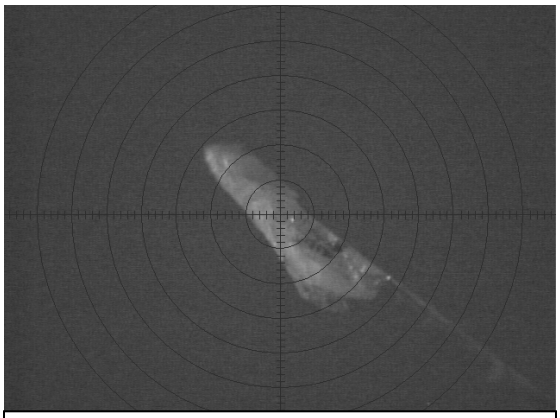

T = 177 K.
The crystal completed the phase transition catastrophically within 1 min.

Figure E.2 Temperature-variable phase transformations in $Tp^{C_2F_5,CH_3}Na(H_2O)$.

APPENDIX F

CRYSTAL STRUCTURE OF HYDROTRIS(3-TRIFLUOROMETHYL-5-METHYLPYRAZOL-1-YL)-BORATO-SILVER(I)-(η^2)-TOLUENE

Tables F.1 to F.5 list the atomic coordinates and crystallographic parameters for $Tp^{CF_3,CH_3}Ag(Tol)\bullet Tol$ **[3-7]** (Figure F.1).

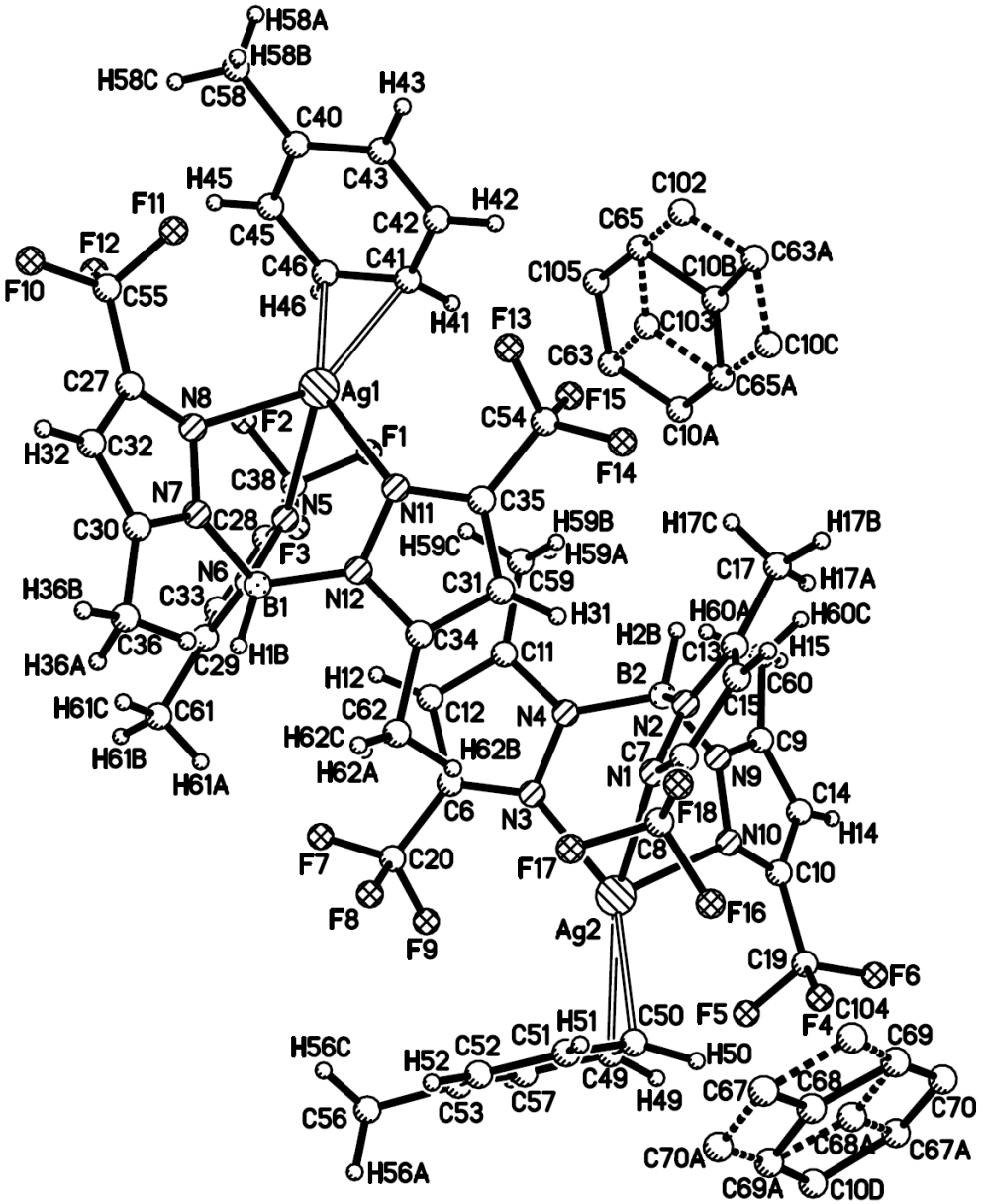

Figure F.1 Crystal structure of $Tp^{CF_3,CH_3}Ag(Tol)\bullet Tol$.

Table F.1 Crystal Data and Structure Refinement for $Tp^{CF_3,CH_3}Ag(Tol)•Tol$

Empirical formula	$C_{34}\ H_{28}\ Ag_{1.33}\ B_{1.33}\ F_{12}\ N_8$	
Formula weight	934.88	
Temperature	100(2) K	
Wavelength	1.54178 Å	
Crystal system	triclinic	
Space group	P-1	
Unit cell dimensions	a = 11.5180(4) Å	α = 96.271(2)°
	b = 11.5270(3) Å	β = 92.511(2)°
	c = 25.0481(9) Å	γ = 119.743(1)°
Volume	2851.63(16) $Å^3$	
Z	3	
Density (calculated)	1.633 g/cm^3	
Absorption coefficient	6.462 mm^{-1}	
F(000)	1396	
Crystal size	0.35 × 0.14 × 0.11 mm^3	
Theta range for data collection	1.79 to 67.90°	
Index ranges	$-13 \le h \le 13, -13 \le k \le 13, -30 \le l \le 29$	
Reflections collected	24097	
Independent reflections	9109 [*R*(int) = 0.0269]	
Completeness to theta = 67.90°	88.0%	
Refinement method	Full-matrix least-squares on F^2	
Data / restraints / parameters	9109 / 0 / 725	
Goodness-of-fit on F^2	1.142	
Final *R* indices [*I*>2sigma(*I*)]	*R*1 = 0.0551, *wR*2 = 0.1345	
R indices (all data)	*R*1 = 0.0582, *wR*2 = 0.1363	
Largest diff. peak and hole	1.682 and −1.455 e.$Å^{-3}$	

Table F.2 Atomic Coordinates (× 10^4) and Equivalent Isotropic Displacement Parameters ($Å^2$ × 10^3) for $Tp^{CF_3,CH_3}Ag(Tol)•Tol^*$

	x	y	z	U(eq)
Ag(1)	9822(1)	6668(1)	3713(1)	24(1)
Ag(2)	2495(1)	2442(1)	1289(1)	24(1)
B(1)	9514(6)	6160(6)	2389(2)	22(1)
F(1)	8023(4)	3100(4)	3910(1)	35(1)
F(3)	8265(4)	1487(4)	3516(2)	46(1)
F(2)	9965(4)	3283(4)	3943(1)	39(1)
F(4)	-1222(4)	548(3)	1101(1)	34(1)
F(6)	-2531(4)	-1128(4)	1496(2)	44(1)
F(5)	-998(4)	-1199(4)	1066(1)	36(1)
F(9)	4205(4)	346(4)	1077(2)	38(1)
F(8)	5646(5)	2354(4)	976(2)	51(1)
F(7)	6268(4)	1216(5)	1406(2)	55(1)
B(2)	2880(6)	2898(6)	2617(2)	21(1)
N(1)	3181(5)	4416(5)	1901(2)	22(1)
N(4)	3997(4)	2652(4)	2402(2)	19(1)
N(2)	2981(4)	4176(5)	2419(2)	20(1)

N(3)	3913(4)	2119(5)	1879(2)	22(1)
F(17)	4453(4)	6100(4)	1124(2)	39(1)
F(16)	2403(4)	5624(4)	1019(1)	41(1)
F(18)	3899(4)	7525(4)	1477(2)	46(1)
N(9)	1473(4)	1650(4)	2431(2)	19(1)
N(10)	871(4)	1360(4)	1911(2)	21(1)
C(6)	5008(6)	2008(5)	1853(2)	23(1)
C(7)	3276(5)	5611(6)	1888(2)	23(1)
C(8)	3531(6)	6219(6)	1384(3)	31(1)
C(9)	637(6)	716(6)	2733(2)	22(1)
C(10)	-322(5)	251(5)	1903(2)	22(1)
C(11)	5142(6)	2882(6)	2691(2)	24(1)
C(12)	5811(6)	2480(6)	2345(2)	25(1)
C(13)	2949(5)	5211(5)	2720(2)	21(1)
C(14)	-515(6)	-197(6)	2403(2)	24(1)
C(15)	3129(6)	6153(6)	2387(2)	24(1)
C(17)	2749(6)	5245(6)	3305(2)	30(1)
C(19)	-1260(6)	-367(6)	1395(2)	27(1)
C(20)	5270(6)	1479(6)	1331(3)	29(1)
N(6)	9378(4)	4871(4)	2578(2)	20(1)
N(7)	10902(5)	7415(5)	2602(2)	21(1)
N(5)	9160(4)	4629(5)	3093(2)	22(1)
N(8)	11443(5)	7678(5)	3128(2)	22(1)
N(12)	8364(4)	6403(5)	2577(2)	21(1)
N(11)	8411(5)	6929(5)	3092(2)	22(1)
C(27)	12649(6)	8781(6)	3149(2)	24(1)
C(28)	9060(5)	3432(5)	3108(2)	22(1)
C(29)	9431(5)	3839(6)	2277(2)	22(1)
C(30)	11760(6)	8360(6)	2311(2)	23(1)
C(31)	6524(6)	6545(6)	2604(2)	24(1)
C(32)	12900(6)	9250(6)	2656(2)	24(1)
C(33)	9218(5)	2900(6)	2611(2)	23(1)
C(34)	7232(5)	6147(5)	2272(2)	20(1)
C(35)	7293(6)	7008(6)	3105(2)	23(1)
C(36)	11442(6)	8334(6)	1723(2)	28(1)
C(38)	8831(6)	2827(6)	3616(2)	27(1)
C(40)	11750(7)	8541(7)	5051(2)	33(1)
C(41)	9163(7)	6469(7)	4621(2)	40(2)
C(42)	9371(7)	7711(8)	4853(3)	40(2)
C(43)	10648(7)	8728(7)	5069(2)	35(1)
C(45)	11533(7)	7300(7)	4821(2)	38(2)
C(46)	10246(8)	6247(7)	4605(3)	43(2)
C(51)	2809(7)	3417(7)	150(3)	38(2)
C(53)	3485(7)	1759(7)	-51(2)	35(1)
C(52)	2394(7)	849(7)	182(2)	40(2)
C(50)	1697(7)	2505(8)	382(3)	40(2)
C(49)	1494(7)	1208(7)	397(3)	41(2)
F(12)	13667(4)	8484(4)	3922(2)	39(1)
F(10)	14780(4)	10329(4)	3594(2)	53(1)
F(11)	13104(4)	9983(4)	4028(2)	46(1)
F(15)	6566(4)	6693(4)	3969(2)	43(1)
F(13)	8088(4)	8684(4)	3871(2)	40(1)
F(14)	6053(4)	7882(4)	3518(2)	45(1)
C(54)	7009(6)	7566(6)	3615(2)	29(1)
C(55)	13544(6)	9378(6)	3673(2)	29(1)
C(56)	4415(8)	1349(9)	-299(3)	51(2)

C(57)	3675(7)	3031(7)	-65(2)	36(1)
C(58)	13128(7)	9650(8)	5297(3)	45(2)
C(59)	5527(6)	3466(6)	3274(2)	28(1)
C(60)	997(6)	779(6)	3320(2)	27(1)
C(61)	9634(6)	3801(6)	1696(2)	26(1)
C(62)	6915(6)	5575(6)	1685(2)	26(1)
C(65)	6004	5544	5319	50
C(69)	-352	5532	323	50
C(63)	5192	3275	4850	50
C(67)	1587	6845	-121	50
C(68)	480	5568	-50	50
C(70)	-1436	4403	386	50
C(102)	5948	6690	5404	113
C(103)	5225	4454	4963	122
C(104)	764	6846	284	138
C(105)	6106(16)	4400(20)	5231(7)	62(5)

* U(eq) is defined as one third of the trace of the orthogonalized U^{ij} tensor.

Table F.3 Bond Lengths (Å) and Angles (°) for $Tp^{CF_3,CH_3}Ag(Tol)\bullet Tol$

Ag(1)-N(8)	2.333(5)	Ag(2)-N(1)	2.346(5)
Ag(1)-N(11)	2.348(4)	Ag(2)-N(3)	2.346(4)
Ag(1)-N(5)	2.415(5)	Ag(2)-C(49)	2.407(6)
Ag(1)-C(46)	2.418(6)	Ag(2)-N(10)	2.418(5)
Ag(1)-C(41)	2.428(6)	Ag(2)-C(50)	2.434(6)
B(1)-N(6)	1.544(7)	N(6)-N(5)	1.358(6)
B(1)-N(7)	1.548(8)	N(6)-C(29)	1.366(7)
B(1)-N(12)	1.565(7)	N(7)-C(30)	1.365(7)
F(1)-C(38)	1.344(7)	N(7)-N(8)	1.368(6)
F(3)-C(38)	1.333(7)	N(5)-C(28)	1.331(7)
F(2)-C(38)	1.336(7)	N(8)-C(27)	1.332(7)
F(4)-C(19)	1.336(7)	N(12)-N(11)	1.351(6)
F(6)-C(19)	1.335(7)	N(12)-C(34)	1.362(7)
F(5)-C(19)	1.351(7)	N(11)-C(35)	1.337(7)
F(9)-C(20)	1.332(7)	C(27)-C(32)	1.388(8)
F(8)-C(20)	1.338(7)	C(27)-C(55)	1.495(8)
F(7)-C(20)	1.337(7)	C(28)-C(33)	1.386(8)
B(2)-N(9)	1.545(8)	C(28)-C(38)	1.490(8)
B(2)-N(4)	1.554(7)	C(29)-C(33)	1.372(8)
B(2)-N(2)	1.557(7)	C(29)-C(61)	1.485(8)
N(1)-C(7)	1.331(7)	C(30)-C(32)	1.376(8)
N(1)-N(2)	1.363(6)	C(30)-C(36)	1.494(8)
N(4)-N(3)	1.362(6)	C(31)-C(34)	1.382(8)
N(4)-C(11)	1.365(7)	C(31)-C(35)	1.390(8)
N(2)-C(13)	1.357(7)	C(34)-C(62)	1.496(8)
N(3)-C(6)	1.334(7)	C(35)-C(54)	1.489(8)
F(17)-C(8)	1.325(7)	C(40)-C(45)	1.376(9)
F(16)-C(8)	1.366(7)	C(40)-C(43)	1.391(9)
F(18)-C(8)	1.334(7)	C(40)-C(58)	1.504(9)
N(9)-C(9)	1.367(7)	C(41)-C(42)	1.383(10)
N(9)-N(10)	1.374(6)	C(41)-C(46)	1.394(11)
N(10)-C(10)	1.331(7)	C(42)-C(43)	1.383(10)
C(6)-C(12)	1.387(8)	C(45)-C(46)	1.402(10)
C(6)-C(20)	1.488(8)	C(51)-C(57)	1.385(9)

C(7)-C(15)	1.390(8)	C(51)-C(50)	1.396(10)
C(7)-C(8)	1.483(8)	C(53)-C(57)	1.376(10)
C(9)-C(14)	1.371(8)	C(53)-C(52)	1.383(10)
C(9)-C(60)	1.494(8)	C(53)-C(56)	1.501(9)
C(10)-C(14)	1.390(8)	C(52)-C(49)	1.401(10)
C(10)-C(19)	1.487(8)	C(50)-C(49)	1.400(10)
C(11)-C(12)	1.373(8)	F(12)-C(55)	1.323(7)
C(11)-C(59)	1.489(8)	F(10)-C(55)	1.337(7)
C(13)-C(15)	1.382(8)	F(11)-C(55)	1.338(7)
C(13)-C(17)	1.492(8)	F(15)-C(54)	1.335(7)
F(13)-C(54)	1.334(7)	N(6)-B(1)-N(7)	111.4(4)
F(14)-C(54)	1.341(7)	N(6)-B(1)-N(12)	110.5(5)
C(65)-C(103)	1.3210	N(7)-B(1)-N(12)	109.9(4)
C(65)-C(102)	1.3484	N(9)-B(2)-N(4)	110.7(4)
C(65)-C(105)	1.38(2)	N(9)-B(2)-N(2)	110.6(4)
C(65)-C(103)#1	1.5548	N(4)-B(2)-N(2)	109.9(4)
C(69)-C(68)#2	1.3089	C(7)-N(1)-N(2)	105.3(4)
C(69)-C(70)	1.3143	C(7)-N(1)-Ag(2)	136.9(4)
C(69)-C(68)	1.3566	N(2)-N(1)-Ag(2)	112.9(3)
C(69)-C(104)	1.4382	N(3)-N(4)-C(11)	110.8(4)
C(63)-C(103)	1.3393	N(3)-N(4)-B(2)	122.2(4)
C(63)-C(105)	1.41(2)	C(11)-N(4)-B(2)	127.0(5)
C(63)-C(102)#1	1.4541	C(13)-N(2)-N(1)	110.6(4)
C(67)-C(104)	1.4183	C(13)-N(2)-B(2)	127.2(5)
C(67)-C(68)	1.4279	N(1)-N(2)-B(2)	122.1(4)
C(67)-C(70)#2	1.4399	C(6)-N(3)-N(4)	105.0(4)
C(68)-C(68)#2	1.2882	C(6)-N(3)-Ag(2)	137.0(4)
C(68)-C(69)#2	1.3089	N(4)-N(3)-Ag(2)	112.9(3)
C(68)-C(70)#2	1.4045	C(9)-N(9)-N(10)	110.1(4)
C(70)-C(68)#2	1.4045	C(9)-N(9)-B(2)	128.1(5)
C(70)-C(67)#2	1.4399	N(10)-N(9)-B(2)	121.8(4)
C(102)-C(63)#1	1.4541	C(10)-N(10)-N(9)	105.0(4)
C(102)-C(103)#1	1.5054	C(10)-N(10)-Ag(2)	138.4(4)
C(103)-C(102)#1	1.5054	N(9)-N(10)-Ag(2)	111.9(3)
C(103)-C(65)#1	1.5548	N(3)-C(6)-C(12)	111.9(5)
C(103)-C(103)#1	1.5774	N(3)-C(6)-C(20)	120.1(5)
		C(12)-C(6)-C(20)	127.9(5)
N(8)-Ag(1)-N(11)	84.55(16)	N(1)-C(7)-C(15)	112.0(5)
N(8)-Ag(1)-N(5)	83.59(15)	N(1)-C(7)-C(8)	120.4(5)
N(11)-Ag(1)-N(5)	83.38(15)	C(15)-C(7)-C(8)	127.6(5)
N(8)-Ag(1)-C(46)	125.5(2)	F(17)-C(8)-F(18)	108.5(5)
N(11)-Ag(1)-C(46)	148.5(2)	F(17)-C(8)-F(16)	105.2(5)
N(5)-Ag(1)-C(46)	107.08(19)	F(18)-C(8)-F(16)	105.4(5)
N(8)-Ag(1)-C(41)	150.4(2)	F(17)-C(8)-C(7)	113.6(5)
N(11)-Ag(1)-C(41)	115.4(2)	F(18)-C(8)-C(7)	111.6(5)
N(5)-Ag(1)-C(41)	118.7(2)	F(16)-C(8)-C(7)	112.0(5)
C(46)-Ag(1)-C(41)	33.4(3)	N(9)-C(9)-C(14)	107.8(5)
N(1)-Ag(2)-N(3)	84.28(15)	N(9)-C(9)-C(60)	122.7(5)
N(1)-Ag(2)-C(49)	147.6(2)	C(14)-C(9)-C(60)	129.5(5)
N(3)-Ag(2)-C(49)	126.3(2)	N(10)-C(10)-C(14)	112.2(5)
N(1)-Ag(2)-N(10)	84.26(15)	N(10)-C(10)-C(19)	120.1(5)
N(3)-Ag(2)-N(10)	83.37(15)	C(14)-C(10)-C(19)	127.7(5)
C(49)-Ag(2)-N(10)	107.5(2)	N(4)-C(11)-C(12)	107.2(5)
N(1)-Ag(2)-C(50)	114.2(2)	N(4)-C(11)-C(59)	123.8(5)
N(3)-Ag(2)-C(50)	151.04(19)	C(12)-C(11)-C(59)	129.0(5)
C(49)-Ag(2)-C(50)	33.6(2)	C(11)-C(12)-C(6)	105.1(5)

N(10)-Ag(2)-C(50)	119.0(2)	N(2)-C(13)-C(15)	107.6(5)
N(2)-C(13)-C(17)	123.3(5)	C(30)-C(32)-C(27)	104.7(5)
C(15)-C(13)-C(17)	129.1(5)	C(29)-C(33)-C(28)	105.5(5)
C(9)-C(14)-C(10)	104.9(5)	N(12)-C(34)-C(31)	107.2(5)
C(13)-C(15)-C(7)	104.5(5)	N(12)-C(34)-C(62)	123.2(5)
F(6)-C(19)-F(4)	107.5(5)	C(31)-C(34)-C(62)	129.6(5)
F(6)-C(19)-F(5)	105.5(5)	N(11)-C(35)-C(31)	111.9(5)
F(4)-C(19)-F(5)	106.0(5)	N(11)-C(35)-C(54)	120.3(5)
F(6)-C(19)-C(10)	111.5(5)	C(31)-C(35)-C(54)	127.7(5)
F(4)-C(19)-C(10)	113.0(5)	F(3)-C(38)-F(2)	106.6(5)
F(5)-C(19)-C(10)	112.8(4)	F(3)-C(38)-F(1)	107.3(5)
F(9)-C(20)-F(7)	107.2(5)	F(2)-C(38)-F(1)	105.8(5)
F(9)-C(20)-F(8)	105.7(5)	F(3)-C(38)-C(28)	111.6(5)
F(7)-C(20)-F(8)	106.1(5)	F(2)-C(38)-C(28)	113.0(5)
F(9)-C(20)-C(6)	113.5(5)	F(1)-C(38)-C(28)	112.2(4)
F(7)-C(20)-C(6)	110.9(5)	C(45)-C(40)-C(43)	118.1(6)
F(8)-C(20)-C(6)	113.0(5)	C(45)-C(40)-C(58)	121.2(6)
N(5)-N(6)-C(29)	110.9(4)	C(43)-C(40)-C(58)	120.7(6)
N(5)-N(6)-B(1)	121.5(4)	C(42)-C(41)-C(46)	119.7(6)
C(29)-N(6)-B(1)	127.6(5)	C(42)-C(41)-Ag(1)	107.9(5)
C(30)-N(7)-N(8)	111.0(5)	C(46)-C(41)-Ag(1)	72.9(4)
C(30)-N(7)-B(1)	127.1(5)	C(43)-C(42)-C(41)	120.1(7)
N(8)-N(7)-B(1)	121.8(4)	C(42)-C(43)-C(40)	121.4(6)
C(28)-N(5)-N(6)	105.2(4)	C(40)-C(45)-C(46)	121.7(6)
C(28)-N(5)-Ag(1)	137.9(4)	C(41)-C(46)-C(45)	119.0(6)
N(6)-N(5)-Ag(1)	112.3(3)	C(41)-C(46)-Ag(1)	73.7(4)
C(27)-N(8)-N(7)	104.4(4)	C(45)-C(46)-Ag(1)	106.8(4)
C(27)-N(8)-Ag(1)	137.6(4)	C(57)-C(51)-C(50)	120.3(6)
N(7)-N(8)-Ag(1)	112.9(3)	C(57)-C(53)-C(52)	118.6(6)
N(11)-N(12)-C(34)	111.2(4)	C(57)-C(53)-C(56)	120.9(7)
N(11)-N(12)-B(1)	121.4(4)	C(52)-C(53)-C(56)	120.5(7)
C(34)-N(12)-B(1)	127.4(4)	C(53)-C(52)-C(49)	120.9(7)
C(35)-N(11)-N(12)	105.1(4)	C(51)-C(50)-C(49)	118.4(6)
C(35)-N(11)-Ag(1)	136.2(4)	C(51)-C(50)-Ag(2)	107.5(4)
N(12)-N(11)-Ag(1)	113.7(3)	C(49)-C(50)-Ag(2)	72.1(4)
N(8)-C(27)-C(32)	112.6(5)	C(50)-C(49)-C(52)	120.1(7)
N(8)-C(27)-C(55)	119.6(5)	C(50)-C(49)-Ag(2)	74.3(4)
C(32)-C(27)-C(55)	127.7(5)	C(52)-C(49)-Ag(2)	106.9(5)
N(5)-C(28)-C(33)	111.6(5)	F(13)-C(54)-F(15)	106.4(5)
N(5)-C(28)-C(38)	121.0(5)	F(13)-C(54)-F(14)	106.9(5)
C(33)-C(28)-C(38)	127.4(5)	F(15)-C(54)-F(14)	106.3(5)
N(6)-C(29)-C(33)	106.8(5)	F(13)-C(54)-C(35)	112.8(5)
N(6)-C(29)-C(61)	123.5(5)	F(15)-C(54)-C(35)	112.8(5)
C(33)-C(29)-C(61)	129.7(5)	F(14)-C(54)-C(35)	111.1(5)
N(7)-C(30)-C(32)	107.2(5)	F(12)-C(55)-F(10)	107.5(5)
N(7)-C(30)-C(36)	123.2(5)	F(12)-C(55)-F(11)	105.8(5)
C(32)-C(30)-C(36)	129.6(5)	F(10)-C(55)-F(11)	106.2(5)
C(34)-C(31)-C(35)	104.5(5)	F(12)-C(55)-C(27)	113.8(5)
F(10)-C(55)-C(27)	110.6(5)	C(69)#2-C(68)-C(70)#2	57.8
F(11)-C(55)-C(27)	112.4(5)	C(69)-C(68)-C(70)#2	173.2
C(53)-C(57)-C(51)	121.7(7)	C(68)#2-C(68)-C(67)	175.8
C(103)-C(65)-C(102)	127.3	C(69)#2-C(68)-C(67)	118.8
C(103)-C(65)-C(105)	53.9(7)	C(69)-C(68)-C(67)	118.8
C(102)-C(65)-C(105)	178.1(7)	C(70)#2-C(68)-C(67)	61.1
C(103)-C(65)-C(103)#1	66.0	C(69)-C(70)-C(68)#2	57.4
C(102)-C(65)-C(103)#1	62.0	C(69)-C(70)-C(67)#2	117.6

C(105)-C(65)-C(103)#1	119.4(7)	C(68)#2-C(70)-C(67)#2	60.2
C(68)#2-C(69)-C(70)	64.7	C(65)-C(102)-C(63)#1	119.5
C(68)#2-C(69)-C(68)	57.8	C(65)-C(102)-C(103)#1	65.8
C(70)-C(69)-C(68)	122.0	C(63)#1-C(102)-C(103)#1	53.8
C(68)#2-C(69)-C(104)	121.6	C(65)-C(103)-C(63)	131.9
C(70)-C(69)-C(104)	173.5	C(65)-C(103)-C(102)#1	164.4
C(68)-C(69)-C(104)	64.1	C(63)-C(103)-C(102)#1	61.2
C(103)-C(63)-C(105)	52.8(7)	C(65)-C(103)-C(65)#1	114.0
C(103)-C(63)-C(102)#1	65.1	C(63)-C(103)-C(65)#1	113.4
C(105)-C(63)-C(102)#1	117.4(7)	C(102)#1-C(103)-C(65)#1	52.3
C(104)-C(67)-C(68)	62.9	C(65)-C(103)-C(103)#1	64.2
C(104)-C(67)-C(70)#2	120.8	C(63)-C(103)-C(103)#1	161.9
C(68)-C(67)-C(70)#2	58.6	C(102)#1-C(103)-C(103)#1	101.7
C(68)#2-C(68)-C(69)#2	63.0	C(65)#1-C(103)-C(103)#1	49.9
C(68)#2-C(68)-C(69)	59.3	C(67)-C(104)-C(69)	114.1
C(69)#2-C(68)-C(69)	122.2	C(65)-C(105)-C(63)	121.3(10)
C(68)#2-C(68)-C(70)#2	120.3		

Symmetry transformations used to generate equivalent atoms: #1 -x+1,-y+1,-z+1; #2 -x,-y+1,-z.

Table F.4 Anisotropic Displacement Parameters ($Å^2 \times 10^3$) for $Tp^{CF_3,CH_3}Ag(Tol)•Tol^*$

	U^{11}	U^{22}	U^{33}	U^{23}	U^{13}	U^{12}
Ag(1)	25(1)	25(1)	22(1)	4(1)	2(1)	13(1)
Ag(2)	23(1)	25(1)	22(1)	2(1)	1(1)	11(1)
B(1)	22(3)	25(3)	21(3)	4(2)	2(2)	14(3)
F(1)	33(2)	46(2)	36(2)	17(2)	14(2)	25(2)
F(3)	66(3)	26(2)	44(2)	13(2)	13(2)	21(2)
F(2)	33(2)	56(3)	35(2)	18(2)	4(2)	26(2)
F(4)	37(2)	25(2)	36(2)	2(1)	-9(2)	16(2)
F(6)	18(2)	52(2)	43(2)	6(2)	-1(2)	4(2)
F(5)	40(2)	28(2)	39(2)	-6(1)	-8(2)	19(2)
F(9)	29(2)	26(2)	45(2)	-6(2)	7(2)	6(2)
F(8)	63(3)	40(2)	37(2)	8(2)	24(2)	16(2)
F(7)	44(3)	85(3)	49(2)	-15(2)	-2(2)	48(3)
B(2)	22(3)	18(3)	26(3)	6(2)	6(2)	12(3)
N(1)	20(3)	24(2)	24(2)	6(2)	3(2)	12(2)
N(4)	15(2)	15(2)	27(2)	4(2)	3(2)	6(2)
N(2)	18(2)	20(2)	23(2)	4(2)	2(2)	10(2)
N(3)	16(2)	20(2)	26(2)	3(2)	2(2)	7(2)
F(17)	40(2)	53(2)	43(2)	23(2)	20(2)	33(2)
F(16)	31(2)	58(3)	35(2)	19(2)	1(2)	21(2)
F(18)	67(3)	29(2)	49(2)	19(2)	19(2)	27(2)
N(9)	15(2)	15(2)	26(2)	3(2)	1(2)	8(2)
N(10)	17(2)	18(2)	26(2)	1(2)	1(2)	9(2)
C(6)	21(3)	14(3)	32(3)	5(2)	3(2)	6(2)
C(7)	14(3)	24(3)	32(3)	7(2)	2(2)	10(2)
C(8)	26(3)	32(3)	37(3)	10(3)	5(2)	15(3)
C(9)	20(3)	22(3)	29(3)	7(2)	7(2)	13(3)
C(10)	17(3)	17(3)	32(3)	2(2)	2(2)	10(2)
C(11)	18(3)	22(3)	28(3)	6(2)	-1(2)	8(3)
C(12)	21(3)	22(3)	32(3)	7(2)	3(2)	11(3)
C(13)	12(3)	18(3)	31(3)	0(2)	0(2)	6(2)
C(14)	20(3)	19(3)	34(3)	8(2)	8(2)	10(2)
C(15)	19(3)	18(3)	34(3)	2(2)	2(2)	9(2)
C(17)	32(4)	29(3)	28(3)	2(2)	4(2)	16(3)

C(19)	25(3)	21(3)	35(3)	3(2)	-1(2)	12(3)
C(20)	23(3)	25(3)	39(3)	1(2)	5(2)	13(3)
N(6)	16(2)	18(2)	26(2)	4(2)	2(2)	8(2)
N(7)	19(3)	23(2)	21(2)	3(2)	2(2)	11(2)
N(5)	18(2)	28(3)	22(2)	6(2)	2(2)	12(2)
N(8)	18(3)	21(2)	25(2)	1(2)	-1(2)	8(2)
N(12)	18(2)	21(2)	22(2)	3(2)	0(2)	10(2)
N(11)	19(3)	22(2)	26(2)	4(2)	3(2)	11(2)
C(27)	19(3)	24(3)	28(3)	1(2)	3(2)	11(3)
C(28)	13(3)	19(3)	30(3)	4(2)	-1(2)	5(2)
C(29)	14(3)	24(3)	28(3)	0(2)	0(2)	11(2)
C(30)	22(3)	21(3)	29(3)	8(2)	7(2)	13(3)
C(31)	16(3)	20(3)	37(3)	6(2)	1(2)	10(2)
C(32)	22(3)	18(3)	35(3)	5(2)	3(2)	12(3)
C(33)	16(3)	22(3)	33(3)	3(2)	2(2)	11(2)
C(34)	16(3)	12(2)	32(3)	6(2)	0(2)	6(2)
C(35)	19(3)	19(3)	31(3)	6(2)	5(2)	10(2)
C(36)	31(3)	27(3)	30(3)	11(2)	6(2)	15(3)
C(38)	28(3)	26(3)	34(3)	7(2)	5(2)	18(3)
C(40)	34(4)	33(3)	26(3)	7(2)	2(2)	13(3)
C(41)	32(4)	41(4)	25(3)	6(3)	0(3)	3(3)
C(42)	34(4)	51(4)	32(3)	3(3)	3(3)	20(4)
C(43)	39(4)	33(3)	29(3)	-1(2)	-1(3)	17(3)
C(45)	43(4)	54(4)	29(3)	8(3)	1(3)	32(4)
C(46)	65(5)	28(3)	31(3)	7(3)	1(3)	19(4)
C(51)	51(4)	38(4)	31(3)	5(3)	7(3)	27(4)
C(53)	40(4)	47(4)	23(3)	2(3)	0(3)	27(3)
C(52)	50(5)	37(4)	28(3)	0(3)	-3(3)	19(4)
C(50)	33(4)	63(5)	29(3)	0(3)	-4(3)	29(4)
C(49)	30(4)	39(4)	34(3)	-1(3)	-1(3)	3(3)
F(12)	43(2)	31(2)	43(2)	4(2)	-12(2)	20(2)
F(10)	29(2)	42(2)	53(2)	12(2)	-10(2)	-8(2)
F(11)	65(3)	47(2)	35(2)	-10(2)	-12(2)	38(2)
F(15)	51(3)	36(2)	36(2)	8(2)	20(2)	17(2)
F(13)	29(2)	36(2)	41(2)	-12(2)	4(2)	10(2)
F(14)	40(2)	61(3)	50(2)	-7(2)	2(2)	40(2)
C(54)	21(3)	33(3)	32(3)	0(2)	2(2)	13(3)
C(55)	20(3)	29(3)	34(3)	3(2)	1(2)	10(3)
C(56)	60(5)	81(6)	31(4)	2(3)	3(3)	52(5)
C(57)	33(4)	41(4)	30(3)	5(3)	4(3)	15(3)
C(58)	33(4)	48(4)	39(4)	6(3)	3(3)	9(4)
C(59)	24(3)	30(3)	30(3)	1(2)	-1(2)	15(3)
C(60)	23(3)	28(3)	30(3)	10(2)	5(2)	12(3)
C(61)	23(3)	23(3)	34(3)	1(2)	3(2)	13(3)
C(62)	19(3)	26(3)	32(3)	3(2)	-3(2)	12(3)
C(65)	50	50	50	8	6	25
C(69)	50	50	50	8	6	25
C(63)	50	50	50	8	6	25
C(67)	50	50	50	8	6	25
C(68)	50	50	50	8	6	25
C(70)	50	50	50	8	6	25
C(102)	111	90	94	-2	19	21
C(103)	160	64	130	25	76	42
C(104)	217	144	93	-3	-29	129
C(105)	38(9)	121(17)	50(9)	48(10)	23(7)	48(11)

* The anisotropic displacement factor exponent takes the form: $-2\pi^2 [h^2 a^{*2} U^{11} + ... + 2 h k a^* b^* U^{12}]$.

Table F.5 Hydrogen Coordinates (× 10^4) and Isotropic Displacement Parameters (Å^2 × 10^3) for $Tp^{CF_3,CH_3}Ag(Tol)$)•Tol

	x	y	z	U(eq)
H(1B)	9426	6027	1985	26
H(12)	6644	2518	2425	30
H(14)	-1278	-967	2495	29
H(15)	3148	6985	2478	29
H(17A)	1994	4373	3361	44
H(17B)	2552	5964	3419	44
H(17C)	3568	5420	3518	44
H(31)	5698	6509	2510	29
H(32)	13685	10017	2575	29
H(33)	9185	2061	2521	28
H(36A)	11418	7551	1514	43
H(36B)	12137	9165	1609	43
H(36C)	10564	8269	1662	43
H(41)	8273	5667	4657	48
H(42)	8635	7866	4864	48
H(43)	10776	9572	5233	42
H(45)	12274	7154	4808	46
H(46)	10047	5309	4635	52
H(51)	2973	4307	139	46
H(52)	2253	-32	197	48
H(50)	873	2587	344	48
H(49)	535	464	368	49
H(56A)	4271	1255	-694	76
H(56B)	4230	483	-195	76
H(56C)	5350	2040	-171	76
H(57)	4420	3661	-226	43
H(58A)	13178	9723	5692	68
H(58B)	13299	10508	5190	68
H(58C)	13806	9440	5170	68
H(59A)	4988	2772	3493	42
H(59B)	5364	4224	3344	42
H(59C)	6484	3788	3370	42
H(60A)	1938	1009	3382	40
H(60B)	413	-101	3431	40
H(60C)	876	1471	3532	40
H(61A)	8796	3563	1479	39
H(61B)	9893	3125	1589	39
H(61C)	10348	4692	1635	39
H(62A)	7515	6265	1476	39
H(62B)	5979	5290	1565	39
H(62C)	7045	4794	1628	39
H(2B)	3030(50)	3070(50)	3057(19)	4(11)

APPENDIX G

CRYSTAL STRUCTURE OF HYDROTRIS(3-PENTAFLUOROETHYL-5-METHYLPYRAZOL-1-YL)-BORATO-SILVER(I)-(η^2)-TOLUENE

Tables G.1 to G.5 list the atomic coordinates and crystallographic parameters for $Tp^{C_2F_5,CH_3}Ag(Tol)$ **[3-8]** (Figure G.1).

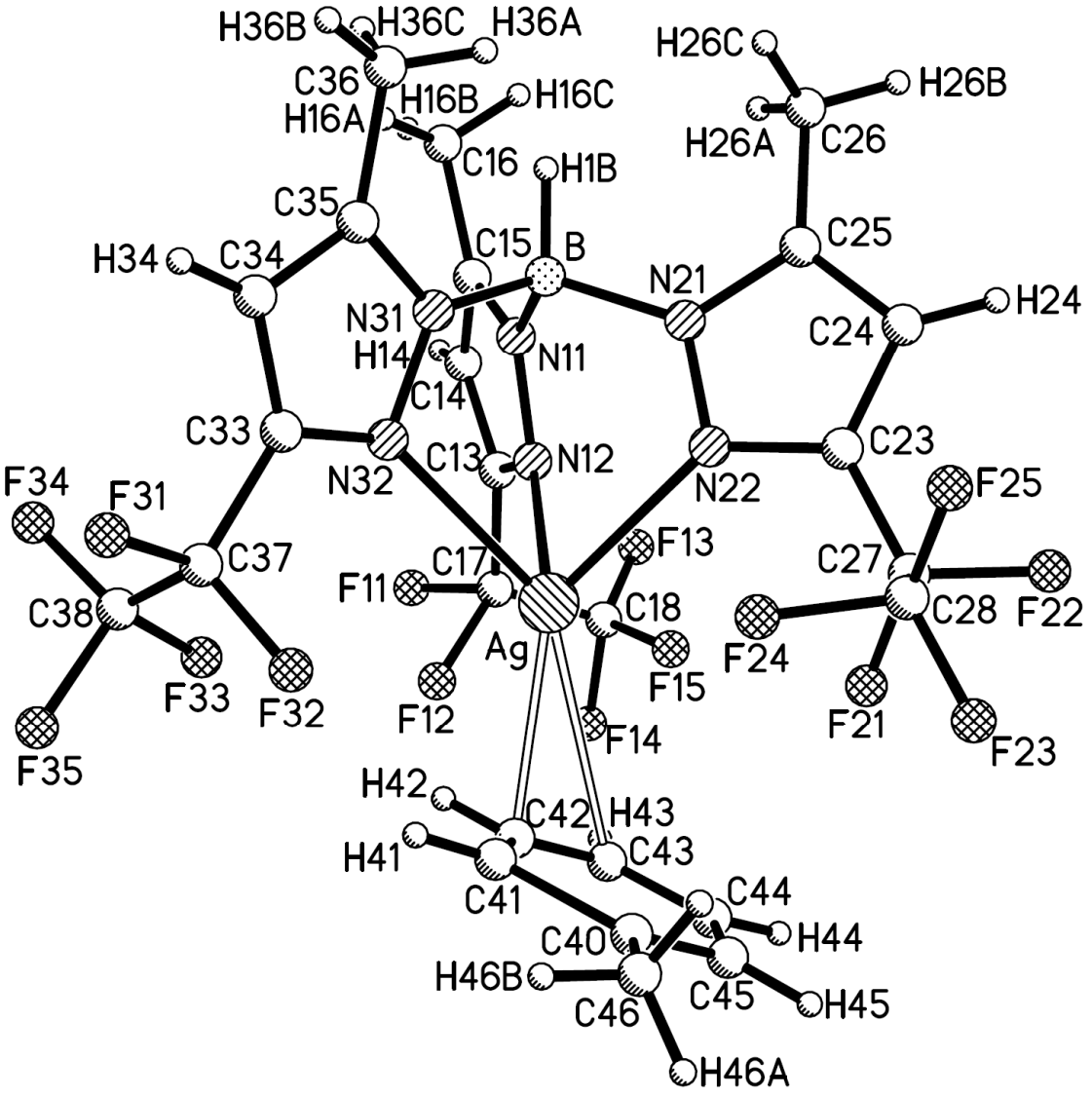

Figure G.1 Crystal structure of $Tp^{C_2F_5,CH_3}Ag(Tol)$.

Table G.1 Crystal Data and Structure Refinement for $Tp^{C_2F_5,CH_3}Ag(Tol)$

Empirical formula	$C_{25}\ H_{21}\ Ag\ B\ F_{15}\ N_6$	
Formula weight	809.16	
Temperature	243(2) K	
Wavelength	1.54178 Å	
Crystal system	triclinic	
Space group	P-1	
Unit cell dimensions	a = 11.5821(1) Å	α = 93.548(4)°
	b = 12.0954(1) Å	β = 116.605(4)°
	c = 12.5582(1) Å	γ = 98.557(4)°
Volume	1539.0(2) $Å^3$	
Z	2	
Density (calculated)	1.746 g/cm^3	
Absorption coefficient	6.369 mm^{-1}	
F(000)	800	
Crystal size	0.36 × 0.25 × 0.15 mm^3	
Theta range for data collection	5.15 to 67.98°	
Index ranges	$-12 \le h \le 12, -14 \le k \le 14, -14 \le l \le 15$	
Reflections collected	24387	
Max. and min. transmission	0.4484 and 0.2076	
Independent reflections	5248 [*R*(int) = 0.0208]	
Completeness to theta = 67.98°	93.7%	
Refinement method	Full-matrix least-squares on F^2	
Data / restraints / parameters	5248 / 22 / 430	
Goodness-of-fit on F^2	1.073	
Final *R* indices [*I*>2sigma(*I*)]	*R*1 = 0.0544, *wR*2 = 0.1524	
R indices (all data)	*R*1 = 0.0602, *wR*2 = 0.1606	
Extinction coefficient	0.0015(3)	
Largest diff. peak and hole	0.883 and −0.614 e.$Å^{-3}$	

Table G.2 Atomic Coordinates (× 10^4) and Equivalent Isotropic Displacement Parameters ($Å^2$ × 10^3) for $Tp^{C_2F_5,CH_3}Ag(Tol)$*

	x	y	z	U(eq)
C(40)	7385(14)	10358(6)	7028(7)	254(12)
C(41)	8283(9)	9920(6)	7986(9)	169(5)
C(42)	7911(8)	9447(5)	8795(6)	124(3)
C(43)	6642(10)	9413(6)	8645(9)	159(4)
C(44)	5744(7)	9851(7)	7687(11)	247(13)
C(45)	6115(12)	10324(6)	6879(7)	253(14)
C(46)	6270(30)	8913(16)	9440(30)	356(19)
Ag	6516(1)	12247(1)	7747(1)	81(1)
B	6502(6)	4965(4)	8252(5)	63(1)
N(11)	6757(4)	4802(3)	7150(3)	63(1)
N(12)	7055(5)	3830(4)	6836(4)	76(1)
C(13)	7174(7)	4004(5)	5837(5)	89(2)
C(14)	6984(7)	5048(6)	5530(5)	90(2)
C(15)	6703(5)	5553(4)	6369(4)	72(1)

C(16)	6363(7)	6675(5)	6453(6)	93(2)
C(17)	7398(11)	3076(9)	5131(8)	125(3)
C(18)	8682(15)	2987(15)	5617(11)	186(6)
N(21)	7601(4)	4622(3)	9376(3)	59(1)
N(22)	7664(4)	3523(3)	9529(3)	64(1)
C(23)	8689(5)	3554(4)	10598(4)	64(1)
C(24)	9306(5)	4653(4)	11140(4)	70(1)
C(25)	8597(5)	5317(4)	10339(4)	65(1)
C(26)	8818(7)	6574(5)	10435(5)	85(2)
C(27)	9039(6)	2504(5)	11101(5)	77(1)
C(28)	8311(14)	2011(10)	11719(14)	151(4)
N(31)	5137(4)	4290(3)	7983(4)	67(1)
N(32)	4716(4)	3189(4)	7488(5)	85(1)
C(33)	3473(5)	2932(5)	7345(6)	96(2)
C(34)	3097(6)	3839(6)	7701(6)	94(2)
C(35)	4176(5)	4694(5)	8125(5)	72(1)
C(36)	4340(7)	5865(5)	8682(5)	89(2)
C(37)	2669(9)	1734(9)	6897(9)	130(3)
C(38)	2245(14)	1476(11)	5674(12)	157(4)
F(11)	6924(7)	3223(7)	3941(4)	177(3)
F(12)	6576(7)	2038(5)	4973(5)	151(2)
F(13)	9453(9)	3919(9)	5616(10)	216(4)
F(14)	8907(9)	2206(9)	4899(6)	249(5)
F(15)	9047(7)	2674(6)	6656(4)	170(3)
F(21)	8970(4)	1722(3)	10270(4)	108(1)
F(22)	10321(4)	2704(4)	11949(4)	125(1)
F(23)	8690(7)	1076(5)	12155(7)	184(3)
F(24)	7024(7)	1695(6)	10863(10)	214(5)
F(25)	8358(12)	2710(7)	12547(8)	234(5)
F(31)	1548(5)	1615(5)	7106(5)	143(2)
F(32)	3325(5)	943(4)	7528(5)	130(2)
F(33)	3251(5)	1374(4)	5468(5)	130(2)
F(34)	1538(5)	2146(6)	5017(5)	157(2)
F(35)	1377(7)	390(7)	5255(9)	241(5)

* U(eq) is defined as one third of the trace of the orthogonalized U^{ij} tensor.

Table G.3 Bond Lengths (Å) and Angles (°) for $Tp^{C_2F_5,CH_3}Ag(Tol)$

Ag-N(22)#1	2.335(4)	C(25)-C(26)	1.491(7)
Ag-N(32)#1	2.428(5)	C(27)-F(21)	1.331(6)
Ag-N(12)#1	2.433(5)	C(27)-F(22)	1.357(7)
		C(27)-C(28)	1.470(10)
C(40)-C(41)	1.3900	C(28)-F(25)	1.276(15)
C(40)-C(45)	1.3900	C(28)-F(23)	1.334(9)
C(41)-C(42)	1.3900	C(28)-F(24)	1.367(16)
C(42)-C(43)	1.3900	N(31)-N(32)	1.353(6)
C(43)-C(46)	1.38(2)	N(31)-C(35)	1.355(6)
C(43)-C(44)	1.3900	N(32)-C(33)	1.352(7)
C(44)-C(45)	1.3900	N(32)-Ag#2	2.428(5)
C(45)-Ag	2.393(6)	C(33)-C(34)	1.360(9)
B-N(31)	1.544(7)	C(33)-C(37)	1.520(10)
B-N(11)	1.546(6)	C(34)-C(35)	1.366(8)
B-N(21)	1.551(7)	C(35)-C(36)	1.487(8)
N(11)-N(12)	1.357(5)	C(37)-F(32)	1.376(11)
N(11)-C(15)	1.366(6)	C(37)-C(38)	1.384(13)

N(12)-C(13)	1.349(7)	C(37)-F(31)	1.425(10)
N(12)-Ag#2	2.433(5)	C(38)-F(34)	1.298(13)
C(13)-C(14)	1.363(8)	C(38)-F(33)	1.322(12)
C(13)-C(17)	1.511(9)	C(38)-F(35)	1.436(13)
C(14)-C(15)	1.369(7)		
C(15)-C(16)	1.478(8)	C(41)-C(40)-C(45)	120.0
C(17)-C(18)	1.356(14)	C(40)-C(41)-C(42)	120.0
C(17)-F(11)	1.376(9)	C(43)-C(42)-C(41)	120.0
C(17)-F(12)	1.403(12)	C(46)-C(43)-C(44)	120.4(15)
C(18)-F(15)	1.280(17)	C(46)-C(43)-C(42)	119.6(15)
C(18)-F(13)	1.330(19)	C(44)-C(43)-C(42)	120.0
C(18)-F(14)	1.397(13)	C(45)-C(44)-C(43)	120.0
N(21)-C(25)	1.355(6)	C(44)-C(45)-C(40)	120.0
N(21)-N(22)	1.362(5)	C(44)-C(45)-Ag	95.9(5)
N(22)-C(23)	1.329(6)	C(40)-C(45)-Ag	95.5(5)
N(22)-Ag#2	2.335(4)	N(22)#1-Ag-C(45)	144.32(18)
C(23)-C(24)	1.382(7)	N(22)#1-Ag-N(32)#1	83.24(15)
C(23)-C(27)	1.483(7)	C(45)-Ag-N(32)#1	121.4(3)
C(24)-C(25)	1.375(7)	N(22)#1-Ag-N(12)#1	83.90(14)
F(11)-C(17)-C(13)	111.1(7)	F(23)-C(28)-F(24)	106.7(11)
F(12)-C(17)-C(13)	111.9(7)	F(25)-C(28)-C(27)	113.2(11)
F(15)-C(18)-F(13)	113.7(10)	F(23)-C(28)-C(27)	112.7(7)
F(15)-C(18)-C(17)	110.1(15)	F(24)-C(28)-C(27)	106.2(10)
F(13)-C(18)-C(17)	112.3(14)	N(32)-N(31)-C(35)	110.4(4)
F(15)-C(18)-F(14)	108.3(12)	N(32)-N(31)-B	122.5(4)
F(13)-C(18)-F(14)	100.1(15)	C(35)-N(31)-B	127.0(4)
C(17)-C(18)-F(14)	112.0(9)	C(33)-N(32)-N(31)	104.4(4)
C(25)-N(21)-N(22)	110.1(4)	C(33)-N(32)-Ag#2	139.1(4)
C(25)-N(21)-B	127.4(4)	N(31)-N(32)-Ag#2	112.6(3)
N(22)-N(21)-B	122.5(4)	N(32)-C(33)-C(34)	112.2(5)
C(23)-N(22)-N(21)	105.8(4)	N(32)-C(33)-C(37)	121.5(6)
C(23)-N(22)-Ag#2	136.2(3)	C(34)-C(33)-C(37)	126.2(6)
N(21)-N(22)-Ag#2	114.1(3)	C(33)-C(34)-C(35)	105.0(5)
N(22)-C(23)-C(24)	111.4(4)	N(31)-C(35)-C(34)	108.0(5)
N(22)-C(23)-C(27)	121.4(4)	N(31)-C(35)-C(36)	123.8(5)
C(24)-C(23)-C(27)	127.1(5)	C(34)-C(35)-C(36)	128.1(5)
C(25)-C(24)-C(23)	105.1(4)	F(32)-C(37)-C(38)	111.7(9)
N(21)-C(25)-C(24)	107.7(4)	F(32)-C(37)-F(31)	102.2(8)
N(21)-C(25)-C(26)	123.2(5)	C(38)-C(37)-F(31)	108.8(8)
C(24)-C(25)-C(26)	129.1(5)	F(32)-C(37)-C(33)	113.2(7)
F(21)-C(27)-F(22)	104.0(5)	C(38)-C(37)-C(33)	109.8(9)
F(21)-C(27)-C(28)	109.8(7)	F(31)-C(37)-C(33)	110.9(7)
F(22)-C(27)-C(28)	104.3(7)	F(34)-C(38)-F(33)	112.4(9)
F(21)-C(27)-C(23)	111.4(4)	F(34)-C(38)-C(37)	114.8(11)
F(22)-C(27)-C(23)	110.2(5)	F(33)-C(38)-C(37)	110.4(11)
C(28)-C(27)-C(23)	116.3(5)	F(34)-C(38)-F(35)	104.0(11)
F(25)-C(28)-F(23)	110.0(10)	F(33)-C(38)-F(35)	106.3(10)
F(25)-C(28)-F(24)	107.7(9)	C(37)-C(38)-F(35)	108.4(10)

Symmetry transformations used to generate equivalent atoms: #1 x,y+1,z; #2 x,y-1,z.

Table G.4 Anisotropic Displacement Parameters ($Å^2 \times 10^3$) for $Tp^{C_2F_5,CH_3}Ag(Tol)$*

	U^{11}	U^{22}	U^{33}	U^{23}	U^{13}	U^{12}
C(40)	520(40)	86(7)	128(10)	-7(6)	119(16)	81(13)
C(41)	244(14)	78(5)	161(10)	-17(6)	75(10)	40(7)
C(42)	127(7)	73(4)	141(7)	-9(4)	33(5)	33(4)
C(43)	174(11)	81(5)	195(12)	-26(6)	71(9)	16(6)
C(44)	166(11)	158(13)	260(20)	-107(14)	-28(13)	79(10)
C(45)	310(20)	117(9)	148(11)	-76(9)	-57(12)	112(13)
C(46)	450(40)	163(16)	600(50)	-20(20)	400(40)	-20(20)
Ag	85(1)	65(1)	77(1)	-11(1)	25(1)	23(1)
B	68(3)	58(3)	64(3)	-1(2)	32(2)	19(2)
N(11)	64(2)	66(2)	59(2)	-1(2)	28(2)	17(2)
N(12)	90(3)	77(3)	67(2)	1(2)	39(2)	29(2)
C(13)	109(5)	99(4)	75(3)	2(3)	54(3)	30(3)
C(14)	108(5)	103(4)	71(3)	10(3)	51(3)	16(3)
C(15)	69(3)	78(3)	65(3)	6(2)	29(2)	13(2)
C(16)	108(5)	82(4)	95(4)	24(3)	48(4)	25(3)
C(17)	157(9)	153(8)	114(6)	39(6)	89(6)	73(7)
C(18)	157(11)	228(16)	116(8)	-53(9)	12(7)	77(11)
N(21)	61(2)	58(2)	57(2)	-4(2)	29(2)	11(2)
N(22)	66(2)	62(2)	61(2)	-2(2)	27(2)	19(2)
C(23)	67(3)	73(3)	59(2)	3(2)	33(2)	21(2)
C(24)	66(3)	80(3)	56(2)	-7(2)	26(2)	9(2)
C(25)	70(3)	69(3)	57(2)	-7(2)	36(2)	6(2)
C(26)	105(4)	69(3)	74(3)	-4(2)	45(3)	-2(3)
C(27)	77(3)	83(3)	72(3)	5(2)	33(3)	29(3)
C(28)	181(11)	148(8)	229(12)	112(9)	155(10)	98(8)
N(31)	63(2)	70(2)	72(2)	8(2)	31(2)	24(2)
N(32)	64(3)	71(3)	107(3)	-4(2)	30(2)	14(2)
C(33)	57(3)	91(4)	121(5)	13(4)	27(3)	12(3)
C(34)	66(4)	116(5)	108(4)	29(4)	43(3)	33(3)
C(35)	71(3)	89(3)	69(3)	19(2)	38(2)	33(3)
C(36)	99(4)	107(4)	85(3)	15(3)	55(3)	51(3)
C(37)	96(6)	161(9)	135(7)	13(6)	55(5)	33(5)
C(38)	168(11)	159(10)	184(12)	44(9)	113(10)	32(8)
F(11)	209(6)	276(8)	79(3)	28(3)	67(3)	141(6)
F(12)	182(5)	138(4)	123(4)	-20(3)	57(4)	60(4)
F(13)	185(8)	262(10)	289(10)	27(8)	174(8)	93(7)
F(14)	254(8)	382(12)	140(5)	-23(6)	77(5)	220(9)
F(15)	199(6)	239(7)	85(3)	14(3)	51(3)	138(5)
F(21)	144(3)	79(2)	104(2)	5(2)	57(2)	41(2)
F(22)	95(3)	120(3)	120(3)	23(2)	9(2)	38(2)
F(23)	237(7)	168(5)	268(8)	145(5)	184(6)	121(5)
F(24)	143(5)	183(6)	393(13)	167(8)	165(7)	67(5)
F(25)	433(14)	251(8)	232(7)	151(7)	277(10)	226(10)
F(31)	112(3)	152(4)	192(5)	14(4)	100(4)	4(3)
F(32)	134(4)	102(3)	171(4)	38(3)	81(3)	25(3)
F(33)	119(3)	126(3)	147(4)	-29(3)	81(3)	-11(3)
F(34)	111(4)	179(5)	124(4)	-2(4)	13(3)	13(3)
F(35)	157(6)	172(6)	321(11)	-102(7)	94(6)	-67(5)

* The anisotropic displacement factor exponent takes the form: $-2\pi^2 [h^2 a^{*2} U^{11} + ... + 2 h k a^* b^* U^{12}]$.

Table G.5 Hydrogen Coordinates ($\times 10^4$) and Isotropic Displacement Parameters ($Å^2 \times 10^3$) for $Tp^{C_2F_5,CH_3}Ag(Tol)$

	x	y	z	U(eq)
H(40)	7636	10677	6482	304
H(41)	9141	9943	8088	203
H(42)	8518	9151	9443	149
H(44)	4885	9828	7586	296
H(45)	5508	10620	6231	303
H(46A)	6696	9395	10209	533
H(46B)	6531	8185	9537	533
H(46C)	5321	8808	9116	533
H(1B)	6570(50)	5890(40)	8440(40)	60(12)
H(14)	7034	5357	4880	109
H(16A)	5567	6594	6544	140
H(16B)	6219	6999	5727	140
H(16C)	7080	7168	7144	140
H(24)	10049	4894	11894	83
H(26A)	8718	6795	9674	127
H(26B)	9701	6897	11063	127
H(26C)	8181	6847	10631	127
H(34)	2274	3870	7664	112
H(36A)	5117	6028	9462	133
H(36B)	3570	5937	8783	133
H(36C)	4441	6395	8166	133

APPENDIX H

CRYSTAL STRUCTURE OF HYDROTRIS(3-TRIFLUOROMETHYL-5-METHYLPYRAZOL-1-YL)-BORATO-SILVER(I)-METHYLDIPHENYLPHOSPHINE

Tables H.1 to H.5 list the atomic coordinates and crystallographic parameters for $Tp^{CF_3,CH_3}Ag(PMePh_2)$ **[3-9]** (Figure H.1).

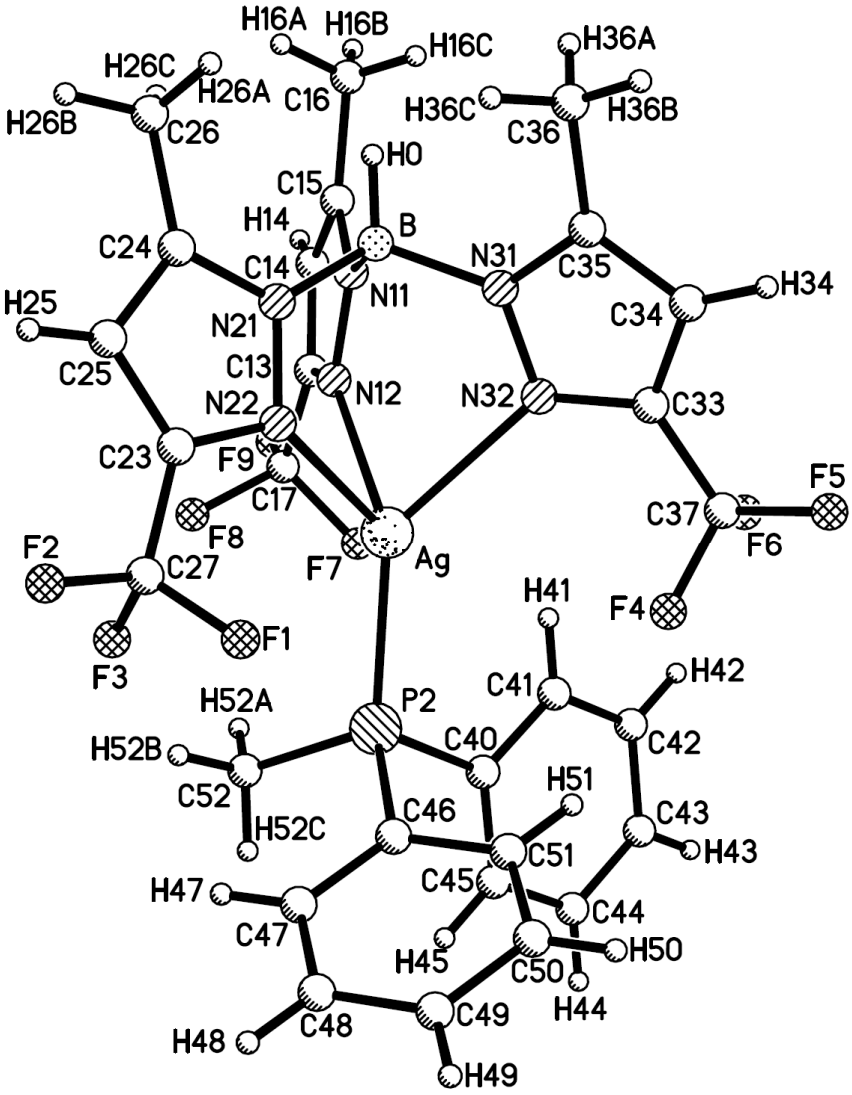

Figure H.1 Crystal structure of $Tp^{CF_3,CH_3}Ag(PMePh_2)$.

Table H.1 Crystal Data and Structure Refinement for $Tp^{CF_3,CH_3}Ag(PMePh_2)$

Empirical formula	$C_{28}\ H_{26}\ Ag\ B\ F_9\ N_6\ P$	
Formula weight	767.20	
Temperature	100(2) K	
Wavelength	1.54178 Å	
Crystal system	monoclinic	
Space group	P2(1)/n	
Unit cell dimensions	a = 12.0444(3) Å	α = 90°
	b = 19.1515(6) Å	β = 94.530(1)°
	c = 13.4945(4) Å	γ = 90°
Volume	3103.0(2) $Å^3$	
Z	4	
Density (calculated)	1.642 g/cm^3	
Absorption coefficient	6.468 mm^{-1}	
F(000)	1536	
Crystal size	0.38 × 0.25 × 0.22 mm^3	
Theta range for data collection	4.02 to 68.05°	
Index ranges	$-14 \le h \le 13, -22 \le k \le 23, -15 \le l \le 16$	
Reflections collected	22882	
Independent reflections	5503 [*R*(int) = 0.0228]	
Completeness to theta = 68.05°	97.1%	
Max. and min. transmission	0.3303 and 0.1925	
Refinement method	Full-matrix least-squares on F^2	
Data / restraints / parameters	5503 / 0 / 420	
Goodness-of-fit on F^2	1.070	
Final *R* indices [*I*>2sigma(*I*)]	*R*1 = 0.0272, *wR*2 = 0.0695	
R indices (all data)	*R*1 = 0.0274, *wR*2 = 0.0696	
Extinction coefficient	0.00009(3)	
Largest diff. peak and hole	0.590 and −0.430 e.$Å^{-3}$	

Table H.2 Atomic Coordinates (× 10^4) and Equivalent Isotropic Displacement Parameters ($Å^2$ × 10^3) for $Tp^{CF_3,CH_3}Ag(PMePh_2)$*

	x	y	z	U(eq)
Ag	2286(1)	1074(1)	3090(1)	21(1)
P(2)	2110(1)	1408(1)	1408(1)	21(1)
F(8)	5046(1)	2151(1)	3065(1)	38(1)
F(6)	2264(1)	-1090(1)	2501(1)	43(1)
F(7)	5016(2)	1145(1)	2409(1)	47(1)
F(1)	-334(2)	2122(1)	3134(1)	52(1)
F(5)	603(1)	-1384(1)	2752(1)	43(1)
F(3)	1024(2)	2817(1)	3054(1)	52(1)
F(9)	6489(1)	1498(1)	3275(2)	55(1)
F(4)	933(2)	-378(1)	2139(1)	46(1)
F(2)	-284(2)	3083(1)	3954(1)	49(1)
B	2614(2)	757(1)	5546(2)	19(1)
N(12)	3882(2)	1116(1)	4228(1)	20(1)
N(21)	1904(1)	1430(1)	5364(1)	19(1)

N(32)	2022(1)	30(1)	4017(1)	19(1)
N(31)	2014(1)	130(1)	5016(1)	18(1)
N(11)	3781(2)	874(1)	5163(1)	18(1)
N(22)	1441(2)	1596(1)	4441(1)	20(1)
C(14)	5591(2)	1013(1)	5035(2)	23(1)
C(17)	5382(2)	1498(1)	3239(2)	26(1)
C(15)	4802(2)	809(1)	5669(2)	20(1)
C(33)	1447(2)	-559(1)	3833(2)	20(1)
C(36)	1241(2)	-407(1)	6519(2)	29(1)
C(24)	1678(2)	1928(1)	6034(2)	23(1)
C(25)	1035(2)	2432(1)	5534(2)	25(1)
C(35)	1429(2)	-384(1)	5436(2)	21(1)
C(34)	1058(2)	-839(1)	4692(2)	23(1)
C(52)	2774(2)	2233(1)	1128(2)	30(1)
C(16)	4976(2)	572(1)	6723(2)	28(1)
C(13)	4973(2)	1198(1)	4160(2)	21(1)
C(49)	-1502(2)	1569(1)	21(2)	33(1)
C(37)	1310(2)	-847(1)	2807(2)	24(1)
C(51)	72(2)	892(1)	661(2)	30(1)
C(23)	918(2)	2203(1)	4553(2)	22(1)
C(27)	326(2)	2547(1)	3682(2)	27(1)
C(26)	2102(2)	1894(2)	7105(2)	37(1)
C(48)	-894(2)	2170(1)	210(2)	37(1)
C(50)	-1016(2)	927(1)	245(2)	34(1)
C(41)	3283(2)	204(1)	975(2)	27(1)
C(45)	2599(2)	875(1)	-452(2)	31(1)
C(40)	2714(2)	787(1)	576(2)	24(1)
C(42)	3728(2)	-280(1)	354(2)	35(1)
C(44)	3044(2)	388(2)	-1067(2)	40(1)
C(43)	3606(2)	-188(2)	-666(2)	40(1)
C(46)	691(2)	1498(1)	845(2)	22(1)
C(47)	198(2)	2139(1)	621(2)	32(1)

* U(eq) is defined as one third of the trace of the orthogonalized U^{ij} tensor.

Table H.3 Bond Lengths (Å) and Angles (°) for $Tp^{CF_3,CH_3}Ag(PMePh_2)$

Ag-P(2)	2.3510(5)	Ag-N(22)	2.3771(18)
Ag-N(12)	2.3647(19)	Ag-N(32)	2.3937(17)
P(2)-C(52)	1.822(2)	C(49)-C(48)	1.378(4)
P(2)-C(46)	1.823(2)	C(49)-C(50)	1.384(4)
P(2)-C(40)	1.826(2)	C(51)-C(50)	1.386(4)
F(8)-C(17)	1.330(3)	C(51)-C(46)	1.391(3)
F(6)-C(37)	1.335(3)	C(23)-C(27)	1.481(3)
F(7)-C(17)	1.351(3)	C(48)-C(47)	1.388(4)
F(1)-C(27)	1.323(3)	C(41)-C(42)	1.384(3)
F(5)-C(37)	1.333(3)	C(41)-C(40)	1.396(3)
F(3)-C(27)	1.342(3)	C(45)-C(44)	1.384(4)
F(9)-C(17)	1.329(3)	C(45)-C(40)	1.394(3)
F(4)-C(37)	1.327(3)	C(42)-C(43)	1.384(4)
F(2)-C(27)	1.331(3)	C(44)-C(43)	1.382(4)
B-N(31)	1.548(3)	C(46)-C(47)	1.387(3)
B-N(11)	1.552(3)	N(12)-C(13)	1.334(3)
B-N(21)	1.555(3)	N(12)-N(11)	1.358(3)
N(21)-C(24)	1.356(3)	P(2)-Ag-N(12)	128.62(5)

N(21)-N(22)	1.362(3)	P(2)-Ag-N(22)	127.90(4)
N(32)-C(33)	1.336(3)	N(12)-Ag-N(22)	82.14(6)
N(32)-N(31)	1.362(2)	P(2)-Ag-N(32)	136.57(4)
N(31)-C(35)	1.361(3)	N(12)-Ag-N(32)	79.85(6)
N(11)-C(15)	1.365(3)	N(22)-Ag-N(32)	82.41(6)
N(22)-C(23)	1.336(3)	C(52)-P(2)-C(46)	104.14(11)
C(14)-C(15)	1.384(3)	C(52)-P(2)-C(40)	103.53(11)
C(14)-C(13)	1.392(3)	C(46)-P(2)-C(40)	102.17(10)
C(17)-C(13)	1.488(3)	C(52)-P(2)-Ag	115.37(8)
C(15)-C(16)	1.492(3)	C(46)-P(2)-Ag	115.98(7)
C(33)-C(34)	1.393(3)	C(40)-P(2)-Ag	113.98(8)
C(33)-C(37)	1.487(3)	N(31)-B-N(11)	111.11(17)
C(36)-C(35)	1.496(3)	N(31)-B-N(21)	109.85(17)
C(24)-C(25)	1.380(3)	N(11)-B-N(21)	109.19(16)
C(24)-C(26)	1.496(3)	C(13)-N(12)-N(11)	105.35(18)
C(25)-C(23)	1.391(3)	C(13)-N(12)-Ag	135.54(15)
C(35)-C(34)	1.377(3)	N(11)-N(12)-Ag	117.64(13)
		C(24)-N(21)-N(22)	110.86(17)
		C(24)-N(21)-B	127.89(19)
N(22)-N(21)-B	121.23(17)	N(12)-C(13)-C(14)	112.1(2)
C(33)-N(32)-N(31)	104.99(17)	N(12)-C(13)-C(17)	119.7(2)
C(33)-N(32)-Ag	134.11(14)	C(14)-C(13)-C(17)	128.1(2)
N(31)-N(32)-Ag	114.29(12)	C(48)-C(49)-C(50)	119.5(2)
C(35)-N(31)-N(32)	110.84(17)	F(4)-C(37)-F(5)	107.48(19)
C(35)-N(31)-B	127.33(18)	F(4)-C(37)-F(6)	106.4(2)
N(32)-N(31)-B	121.83(16)	F(5)-C(37)-F(6)	105.99(18)
N(12)-N(11)-C(15)	110.69(17)	F(4)-C(37)-C(33)	112.83(18)
N(12)-N(11)-B	120.56(17)	F(5)-C(37)-C(33)	111.24(19)
C(15)-N(11)-B	128.61(18)	F(6)-C(37)-C(33)	112.51(19)
C(23)-N(22)-N(21)	105.18(17)	C(50)-C(51)-C(46)	120.6(2)
C(23)-N(22)-Ag	133.41(14)	N(22)-C(23)-C(25)	111.7(2)
N(21)-N(22)-Ag	115.71(12)	N(22)-C(23)-C(27)	119.9(2)
C(15)-C(14)-C(13)	104.41(19)	C(25)-C(23)-C(27)	128.4(2)
F(9)-C(17)-F(8)	107.22(19)	F(1)-C(27)-F(2)	108.0(2)
F(9)-C(17)-F(7)	107.0(2)	F(1)-C(27)-F(3)	105.2(2)
F(8)-C(17)-F(7)	104.4(2)	F(2)-C(27)-F(3)	105.38(19)
F(9)-C(17)-C(13)	111.5(2)	F(1)-C(27)-C(23)	113.56(18)
F(8)-C(17)-C(13)	113.19(19)	F(2)-C(27)-C(23)	111.4(2)
F(7)-C(17)-C(13)	112.99(19)	F(3)-C(27)-C(23)	112.72(19)
N(11)-C(15)-C(14)	107.48(19)	C(49)-C(48)-C(47)	120.7(2)
N(11)-C(15)-C(16)	123.93(19)	C(49)-C(50)-C(51)	120.1(2)
C(14)-C(15)-C(16)	128.6(2)	C(42)-C(41)-C(40)	120.3(2)
N(32)-C(33)-C(34)	111.98(19)	C(44)-C(45)-C(40)	120.2(2)
N(32)-C(33)-C(37)	120.27(19)	C(45)-C(40)-C(41)	119.2(2)
C(34)-C(33)-C(37)	127.73(19)	C(45)-C(40)-P(2)	121.35(18)
N(21)-C(24)-C(25)	107.5(2)	C(41)-C(40)-P(2)	119.46(18)
N(21)-C(24)-C(26)	122.9(2)	C(43)-C(42)-C(41)	120.1(2)
C(25)-C(24)-C(26)	129.6(2)	C(43)-C(44)-C(45)	120.3(3)
C(24)-C(25)-C(23)	104.74(19)	C(44)-C(43)-C(42)	120.1(2)
N(31)-C(35)-C(34)	107.59(19)	C(47)-C(46)-C(51)	119.0(2)
N(31)-C(35)-C(36)	123.5(2)	C(47)-C(46)-P(2)	123.05(18)
C(34)-C(35)-C(36)	128.9(2)	C(51)-C(46)-P(2)	117.90(17)
C(35)-C(34)-C(33)	104.60(19)	C(46)-C(47)-C(48)	120.1(2)

Table H.4 Anisotropic Displacement Parameters ($Å^2 \times 10^3$) for $Tp^{CF_3,CH_3}Ag(PMePh_2)$*

	U^{11}	U^{22}	U^{33}	U^{23}	U^{13}	U^{12}
Ag	25(1)	22(1)	17(1)	1(1)	3(1)	0(1)
P(2)	25(1)	19(1)	19(1)	1(1)	2(1)	-2(1)
F(8)	49(1)	26(1)	41(1)	11(1)	16(1)	5(1)
F(6)	34(1)	55(1)	41(1)	-21(1)	7(1)	3(1)
F(7)	72(1)	42(1)	31(1)	-6(1)	23(1)	-15(1)
F(1)	63(1)	34(1)	55(1)	9(1)	-28(1)	-3(1)
F(5)	50(1)	41(1)	39(1)	-12(1)	5(1)	-26(1)
F(3)	46(1)	62(1)	49(1)	32(1)	12(1)	8(1)
F(9)	22(1)	78(1)	67(1)	38(1)	15(1)	3(1)
F(4)	79(1)	32(1)	25(1)	-1(1)	-8(1)	12(1)
F(2)	59(1)	41(1)	47(1)	4(1)	4(1)	31(1)
B	20(1)	18(1)	17(1)	-1(1)	2(1)	1(1)
N(12)	21(1)	18(1)	20(1)	1(1)	3(1)	-1(1)
N(21)	19(1)	19(1)	19(1)	-1(1)	4(1)	0(1)
N(32)	20(1)	18(1)	20(1)	-1(1)	2(1)	0(1)
N(31)	19(1)	17(1)	18(1)	1(1)	2(1)	1(1)
N(11)	20(1)	16(1)	18(1)	-1(1)	2(1)	0(1)
N(22)	21(1)	18(1)	22(1)	2(1)	3(1)	1(1)
C(14)	19(1)	17(1)	32(1)	-4(1)	2(1)	1(1)
C(17)	22(1)	24(1)	33(1)	2(1)	8(1)	1(1)
C(15)	21(1)	14(1)	26(1)	-2(1)	1(1)	2(1)
C(33)	18(1)	16(1)	26(1)	0(1)	1(1)	1(1)
C(36)	33(1)	27(1)	28(1)	3(1)	10(1)	-4(1)
C(24)	20(1)	25(1)	26(1)	-7(1)	5(1)	1(1)
C(25)	22(1)	21(1)	32(1)	-6(1)	5(1)	1(1)
C(35)	20(1)	19(1)	26(1)	4(1)	5(1)	2(1)
C(34)	22(1)	19(1)	29(1)	2(1)	4(1)	-3(1)
C(52)	35(1)	25(1)	31(1)	3(1)	3(1)	-8(1)
C(16)	26(1)	29(1)	28(1)	2(1)	-2(1)	3(1)
C(13)	21(1)	15(1)	27(1)	-2(1)	5(1)	-1(1)
C(49)	26(1)	38(1)	36(1)	3(1)	0(1)	9(1)
C(37)	25(1)	18(1)	29(1)	-2(1)	1(1)	-2(1)
C(51)	29(1)	19(1)	40(1)	0(1)	-3(1)	4(1)
C(23)	19(1)	17(1)	29(1)	2(1)	6(1)	-1(1)
C(27)	29(1)	19(1)	33(1)	3(1)	4(1)	3(1)
C(26)	37(1)	43(1)	29(1)	-16(1)	-4(1)	16(1)
C(48)	37(1)	25(1)	48(2)	12(1)	5(1)	10(1)
C(50)	29(1)	27(1)	45(2)	-5(1)	-3(1)	0(1)
C(41)	23(1)	30(1)	27(1)	-2(1)	-1(1)	-1(1)
C(45)	37(1)	33(1)	24(1)	0(1)	6(1)	-2(1)
C(40)	22(1)	24(1)	25(1)	-2(1)	4(1)	-3(1)
C(42)	23(1)	33(1)	48(2)	-9(1)	2(1)	2(1)
C(44)	45(2)	49(2)	26(1)	-7(1)	11(1)	-6(1)
C(43)	31(1)	47(2)	45(2)	-19(1)	14(1)	-2(1)
C(46)	26(1)	21(1)	20(1)	1(1)	2(1)	1(1)
C(47)	34(1)	21(1)	42(1)	6(1)	6(1)	1(1)

* The anisotropic displacement factor exponent takes the form: $-2\pi^2 [h^2 a^{*2} U^{11} + ... + 2 h k a^* b^* U^{12}]$.

Table H.5 Hydrogen Coordinates ($\times 10^4$) and Isotropic Displacement Parameters ($Å^2 \times 10^3$) for $Tp^{CF_3,CH_3}Ag(PMePh_2)$

	x	y	z	U(eq)
H(0)	2705	661	6276	22
H(14)	6377	1024	5168	27
H(36A)	1936	-534	6902	43
H(36B)	667	-754	6631	43
H(36C)	996	54	6733	43
H(25)	738	2845	5801	30
H(34)	631	-1252	4752	28
H(52A)	3577	2199	1304	45
H(52B)	2461	2609	1513	45
H(52C)	2640	2334	417	45
H(16A)	4762	947	7164	42
H(16B)	5763	456	6878	42
H(16C)	4517	159	6819	42
H(49)	-2249	1594	-261	40
H(51)	398	451	821	36
H(26A)	1735	1509	7430	55
H(26B)	1941	2335	7432	55
H(26C)	2909	1815	7154	55
H(48)	-1227	2611	59	44
H(50)	-1429	510	113	41
H(41)	3365	138	1674	32
H(45)	2215	1271	-732	38
H(42)	4118	-675	629	42
H(44)	2964	451	-1768	48
H(43)	3908	-521	-1091	48
H(47)	609	2557	748	39

APPENDIX I

CRYSTAL STRUCTURE OF HYDROTRIS(3-PENTAFLUOROETHYL-5-METHYLPYRAZOL-1-YL)-BORATO-SILVER(I)-METHYLDIPHENYLPHOSPHINE

Tables I.1 to I.5 list the atomic coordinates and crystallographic parameters for $Tp^{C_2F_5,CH_3}Ag(PMePh_2)$ **[3-10]** (Figure I.1).

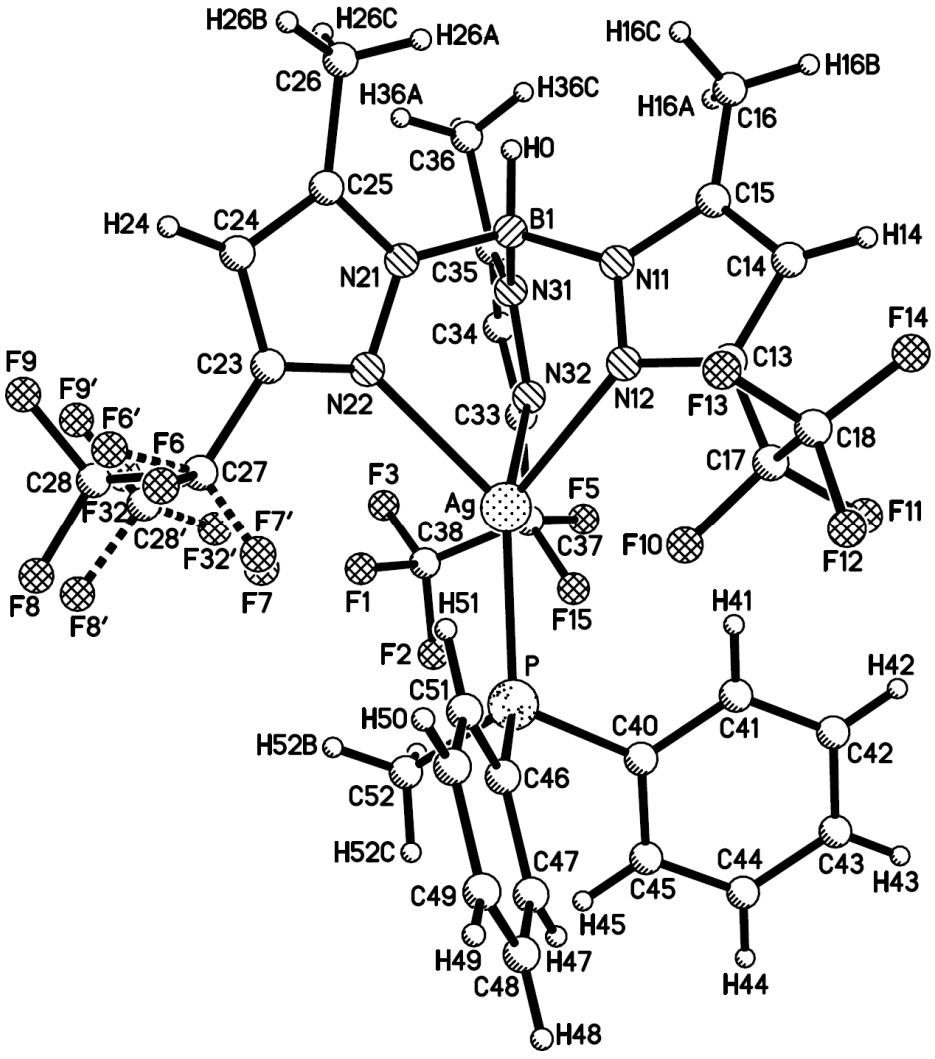

Figure I.1 Crystal structure of $Tp^{C_2F_5,CH_3}Ag(PMePh_2)$.

Table I.1 Crystal Data and Structure Refinement for $Tp^{C_2F_5,CH_3}Ag(PMePh_2)$

Empirical formula	$C_{62}\ H_{52}\ Ag_2\ B_2\ F_{30}\ N_{12}\ P_2$	
Formula weight	1834.46	
Temperature	100(2) K	
Wavelength	1.54178 Å	
Crystal system	primitive	
Space group	P-1	
Unit cell dimensions	a = 10.9393(2) Å	α = 97.393(1)°
	b = 11.8589(3) Å	β = 105.308(1)°
	c = 14.7060(3) Å	γ = 91.537(1)°
Volume	1821.11(7) $Å^3$	
Z	2	
Density (calculated)	1.673 g/cm^3	
Absorption coefficient	5.868 mm^{-1}	
F(000)	912	
Crystal size	0.26 × 0.23 × 0.46 mm^3	
Theta range for data collection	3.15 to 67.65°	
Index ranges	$-12 \le h \le 13, -14 \le k \le 13, -17 \le l \le 17$	
Reflections collected	13987	
Independent reflections	5905 [*R*(int) = 0.0178]	
Completeness to theta = 67.65°	89.7%	
Refinement method	Full-matrix least-squares on F^2	
Data / restraints / parameters	5905 / 9 / 526	
Goodness-of-fit on F^2	1.095	
Final *R* indices [*I*>2sigma(*I*)]	*R*1 = 0.0241, *wR*2 = 0.0614	
R indices (all data)	*R*1 = 0.0244, *wR*2 = 0.0617	
Extinction coefficient	0.00000(8)	
Largest diff. peak and hole	0.526 and −0.278 e.$Å^{-3}$	

Table I.2 Atomic Coordinates (× 10^4) and Equivalent Isotropic Displacement Parameters ($Å^2$ × 10^3) for $Tp^{C_2F_5,CH_3}Ag(PMePh_2)$*

	x	y	z	U(eq)
Ag	2051(1)	2869(1)	7283(1)	21(1)
P	4084(1)	2911(1)	8378(1)	22(1)
B(1)	-875(2)	2583(2)	5768(2)	21(1)
F(6)	2163(2)	6877(2)	7348(1)	51(1)
F(7)	2515(2)	5455(2)	8140(2)	50(1)
C(28)	1074(3)	6712(3)	8471(2)	42(1)
F(8)	2002(2)	7331(2)	9127(1)	45(1)
F(9)	211(2)	7402(2)	8104(2)	82(1)
F(32)	532(3)	5996(3)	8878(2)	78(1)
F(1)	1105(2)	2905(1)	9545(1)	48(1)
F(2)	1643(2)	1602(2)	10442(1)	51(1)
F(3)	-335(2)	1856(2)	9861(1)	46(1)
F(5)	429(1)	-33(1)	8994(1)	41(1)
F(10)	3842(1)	2535(1)	5791(1)	37(1)
F(11)	3752(1)	758(1)	5171(1)	39(1)

F(12)	4830(1)	2263(1)	4320(1)	38(1)
F(13)	3091(2)	3116(2)	3985(1)	56(1)
F(14)	3123(2)	1362(2)	3409(1)	54(1)
F(15)	1931(1)	982(1)	8693(1)	34(1)
N(11)	61(2)	2022(1)	5244(1)	19(1)
N(21)	-490(2)	3869(1)	6090(1)	20(1)
N(22)	534(2)	4227(1)	6837(1)	21(1)
N(12)	1342(2)	2279(1)	5573(1)	21(1)
N(32)	182(2)	1786(1)	7275(1)	20(1)
N(31)	-910(2)	1986(1)	6633(1)	20(1)
C(46)	5337(2)	3750(2)	8102(2)	28(1)
C(51)	4987(2)	4487(2)	7435(2)	37(1)
C(50)	5910(3)	5147(3)	7211(2)	52(1)
C(49)	7180(3)	5061(3)	7651(2)	52(1)
C(48)	7533(3)	4327(3)	8308(2)	50(1)
C(47)	6618(2)	3669(2)	8538(2)	40(1)
C(40)	4717(2)	1507(2)	8466(2)	24(1)
C(41)	4331(2)	683(2)	7671(2)	28(1)
C(42)	4794(2)	-397(2)	7684(2)	36(1)
C(43)	5651(2)	-656(2)	8493(2)	40(1)
C(44)	6029(3)	155(2)	9290(2)	41(1)
C(45)	5566(2)	1233(2)	9283(2)	32(1)
C(16)	-1542(2)	832(2)	3895(2)	26(1)
C(15)	-223(2)	1278(2)	4425(2)	21(1)
C(14)	900(2)	1043(2)	4202(2)	23(1)
C(13)	1831(2)	1680(2)	4931(1)	21(1)
C(17)	3227(2)	1772(2)	5039(2)	24(1)
C(18)	3573(2)	2134(2)	4172(2)	33(1)
C(25)	-1058(2)	4772(2)	5707(2)	22(1)
C(26)	-2219(2)	4652(2)	4884(2)	29(1)
C(24)	-381(2)	5750(2)	6225(2)	24(1)
C(23)	592(2)	5366(2)	6916(2)	22(1)
C(27)	1570(2)	6066(2)	7689(2)	27(1)
C(36)	-3280(2)	1761(2)	6345(2)	32(1)
C(37)	738(2)	1006(2)	8793(2)	26(1)
C(38)	795(2)	1857(2)	9680(2)	36(1)
C(35)	-1944(2)	1627(2)	6894(2)	23(1)
C(34)	-1516(2)	1166(2)	7724(2)	25(1)
C(33)	-195(2)	1284(2)	7930(2)	22(1)
C(52)	4194(2)	3498(2)	9610(2)	31(1)

* U(eq) is defined as one third of the trace of the orthogonalized U^{ij} tensor.

Table I.3 Bond Lengths (Å) and Angles (°) for $Tp^{C_2F_5,CH_3}Ag(PMePh_2)$

Ag-N(22)	2.3703(17)	Ag-N(32)	2.3808(17)
Ag-P	2.3711(5)	Ag-N(12)	2.4305(17)
F(6)-C(27)	1.364(3)	C(48)-C(47)	1.390(4)
F(7)-C(27)	1.354(3)	C(48)-H(48)	0.9500
C(28)-F(32)	1.313(5)	C(47)-H(47)	0.9500
C(28)-F(9)	1.319(4)	C(40)-C(41)	1.387(3)
C(28)-F(8)	1.327(4)	C(40)-C(45)	1.393(3)
C(28)-C(27)	1.525(4)	C(41)-C(42)	1.390(3)
F(6')-C(27)	1.349(10)	C(41)-H(41)	0.9500
F(7')-C(27)	1.230(12)	C(42)-C(43)	1.383(4)
C(28')-F(32')	1.268(16)	C(42)-H(42)	0.9500

C(28')-F(9')	1.332(15)	C(43)-C(44)	1.379(4)
C(28')-F(8')	1.347(15)	C(43)-H(43)	0.9500
C(28')-C(27)	1.561(16)	C(44)-C(45)	1.388(4)
P-C(40)	1.827(2)	C(44)-H(44)	0.9500
P-C(52)	1.828(2)	C(45)-H(45)	0.9500
P-C(46)	1.832(2)	C(16)-C(15)	1.493(3)
F(1)-C(38)	1.332(3)	C(16)-H(16A)	0.9800
F(2)-C(38)	1.326(3)	C(16)-H(16B)	0.9800
F(3)-C(38)	1.331(3)	C(16)-H(16C)	0.9800
F(5)-C(37)	1.358(3)	C(15)-C(14)	1.378(3)
F(10)-C(17)	1.346(3)	C(14)-C(13)	1.390(3)
F(11)-C(17)	1.361(2)	C(14)-H(14)	0.9500
F(12)-C(18)	1.336(3)	C(13)-C(17)	1.493(3)
F(13)-C(18)	1.322(3)	C(17)-C(18)	1.530(3)
F(14)-C(18)	1.326(3)	C(25)-C(24)	1.380(3)
F(15)-C(37)	1.353(3)	C(25)-C(26)	1.494(3)
N(11)-C(15)	1.356(3)	C(26)-H(26A)	0.9800
N(11)-N(12)	1.368(2)	C(26)-H(26B)	0.9800
N(11)-B(1)	1.551(3)	C(26)-H(26C)	0.9800
N(21)-N(22)	1.359(3)	C(24)-C(23)	1.394(3)
N(21)-C(25)	1.362(3)	C(24)-H(24)	0.9500
N(21)-B(1)	1.550(3)	C(23)-C(27)	1.482(3)
N(22)-C(23)	1.338(3)	C(36)-C(35)	1.495(3)
N(12)-C(13)	1.340(3)	C(36)-H(36A)	0.9800
N(32)-C(33)	1.341(3)	C(36)-H(36B)	0.9800
N(32)-N(31)	1.361(2)	C(36)-H(36C)	0.9800
N(31)-C(35)	1.361(3)	C(37)-C(33)	1.484(3)
N(31)-B(1)	1.541(3)	C(37)-C(38)	1.529(3)
C(46)-C(51)	1.384(3)	C(35)-C(34)	1.375(3)
C(46)-C(47)	1.390(3)	C(34)-C(33)	1.395(3)
C(51)-C(50)	1.393(4)	C(34)-H(34)	0.9500
C(51)-H(51)	0.9500	C(52)-H(52A)	0.9800
C(50)-C(49)	1.383(4)	C(52)-H(52B)	0.9800
C(50)-H(50)	0.9500	C(52)-H(52C)	0.9800
C(49)-C(48)	1.370(4)	B(1)-H(0)	1.0000
C(49)-H(49)	0.9500		
N(22)-Ag-P	135.35(4)	N(22)-Ag-N(12)	79.61(6)
N(22)-Ag-N(32)	80.88(6)	P-Ag-N(12)	131.21(4)
P-Ag-N(32)	127.15(4)	N(32)-Ag-N(12)	83.31(6)
F(32)-C(28)-F(9)	107.6(3)	C(48)-C(49)-H(49)	119.9
F(32)-C(28)-F(8)	109.2(3)	C(50)-C(49)-H(49)	119.9
F(9)-C(28)-F(8)	108.2(3)	C(49)-C(48)-C(47)	120.3(3)
F(32)-C(28)-C(27)	110.2(3)	C(49)-C(48)-H(48)	119.9
F(9)-C(28)-C(27)	110.1(3)	C(47)-C(48)-H(48)	119.9
F(8)-C(28)-C(27)	111.4(2)	C(48)-C(47)-C(46)	120.2(2)
F(32')-C(28')-F(9')	115.9(14)	C(48)-C(47)-H(47)	119.9
F(32')-C(28')-F(8')	107.0(13)	C(46)-C(47)-H(47)	119.9
F(9')-C(28')-F(8')	106.9(12)	C(41)-C(40)-C(45)	118.9(2)
F(32')-C(28')-C(27)	112.4(12)	C(41)-C(40)-P	117.69(16)
F(9')-C(28')-C(27)	106.2(11)	C(45)-C(40)-P	123.36(18)
F(8')-C(28')-C(27)	108.2(11)	C(40)-C(41)-C(42)	120.7(2)
C(40)-P-C(52)	103.98(11)	C(40)-C(41)-H(41)	119.7
C(40)-P-C(46)	103.70(10)	C(42)-C(41)-H(41)	119.7
C(52)-P-C(46)	102.85(11)	C(43)-C(42)-C(41)	120.0(2)
C(40)-P-Ag	113.65(8)	C(43)-C(42)-H(42)	120.0

C(52)-P-Ag	116.10(8)	C(41)-C(42)-H(42)	120.0
C(46)-P-Ag	115.03(8)	C(44)-C(43)-C(42)	119.7(2)
C(15)-N(11)-N(12)	110.92(16)	C(44)-C(43)-H(43)	120.2
C(15)-N(11)-B(1)	127.73(17)	C(42)-C(43)-H(43)	120.2
N(12)-N(11)-B(1)	121.31(16)	C(43)-C(44)-C(45)	120.6(2)
N(22)-N(21)-C(25)	110.88(17)	C(43)-C(44)-H(44)	119.7
N(22)-N(21)-B(1)	121.03(16)	C(45)-C(44)-H(44)	119.7
C(25)-N(21)-B(1)	128.09(17)	C(44)-C(45)-C(40)	120.1(2)
C(23)-N(22)-N(21)	105.29(17)	C(44)-C(45)-H(45)	120.0
C(23)-N(22)-Ag	134.00(14)	C(40)-C(45)-H(45)	120.0
N(21)-N(22)-Ag	116.57(12)	C(15)-C(16)-H(16A)	109.5
C(13)-N(12)-N(11)	104.60(16)	C(15)-C(16)-H(16B)	109.5
C(13)-N(12)-Ag	134.88(14)	H(16A)-C(16)-H(16B)	109.5
N(11)-N(12)-Ag	113.22(11)	C(15)-C(16)-H(16C)	109.5
C(33)-N(32)-N(31)	105.08(16)	H(16A)-C(16)-H(16C)	109.5
C(33)-N(32)-Ag	134.21(14)	H(16B)-C(16)-H(16C)	109.5
N(31)-N(32)-Ag	116.62(12)	N(11)-C(15)-C(14)	107.75(18)
N(32)-N(31)-C(35)	110.77(17)	N(11)-C(15)-C(16)	123.65(18)
N(32)-N(31)-B(1)	120.95(16)	C(14)-C(15)-C(16)	128.61(19)
C(35)-N(31)-B(1)	128.25(17)	C(15)-C(14)-C(13)	104.61(18)
C(51)-C(46)-C(47)	119.3(2)	C(15)-C(14)-H(14)	127.7
C(51)-C(46)-P	118.39(17)	C(13)-C(14)-H(14)	127.7
C(47)-C(46)-P	122.34(18)	N(12)-C(13)-C(14)	112.12(18)
C(46)-C(51)-C(50)	120.2(2)	N(12)-C(13)-C(17)	120.14(19)
C(46)-C(51)-H(51)	119.9	C(14)-C(13)-C(17)	127.72(18)
C(50)-C(51)-H(51)	119.9	F(10)-C(17)-F(11)	106.93(17)
C(49)-C(50)-C(51)	120.0(3)	F(10)-C(17)-C(13)	112.04(17)
C(49)-C(50)-H(50)	120.0	F(11)-C(17)-C(13)	111.49(17)
C(51)-C(50)-H(50)	120.0	F(10)-C(17)-C(18)	106.38(18)
C(48)-C(49)-C(50)	120.1(2)	F(11)-C(17)-C(18)	106.08(17)
C(13)-C(17)-C(18)	113.49(18)	C(23)-C(27)-C(28')	109.5(6)
F(13)-C(18)-F(14)	108.4(2)	C(28)-C(27)-C(28')	30.5(5)
F(13)-C(18)-F(12)	107.98(19)	C(35)-C(36)-H(36A)	109.5
F(14)-C(18)-F(12)	107.80(19)	C(35)-C(36)-H(36B)	109.5
F(13)-C(18)-C(17)	110.31(19)	H(36A)-C(36)-H(36B)	109.5
F(14)-C(18)-C(17)	110.9(2)	C(35)-C(36)-H(36C)	109.5
F(12)-C(18)-C(17)	111.36(19)	H(36A)-C(36)-H(36C)	109.5
N(21)-C(25)-C(24)	107.46(18)	H(36B)-C(36)-H(36C)	109.5
N(21)-C(25)-C(26)	123.49(19)	F(15)-C(37)-F(5)	107.21(17)
C(24)-C(25)-C(26)	129.04(19)	F(15)-C(37)-C(33)	112.47(17)
C(25)-C(26)-H(26A)	109.5	F(5)-C(37)-C(33)	110.75(19)
C(25)-C(26)-H(26B)	109.5	F(15)-C(37)-C(38)	106.8(2)
H(26A)-C(26)-H(26B)	109.5	F(5)-C(37)-C(38)	106.45(18)
C(25)-C(26)-H(26C)	109.5	C(33)-C(37)-C(38)	112.75(18)
H(26A)-C(26)-H(26C)	109.5	F(2)-C(38)-F(3)	108.06(19)
H(26B)-C(26)-H(26C)	109.5	F(2)-C(38)-F(1)	108.1(2)
C(25)-C(24)-C(23)	104.77(18)	F(3)-C(38)-F(1)	108.5(2)
C(25)-C(24)-H(24)	127.6	F(2)-C(38)-C(37)	111.9(2)
C(23)-C(24)-H(24)	127.6	F(3)-C(38)-C(37)	109.8(2)
N(22)-C(23)-C(24)	111.6(2)	F(1)-C(38)-C(37)	110.35(19)
N(22)-C(23)-C(27)	120.86(19)	N(31)-C(35)-C(34)	107.79(19)
C(24)-C(23)-C(27)	127.48(19)	N(31)-C(35)-C(36)	123.35(19)
F(7')-C(27)-F(6')	109.6(7)	C(34)-C(35)-C(36)	128.85(19)
F(7')-C(27)-F(7)	31.6(5)	C(35)-C(34)-C(33)	104.65(18)
F(6')-C(27)-F(7)	132.7(5)	C(35)-C(34)-H(34)	127.7
F(7')-C(27)-F(6)	76.2(6)	C(33)-C(34)-H(34)	127.7

F(6')-C(27)-F(6)	35.9(5)	N(32)-C(33)-C(34)	111.70(19)
F(7)-C(27)-F(6)	105.1(2)	N(32)-C(33)-C(37)	121.07(19)
F(7')-C(27)-C(23)	113.5(6)	C(34)-C(33)-C(37)	127.03(19)
F(6')-C(27)-C(23)	108.0(5)	P-C(52)-H(52A)	109.5
F(7)-C(27)-C(23)	113.31(18)	P-C(52)-H(52B)	109.5
F(6)-C(27)-C(23)	111.4(2)	H(52A)-C(52)-H(52B)	109.5
F(7')-C(27)-C(28)	126.3(6)	P-C(52)-H(52C)	109.5
F(6')-C(27)-C(28)	75.4(5)	H(52A)-C(52)-H(52C)	109.5
F(7)-C(27)-C(28)	105.8(2)	H(52B)-C(52)-H(52C)	109.5
F(6)-C(27)-C(28)	105.4(2)	N(31)-B(1)-N(21)	110.28(17)
C(23)-C(27)-C(28)	115.0(2)	N(31)-B(1)-N(11)	110.57(16)
F(7')-C(27)-C(28')	110.4(8)	N(21)-B(1)-N(11)	110.27(16)
F(6')-C(27)-C(28')	105.5(7)	N(31)-B(1)-H(0)	108.6
F(7)-C(27)-C(28')	81.9(6)	N(21)-B(1)-H(0)	108.6
F(6)-C(27)-C(28')	131.0(6)	N(11)-B(1)-H(0)	108.6

Table I.4 Anisotropic Displacement Parameters ($Å^2 \times 10^3$) for $Tp^{C_2F_5,CH_3}Ag(PMePh_2)^*$

	U^{11}	U^{22}	U^{33}	U^{23}	U^{13}	U^{12}
F(6)	65(2)	48(1)	39(1)	-3(1)	18(1)	-31(1)
F(7)	33(1)	33(1)	62(2)	-7(1)	-19(1)	10(1)
C(28)	26(2)	60(2)	33(2)	-12(2)	5(1)	-1(2)
F(8)	32(1)	56(1)	35(1)	-18(1)	1(1)	-5(1)
F(9)	54(1)	89(2)	71(2)	-44(1)	-15(1)	42(1)
F(32)	81(2)	112(2)	37(1)	-19(1)	31(1)	-56(2)
Ag	15(1)	25(1)	23(1)	6(1)	2(1)	2(1)
P	16(1)	25(1)	22(1)	7(1)	2(1)	0(1)
F(1)	54(1)	38(1)	42(1)	-4(1)	3(1)	0(1)
F(2)	47(1)	78(1)	25(1)	9(1)	2(1)	18(1)
F(3)	41(1)	71(1)	32(1)	5(1)	18(1)	16(1)
F(5)	46(1)	35(1)	47(1)	22(1)	15(1)	6(1)
F(10)	22(1)	51(1)	35(1)	-6(1)	8(1)	-3(1)
F(11)	27(1)	36(1)	58(1)	17(1)	16(1)	12(1)
F(12)	23(1)	55(1)	41(1)	10(1)	16(1)	1(1)
F(13)	43(1)	64(1)	83(1)	51(1)	34(1)	18(1)
F(14)	37(1)	94(1)	30(1)	-7(1)	16(1)	-11(1)
F(15)	24(1)	49(1)	33(1)	16(1)	10(1)	11(1)
N(11)	16(1)	22(1)	20(1)	5(1)	3(1)	1(1)
N(21)	15(1)	25(1)	21(1)	4(1)	4(1)	3(1)
N(22)	17(1)	24(1)	21(1)	2(1)	2(1)	1(1)
N(12)	16(1)	24(1)	22(1)	6(1)	5(1)	2(1)
N(32)	18(1)	22(1)	22(1)	5(1)	5(1)	3(1)
N(31)	16(1)	22(1)	22(1)	3(1)	4(1)	2(1)
C(46)	21(1)	29(1)	32(1)	6(1)	6(1)	-4(1)
C(51)	26(1)	43(1)	44(1)	18(1)	6(1)	-4(1)
C(50)	43(2)	57(2)	59(2)	30(2)	11(1)	-10(1)
C(49)	37(2)	62(2)	63(2)	21(2)	17(1)	-16(1)
C(48)	23(1)	65(2)	61(2)	17(2)	6(1)	-10(1)
C(47)	22(1)	47(1)	48(2)	18(1)	2(1)	-5(1)
C(40)	17(1)	29(1)	28(1)	10(1)	6(1)	2(1)
C(41)	20(1)	35(1)	29(1)	8(1)	5(1)	4(1)
C(42)	29(1)	35(1)	42(1)	0(1)	8(1)	5(1)
C(43)	34(1)	34(1)	54(2)	13(1)	12(1)	12(1)
C(44)	35(1)	47(1)	40(1)	19(1)	1(1)	11(1)

C(45)	29(1)	37(1)	27(1)	7(1)	1(1)	4(1)
C(16)	22(1)	28(1)	27(1)	1(1)	4(1)	-2(1)
C(15)	22(1)	20(1)	22(1)	5(1)	4(1)	0(1)
C(14)	24(1)	22(1)	22(1)	2(1)	7(1)	2(1)
C(13)	21(1)	22(1)	21(1)	7(1)	7(1)	3(1)
C(17)	20(1)	26(1)	25(1)	4(1)	5(1)	3(1)
C(18)	22(1)	44(1)	36(1)	11(1)	11(1)	4(1)
C(25)	22(1)	26(1)	21(1)	7(1)	8(1)	7(1)
C(26)	27(1)	32(1)	26(1)	8(1)	2(1)	8(1)
C(24)	26(1)	22(1)	27(1)	6(1)	9(1)	5(1)
C(23)	20(1)	23(1)	24(1)	4(1)	7(1)	2(1)
C(27)	24(1)	24(1)	32(1)	4(1)	6(1)	3(1)
C(36)	18(1)	43(1)	39(1)	9(1)	9(1)	3(1)
C(37)	25(1)	30(1)	29(1)	12(1)	13(1)	5(1)
C(38)	35(1)	46(1)	27(1)	9(1)	7(1)	9(1)
C(35)	18(1)	25(1)	29(1)	2(1)	10(1)	1(1)
C(34)	23(1)	28(1)	28(1)	5(1)	13(1)	1(1)
C(33)	22(1)	21(1)	24(1)	4(1)	9(1)	3(1)
C(52)	31(1)	33(1)	26(1)	2(1)	5(1)	-1(1)
B(1)	16(1)	24(1)	22(1)	4(1)	3(1)	2(1)

* The anisotropic displacement factor exponent takes the form: $-2\pi^2 [h^2 a^{*2} U^{11} + ... + 2 h k a^* b^* U^{12}]$.

Table I.5 Hydrogen Coordinates ($\times 10^4$) and Isotropic Displacement Parameters ($Å^2 \times 10^3$) for $Tp^{C_2F_5,CH_3}Ag(PMePh_2)$

	x	y	z	U(eq)
H(51)	4114	4543	7128	44
H(50)	5666	5657	6756	62
H(49)	7810	5510	7498	63
H(48)	8408	4267	8607	60
H(47)	6868	3162	8995	48
H(41)	3744	858	7112	33
H(42)	4521	-956	7136	43
H(43)	5979	-1390	8501	48
H(44)	6611	-26	9848	49
H(45)	5829	1785	9837	39
H(16A)	-1960	525	4332	40
H(16B)	-1511	227	3382	40
H(16C)	-2021	1451	3622	40
H(14)	1012	554	3670	27
H(26A)	-2123	4048	4392	43
H(26B)	-2331	5373	4622	43
H(26C)	-2963	4458	5099	43
H(24)	-541	6516	6132	29
H(36A)	-3421	2573	6337	49
H(36B)	-3869	1420	6648	49
H(36C)	-3427	1378	5691	49
H(34)	-2011	839	8077	30
H(52A)	3695	2997	9878	46
H(52B)	3861	4257	9629	46
H(52C)	5084	3555	9985	46
H(0)	-1745	2502	5316	25

APPENDIX J

CRYSTAL STRUCTURE OF HYDROTRIS(3-TRIFLUOROMETHYL-5-METHYLPYRAZOL-1-YL)-BORATO-SILVER(I)-TRIPHENYLPHOSPHINE

Tables J.1 to J.5 list the atomic coordinates and crystallographic parameters for $Tp^{CF_3,CH_3}Ag(PPh_3)$•Tol **[3-11]** (Figure J.1).

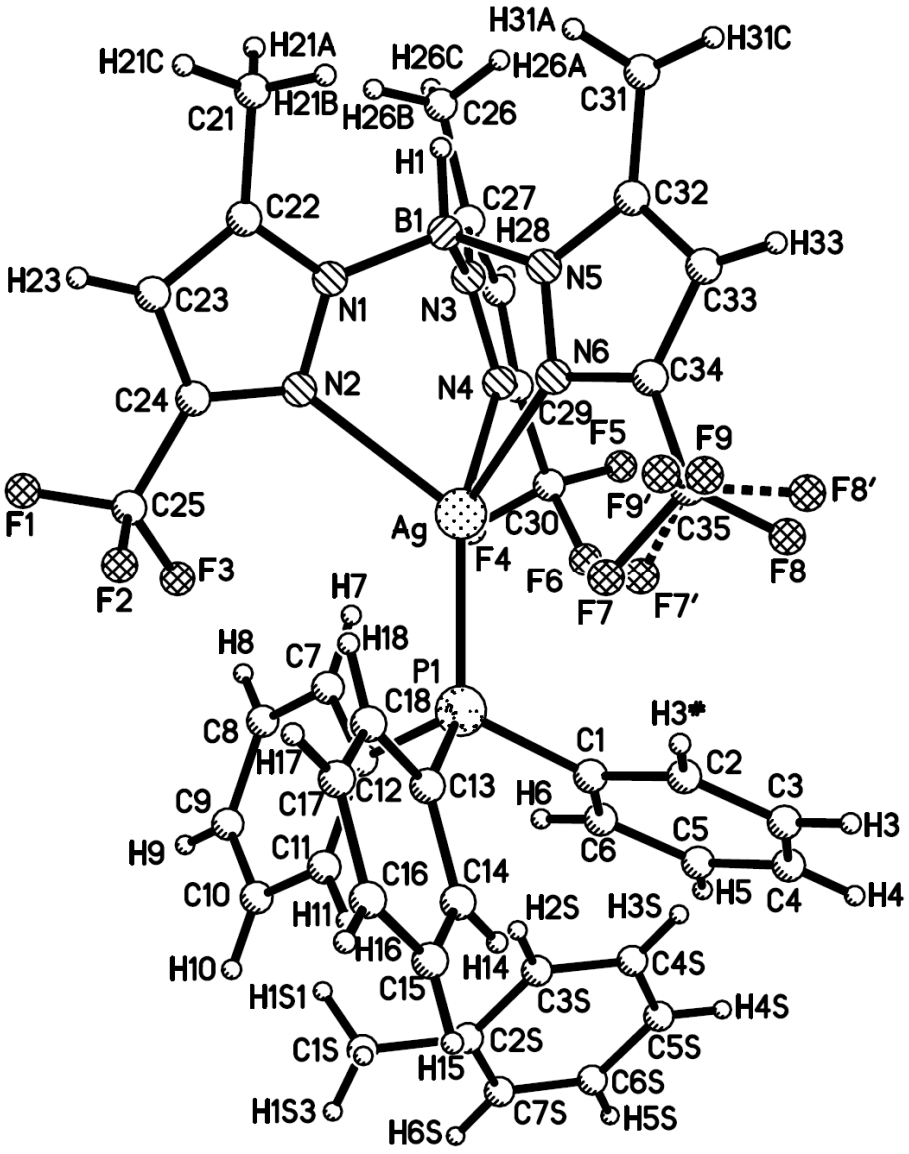

Figure J.1 Crystal structure of $Tp^{CF_3,CH_3}Ag(PPh_3)$•Tol.

Table J.1 Crystal Data and Structure Refinement for $Tp^{CF_3,CH_3}Ag(PPh_3)$•Tol

Empirical formula	$C_{40}\ H_{36}\ Ag\ B\ F_9\ N_6\ P$	
Formula weight	1842.80	
Temperature	173(2) K	
Wavelength	1.54178 Å	
Crystal system	triclinic	
Space group	P-1	
Unit cell dimensions	a = 11.0205(2) Å	α = 95.635(1)°
	b = 11.5728(2) Å	β = 106.430(1)°
	c = 16.5400(3) Å	γ = 92.038(1)°
Volume	2009.13(6) $Å^3$	
Z	1	
Density (calculated)	1.523 g/cm^3	
Absorption coefficient	5.103 mm^{-1}	
F(000)	932	
Crystal size	0.20 × 0.24 × 0.29 mm^3	
Theta range for data collection	3.85 to 67.92°	
Index ranges	$-13 \le h \le 13, -13 \le k \le 13, -18 \le l \le 19$	
Reflections collected	18654	
Independent reflections	6634 [*R*(int) = 0.0277]	
Completeness to theta = 67.92°	90.7%	
Refinement method	Full-matrix least-squares on F^2	
Data / restraints / parameters	6634 / 3 / 556	
Goodness-of-fit on F^2	1.053	
Final *R* indices [*I*>2sigma(*I*)]	*R*1 = 0.0256, *wR*2 = 0.0656	
R indices (all data)	*R*1 = 0.0257, *wR*2 = 0.0657	
Extinction coefficient	0.00055(8)	
Largest diff. peak and hole	0.484 and −0.308 e.$Å^{-3}$	

Table J.2 Atomic Coordinates (× 10^4) and Equivalent Isotropic Displacement Parameters ($Å^2$ × 10^3) for $Tp^{CF_3,CH_3}Ag(PPh_3)$•Tol*

	x	y	z	U(eq)
Ag	9516(1)	7736(1)	2021(1)	20(1)
P(1)	8134(1)	7821(1)	2886(1)	18(1)
F(1)	5859(1)	7863(2)	-742(1)	61(1)
F(2)	6384(1)	9266(1)	241(1)	44(1)
F(3)	6539(1)	7541(1)	558(1)	51(1)
F(7)	10470(5)	10274(8)	3153(4)	42(1)
F(8)	12254(14)	10140(10)	4042(3)	54(2)
F(9)	11974(11)	11535(6)	3273(9)	55(2)
F(7')	10760(20)	9979(19)	3356(17)	70(6)
F(8')	12703(18)	10491(16)	3963(10)	62(4)
F(9')	11630(20)	11445(12)	3025(11)	59(3)
F(4)	9242(1)	3994(1)	2114(1)	39(1)
F(5)	11165(2)	3882(2)	2829(1)	54(1)
F(6)	10184(2)	5409(1)	3022(1)	39(1)
N(1)	10013(2)	7997(1)	221(1)	18(1)

N(2)	8971(2)	7843(1)	499(1)	19(1)
N(3)	11189(1)	6382(1)	995(1)	19(1)
N(4)	10711(2)	6243(1)	1659(1)	19(1)
N(5)	11969(2)	8493(1)	1474(1)	20(1)
N(6)	11317(2)	8928(1)	2006(1)	20(1)
C(1)	8799(2)	7538(2)	3989(1)	21(1)
C(2)	9688(2)	8360(2)	4536(1)	26(1)
C(3)	10240(2)	8170(2)	5372(1)	29(1)
C(4)	9921(2)	7163(2)	5666(1)	31(1)
C(5)	9055(3)	6341(2)	5127(2)	40(1)
C(6)	8492(2)	6530(2)	4290(1)	33(1)
C(7)	6874(2)	5807(2)	1941(1)	28(1)
C(8)	5899(2)	4935(2)	1657(2)	34(1)
C(9)	4806(2)	5028(2)	1908(1)	31(1)
C(10)	4688(2)	5985(2)	2441(2)	32(1)
C(11)	5670(2)	6848(2)	2733(1)	28(1)
C(12)	6771(2)	6758(2)	2484(1)	21(1)
C(13)	7482(2)	9242(2)	2991(1)	21(1)
C(14)	6997(2)	9617(2)	3658(1)	24(1)
C(15)	6527(2)	10713(2)	3705(1)	29(1)
C(16)	6528(2)	11436(2)	3082(2)	32(1)
C(17)	7012(2)	11071(2)	2423(2)	32(1)
C(18)	7494(2)	9981(2)	2379(1)	26(1)
C(21)	10661(2)	8790(2)	-970(1)	26(1)
C(22)	9713(2)	8501(2)	-514(1)	20(1)
C(23)	8434(2)	8670(2)	-728(1)	22(1)
C(24)	8025(2)	8246(2)	-80(1)	20(1)
C(25)	6711(2)	8215(2)	-5(1)	24(1)
C(26)	12161(2)	5242(2)	-5(1)	27(1)
C(27)	11573(2)	5361(2)	706(1)	20(1)
C(28)	11333(2)	4528(2)	1192(1)	22(1)
C(29)	10812(2)	5114(2)	1767(1)	20(1)
C(30)	10362(2)	4617(2)	2437(1)	24(1)
C(31)	14119(2)	8664(2)	1242(2)	34(1)
C(32)	13186(2)	8959(2)	1720(1)	25(1)
C(33)	13328(2)	9728(2)	2436(1)	27(1)
C(34)	12144(2)	9679(2)	2585(1)	24(1)
C(35)	11747(2)	10391(2)	3249(1)	30(1)
B(1)	11324(2)	7594(2)	701(1)	19(1)
C(1S)	4123(3)	3764(2)	3903(2)	46(1)
C(2S)	5180(2)	3359(2)	4586(1)	32(1)
C(3S)	6440(3)	3748(2)	4713(2)	39(1)
C(4S)	7411(2)	3371(2)	5343(2)	44(1)
C(5S)	7149(3)	2597(2)	5861(2)	43(1)
C(6S)	5912(3)	2195(2)	5741(2)	43(1)
C(7S)	4940(2)	2574(2)	5115(2)	36(1)

* U(eq) is defined as one third of the trace of the orthogonalized U^{ij} tensor.

Table J.3 Bond Lengths (Å) and Angles (°) for $Tp^{CF_3,CH_3}Ag(PPh_3)$•Tol

Ag-N(4)	2.341(2)	Ag-N(6)	2.384(2)
Ag-P(1)	2.3642(5)	Ag-N(2)	2.434(2)
F(1)-C(25)	1.328(2)	C(14)-C(15)	1.390(3)
F(2)-C(25)	1.339(2)	C(14)-H(14)	0.9500
F(3)-C(25)	1.320(3)	C(15)-C(16)	1.390(3)
F(7)-C(35)	1.371(7)	C(15)-H(15)	0.9500
F(8)-C(35)	1.338(5)	C(16)-C(17)	1.381(4)
F(9)-C(35)	1.333(7)	C(16)-H(16)	0.9500
F(7')-C(35)	1.239(12)	C(17)-C(18)	1.389(3)
F(8')-C(35)	1.334(8)	C(17)-H(17)	0.9500
F(9')-C(35)	1.309(11)	C(18)-H(18)	0.9500
P(1)-C(1)	1.8297(19)	C(21)-C(22)	1.498(3)
P(1)-C(13)	1.831(2)	C(21)-H(21A)	0.9800
P(1)-C(12)	1.8323(19)	C(21)-H(21B)	0.9800
F(4)-C(30)	1.348(2)	C(21)-H(21C)	0.9800
F(5)-C(30)	1.329(2)	C(22)-C(23)	1.379(3)
F(6)-C(30)	1.327(3)	C(23)-C(24)	1.397(3)
N(1)-C(22)	1.360(2)	C(23)-H(23)	0.9500
N(1)-N(2)	1.365(2)	C(24)-C(25)	1.488(3)
N(1)-B(1)	1.551(3)	C(26)-C(27)	1.493(3)
N(2)-C(24)	1.334(2)	C(26)-H(26A)	0.9800
N(3)-C(27)	1.356(3)	C(26)-H(26B)	0.9800
N(3)-N(4)	1.367(2)	C(26)-H(26C)	0.9800
N(3)-B(1)	1.544(3)	C(27)-C(28)	1.378(3)
N(4)-C(29)	1.341(2)	C(28)-C(29)	1.381(3)
N(5)-N(6)	1.356(2)	C(28)-H(28)	0.9500
N(5)-C(32)	1.361(3)	C(29)-C(30)	1.489(3)
N(5)-B(1)	1.548(3)	C(31)-C(32)	1.493(3)
N(6)-C(34)	1.338(3)	C(31)-H(31A)	0.9800
C(1)-C(6)	1.380(3)	C(31)-H(31B)	0.9800
C(1)-C(2)	1.396(3)	C(31)-H(31C)	0.9800
C(2)-C(3)	1.387(3)	C(32)-C(33)	1.377(3)
C(2)-H(3#)	0.9500	C(33)-C(34)	1.396(3)
C(3)-C(4)	1.377(3)	C(33)-H(33)	0.9500
C(3)-H(3)	0.9500	C(34)-C(35)	1.481(3)
C(4)-C(5)	1.377(3)	B(1)-H(1)	0.9997
C(4)-H(4)	0.9500	C(1S)-C(2S)	1.500(3)
C(5)-C(6)	1.391(3)	C(1S)-H(1S1)	0.9800
C(5)-H(5)	0.9500	C(1S)-H(1S2)	0.9800
C(6)-H(6)	0.9500	C(1S)-H(1S3)	0.9800
C(7)-C(12)	1.379(3)	C(2S)-C(7S)	1.390(3)
C(7)-C(8)	1.392(3)	C(2S)-C(3S)	1.396(4)
C(7)-H(7)	0.9500	C(3S)-C(4S)	1.384(4)
C(8)-C(9)	1.385(3)	C(3S)-H(2S)	0.9500
C(8)-H(8)	0.9500	C(4S)-C(5S)	1.374(4)
C(9)-C(10)	1.381(3)	C(4S)-H(3S)	0.9500
C(9)-H(9)	0.9500	C(5S)-C(6S)	1.378(4)
C(10)-C(11)	1.391(3)	C(5S)-H(4S)	0.9500
C(10)-H(10)	0.9500	C(6S)-C(7S)	1.381(4)
C(11)-C(12)	1.391(3)	C(6S)-H(5S)	0.9500
C(11)-H(11)	0.9500	C(7S)-H(6S)	0.9500
C(13)-C(18)	1.390(3)		
C(13)-C(14)	1.396(3)		

N(4)-Ag-P(1)	131.54(4)	N(4)-Ag-N(2)	81.14(5)
N(4)-Ag-N(6)	82.52(6)	P(1)-Ag-N(2)	127.49(4)
P(1)-Ag-N(6)	133.26(4)	N(6)-Ag-N(2)	81.95(5)
C(1)-P(1)-C(13)	103.01(9)	C(9)-C(10)-H(10)	120.0
C(1)-P(1)-C(12)	103.54(9)	C(11)-C(10)-H(10)	120.0
C(13)-P(1)-C(12)	106.19(9)	C(12)-C(11)-C(10)	120.3(2)
C(1)-P(1)-Ag	116.92(7)	C(12)-C(11)-H(11)	119.8
C(13)-P(1)-Ag	113.55(7)	C(10)-C(11)-H(11)	119.8
C(12)-P(1)-Ag	112.45(7)	C(7)-C(12)-C(11)	119.31(18)
C(22)-N(1)-N(2)	110.84(15)	C(7)-C(12)-P(1)	117.96(15)
C(22)-N(1)-B(1)	127.38(16)	C(11)-C(12)-P(1)	122.67(15)
N(2)-N(1)-B(1)	121.76(15)	C(18)-C(13)-C(14)	119.13(19)
C(24)-N(2)-N(1)	105.04(15)	C(18)-C(13)-P(1)	117.72(16)
C(24)-N(2)-Ag	135.86(13)	C(14)-C(13)-P(1)	123.14(15)
N(1)-N(2)-Ag	112.64(11)	C(15)-C(14)-C(13)	120.2(2)
C(27)-N(3)-N(4)	110.87(15)	C(15)-C(14)-H(14)	119.9
C(27)-N(3)-B(1)	127.98(16)	C(13)-C(14)-H(14)	119.9
N(4)-N(3)-B(1)	121.01(15)	C(14)-C(15)-C(16)	120.0(2)
C(29)-N(4)-N(3)	104.48(16)	C(14)-C(15)-H(15)	120.0
C(29)-N(4)-Ag	136.38(13)	C(16)-C(15)-H(15)	120.0
N(3)-N(4)-Ag	116.38(11)	C(17)-C(16)-C(15)	120.0(2)
N(6)-N(5)-C(32)	111.03(16)	C(17)-C(16)-H(16)	120.0
N(6)-N(5)-B(1)	121.04(15)	C(15)-C(16)-H(16)	120.0
C(32)-N(5)-B(1)	127.92(18)	C(16)-C(17)-C(18)	120.1(2)
C(34)-N(6)-N(5)	105.27(16)	C(16)-C(17)-H(17)	119.9
C(34)-N(6)-Ag	134.05(14)	C(18)-C(17)-H(17)	119.9
N(5)-N(6)-Ag	115.08(11)	C(17)-C(18)-C(13)	120.5(2)
C(6)-C(1)-C(2)	118.93(18)	C(17)-C(18)-H(18)	119.8
C(6)-C(1)-P(1)	122.74(15)	C(13)-C(18)-H(18)	119.8
C(2)-C(1)-P(1)	118.28(15)	C(22)-C(21)-H(21A)	109.5
C(3)-C(2)-C(1)	120.33(19)	C(22)-C(21)-H(21B)	109.5
C(3)-C(2)-H(3#)	119.8	H(21A)-C(21)-H(21B)	109.5
C(1)-C(2)-H(3#)	119.8	C(22)-C(21)-H(21C)	109.5
C(4)-C(3)-C(2)	120.16(19)	H(21A)-C(21)-H(21C)	109.5
C(4)-C(3)-H(3)	119.9	H(21B)-C(21)-H(21C)	109.5
C(2)-C(3)-H(3)	119.9	N(1)-C(22)-C(23)	107.64(17)
C(3)-C(4)-C(5)	119.9(2)	N(1)-C(22)-C(21)	123.35(17)
C(3)-C(4)-H(4)	120.0	C(23)-C(22)-C(21)	129.01(17)
C(5)-C(4)-H(4)	120.0	C(22)-C(23)-C(24)	104.50(16)
C(4)-C(5)-C(6)	120.2(2)	C(22)-C(23)-H(23)	127.8
C(4)-C(5)-H(5)	119.9	C(24)-C(23)-H(23)	127.8
C(6)-C(5)-H(5)	119.9	N(2)-C(24)-C(23)	111.98(17)
C(1)-C(6)-C(5)	120.5(2)	N(2)-C(24)-C(25)	121.29(17)
C(1)-C(6)-H(6)	119.8	C(23)-C(24)-C(25)	126.73(17)
C(5)-C(6)-H(6)	119.8	F(3)-C(25)-F(1)	108.03(18)
C(12)-C(7)-C(8)	120.5(2)	F(3)-C(25)-F(2)	105.37(18)
C(12)-C(7)-H(7)	119.8	F(1)-C(25)-F(2)	105.37(17)
C(8)-C(7)-H(7)	119.8	F(3)-C(25)-C(24)	113.42(16)
C(9)-C(8)-C(7)	120.0(2)	F(1)-C(25)-C(24)	111.82(18)
C(9)-C(8)-H(8)	120.0	F(2)-C(25)-C(24)	112.29(16)
C(7)-C(8)-H(8)	120.0	C(27)-C(26)-H(26A)	109.5
C(10)-C(9)-C(8)	119.88(19)	C(27)-C(26)-H(26B)	109.5
C(10)-C(9)-H(9)	120.1	H(26A)-C(26)-H(26B)	109.5
C(8)-C(9)-H(9)	120.1	C(27)-C(26)-H(26C)	109.5
C(9)-C(10)-C(11)	120.0(2)	H(26A)-C(26)-H(26C)	109.5

H(26B)-C(26)-H(26C)	109.5	F(7')-C(35)-F(7)	23.5(16)
N(3)-C(27)-C(28)	107.55(17)	F(9')-C(35)-F(7)	90.1(8)
N(3)-C(27)-C(26)	123.37(17)	F(9)-C(35)-F(7)	103.3(5)
C(28)-C(27)-C(26)	129.08(18)	F(8')-C(35)-F(7)	128.6(12)
C(27)-C(28)-C(29)	104.82(17)	F(8)-C(35)-F(7)	102.8(6)
C(27)-C(28)-H(28)	127.6	F(7')-C(35)-C(34)	112.4(6)
C(29)-C(28)-H(28)	127.6	F(9')-C(35)-C(34)	107.1(7)
N(4)-C(29)-C(28)	112.27(17)	F(9)-C(35)-C(34)	114.5(4)
N(4)-C(29)-C(30)	120.54(18)	F(8')-C(35)-C(34)	108.0(7)
C(28)-C(29)-C(30)	127.18(18)	F(8)-C(35)-C(34)	115.3(3)
F(6)-C(30)-F(5)	107.92(18)	F(7)-C(35)-C(34)	113.6(4)
F(6)-C(30)-F(4)	105.40(17)	N(3)-B(1)-N(5)	110.03(15)
F(5)-C(30)-F(4)	105.48(17)	N(3)-B(1)-N(1)	111.13(15)
F(6)-C(30)-C(29)	114.11(16)	N(5)-B(1)-N(1)	109.72(16)
F(5)-C(30)-C(29)	111.22(18)	N(3)-B(1)-H(1)	108.5
F(4)-C(30)-C(29)	112.16(16)	N(5)-B(1)-H(1)	108.6
C(32)-C(31)-H(31A)	109.5	N(1)-B(1)-H(1)	108.8
C(32)-C(31)-H(31B)	109.5	C(2S)-C(1S)-H(1S1)	109.5
H(31A)-C(31)-H(31B)	109.5	C(2S)-C(1S)-H(1S2)	109.5
C(32)-C(31)-H(31C)	109.5	H(1S1)-C(1S)-H(1S2)	109.5
H(31A)-C(31)-H(31C)	109.5	C(2S)-C(1S)-H(1S3)	109.5
H(31B)-C(31)-H(31C)	109.5	H(1S1)-C(1S)-H(1S3)	109.5
N(5)-C(32)-C(33)	107.40(19)	H(1S2)-C(1S)-H(1S3)	109.5
N(5)-C(32)-C(31)	123.1(2)	C(7S)-C(2S)-C(3S)	117.4(2)
C(33)-C(32)-C(31)	129.53(19)	C(7S)-C(2S)-C(1S)	121.1(2)
C(32)-C(33)-C(34)	104.80(17)	C(3S)-C(2S)-C(1S)	121.5(2)
C(32)-C(33)-H(33)	127.6	C(4S)-C(3S)-C(2S)	121.2(2)
C(34)-C(33)-H(33)	127.6	C(4S)-C(3S)-H(2S)	119.4
N(6)-C(34)-C(33)	111.50(19)	C(2S)-C(3S)-H(2S)	119.4
N(6)-C(34)-C(35)	121.02(19)	C(5S)-C(4S)-C(3S)	120.3(2)
C(33)-C(34)-C(35)	127.37(18)	C(5S)-C(4S)-H(3S)	119.8
F(7')-C(35)-F(9')	112.0(13)	C(3S)-C(4S)-H(3S)	119.8
F(7')-C(35)-F(9)	121.5(12)	C(4S)-C(5S)-C(6S)	119.3(2)
F(9')-C(35)-F(9)	20.6(7)	C(4S)-C(5S)-H(4S)	120.3
F(7')-C(35)-F(8')	111.5(7)	C(6S)-C(5S)-H(4S)	120.3
F(9')-C(35)-F(8')	105.3(6)	C(5S)-C(6S)-C(7S)	120.6(2)
F(9)-C(35)-F(8')	84.8(6)	C(5S)-C(6S)-H(5S)	119.7
F(7')-C(35)-F(8)	82.9(10)	C(7S)-C(6S)-H(5S)	119.7
F(9')-C(35)-F(8)	124.8(6)	C(6S)-C(7S)-C(2S)	121.2(2)
F(9)-C(35)-F(8)	105.8(4)	C(6S)-C(7S)-H(6S)	119.4
F(8')-C(35)-F(8)	29.4(7)	C(2S)-C(7S)-H(6S)	119.4

Table J.4 Anisotropic Displacement Parameters ($Å^2 \times 10^3$) for $Tp^{CF_3,CH_3}Ag(PPh_3)$•Tol^*

	U^{11}	U^{22}	U^{33}	U^{23}	U^{13}	U^{12}
F(1)	24(1)	107(1)	41(1)	-21(1)	3(1)	-7(1)
F(2)	35(1)	33(1)	73(1)	4(1)	29(1)	11(1)
F(3)	32(1)	60(1)	80(1)	44(1)	31(1)	17(1)
F(7)	31(2)	55(3)	37(2)	-19(2)	12(2)	-5(2)
F(8)	70(5)	68(4)	22(1)	2(2)	7(2)	29(3)
F(9)	83(4)	22(2)	73(5)	-10(2)	50(4)	-17(2)
F(7')	82(9)	60(7)	82(9)	-45(6)	68(8)	-44(6)
F(8')	65(6)	74(6)	30(4)	-21(3)	-7(4)	14(5)
F(9')	104(8)	24(4)	54(6)	3(3)	32(5)	25(5)

Ag	20(1)	22(1)	20(1)	2(1)	11(1)	0(1)
P(1)	19(1)	20(1)	18(1)	1(1)	9(1)	-1(1)
F(4)	41(1)	42(1)	35(1)	4(1)	15(1)	-16(1)
F(5)	51(1)	67(1)	62(1)	49(1)	29(1)	31(1)
F(6)	64(1)	32(1)	28(1)	0(1)	24(1)	-7(1)
N(1)	19(1)	18(1)	19(1)	2(1)	9(1)	2(1)
N(2)	18(1)	20(1)	20(1)	2(1)	8(1)	2(1)
N(3)	18(1)	22(1)	19(1)	5(1)	8(1)	4(1)
N(4)	20(1)	21(1)	19(1)	5(1)	8(1)	2(1)
N(5)	17(1)	20(1)	24(1)	7(1)	8(1)	2(1)
N(6)	20(1)	20(1)	22(1)	3(1)	7(1)	0(1)
C(1)	20(1)	25(1)	20(1)	2(1)	10(1)	2(1)
C(2)	23(1)	27(1)	28(1)	5(1)	7(1)	0(1)
C(3)	24(1)	33(1)	26(1)	1(1)	3(1)	0(1)
C(4)	32(1)	42(1)	21(1)	7(1)	7(1)	2(1)
C(5)	51(1)	37(1)	30(1)	13(1)	9(1)	-11(1)
C(6)	42(1)	31(1)	25(1)	3(1)	6(1)	-11(1)
C(7)	25(1)	30(1)	28(1)	-3(1)	12(1)	-2(1)
C(8)	35(1)	30(1)	35(1)	-8(1)	12(1)	-6(1)
C(9)	27(1)	30(1)	33(1)	3(1)	4(1)	-7(1)
C(10)	24(1)	34(1)	40(1)	5(1)	14(1)	-1(1)
C(11)	28(1)	27(1)	33(1)	-1(1)	14(1)	-2(1)
C(12)	21(1)	23(1)	20(1)	4(1)	7(1)	-1(1)
C(13)	18(1)	20(1)	24(1)	-1(1)	5(1)	-1(1)
C(14)	19(1)	26(1)	25(1)	-2(1)	7(1)	0(1)
C(15)	20(1)	31(1)	31(1)	-8(1)	6(1)	0(1)
C(16)	24(1)	24(1)	43(1)	-1(1)	3(1)	4(1)
C(17)	35(1)	25(1)	34(1)	7(1)	6(1)	2(1)
C(18)	28(1)	26(1)	25(1)	2(1)	9(1)	-1(1)
C(21)	30(1)	27(1)	25(1)	9(1)	13(1)	3(1)
C(22)	26(1)	14(1)	20(1)	4(1)	8(1)	1(1)
C(23)	25(1)	19(1)	21(1)	5(1)	6(1)	4(1)
C(24)	21(1)	17(1)	22(1)	1(1)	6(1)	2(1)
C(25)	22(1)	24(1)	25(1)	4(1)	5(1)	4(1)
C(26)	32(1)	25(1)	27(1)	2(1)	14(1)	7(1)
C(27)	18(1)	21(1)	21(1)	1(1)	5(1)	3(1)
C(28)	22(1)	19(1)	23(1)	2(1)	4(1)	2(1)
C(29)	18(1)	20(1)	21(1)	4(1)	3(1)	1(1)
C(30)	27(1)	22(1)	24(1)	7(1)	8(1)	3(1)
C(31)	18(1)	44(1)	43(1)	14(1)	11(1)	4(1)
C(32)	17(1)	27(1)	31(1)	14(1)	4(1)	2(1)
C(33)	20(1)	28(1)	30(1)	10(1)	0(1)	-4(1)
C(34)	25(1)	21(1)	22(1)	6(1)	3(1)	-3(1)
C(35)	33(1)	24(1)	28(1)	1(1)	4(1)	-5(1)
B(1)	18(1)	21(1)	22(1)	5(1)	10(1)	4(1)
C(1S)	55(2)	40(1)	40(1)	5(1)	7(1)	5(1)
C(2S)	40(1)	24(1)	32(1)	-2(1)	12(1)	3(1)
C(3S)	51(2)	24(1)	45(1)	1(1)	20(1)	-5(1)
C(4S)	35(1)	37(1)	56(2)	-10(1)	10(1)	0(1)
C(5S)	45(1)	44(1)	37(1)	-1(1)	7(1)	17(1)
C(6S)	54(2)	49(1)	37(1)	13(1)	27(1)	21(1)
C(7S)	36(1)	38(1)	42(1)	5(1)	23(1)	8(1)

* The anisotropic displacement factor exponent takes the form: $-2\pi^2 [h^2 a^{*2} U^{11} + ... + 2 h k a^* b^* U^{12}]$.

Table J.5 Hydrogen Coordinates ($\times 10^4$) and Isotropic Displacement Parameters ($Å^2 \times 10^3$) for $Tp^{CF_3,CH_3}Ag(PPh_3)$•Tol

	x	y	z	U(eq)
H(3#)	9915	9054	4335	31
H(3)	10841	8735	5742	35
H(4)	10298	7036	6239	37
H(5)	8842	5642	5328	48
H(6)	7891	5962	3923	40
H(7)	7617	5747	1760	33
H(8)	5984	4277	1291	41
H(9)	4140	4434	1714	37
H(10)	3934	6055	2609	38
H(11)	5589	7502	3105	34
H(14)	6989	9122	4082	28
H(15)	6204	10968	4163	34
H(16)	6196	12180	3110	38
H(17)	7015	11567	1998	38
H(18)	7835	9739	1928	31
H(21A)	10941	8069	-1202	38
H(21B)	11393	9245	-574	38
H(21C)	10270	9245	-1434	38
H(23)	7941	9000	-1208	26
H(26A)	13025	5607	188	40
H(26B)	11656	5624	-480	40
H(26C)	12188	4415	-191	40
H(28)	11492	3726	1141	26
H(31A)	13806	8880	665	50
H(31B)	14230	7826	1218	50
H(31C)	14935	9092	1531	50
H(33)	14069	10189	2757	33
H(1)	11870	7545	310	23
H(1S1)	4131	3379	3350	70
H(1S2)	4237	4608	3909	70
H(1S3)	3310	3568	4004	70
H(2S)	6636	4282	4359	47
H(3S)	8262	3648	5419	53
H(4S)	7815	2342	6297	51
H(5S)	5727	1652	6091	51
H(6S)	4092	2292	5045	43

APPENDIX K

CRYSTAL STRUCTURE OF HYDROTRIS(3-TRIFLUOROMETHYL-5-METHYLPYRAZOL-1-YL)-BORATO-SILVER(I)-TRIPHENYLPHOSPHINE OXIDE

Tables K.1 to K.5 list the atomic coordinates and crystallographic parameters for $Tp^{CF_3,CH_3}Ag(OPPh_3)$•Tol **[3-12]** (Figure K.1).

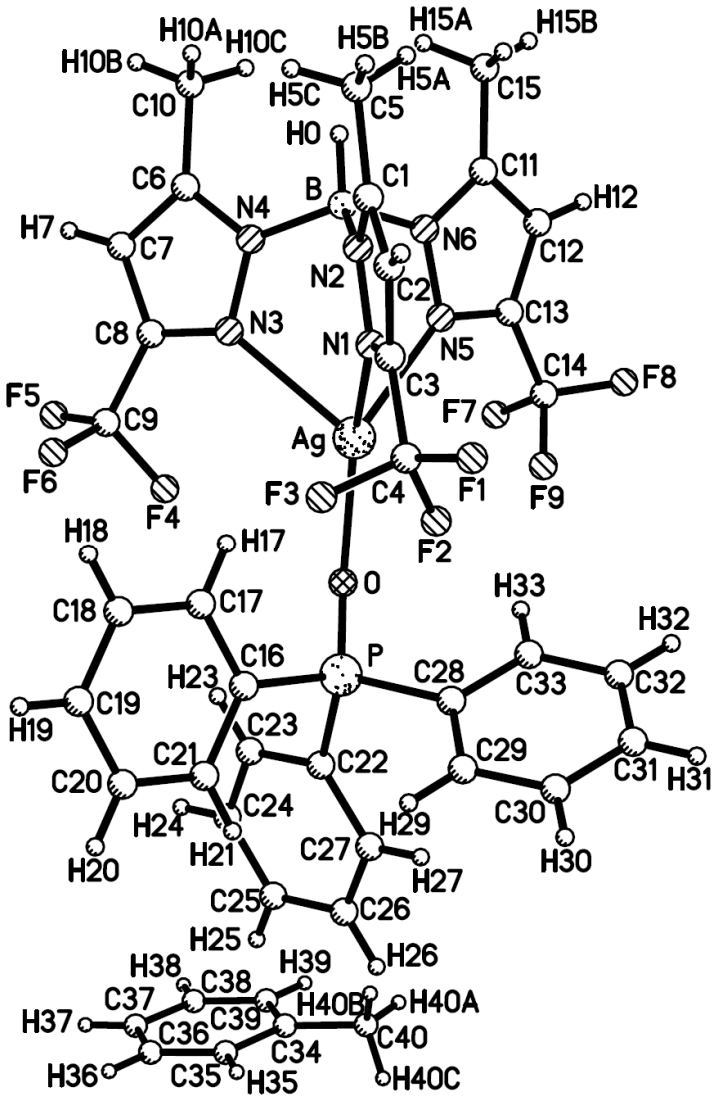

Figure K.1 Crystal structure of $Tp^{CF_3,CH_3}Ag(OPPh_3)$•Tol.

Table K.1 Crystal Data and Structure Refinement for $Tp^{CF_3,CH_3}Ag(OPPh_3)$•Tol

Empirical formula	$C_{40}\ H_{36}\ Ag\ B\ F_9\ N_6\ O\ P$	
Formula weight	937.40	
Temperature	100(2) K	
Wavelength	1.54178 Å	
Crystal system	orthorhombic	
Space group	Pna2(1)	
Unit cell dimensions	a = 15.7204(4) Å	α = 90°
	b = 17.0401(5) Å	β = 90°
	c = 15.1258(4) Å	γ = 90°
Volume	4051.9(2) $Å^3$	
Z	4	
Density (calculated)	1.537 g/cm^3	
Absorption coefficient	5.091 mm^{-1}	
F(000)	1896	
Crystal size	0.50 × 0.27 × 0.24 mm^3	
Theta range for data collection	3.83 to 71.24°	
Index ranges	$-18 \le h \le 18, -20 \le k \le 20, -18 \le l \le 17$	
Reflections collected	35247	
Independent reflections	6445 [*R*(int) = 0.0251]	
Completeness to theta = 71.24°	93.3%	
Max. and min. transmission	0.3698 and 0.1851	
Refinement method	Full-matrix least-squares on F^2	
Data / restraints / parameters	6445 / 1 / 537	
Goodness-of-fit on F^2	1.071	
Final *R* indices [*I*>2sigma(*I*)]	*R*1 = 0.0202, *wR*2 = 0.0538	
R indices (all data)	*R*1 = 0.0204, *wR*2 = 0.0540	
Absolute structure parameter	0.019(4)	
Extinction coefficient	0.00009(2)	
Largest diff. peak and hole	0.568 and −0.324 e.$Å^{-3}$	

Table K.2 Atomic Coordinates (× 10^4) and Equivalent Isotropic Displacement Parameters ($Å^2$ × 10^3) for $Tp^{CF_3,CH_3}Ag(OPPh_3)$•Tol*

	x	y	z	U(eq)
Ag	8584(1)	4203(1)	10027(1)	20(1)
N(1)	9919(1)	3579(1)	9988(2)	18(1)
N(2)	9911(1)	2782(1)	9862(1)	16(1)
N(3)	8311(1)	3293(1)	8845(1)	19(1)
N(4)	8520(1)	2533(1)	9019(1)	18(1)
N(5)	8215(1)	3111(1)	10906(1)	21(1)
N(6)	8556(1)	2405(1)	10688(2)	19(1)
O	8027(1)	5397(1)	10007(1)	21(1)
P	8402(1)	6205(1)	9946(1)	15(1)
B	9072(1)	2301(1)	9826(2)	18(1)
C(1)	10723(1)	2501(1)	9841(2)	23(1)
C(2)	11267(1)	3123(1)	9956(2)	24(1)

C(3)	10739(1)	3771(1)	10049(2)	19(1)
C(4)	10996(1)	4605(1)	10165(2)	23(1)
C(5)	10934(2)	1652(1)	9695(2)	36(1)
C(6)	8141(2)	2043(1)	8424(2)	21(1)
C(7)	7678(2)	2500(2)	7849(2)	26(1)
C(8)	7806(2)	3268(2)	8139(2)	23(1)
C(9)	7485(2)	4009(2)	7740(2)	30(1)
C(10)	8225(2)	1170(1)	8447(2)	32(1)
C(11)	8332(2)	1853(1)	11291(2)	26(1)
C(12)	7834(2)	2204(2)	11918(2)	30(1)
C(13)	7788(2)	2989(2)	11655(2)	27(1)
C(14)	7338(2)	3647(2)	12088(2)	38(1)
C(15)	8621(2)	1013(2)	11248(2)	36(1)
C(16)	9019(1)	6340(1)	8954(2)	18(1)
C(17)	9347(2)	5691(1)	8508(2)	29(1)
C(18)	9778(2)	5791(2)	7718(2)	37(1)
C(19)	9882(2)	6527(2)	7358(2)	32(1)
C(20)	9557(2)	7179(2)	7793(2)	27(1)
C(21)	9124(1)	7090(1)	8583(2)	22(1)
C(22)	7588(1)	6945(1)	9868(2)	17(1)
C(23)	6957(2)	6814(1)	9243(2)	26(1)
C(24)	6338(2)	7381(2)	9094(2)	36(1)
C(25)	6352(2)	8073(2)	9561(2)	34(1)
C(26)	6967(2)	8204(1)	10195(2)	28(1)
C(27)	7591(1)	7640(1)	10353(2)	24(1)
C(28)	9025(2)	6435(1)	10911(2)	20(1)
C(29)	9643(2)	7018(2)	10924(2)	31(1)
C(30)	10066(2)	7180(2)	11709(2)	45(1)
C(31)	9879(2)	6781(2)	12468(2)	43(1)
C(32)	9263(2)	6204(2)	12461(2)	41(1)
C(33)	8836(2)	6026(2)	11681(2)	29(1)
C(34)	271(2)	9408(2)	10421(2)	39(1)
C(35)	715(2)	9668(1)	9690(2)	36(1)
C(36)	345(2)	9685(2)	8861(2)	36(1)
C(37)	-483(2)	9442(1)	8755(2)	33(1)
C(38)	-946(2)	9196(1)	9476(2)	34(1)
C(39)	-572(2)	9175(2)	10298(2)	41(1)
C(40)	687(3)	9383(2)	11308(3)	76(1)
F(1)	11701(1)	4664(1)	10640(2)	53(1)
F(2)	10413(1)	5049(1)	10533(1)	46(1)
F(3)	11185(1)	4949(1)	9386(1)	52(1)
F(4)	7295(1)	4553(1)	8338(1)	40(1)
F(5)	6783(2)	3880(1)	7273(2)	71(1)
F(6)	8043(2)	4335(1)	7199(1)	61(1)
F(7)	6543(2)	3749(2)	11741(2)	79(1)
F(8)	7176(1)	3500(1)	12927(1)	53(1)
F(9)	7715(2)	4315(1)	12014(2)	110(2)

* U(eq) is defined as one third of the trace of the orthogonalized U^{ij} tensor.

Table K.3 Bond Lengths (Å) and Angles (°) for $Tp^{CF_3,CH_3}Ag(OPPh_3)$•Tol

Ag-O	2.2166(12)	Ag-N(5)	2.358(2)
Ag-N(1)	2.3538(14)	Ag-N(3)	2.404(2)
N(1)-C(3)	1.333(2)	C(29)-C(30)	1.390(4)
N(1)-N(2)	1.371(2)	C(30)-C(31)	1.365(5)
N(2)-C(1)	1.362(3)	C(31)-C(32)	1.380(5)
N(2)-B	1.555(3)	C(32)-C(33)	1.391(4)
N(3)-C(8)	1.332(3)	C(34)-C(35)	1.380(4)
N(3)-N(4)	1.362(3)	C(34)-C(39)	1.396(5)
N(4)-C(6)	1.364(3)	C(34)-C(40)	1.494(5)
N(4)-B	1.549(3)	C(35)-C(36)	1.382(4)
N(5)-C(13)	1.333(3)	C(36)-C(37)	1.376(4)
N(5)-N(6)	1.359(3)	C(37)-C(38)	1.377(4)
N(6)-C(11)	1.357(3)	C(38)-C(39)	1.376(5)
N(6)-B	1.545(3)		
O-P	1.4996(13)	O-Ag-N(1)	140.06(5)
P-C(28)	1.800(3)	O-Ag-N(5)	129.40(7)
P-C(22)	1.8001(19)	N(1)-Ag-N(5)	82.96(7)
P-C(16)	1.802(3)	O-Ag-N(3)	120.78(7)
C(1)-C(2)	1.373(3)	N(1)-Ag-N(3)	81.33(7)
C(1)-C(5)	1.501(3)	N(5)-Ag-N(3)	82.36(7)
C(2)-C(3)	1.390(3)	C(3)-N(1)-N(2)	105.20(14)
C(3)-C(4)	1.486(3)	C(3)-N(1)-Ag	138.55(12)
C(4)-F(2)	1.312(3)	N(2)-N(1)-Ag	116.25(11)
C(4)-F(1)	1.324(3)	C(1)-N(2)-N(1)	110.03(15)
C(4)-F(3)	1.349(3)	C(1)-N(2)-B	127.47(16)
C(6)-C(7)	1.376(4)	N(1)-N(2)-B	122.35(15)
C(6)-C(10)	1.494(3)	C(8)-N(3)-N(4)	105.53(19)
C(7)-C(8)	1.394(4)	C(8)-N(3)-Ag	136.31(16)
C(8)-C(9)	1.488(4)	N(4)-N(3)-Ag	115.28(15)
C(9)-F(6)	1.322(4)	N(3)-N(4)-C(6)	110.5(2)
C(9)-F(5)	1.328(3)	N(3)-N(4)-B	121.96(19)
C(9)-F(4)	1.330(3)	C(6)-N(4)-B	127.47(19)
C(14)-F(8)	1.318(3)	C(13)-N(5)-N(6)	105.46(19)
C(14)-F(7)	1.366(4)	C(13)-N(5)-Ag	136.57(16)
C(16)-C(17)	1.394(3)	N(6)-N(5)-Ag	117.70(15)
C(16)-C(21)	1.406(3)	C(11)-N(6)-N(5)	110.4(2)
C(17)-C(18)	1.385(4)	C(11)-N(6)-B	128.6(2)
C(18)-C(19)	1.377(4)	N(5)-N(6)-B	120.89(19)
C(19)-C(20)	1.388(4)	P-O-Ag	133.49(8)
C(20)-C(21)	1.383(3)	O-P-C(28)	111.34(11)
C(22)-C(23)	1.388(3)	O-P-C(22)	111.52(8)
C(22)-C(27)	1.394(3)	C(28)-P-C(22)	106.72(10)
C(23)-C(24)	1.390(3)	O-P-C(16)	112.33(11)
C(24)-C(25)	1.374(4)	C(28)-P-C(16)	110.78(9)
C(25)-C(26)	1.381(4)	C(22)-P-C(16)	103.77(11)
C(26)-C(27)	1.394(3)	N(6)-B-N(4)	109.99(16)
C(28)-C(33)	1.389(4)	N(6)-B-N(2)	110.83(17)
C(28)-C(29)	1.390(4)	N(4)-B-N(2)	111.61(17)
C(11)-C(12)	1.369(4)	N(2)-C(1)-C(2)	108.06(17)
C(11)-C(15)	1.503(4)	N(2)-C(1)-C(5)	123.34(19)
C(12)-C(13)	1.397(4)	C(2)-C(1)-C(5)	128.59(19)
C(13)-C(14)	1.478(4)	C(1)-C(2)-C(3)	104.70(17)
C(14)-F(9)	1.288(3)	N(1)-C(3)-C(2)	112.00(16)

N(1)-C(3)-C(4)	120.36(17)	F(7)-C(14)-C(13)	111.3(3)
C(2)-C(3)-C(4)	127.59(18)	C(17)-C(16)-C(21)	119.0(2)
F(2)-C(4)-F(1)	108.1(2)	C(17)-C(16)-P	120.03(19)
F(2)-C(4)-F(3)	105.9(2)	C(21)-C(16)-P	120.79(18)
F(1)-C(4)-F(3)	104.8(2)	C(18)-C(17)-C(16)	120.0(2)
F(2)-C(4)-C(3)	114.33(18)	C(19)-C(18)-C(17)	120.8(2)
F(1)-C(4)-C(3)	111.35(19)	C(18)-C(19)-C(20)	119.8(3)
F(3)-C(4)-C(3)	111.8(2)	C(21)-C(20)-C(19)	120.2(2)
N(4)-C(6)-C(7)	107.5(2)	C(20)-C(21)-C(16)	120.1(2)
N(4)-C(6)-C(10)	123.7(2)	C(23)-C(22)-C(27)	119.81(19)
C(7)-C(6)-C(10)	128.7(2)	C(23)-C(22)-P	116.17(16)
C(6)-C(7)-C(8)	104.9(2)	C(27)-C(22)-P	123.91(17)
N(3)-C(8)-C(7)	111.6(2)	C(22)-C(23)-C(24)	120.0(2)
N(3)-C(8)-C(9)	120.0(2)	C(25)-C(24)-C(23)	120.1(3)
C(7)-C(8)-C(9)	128.3(2)	C(24)-C(25)-C(26)	120.5(2)
F(6)-C(9)-F(5)	106.9(3)	C(25)-C(26)-C(27)	120.0(2)
F(6)-C(9)-F(4)	106.1(2)	C(22)-C(27)-C(26)	119.6(2)
F(5)-C(9)-F(4)	106.9(2)	C(33)-C(28)-C(29)	119.7(2)
F(6)-C(9)-C(8)	112.5(2)	C(33)-C(28)-P	117.0(2)
F(5)-C(9)-C(8)	110.9(2)	C(29)-C(28)-P	123.2(2)
F(4)-C(9)-C(8)	113.1(2)	C(30)-C(29)-C(28)	119.3(3)
N(6)-C(11)-C(12)	108.1(2)	C(31)-C(30)-C(29)	121.1(3)
N(6)-C(11)-C(15)	123.5(2)	C(30)-C(31)-C(32)	119.9(3)
C(12)-C(11)-C(15)	128.3(2)	C(31)-C(32)-C(33)	120.0(3)
C(11)-C(12)-C(13)	104.5(2)	C(28)-C(33)-C(32)	119.9(3)
N(5)-C(13)-C(12)	111.5(2)	C(35)-C(34)-C(39)	117.7(3)
N(5)-C(13)-C(14)	119.9(2)	C(35)-C(34)-C(40)	120.5(3)
C(12)-C(13)-C(14)	128.6(2)	C(39)-C(34)-C(40)	121.8(3)
F(9)-C(14)-F(8)	109.9(3)	C(34)-C(35)-C(36)	121.3(2)
F(9)-C(14)-F(7)	106.0(3)	C(37)-C(36)-C(35)	119.9(3)
F(8)-C(14)-F(7)	102.6(2)	C(36)-C(37)-C(38)	119.9(3)
F(9)-C(14)-C(13)	114.3(2)	C(39)-C(38)-C(37)	119.9(2)
F(8)-C(14)-C(13)	112.0(2)	C(38)-C(39)-C(34)	121.2(3)

Table K.4 Anisotropic Displacement Parameters ($Å^2 \times 10^3$) for $Tp^{CF_3,CH_3}Ag(OPPh_3)\bullet Tol^*$

	U^{11}	U^{22}	U^{33}	U^{23}	U^{13}	U^{12}
Ag	24(1)	14(1)	22(1)	1(1)	0(1)	4(1)
N(1)	18(1)	16(1)	19(1)	-2(1)	-1(1)	1(1)
N(2)	17(1)	16(1)	15(1)	0(1)	-1(1)	2(1)
N(3)	22(1)	16(1)	19(1)	0(1)	0(1)	3(1)
N(4)	18(1)	16(1)	20(1)	1(1)	1(1)	0(1)
N(5)	22(1)	20(1)	21(1)	2(1)	6(1)	1(1)
N(6)	20(1)	15(1)	20(1)	2(1)	0(1)	1(1)
O	23(1)	14(1)	27(1)	1(1)	0(1)	2(1)
P	17(1)	14(1)	15(1)	0(1)	-1(1)	3(1)
B	19(1)	14(1)	21(2)	0(1)	0(1)	2(1)
C(1)	21(1)	21(1)	27(2)	-2(1)	2(1)	4(1)
C(2)	16(1)	26(1)	31(1)	1(1)	0(1)	1(1)
C(3)	20(1)	20(1)	18(1)	-3(1)	4(1)	-2(1)
C(4)	22(1)	23(1)	24(2)	-3(1)	-1(1)	-3(1)
C(5)	21(1)	24(1)	62(2)	-6(1)	1(1)	7(1)
C(6)	24(1)	19(1)	19(1)	-4(1)	0(1)	-2(1)
C(7)	30(1)	26(1)	23(1)	-1(1)	-5(1)	-3(1)

C(8)	25(1)	26(1)	17(1)	1(1)	-3(1)	1(1)
C(9)	43(2)	24(1)	24(1)	0(1)	-9(1)	6(1)
C(10)	45(2)	20(1)	30(2)	-3(1)	-7(1)	-2(1)
C(11)	29(1)	24(1)	24(1)	6(1)	1(1)	-2(1)
C(12)	36(1)	27(1)	28(2)	10(1)	12(1)	2(1)
C(13)	28(1)	28(1)	25(1)	4(1)	7(1)	2(1)
C(14)	47(2)	33(1)	36(2)	5(1)	22(1)	7(1)
C(15)	48(2)	22(1)	38(2)	13(1)	6(1)	2(1)
C(16)	16(1)	24(1)	15(1)	-1(1)	-1(1)	0(1)
C(17)	35(1)	26(1)	26(1)	-3(1)	6(1)	2(1)
C(18)	44(2)	40(2)	27(2)	-10(1)	10(1)	6(1)
C(19)	26(1)	52(2)	18(1)	-2(1)	3(1)	-4(1)
C(20)	24(1)	36(1)	22(1)	8(1)	-3(1)	-6(1)
C(21)	22(1)	25(1)	20(1)	0(1)	-2(1)	1(1)
C(22)	17(1)	15(1)	18(1)	4(1)	3(1)	2(1)
C(23)	25(1)	22(1)	32(1)	-2(1)	-5(1)	4(1)
C(24)	27(1)	36(1)	46(2)	1(1)	-13(1)	8(1)
C(25)	26(1)	27(1)	49(2)	8(1)	6(1)	13(1)
C(26)	31(1)	20(1)	33(2)	-1(1)	6(1)	7(1)
C(27)	24(1)	22(1)	25(1)	1(1)	3(1)	3(1)
C(28)	21(1)	21(1)	19(1)	-2(1)	-2(1)	10(1)
C(29)	28(1)	40(1)	25(1)	-5(1)	-3(1)	-3(1)
C(30)	33(1)	58(2)	46(2)	-17(2)	-14(1)	-3(1)
C(31)	40(2)	60(2)	28(2)	-17(2)	-18(1)	23(2)
C(32)	59(2)	48(2)	18(1)	1(1)	-2(1)	24(2)
C(33)	36(1)	28(1)	22(1)	1(1)	-1(1)	11(1)
C(34)	54(2)	22(1)	40(2)	-8(1)	-7(1)	-7(1)
C(35)	31(1)	21(1)	56(2)	-7(1)	-6(1)	-2(1)
C(36)	36(1)	28(1)	44(2)	-3(1)	6(1)	-3(1)
C(37)	41(1)	23(1)	35(2)	-2(1)	-6(1)	1(1)
C(38)	33(2)	25(1)	43(2)	-6(1)	3(1)	-2(1)
C(39)	54(2)	32(1)	37(2)	-7(1)	11(1)	-11(1)
C(40)	118(4)	54(2)	56(2)	2(2)	-37(3)	-32(2)
F(1)	44(1)	33(1)	82(2)	-14(1)	-32(1)	-6(1)
F(2)	38(1)	23(1)	76(1)	-16(1)	16(1)	-2(1)
F(3)	87(1)	28(1)	41(1)	1(1)	11(1)	-21(1)
F(4)	56(1)	33(1)	32(1)	-2(1)	-5(1)	20(1)
F(5)	87(1)	41(1)	86(2)	-6(1)	-70(1)	13(1)
F(6)	90(2)	45(1)	49(1)	23(1)	27(1)	22(1)
F(7)	83(2)	92(2)	62(2)	-5(1)	0(1)	59(1)
F(8)	66(1)	55(1)	37(1)	2(1)	25(1)	14(1)
F(9)	150(3)	30(1)	152(3)	-26(1)	124(3)	-18(1)

* The anisotropic displacement factor exponent takes the form: $-2\pi^2 [h^2 a^{*2} U^{11} + ... + 2 h k a^* b^* U^{12}]$.

Table K.5 Hydrogen Coordinates ($\times 10^4$) and Isotropic Displacement Parameters ($Å^2 \times 10^3$) for $Tp^{CF_3,CH_3}Ag(OPPh_3)$•Tol

	x	y	z	U(eq)
H(0)	9223	1733	9768	22
H(2)	11871	3111	9969	29
H(5A)	10695	1337	10178	53
H(5B)	11553	1586	9683	53
H(5C)	10693	1478	9131	53
H(7)	7343	2330	7362	32
H(10A)	8827	1026	8403	48
H(10B)	7911	941	7950	48
H(10C)	7992	970	9004	48
H(12)	7576	1968	12420	36
H(15A)	8463	788	10675	54
H(15B)	8349	713	11723	54
H(15C)	9241	990	11318	54
H(17)	9275	5179	8747	35
H(18)	10004	5347	7420	45
H(19)	10176	6589	6813	39
H(20)	9631	7687	7547	33
H(21)	8898	7537	8875	27
H(23)	6948	6337	8918	32
H(24)	5905	7291	8668	43
H(25)	5935	8463	9447	40
H(26)	6966	8680	10523	33
H(27)	8015	7728	10790	29
H(29)	9774	7303	10401	37
H(30)	10493	7574	11719	54
H(31)	10172	6902	13000	51
H(32)	9130	5929	12989	50
H(33)	8416	5625	11675	34
H(35)	1286	9840	9758	43
H(36)	662	9863	8366	43
H(37)	-735	9445	8184	40
H(38)	-1523	9041	9406	40
H(39)	-893	8997	10791	49
H(40A)	1196	9053	11279	114
H(40B)	289	9164	11742	114
H(40C)	847	9916	11486	114

APPENDIX L

CRYSTAL STRUCTURE OF HYDROTRIS(3-PENTAFLUOROETHYL-5-METHYLPYRAZOL-1-YL)-BORATO-SILVER(I)-TRIPHENYLPHOSPHINE OXIDE

Tables L.1 to L.5 list the atomic coordinates and crystallographic parameters for $Tp^{C_2F_5,CH_3}Ag(OPPh_3)$ **[3-13]** (Figure L.1).

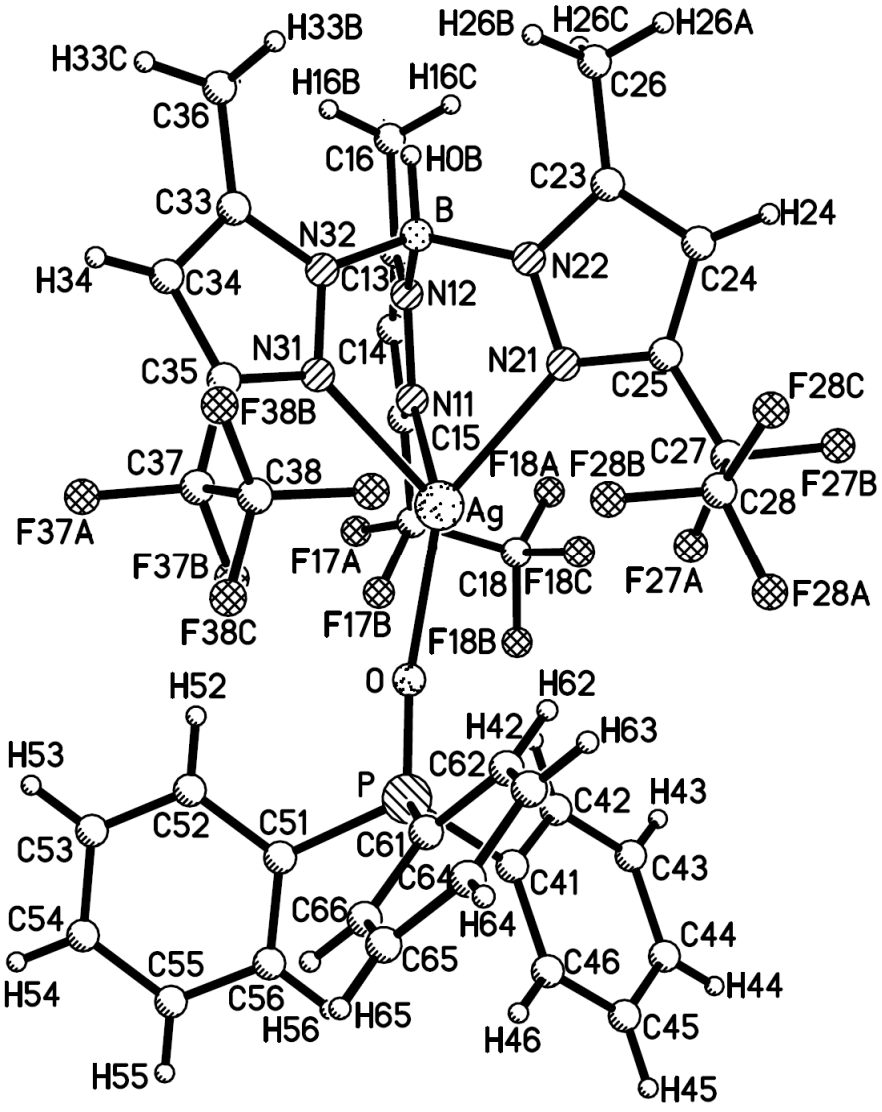

Figure L.1 Crystal structure of $Tp^{C_2F_5,CH_3}Ag(OPPh_3)$.

Table L.1 Crystal Data and Structure Refinement for $Tp^{C_2F_5,CH_3}Ag(OPPh_3)$

Empirical formula	$C_{36}\ H_{28}\ Ag\ B\ F_{15}\ N_6\ O\ P$	
Formula weight	995.29	
Temperature	100(2) K	
Wavelength	1.54178 Å	
Crystal system	monoclinic	
Space group	C2/c	
Unit cell dimensions	a = 20.4765(1) Å	α = 90°
	b = 11.2975(6) Å	β = 97.184(3)°
	c = 34.8025(1) Å	γ = 90°
Volume	7987.8(8) $Å^3$	
Z	8	
Density (calculated)	1.655 g/cm^3	
Absorption coefficient	5.427 mm^{-1}	
F(000)	3968	
Crystal size	0.32 × 0.25 × 0.15 mm^3	
Theta range for data collection	4.35 to 68.29°	
Index ranges	$-24 \le h \le 23, -13 \le k \le 12, -41 \le l \le 41$	
Reflections collected	37831	
Independent reflections	7203 [*R*(int) = 0.0304]	
Completeness to theta = 68.29°	98.5%	
Refinement method	Full-matrix least-squares on F^2	
Data / restraints / parameters	7203 / 0 / 554	
Goodness-of-fit on F^2	1.167	
Final *R* indices [*I*>2sigma(*I*)]	*R*1 = 0.0307, *wR*2 = 0.0764	
R indices (all data)	*R*1 = 0.0312, *wR*2 = 0.0766	
Extinction coefficient	0.000032(7)	
Largest diff. peak and hole	0.550 and −0.472 e.$Å^{-3}$	

Table L.2 Atomic Coordinates (× 10^4) and Equivalent Isotropic Displacement Parameters ($Å^2$ × 10^3) for $Tp^{C_2F_5,CH_3}Ag(OPPh_3)$*

	x	y	z	U(eq)
Ag	3000(1)	5897(1)	8666(1)	21(1)
P	3901(1)	8591(1)	8957(1)	21(1)
O	3436(1)	7642(2)	8804(1)	30(1)
B	2164(1)	3598(2)	8220(1)	21(1)
N(11)	1866(1)	5682(2)	8418(1)	22(1)
N(12)	1669(1)	4630(2)	8252(1)	20(1)
N(21)	2814(1)	3983(2)	8885(1)	21(1)
N(22)	2482(1)	3207(2)	8630(1)	19(1)
N(31)	3160(1)	4807(2)	8101(1)	21(1)
N(32)	2703(1)	3985(2)	7970(1)	21(1)
C(13)	1006(1)	4641(2)	8136(1)	22(1)
C(14)	772(1)	5731(2)	8227(1)	25(1)
C(15)	1320(1)	6339(2)	8402(1)	22(1)
C(16)	637(1)	3603(3)	7952(1)	33(1)
C(17)	1354(1)	7535(2)	8582(1)	27(1)

C(18)	1225(2)	7562(3)	9004(1)	39(1)
C(23)	2474(1)	2110(2)	8789(1)	22(1)
C(24)	2807(1)	2178(2)	9160(1)	23(1)
C(25)	3004(1)	3351(2)	9202(1)	21(1)
C(26)	2164(1)	1057(2)	8583(1)	28(1)
C(27)	3422(1)	3916(2)	9534(1)	26(1)
C(28)	4163(1)	3759(2)	9524(1)	28(1)
C(33)	2804(1)	3597(2)	7611(1)	25(1)
C(34)	3342(1)	4198(2)	7507(1)	26(1)
C(35)	3543(1)	4932(2)	7822(1)	23(1)
C(36)	2405(1)	2634(3)	7400(1)	34(1)
C(37)	4132(1)	5709(2)	7891(1)	26(1)
C(38)	4740(1)	5081(2)	8105(1)	26(1)
C(41)	3681(1)	9174(2)	9406(1)	24(1)
C(42)	3047(1)	8929(2)	9491(1)	31(1)
C(43)	2844(1)	9373(3)	9829(1)	38(1)
C(44)	3267(2)	10048(3)	10080(1)	38(1)
C(45)	3898(1)	10289(3)	9998(1)	34(1)
C(46)	4110(1)	9843(2)	9662(1)	28(1)
C(51)	3902(1)	9796(2)	8617(1)	22(1)
C(52)	3747(1)	9523(3)	8224(1)	34(1)
C(53)	3752(2)	10404(3)	7948(1)	39(1)
C(54)	3905(1)	11549(3)	8057(1)	35(1)
C(55)	4053(1)	11831(2)	8446(1)	31(1)
C(56)	4052(1)	10955(2)	8725(1)	26(1)
C(61)	4738(1)	8077(2)	9055(1)	23(1)
C(62)	4838(1)	6963(3)	9220(1)	35(1)
C(63)	5468(1)	6509(3)	9300(1)	39(1)
C(64)	6000(1)	7164(3)	9218(1)	35(1)
C(65)	5908(1)	8274(3)	9053(1)	33(1)
C(66)	5276(1)	8734(2)	8969(1)	27(1)
F(17A)	902(1)	8262(2)	8385(1)	51(1)
F(17B)	1946(1)	8050(1)	8572(1)	37(1)
F(18A)	634(1)	7129(2)	9038(1)	72(1)
F(18B)	1257(1)	8657(2)	9144(1)	53(1)
F(18C)	1676(1)	6920(2)	9220(1)	56(1)
F(27A)	3314(1)	5105(1)	9544(1)	34(1)
F(27B)	3288(1)	3466(2)	9876(1)	35(1)
F(28A)	4510(1)	4375(2)	9806(1)	41(1)
F(28B)	4333(1)	4138(2)	9189(1)	37(1)
F(28C)	4332(1)	2631(1)	9567(1)	38(1)
F(37A)	4307(1)	6099(1)	7550(1)	34(1)
F(37B)	4026(1)	6670(1)	8106(1)	35(1)
F(38A)	4614(1)	4709(1)	8451(1)	33(1)
F(38B)	4897(1)	4154(1)	7902(1)	34(1)
F(38C)	5258(1)	5797(2)	8160(1)	37(1)

* U(eq) is defined as one third of the trace of the orthogonalized U^{ij} tensor.

Table L.3 Bond Lengths (Å) and Angles (°) for $Tp^{C_2F_5,CH_3}Ag(OPPh_3)$

Ag-O	2.1925(18)	Ag-N(31)	2.377(2)
Ag-N(21)	2.339(2)	Ag-N(11)	2.3875(19)
P-O	1.4883(18)	C(33)-C(36)	1.497(4)
P-C(61)	1.800(2)	C(34)-C(35)	1.395(4)
P-C(51)	1.803(3)	C(34)-H(34)	0.9500
P-C(41)	1.805(3)	C(35)-C(37)	1.488(4)
B-N(32)	1.553(3)	C(36)-H(33B)	0.9800
B-N(22)	1.553(3)	C(36)-H(33C)	0.9800
B-N(12)	1.558(3)	C(36)-H(33A)	0.9800
B-H(0B)	1.0000	C(37)-F(37B)	1.350(3)
N(11)-C(15)	1.336(3)	C(37)-F(37A)	1.356(3)
N(11)-N(12)	1.361(3)	C(37)-C(38)	1.541(3)
N(12)-C(13)	1.366(3)	C(38)-F(38B)	1.324(3)
N(21)-C(25)	1.331(3)	C(38)-F(38A)	1.329(3)
N(21)-N(22)	1.367(3)	C(38)-F(38C)	1.329(3)
N(22)-C(23)	1.359(3)	C(41)-C(42)	1.393(4)
N(31)-C(35)	1.331(3)	C(41)-C(46)	1.394(4)
N(31)-N(32)	1.356(3)	C(42)-C(43)	1.390(4)
N(32)-C(33)	1.363(3)	C(42)-H(42)	0.9500
C(13)-C(14)	1.372(4)	C(43)-C(44)	1.379(5)
C(13)-C(16)	1.495(4)	C(43)-H(43)	0.9500
C(14)-C(15)	1.390(3)	C(44)-C(45)	1.385(4)
C(14)-H(14)	0.9500	C(44)-H(44)	0.9500
C(15)-C(17)	1.487(4)	C(45)-C(46)	1.389(4)
C(16)-H(16B)	0.9800	C(45)-H(45)	0.9500
C(16)-H(16A)	0.9800	C(46)-H(46)	0.9500
C(16)-H(16C)	0.9800	C(51)-C(56)	1.386(4)
C(17)-F(17B)	1.350(3)	C(51)-C(52)	1.398(4)
C(17)-F(17A)	1.356(3)	C(52)-C(53)	1.384(4)
C(17)-C(18)	1.523(4)	C(52)-H(52)	0.9500
C(18)-F(18A)	1.324(3)	C(53)-C(54)	1.373(5)
C(18)-F(18B)	1.329(3)	C(53)-H(53)	0.9500
C(18)-F(18C)	1.331(4)	C(54)-C(55)	1.385(4)
C(23)-C(24)	1.384(3)	C(54)-H(54)	0.9500
C(23)-C(26)	1.489(3)	C(55)-C(56)	1.387(4)
C(24)-C(25)	1.388(4)	C(55)-H(55)	0.9500
C(24)-H(24)	0.9500	C(56)-H(56)	0.9500
C(25)-C(27)	1.493(3)	C(61)-C(62)	1.389(4)
C(26)-H(26C)	0.9800	C(61)-C(66)	1.391(4)
C(26)-H(26A)	0.9800	C(62)-C(63)	1.385(4)
C(26)-H(26B)	0.9800	C(62)-H(62)	0.9500
C(27)-F(27B)	1.354(3)	C(63)-C(64)	1.375(4)
C(27)-F(27A)	1.363(3)	C(63)-H(63)	0.9500
C(27)-C(28)	1.533(4)	C(64)-C(65)	1.382(4)
C(28)-F(28C)	1.324(3)	C(64)-H(64)	0.9500
C(28)-F(28B)	1.329(3)	C(65)-C(66)	1.391(4)
C(28)-F(28A)	1.332(3)	C(65)-H(65)	0.9500
C(33)-C(34)	1.380(4)	C(66)-H(66)	0.9500
O-Ag-N(21)	147.03(7)	N(21)-Ag-N(11)	80.36(7)
O-Ag-N(31)	123.50(7)	N(31)-Ag-N(11)	82.93(7)
N(21)-Ag-N(31)	80.50(7)	O-P-C(61)	112.73(11)
O-Ag-N(11)	121.43(7)	O-P-C(51)	111.24(11)

C(61)-P-C(51)	106.77(11)	N(22)-C(23)-C(24)	107.5(2)
O-P-C(41)	110.73(11)	N(22)-C(23)-C(26)	123.9(2)
C(61)-P-C(41)	106.81(11)	C(24)-C(23)-C(26)	128.6(2)
C(51)-P-C(41)	108.32(11)	C(25)-C(24)-C(23)	104.7(2)
P-O-Ag	162.02(12)	C(25)-C(24)-H(24)	127.7
N(32)-B-N(22)	110.45(18)	C(23)-C(24)-H(24)	127.7
N(32)-B-N(12)	110.1(2)	N(21)-C(25)-C(24)	112.0(2)
N(22)-B-N(12)	110.46(19)	N(21)-C(25)-C(27)	119.5(2)
N(32)-B-H(0B)	108.6	C(24)-C(25)-C(27)	128.4(2)
N(22)-B-H(0B)	108.6	C(23)-C(26)-H(26C)	109.5
N(12)-B-H(0B)	108.6	C(23)-C(26)-H(26A)	109.5
C(15)-N(11)-N(12)	105.39(19)	H(26C)-C(26)-H(26A)	109.5
C(15)-N(11)-Ag	136.83(17)	C(23)-C(26)-H(26B)	109.5
N(12)-N(11)-Ag	117.75(14)	H(26C)-C(26)-H(26B)	109.5
N(11)-N(12)-C(13)	110.39(19)	H(26A)-C(26)-H(26B)	109.5
N(11)-N(12)-B	121.51(18)	F(27B)-C(27)-F(27A)	107.2(2)
C(13)-N(12)-B	128.1(2)	F(27B)-C(27)-C(25)	111.0(2)
C(25)-N(21)-N(22)	105.34(19)	F(27A)-C(27)-C(25)	111.3(2)
C(25)-N(21)-Ag	136.27(16)	F(27B)-C(27)-C(28)	106.7(2)
N(22)-N(21)-Ag	118.04(14)	F(27A)-C(27)-C(28)	106.2(2)
C(23)-N(22)-N(21)	110.48(19)	C(25)-C(27)-C(28)	114.0(2)
C(23)-N(22)-B	127.5(2)	F(28C)-C(28)-F(28B)	108.5(2)
N(21)-N(22)-B	121.99(19)	F(28C)-C(28)-F(28A)	108.2(2)
C(35)-N(31)-N(32)	105.69(19)	F(28B)-C(28)-F(28A)	107.7(2)
C(35)-N(31)-Ag	134.78(17)	F(28C)-C(28)-C(27)	110.7(2)
N(32)-N(31)-Ag	118.22(14)	F(28B)-C(28)-C(27)	110.5(2)
N(31)-N(32)-C(33)	110.6(2)	F(28A)-C(28)-C(27)	111.1(2)
N(31)-N(32)-B	120.82(19)	N(32)-C(33)-C(34)	107.5(2)
C(33)-N(32)-B	128.6(2)	N(32)-C(33)-C(36)	123.2(2)
N(12)-C(13)-C(14)	107.6(2)	C(34)-C(33)-C(36)	129.2(2)
N(12)-C(13)-C(16)	123.3(2)	C(33)-C(34)-C(35)	104.6(2)
C(14)-C(13)-C(16)	129.1(2)	C(33)-C(34)-H(34)	127.7
C(13)-C(14)-C(15)	105.0(2)	C(35)-C(34)-H(34)	127.7
C(13)-C(14)-H(14)	127.5	N(31)-C(35)-C(34)	111.6(2)
C(15)-C(14)-H(14)	127.5	N(31)-C(35)-C(37)	118.9(2)
N(11)-C(15)-C(14)	111.7(2)	C(34)-C(35)-C(37)	129.2(2)
N(11)-C(15)-C(17)	119.5(2)	C(33)-C(36)-H(33B)	109.5
C(14)-C(15)-C(17)	128.7(2)	C(33)-C(36)-H(33C)	109.5
C(13)-C(16)-H(16B)	109.5	H(33B)-C(36)-H(33C)	109.5
C(13)-C(16)-H(16A)	109.5	C(33)-C(36)-H(33A)	109.5
H(16B)-C(16)-H(16A)	109.5	H(33B)-C(36)-H(33A)	109.5
C(13)-C(16)-H(16C)	109.5	H(33C)-C(36)-H(33A)	109.5
H(16B)-C(16)-H(16C)	109.5	F(37B)-C(37)-F(37A)	107.6(2)
H(16A)-C(16)-H(16C)	109.5	F(37B)-C(37)-C(35)	112.4(2)
F(17B)-C(17)-F(17A)	106.5(2)	F(37A)-C(37)-C(35)	110.3(2)
F(17B)-C(17)-C(15)	112.0(2)	F(37B)-C(37)-C(38)	106.2(2)
F(17A)-C(17)-C(15)	110.2(2)	F(37A)-C(37)-C(38)	106.68(19)
F(17B)-C(17)-C(18)	106.3(2)	C(35)-C(37)-C(38)	113.4(2)
F(17A)-C(17)-C(18)	106.6(2)	F(38B)-C(38)-F(38A)	108.7(2)
C(15)-C(17)-C(18)	114.8(2)	F(38B)-C(38)-F(38C)	108.4(2)
F(18A)-C(18)-F(18B)	108.3(2)	F(38A)-C(38)-F(38C)	107.6(2)
F(18A)-C(18)-F(18C)	109.0(3)	F(38B)-C(38)-C(37)	110.0(2)
F(18B)-C(18)-F(18C)	107.6(2)	F(38A)-C(38)-C(37)	110.3(2)
F(18A)-C(18)-C(17)	110.4(2)	F(38C)-C(38)-C(37)	111.8(2)
F(18B)-C(18)-C(17)	111.5(3)	C(42)-C(41)-C(46)	120.0(2)
F(18C)-C(18)-C(17)	110.0(2)	C(42)-C(41)-P	116.9(2)

C(46)-C(41)-P	123.06(19)	C(53)-C(54)-H(54)	120.0
C(43)-C(42)-C(41)	119.6(3)	C(55)-C(54)-H(54)	120.0
C(43)-C(42)-H(42)	120.2	C(56)-C(55)-C(54)	120.0(3)
C(41)-C(42)-H(42)	120.2	C(56)-C(55)-H(55)	120.0
C(44)-C(43)-C(42)	120.2(3)	C(54)-C(55)-H(55)	120.0
C(44)-C(43)-H(43)	119.9	C(55)-C(56)-C(51)	120.3(2)
C(42)-C(43)-H(43)	119.9	C(55)-C(56)-H(56)	119.8
C(43)-C(44)-C(45)	120.4(3)	C(51)-C(56)-H(56)	119.8
C(43)-C(44)-H(44)	119.8	C(62)-C(61)-C(66)	119.4(2)
C(45)-C(44)-H(44)	119.8	C(62)-C(61)-P	117.34(19)
C(44)-C(45)-C(46)	120.0(3)	C(66)-C(61)-P	123.2(2)
C(44)-C(45)-H(45)	120.0	C(63)-C(62)-C(61)	120.4(3)
C(46)-C(45)-H(45)	120.0	C(63)-C(62)-H(62)	119.8
C(45)-C(46)-C(41)	119.7(2)	C(61)-C(62)-H(62)	119.8
C(45)-C(46)-H(46)	120.1	C(64)-C(63)-C(62)	120.0(3)
C(41)-C(46)-H(46)	120.1	C(64)-C(63)-H(63)	120.0
C(56)-C(51)-C(52)	119.2(2)	C(62)-C(63)-H(63)	120.0
C(56)-C(51)-P	123.63(19)	C(63)-C(64)-C(65)	120.3(2)
C(52)-C(51)-P	117.1(2)	C(63)-C(64)-H(64)	119.9
C(53)-C(52)-C(51)	120.0(3)	C(65)-C(64)-H(64)	119.9
C(53)-C(52)-H(52)	120.0	C(64)-C(65)-C(66)	120.1(3)
C(51)-C(52)-H(52)	120.0	C(64)-C(65)-H(65)	120.0
C(54)-C(53)-C(52)	120.5(3)	C(66)-C(65)-H(65)	120.0
C(54)-C(53)-H(53)	119.8	C(61)-C(66)-C(65)	119.8(3)
C(52)-C(53)-H(53)	119.8	C(61)-C(66)-H(66)	120.1
C(53)-C(54)-C(55)	120.0(3)	C(65)-C(66)-H(66)	120.1

Table L.4 Anisotropic Displacement Parameters ($Å^2 \times 10^3$) for $Tp^{C_2F_5,CH_3}Ag(OPPh_3)^*$

	U^{11}	U^{22}	U^{33}	U^{23}	U^{13}	U^{12}
Ag	17(1)	16(1)	30(1)	-3(1)	2(1)	-3(1)
P	17(1)	16(1)	30(1)	-1(1)	3(1)	-2(1)
O	25(1)	19(1)	47(1)	-4(1)	3(1)	-5(1)
B	17(1)	19(1)	27(1)	-2(1)	0(1)	-1(1)
N(11)	17(1)	18(1)	29(1)	-1(1)	1(1)	0(1)
N(12)	15(1)	18(1)	25(1)	-1(1)	0(1)	-1(1)
N(21)	19(1)	18(1)	25(1)	-1(1)	2(1)	-3(1)
N(22)	14(1)	15(1)	28(1)	-2(1)	3(1)	-1(1)
N(31)	17(1)	18(1)	28(1)	-1(1)	4(1)	-1(1)
N(32)	19(1)	19(1)	26(1)	-3(1)	1(1)	1(1)
C(13)	15(1)	26(1)	25(1)	2(1)	0(1)	-2(1)
C(14)	15(1)	28(1)	31(1)	2(1)	0(1)	3(1)
C(15)	18(1)	22(1)	27(1)	4(1)	3(1)	3(1)
C(16)	20(1)	35(2)	43(2)	-7(1)	-4(1)	-5(1)
C(17)	18(1)	22(1)	39(1)	2(1)	-2(1)	7(1)
C(18)	36(2)	34(2)	48(2)	-12(1)	11(1)	-6(1)
C(23)	16(1)	17(1)	32(1)	0(1)	5(1)	-1(1)
C(24)	18(1)	21(1)	30(1)	4(1)	3(1)	2(1)
C(25)	18(1)	20(1)	26(1)	0(1)	3(1)	1(1)
C(26)	26(1)	18(1)	40(1)	0(1)	2(1)	-3(1)
C(27)	29(1)	21(1)	26(1)	0(1)	1(1)	0(1)
C(28)	27(1)	25(1)	31(1)	-5(1)	-4(1)	-6(1)
C(33)	24(1)	25(1)	24(1)	-2(1)	-2(1)	8(1)
C(34)	28(1)	26(1)	25(1)	1(1)	6(1)	8(1)

C(35)	21(1)	20(1)	27(1)	5(1)	5(1)	7(1)
C(36)	33(1)	38(2)	31(1)	-10(1)	-1(1)	3(1)
C(37)	25(1)	22(1)	32(1)	6(1)	12(1)	4(1)
C(38)	22(1)	25(1)	33(1)	3(1)	7(1)	-2(1)
C(41)	23(1)	19(1)	30(1)	3(1)	6(1)	3(1)
C(42)	25(1)	28(1)	41(2)	2(1)	8(1)	-3(1)
C(43)	31(1)	39(2)	48(2)	7(1)	16(1)	2(1)
C(44)	41(2)	44(2)	31(1)	4(1)	14(1)	11(1)
C(45)	35(1)	37(2)	28(1)	-1(1)	1(1)	6(1)
C(46)	24(1)	28(1)	31(1)	1(1)	4(1)	1(1)
C(51)	17(1)	19(1)	30(1)	-1(1)	1(1)	3(1)
C(52)	41(2)	25(1)	34(1)	-5(1)	-4(1)	8(1)
C(53)	46(2)	41(2)	30(1)	2(1)	-1(1)	14(1)
C(54)	28(1)	35(2)	42(2)	13(1)	7(1)	13(1)
C(55)	28(1)	20(1)	46(2)	3(1)	9(1)	1(1)
C(56)	25(1)	23(1)	31(1)	-3(1)	6(1)	-1(1)
C(61)	21(1)	22(1)	25(1)	-1(1)	3(1)	2(1)
C(62)	28(1)	26(1)	51(2)	8(1)	7(1)	3(1)
C(63)	34(2)	35(2)	49(2)	10(1)	8(1)	13(1)
C(64)	25(1)	50(2)	29(1)	1(1)	5(1)	14(1)
C(65)	21(1)	49(2)	30(1)	3(1)	8(1)	-2(1)
C(66)	24(1)	29(1)	30(1)	4(1)	5(1)	-1(1)
F(17A)	50(1)	32(1)	64(1)	-6(1)	-19(1)	24(1)
F(17B)	33(1)	22(1)	57(1)	-4(1)	12(1)	-6(1)
F(18A)	60(1)	84(2)	82(2)	-41(1)	47(1)	-35(1)
F(18B)	55(1)	42(1)	62(1)	-26(1)	14(1)	-4(1)
F(18C)	88(2)	42(1)	34(1)	1(1)	-5(1)	-4(1)
F(27A)	42(1)	22(1)	35(1)	-8(1)	-4(1)	3(1)
F(27B)	39(1)	43(1)	24(1)	3(1)	3(1)	-4(1)
F(28A)	38(1)	40(1)	40(1)	-9(1)	-11(1)	-11(1)
F(28B)	29(1)	46(1)	37(1)	1(1)	5(1)	-12(1)
F(28C)	28(1)	27(1)	54(1)	-2(1)	-8(1)	3(1)
F(37A)	28(1)	36(1)	41(1)	18(1)	14(1)	6(1)
F(37B)	28(1)	20(1)	59(1)	-5(1)	17(1)	-3(1)
F(38A)	30(1)	37(1)	31(1)	8(1)	4(1)	-8(1)
F(38B)	28(1)	33(1)	42(1)	0(1)	3(1)	13(1)
F(38C)	24(1)	37(1)	48(1)	8(1)	5(1)	-9(1)

* The anisotropic displacement factor exponent takes the form: $-2\pi^2 [h^2 a^{*2} U^{11} + ... + 2 h k a^* b^* U^{12}]$.

Table L.5 Hydrogen Coordinates ($\times 10^4$) and Isotropic Displacement Parameters ($Å^2 \times 10^3$) for $Tp^{C_2F_5,CH_3}Ag(OPPh_3)$

	x	y	z	U(eq)
H(0B)	1919	2910	8092	26
H(14)	332	6009	8180	30
H(16B)	796	3424	7705	50
H(16A)	166	3791	7907	50
H(16C)	707	2916	8124	50
H(24)	2884	1559	9345	27
H(26C)	1695	1209	8508	42
H(26A)	2218	367	8754	42
H(26B)	2377	903	8350	42
H(34)	3532	4127	7273	31
H(33B)	2506	1877	7532	51

H(33C)	2512	2585	7134	51
H(33A)	1936	2810	7396	51
H(42)	2756	8462	9319	37
H(43)	2412	9212	9888	46
H(44)	3125	10349	10310	46
H(45)	4186	10758	10170	40
H(46)	4545	9994	9608	33
H(52)	3639	8734	8147	41
H(53)	3648	10216	7682	47
H(54)	3910	12149	7866	42
H(55)	4155	12625	8521	37
H(56)	4155	11150	8991	32
H(62)	4472	6510	9278	42
H(63)	5534	5744	9412	47
H(64)	6432	6852	9275	42
H(65)	6276	8723	8997	40
H(66)	5212	9494	8854	33

APPENDIX M

CRYSTAL STRUCTURE OF 1,2-BIS(TRIFLUOROMETHYL)-4,5-DIMETHYLBENZENE

Tables M.1 to M.5 list the atomic coordinates and crystallographic parameters for 1,2-bis(trifluoromethyl)-4,5-dimethylbenzene **[4-3]** (Figure M.1).

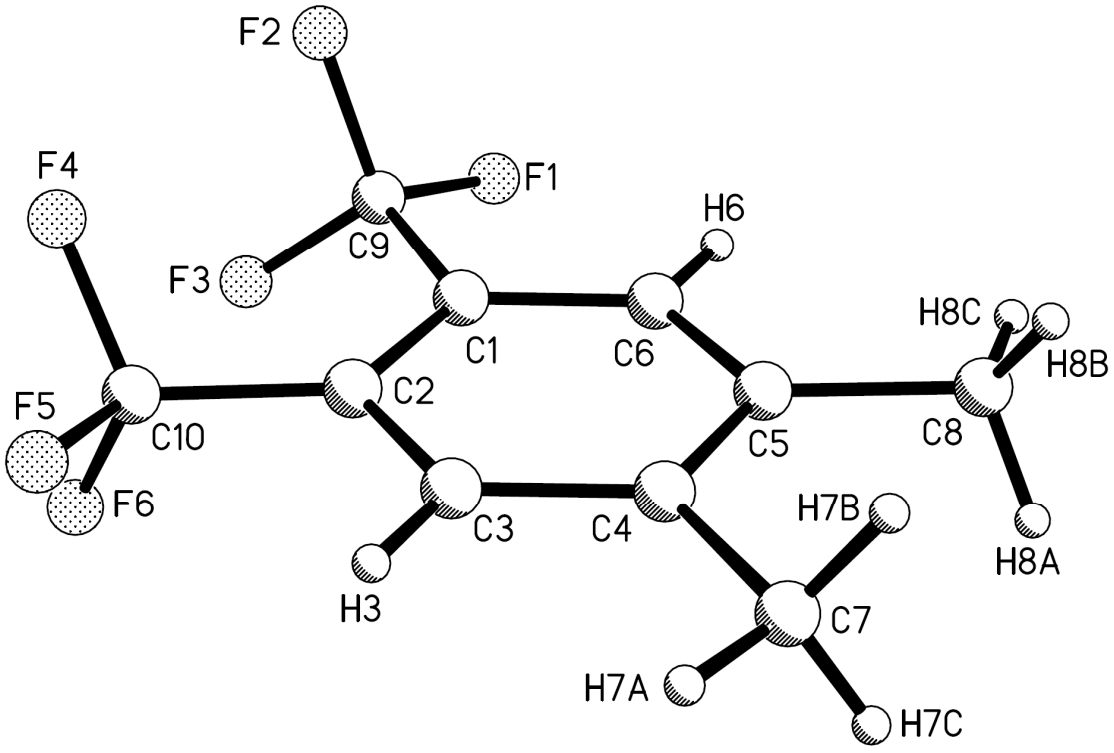

Figure M.1 Crystal structure of 1,2-bis(trifluoromethyl)-4,5-dimethylbenzene.

Table M.1 Crystal Data and Structure Refinement for 1,2-Bis(trifluoromethyl)-4,5-dimethylbenzene

Empirical formula	$C_{10}H_8F_6$	
Formula weight	242.16	
Temperature	100(2) K	
Wavelength	1.54178 Å	
Crystal system	monoclinic	
Space group	P21/c	
Unit cell dimensions	a = 7.4166(3) Å	α = 90°
	b = 9.5676(4) Å	β = 90.908(2)°
	c = 13.7504(5) Å	γ = 90°
Volume	975.59(7) $Å^3$	
Z	4	
Density (calculated)	1.649 g/cm^3	
Absorption coefficient	1.596 mm^{-1}	
F(000)	488	
Crystal size	0.23 × 0.20 × 0.15 mm^3	
Theta range for data collection	5.63 to 73.48°	
Index ranges	$-6 \le h \le 8, -11 \le k \le 11, -16 \le l \le 16$	
Reflections collected	5568	
Independent reflections	1661 [*R*(int) = 0.0271]	
Completeness to theta = 73.48°	84.5%	
Max. and min. transmission	0.7958 and 0.7104	
Refinement method	Full-matrix least-squares on F^2	
Data / restraints / parameters	1661 / 0 / 147	
Goodness-of-fit on F^2	1.026	
Final *R* indices [*I*>2sigma(*I*)]	*R*1 = 0.0549, *wR*2 = 0.1407	
R indices (all data)	*R*1 = 0.0557, *wR*2 = 0.1414	
Largest diff. peak and hole	0.357 and −0.261 e.$Å^{-3}$	

Table M.2 Atomic Coordinates (× 10^4) and Equivalent Isotropic Displacement Parameters ($Å^2$ × 10^3) for 1,2-Bis(trifluoromethyl)-4,5-dimethylbenzene*

	x	y	z	U(eq)
C(3)	2411(3)	-889(3)	8359(2)	22(1)
C(6)	2661(3)	983(3)	9870(2)	23(1)
C(4)	2302(3)	-1382(3)	9306(2)	23(1)
C(2)	2627(3)	521(3)	8145(2)	20(1)
C(1)	2764(3)	1482(3)	8918(2)	21(1)
C(5)	2425(3)	-426(3)	10077(2)	22(1)
C(9)	2926(4)	3061(3)	8782(2)	26(1)
C(10)	2725(4)	942(3)	7089(2)	24(1)
C(8)	2303(4)	-895(3)	11123(2)	29(1)
C(7)	2043(4)	-2922(3)	9490(2)	29(1)
F(6)	4392(2)	1299(2)	6829(1)	30(1)
F(2)	1340(2)	3632(2)	8535(1)	34(1)
F(4)	1657(2)	2046(2)	6883(1)	32(1)
F(3)	4091(2)	3397(2)	8092(1)	32(1)

F(1)	3490(3)	3678(2)	9600(1)	38(1)
F(5)	2203(3)	-87(2)	6493(1)	34(1)

* U(eq) is defined as one third of the trace of the orthogonalized U^{ij} tensor.

Table M.3 Bond Lengths (Å) and Angles (°) for 1,2-Bis(trifluoromethyl)-4,5-dimethyl-benzene

C(3)-C(4)	1.389(4)	C(3)-C(2)-C(1)	118.8(2)
C(3)-C(2)	1.390(4)	C(3)-C(2)-C(10)	118.0(2)
C(6)-C(5)	1.390(4)	C(1)-C(2)-C(10)	123.2(2)
C(6)-C(1)	1.396(4)	C(6)-C(1)-C(2)	118.7(2)
C(4)-C(5)	1.402(4)	C(6)-C(1)-C(9)	117.3(2)
C(4)-C(7)	1.508(4)	C(2)-C(1)-C(9)	123.9(2)
C(2)-C(1)	1.408(4)	C(6)-C(5)-C(4)	119.0(2)
C(2)-C(10)	1.511(4)	C(6)-C(5)-C(8)	119.6(2)
C(1)-C(9)	1.528(4)	C(4)-C(5)-C(8)	121.5(3)
C(5)-C(8)	1.510(4)	F(1)-C(9)-F(3)	107.2(2)
C(9)-F(1)	1.331(3)	F(1)-C(9)-F(2)	107.3(2)
C(9)-F(3)	1.332(3)	F(3)-C(9)-F(2)	107.4(2)
C(9)-F(2)	1.336(3)	F(1)-C(9)-C(1)	111.1(2)
C(10)-F(5)	1.335(3)	F(3)-C(9)-C(1)	112.3(2)
C(10)-F(6)	1.337(3)	F(2)-C(9)-C(1)	111.4(2)
C(10)-F(4)	1.348(3)	F(5)-C(10)-F(6)	106.6(2)
		F(5)-C(10)-F(4)	106.6(2)
C(4)-C(3)-C(2)	122.4(2)	F(6)-C(10)-F(4)	106.7(2)
C(5)-C(6)-C(1)	122.2(2)	F(5)-C(10)-C(2)	112.1(2)
C(3)-C(4)-C(5)	118.9(2)	F(6)-C(10)-C(2)	112.6(2)
C(3)-C(4)-C(7)	119.9(3)	F(4)-C(10)-C(2)	111.9(2)
C(5)-C(4)-C(7)	121.2(3)		

Table M.4 Anisotropic Displacement Parameters ($Å^2 \times 10^3$) for 1,2-Bis(trifluoro-methyl)-4,5-dimethylbenzene*

	U^{11}	U^{22}	U^{33}	U^{23}	U^{13}	U^{12}
C(3)	24(1)	19(1)	24(1)	-3(1)	1(1)	0(1)
C(6)	24(1)	20(1)	25(1)	-3(1)	-2(1)	0(1)
C(4)	21(1)	21(1)	28(1)	2(1)	0(1)	1(1)
C(2)	20(1)	19(1)	22(1)	1(1)	0(1)	0(1)
C(1)	19(1)	20(1)	25(1)	-1(1)	0(1)	-1(1)
C(5)	20(1)	25(1)	23(1)	0(1)	1(1)	2(1)
C(9)	26(1)	26(1)	26(1)	0(1)	-1(1)	2(1)
C(10)	28(1)	19(1)	24(1)	-2(1)	-1(1)	-1(1)
C(8)	30(1)	33(2)	23(1)	4(1)	1(1)	2(1)
C(7)	35(2)	20(1)	34(2)	5(1)	2(1)	0(1)
F(6)	34(1)	31(1)	27(1)	4(1)	7(1)	-4(1)
F(2)	34(1)	19(1)	49(1)	4(1)	-1(1)	6(1)
F(4)	39(1)	28(1)	28(1)	9(1)	-4(1)	4(1)
F(3)	36(1)	20(1)	40(1)	2(1)	6(1)	-6(1)
F(1)	58(1)	22(1)	34(1)	-6(1)	-5(1)	-6(1)
F(5)	50(1)	30(1)	22(1)	-4(1)	-1(1)	-9(1)

* The anisotropic displacement factor exponent takes the form: $-2\pi^2 [h^2 a^{*2} U^{11} + ... + 2 h k a^* b^* U^{12}]$.

Table M.5 Hydrogen Coordinates ($\times 10^4$) and Isotropic Displacement Parameters ($Å^2 \times 10^3$) for 1,2-Bis(trifluoromethyl)-4,5-dimethylbenzene

	x	y	z	U(eq)
H(3)	2336	-1539	7838	27
H(6)	2755	1629	10393	28
H(8A)	3274	-1560	11269	43
H(8B)	1135	-1346	11225	43
H(8C)	2420	-83	11553	43
H(7A)	1958	-3418	8867	44
H(7B)	931	-3067	9852	44
H(7C)	3071	-3283	9869	44

APPENDIX N

CRYSTAL STRUCTURE OF 1,2-BIS(TRIFLUOROMETHYL)-3-NITRO-4,5-DIMETHYLBENZENE

Tables N.1 to N.5 list the atomic coordinates and crystallographic parameters for 1,2-bis(trifluoromethyl)-3-nitro-4,5-dimethylbenzene **[4-7]** (Figure N.1).

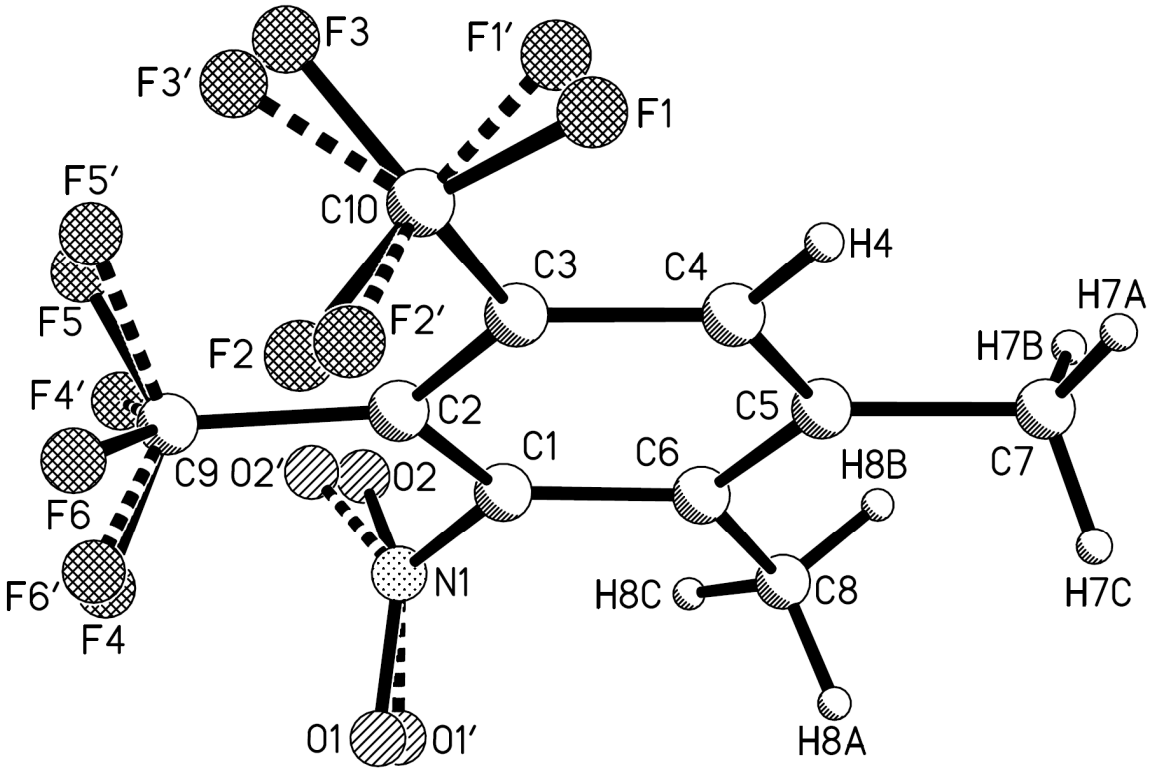

Figure N.1 Crystal structure of 1,2-bis(trifluoromethyl)-3-nitro-4,5-dimethylbenzene.

Table N.1 Crystal Data and Structure Refinement for 1,2-Bis(trifluoromethyl)-3-nitro-4,5-dimethylbenzene

Empirical formula	$C_{10}\,H_7\,F_6\,N\,O_2$	
Formula weight	287.17	
Temperature	100(2) K	
Wavelength	1.54178 Å	
Crystal system	monoclinic	
Space group	P2(1)/n	
Unit cell dimensions	a = 8.86990(10) Å	α = 90°
	b = 9.68820(10) Å	β = 108.895(1)°
	c = 13.63110(10) Å	γ = 90°
Volume	1108.245(19) $Å^3$	
Z	4	
Density (calculated)	1.721 g/cm^3	
Absorption coefficient	1.686 mm^{-1}	
F(000)	576	
Crystal size	0.35 × 0.30 × 0.22 mm^3	
Theta range for data collection	5.28 to 71.22°	
Index ranges	$-10 \le h \le 10, -11 \le k \le 11, -15 \le l \le 16$	
Reflections collected	9011	
Independent reflections	1957 [*R*(int) = 0.0208]	
Completeness to theta = 71.22°	91.0%	
Refinement method	Full-matrix least-squares on F^2	
Data / restraints / parameters	1957 / 22 / 203	
Goodness-of-fit on F^2	1.074	
Final *R* indices [*I*>2sigma(*I*)]	*R*1 = 0.0506, *wR*2 = 0.1310	
R indices (all data)	*R*1 = 0.0573, *wR*2 = 0.1370	
Extinction coefficient	0.0012(6)	
Largest diff. peak and hole	0.297 and −0.371 e.$Å^{-3}$	

Table N.2 Atomic Coordinates (× 10^4) and Equivalent Isotropic Displacement Parameters ($Å^2$ × 10^3) for 1,2-Bis(trifluoromethyl)-3-nitro-4,5-dimethylbenzene*

	x	y	z	U(eq)
C(1)	3748(3)	9237(2)	3206(2)	29(1)
C(2)	2912(3)	9026(2)	3901(2)	28(1)
C(3)	3547(3)	8052(3)	4685(2)	28(1)
C(4)	4934(3)	7359(3)	4733(2)	31(1)
C(5)	5726(3)	7565(3)	4019(2)	31(1)
C(6)	5130(3)	8537(3)	3232(2)	30(1)
C(9)	1362(3)	9789(3)	3769(2)	38(1)
F(4)	578(3)	10125(2)	2760(2)	45(1)
F(5)	252(2)	8983(2)	3992(2)	45(1)
F(6)	1514(3)	10900(2)	4313(2)	47(1)
F(4')	227(7)	9244(6)	3259(5)	43(2)
F(5')	1380(7)	10119(7)	4786(5)	44(2)
F(6')	1590(8)	11138(6)	3449(5)	45(2)
C(10)	2768(3)	7636(2)	5496(2)	36(1)

F(1)	3650(6)	6677(7)	6117(4)	78(2)
F(2)	1321(5)	7138(8)	5021(2)	80(2)
F(3)	2661(9)	8734(4)	6052(4)	96(2)
F(1')	3704(10)	7040(9)	6298(6)	39(2)
F(2')	1538(8)	6811(6)	5166(5)	19(2)
F(3')	2153(7)	8688(6)	5881(4)	25(2)
C(7)	7201(3)	6740(3)	4093(2)	44(1)
C(8)	5935(4)	8794(3)	2428(2)	42(1)
N(1)	3165(3)	10272(2)	2377(2)	37(1)
O(2)	3660(16)	11433(7)	2558(8)	97(3)
O(1)	2341(14)	9836(10)	1552(6)	79(3)
O(1')	2582(14)	9943(14)	1469(9)	36(3)
O(2')	3217(11)	11488(10)	2631(8)	30(3)

* U(eq) is defined as one third of the trace of the orthogonalized U^{ij} tensor.

Table N.3 Bond Lengths (Å) and Angles (°) for 1,2-Bis(trifluoromethyl)-3-nitro-4,5-dimethylbenzene

C(1)-C(6)	1.392(4)	C(3)-C(2)-C(9)	122.9(2)
C(1)-C(2)	1.394(4)	C(4)-C(3)-C(2)	119.7(2)
C(1)-N(1)	1.474(3)	C(4)-C(3)-C(10)	116.0(2)
C(2)-C(3)	1.399(3)	C(2)-C(3)-C(10)	124.3(2)
C(2)-C(9)	1.519(4)	C(3)-C(4)-C(5)	122.8(2)
C(3)-C(4)	1.385(4)	C(4)-C(5)-C(6)	119.0(2)
C(3)-C(10)	1.535(3)	C(4)-C(5)-C(7)	120.1(2)
C(4)-C(5)	1.386(4)	C(6)-C(5)-C(7)	120.9(2)
C(5)-C(6)	1.397(4)	C(1)-C(6)-C(5)	117.3(2)
C(5)-C(7)	1.509(4)	C(1)-C(6)-C(8)	121.4(2)
C(6)-C(8)	1.509(3)	C(5)-C(6)-C(8)	121.3(2)
N(1)-O(1)	1.202(7)	O(1)-N(1)-O(2)	126.2(6)
N(1)-O(2)	1.204(6)	O(1)-N(1)-O(1')	13.8(10)
N(1)-O(1')	1.219(10)	O(2)-N(1)-O(1')	117.3(9)
N(1)-O(2')	1.224(9)	O(1)-N(1)-O(2')	123.9(7)
		O(2)-N(1)-O(2')	20.8(9)
C(6)-C(1)-C(2)	124.7(2)	O(1')-N(1)-O(2')	120.2(9)
C(6)-C(1)-N(1)	116.0(2)	O(1)-N(1)-C(1)	115.8(5)
C(2)-C(1)-N(1)	119.3(2)	O(2)-N(1)-C(1)	117.7(4)
C(1)-C(2)-C(3)	116.5(2)	O(1')-N(1)-C(1)	122.0(7)
C(1)-C(2)-C(9)	120.6(2)	O(2')-N(1)-C(1)	117.8(5)

Table N.4 Anisotropic Displacement Parameters ($Å^2 \times 10^3$) for 1,2-Bis(trifluoromethyl)-3-nitro-4,5-dimethylbenzene*

	U^{11}	U^{22}	U^{33}	U^{23}	U^{13}	U^{12}
C(1)	34(1)	27(1)	25(1)	-1(1)	9(1)	-2(1)
C(2)	29(1)	28(1)	29(1)	-7(1)	10(1)	0(1)
C(3)	31(1)	29(1)	26(1)	-4(1)	11(1)	-4(1)
C(4)	32(1)	29(1)	30(1)	0(1)	8(1)	-1(1)
C(5)	27(1)	30(1)	36(1)	-7(1)	10(1)	-1(1)
C(6)	31(1)	31(1)	30(1)	-8(1)	13(1)	-6(1)
C(9)	40(2)	38(2)	39(1)	-1(1)	15(1)	6(1)
F(4)	34(1)	57(2)	38(1)	2(1)	2(1)	13(1)
F(5)	24(1)	50(1)	63(2)	3(1)	17(1)	0(1)

F(6)	39(1)	41(1)	60(2)	-21(1)	15(1)	7(1)
C(10)	36(2)	43(2)	32(1)	-1(1)	13(1)	-5(1)
F(1)	76(3)	101(5)	75(3)	61(3)	48(3)	36(3)
F(2)	36(2)	158(5)	48(2)	12(2)	18(2)	-16(3)
F(3)	139(5)	90(3)	110(4)	-65(3)	109(4)	-74(3)
C(7)	34(2)	45(2)	52(2)	-8(1)	13(1)	7(1)
C(8)	42(2)	52(2)	39(1)	-8(1)	24(1)	-11(1)
N(1)	42(1)	36(1)	32(1)	3(1)	10(1)	-2(1)
O(2)	111(7)	38(3)	93(4)	25(2)	-35(4)	-25(4)
O(1)	108(6)	57(3)	35(3)	8(2)	-27(3)	-18(3)

* The anisotropic displacement factor exponent takes the form: $-2\pi^2 [h^2 a^{*2} U^{11} + ... + 2 h k a^* b^* U^{12}]$.

Table N.5 Hydrogen Coordinates ($\times 10^4$) and Isotropic Displacement Parameters ($Å^2 \times 10^3$) for 1,2-Bis(trifluoromethyl)-3-nitro-4,5-dimethylbenzene

	x	y	z	U(eq)
H(4)	5362	6715	5278	37
H(7A)	7463	6139	4704	66
H(7B)	8092	7369	4156	66
H(7C)	7006	6174	3468	66
H(8A)	5678	8042	1920	63
H(8B)	7091	8837	2767	63
H(8C)	5558	9671	2075	63

APPENDIX O

CRYSTAL STRUCTURE OF 1,2-BIS(TRIFLUOROMETHYL)-3-FLUORO-4,5-DIMETHYLBENZENE

Tables O.1 to O.5 list the atomic coordinates and crystallographic parameters for 1,2-bis(trifluoromethyl)-3-fluoro-4,5-dimethylbenzene **[4-8]** (Figure O.1).

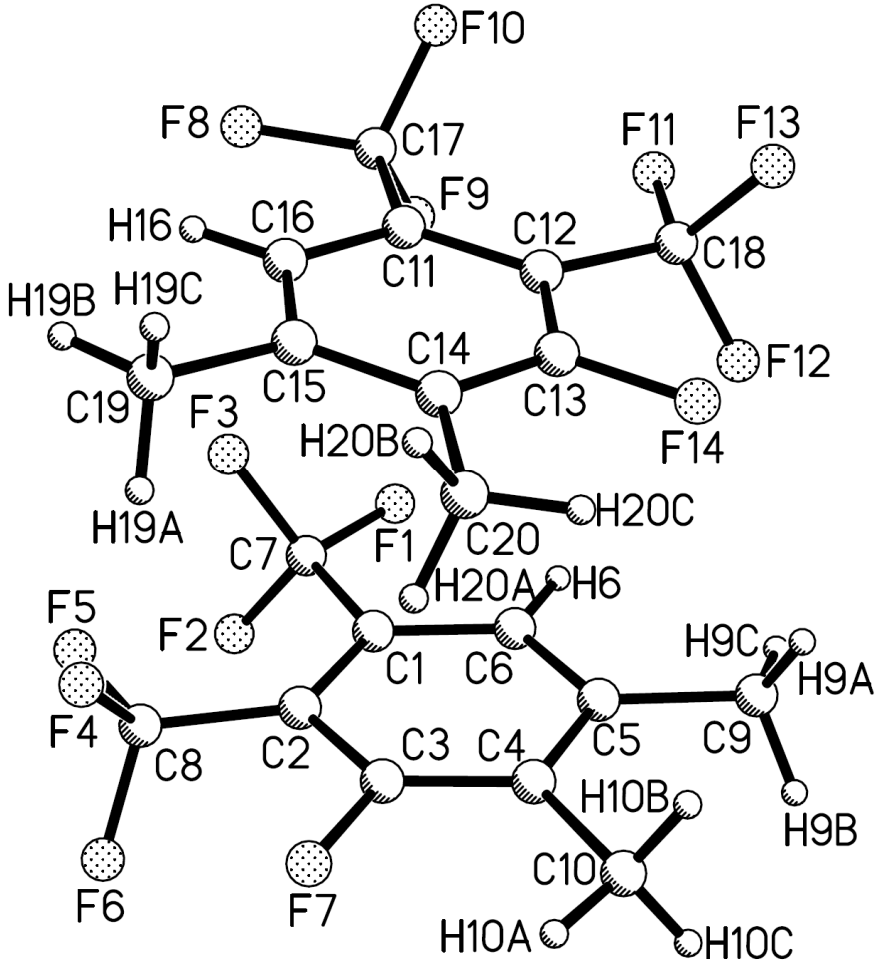

Figure O.1 Crystal structure of 1,2-bis(trifluoromethyl)-3-fluoro-4,5-dimethylbenzene.

Table O.1 Crystal Data and Structure Refinement for 1,2-Bis(trifluoromethyl)-3-fluoro-4,5-dimethylbenzene

Empirical formula	$C_{10}\,H_7\,F_7$	
Formula weight	260.16	
Temperature	100(2) K	
Wavelength	1.54178 Å	
Crystal system	triclinic	
Space group	P-1	
Unit cell dimensions	a = 7.8599(3) Å	α = 88.231(2)°
	b = 9.0897(3) Å	β = 85.687(2)°
	c = 13.9740(5) Å	γ = 84.709(2)°
Volume	991.00(6) $Å^3$	
Z	4	
Density (calculated)	1.744 g/cm^3	
Absorption coefficient	1.772 mm^{-1}	
F(000)	520	
Crystal size	0.40 × 0.35 × 0.35 mm^3	
Theta range for data collection	3.17 to 71.41°	
Index ranges	$-9 \le h \le 9, -11 \le k \le 10, -16 \le l \le 16$	
Reflections collected	9187	
Independent reflections	3276 [*R*(int) = 0.0212]	
Completeness to theta = 71.41°	84.9%	
Absorption correction	SADABS	
Max. and min. transmission	0.5760 and 0.5376	
Refinement method	Full-matrix least-squares on F^2	
Data / restraints / parameters	3276 / 0 / 312	
Goodness-of-fit on F^2	1.108	
Final *R* indices [*I*>2sigma(*I*)]	*R*1 = 0.0513, *wR*2 = 0.1365	
R indices (all data)	*R*1 = 0.0549, *wR*2 = 0.1394	
Extinction coefficient	0.0000(4)	
Largest diff. peak and hole	0.605 and −0.275 e.$Å^{-3}$	

Table O.2 Atomic Coordinates (× 10^4) and Equivalent Isotropic Displacement Parameters ($Å^2$ × 10^3) for 1,2-Bis(trifluoromethyl)-3-fluoro-4,5-dimethylbenzene*

	x	y	z	U(eq)
C(1)	7530(3)	8900(3)	7096(2)	24(1)
C(2)	7843(3)	7925(3)	6329(2)	26(1)
C(3)	8421(3)	6474(3)	6559(2)	27(1)
C(4)	8734(3)	5927(3)	7471(2)	25(1)
C(5)	8417(3)	6925(3)	8222(2)	25(1)
C(6)	7813(3)	8380(3)	8015(2)	25(1)
C(7)	6904(3)	10518(3)	6980(2)	28(1)
C(8)	7643(4)	8298(3)	5281(2)	32(1)
C(9)	8740(4)	6443(3)	9235(2)	33(1)
C(10)	9394(4)	4339(3)	7635(2)	33(1)
C(11)	2524(3)	8786(3)	7968(2)	24(1)
C(12)	3231(3)	7814(3)	8662(2)	24(1)

C(13)	3844(3)	6405(3)	8361(2)	26(1)
C(14)	3788(3)	5894(3)	7444(2)	24(1)
C(15)	3058(3)	6884(3)	6765(2)	25(1)
C(16)	2453(3)	8305(3)	7044(2)	25(1)
C(17)	1832(4)	10369(3)	8169(2)	32(1)
C(18)	3386(4)	8117(3)	9709(2)	31(1)
C(19)	2904(4)	6405(3)	5761(2)	37(1)
C(20)	4488(4)	4347(3)	7192(2)	35(1)
F(1)	6774(2)	11198(2)	7824(1)	38(1)
F(2)	7967(2)	11269(2)	6404(1)	36(1)
F(3)	5351(2)	10727(2)	6641(1)	36(1)
F(4)	6983(3)	9658(2)	5104(1)	54(1)
F(5)	6591(3)	7438(2)	4905(1)	61(1)
F(6)	9115(3)	8115(3)	4772(1)	76(1)
F(7)	8707(2)	5521(2)	5831(1)	40(1)
F(8)	1300(3)	11060(2)	7371(1)	57(1)
F(9)	3005(2)	11181(2)	8476(1)	33(1)
F(10)	501(2)	10460(2)	8818(2)	51(1)
F(11)	2786(3)	9470(2)	9962(1)	51(1)
F(12)	5003(2)	7938(3)	9940(1)	53(1)
F(13)	2511(2)	7210(2)	10278(1)	44(1)
F(14)	4529(2)	5463(2)	9021(1)	39(1)

* U(eq) is defined as one third of the trace of the orthogonalized U^{ij} tensor.

Table O.3 Bond Lengths (Å) and Angles (°) for 1,2-Bis(trifluoromethyl)-3-fluoro-4,5-dimethylbenzene

C(1)-C(6)	1.381(4)	C(15)-C(19)	1.498(4)
C(1)-C(2)	1.405(4)	C(17)-F(10)	1.329(3)
C(1)-C(7)	1.515(3)	C(17)-F(9)	1.335(3)
C(2)-C(3)	1.391(4)	C(17)-F(8)	1.339(3)
C(2)-C(8)	1.509(4)	C(18)-F(11)	1.325(3)
C(3)-F(7)	1.350(3)	C(18)-F(13)	1.329(3)
C(3)-C(4)	1.384(4)	C(18)-F(12)	1.329(3)
C(4)-C(5)	1.401(4)		
C(4)-C(10)	1.505(3)	C(6)-C(1)-C(2)	119.2(2)
C(5)-C(6)	1.392(4)	C(6)-C(1)-C(7)	117.0(2)
C(5)-C(9)	1.502(4)	C(2)-C(1)-C(7)	123.8(2)
C(7)-F(2)	1.335(3)	C(3)-C(2)-C(1)	116.5(2)
C(7)-F(3)	1.338(3)	C(3)-C(2)-C(8)	116.8(2)
C(7)-F(1)	1.341(3)	C(1)-C(2)-C(8)	126.7(2)
C(8)-F(6)	1.312(3)	F(7)-C(3)-C(4)	117.3(2)
C(8)-F(4)	1.320(3)	F(7)-C(3)-C(2)	117.1(2)
C(8)-F(5)	1.334(3)	C(4)-C(3)-C(2)	125.6(2)
C(11)-C(16)	1.383(4)	C(3)-C(4)-C(5)	116.7(2)
C(11)-C(12)	1.403(4)	C(3)-C(4)-C(10)	121.1(2)
C(11)-C(17)	1.518(3)	C(5)-C(4)-C(10)	122.2(2)
C(12)-C(13)	1.392(4)	C(6)-C(5)-C(4)	119.0(2)
C(12)-C(18)	1.513(4)	C(6)-C(5)-C(9)	120.3(2)
C(13)-F(14)	1.347(3)	C(4)-C(5)-C(9)	120.7(2)
C(13)-C(14)	1.381(4)	C(1)-C(6)-C(5)	123.0(2)
C(14)-C(15)	1.405(4)	F(2)-C(7)-F(3)	107.6(2)
C(14)-C(20)	1.505(3)	F(2)-C(7)-F(1)	105.6(2)
C(15)-C(16)	1.392(4)	F(3)-C(7)-F(1)	106.0(2)
F(2)-C(7)-C(1)	112.8(2)	C(13)-C(14)-C(20)	121.0(2)

F(3)-C(7)-C(1)	113.0(2)	C(15)-C(14)-C(20)	122.0(2)
F(1)-C(7)-C(1)	111.2(2)	C(16)-C(15)-C(14)	119.0(2)
F(6)-C(8)-F(4)	107.1(3)	C(16)-C(15)-C(19)	120.6(2)
F(6)-C(8)-F(5)	106.7(3)	C(14)-C(15)-C(19)	120.4(2)
F(4)-C(8)-F(5)	104.5(2)	C(11)-C(16)-C(15)	122.8(2)
F(6)-C(8)-C(2)	111.5(2)	F(10)-C(17)-F(9)	107.3(2)
F(4)-C(8)-C(2)	114.7(2)	F(10)-C(17)-F(8)	106.7(2)
F(5)-C(8)-C(2)	111.8(2)	F(9)-C(17)-F(8)	105.7(2)
C(16)-C(11)-C(12)	119.4(2)	F(10)-C(17)-C(11)	112.8(2)
C(16)-C(11)-C(17)	117.1(2)	F(9)-C(17)-C(11)	113.1(2)
C(12)-C(11)-C(17)	123.5(2)	F(8)-C(17)-C(11)	110.8(2)
C(13)-C(12)-C(11)	116.7(2)	F(11)-C(18)-F(13)	105.7(2)
C(13)-C(12)-C(18)	116.0(2)	F(11)-C(18)-F(12)	106.6(2)
C(11)-C(12)-C(18)	127.3(2)	F(13)-C(18)-F(12)	107.2(2)
F(14)-C(13)-C(14)	117.6(2)	F(11)-C(18)-C(12)	113.8(2)
F(14)-C(13)-C(12)	117.2(2)	F(13)-C(18)-C(12)	111.2(2)
C(14)-C(13)-C(12)	125.2(2)	F(12)-C(18)-C(12)	111.9(2)
C(13)-C(14)-C(15)	117.0(2)		

Table O.4 Anisotropic Displacement Parameters ($Å^2 \times 10^3$) for 1,2-Bis(trifluoromethyl)-3-fluoro-4,5-dimethylbenzene*

	U^{11}	U^{22}	U^{33}	U^{23}	U^{13}	U^{12}
C(1)	20(1)	23(1)	29(1)	1(1)	-1(1)	-5(1)
C(2)	25(1)	28(1)	26(1)	-1(1)	-2(1)	-6(1)
C(3)	27(1)	26(1)	28(1)	-7(1)	0(1)	-5(1)
C(4)	21(1)	21(1)	34(1)	1(1)	-1(1)	-4(1)
C(5)	22(1)	25(1)	28(1)	1(1)	-2(1)	-5(1)
C(6)	26(1)	24(1)	25(1)	-4(1)	0(1)	-4(1)
C(7)	28(1)	26(1)	30(1)	2(1)	-4(1)	-4(1)
C(8)	34(1)	35(2)	28(1)	-1(1)	-2(1)	-3(1)
C(9)	36(2)	32(1)	30(1)	4(1)	-4(1)	-2(1)
C(10)	37(2)	21(1)	41(2)	0(1)	-3(1)	1(1)
C(11)	19(1)	22(1)	30(1)	-2(1)	1(1)	-4(1)
C(12)	25(1)	24(1)	24(1)	-1(1)	1(1)	-7(1)
C(13)	25(1)	26(1)	28(1)	5(1)	-5(1)	-3(1)
C(14)	23(1)	20(1)	31(1)	-3(1)	-1(1)	-3(1)
C(15)	26(1)	24(1)	26(1)	-2(1)	0(1)	-5(1)
C(16)	24(1)	25(1)	26(1)	2(1)	-2(1)	-2(1)
C(17)	30(1)	28(1)	39(2)	-6(1)	-7(1)	1(1)
C(18)	36(2)	29(1)	28(1)	-2(1)	-2(1)	-9(1)
C(19)	45(2)	37(2)	28(2)	-7(1)	-5(1)	1(1)
C(20)	38(2)	24(1)	41(2)	-5(1)	-5(1)	2(1)
F(1)	54(1)	24(1)	35(1)	-5(1)	-8(1)	7(1)
F(2)	37(1)	27(1)	44(1)	9(1)	-1(1)	-6(1)
F(3)	30(1)	31(1)	46(1)	5(1)	-12(1)	2(1)
F(4)	90(2)	39(1)	31(1)	4(1)	-14(1)	7(1)
F(5)	94(2)	56(1)	42(1)	1(1)	-33(1)	-25(1)
F(6)	47(1)	145(2)	30(1)	19(1)	8(1)	16(1)
F(7)	54(1)	32(1)	34(1)	-13(1)	-3(1)	3(1)
F(8)	86(2)	30(1)	56(1)	-8(1)	-36(1)	21(1)
F(9)	40(1)	23(1)	38(1)	-5(1)	-2(1)	-7(1)
F(10)	30(1)	44(1)	78(1)	-30(1)	11(1)	-1(1)
F(11)	93(2)	31(1)	28(1)	-7(1)	1(1)	-2(1)

F(12)	44(1)	84(2)	35(1)	-12(1)	-12(1)	-14(1)
F(13)	63(1)	46(1)	25(1)	4(1)	0(1)	-22(1)
F(14)	54(1)	29(1)	35(1)	5(1)	-15(1)	1(1)

* The anisotropic displacement factor exponent takes the form: $-2\pi^2 [h^2 a^{*2} U^{11} + ... + 2 h k a^* b^* U^{12}]$.

Table O.5 Hydrogen Coordinates ($\times 10^4$) and Isotropic Displacement Parameters ($Å^2 \times 10^3$) for 1,2-Bis(trifluoromethyl)-3-fluoro-4,5-dimethylbenzene

	x	y	z	U(eq)
H(6)	7585	9046	8529	30
H(9A)	8612	7307	9645	49
H(9B)	9905	5961	9252	49
H(9C)	7914	5746	9468	49
H(10A)	9590	3846	7018	49
H(10B)	8549	3840	8047	49
H(10C)	10473	4298	7948	49
H(16)	1970	8973	6580	30
H(19A)	4041	6063	5472	55
H(19B)	2415	7241	5380	55
H(19C)	2157	5599	5774	55
H(20A)	5498	4383	6739	52
H(20B)	3610	3850	6898	52
H(20C)	4810	3799	7776	52

APPENDIX P

CRYSTAL STRUCTURE OF 4,5-BIS(TRIFLUOROMETHYL)-3-FLUOROPHTHALIC ACID

Tables P.1 to P.5 list the atomic coordinates and crystallographic parameters for 4,5-bis(trifluoromethyl)-3-fluorophthalic acid **[4-9]** (Figure P.1).

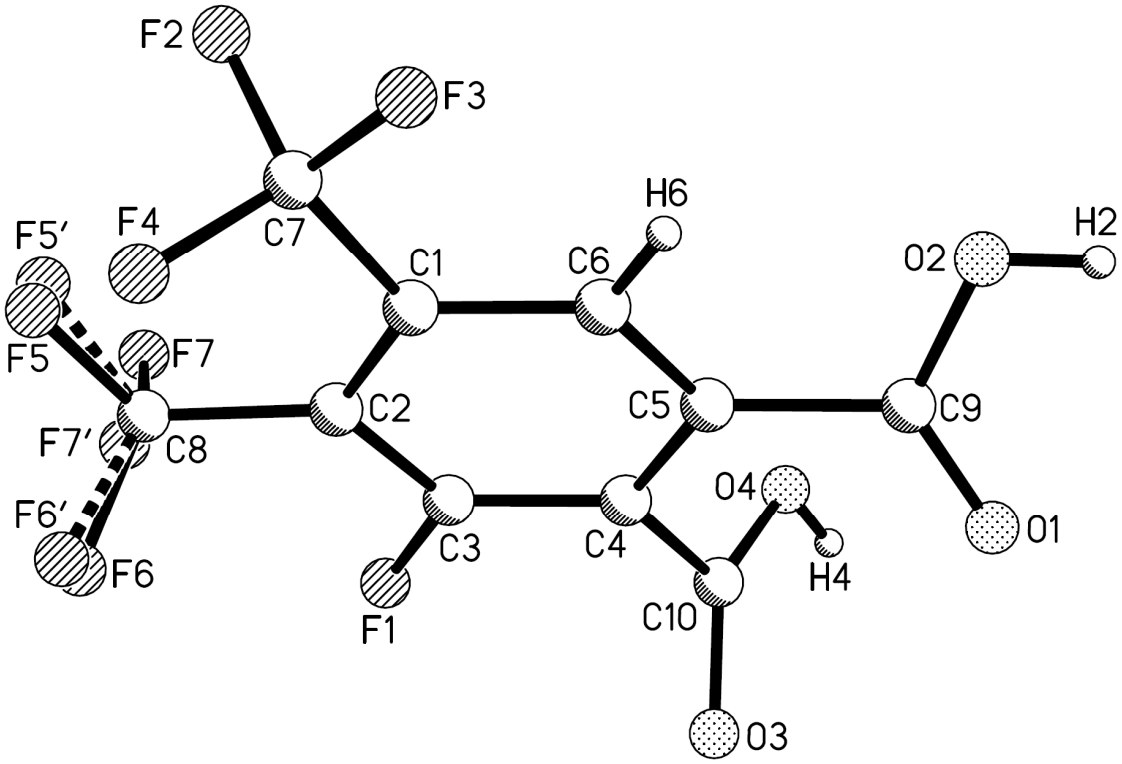

Figure P.1 Crystal structure of 4,5-bis(trifluoromethyl)-3-fluorophthalic acid.

Table P.1 Crystal Data and Structure Refinement for 4,5-Bis(trifluoromethyl)-3-fluorophthalic Acid

Empirical formula	$C_{10}\,H_3\,F_7\,O_4$	
Formula weight	320.12	
Temperature	100(2) K	
Wavelength	1.54178 Å	
Crystal system	monoclinic	
Space group	C2/c	
Unit cell dimensions	a = 12.0233(2) Å	α = 90°
	b = 14.4173(3) Å	β = 106.340(1)°
	c = 13.2233(3) Å	γ = 90°
Volume	2199.59(8) $Å^3$	
Z	8	
Density (calculated)	1.933 g/cm^3	
Absorption coefficient	2.038 mm^{-1}	
F(000)	1264	
Crystal size	0.48 × 0.43 × 0.14 mm^3	
Theta range for data collection	4.91 to 67.21°	
Index ranges	$-14 \le h \le 14, -16 \le k \le 17, -15 \le l \le 15$	
Reflections collected	9633	
Independent reflections	1894 [*R*(int) = 0.0188]	
Completeness to theta = 67.21°	96.1%	
Absorption correction	SADABS	
Max. and min. transmission	0.7635 and 0.4413	
Refinement method	Full-matrix least-squares on F^2	
Data / restraints / parameters	1894 / 91 / 221	
Goodness-of-fit on F^2	1.071	
Final *R* indices [*I*>2sigma(*I*)]	*R*1 = 0.0561, *wR*2 = 0.1635	
R indices (all data)	*R*1 = 0.0575, *wR*2 = 0.1649	
Extinction coefficient	0.00000(17)	
Largest diff. peak and hole	0.567 and −0.451 e.$Å^{-3}$	

Table P.2 Atomic Coordinates (× 10^4) and Equivalent Isotropic Displacement Parameters ($Å^2$ × 10^3) for 4,5-Bis(trifluoromethyl)-3-fluorophthalic Acid*

	x	y	z	U(eq)
F(1)	1451(2)	643(1)	-159(2)	52(1)
C(5)	878(2)	2834(2)	862(2)	24(1)
C(3)	1374(2)	1290(2)	537(2)	30(1)
C(6)	1190(2)	2633(2)	1932(2)	26(1)
C(10)	573(2)	2291(2)	-1029(2)	29(1)
C(4)	969(2)	2153(2)	138(2)	26(1)
C(2)	1660(2)	1057(2)	1590(2)	31(1)
C(1)	1579(2)	1761(2)	2312(2)	29(1)
C(7)	1848(3)	1612(2)	3495(2)	40(1)
F(2)	1074(2)	1058(1)	3743(1)	47(1)
F(3)	1803(2)	2416(1)	3985(1)	57(1)
F(4)	2890(2)	1240(2)	3911(2)	61(1)

O(4)	-514(2)	2363(2)	-1443(2)	47(1)
C(8)	2014(3)	59(2)	1876(3)	47(1)
F(5)	2180(16)	-142(15)	2867(7)	64(3)
F(6)	2901(8)	-191(6)	1598(8)	55(2)
F(7)	1110(6)	-472(5)	1362(9)	87(3)
O(3)	1323(2)	2298(2)	-1496(2)	49(1)
C(9)	489(2)	3787(2)	480(2)	24(1)
O(1)	611(2)	4086(1)	-342(1)	32(1)
O(2)	26(2)	4243(1)	1112(2)	35(1)
F(7')	1600(20)	-545(6)	1137(8)	142(8)
F(6')	3177(11)	-9(12)	2026(16)	90(4)
F(5')	1881(18)	-234(19)	2756(10)	72(4)

* U(eq) is defined as one third of the trace of the orthogonalized U^{ij} tensor.

Table P.3 Bond Lengths (Å) and Angles (°) for 4,5-Bis(trifluoromethyl)-3-fluoro-phthalic Acid

F(1)-C(3)	1.331(3)	C(5)-C(4)-C(10)	123.4(2)
C(5)-C(6)	1.389(4)	C(3)-C(2)-C(1)	117.5(2)
C(5)-C(4)	1.396(4)	C(3)-C(2)-C(8)	117.1(2)
C(5)-C(9)	1.494(3)	C(1)-C(2)-C(8)	125.4(3)
C(3)-C(2)	1.379(4)	C(6)-C(1)-C(2)	119.1(2)
C(3)-C(4)	1.386(4)	C(6)-C(1)-C(7)	116.9(2)
C(6)-C(1)	1.385(4)	C(2)-C(1)-C(7)	123.9(2)
C(10)-O(3)	1.227(4)	F(4)-C(7)-F(2)	107.3(2)
C(10)-O(4)	1.272(4)	F(4)-C(7)-F(3)	108.1(3)
C(10)-C(4)	1.494(4)	F(2)-C(7)-F(3)	105.9(3)
C(2)-C(1)	1.415(4)	F(4)-C(7)-C(1)	112.6(2)
C(2)-C(8)	1.518(4)	F(2)-C(7)-C(1)	112.1(2)
C(1)-C(7)	1.522(4)	F(3)-C(7)-C(1)	110.5(2)
C(7)-F(4)	1.331(3)	F(6)-C(8)-F(5')	119.6(12)
C(7)-F(2)	1.335(4)	F(6)-C(8)-F(7')	76.8(11)
C(7)-F(3)	1.336(4)	F(5')-C(8)-F(7')	109.8(11)
C(8)-F(6)	1.273(7)	F(6)-C(8)-F(5)	108.9(9)
C(8)-F(5')	1.289(11)	F(5')-C(8)-F(5)	16.5(14)
C(8)-F(7')	1.300(8)	F(7')-C(8)-F(5)	121.6(12)
C(8)-F(5)	1.302(9)	F(6)-C(8)-F(7)	108.4(5)
C(8)-F(7)	1.348(7)	F(5')-C(8)-F(7)	89.0(11)
C(8)-F(6')	1.360(10)	F(7')-C(8)-F(7)	32.1(11)
C(9)-O(1)	1.216(3)	F(5)-C(8)-F(7)	104.8(8)
C(9)-O(2)	1.304(3)	F(6)-C(8)-F(6')	27.3(7)
		F(5')-C(8)-F(6')	103.2(9)
C(6)-C(5)-C(4)	120.1(2)	F(7')-C(8)-F(6')	103.1(7)
C(6)-C(5)-C(9)	120.4(2)	F(5)-C(8)-F(6')	88.7(10)
C(4)-C(5)-C(9)	119.5(2)	F(7)-C(8)-F(6')	133.1(8)
F(1)-C(3)-C(2)	118.8(2)	F(6)-C(8)-C(2)	113.3(4)
F(1)-C(3)-C(4)	116.8(2)	F(5')-C(8)-C(2)	116.0(13)
C(2)-C(3)-C(4)	124.3(2)	F(7')-C(8)-C(2)	115.2(5)
C(1)-C(6)-C(5)	121.7(2)	F(5)-C(8)-C(2)	114.5(10)
O(3)-C(10)-O(4)	126.4(3)	F(7)-C(8)-C(2)	106.4(4)
O(3)-C(10)-C(4)	117.1(2)	F(6')-C(8)-C(2)	108.1(6)
O(4)-C(10)-C(4)	116.5(2)	O(1)-C(9)-O(2)	125.1(2)
C(3)-C(4)-C(5)	117.2(2)	O(1)-C(9)-C(5)	121.6(2)
C(3)-C(4)-C(10)	119.2(2)	O(2)-C(9)-C(5)	113.4(2)

Table P.4 Anisotropic Displacement Parameters ($Å^2 \times 10^3$) for 4,5-Bis(trifluoromethyl)-3-fluorophthalic Acid*

	U^{11}	U^{22}	U^{33}	U^{23}	U^{13}	U^{12}
F(1)	81(1)	28(1)	43(1)	-8(1)	10(1)	11(1)
C(5)	28(1)	17(1)	24(1)	1(1)	4(1)	0(1)
C(3)	38(1)	17(1)	32(1)	-2(1)	7(1)	2(1)
C(6)	30(1)	23(1)	24(1)	-1(1)	5(1)	-1(1)
C(10)	39(1)	20(1)	26(1)	-2(1)	4(1)	-1(1)
C(4)	31(1)	19(1)	27(1)	1(1)	5(1)	-1(1)
C(2)	33(1)	20(1)	37(2)	6(1)	6(1)	3(1)
C(1)	29(1)	29(1)	28(1)	7(1)	5(1)	2(1)
C(7)	40(2)	43(2)	32(2)	7(1)	0(1)	9(1)
F(2)	52(1)	52(1)	40(1)	21(1)	20(1)	10(1)
F(3)	83(2)	53(1)	24(1)	0(1)	-1(1)	4(1)
F(4)	43(1)	87(2)	45(1)	29(1)	2(1)	18(1)
O(4)	49(1)	53(1)	36(1)	-2(1)	8(1)	6(1)
C(8)	67(2)	29(2)	45(2)	13(1)	15(2)	13(2)
F(5)	99(7)	43(7)	60(4)	34(3)	41(3)	34(5)
F(6)	85(4)	32(3)	63(4)	20(3)	47(4)	31(3)
F(7)	62(4)	14(3)	159(8)	9(3)	-13(3)	-12(2)
O(3)	47(1)	59(2)	39(1)	1(1)	10(1)	0(1)
C(9)	31(1)	17(1)	21(1)	-2(1)	2(1)	-1(1)
O(1)	52(1)	19(1)	26(1)	2(1)	14(1)	7(1)
O(2)	55(1)	23(1)	30(1)	6(1)	17(1)	13(1)
F(7')	277(19)	25(3)	70(5)	-2(3)	-37(8)	46(7)
F(6')	107(7)	87(8)	100(10)	49(7)	67(6)	71(6)
F(5')	114(10)	34(4)	90(7)	31(5)	67(7)	15(7)

* The anisotropic displacement factor exponent takes the form: $-2\pi^2 [h^2 a^{*2} U^{11} + ... + 2 h k a^* b^* U^{12}]$.

Table P.5 Hydrogen Coordinates ($\times 10^4$) and Isotropic Displacement Parameters ($Å^2 \times 10^3$) for 4,5-Bis(trifluoromethyl)-3-fluorophthalic Acid

	x	y	z	U(eq)
H(6)	1134	3105	2417	31
H(4)	-650	2444	-2096	70
H(2)	-227	4754	838	52

APPENDIX Q

CRYSTAL STRUCTURE OF 4,5-BIS(TRIFLUOROMETHYL)-3-FLUOROPHTHALONITRILE

Tables Q.1 to Q.5 list the atomic coordinates and crystallographic parameters for 4,5-bis(trifluoromethyl)-3-fluorophthalonitrile **[4-13]** (Figure Q.1).

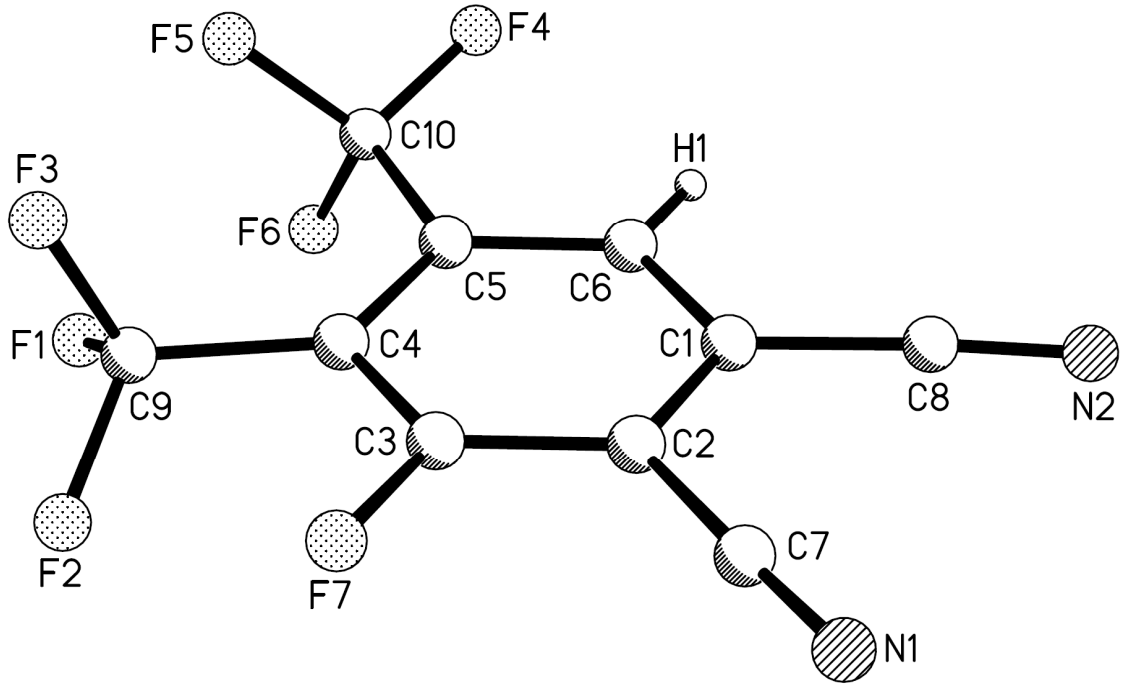

Figure Q.1 Crystal structure of 4,5-bis(trifluoromethyl)-3-fluorophthalonitrile.

Table Q.1 Crystal Data and Structure Refinement for 4,5-Bis(trifluoromethyl)-3-fluorophthalonitrile

Empirical formula	C_{10} H F_7 N_2	
Formula weight	282.13	
Temperature	100(2) K	
Wavelength	1.54178 Å	
Crystal system	orthorhombic	
Space group	Pna2(1)	
Unit cell dimensions	a = 20.2206(9) Å	α = 90°
	b = 7.1307(3) Å	β = 90°
	c = 7.1706(3) Å	γ = 90°
Volume	1033.91(8) $Å^3$	
Z	4	
Density (calculated)	1.812 g/cm^3	
Absorption coefficient	1.831 mm^{-1}	
F(000)	552	
Crystal size	0.56 × 0.25 × 0.16 mm^3	
Theta range for data collection	4.37 to 67.32°	
Index ranges	$-23 \le h \le 22$, $-8 \le k \le 8$, $-8 \le l \le 8$	
Reflections collected	8198	
Independent reflections	1718 [*R*(int) = 0.0277]	
Completeness to theta = 67.32°	98.1%	
Max. and min. transmission	0.7583 and 0.4255	
Refinement method	Full-matrix least-squares on F^2	
Data / restraints / parameters	1718 / 1 / 174	
Goodness-of-fit on F^2	1.152	
Final *R* indices [*I*>2sigma(*I*)]	*R*1 = 0.0414, *wR*2 = 0.1145	
R indices (all data)	*R*1 = 0.0416, *wR*2 = 0.1147	
Absolute structure parameter	0.1(2)	
Extinction coefficient	0.0022(6)	
Largest diff. peak and hole	0.780 and −0.312 e.$Å^{-3}$	

Table Q.2 Atomic Coordinates (× 10^4) and Equivalent Isotropic Displacement Parameters ($Å^2$ × 10^3) for 4,5-Bis(trifluoromethyl)-3-fluorophthalonitrile*

	x	y	z	U(eq)
C(1)	3272(1)	4476(5)	6179(5)	34(1)
C(2)	3506(2)	2634(5)	6259(4)	30(1)
C(3)	3957(2)	2060(4)	4935(5)	25(1)
C(4)	4189(1)	3225(4)	3540(4)	23(1)
C(5)	3921(1)	5050(4)	3433(4)	26(1)
C(6)	3472(2)	5648(4)	4768(5)	32(1)
C(7)	3273(2)	1327(7)	7638(5)	45(1)
C(8)	2795(2)	5081(7)	7553(6)	54(1)
C(9)	4708(2)	2449(4)	2206(5)	29(1)
C(10)	4086(2)	6407(4)	1873(6)	37(1)
N(1)	3073(2)	303(8)	8730(6)	77(2)
N(2)	2419(2)	5473(9)	8680(7)	88(2)

F(1)	5104(1)	3773(3)	1559(3)	43(1)
F(2)	5097(1)	1219(3)	3046(3)	42(1)
F(3)	4433(1)	1595(3)	762(3)	45(1)
F(4)	3645(1)	7770(3)	1775(4)	59(1)
F(5)	4099(1)	5558(3)	206(3)	46(1)
F(6)	4679(1)	7210(3)	2125(3)	44(1)
F(7)	4143(1)	284(3)	5018(4)	44(1)

* U(eq) is defined as one third of the trace of the orthogonalized U^{ij} tensor.

Table Q.3 Bond Lengths (Å) and Angles (°) for 4,5-Bis(trifluoromethyl)-3-fluoro-phthalonitrile

C(1)-C(6)	1.373(5)	F(7)-C(3)-C(2)	116.2(3)
C(1)-C(2)	1.397(5)	F(7)-C(3)-C(4)	120.8(3)
C(1)-C(8)	1.445(5)	C(2)-C(3)-C(4)	123.0(3)
C(2)-C(3)	1.379(5)	C(3)-C(4)-C(5)	117.6(3)
C(2)-C(7)	1.437(5)	C(3)-C(4)-C(9)	118.0(3)
C(3)-F(7)	1.322(3)	C(5)-C(4)-C(9)	124.4(3)
C(3)-C(4)	1.382(4)	C(6)-C(5)-C(4)	119.8(3)
C(4)-C(5)	1.412(4)	C(6)-C(5)-C(10)	117.2(3)
C(4)-C(9)	1.525(4)	C(4)-C(5)-C(10)	122.9(3)
C(5)-C(6)	1.386(5)	C(1)-C(6)-C(5)	121.0(3)
C(5)-C(10)	1.516(5)	C(1)-C(6)-H(1)	119.5
C(6)-H(1)	0.9500	C(5)-C(6)-H(1)	119.5
C(7)-N(1)	1.145(6)	N(1)-C(7)-C(2)	178.4(4)
C(8)-N(2)	1.145(6)	N(2)-C(8)-C(1)	176.5(6)
C(9)-F(1)	1.322(4)	F(1)-C(9)-F(2)	105.9(2)
C(9)-F(2)	1.323(4)	F(1)-C(9)-F(3)	108.0(3)
C(9)-F(3)	1.324(4)	F(2)-C(9)-F(3)	107.6(3)
C(10)-F(4)	1.320(4)	F(1)-C(9)-C(4)	112.2(2)
C(10)-F(5)	1.340(5)	F(2)-C(9)-C(4)	111.3(3)
C(10)-F(6)	1.341(4)	F(3)-C(9)-C(4)	111.6(2)
		F(4)-C(10)-F(5)	107.3(3)
C(6)-C(1)-C(2)	120.2(3)	F(4)-C(10)-F(6)	107.2(3)
C(6)-C(1)-C(8)	121.1(4)	F(5)-C(10)-F(6)	107.2(3)
C(2)-C(1)-C(8)	118.6(4)	F(4)-C(10)-C(5)	111.2(3)
C(3)-C(2)-C(1)	118.3(3)	F(5)-C(10)-C(5)	112.0(3)
C(3)-C(2)-C(7)	119.8(3)	F(6)-C(10)-C(5)	111.7(3)
C(1)-C(2)-C(7)	121.8(3)		

Table Q.4 Anisotropic Displacement Parameters ($Å^2 \times 10^3$) for 4,5-Bis(trifluoromethyl)-3-fluorophthalonitrile*

	U^{11}	U^{22}	U^{33}	U^{23}	U^{13}	U^{12}
C(1)	18(1)	54(2)	30(2)	-19(2)	1(1)	-5(1)
C(2)	24(1)	47(2)	20(2)	-1(1)	-4(1)	-7(1)
C(3)	23(2)	24(1)	27(2)	2(1)	-7(1)	-3(1)
C(4)	21(1)	25(1)	23(2)	-4(1)	0(1)	-2(1)
C(5)	23(1)	26(1)	29(2)	-1(1)	-5(1)	-5(1)
C(6)	22(2)	26(1)	48(2)	-11(2)	-6(1)	3(1)
C(7)	29(2)	78(3)	29(2)	13(2)	-6(2)	-16(2)
C(8)	27(2)	93(3)	44(2)	-33(2)	5(2)	-1(2)
C(9)	25(2)	31(1)	30(2)	-5(1)	5(1)	-2(1)

C(10)	40(2)	32(2)	40(2)	10(2)	-9(2)	-2(1)
N(1)	37(2)	140(4)	54(2)	51(3)	-6(2)	-19(2)
N(2)	38(2)	158(5)	67(3)	-59(3)	8(2)	7(2)
F(1)	34(1)	47(1)	48(1)	0(1)	19(1)	-7(1)
F(2)	35(1)	47(1)	45(1)	-3(1)	4(1)	17(1)
F(3)	41(1)	62(1)	33(1)	-20(1)	1(1)	-1(1)
F(4)	60(1)	38(1)	80(2)	24(1)	-14(1)	11(1)
F(5)	56(1)	52(1)	32(1)	14(1)	-8(1)	-13(1)
F(6)	45(1)	37(1)	51(1)	13(1)	-6(1)	-17(1)
F(7)	47(1)	36(1)	50(1)	9(1)	-3(1)	1(1)

* The anisotropic displacement factor exponent takes the form: $-2\pi^2 [h^2 a^{*2} U^{11} + ... + 2 h k a^* b^* U^{12}]$.

Table Q.5 Hydrogen Coordinates ($\times 10^4$) and Isotropic Displacement Parameters ($Å^2 \times 10^3$) for 4,5-Bis(trifluoromethyl)-3-fluorophthalonitrile

	x	y	z	U(eq)
H(1)	3300	6886	4705	39

APPENDIX R

CRYSTAL STRUCTURE OF 2,3,9,10,16,17,23,24-OCTAKIS-(TRIFLUOROMETHYL)-TETRAFLUOROPHTHALOCYANINATO-ZINC(II)

Tables R.1 to R.5 list the atomic coordinates and crystallographic parameters for $F_{28}H_4PcZn(CH_3CN)(H_2O)_{0.5}\bullet 0.5H_2O$ **[4-14]** (Figure R.1).

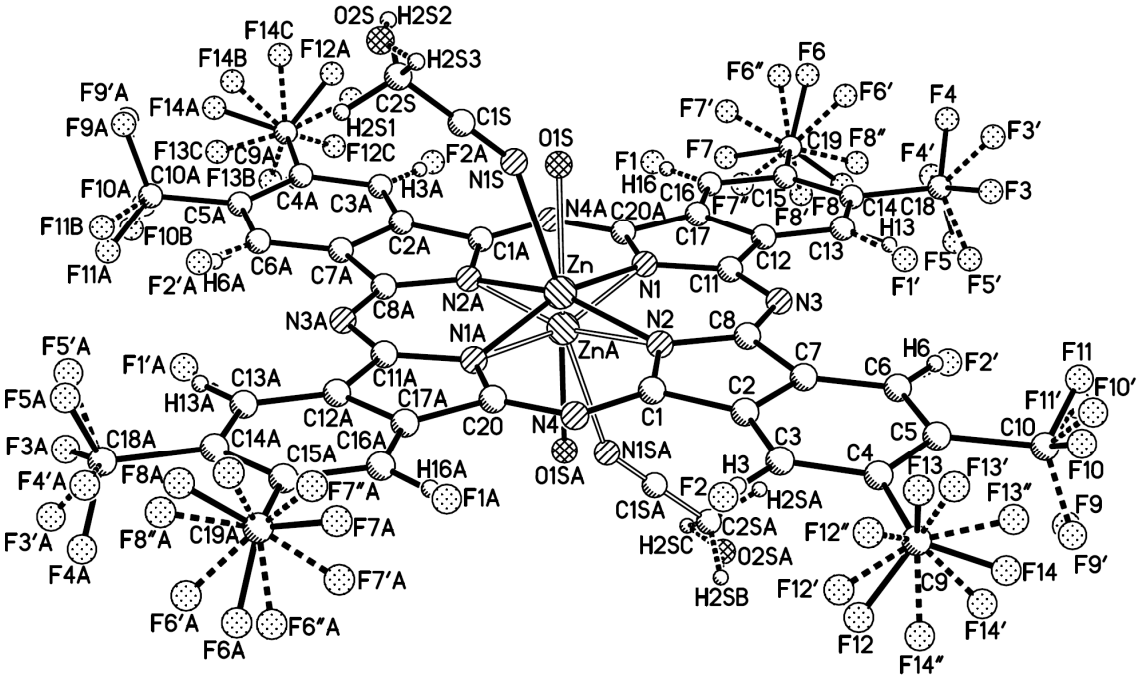

Figure R.1 Crystal structure of $F_{28}H_4PcZn(CH_3CN)(H_2O)_{0.5}\bullet 0.5H_2O$.

Table R.1 Crystal Data and Structure Refinement for $F_{28}H_4PcZn(CH_3CN)(H_2O)_{0.5}$•$0.5H_2O$

Empirical formula	$C_{42}\ H_7\ F_{28}\ N_9\ O\ Zn$	
Formula weight	1250.93	
Temperature	100(2) K	
Wavelength	0.41328 Å	
Crystal system	monoclinic	
Space group	P21/c	
Unit cell dimensions	a = 7.2524(3) Å	α = 90°
	b = 17.3057(7) Å	β = 91.886(1)°
	c = 17.7529(7) Å	γ = 90°
Volume	2226.92(16) $Å^3$	
Z	2	
Density (calculated)	1.866 g/cm^3	
Absorption coefficient	0.385 mm^{-1}	
F(000)	1224	
Crystal size	0.05 × 0.02 × 0.02 mm^3	
Theta range for data collection	1.50 to 17.17°	
Index ranges	$-10 \le h \le 10$, $-20 \le k \le 24$, $-25 \le l \le 20$	
Reflections collected	59369	
Independent reflections	6701 [*R*(int) = 0.0611]	
Completeness to theta = 17.17°	98.3%	
Max. and min. transmission	0.9962 and 0.9553	
Refinement method	Full-matrix least-squares on F^2	
Data / restraints / parameters	6701 / 477 / 523	
Goodness-of-fit on F^2	1.061	
Final *R* indices [*I*>2sigma(*I*)]	*R*1 = 0.0755, *wR*2 = 0.1727	
R indices (all data)	*R*1 = 0.1044, *wR*2 = 0.1854	
Largest diff. peak and hole	0.870 and −0.873 e.$Å^{-3}$	

Table R.2 Atomic Coordinates (× 10^4) and Equivalent Isotropic Displacement Parameters ($Å^2$ × 10^3) for $F_{28}H_4PcZn(CH_3CN)(H_2O)_{0.5}$•$0.5H_2O$*

	x	y	z	U(eq)
Zn	5191(2)	10010(1)	10162(1)	26(1)
N(1)	6739(3)	10773(1)	9594(2)	26(1)
N(2)	6743(3)	9158(1)	9754(2)	26(1)
N(4)	4995(3)	8058(1)	10186(1)	22(1)
N(3)	9092(3)	9908(1)	9141(2)	25(1)
N(1S)	5875(9)	10164(4)	11434(4)	35(1)
C(1S)	5441(7)	10115(3)	12015(3)	21(1)
C(2S)	4937(12)	10029(4)	12704(5)	37(2)
C(1)	6424(4)	8390(2)	9862(2)	22(1)
C(2)	7949(4)	7953(2)	9548(2)	21(1)
C(3)	8310(4)	7171(2)	9495(2)	24(1)
C(4)	9866(4)	6920(2)	9126(2)	26(1)
C(5)	11090(4)	7469(2)	8833(2)	26(1)
C(6)	10725(4)	8252(2)	8891(2)	26(1)

C(7)	9142(4)	8487(2)	9246(2)	22(1)
C(8)	8346(4)	9252(2)	9377(2)	24(1)
C(9)	10098(4)	6048(2)	9041(2)	36(1)
F(12)	8508(9)	5738(3)	8856(15)	73(7)
F(13)	10710(40)	5756(3)	9678(5)	65(7)
F(14)	11270(30)	5906(2)	8516(10)	61(6)
F(12')	8509(11)	5676(5)	9224(8)	51(3)
F(13')	11304(13)	5763(7)	9561(5)	43(2)
F(14')	10580(20)	5813(5)	8398(4)	45(3)
F(12'')	9560(30)	5656(8)	9602(8)	73(7)
F(13'')	11895(13)	5856(6)	8971(12)	66(5)
F(14'')	9270(30)	5778(6)	8404(8)	71(5)
C(10)	12851(4)	7243(2)	8432(2)	38(1)
F(9)	12446(4)	7090(4)	7725(3)	33(2)
F(10)	13580(8)	6632(4)	8755(4)	61(3)
F(11)	14029(5)	7814(3)	8474(4)	48(3)
F(9')	12494(7)	6856(6)	7794(3)	54(2)
F(10')	14036(10)	6838(6)	8830(3)	60(2)
F(11')	13742(12)	7879(3)	8203(8)	142(5)
C(11)	8334(4)	10600(2)	9244(2)	24(1)
C(12)	9128(4)	11318(2)	8963(2)	24(1)
C(13)	10709(4)	11476(2)	8572(2)	28(1)
C(14)	11108(4)	12234(2)	8386(2)	26(1)
C(15)	9884(4)	12839(2)	8574(2)	25(1)
C(16)	8322(4)	12664(2)	8978(2)	25(1)
C(17)	7942(4)	11910(2)	9168(2)	22(1)
C(18)	12966(2)	12358(1)	7967(1)	34(1)
F(1)	7264(4)	13225(2)	9176(2)	32(1)
F(1')	11664(8)	10951(3)	8288(4)	47(2)
F(2')	11770(8)	8722(3)	8574(4)	44(2)
F(2)	7217(4)	6662(2)	9775(2)	30(1)
F(3)	13999(2)	11740(1)	8047(1)	53(1)
F(4)	13843(2)	12955(1)	8257(1)	52(1)
F(5)	12603(2)	12481(1)	7250(1)	43(1)
F(3')	14620(40)	12270(20)	8260(20)	121(18)
F(4')	12840(50)	13081(9)	7691(19)	91(14)
F(5')	12790(40)	11901(13)	7363(11)	52(8)
C(19)	10153(4)	13685(2)	8364(2)	34(1)
F(6)	11350(16)	14002(3)	8836(5)	46(3)
F(7)	8579(8)	14049(3)	8396(9)	77(5)
F(8)	10760(20)	13730(2)	7681(4)	60(4)
F(6')	11910(20)	13870(20)	8500(20)	71(11)
F(8')	9720(50)	13926(17)	7682(9)	43(8)
F(7')	9180(50)	14100(20)	8834(17)	71(11)
F(6'')	10730(20)	14117(5)	8913(4)	67(3)
F(8'')	11334(17)	13791(4)	7798(5)	46(2)
F(7'')	8592(10)	13984(5)	8070(11)	79(4)
C(20)	3578(4)	8456(2)	10440(2)	23(1)
O(1S)	6637(19)	10150(7)	11220(7)	45(3)
O(2S)	5030(20)	10084(8)	13041(8)	54(4)

* U(eq) is defined as one third of the trace of the orthogonalized U^{ij} tensor.

Table R.3 Bond Lengths (Å) and Angles (°) for $F_{28}H_4PcZn(CH_3CN)(H_2O)_{0.5}$•$0.5H_2O$

Zn-N(2)	2.006(3)	Zn-N(1)	2.023(3)
Zn-N(1)#1	2.006(3)	Zn-O(1S)	2.135(12)
Zn-N(2)#1	2.019(3)	Zn-N(1S)	2.311(6)
N(1)-C(20)#1	1.355(4)	C(5)-C(6)	1.386(4)
N(1)-C(11)	1.364(3)	C(5)-C(10)	1.534(4)
N(2)-C(1)	1.364(4)	C(6)-C(7)	1.389(4)
N(2)-C(8)	1.370(4)	C(6)-H(6)	0.9500
N(4)-C(20)	1.328(3)	C(7)-C(8)	1.465(4)
N(4)-C(1)	1.332(3)	C(11)-C(12)	1.464(4)
N(3)-C(11)	1.332(4)	C(12)-C(13)	1.388(4)
N(3)-C(8)	1.333(4)	C(12)-C(17)	1.394(4)
N(1S)-C(1S)	1.092(9)	C(13)-C(14)	1.386(4)
C(1S)-C(2S)	1.297(10)	C(13)-H(13)	0.9500
C(2S)-H(2S1)	0.9800	C(14)-C(15)	1.419(4)
C(2S)-H(2S2)	0.9800	C(14)-C(18)	1.575(3)
C(2S)-H(2S3)	0.9800	C(15)-C(16)	1.394(4)
C(1)-C(2)	1.464(4)	C(15)-C(19)	1.525(4)
C(2)-C(3)	1.381(4)	C(16)-C(17)	1.378(4)
C(2)-C(7)	1.387(4)	C(16)-H(16)	0.9500
C(3)-C(4)	1.393(4)	C(17)-C(20)#1	1.467(4)
C(3)-H(3)	0.9500	C(20)-N(1)#1	1.355(4)
C(4)-C(5)	1.411(4)	C(20)-C(17)#1	1.467(4)
C(4)-C(9)	1.525(4)		
N(2)-Zn-N(1)#1	89.12(11)	C(1S)-C(2S)-H(2S3)	109.5
N(2)-Zn-N(2)#1	161.99(5)	H(2S1)-C(2S)-H(2S3)	109.5
N(1)#1-Zn-N(2)#1	88.55(11)	H(2S2)-C(2S)-H(2S3)	109.5
N(2)-Zn-N(1)	88.45(11)	N(4)-C(1)-N(2)	128.2(3)
N(1)#1-Zn-N(1)	162.01(5)	N(4)-C(1)-C(2)	123.4(2)
N(2)#1-Zn-N(1)	88.27(11)	N(2)-C(1)-C(2)	108.4(2)
N(2)-Zn-O(1S)	97.8(4)	C(3)-C(2)-C(7)	120.3(2)
N(1)#1-Zn-O(1S)	102.3(4)	C(3)-C(2)-C(1)	132.8(3)
N(2)#1-Zn-O(1S)	100.1(4)	C(7)-C(2)-C(1)	106.9(2)
N(1)-Zn-O(1S)	95.7(4)	C(2)-C(3)-C(4)	119.8(3)
N(2)-Zn-N(1S)	109.42(18)	C(2)-C(3)-H(3)	120.1
N(1)#1-Zn-N(1S)	89.72(18)	C(4)-C(3)-H(3)	120.1
N(2)#1-Zn-N(1S)	88.44(18)	C(3)-C(4)-C(5)	119.4(3)
N(1)-Zn-N(1S)	107.89(19)	C(3)-C(4)-C(9)	116.7(3)
O(1S)-Zn-N(1S)	17.0(3)	C(5)-C(4)-C(9)	123.8(3)
C(20)#1-N(1)-C(11)	110.0(2)	C(6)-C(5)-C(4)	120.5(3)
C(20)#1-N(1)-Zn	124.60(19)	C(6)-C(5)-C(10)	116.6(3)
C(11)-N(1)-Zn	125.2(2)	C(4)-C(5)-C(10)	122.9(3)
C(1)-N(2)-C(8)	109.6(2)	C(5)-C(6)-C(7)	118.9(3)
C(1)-N(2)-Zn	124.54(19)	C(5)-C(6)-H(6)	120.6
C(8)-N(2)-Zn	125.7(2)	C(7)-C(6)-H(6)	120.6
C(20)-N(4)-C(1)	123.0(2)	C(2)-C(7)-C(6)	121.1(3)
C(11)-N(3)-C(8)	123.3(2)	C(2)-C(7)-C(8)	106.6(2)
C(1S)-N(1S)-Zn	148.7(6)	C(6)-C(7)-C(8)	132.3(3)
N(1S)-C(1S)-C(2S)	177.9(7)	N(3)-C(8)-N(2)	127.9(3)
C(1S)-C(2S)-H(2S1)	109.5	N(3)-C(8)-C(7)	123.6(2)
C(1S)-C(2S)-H(2S2)	109.5	N(2)-C(8)-C(7)	108.4(2)
H(2S1)-C(2S)-H(2S2)	109.5	N(3)-C(11)-N(1)	128.3(3)
N(3)-C(11)-C(12)	123.2(2)	C(16)-C(15)-C(19)	116.5(3)

N(1)-C(11)-C(12)	108.5(2)	C(14)-C(15)-C(19)	124.4(3)
C(13)-C(12)-C(17)	120.9(3)	C(17)-C(16)-C(15)	120.2(3)
C(13)-C(12)-C(11)	132.7(3)	C(17)-C(16)-H(16)	119.9
C(17)-C(12)-C(11)	106.4(2)	C(15)-C(16)-H(16)	119.9
C(14)-C(13)-C(12)	119.2(3)	C(16)-C(17)-C(12)	120.2(3)
C(14)-C(13)-H(13)	120.4	C(16)-C(17)-C(20)#1	133.2(3)
C(12)-C(13)-H(13)	120.4	C(12)-C(17)-C(20)#1	106.7(2)
C(13)-C(14)-C(15)	120.4(3)	N(4)-C(20)-N(1)#1	128.9(3)
C(13)-C(14)-C(18)	115.4(2)	N(4)-C(20)-C(17)#1	122.6(3)
C(15)-C(14)-C(18)	124.2(2)	N(1)#1-C(20)-C(17)#1	108.5(2)
C(16)-C(15)-C(14)	119.1(3)		

Symmetry transformations used to generate equivalent atoms: #1 -x+1, -y+2, -z+2.

Table R.4 Anisotropic Displacement Parameters ($Å^2 \times 10^3$) for $F_{28}H_4PcZn(CH_3CN)(H_2O)_{0.5}•0.5H_2O$*

	U^{11}	U^{22}	U^{33}	U^{23}	U^{13}	U^{12}
F(1)	27(2)	21(1)	50(2)	-1(1)	17(1)	5(1)
F(1')	41(3)	30(3)	71(4)	4(3)	28(3)	11(2)
F(2')	36(3)	31(3)	64(4)	7(3)	19(3)	-1(2)
F(2)	23(1)	19(1)	48(2)	5(1)	13(1)	-2(1)
Zn	19(1)	18(1)	41(1)	3(1)	13(1)	2(1)
N(1)	19(1)	20(1)	39(1)	3(1)	11(1)	2(1)
N(2)	21(1)	19(1)	38(1)	1(1)	11(1)	1(1)
N(4)	20(1)	20(1)	28(1)	0(1)	8(1)	0(1)
N(3)	20(1)	19(1)	36(1)	2(1)	10(1)	1(1)
N(1S)	26(3)	46(4)	33(3)	3(2)	8(2)	4(2)
C(1S)	12(2)	14(2)	38(3)	1(2)	-1(2)	-2(2)
C(2S)	47(4)	35(3)	29(4)	-5(3)	-5(3)	6(3)
C(1)	19(1)	19(1)	29(1)	4(1)	6(1)	0(1)
C(2)	17(1)	21(1)	26(1)	-2(1)	5(1)	-1(1)
C(3)	21(1)	20(1)	30(1)	1(1)	3(1)	3(1)
C(4)	26(1)	24(1)	28(1)	-2(1)	3(1)	6(1)
C(5)	19(1)	29(1)	29(1)	-2(1)	7(1)	6(1)
C(6)	20(1)	25(1)	34(2)	5(1)	8(1)	4(1)
C(7)	18(1)	19(1)	28(1)	1(1)	6(1)	3(1)
C(8)	19(1)	21(1)	34(2)	-1(1)	9(1)	3(1)
C(9)	36(2)	23(1)	51(2)	-4(1)	11(2)	7(1)
F(12)	43(6)	40(7)	133(19)	-49(11)	-5(8)	-2(5)
F(13)	125(18)	25(5)	47(6)	13(4)	33(11)	9(12)
F(14)	79(12)	32(5)	76(10)	-42(6)	50(9)	-31(6)
F(12')	56(5)	21(3)	77(8)	-5(4)	3(4)	-1(3)
F(13')	47(4)	36(3)	46(5)	13(3)	16(4)	22(3)
F(14')	81(8)	19(3)	35(3)	-12(3)	2(4)	-5(4)
F(12'')	136(18)	26(6)	60(9)	19(6)	56(11)	18(10)
F(13'')	56(7)	35(5)	107(13)	-17(7)	19(8)	23(5)
F(14'')	109(14)	24(4)	77(9)	-15(5)	-43(9)	-18(8)
C(10)	26(2)	43(2)	44(2)	-4(2)	11(1)	10(1)
F(9)	31(3)	41(4)	29(3)	6(2)	7(2)	19(3)
F(10)	39(5)	101(7)	43(5)	1(5)	-1(4)	48(5)
F(11)	12(3)	92(6)	40(4)	-35(3)	5(2)	-12(3)
F(9')	44(3)	89(5)	30(2)	-5(3)	4(2)	41(3)
F(10')	28(3)	109(5)	44(3)	-30(3)	-16(2)	37(3)
F(11')	111(6)	41(3)	285(12)	5(5)	157(7)	3(3)

C(11)	18(1)	22(1)	35(2)	2(1)	8(1)	1(1)
C(12)	19(1)	20(1)	32(2)	1(1)	9(1)	0(1)
C(13)	23(1)	27(1)	35(2)	-2(1)	11(1)	1(1)
C(14)	21(1)	30(1)	25(1)	1(1)	8(1)	-4(1)
C(15)	25(1)	24(1)	27(1)	2(1)	6(1)	-4(1)
C(16)	23(1)	23(1)	29(1)	1(1)	6(1)	0(1)
C(17)	20(1)	22(1)	27(1)	-1(1)	7(1)	-1(1)
C(18)	31(2)	37(2)	34(2)	1(1)	13(1)	-8(1)
F(3)	27(1)	67(2)	65(2)	18(1)	23(1)	11(1)
F(4)	38(1)	74(2)	47(2)	-10(1)	14(1)	-34(1)
F(5)	30(1)	75(2)	25(1)	7(1)	9(1)	-5(1)
C(19)	34(2)	27(2)	42(2)	8(1)	8(1)	-5(1)
F(6)	73(6)	22(3)	43(4)	-16(3)	10(4)	-16(3)
F(7)	45(5)	38(4)	147(14)	54(5)	1(5)	-2(3)
F(8)	90(10)	58(6)	32(3)	11(3)	4(4)	-50(6)
F(6")	138(9)	19(2)	44(4)	-4(2)	-4(4)	4(4)
F(8")	53(5)	26(3)	61(4)	10(2)	27(4)	-11(2)
F(7")	44(4)	59(4)	135(10)	69(4)	6(4)	10(3)
C(20)	19(1)	19(1)	30(1)	0(1)	7(1)	-1(1)

* The anisotropic displacement factor exponent takes the form: $-2\pi^2 [h^2 a^{*2} U^{11} + ... + 2 h k a^* b^* U^{12}]$.

Table R.5 Hydrogen Coordinates ($\times 10^4$) and Isotropic Displacement Parameters ($Å^2 \times 10^3$) for $F_{28}H_4PcZn(CH_3CN)(H_2O)_{0.5}\bullet 0.5H_2O$

	x	y	z	U(eq)
H(2S1)	3613	9917	12707	55
H(2S2)	5193	10505	12987	55
H(2S3)	5625	9600	12939	55
H(3)	7501	6807	9709	28
H(6)	11544	8623	8691	31
H(13)	11508	11069	8432	33
H(16)	7516	13067	9124	30

APPENDIX S

CRYSTAL STRUCTURE OF 1,3,4-TRIS-(PERFLUOROISOPROPYL)-TRIDECAFLUOROPHTHALOCYANINATO-ZINC(II)

Tables S.1 to S.5 list the atomic coordinates and crystallographic parameters for $F_{34}PcZn(H_2O)\bullet 2(CH_3)_2CO$ **[5-10]** (Figure S.1).

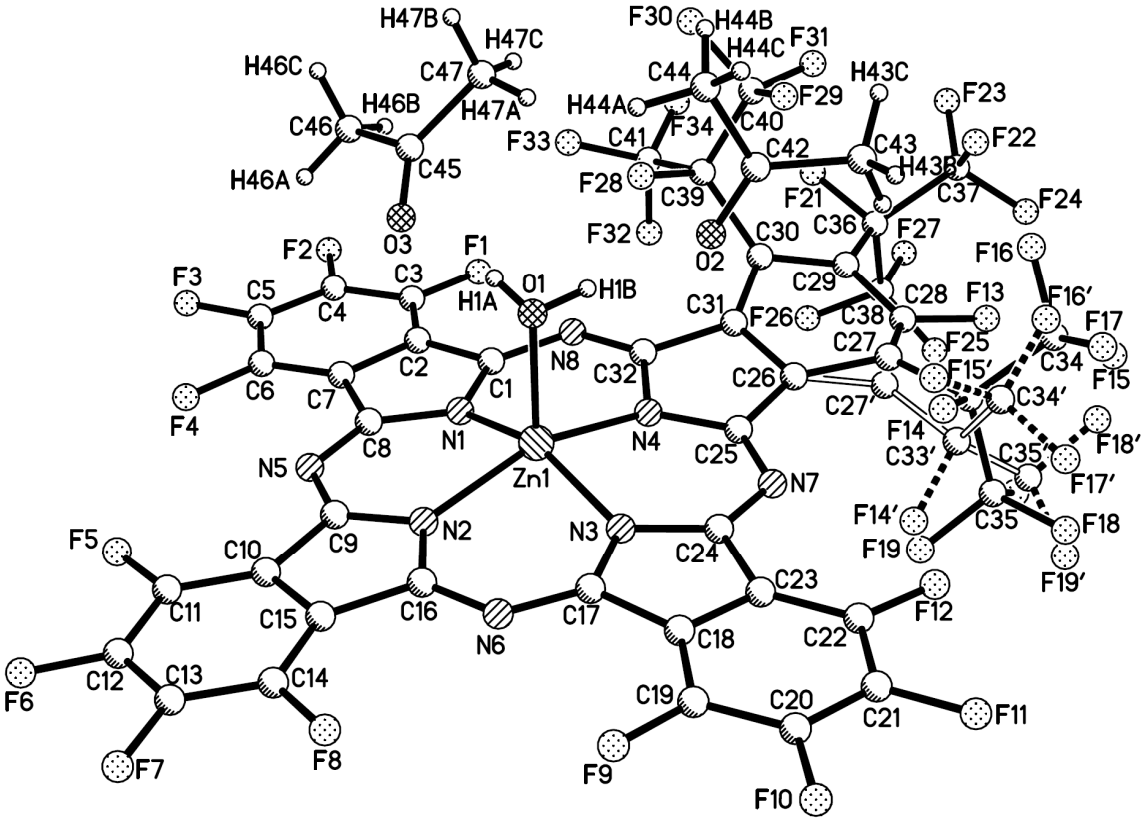

Figure S.1 Crystal structure of $F_{34}PcZn(H_2O)\bullet 2(CH_3)_2CO$.

Table S.1 Crystal Data and Structure Refinement for $F_{34}PcZn(H_2O)\bullet 2(CH_3)_2CO$

Empirical formula	$C_{47}\ H_{14}\ F_{34}\ N_8\ O_3\ Zn$	
Formula weight	1450.03	
Temperature	100(2) K	
Wavelength	1.54178 Å	
Crystal system	monoclinic	
Space group	P2(1)/c	
Unit cell dimensions	a = 11.0463(2) Å	α = 90°
	b = 11.4442(2) Å	β = 103.436(1)°
	c = 41.9063(6) Å	γ = 90°
Volume	5152.63(15) $Å^3$	
Z	4	
Density (calculated)	1.869 g/cm^3	
Absorption coefficient	2.310 mm^{-1}	
F(000)	2848	
Crystal size	0.14 × 0.06 × 0.02 mm^3	
Theta range for data collection	4.01 to 66.59°	
Index ranges	$-12 \le h \le 13, -13 \le k \le 13, -48 \le l \le 49$	
Reflections collected	42463	
Independent reflections	8939 [*R*(int) = 0.0238]	
Completeness to theta = 66.59°	98.3%	
Refinement method	Full-matrix least-squares on F^2	
Data / restraints / parameters	8939 / 294 / 906	
Goodness-of-fit on F^2	1.155	
Final *R* indices [*I*>2sigma(*I*)]	*R*1 = 0.0876, *wR*2 = 0.2343	
R indices (all data)	*R*1 = 0.0911, *wR*2 = 0.2364	
Largest diff. peak and hole	1.164 and −0.562 e.$Å^{-3}$	

Table S.2 Atomic Coordinates (× 10^4) and Equivalent Isotropic Displacement Parameters ($Å^2$ × 10^3) for $F_{34}PcZn(H_2O)\bullet 2(CH_3)_2CO$*

	x	y	z	U(eq)
Zn(1)	7114(1)	4236(1)	463(1)	31(1)
O(1)	8171(4)	2770(4)	603(1)	43(1)
N(1)	5390(4)	3519(4)	382(1)	30(1)
N(2)	6833(4)	4381(4)	-33(1)	32(1)
N(3)	8339(4)	5554(4)	498(1)	36(1)
N(4)	6914(4)	4653(4)	923(1)	36(1)
N(5)	4975(4)	3205(4)	-206(1)	30(1)
N(6)	8583(4)	5615(4)	-61(1)	37(1)
N(7)	8588(5)	6052(4)	1074(1)	44(1)
N(8)	5224(4)	3370(4)	948(1)	33(1)
C(1)	4840(5)	3188(4)	626(1)	31(1)
C(2)	3724(5)	2503(4)	480(1)	30(1)
C(3)	2786(5)	1993(5)	606(1)	33(1)
F(1)	2736(3)	2108(3)	917(1)	45(1)
C(4)	1883(5)	1349(5)	397(2)	39(1)
F(2)	980(3)	832(3)	514(1)	47(1)

C(5)	1876(5)	1222(5)	70(2)	34(1)
F(3)	996(3)	572(3)	-123(1)	43(1)
C(6)	2763(5)	1783(5)	-63(1)	34(1)
F(4)	2677(3)	1695(3)	-384(1)	37(1)
C(7)	3683(5)	2411(4)	144(1)	29(1)
C(8)	4751(5)	3083(4)	89(1)	29(1)
C(9)	5937(5)	3817(5)	-258(1)	32(1)
C(10)	6173(5)	3987(5)	-587(2)	36(1)
C(11)	5571(6)	3604(5)	-897(2)	41(1)
F(5)	4549(3)	2949(3)	-954(1)	46(1)
C(12)	6053(7)	3935(6)	-1162(2)	48(2)
F(6)	5500(4)	3588(4)	-1464(1)	61(1)
C(13)	7109(6)	4621(6)	-1115(2)	48(2)
F(7)	7567(4)	4914(4)	-1377(1)	65(1)
C(14)	7713(6)	5012(5)	-809(2)	44(2)
F(8)	8740(3)	5659(3)	-774(1)	51(1)
C(15)	7240(5)	4687(5)	-540(2)	37(1)
C(16)	7630(5)	4931(5)	-190(2)	36(1)
C(17)	8876(5)	5906(5)	253(2)	36(1)
C(18)	9859(5)	6742(5)	392(2)	42(2)
C(19)	10697(6)	7366(5)	251(2)	49(2)
F(9)	10708(3)	7268(3)	-62(1)	56(1)
C(20)	11539(6)	8099(5)	454(2)	55(2)
F(10)	12371(3)	8683(3)	331(1)	72(1)
C(21)	11533(6)	8237(6)	780(2)	64(2)
F(11)	12370(4)	8952(4)	969(1)	81(2)
C(22)	10685(7)	7646(6)	921(2)	57(2)
F(12)	10696(4)	7826(4)	1236(1)	73(1)
C(23)	9848(5)	6894(5)	721(2)	46(2)
C(24)	8857(5)	6129(5)	784(2)	40(1)
C(25)	7714(6)	5357(6)	1140(2)	46(2)
C(26)	7458(6)	5180(7)	1470(2)	55(2)
C(27)	8034(8)	5548(7)	1800(2)	54(3)
C(33)	9087(6)	6407(6)	1899(2)	85(4)
F(14)	9877(8)	6229(7)	1687(2)	89(2)
C(34)	9942(8)	6212(5)	2233(3)	107(2)
F(15)	11140(6)	6464(7)	2230(2)	113(3)
F(16)	9920(7)	5085(5)	2331(2)	97(2)
F(17)	9630(8)	6884(7)	2467(2)	113(3)
C(35)	8709(6)	7674(10)	1844(1)	104(3)
F(18)	9705(8)	8397(6)	1921(2)	111(3)
F(19)	8131(8)	7871(5)	1526(2)	89(2)
F(20)	7903(8)	7994(7)	2028(2)	107(2)
C(27')	7695(11)	5875(9)	1768(2)	54(3)
C(33')	8616(9)	6868(7)	1822(2)	85(4)
F(14')	8469(11)	7449(9)	1522(3)	89(2)
C(34')	9970(12)	6507(8)	1903(2)	102(3)
F(15')	10234(12)	5795(13)	1670(4)	89(2)
F(16')	10274(13)	5922(12)	2192(3)	107(2)
F(17')	10739(9)	7443(11)	1929(4)	110(4)
C(35')	8386(9)	7827(10)	2049(2)	107(2)
F(18')	8944(14)	7593(11)	2367(2)	111(4)
F(19')	8843(15)	8865(7)	1974(3)	105(4)
F(20')	7157(10)	7978(12)	2032(4)	96(4)
C(28)	7304(8)	5313(8)	2018(2)	68(2)
F(13)	7605(6)	5864(5)	2313(1)	91(2)

C(29)	6541(8)	4355(9)	1998(2)	67(2)
C(36)	5928(11)	4120(9)	2275(2)	87(3)
F(21)	5171(5)	3111(5)	2221(1)	82(2)
C(37)	6788(13)	3961(12)	2627(2)	101(4)
F(22)	7934(7)	3710(7)	2601(1)	115(2)
F(23)	6367(8)	3116(8)	2789(1)	138(3)
F(24)	6886(7)	4974(7)	2806(1)	128(3)
C(38)	4857(11)	5075(13)	2283(2)	97(3)
F(25)	5314(7)	6157(6)	2318(2)	108(2)
F(26)	4018(5)	4952(6)	2009(1)	88(2)
F(27)	4318(7)	4828(7)	2530(1)	120(2)
C(30)	6287(7)	3684(7)	1708(2)	55(2)
C(39)	6050(8)	2322(7)	1683(2)	62(2)
F(28)	6408(4)	1963(4)	1406(1)	66(1)
C(40)	6951(11)	1676(9)	1944(2)	90(3)
F(29)	8154(6)	1925(5)	1915(2)	99(2)
F(30)	6869(7)	478(5)	1857(2)	111(2)
F(31)	6944(6)	1746(6)	2241(1)	104(2)
C(41)	4712(8)	1850(8)	1636(2)	66(2)
F(32)	3899(4)	2757(4)	1566(1)	68(1)
F(33)	4431(5)	1114(4)	1387(1)	74(1)
F(34)	4525(6)	1329(5)	1891(1)	92(2)
C(31)	6619(6)	4253(6)	1438(2)	47(2)
C(32)	6220(5)	4009(5)	1081(1)	38(1)
O(2)	9339(8)	2946(7)	1252(2)	102(2)
C(42)	10178(9)	2470(10)	1443(2)	77(3)
C(43)	10792(12)	2993(13)	1760(3)	116(4)
C(44)	10662(10)	1337(13)	1362(3)	113(4)
O(3)	6535(5)	969(4)	460(2)	74(2)
C(45)	6242(7)	233(6)	641(2)	64(2)
C(46)	5024(7)	-384(6)	554(3)	82(3)
C(47)	7117(10)	-139(9)	958(2)	84(3)

* U(eq) is defined as one third of the trace of the orthogonalized U^{ij} tensor.

Table S.3 Bond Lengths (Å) and Angles (°) for $F_{34}PcZn(H_2O)\bullet 2(CH_3)_2CO$

Zn(1)-N(3)	2.009(4)	Zn(1)-N(2)	2.034(5)
Zn(1)-N(1)	2.028(4)	Zn(1)-N(4)	2.048(5)
Zn(1)-O(1)	2.051(4)		
O(1)-H(1A)	0.8401	N(7)-C(25)	1.328(9)
O(1)-H(1B)	0.8401	N(8)-C(32)	1.331(7)
N(1)-C(1)	1.358(7)	N(8)-C(1)	1.335(7)
N(1)-C(8)	1.363(7)	C(1)-C(2)	1.468(7)
N(2)-C(9)	1.360(7)	C(2)-C(3)	1.396(8)
N(2)-C(16)	1.367(7)	C(2)-C(7)	1.403(8)
N(3)-C(17)	1.360(8)	C(3)-F(1)	1.320(7)
N(3)-C(24)	1.369(8)	C(3)-C(4)	1.379(8)
N(4)-C(32)	1.345(8)	C(4)-F(2)	1.346(6)
N(4)-C(25)	1.373(7)	C(4)-C(5)	1.377(9)
N(5)-C(8)	1.320(7)	C(5)-F(3)	1.336(6)
N(5)-C(9)	1.332(7)	C(5)-C(6)	1.390(8)
N(6)-C(16)	1.322(7)	C(6)-F(4)	1.331(7)
N(6)-C(17)	1.323(8)	C(6)-C(7)	1.375(7)
N(7)-C(24)	1.323(9)	C(7)-C(8)	1.471(7)

C(9)-C(10)	1.475(8)	C(36)-C(38)	1.616(16)
C(10)-C(11)	1.386(9)	C(37)-F(22)	1.326(15)
C(10)-C(15)	1.401(8)	C(37)-F(23)	1.327(14)
C(11)-F(5)	1.330(7)	C(37)-F(24)	1.371(14)
C(11)-C(12)	1.391(9)	C(38)-F(26)	1.303(11)
C(12)-F(6)	1.332(8)	C(38)-F(25)	1.333(15)
C(12)-C(13)	1.381(10)	C(38)-F(27)	1.340(11)
C(13)-F(7)	1.352(7)	C(30)-C(31)	1.424(10)
C(13)-C(14)	1.377(10)	C(30)-C(39)	1.580(11)
C(14)-F(8)	1.335(7)	C(39)-F(28)	1.372(9)
C(14)-C(15)	1.398(8)	C(39)-C(40)	1.493(11)
C(15)-C(16)	1.456(9)	C(39)-C(41)	1.543(12)
C(17)-C(18)	1.463(8)	C(40)-F(31)	1.251(11)
C(18)-C(23)	1.393(10)	C(40)-F(29)	1.391(13)
C(18)-C(19)	1.403(9)	C(40)-F(30)	1.415(12)
C(19)-F(9)	1.319(9)	C(41)-F(34)	1.283(9)
C(19)-C(20)	1.387(10)	C(41)-F(33)	1.321(9)
C(20)-F(10)	1.332(8)	C(41)-F(32)	1.360(10)
C(20)-C(21)	1.378(12)	C(31)-C(32)	1.485(8)
C(21)-F(11)	1.345(8)	O(2)-C(42)	1.205(11)
C(21)-C(22)	1.394(11)	C(42)-C(43)	1.471(14)
C(22)-F(12)	1.331(9)	C(42)-C(44)	1.472(16)
C(22)-C(23)	1.392(9)	C(43)-H(43A)	0.9800
C(23)-C(24)	1.472(8)	C(43)-H(43B)	0.9800
C(25)-C(26)	1.489(10)	C(43)-H(43C)	0.9800
C(26)-C(31)	1.395(10)	C(44)-H(44A)	0.9800
C(26)-C(27)	1.444(10)	C(44)-H(44B)	0.9800
C(26)-C(27')	1.450(10)	C(44)-H(44C)	0.9800
C(27)-C(28)	1.377(12)	O(3)-C(45)	1.226(10)
C(27)-C(33)	1.505(11)	C(45)-C(46)	1.488(10)
C(33)-F(14)	1.400(13)	C(45)-C(47)	1.512(13)
C(33)-C(34)	1.510(12)	C(46)-H(46A)	0.9800
C(33)-C(35)	1.512(12)	C(46)-H(46B)	0.9800
C(34)-F(17)	1.354(6)	C(46)-H(46C)	0.9800
C(34)-F(16)	1.356(6)	C(47)-H(47A)	0.9800
C(34)-F(15)	1.356(6)	C(47)-H(47B)	0.9800
C(35)-F(18)	1.354(6)	C(47)-H(47C)	0.9800
C(35)-F(19)	1.356(6)		
C(35)-F(20)	1.357(6)	N(3)-Zn(1)-N(1)	154.99(18)
C(27')-C(28)	1.382(13)	N(3)-Zn(1)-N(2)	87.39(19)
C(27')-C(33')	1.507(11)	N(1)-Zn(1)-N(2)	87.12(18)
C(33')-F(14')	1.400(13)	N(3)-Zn(1)-N(4)	88.44(19)
C(33')-C(34')	1.512(12)	N(1)-Zn(1)-N(4)	87.03(18)
C(33')-C(35')	1.512(12)	N(2)-Zn(1)-N(4)	156.66(19)
C(34')-F(15')	1.355(6)	N(3)-Zn(1)-O(1)	105.29(17)
C(34')-F(17')	1.355(6)	N(1)-Zn(1)-O(1)	99.63(17)
C(34')-F(16')	1.357(6)	N(2)-Zn(1)-O(1)	107.50(18)
C(35')-F(20')	1.354(6)	N(4)-Zn(1)-O(1)	95.75(19)
C(35')-F(18')	1.355(6)	Zn(1)-O(1)-H(1A)	109.7
C(35')-F(19')	1.357(6)	Zn(1)-O(1)-H(1B)	109.5
C(28)-F(13)	1.360(8)	H(1A)-O(1)-H(1B)	108.2
C(28)-C(29)	1.373(13)	C(1)-N(1)-C(8)	110.4(4)
C(29)-C(30)	1.408(10)	C(1)-N(1)-Zn(1)	123.7(4)
C(29)-C(36)	1.500(14)	C(8)-N(1)-Zn(1)	124.5(4)
C(36)-F(21)	1.413(12)	C(9)-N(2)-C(16)	109.4(5)
C(36)-C(37)	1.566(12)	C(9)-N(2)-Zn(1)	125.5(4)

C(16)-N(2)-Zn(1)	124.5(4)	N(6)-C(16)-N(2)	128.1(6)
C(17)-N(3)-C(24)	110.5(5)	N(6)-C(16)-C(15)	123.1(5)
C(17)-N(3)-Zn(1)	124.8(4)	N(2)-C(16)-C(15)	108.8(5)
C(24)-N(3)-Zn(1)	124.3(4)	N(6)-C(17)-N(3)	128.8(5)
C(32)-N(4)-C(25)	110.3(5)	N(6)-C(17)-C(18)	123.2(5)
C(32)-N(4)-Zn(1)	122.4(4)	N(3)-C(17)-C(18)	107.9(5)
C(25)-N(4)-Zn(1)	124.6(4)	C(23)-C(18)-C(19)	120.8(6)
C(8)-N(5)-C(9)	122.6(5)	C(23)-C(18)-C(17)	107.4(5)
C(16)-N(6)-C(17)	122.9(5)	C(19)-C(18)-C(17)	131.9(7)
C(24)-N(7)-C(25)	124.1(5)	F(9)-C(19)-C(20)	120.1(6)
C(32)-N(8)-C(1)	123.2(5)	F(9)-C(19)-C(18)	122.3(6)
N(8)-C(1)-N(1)	128.7(5)	C(20)-C(19)-C(18)	117.6(7)
N(8)-C(1)-C(2)	122.9(5)	F(10)-C(20)-C(21)	119.2(6)
N(1)-C(1)-C(2)	108.4(5)	F(10)-C(20)-C(19)	119.4(8)
C(3)-C(2)-C(7)	119.7(5)	C(21)-C(20)-C(19)	121.4(6)
C(3)-C(2)-C(1)	133.7(5)	F(11)-C(21)-C(20)	119.4(7)
C(7)-C(2)-C(1)	106.6(5)	F(11)-C(21)-C(22)	119.0(9)
F(1)-C(3)-C(4)	119.4(5)	C(20)-C(21)-C(22)	121.6(6)
F(1)-C(3)-C(2)	122.4(5)	F(12)-C(22)-C(23)	123.0(7)
C(4)-C(3)-C(2)	118.2(5)	F(12)-C(22)-C(21)	119.5(7)
F(2)-C(4)-C(5)	118.8(5)	C(23)-C(22)-C(21)	117.5(8)
F(2)-C(4)-C(3)	119.4(6)	C(22)-C(23)-C(18)	121.1(6)
C(5)-C(4)-C(3)	121.8(5)	C(22)-C(23)-C(24)	132.6(7)
F(3)-C(5)-C(4)	119.7(5)	C(18)-C(23)-C(24)	106.3(5)
F(3)-C(5)-C(6)	119.9(5)	N(7)-C(24)-N(3)	129.4(5)
C(4)-C(5)-C(6)	120.4(5)	N(7)-C(24)-C(23)	122.7(6)
F(4)-C(6)-C(7)	123.1(5)	N(3)-C(24)-C(23)	107.9(6)
F(4)-C(6)-C(5)	118.5(5)	N(7)-C(25)-N(4)	126.9(6)
C(7)-C(6)-C(5)	118.5(5)	N(7)-C(25)-C(26)	125.3(6)
C(6)-C(7)-C(2)	121.2(5)	N(4)-C(25)-C(26)	107.8(6)
C(6)-C(7)-C(8)	132.5(5)	C(31)-C(26)-C(27)	116.6(7)
C(2)-C(7)-C(8)	106.3(4)	C(31)-C(26)-C(27')	118.9(7)
N(5)-C(8)-N(1)	129.4(5)	C(27)-C(26)-C(27')	20.9(7)
N(5)-C(8)-C(7)	122.3(5)	C(31)-C(26)-C(25)	106.2(6)
N(1)-C(8)-C(7)	108.3(5)	C(27)-C(26)-C(25)	135.6(7)
N(5)-C(9)-N(2)	128.0(5)	C(27')-C(26)-C(25)	133.6(7)
N(5)-C(9)-C(10)	122.9(5)	C(28)-C(27)-C(26)	112.4(7)
N(2)-C(9)-C(10)	109.0(5)	C(28)-C(27)-C(33)	118.6(7)
C(11)-C(10)-C(15)	121.1(6)	C(26)-C(27)-C(33)	126.5(7)
C(11)-C(10)-C(9)	133.2(5)	F(14)-C(33)-C(27)	106.6(7)
C(15)-C(10)-C(9)	105.6(5)	F(14)-C(33)-C(34)	102.7(4)
F(5)-C(11)-C(10)	123.3(5)	C(27)-C(33)-C(34)	115.8(4)
F(5)-C(11)-C(12)	118.5(6)	F(14)-C(33)-C(35)	103.4(4)
C(10)-C(11)-C(12)	118.3(6)	C(27)-C(33)-C(35)	114.6(4)
F(6)-C(12)-C(13)	119.4(6)	C(34)-C(33)-C(35)	112.0(4)
F(6)-C(12)-C(11)	120.1(6)	F(17)-C(34)-F(16)	107.2(6)
C(13)-C(12)-C(11)	120.5(6)	F(17)-C(34)-F(15)	107.3(6)
F(7)-C(13)-C(14)	119.0(6)	F(16)-C(34)-F(15)	106.9(6)
F(7)-C(13)-C(12)	119.2(6)	F(17)-C(34)-C(33)	112.2(5)
C(14)-C(13)-C(12)	121.8(6)	F(16)-C(34)-C(33)	111.6(5)
F(8)-C(14)-C(13)	119.7(6)	F(15)-C(34)-C(33)	111.3(5)
F(8)-C(14)-C(15)	121.9(6)	F(18)-C(35)-F(19)	107.7(6)
C(13)-C(14)-C(15)	118.4(6)	F(18)-C(35)-F(20)	107.6(6)
C(14)-C(15)-C(10)	119.9(6)	F(19)-C(35)-F(20)	107.0(6)
C(14)-C(15)-C(16)	133.0(6)	F(18)-C(35)-C(33)	111.7(5)
C(10)-C(15)-C(16)	107.1(5)	F(19)-C(35)-C(33)	111.2(5)

F(20)-C(35)-C(33)	111.4(5)	F(28)-C(39)-C(41)	104.1(6)
C(28)-C(27')-C(26)	111.8(8)	C(40)-C(39)-C(41)	112.0(7)
C(28)-C(27')-C(33')	123.7(8)	F(28)-C(39)-C(30)	106.1(6)
C(26)-C(27')-C(33')	121.7(7)	C(40)-C(39)-C(30)	111.6(7)
F(14')-C(33')-C(27')	106.8(7)	C(41)-C(39)-C(30)	119.5(7)
F(14')-C(33')-C(34')	103.5(5)	F(31)-C(40)-F(29)	107.4(8)
C(27')-C(33')-C(34')	115.2(4)	F(31)-C(40)-F(30)	107.6(8)
F(14')-C(33')-C(35')	102.8(4)	F(29)-C(40)-F(30)	100.5(10)
C(27')-C(33')-C(35')	115.9(4)	F(31)-C(40)-C(39)	122.7(11)
C(34')-C(33')-C(35')	111.0(5)	F(29)-C(40)-C(39)	108.8(7)
F(15')-C(34')-F(17')	107.3(6)	F(30)-C(40)-C(39)	107.5(7)
F(15')-C(34')-F(16')	107.2(6)	F(34)-C(41)-F(33)	108.0(8)
F(17')-C(34')-F(16')	107.3(6)	F(34)-C(41)-F(32)	108.0(7)
F(15')-C(34')-C(33')	111.8(6)	F(33)-C(41)-F(32)	107.0(6)
F(17')-C(34')-C(33')	111.8(6)	F(34)-C(41)-C(39)	113.1(7)
F(16')-C(34')-C(33')	111.2(6)	F(33)-C(41)-C(39)	111.5(7)
F(20')-C(35')-F(18')	107.5(6)	F(32)-C(41)-C(39)	109.0(7)
F(20')-C(35')-F(19')	107.3(6)	C(26)-C(31)-C(30)	124.1(6)
F(18')-C(35')-F(19')	107.0(6)	C(26)-C(31)-C(32)	105.9(6)
F(20')-C(35')-C(33')	111.8(6)	C(30)-C(31)-C(32)	130.0(6)
F(18')-C(35')-C(33')	111.7(6)	N(8)-C(32)-N(4)	127.2(5)
F(19')-C(35')-C(33')	111.3(6)	N(8)-C(32)-C(31)	123.3(6)
F(13)-C(28)-C(29)	116.3(8)	N(4)-C(32)-C(31)	109.0(5)
F(13)-C(28)-C(27)	117.1(9)	O(2)-C(42)-C(43)	122.6(11)
C(29)-C(28)-C(27)	124.1(7)	O(2)-C(42)-C(44)	120.6(10)
F(13)-C(28)-C(27')	114.9(9)	C(43)-C(42)-C(44)	116.8(10)
C(29)-C(28)-C(27')	128.3(7)	C(42)-C(43)-H(43A)	109.5
C(27)-C(28)-C(27')	21.9(6)	C(42)-C(43)-H(43B)	109.5
C(28)-C(29)-C(30)	119.0(8)	H(43A)-C(43)-H(43B)	109.5
C(28)-C(29)-C(36)	118.4(8)	C(42)-C(43)-H(43C)	109.5
C(30)-C(29)-C(36)	122.4(9)	H(43A)-C(43)-H(43C)	109.5
F(21)-C(36)-C(29)	112.3(7)	H(43B)-C(43)-H(43C)	109.5
F(21)-C(36)-C(37)	105.2(8)	C(42)-C(44)-H(44A)	109.5
C(29)-C(36)-C(37)	117.8(10)	C(42)-C(44)-H(44B)	109.5
F(21)-C(36)-C(38)	98.4(9)	H(44A)-C(44)-H(44B)	109.5
C(29)-C(36)-C(38)	110.9(7)	C(42)-C(44)-H(44C)	109.5
C(37)-C(36)-C(38)	110.3(8)	H(44A)-C(44)-H(44C)	109.5
F(22)-C(37)-F(23)	109.7(11)	H(44B)-C(44)-H(44C)	109.5
F(22)-C(37)-F(24)	105.7(10)	O(3)-C(45)-C(46)	121.9(9)
F(23)-C(37)-F(24)	109.1(9)	O(3)-C(45)-C(47)	122.1(7)
F(22)-C(37)-C(36)	109.3(9)	C(46)-C(45)-C(47)	116.0(8)
F(23)-C(37)-C(36)	111.0(10)	C(45)-C(46)-H(46A)	109.5
F(24)-C(37)-C(36)	111.7(10)	C(45)-C(46)-H(46B)	109.5
F(26)-C(38)-F(25)	111.8(10)	H(46A)-C(46)-H(46B)	109.5
F(26)-C(38)-F(27)	107.7(10)	C(45)-C(46)-H(46C)	109.5
F(25)-C(38)-F(27)	109.5(9)	H(46A)-C(46)-H(46C)	109.5
F(26)-C(38)-C(36)	106.6(8)	H(46B)-C(46)-H(46C)	109.5
F(25)-C(38)-C(36)	111.7(10)	C(45)-C(47)-H(47A)	109.5
F(27)-C(38)-C(36)	109.3(10)	C(45)-C(47)-H(47B)	109.5
C(29)-C(30)-C(31)	113.5(8)	H(47A)-C(47)-H(47B)	109.5
C(29)-C(30)-C(39)	126.3(7)	C(45)-C(47)-H(47C)	109.5
C(31)-C(30)-C(39)	117.8(6)	H(47A)-C(47)-H(47C)	109.5
F(28)-C(39)-C(40)	101.3(7)	H(47B)-C(47)-H(47C)	109.5

Table S.4 Anisotropic Displacement Parameters ($Å^2 \times 10^3$) for $F_{34}PcZn(H_2O)$ $\bullet 2(CH_3)_2CO^*$

	U^{11}	U^{22}	U^{33}	U^{23}	U^{13}	U^{12}
Zn(1)	27(1)	24(1)	42(1)	-2(1)	6(1)	-5(1)
O(1)	39(2)	31(2)	56(3)	3(2)	8(2)	-2(2)
N(1)	25(2)	25(2)	40(2)	-2(2)	6(2)	-4(2)
N(2)	26(2)	26(2)	42(3)	3(2)	7(2)	-2(2)
N(3)	31(2)	21(2)	53(3)	-2(2)	4(2)	-4(2)
N(4)	30(2)	31(2)	45(3)	-10(2)	5(2)	-7(2)
N(5)	29(2)	20(2)	40(2)	1(2)	6(2)	1(2)
N(6)	30(2)	23(2)	59(3)	8(2)	13(2)	1(2)
N(7)	36(3)	30(3)	58(3)	-10(2)	-3(2)	-3(2)
N(8)	30(2)	28(2)	42(3)	-1(2)	9(2)	-1(2)
C(1)	27(3)	23(3)	41(3)	1(2)	5(2)	0(2)
C(2)	28(3)	19(2)	41(3)	3(2)	5(2)	0(2)
C(3)	31(3)	23(3)	45(3)	1(2)	9(2)	-3(2)
F(1)	46(2)	43(2)	47(2)	6(2)	16(2)	-9(2)
C(4)	25(3)	26(3)	64(4)	8(3)	10(3)	-3(2)
F(2)	34(2)	39(2)	69(2)	8(2)	15(2)	-11(2)
C(5)	27(3)	22(3)	51(3)	-2(2)	4(2)	-3(2)
F(3)	30(2)	27(2)	67(2)	-3(2)	0(2)	-8(1)
C(6)	28(3)	22(3)	47(3)	-2(2)	0(2)	5(2)
F(4)	33(2)	33(2)	43(2)	-5(1)	2(1)	-1(1)
C(7)	22(2)	16(2)	47(3)	0(2)	6(2)	3(2)
C(8)	27(3)	19(2)	40(3)	-1(2)	6(2)	2(2)
C(9)	31(3)	22(3)	41(3)	1(2)	7(2)	2(2)
C(10)	38(3)	22(3)	47(3)	5(2)	10(3)	6(2)
C(11)	48(3)	31(3)	43(3)	6(2)	9(3)	14(3)
F(5)	55(2)	38(2)	41(2)	-2(2)	4(2)	-4(2)
C(12)	58(4)	42(4)	43(3)	7(3)	11(3)	10(3)
F(6)	74(3)	67(3)	42(2)	5(2)	12(2)	4(2)
C(13)	54(4)	47(4)	45(3)	15(3)	18(3)	17(3)
F(7)	71(3)	76(3)	52(2)	18(2)	26(2)	4(2)
C(14)	40(3)	31(3)	65(4)	14(3)	21(3)	11(3)
F(8)	45(2)	45(2)	69(2)	18(2)	26(2)	4(2)
C(15)	36(3)	26(3)	50(3)	7(2)	14(3)	9(2)
C(16)	31(3)	22(3)	54(3)	9(2)	13(2)	5(2)
C(17)	22(3)	20(3)	64(4)	5(2)	7(3)	2(2)
C(18)	27(3)	21(3)	74(4)	6(3)	4(3)	-2(2)
C(19)	31(3)	28(3)	85(5)	13(3)	8(3)	2(2)
F(9)	37(2)	40(2)	98(3)	15(2)	26(2)	1(2)
C(20)	28(3)	26(3)	105(6)	16(3)	4(3)	-4(2)
F(10)	35(2)	38(2)	139(4)	23(2)	14(2)	-10(2)
C(21)	32(3)	29(3)	113(7)	14(4)	-16(4)	-15(3)
F(11)	54(2)	43(2)	123(4)	10(2)	-23(3)	-27(2)
C(22)	49(4)	37(4)	75(5)	4(3)	-10(3)	-9(3)
F(12)	74(3)	54(3)	74(3)	-4(2)	-16(2)	-29(2)
C(23)	29(3)	25(3)	73(5)	8(3)	-9(3)	-5(2)
C(24)	29(3)	28(3)	58(4)	-1(3)	-2(3)	1(2)
C(25)	38(3)	43(3)	54(4)	-18(3)	3(3)	-3(3)
C(26)	45(4)	62(4)	57(4)	-24(3)	7(3)	-8(3)
C(27)	40(6)	57(7)	59(5)	-14(5)	1(4)	10(5)
C(33)	78(10)	85(11)	73(8)	-15(7)	-19(7)	-5(8)
F(14)	98(5)	78(6)	74(3)	-4(4)	-16(4)	-18(4)

C(34)	112(4)	99(4)	84(4)	-10(3)	-29(4)	-20(4)
F(15)	113(5)	106(5)	91(5)	-6(4)	-33(4)	-30(5)
F(16)	106(5)	78(4)	78(4)	0(4)	-40(4)	-14(4)
F(17)	129(6)	99(5)	87(5)	-16(4)	-24(4)	-15(5)
C(35)	146(6)	59(4)	88(4)	-14(4)	-8(4)	-8(4)
F(18)	144(7)	63(4)	99(5)	-8(4)	-24(5)	-22(5)
F(19)	135(6)	38(4)	80(3)	-13(3)	-4(4)	-2(4)
F(20)	152(7)	72(3)	86(3)	-16(3)	6(4)	-2(4)
C(27')	40(6)	57(7)	59(5)	-14(5)	1(4)	10(5)
C(33')	78(10)	85(11)	73(8)	-15(7)	-19(7)	-5(8)
F(14')	135(6)	38(4)	80(3)	-13(3)	-4(4)	-2(4)
C(34')	106(5)	93(5)	86(5)	-11(5)	-19(5)	-19(5)
F(15')	98(5)	78(6)	74(3)	-4(4)	-16(4)	-18(4)
F(16')	112(4)	99(4)	84(4)	-10(3)	-29(4)	-20(4)
F(17')	111(7)	98(7)	103(7)	-16(6)	-14(6)	-21(7)
C(35')	152(7)	72(3)	86(3)	-16(3)	6(4)	-2(4)
F(18')	150(8)	84(6)	87(6)	-13(6)	1(6)	1(7)
F(19')	153(9)	65(6)	88(6)	-26(5)	8(7)	-10(6)
F(20')	137(9)	69(5)	81(6)	-14(5)	23(7)	0(7)
C(28)	76(5)	79(6)	43(4)	-21(4)	-2(4)	21(5)
F(13)	121(4)	98(4)	43(2)	-22(2)	-2(3)	9(3)
C(29)	64(5)	90(6)	39(4)	-8(4)	-7(3)	24(5)
C(36)	135(9)	80(6)	33(4)	-3(4)	-7(5)	19(6)
F(21)	105(4)	96(4)	42(2)	11(2)	9(2)	-1(3)
C(37)	124(10)	125(10)	40(5)	5(6)	-9(5)	-3(8)
F(22)	121(5)	137(6)	62(3)	4(3)	-27(3)	32(5)
F(23)	193(8)	159(7)	46(3)	22(4)	-7(4)	-8(6)
F(24)	161(6)	166(7)	40(3)	-19(4)	-12(3)	37(5)
C(38)	107(8)	140(11)	49(5)	-7(6)	27(5)	10(8)
F(25)	135(6)	109(5)	83(4)	-28(4)	31(4)	25(4)
F(26)	91(4)	134(5)	38(2)	-4(3)	15(2)	22(3)
F(27)	134(5)	180(7)	54(3)	-14(4)	36(3)	7(5)
C(30)	50(4)	70(5)	40(3)	-6(3)	-1(3)	5(3)
C(39)	68(5)	55(4)	54(4)	9(3)	-3(4)	9(4)
F(28)	74(3)	50(2)	64(3)	-4(2)	-1(2)	11(2)
C(40)	113(9)	86(7)	53(5)	26(5)	-18(5)	-19(6)
F(29)	84(4)	87(4)	109(4)	14(3)	-9(3)	22(3)
F(30)	132(5)	64(3)	116(5)	22(3)	-13(4)	19(3)
F(31)	118(5)	103(4)	78(4)	20(3)	-3(3)	9(4)
C(41)	77(5)	75(5)	45(4)	9(4)	13(4)	7(4)
F(32)	64(3)	82(3)	57(2)	-4(2)	12(2)	8(2)
F(33)	89(3)	58(3)	69(3)	5(2)	4(2)	2(2)
F(34)	114(4)	86(4)	69(3)	25(3)	3(3)	-16(3)
C(31)	38(3)	57(4)	42(3)	-9(3)	4(3)	5(3)
C(32)	35(3)	38(3)	38(3)	-9(2)	4(2)	1(2)
O(2)	116(6)	102(5)	73(4)	5(4)	-5(4)	25(5)
C(42)	68(5)	111(8)	55(5)	16(5)	16(4)	6(5)
C(43)	120(10)	144(12)	77(7)	-6(7)	10(6)	0(9)
C(44)	69(6)	160(13)	118(9)	-18(9)	38(6)	1(7)
O(3)	45(3)	28(2)	144(6)	8(3)	11(3)	-5(2)
C(45)	49(4)	28(3)	122(7)	-14(4)	30(4)	-4(3)
C(46)	45(4)	32(4)	173(10)	3(5)	31(5)	-3(3)
C(47)	100(7)	75(6)	80(6)	-23(5)	25(5)	-22(5)

* The anisotropic displacement factor exponent takes the form: $-2\pi^2 [h^2 a^{*2} U^{11} + ... + 2 h k a^* b^* U^{12}]$.

Table S.5 Hydrogen Coordinates (× 10^4) and Isotropic Displacement Parameters (Å^2 × 10^3) for $F_{34}PcZn(H_2O)•2(CH_3)_2CO$

	x	y	z	U(eq)
H(1A)	7712	2176	576	51
H(1B)	8524	2817	803	51
H(43A)	10272	3624	1813	174
H(43B)	11603	3308	1746	174
H(43C)	10909	2394	1931	174
H(44A)	10327	1165	1129	169
H(44B)	10408	723	1495	169
H(44C)	11572	1370	1407	169
H(46A)	4549	-111	340	123
H(46B)	4554	-221	721	123
H(46C)	5166	-1227	545	123
H(47A)	7825	399	1011	126
H(47B)	7417	-933	934	126
H(47C)	6674	-126	1136	126

APPENDIX T

CRYSTAL STRUCTURE OF 1,3,4-TRIS-(PERFLUOROISOPROPYL)-TRIDECAFLUOROPHTHALOCYANINATO-COBALT(II)

Tables T.1 to T.5 list the atomic coordinates and crystallographic parameters for $F_{34}PcCo(CH_3CN)$•2Tol **[5-11]** (Figure T.1).

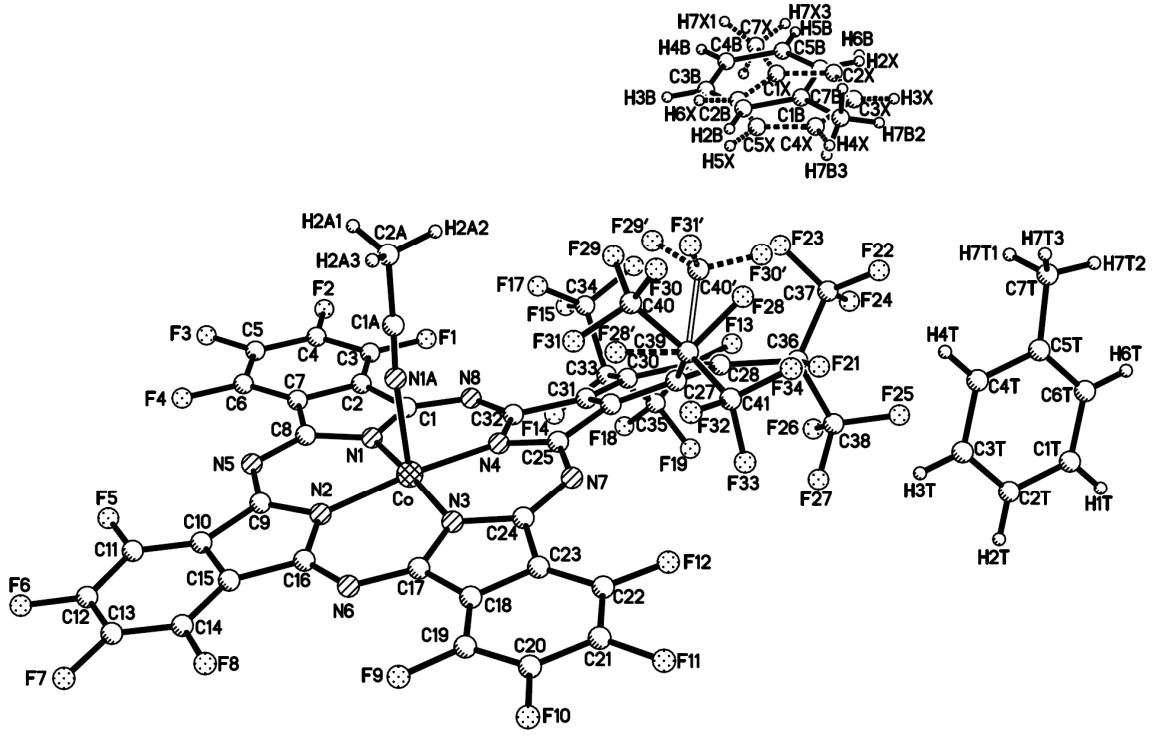

Figure T.1 Crystal structure of $F_{34}PcCo(CH_3CN)$•2Tol.

Table T.1 Crystal Data and Structure Refinement for $F_{34}PcCo(CH_3CN)$•2Tol

Empirical formula	$C_{57}\ H_{19}\ Co\ F_{34}\ N_9$	
Formula weight	1534.74	
Temperature	100(2) K	
Wavelength	0.71073 Å	
Crystal system	triclinic	
Space group	P-1	
Unit cell dimensions	a = 10.540(2) Å	α = 95.096(4)°
	b = 14.554(3) Å	β = 94.831(4)°
	c = 18.695(4) Å	γ = 106.229(4)°
Volume	2724.8(10) $Å^3$	
Z	2	
Density (calculated)	1.871 g/cm^3	
Absorption coefficient	0.485 mm^{-1}	
F(000)	1514	
Crystal size	0.035 × 0.020 × 0.005 mm^3	
Theta range for data collection	1.73 to 27.48°	
Index ranges	$-10 \le h \le 13, -18 \le k \le 13, -23 \le l \le 24$	
Reflections collected	21427	
Independent reflections	10873 [*R*(int) = 0.0689]	
Completeness to theta = 27.48°	87.1%	
Max. and min. transmission	0.9622 and 0.9531	
Refinement method	Full-matrix least-squares on F^2	
Data / restraints / parameters	10873 / 540 / 866	
Goodness-of-fit on F^2	1.031	
Final *R* indices [*I*>2sigma(*I*)]	*R*1 = 0.0950, *wR*2 = 0.2441	
R indices (all data)	*R*1 = 0.1419, *wR*2 = 0.2658	
Largest diff. peak and hole	1.155 and −1.144 e.$Å^{-3}$	

Table T.2 Atomic Coordinates (× 10^4) and Equivalent Isotropic Displacement Parameters ($Å^2$ × 10^3) for $F_{34}PcCo(CH_3CN)$•2Tol*

	x	y	z	U(eq)
Co	6082(1)	15(1)	1229(1)	15(1)
N(1)	5123(4)	-917(3)	1789(3)	17(1)
N(2)	5938(5)	-982(3)	458(3)	18(1)
N(3)	6844(4)	964(3)	624(3)	16(1)
N(4)	6037(4)	1014(3)	1955(3)	17(1)
N(5)	4971(5)	-2403(3)	1044(3)	21(1)
N(6)	6863(5)	-50(3)	-479(2)	18(1)
N(7)	7302(4)	2412(3)	1456(3)	17(1)
N(8)	4751(4)	109(3)	2794(3)	17(1)
C(1)	4676(5)	-732(4)	2437(3)	18(1)
C(2)	4081(6)	-1636(4)	2727(3)	19(1)
C(3)	3468(6)	-1847(4)	3349(3)	25(1)
C(4)	3047(6)	-2810(5)	3458(4)	29(2)
C(5)	3167(6)	-3526(5)	2979(4)	30(2)
C(6)	3731(6)	-3329(4)	2338(4)	23(1)

C(7)	4189(5)	-2371(4)	2229(3)	21(1)
C(8)	4833(5)	-1888(4)	1644(3)	17(1)
C(9)	5453(5)	-1955(4)	488(3)	18(1)
C(10)	5486(5)	-2495(4)	-197(3)	17(1)
C(11)	5066(6)	-3456(4)	-444(3)	21(1)
C(12)	5229(6)	-3738(4)	-1152(3)	24(1)
C(13)	5811(6)	-3055(5)	-1590(3)	23(1)
C(14)	6231(6)	-2095(4)	-1347(3)	21(1)
C(15)	6037(5)	-1793(4)	-644(3)	18(1)
C(16)	6314(5)	-868(4)	-221(3)	17(1)
C(17)	7085(5)	800(4)	-86(3)	16(1)
C(18)	7650(5)	1690(4)	-359(3)	20(1)
C(19)	8110(6)	1925(4)	-1014(3)	21(1)
C(20)	8572(6)	2876(5)	-1117(3)	24(1)
C(21)	8595(6)	3602(4)	-577(3)	21(1)
C(22)	8185(6)	3380(4)	89(3)	24(1)
C(23)	7720(5)	2423(4)	195(3)	17(1)
C(24)	7259(5)	1940(4)	819(3)	16(1)
C(25)	6753(5)	1961(4)	1992(3)	16(1)
C(26)	6651(6)	2474(4)	2683(3)	19(1)
C(27)	7353(6)	3406(4)	3005(3)	19(1)
C(28)	6785(6)	3795(4)	3570(3)	22(1)
C(29)	5706(7)	3174(4)	3832(3)	24(1)
C(30)	5093(6)	2219(4)	3588(3)	21(1)
C(31)	5621(5)	1872(4)	2989(3)	18(1)
C(32)	5391(5)	911(4)	2566(3)	18(1)
C(33)	3913(6)	1631(4)	3929(3)	19(1)
C(34)	4405(2)	1177(2)	4590(1)	26(1)
F(15)	3374(3)	633(2)	4853(1)	40(1)
F(16)	5093(3)	1867(2)	5092(1)	37(1)
F(17)	5163(3)	648(2)	4377(1)	34(1)
C(35)	2835(2)	2159(2)	4125(1)	32(2)
F(18)	1658(3)	1524(2)	4061(2)	39(1)
F(19)	2818(3)	2808(2)	3682(2)	41(1)
F(20)	3138(3)	2581(2)	4792(2)	35(1)
C(36)	7121(7)	4873(4)	3823(3)	27(1)
C(37)	7578(3)	5147(2)	4673(1)	38(2)
F(22)	8572(4)	5947(2)	4783(1)	44(1)
F(23)	7964(4)	4444(2)	4932(1)	53(1)
F(24)	6573(4)	5275(2)	5001(1)	45(1)
C(38)	5977(3)	5324(2)	3568(1)	32(2)
F(25)	6299(3)	6233(2)	3838(2)	40(1)
F(26)	4860(3)	4853(2)	3795(2)	50(1)
F(27)	5826(3)	5261(2)	2860(2)	46(1)
C(39)	8830(6)	3790(4)	2897(4)	26(1)
C(40)	9710(6)	3122(5)	2959(4)	29(4)
F(29)	9497(8)	2677(6)	3543(5)	36(3)
F(30)	10974(8)	3632(6)	3007(5)	35(3)
F(31)	9423(8)	2476(6)	2380(5)	27(3)
C(40')	9811(4)	3877(3)	3596(3)	28(2)
F(29')	9434(5)	3101(4)	3915(3)	38(2)
F(30')	9805(5)	4623(4)	4034(3)	41(2)
F(31')	11008(4)	3979(4)	3420(3)	36(2)
C(41)	9231(6)	4570(4)	2370(4)	27(1)
F(1)	3315(4)	-1183(3)	3821(2)	33(1)
F(2)	2443(4)	-3037(3)	4054(2)	37(1)

F(3)	2731(4)	-4446(3)	3102(2)	37(1)
F(4)	3829(4)	-4045(2)	1882(2)	34(1)
F(5)	4514(3)	-4129(2)	-28(2)	24(1)
F(6)	4819(4)	-4667(2)	-1400(2)	33(1)
F(7)	5973(4)	-3358(3)	-2260(2)	33(1)
F(8)	6797(3)	-1467(2)	-1792(2)	24(1)
F(9)	8094(3)	1253(2)	-1554(2)	25(1)
F(10)	9030(4)	3126(3)	-1740(2)	31(1)
F(11)	9041(4)	4522(2)	-706(2)	32(1)
F(12)	8208(4)	4098(2)	591(2)	27(1)
F(13)	5269(4)	3550(2)	4415(2)	29(1)
F(14)	3196(3)	880(2)	3427(2)	25(1)
F(21)	8137(4)	5369(3)	3481(2)	35(1)
F(28)	9413(11)	4436(7)	3578(6)	33(3)
F(28')	9145(6)	2971(5)	2508(3)	28(2)
F(32)	9866(4)	4269(3)	1855(2)	42(1)
F(33)	8142(4)	4720(3)	2040(2)	31(1)
F(34)	10007(4)	5385(3)	2692(3)	43(1)
N(1A)	7999(5)	13(3)	1716(3)	20(1)
C(1A)	9003(7)	70(5)	2013(4)	30(1)
C(2A)	10305(7)	121(6)	2390(4)	45(2)
C(1T)	7853(10)	8797(10)	3403(7)	196(13)
C(2T)	7714(6)	8065(9)	2845(6)	204(14)
C(3T)	8585(9)	7503(6)	2854(4)	167(10)
C(4T)	9595(7)	7672(5)	3420(4)	71(3)
C(5T)	9734(9)	8404(6)	3978(4)	89(4)
C(6T)	8863(14)	8966(8)	3969(5)	262(17)
C(7T)	10576(13)	8458(10)	4630(9)	112(5)
C(1X)	1064(9)	2249(5)	10242(4)	32(4)
C(2X)	1502(10)	3249(5)	10356(4)	27(3)
C(3X)	2021(10)	3771(5)	9807(5)	31(3)
C(4X)	2103(10)	3292(7)	9143(5)	42(4)
C(5X)	1665(11)	2292(7)	9028(4)	35(4)
C(6X)	1145(10)	1770(5)	9578(5)	31(4)
C(7X)	535(17)	1672(11)	10821(8)	41(4)
C(1B)	1542(8)	2846(5)	9780(4)	32(3)
C(2B)	1298(8)	1927(6)	9416(4)	18(3)
C(3B)	739(9)	1122(4)	9756(5)	33(3)
C(4B)	425(10)	1236(6)	10459(5)	41(4)
C(5B)	670(11)	2154(7)	10823(4)	46(4)
C(6B)	1228(10)	2959(5)	10483(4)	34(3)
C(7B)	2158(15)	3659(11)	9381(9)	38(3)

* U(eq) is defined as one third of the trace of the orthogonalized U^{ij} tensor.

Table T.3 Bond Lengths (Å) and Angles (°) for $F_{34}PcCo(CH_3CN)$•2Tol

Co-N(1)	1.903(4)	Co-N(2)	1.916(5)
Co-N(3)	1.908(5)	Co-N(1A)	2.146(5)
Co-N(4)	1.913(5)		
N(1)-C(8)	1.357(7)	N(3)-C(17)	1.386(7)
N(1)-C(1)	1.368(8)	N(4)-C(25)	1.366(7)
N(2)-C(9)	1.372(7)	N(4)-C(32)	1.376(7)
N(2)-C(16)	1.372(7)	N(5)-C(8)	1.333(8)
N(3)-C(24)	1.370(7)	N(5)-C(9)	1.337(8)

N(6)-C(16)	1.323(7)	C(1A)-C(2A)	1.468(10)
N(6)-C(17)	1.331(7)	C(2A)-H(2A1)	0.9800
N(7)-C(24)	1.313(7)	C(2A)-H(2A2)	0.9800
N(7)-C(25)	1.330(7)	C(2A)-H(2A3)	0.9800
N(8)-C(32)	1.303(7)	C(1T)-C(2T)	1.3900
N(8)-C(1)	1.319(7)	C(1T)-C(6T)	1.3900
C(1)-C(2)	1.462(8)	C(1T)-H(1T)	0.9500
C(2)-C(7)	1.390(9)	C(2T)-C(3T)	1.3900
C(2)-C(3)	1.395(9)	C(2T)-H(2T)	0.9500
C(3)-C(4)	1.386(9)	C(3T)-C(4T)	1.3900
C(4)-C(5)	1.353(10)	C(3T)-H(3T)	0.9500
C(5)-C(6)	1.400(9)	C(4T)-C(5T)	1.3900
C(6)-C(7)	1.381(8)	C(4T)-H(4T)	0.9500
C(7)-C(8)	1.466(8)	C(5T)-C(6T)	1.3900
C(9)-C(10)	1.451(8)	C(5T)-C(7T)	1.429(17)
C(10)-C(11)	1.368(8)	C(6T)-H(6T)	0.9500
C(10)-C(15)	1.409(8)	C(7T)-H(7T1)	0.9800
C(11)-C(12)	1.389(9)	C(7T)-H(7T2)	0.9800
C(12)-C(13)	1.386(9)	C(7T)-H(7T3)	0.9800
C(13)-C(14)	1.364(9)	C(1X)-C(2X)	1.3900
C(14)-C(15)	1.397(8)	C(1X)-C(6X)	1.3900
C(15)-C(16)	1.441(8)	C(1X)-C(7X)	1.480(17)
C(17)-C(18)	1.424(8)	C(2X)-C(3X)	1.3900
C(18)-C(19)	1.391(8)	C(2X)-H(2X)	0.9500
C(18)-C(23)	1.401(8)	C(3X)-C(4X)	1.3900
C(19)-C(20)	1.370(8)	C(3X)-H(3X)	0.9500
C(20)-C(21)	1.389(9)	C(4X)-C(5X)	1.3900
C(21)-C(22)	1.386(9)	C(4X)-H(4X)	0.9500
C(22)-C(23)	1.381(8)	C(5X)-C(6X)	1.3900
C(23)-C(24)	1.462(8)	C(5X)-H(5X)	0.9500
C(25)-C(26)	1.461(8)	C(6X)-H(6X)	0.9500
C(26)-C(31)	1.392(8)	C(7X)-H(7X1)	0.9800
C(26)-C(27)	1.403(8)	C(7X)-H(7X2)	0.9800
C(27)-C(28)	1.408(8)	C(7X)-H(7X3)	0.9800
C(27)-C(39)	1.537(8)	C(1B)-C(2B)	1.3900
C(28)-C(29)	1.396(9)	C(1B)-C(6B)	1.3900
C(28)-C(36)	1.530(8)	C(1B)-C(7B)	1.478(15)
C(29)-C(30)	1.376(8)	C(2B)-C(3B)	1.3900
C(30)-C(31)	1.406(8)	C(2B)-H(2B)	0.9500
C(30)-C(33)	1.525(8)	C(3B)-C(4B)	1.3900
C(31)-C(32)	1.491(8)	C(3B)-H(3B)	0.9500
C(33)-C(34)	1.569(6)	C(4B)-C(5B)	1.3900
C(33)-C(35)	1.588(6)	C(4B)-H(4B)	0.9500
C(36)-C(38)	1.586(8)	C(5B)-C(6B)	1.3900
C(36)-C(37)	1.601(7)	C(5B)-H(5B)	0.9500
C(39)-C(40)	1.526(10)	C(6B)-H(6B)	0.9500
C(39)-C(41)	1.562(8)	C(7B)-H(7B1)	0.9800
C(39)-C(40')	1.570(8)	C(7B)-H(7B2)	0.9800
N(1A)-C(1A)	1.131(8)	C(7B)-H(7B3)	0.9800
N(1)-Co-N(3)	173.2(2)	N(4)-Co-N(2)	173.7(2)
N(1)-Co-N(4)	89.4(2)	N(1)-Co-N(1A)	94.35(19)
N(3)-Co-N(4)	89.8(2)	N(3)-Co-N(1A)	92.40(19)
N(1)-Co-N(2)	90.1(2)	N(4)-Co-N(1A)	90.41(19)
N(3)-Co-N(2)	90.0(2)	N(2)-Co-N(1A)	95.87(19)

C(8)-N(1)-C(1)	107.2(5)	C(22)-C(21)-C(20)	120.6(5)
C(8)-N(1)-Co	126.3(4)	C(23)-C(22)-C(21)	118.5(6)
C(1)-N(1)-Co	126.4(4)	C(22)-C(23)-C(18)	120.8(5)
C(9)-N(2)-C(16)	106.8(5)	C(22)-C(23)-C(24)	133.0(5)
C(9)-N(2)-Co	126.1(4)	C(18)-C(23)-C(24)	106.2(5)
C(16)-N(2)-Co	127.1(4)	N(7)-C(24)-N(3)	128.0(5)
C(24)-N(3)-C(17)	107.3(4)	N(7)-C(24)-C(23)	122.7(5)
C(24)-N(3)-Co	125.9(4)	N(3)-C(24)-C(23)	109.3(5)
C(17)-N(3)-Co	126.8(4)	N(7)-C(25)-N(4)	126.9(5)
C(25)-N(4)-C(32)	107.2(5)	N(7)-C(25)-C(26)	122.6(5)
C(25)-N(4)-Co	125.3(4)	N(4)-C(25)-C(26)	109.8(5)
C(32)-N(4)-Co	127.3(4)	C(31)-C(26)-C(27)	122.7(5)
C(8)-N(5)-C(9)	119.8(5)	C(31)-C(26)-C(25)	106.8(5)
C(16)-N(6)-C(17)	121.7(5)	C(27)-C(26)-C(25)	130.4(5)
C(24)-N(7)-C(25)	121.0(4)	C(26)-C(27)-C(28)	116.4(5)
C(32)-N(8)-C(1)	121.0(5)	C(26)-C(27)-C(39)	117.9(5)
N(8)-C(1)-N(1)	128.5(5)	C(28)-C(27)-C(39)	122.7(5)
N(8)-C(1)-C(2)	121.4(5)	C(29)-C(28)-C(27)	117.2(5)
N(1)-C(1)-C(2)	110.0(5)	C(29)-C(28)-C(36)	118.0(5)
C(7)-C(2)-C(3)	120.6(5)	C(27)-C(28)-C(36)	124.0(5)
C(7)-C(2)-C(1)	106.5(5)	C(30)-C(29)-C(28)	127.6(6)
C(3)-C(2)-C(1)	132.9(6)	C(29)-C(30)-C(31)	113.7(5)
C(4)-C(3)-C(2)	116.6(6)	C(29)-C(30)-C(33)	121.5(5)
C(5)-C(4)-C(3)	122.8(6)	C(31)-C(30)-C(33)	124.7(5)
C(4)-C(5)-C(6)	121.2(6)	C(26)-C(31)-C(30)	121.1(5)
C(7)-C(6)-C(5)	116.8(6)	C(26)-C(31)-C(32)	103.9(5)
C(6)-C(7)-C(2)	121.8(5)	C(30)-C(31)-C(32)	134.9(5)
C(6)-C(7)-C(8)	132.8(6)	N(8)-C(32)-N(4)	127.1(5)
C(2)-C(7)-C(8)	105.4(5)	N(8)-C(32)-C(31)	122.8(5)
N(5)-C(8)-N(1)	128.6(5)	N(4)-C(32)-C(31)	109.9(5)
N(5)-C(8)-C(7)	120.3(5)	C(30)-C(33)-C(34)	110.4(4)
N(1)-C(8)-C(7)	110.9(5)	C(30)-C(33)-C(35)	116.2(4)
N(5)-C(9)-N(2)	128.0(5)	C(34)-C(33)-C(35)	111.9(4)
N(5)-C(9)-C(10)	121.0(5)	C(28)-C(36)-C(38)	112.8(5)
N(2)-C(9)-C(10)	111.0(5)	C(28)-C(36)-C(37)	113.9(5)
C(11)-C(10)-C(15)	121.8(5)	C(38)-C(36)-C(37)	111.4(4)
C(11)-C(10)-C(9)	133.1(5)	C(40)-C(39)-C(27)	118.9(5)
C(15)-C(10)-C(9)	105.0(5)	C(40)-C(39)-C(41)	115.6(5)
C(10)-C(11)-C(12)	118.3(5)	C(27)-C(39)-C(41)	118.3(5)
C(13)-C(12)-C(11)	120.3(5)	C(40)-C(39)-C(40')	58.9(3)
C(14)-C(13)-C(12)	121.6(5)	C(27)-C(39)-C(40')	114.1(5)
C(13)-C(14)-C(15)	119.0(5)	C(41)-C(39)-C(40')	117.5(5)
C(14)-C(15)-C(10)	118.7(5)	C(1A)-N(1A)-Co	174.4(5)
C(14)-C(15)-C(16)	134.3(5)	N(1A)-C(1A)-C(2A)	178.6(7)
C(10)-C(15)-C(16)	107.0(5)	C(2T)-C(1T)-C(6T)	120.0
N(6)-C(16)-N(2)	127.3(5)	C(2T)-C(1T)-H(1T)	120.0
N(6)-C(16)-C(15)	122.4(5)	C(6T)-C(1T)-H(1T)	120.0
N(2)-C(16)-C(15)	110.2(5)	C(3T)-C(2T)-C(1T)	120.0
N(6)-C(17)-N(3)	127.1(5)	C(3T)-C(2T)-H(2T)	120.0
N(6)-C(17)-C(18)	122.5(5)	C(1T)-C(2T)-H(2T)	120.0
N(3)-C(17)-C(18)	110.4(5)	C(2T)-C(3T)-C(4T)	120.0
C(19)-C(18)-C(23)	119.8(5)	C(2T)-C(3T)-H(3T)	120.0
C(19)-C(18)-C(17)	133.5(6)	C(4T)-C(3T)-H(3T)	120.0
C(23)-C(18)-C(17)	106.7(5)	C(5T)-C(4T)-C(3T)	120.0
C(20)-C(19)-C(18)	119.1(6)	C(5T)-C(4T)-H(4T)	120.0
C(19)-C(20)-C(21)	121.0(5)	C(3T)-C(4T)-H(4T)	120.0

C(4T)-C(5T)-C(6T)	120.0	C(5X)-C(6X)-C(1X)	120.0
C(4T)-C(5T)-C(7T)	120.3(6)	C(5X)-C(6X)-H(6X)	120.0
C(6T)-C(5T)-C(7T)	118.4(6)	C(1X)-C(6X)-H(6X)	120.0
C(5T)-C(6T)-C(1T)	120.0	C(2B)-C(1B)-C(6B)	120.0
C(5T)-C(6T)-H(6T)	120.0	C(2B)-C(1B)-C(7B)	116.3(8)
C(1T)-C(6T)-H(6T)	120.0	C(6B)-C(1B)-C(7B)	123.7(8)
C(2X)-C(1X)-C(6X)	120.0	C(1B)-C(2B)-C(3B)	120.0
C(2X)-C(1X)-C(7X)	121.3(6)	C(1B)-C(2B)-H(2B)	120.0
C(6X)-C(1X)-C(7X)	118.7(6)	C(3B)-C(2B)-H(2B)	120.0
C(3X)-C(2X)-C(1X)	120.0	C(4B)-C(3B)-C(2B)	120.0
C(3X)-C(2X)-H(2X)	120.0	C(4B)-C(3B)-H(3B)	120.0
C(1X)-C(2X)-H(2X)	120.0	C(2B)-C(3B)-H(3B)	120.0
C(4X)-C(3X)-C(2X)	120.0	C(5B)-C(4B)-C(3B)	120.0
C(4X)-C(3X)-H(3X)	120.0	C(5B)-C(4B)-H(4B)	120.0
C(2X)-C(3X)-H(3X)	120.0	C(3B)-C(4B)-H(4B)	120.0
C(3X)-C(4X)-C(5X)	120.0	C(6B)-C(5B)-C(4B)	120.0
C(3X)-C(4X)-H(4X)	120.0	C(6B)-C(5B)-H(5B)	120.0
C(5X)-C(4X)-H(4X)	120.0	C(4B)-C(5B)-H(5B)	120.0
C(6X)-C(5X)-C(4X)	120.0	C(5B)-C(6B)-C(1B)	120.0
C(6X)-C(5X)-H(5X)	120.0	C(5B)-C(6B)-H(6B)	120.0
C(4X)-C(5X)-H(5X)	120.0	C(1B)-C(6B)-H(6B)	120.0

Table T.4 Anisotropic Displacement Parameters ($Å^2 \times 10^3$) for $F_{34}PcCo(CH_3CN)$•2Tol*

	U^{11}	U^{22}	U^{33}	U^{23}	U^{13}	U^{12}
Co	16(1)	15(1)	17(1)	4(1)	5(1)	8(1)
N(1)	16(2)	13(2)	24(3)	7(2)	3(2)	5(2)
N(2)	18(2)	20(2)	18(2)	4(2)	2(2)	7(2)
N(3)	13(2)	14(2)	21(3)	5(2)	0(2)	6(2)
N(4)	15(2)	20(2)	18(2)	0(2)	3(2)	8(2)
N(5)	20(2)	17(2)	29(3)	3(2)	6(2)	9(2)
N(6)	17(2)	25(2)	14(2)	3(2)	1(2)	11(2)
N(7)	16(2)	14(2)	25(3)	9(2)	5(2)	5(2)
N(8)	14(2)	19(2)	21(3)	7(2)	4(2)	7(2)
C(1)	17(3)	25(3)	18(3)	3(2)	6(2)	14(2)
C(2)	19(3)	20(3)	21(3)	9(2)	2(2)	8(2)
C(3)	25(3)	26(3)	24(3)	6(3)	2(2)	7(3)
C(4)	24(3)	30(3)	33(4)	19(3)	5(3)	3(3)
C(5)	25(3)	30(3)	32(4)	13(3)	2(3)	2(3)
C(6)	19(3)	20(3)	33(4)	8(2)	1(2)	8(3)
C(7)	15(3)	26(3)	22(3)	6(2)	1(2)	7(2)
C(8)	11(2)	13(2)	30(3)	6(2)	5(2)	6(2)
C(9)	17(3)	20(3)	24(3)	-1(2)	1(2)	14(2)
C(10)	15(2)	19(3)	20(3)	1(2)	1(2)	10(2)
C(11)	20(3)	21(3)	24(3)	3(2)	-1(2)	11(2)
C(12)	26(3)	18(3)	33(4)	-4(2)	1(3)	15(3)
C(13)	25(3)	36(3)	15(3)	0(2)	0(2)	19(3)
C(14)	19(3)	22(3)	22(3)	2(2)	3(2)	5(2)
C(15)	9(2)	21(3)	26(3)	2(2)	1(2)	8(2)
C(16)	16(2)	23(3)	14(3)	0(2)	6(2)	6(2)
C(17)	17(3)	19(3)	16(3)	5(2)	4(2)	11(2)
C(18)	12(2)	27(3)	23(3)	5(2)	5(2)	8(2)
C(19)	19(3)	29(3)	17(3)	10(2)	2(2)	10(3)
C(20)	17(3)	34(3)	26(3)	11(3)	8(2)	8(3)

C(21)	18(3)	16(3)	30(3)	13(2)	0(2)	4(2)
C(22)	18(3)	24(3)	32(4)	4(3)	3(2)	10(3)
C(23)	15(2)	20(3)	19(3)	10(2)	4(2)	7(2)
C(24)	17(2)	11(2)	20(3)	4(2)	3(2)	6(2)
C(25)	17(2)	11(2)	23(3)	5(2)	6(2)	6(2)
C(26)	21(3)	20(3)	20(3)	4(2)	4(2)	10(2)
C(27)	27(3)	14(2)	18(3)	4(2)	3(2)	7(2)
C(28)	23(3)	29(3)	15(3)	2(2)	-1(2)	11(3)
C(29)	39(3)	28(3)	11(3)	2(2)	4(2)	20(3)
C(30)	25(3)	28(3)	12(3)	6(2)	0(2)	11(3)
C(31)	18(3)	21(3)	19(3)	4(2)	-3(2)	11(2)
C(32)	17(3)	26(3)	16(3)	2(2)	1(2)	14(2)
C(33)	24(3)	19(3)	17(3)	-1(2)	4(2)	10(2)
C(34)	34(3)	26(3)	19(3)	-1(2)	4(3)	11(3)
F(15)	46(2)	43(2)	35(2)	17(2)	24(2)	12(2)
F(16)	46(2)	40(2)	23(2)	4(2)	-8(2)	14(2)
F(17)	39(2)	40(2)	28(2)	12(2)	2(2)	21(2)
C(35)	38(4)	41(4)	24(4)	1(3)	10(3)	22(3)
F(18)	27(2)	50(2)	42(2)	-6(2)	13(2)	13(2)
F(19)	48(2)	49(2)	38(2)	11(2)	11(2)	31(2)
F(20)	45(2)	38(2)	26(2)	-6(2)	15(2)	19(2)
C(36)	39(4)	21(3)	19(3)	-1(2)	6(3)	9(3)
C(37)	58(5)	28(3)	30(4)	3(3)	2(3)	19(4)
F(22)	64(3)	27(2)	34(2)	-7(2)	-10(2)	7(2)
F(23)	90(4)	36(2)	32(2)	3(2)	-18(2)	24(2)
F(24)	75(3)	34(2)	30(2)	-6(2)	13(2)	21(2)
C(38)	57(4)	22(3)	23(3)	3(3)	8(3)	21(3)
F(25)	62(3)	32(2)	32(2)	-1(2)	3(2)	26(2)
F(26)	47(3)	41(2)	75(3)	12(2)	18(2)	27(2)
F(27)	74(3)	42(2)	29(2)	2(2)	-10(2)	32(2)
C(39)	26(3)	27(3)	29(3)	14(3)	4(3)	8(3)
F(29)	53(7)	31(6)	24(6)	15(5)	-6(5)	11(5)
F(30)	40(6)	26(6)	39(7)	-4(5)	-7(5)	14(5)
F(31)	29(6)	17(5)	37(6)	-1(4)	-3(4)	12(5)
F(29')	39(4)	45(4)	28(4)	18(3)	-2(3)	9(3)
F(30')	45(4)	38(4)	39(5)	-9(3)	-16(3)	22(3)
F(31')	16(3)	36(4)	51(5)	10(3)	-8(3)	4(3)
C(41)	29(3)	27(3)	34(4)	14(3)	12(3)	15(3)
F(1)	42(2)	32(2)	23(2)	7(2)	14(2)	7(2)
F(2)	46(2)	41(2)	26(2)	19(2)	13(2)	9(2)
F(3)	41(2)	26(2)	46(2)	20(2)	5(2)	8(2)
F(4)	41(2)	23(2)	43(2)	8(2)	10(2)	14(2)
F(5)	29(2)	16(2)	27(2)	4(1)	3(1)	5(2)
F(6)	50(2)	23(2)	28(2)	-6(2)	1(2)	15(2)
F(7)	48(2)	34(2)	22(2)	-7(2)	4(2)	21(2)
F(8)	27(2)	30(2)	21(2)	5(1)	6(1)	14(2)
F(9)	25(2)	34(2)	22(2)	6(2)	7(1)	15(2)
F(10)	30(2)	44(2)	20(2)	18(2)	8(2)	10(2)
F(11)	35(2)	25(2)	35(2)	14(2)	6(2)	4(2)
F(12)	36(2)	18(2)	27(2)	4(1)	0(2)	10(2)
F(13)	37(2)	27(2)	25(2)	0(2)	13(2)	14(2)
F(14)	24(2)	30(2)	19(2)	-5(1)	4(1)	7(2)
F(21)	44(2)	29(2)	32(2)	-1(2)	11(2)	9(2)
F(28)	39(6)	34(6)	20(6)	-3(4)	-11(5)	8(5)
F(28')	20(3)	31(4)	29(3)	-1(3)	0(2)	4(3)
F(32)	38(2)	61(3)	39(2)	20(2)	18(2)	28(2)

F(33)	34(2)	33(2)	35(2)	19(2)	9(2)	16(2)
F(34)	34(2)	23(2)	69(3)	8(2)	7(2)	4(2)
N(1A)	22(2)	18(2)	22(3)	0(2)	3(2)	9(2)
C(1A)	34(3)	34(3)	27(4)	1(3)	9(3)	16(3)
C(2A)	37(4)	57(5)	47(5)	-1(4)	-10(3)	30(4)
C(1T)	250(20)	320(30)	190(20)	190(20)	190(19)	250(20)
C(2T)	23(5)	280(20)	330(30)	270(30)	11(9)	9(9)
C(3T)	134(13)	145(14)	167(17)	116(14)	-69(12)	-53(12)
C(4T)	69(6)	56(6)	75(7)	11(5)	-3(5)	1(5)
C(5T)	116(9)	126(10)	63(7)	15(7)	6(7)	96(9)
C(6T)	580(50)	270(20)	87(12)	68(15)	70(20)	350(30)
C(7T)	78(8)	125(12)	135(14)	2(10)	22(9)	35(9)

* The anisotropic displacement factor exponent takes the form: $-2\pi^2 [h^2 a^{*2} U^{11} + ... + 2 h k a^* b^* U^{12}]$.

Table T.5 Hydrogen Coordinates ($\times 10^4$) and Isotropic Displacement Parameters ($Å^2 \times 10^3$) for $F_{34}PcCo(CH_3CN)$•2Tol

	x	y	z	U(eq)
H(2A1)	10244	-473	2611	67
H(2A2)	10576	673	2766	67
H(2A3)	10964	196	2043	67
H(1T)	7258	9181	3397	236
H(2T)	7024	7949	2458	245
H(3T)	8490	7003	2473	200
H(4T)	10190	7288	3426	85
H(6T)	8958	9466	4350	314
H(7T1)	10208	7898	4883	168
H(7T2)	10630	9050	4941	168
H(7T3)	11468	8464	4514	168
H(2X)	1446	3576	10810	32
H(3X)	2320	4455	9886	37
H(4X)	2458	3649	8768	50
H(5X)	1721	1964	8574	42
H(6X)	846	1086	9499	37
H(7X1)	988	1174	10873	61
H(7X2)	-422	1366	10696	61
H(7X3)	688	2094	11278	61
H(2B)	1512	1850	8935	22
H(3B)	572	495	9507	40
H(4B)	44	685	10691	49
H(5B)	455	2231	11304	56
H(6B)	1395	3587	10732	41
H(7B1)	3127	3836	9489	58
H(7B2)	1842	4212	9529	58
H(7B3)	1912	3466	8861	58

APPENDIX U

CRYSTAL STRUCTURE OF 1,2,4,8,10,11-HEXA-(PERFLUOROISOPROPYL)-DECAFLUOROPHTHALOCYANINATO-ZINC(II)

Tables U.1 to U.5 list the atomic coordinates and crystallographic parameters for $F_{52}PcZn(OPPh_3)$•3Tol **[5-12]** (Figure U.1).

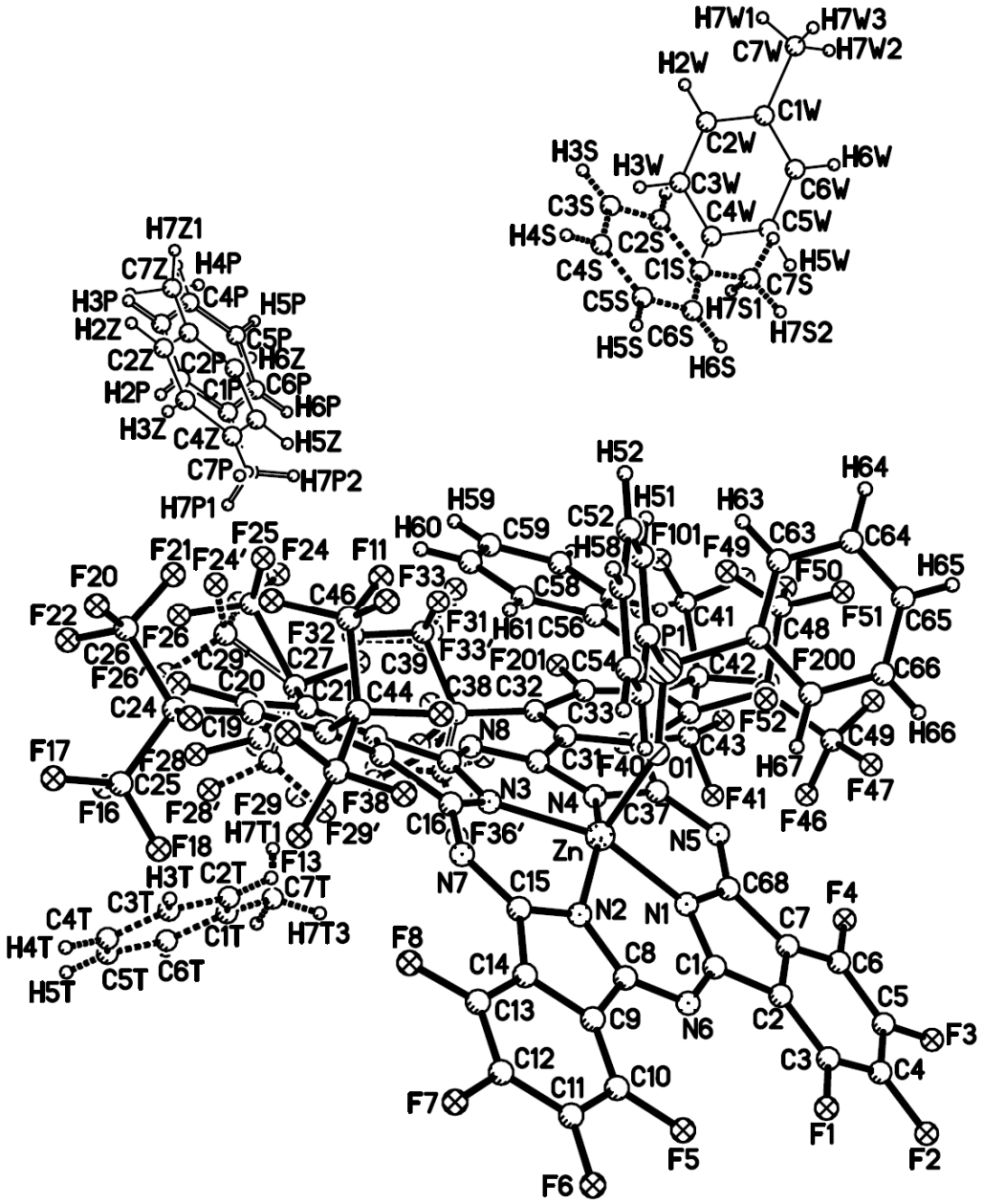

Figure U.1 Crystal structure of $F_{52}PcZn(OPPh_3)$•3Tol.

Table U.1 Crystal Data and Structure Refinement for $F_{52}PcZn(OPPh_3)$•3Tol

Empirical formula	$C_{68}\ H_{15}\ F_{52}\ N_8\ O\ P\ Zn$	
Formula weight	2063.22	
Temperature	100(2) K	
Wavelength	1.54178 Å	
Crystal system	monoclinic	
Space group	$P2_1/n$	
Unit cell dimensions	a = 15.852(2) Å	α = 90°
	b = 22.978(3) Å	β = 96.704(1)°
	c = 24.032(3) Å	γ = 90°
Volume	8694.00(19) $Å^3$	
Z	4	
Density (calculated)	1.576 g/cm^3	
Absorption coefficient	2.042 mm^{-1}	
F(000)	4036	
Theta range for data collection	2.67 to 51.83°	
Index ranges	$-15 \le h \le 13, -22 \le k \le 22, -24 \le l \le 24$	
Reflections collected	36044	
Independent reflections	9072 [*R*(int) = 0.0198]	
Completeness to theta = 51.83°	93.9%	
Refinement method	Full-matrix least-squares on F^2	
Data / restraints / parameters	9072 / 7 / 1092	
Goodness-of-fit on F^2	1.026	
Final *R* indices [*I*>2sigma(*I*)]	*R*1 = 0.0922, *wR*2 = 0.2298	
R indices (all data)	*R*1 = 0.0978, *wR*2 = 0.2348	
Extinction coefficient	0.00006(2)	
Largest diff. peak and hole	1.618 and −1.147 e.$Å^{-3}$	

Table U.2 Atomic Coordinates (× 10^4) and Equivalent Isotropic Displacement Parameters ($Å^2 \times 10^3$) for $F_{52}PcZn(OPPh_3)$•3Tol*

	x	y	z	U(eq)
Zn	6388(1)	751(1)	685(1)	27(1)
O(1)	7652(4)	771(2)	824(2)	40(2)
N(1)	6202(4)	608(3)	-153(3)	27(2)
N(2)	6149(4)	-101(3)	785(2)	24(2)
N(3)	6037(4)	885(3)	1461(3)	24(2)
N(4)	6062(5)	1591(3)	524(3)	33(2)
N(5)	6313(5)	1606(3)	-450(3)	36(2)
N(6)	6031(4)	-432(3)	-177(3)	24(2)
N(7)	6205(4)	-104(3)	1795(3)	24(2)
N(8)	5654(4)	1902(3)	1412(3)	25(2)
P(1)	8389(1)	1108(1)	1114(1)	34(1)
C(1)	6106(5)	86(3)	-405(3)	24(2)
C(2)	6056(5)	175(4)	-1018(3)	28(2)
C(3)	5933(5)	-203(4)	-1466(3)	31(2)
C(4)	5840(5)	29(4)	-2002(3)	36(2)
C(5)	5878(6)	625(4)	-2085(3)	39(2)

C(6)	6024(6)	998(4)	-1641(4)	40(2)
C(7)	6125(5)	775(4)	-1102(3)	31(2)
C(8)	6056(5)	-509(3)	375(3)	25(2)
C(9)	5968(5)	-1083(3)	633(3)	28(2)
C(10)	5857(6)	-1631(4)	409(3)	36(2)
C(11)	5780(6)	-2095(4)	765(4)	41(2)
C(12)	5813(6)	-2003(4)	1339(4)	38(2)
C(13)	5930(5)	-1455(4)	1564(3)	30(2)
C(14)	6015(5)	-988(3)	1211(3)	27(2)
C(15)	6135(5)	-362(3)	1295(3)	26(2)
C(16)	6178(5)	473(3)	1865(3)	25(2)
C(17)	6109(5)	744(3)	2406(3)	25(2)
C(18)	6286(5)	511(3)	2952(3)	28(2)
C(19)	5860(7)	767(4)	3364(4)	45(3)
C(20)	5446(7)	1298(4)	3230(4)	54(3)
C(21)	5446(6)	1609(4)	2736(3)	42(2)
C(22)	5764(5)	1306(3)	2294(3)	29(2)
C(23)	5809(5)	1401(3)	1683(3)	24(2)
C(24)	5728(7)	495(4)	3928(4)	51(3)
C(25)	4803(2)	250(2)	3939(1)	67(4)
F(18)	4646(2)	-148(2)	3544(2)	65(2)
F(16)	4249(3)	680(2)	3849(2)	106(3)
F(17)	4737(3)	15(2)	4434(2)	82(2)
C(26)	6019(3)	887(2)	4468(1)	71(4)
F(22)	5345(4)	1118(2)	4654(2)	103(3)
F(21)	6525(4)	1305(2)	4330(2)	86(2)
F(20)	6428(4)	561(2)	4862(2)	71(2)
C(27)	5072(8)	2212(4)	2669(3)	60(3)
C(28)	4159(5)	2284(5)	2561(5)	1(7)
F(27)	3982(5)	2816(6)	2542(6)	6(6)
F(28)	3813(5)	2048(7)	2947(6)	10(6)
F(29)	3894(5)	2051(7)	2103(7)	31(7)
C(28')	4073(3)	2137(2)	2423(2)	53(4)
F(27')	3704(3)	2658(3)	2379(2)	59(2)
F(28')	3685(3)	1805(3)	2769(3)	75(3)
F(29')	4016(3)	1888(3)	1920(3)	39(2)
C(29)	5397(5)	2679(3)	3205(2)	59(5)
F(24)	5443(6)	3215(3)	3004(3)	55(3)
F(25)	6156(6)	2517(3)	3448(3)	63(3)
F(26)	4843(6)	2668(3)	3579(3)	65(4)
C(29')	4967(4)	2574(3)	3231(2)	43(5)
F(26')	4270(6)	2417(3)	3426(3)	45(4)
F(25')	4934(6)	3127(3)	3117(3)	33(3)
F(24')	5611(6)	2471(3)	3604(3)	37(3)
C(30)	5784(5)	1992(3)	878(3)	30(2)
C(31)	5742(5)	2570(3)	587(3)	28(2)
C(32)	5388(5)	3120(3)	664(3)	25(2)
C(33)	5570(5)	3543(3)	282(3)	28(2)
C(34)	6069(5)	3482(3)	-153(3)	28(2)
C(35)	6459(5)	2940(3)	-215(3)	30(2)
C(36)	6180(5)	2486(3)	116(3)	31(2)
C(37)	6248(6)	1855(4)	49(4)	34(2)
C(38)	4759(5)	3249(3)	1078(3)	30(2)
C(39)	5238(5)	3624(3)	1610(3)	37(5)
F(31)	5943(5)	3355(3)	1811(3)	39(3)
F(32)	4731(7)	3668(5)	2005(4)	87(12)

F(33)	5423(6)	4148(4)	1437(3)	43(4)
C(39')	5026(3)	3754(2)	1501(2)	30(4)
F(31')	5856(5)	3770(3)	1606(3)	50(3)
F(32')	4695(4)	3663(2)	1969(3)	15(5)
F(33')	4750(5)	4252(3)	1283(3)	41(3)
C(40)	3895(3)	3540(3)	860(2)	37(5)
F(36)	3700(4)	3416(4)	334(4)	51(4)
F(37)	3959(4)	4100(4)	921(4)	51(4)
F(38)	3307(4)	3345(4)	1144(3)	37(3)
C(40')	3808(3)	3385(3)	748(2)	30(4)
F(36')	3506(4)	2908(3)	479(3)	45(3)
F(37')	3862(3)	3814(4)	380(3)	46(3)
F(38')	3288(4)	3544(4)	1118(3)	52(4)
C(41)	6447(2)	4584(1)	-302(1)	42(2)
F(100)	6925(3)	4835(1)	-647(2)	53(2)
F(101)	6908(3)	4477(1)	181(2)	52(1)
F(102)	5813(3)	4934(1)	-218(2)	50(1)
C(42)	6075(5)	3986(3)	-569(3)	31(2)
C(43)	5188(2)	4074(1)	-940(1)	35(2)
F(41)	4993(2)	3601(2)	-1233(2)	44(1)
F(39)	5239(2)	4515(2)	-1281(2)	48(1)
F(40)	4599(2)	4179(2)	-614(2)	48(1)
C(44)	7071(6)	106(4)	3052(3)	33(2)
C(45)	6920(2)	-576(1)	3156(1)	35(2)
F(13)	6104(3)	-691(1)	3072(2)	38(1)
F(14)	7213(3)	-711(1)	3673(2)	44(1)
F(15)	7318(2)	-884(1)	2809(2)	40(1)
C(46)	7808(2)	382(1)	3474(1)	42(2)
F(12)	7558(2)	417(2)	3979(2)	53(2)
F(11)	7990(2)	907(2)	3300(2)	51(1)
F(10)	8491(2)	49(2)	3495(2)	54(1)
C(47)	7266(6)	2826(4)	-497(4)	37(2)
C(48)	8051(2)	3237(1)	-270(1)	49(3)
F(49)	8153(2)	3229(2)	282(2)	54(1)
F(50)	7897(2)	3773(2)	-445(2)	59(2)
F(51)	8747(2)	3046(2)	-459(2)	63(2)
C(49)	7156(2)	2737(1)	-1165(1)	48(3)
F(46)	6342(3)	2729(2)	-1353(1)	46(1)
F(47)	7506(3)	2240(2)	-1287(1)	62(2)
F(48)	7529(3)	3168(2)	-1402(1)	56(2)
F(1)	5899(3)	-779(2)	-1408(2)	40(1)
F(2)	5710(3)	-329(2)	-2445(2)	45(1)
F(3)	5774(4)	829(2)	-2609(2)	53(2)
F(4)	6053(4)	1568(2)	-1739(2)	57(2)
F(5)	5832(4)	-1740(2)	-141(2)	49(1)
F(6)	5676(4)	-2638(2)	567(2)	56(2)
F(7)	5727(4)	-2465(2)	1672(2)	48(1)
F(8)	5946(3)	-1391(2)	2119(2)	35(1)
F(9)	7474(3)	125(2)	2573(2)	35(1)
F(19)	6193(3)	-9(2)	3993(2)	43(1)
F(23)	5056(6)	1542(3)	3637(2)	103(3)
F(30)	5463(3)	2514(2)	2300(2)	44(1)
F(34)	4583(3)	2760(2)	1341(2)	30(1)
F(52)	7607(3)	2308(2)	-278(2)	44(1)
F(200)	6570(3)	3838(2)	-976(2)	37(1)
F(201)	5264(3)	4079(2)	358(2)	36(1)

C(50)	9020(2)	648(1)	1606(1)	42(2)
C(51)	9678(2)	882(2)	1971(1)	66(3)
C(52)	10170(3)	522(2)	2344(2)	73(4)
C(53)	10005(4)	-71(2)	2351(2)	88(4)
C(54)	9348(4)	-306(2)	1986(2)	132(7)
C(55)	8855(3)	54(1)	1614(2)	90(5)
C(56)	8071(2)	1723(1)	1516(1)	36(2)
C(57)	7932(2)	2265(1)	1267(1)	45(2)
C(58)	7658(3)	2727(1)	1574(2)	51(3)
C(59)	7523(3)	2646(2)	2130(2)	49(3)
C(60)	7662(2)	2104(2)	2379(1)	46(2)
C(61)	7936(2)	1642(1)	2072(1)	38(2)
C(62)	9019(2)	1393(1)	604(1)	38(2)
C(63)	9713(2)	1753(2)	752(2)	65(3)
C(64)	10191(3)	1956(2)	343(2)	77(4)
C(65)	9975(4)	1799(2)	-214(2)	85(5)
C(66)	9281(4)	1439(2)	-362(1)	110(6)
C(67)	8803(3)	1235(2)	47(1)	71(4)
C(68)	6231(5)	1040(4)	-540(3)	32(2)
C(1P)	1921(13)	9518(5)	2026(6)	18(7)
C(2P)	2108(12)	9449(6)	2602(6)	21(7)
C(3P)	2368(13)	9924(8)	2937(5)	8(6)
C(4P)	2442(16)	10469(6)	2696(7)	80(20)
C(5P)	2256(14)	10538(5)	2120(7)	23(7)
C(6P)	1995(11)	10063(6)	1785(5)	0(5)
C(7P)	1620(20)	9031(14)	1657(14)	34(8)
C(1T)	1003(7)	2984(4)	1431(4)	102(5)
C(2T)	1617(5)	2604(5)	1680(4)	116(5)
C(3T)	1444(6)	2259(4)	2128(4)	103(5)
C(4T)	657(6)	2293(4)	2327(4)	87(4)
C(5T)	43(5)	2673(5)	2078(4)	114(5)
C(6T)	215(6)	3018(4)	1630(4)	125(6)
C(7T)	1009(15)	3446(10)	1019(9)	167(8)
C(1S)	7823(8)	8573(5)	-45(4)	68(6)
C(2S)	7982(9)	8913(5)	434(5)	64(6)
C(3S)	7984(10)	8662(6)	960(4)	72(7)
C(4S)	7827(10)	8070(6)	1008(5)	77(7)
C(5S)	7668(11)	7729(5)	529(6)	81(7)
C(6S)	7666(10)	7981(5)	3(5)	87(8)
C(7S)	7871(13)	8876(8)	-568(5)	96(9)
C(1W)	9528(14)	9699(12)	67(10)	52(11)
C(2W)	9195(16)	9456(13)	525(8)	58(11)
C(3W)	8447(16)	9137(12)	445(8)	66(13)
C(4W)	8031(13)	9059(10)	-92(10)	38(9)
C(5W)	8364(14)	9302(11)	-549(7)	50(10)
C(6W)	9113(15)	9621(11)	-469(9)	43(9)
C(7W)	10390(30)	10090(20)	150(19)	57(11)
C(1Z)	2335(9)	10053(4)	2642(5)	48(5)
C(2Z)	2376(9)	9510(5)	2899(4)	53(5)
C(3Z)	2206(9)	9010(4)	2579(5)	53(5)
C(4Z)	1996(9)	9054(4)	2002(5)	57(6)
C(5Z)	1955(9)	9596(5)	1746(4)	53(5)
C(6Z)	2125(9)	10096(4)	2065(5)	53(5)
C(7Z)	2470(20)	10528(13)	2897(15)	93(9)

* U(eq) is defined as one third of the trace of the orthogonalized U^{ij} tensor.

Table U.3 Bond Lengths (Å) and Angles (°) for $F_{52}PcZn(OPPh_3)$•3Tol

Zn-O(1)	1.993(6)	Zn-N(1)	2.026(6)
Zn-N(2)	2.014(6)	Zn-N(3)	2.030(6)
Zn-N(4)	2.024(6)	O(1)-P(1)	1.504(6)
N(1)-C(1)	1.346(10)	C(27)-C(28')	1.633(13)
N(1)-C(68)	1.365(10)	C(27)-C(29)	1.710(11)
N(2)-C(8)	1.355(10)	C(30)-C(31)	1.498(11)
N(2)-C(15)	1.367(10)	C(31)-C(32)	1.403(11)
N(3)-C(16)	1.356(10)	C(31)-C(36)	1.409(11)
N(3)-C(23)	1.367(10)	C(32)-C(33)	1.391(11)
N(4)-C(37)	1.356(10)	C(32)-C(38)	1.517(11)
N(4)-C(30)	1.362(10)	C(33)-C(34)	1.389(11)
N(5)-C(68)	1.323(11)	C(34)-C(35)	1.405(11)
N(5)-C(37)	1.344(11)	C(34)-C(42)	1.531(11)
N(6)-C(1)	1.322(10)	C(35)-C(36)	1.415(11)
N(6)-C(8)	1.333(10)	C(35)-C(47)	1.539(12)
N(7)-C(15)	1.332(10)	C(36)-C(37)	1.463(12)
N(7)-C(16)	1.338(10)	C(38)-C(40)	1.558(10)
N(8)-C(23)	1.331(10)	C(38)-C(39')	1.569(9)
N(8)-C(30)	1.339(10)	C(38)-C(40')	1.649(10)
P(1)-C(62)	1.793(4)	C(38)-C(39)	1.651(10)
P(1)-C(50)	1.800(4)	C(41)-C(42)	1.600(9)
P(1)-C(56)	1.816(3)	C(42)-C(43)	1.588(9)
C(1)-C(2)	1.479(11)	C(44)-C(46)	1.587(9)
C(2)-C(3)	1.379(12)	C(44)-C(45)	1.611(9)
C(2)-C(7)	1.400(12)	C(47)-C(48)	1.607(10)
C(3)-C(4)	1.388(12)	C(47)-C(49)	1.607(9)
C(4)-C(5)	1.385(13)	C(50)-C(51)	1.3900
C(5)-C(6)	1.368(13)	C(50)-C(55)	1.3900
C(6)-C(7)	1.386(12)	C(51)-C(52)	1.3900
C(7)-C(68)	1.472(12)	C(52)-C(53)	1.3900
C(8)-C(9)	1.471(11)	C(53)-C(54)	1.3900
C(9)-C(10)	1.373(12)	C(54)-C(55)	1.3900
C(9)-C(14)	1.399(11)	C(56)-C(61)	1.3899
C(10)-C(11)	1.381(12)	C(56)-C(57)	1.3900
C(11)-C(12)	1.389(12)	C(57)-C(58)	1.3901
C(12)-C(13)	1.375(12)	C(58)-C(59)	1.3899
C(13)-C(14)	1.386(11)	C(59)-C(60)	1.3898
C(14)-C(15)	1.464(11)	C(60)-C(61)	1.3900
C(16)-C(17)	1.458(11)	C(62)-C(67)	1.3900
C(17)-C(22)	1.414(11)	C(62)-C(63)	1.3901
C(17)-C(18)	1.417(11)	C(63)-C(64)	1.3900
C(18)-C(19)	1.392(12)	C(64)-C(65)	1.3900
C(18)-C(44)	1.548(12)	C(65)-C(66)	1.3900
C(19)-C(20)	1.405(13)	C(66)-C(67)	1.3900
C(19)-C(24)	1.530(13)	C(1P)-C(2P)	1.3900
C(20)-C(21)	1.386(13)	C(1P)-C(6P)	1.3900
C(21)-C(22)	1.411(12)	C(1P)-C(7P)	1.47(4)
C(21)-C(27)	1.508(13)	C(2P)-C(3P)	1.3900
C(22)-C(23)	1.495(11)	C(3P)-C(4P)	1.3900
C(24)-C(25)	1.573(13)	C(4P)-C(5P)	1.3900
C(24)-C(26)	1.602(10)	C(5P)-C(6P)	1.3900
C(27)-C(28)	1.449(14)	C(1T)-C(2T)	1.3900
C(27)-C(29')	1.613(10)	C(1T)-C(6T)	1.3900

C(1T)-C(7T)	1.45(2)	C(1W)-C(6W)	1.3900
C(2T)-C(3T)	1.3900	C(1W)-C(7W)	1.62(5)
C(3T)-C(4T)	1.3900	C(2W)-C(3W)	1.3900
C(4T)-C(5T)	1.3900	C(3W)-C(4W)	1.3900
C(5T)-C(6T)	1.3900	C(4W)-C(5W)	1.3900
C(1S)-C(2S)	1.3900	C(5W)-C(6W)	1.3900
C(1S)-C(6S)	1.3900	C(1Z)-C(7Z)	1.26(3)
C(1S)-C(7S)	1.4468	C(1Z)-C(2Z)	1.3900
C(2S)-C(3S)	1.3900	C(1Z)-C(6Z)	1.3900
C(3S)-C(4S)	1.3900	C(2Z)-C(3Z)	1.3900
C(4S)-C(5S)	1.3900	C(3Z)-C(4Z)	1.3900
C(5S)-C(6S)	1.3900	C(4Z)-C(5Z)	1.3900
C(1W)-C(2W)	1.3900	C(5Z)-C(6Z)	1.3900
O(1)-Zn-N(2)	101.7(2)	N(4)-Zn-N(1)	87.7(3)
O(1)-Zn-N(4)	103.8(3)	O(1)-Zn-N(3)	102.7(2)
N(2)-Zn-N(4)	154.5(3)	N(2)-Zn-N(3)	87.8(2)
O(1)-Zn-N(1)	101.3(3)	N(4)-Zn-N(3)	86.5(2)
N(2)-Zn-N(1)	87.4(2)	N(1)-Zn-N(3)	155.9(3)
P(1)-O(1)-Zn	143.3(4)	N(6)-C(8)-N(2)	128.4(7)
C(1)-N(1)-C(68)	110.6(6)	N(6)-C(8)-C(9)	122.9(7)
C(1)-N(1)-Zn	126.0(5)	N(2)-C(8)-C(9)	108.7(6)
C(68)-N(1)-Zn	123.2(5)	C(10)-C(9)-C(14)	121.3(7)
C(8)-N(2)-C(15)	109.8(6)	C(10)-C(9)-C(8)	132.2(7)
C(8)-N(2)-Zn	126.2(5)	C(14)-C(9)-C(8)	106.5(7)
C(15)-N(2)-Zn	123.7(5)	C(9)-C(10)-C(11)	118.8(8)
C(16)-N(3)-C(23)	110.8(6)	C(10)-C(11)-C(12)	120.2(8)
C(16)-N(3)-Zn	120.8(5)	C(13)-C(12)-C(11)	121.2(8)
C(23)-N(3)-Zn	127.1(5)	C(12)-C(13)-C(14)	119.0(7)
C(37)-N(4)-C(30)	109.9(6)	C(13)-C(14)-C(9)	119.5(7)
C(37)-N(4)-Zn	120.8(5)	C(13)-C(14)-C(15)	134.2(7)
C(30)-N(4)-Zn	128.3(5)	C(9)-C(14)-C(15)	106.3(7)
C(68)-N(5)-C(37)	123.2(7)	N(7)-C(15)-N(2)	127.4(7)
C(1)-N(6)-C(8)	122.5(7)	N(7)-C(15)-C(14)	123.9(7)
C(15)-N(7)-C(16)	123.5(7)	N(2)-C(15)-C(14)	108.7(7)
C(23)-N(8)-C(30)	124.3(7)	N(7)-C(16)-N(3)	127.4(7)
O(1)-P(1)-C(62)	109.6(3)	N(7)-C(16)-C(17)	122.8(7)
O(1)-P(1)-C(50)	110.1(3)	N(3)-C(16)-C(17)	108.5(6)
C(62)-P(1)-C(50)	110.6(2)	C(22)-C(17)-C(18)	123.5(7)
O(1)-P(1)-C(56)	113.4(3)	C(22)-C(17)-C(16)	106.8(7)
C(62)-P(1)-C(56)	107.02(17)	C(18)-C(17)-C(16)	129.6(7)
C(50)-P(1)-C(56)	105.96(18)	C(19)-C(18)-C(17)	116.0(7)
N(6)-C(1)-N(1)	128.8(7)	C(19)-C(18)-C(44)	126.3(7)
N(6)-C(1)-C(2)	122.8(7)	C(17)-C(18)-C(44)	116.1(7)
N(1)-C(1)-C(2)	108.4(7)	C(18)-C(19)-C(20)	117.2(8)
C(3)-C(2)-C(7)	121.0(7)	C(18)-C(19)-C(24)	125.8(8)
C(3)-C(2)-C(1)	132.5(8)	C(20)-C(19)-C(24)	116.6(8)
C(7)-C(2)-C(1)	106.5(7)	C(21)-C(20)-C(19)	126.7(8)
C(2)-C(3)-C(4)	118.2(8)	C(20)-C(21)-C(22)	115.2(8)
C(5)-C(4)-C(3)	120.7(8)	C(20)-C(21)-C(27)	121.7(7)
C(6)-C(5)-C(4)	121.0(8)	C(22)-C(21)-C(27)	122.9(7)
C(5)-C(6)-C(7)	119.2(8)	C(21)-C(22)-C(17)	118.1(7)
C(6)-C(7)-C(2)	119.8(8)	C(21)-C(22)-C(23)	136.8(7)
C(6)-C(7)-C(68)	133.9(8)	C(17)-C(22)-C(23)	105.0(7)
C(2)-C(7)-C(68)	106.1(7)	N(8)-C(23)-N(3)	126.9(7)

N(8)-C(23)-C(22)	125.5(7)	C(51)-C(50)-C(55)	120.0
N(3)-C(23)-C(22)	107.6(6)	C(51)-C(50)-P(1)	120.33(11)
C(19)-C(24)-C(25)	112.7(7)	C(55)-C(50)-P(1)	119.66(11)
C(19)-C(24)-C(26)	115.5(8)	C(52)-C(51)-C(50)	120.0
C(25)-C(24)-C(26)	111.7(6)	C(53)-C(52)-C(51)	120.0
C(28)-C(27)-C(21)	119.8(10)	C(52)-C(53)-C(54)	120.0
C(28)-C(27)-C(29')	83.8(7)	C(55)-C(54)-C(53)	120.0
C(21)-C(27)-C(29')	117.6(7)	C(54)-C(55)-C(50)	120.0
C(28)-C(27)-C(28')	16.7(5)	C(61)-C(56)-C(57)	120.0
C(21)-C(27)-C(28')	107.2(8)	C(61)-C(56)-P(1)	119.43(11)
C(29')-C(27)-C(28')	99.6(6)	C(57)-C(56)-P(1)	120.52(11)
C(28)-C(27)-C(29)	105.6(8)	C(56)-C(57)-C(58)	120.0
C(21)-C(27)-C(29)	114.6(7)	C(59)-C(58)-C(57)	120.0
C(29')-C(27)-C(29)	25.3(3)	C(60)-C(59)-C(58)	120.0
C(28')-C(27)-C(29)	122.2(6)	C(59)-C(60)-C(61)	120.0
N(8)-C(30)-N(4)	126.1(7)	C(56)-C(61)-C(60)	120.0
N(8)-C(30)-C(31)	125.6(7)	C(67)-C(62)-C(63)	120.0
N(4)-C(30)-C(31)	108.0(7)	C(67)-C(62)-P(1)	118.04(12)
C(32)-C(31)-C(36)	118.2(7)	C(63)-C(62)-P(1)	121.95(12)
C(32)-C(31)-C(30)	137.1(7)	C(64)-C(63)-C(62)	120.0
C(36)-C(31)-C(30)	104.7(7)	C(65)-C(64)-C(63)	120.0
C(33)-C(32)-C(31)	115.1(7)	C(64)-C(65)-C(66)	120.0
C(33)-C(32)-C(38)	119.9(7)	C(65)-C(66)-C(67)	120.0
C(31)-C(32)-C(38)	124.5(7)	C(62)-C(67)-C(66)	120.0
C(34)-C(33)-C(32)	127.4(7)	N(5)-C(68)-N(1)	127.9(7)
C(33)-C(34)-C(35)	117.7(7)	N(5)-C(68)-C(7)	123.7(7)
C(33)-C(34)-C(42)	117.6(7)	N(1)-C(68)-C(7)	108.4(7)
C(35)-C(34)-C(42)	124.4(7)	C(2P)-C(1P)-C(6P)	120.0
C(34)-C(35)-C(36)	115.1(7)	C(2P)-C(1P)-C(7P)	121.9(16)
C(34)-C(35)-C(47)	126.6(7)	C(6P)-C(1P)-C(7P)	118.1(16)
C(36)-C(35)-C(47)	116.9(7)	C(1P)-C(2P)-C(3P)	120.0
C(31)-C(36)-C(35)	124.4(7)	C(4P)-C(3P)-C(2P)	120.0
C(31)-C(36)-C(37)	106.0(7)	C(5P)-C(4P)-C(3P)	120.0
C(35)-C(36)-C(37)	129.6(7)	C(4P)-C(5P)-C(6P)	120.0
N(5)-C(37)-N(4)	127.4(7)	C(5P)-C(6P)-C(1P)	120.0
N(5)-C(37)-C(36)	122.3(7)	C(2T)-C(1T)-C(6T)	120.0
N(4)-C(37)-C(36)	109.0(7)	C(2T)-C(1T)-C(7T)	133.8(12)
C(32)-C(38)-C(40)	118.9(6)	C(6T)-C(1T)-C(7T)	105.7(12)
C(32)-C(38)-C(39')	114.9(6)	C(3T)-C(2T)-C(1T)	120.0
C(40)-C(38)-C(39')	93.5(5)	C(2T)-C(3T)-C(4T)	120.0
C(32)-C(38)-C(40')	110.9(6)	C(5T)-C(4T)-C(3T)	120.0
C(40)-C(38)-C(40')	16.1(3)	C(6T)-C(5T)-C(4T)	120.0
C(39')-C(38)-C(40')	109.5(5)	C(5T)-C(6T)-C(1T)	120.0
C(32)-C(38)-C(39)	109.3(6)	C(2S)-C(1S)-C(6S)	120.0
C(40)-C(38)-C(39)	110.1(6)	C(2S)-C(1S)-C(7S)	115.1
C(39')-C(38)-C(39)	17.6(3)	C(6S)-C(1S)-C(7S)	124.8
C(40')-C(38)-C(39)	125.8(6)	C(1S)-C(2S)-C(3S)	120.0
C(34)-C(42)-C(43)	113.0(6)	C(4S)-C(3S)-C(2S)	120.0
C(34)-C(42)-C(41)	114.6(6)	C(3S)-C(4S)-C(5S)	120.0
C(43)-C(42)-C(41)	112.1(5)	C(6S)-C(5S)-C(4S)	120.0
C(18)-C(44)-C(46)	112.3(6)	C(5S)-C(6S)-C(1S)	120.0
C(18)-C(44)-C(45)	118.5(6)	C(2W)-C(1W)-C(6W)	120.0
C(46)-C(44)-C(45)	113.6(5)	C(2W)-C(1W)-C(7W)	121(2)
C(35)-C(47)-C(48)	113.6(6)	C(6W)-C(1W)-C(7W)	119(2)
C(35)-C(47)-C(49)	117.6(7)	C(1W)-C(2W)-C(3W)	120.0
C(48)-C(47)-C(49)	113.9(5)	C(4W)-C(3W)-C(2W)	120.0

C(3W)-C(4W)-C(5W)	120.0	C(1Z)-C(2Z)-C(3Z)	120.0
C(6W)-C(5W)-C(4W)	120.0	C(4Z)-C(3Z)-C(2Z)	120.0
C(5W)-C(6W)-C(1W)	120.0	C(3Z)-C(4Z)-C(5Z)	120.0
C(7Z)-C(1Z)-C(2Z)	124.4(18)	C(4Z)-C(5Z)-C(6Z)	120.0
C(7Z)-C(1Z)-C(6Z)	115.6(18)	C(5Z)-C(6Z)-C(1Z)	120.0
C(2Z)-C(1Z)-C(6Z)	120.0		

Table U.4 Anisotropic Displacement Parameters ($Å^2 \times 10^3$) for $F_{52}PcZn(OPPh_3)$•3Tol*

	U^{11}	U^{22}	U^{33}	U^{23}	U^{13}	U^{12}
Zn	41(1)	20(1)	23(1)	2(1)	11(1)	3(1)
O(1)	43(4)	31(3)	46(4)	-11(3)	9(3)	-2(3)
N(1)	34(4)	25(4)	24(4)	4(3)	8(3)	6(3)
N(2)	28(4)	22(4)	22(4)	1(3)	2(3)	3(3)
N(3)	28(4)	22(4)	23(4)	1(3)	4(3)	1(3)
N(4)	53(5)	22(4)	27(4)	1(3)	20(3)	8(3)
N(5)	59(5)	27(5)	26(4)	4(3)	18(4)	14(3)
N(6)	26(4)	25(4)	21(4)	0(3)	4(3)	-2(3)
N(7)	29(4)	19(4)	26(4)	2(3)	4(3)	2(3)
N(8)	31(4)	24(4)	22(4)	3(3)	6(3)	-2(3)
P(1)	39(1)	25(1)	40(1)	0(1)	13(1)	0(1)
C(1)	22(5)	27(5)	22(4)	1(4)	4(3)	3(3)
C(2)	25(5)	34(5)	25(5)	1(4)	4(4)	6(4)
C(3)	32(5)	37(6)	24(5)	1(4)	5(4)	-4(4)
C(4)	30(5)	56(7)	22(5)	-4(5)	0(4)	0(4)
C(5)	41(6)	56(7)	20(5)	15(5)	10(4)	21(5)
C(6)	56(6)	35(6)	30(6)	12(5)	15(4)	21(5)
C(7)	36(5)	34(5)	26(5)	5(4)	12(4)	10(4)
C(8)	26(5)	24(5)	26(5)	1(4)	5(4)	-1(3)
C(9)	37(5)	26(5)	20(5)	-1(4)	1(4)	-6(4)
C(10)	49(6)	31(5)	27(5)	-2(4)	8(4)	-11(4)
C(11)	69(7)	20(5)	34(6)	-7(4)	12(5)	-13(4)
C(12)	52(6)	23(5)	40(6)	8(4)	11(4)	-2(4)
C(13)	39(5)	29(5)	23(5)	0(4)	5(4)	-1(4)
C(14)	34(5)	22(5)	27(5)	2(4)	4(4)	-1(4)
C(15)	28(5)	22(5)	29(5)	1(4)	5(4)	4(4)
C(16)	26(5)	28(5)	24(5)	0(4)	8(4)	1(4)
C(17)	28(5)	24(5)	23(5)	2(4)	2(4)	-1(4)
C(18)	33(5)	27(5)	22(5)	0(4)	-4(4)	2(4)
C(19)	76(7)	39(6)	19(5)	2(4)	2(5)	18(5)
C(20)	86(8)	53(7)	24(5)	-8(5)	11(5)	33(6)
C(21)	74(7)	36(5)	17(5)	-2(4)	9(4)	29(5)
C(22)	36(5)	30(5)	22(5)	1(4)	1(4)	-3(4)
C(23)	26(5)	23(5)	22(4)	0(4)	5(4)	-4(4)
C(24)	80(8)	50(6)	22(5)	7(4)	3(5)	33(6)
C(25)	63(8)	110(10)	30(6)	27(7)	15(5)	39(7)
F(18)	65(4)	106(5)	26(3)	10(3)	10(3)	8(3)
F(16)	107(6)	167(8)	52(4)	35(4)	39(4)	82(6)
F(17)	90(5)	134(6)	27(3)	24(3)	22(3)	22(4)
C(26)	129(12)	61(8)	25(6)	10(6)	15(7)	41(8)
F(22)	194(8)	94(5)	23(3)	4(3)	28(4)	78(6)
F(21)	189(8)	43(4)	26(3)	-2(3)	5(4)	13(4)
F(20)	133(6)	56(4)	21(3)	2(3)	-5(3)	14(4)
C(27)	125(10)	50(6)	6(4)	-1(4)	15(5)	41(6)

C(30)	40(5)	18(5)	33(5)	2(4)	10(4)	3(4)
C(31)	33(5)	26(5)	26(5)	1(4)	12(4)	2(4)
C(32)	33(5)	20(5)	23(4)	-1(4)	10(4)	4(4)
C(33)	38(5)	16(5)	31(5)	-1(4)	9(4)	2(4)
C(34)	38(5)	19(5)	27(5)	5(4)	8(4)	2(4)
C(35)	37(5)	29(5)	24(4)	5(4)	12(4)	4(4)
C(36)	42(5)	25(5)	28(5)	8(4)	11(4)	8(4)
C(37)	46(6)	27(5)	33(6)	8(4)	19(4)	6(4)
C(38)	43(5)	15(4)	35(5)	5(4)	13(4)	1(4)
C(41)	57(7)	27(5)	44(6)	10(4)	13(5)	4(5)
F(100)	75(4)	32(3)	57(3)	8(3)	29(3)	-13(3)
F(101)	71(4)	36(3)	47(3)	2(2)	6(3)	-15(3)
F(102)	77(4)	24(3)	53(3)	2(2)	26(3)	4(3)
C(42)	43(6)	24(5)	29(5)	3(4)	23(4)	5(4)
C(43)	42(6)	31(5)	35(5)	8(5)	19(5)	7(4)
F(41)	58(3)	36(3)	37(3)	3(2)	5(2)	4(2)
F(39)	64(4)	38(3)	45(3)	21(3)	15(3)	12(3)
F(40)	51(3)	53(3)	41(3)	8(2)	13(3)	14(3)
C(44)	47(6)	30(5)	24(5)	3(4)	5(4)	-1(4)
C(45)	44(7)	32(5)	27(5)	2(4)	-6(4)	-3(4)
F(13)	47(3)	34(3)	32(3)	1(2)	3(2)	-4(2)
F(14)	62(4)	37(3)	31(3)	7(2)	-6(2)	3(2)
F(15)	52(3)	31(3)	38(3)	-2(2)	8(2)	7(2)
C(46)	59(7)	45(6)	19(5)	3(4)	-6(5)	-2(5)
F(12)	75(4)	46(3)	33(3)	4(2)	-11(3)	-2(3)
F(11)	69(4)	37(3)	41(3)	8(2)	-13(3)	-15(3)
F(10)	46(3)	53(3)	57(3)	6(3)	-16(3)	6(3)
C(47)	45(6)	29(5)	42(5)	14(4)	23(4)	14(4)
C(48)	52(7)	45(6)	55(7)	22(5)	24(5)	7(5)
F(49)	55(4)	54(3)	53(4)	15(3)	13(3)	-5(3)
F(50)	53(4)	46(4)	80(4)	32(3)	21(3)	5(3)
F(51)	42(3)	78(4)	76(4)	31(3)	32(3)	17(3)
C(49)	65(8)	36(6)	50(6)	17(5)	35(6)	20(5)
F(46)	63(4)	43(3)	35(3)	7(2)	21(3)	15(3)
F(47)	93(5)	51(4)	52(3)	16(3)	44(3)	35(3)
F(48)	72(4)	51(3)	51(3)	25(3)	38(3)	20(3)
F(1)	52(3)	40(3)	28(3)	-5(2)	6(2)	-16(2)
F(2)	45(3)	67(4)	23(3)	-6(3)	2(2)	-9(3)
F(3)	69(4)	68(4)	25(3)	13(3)	12(3)	24(3)
F(4)	102(5)	41(3)	31(3)	16(2)	28(3)	29(3)
F(5)	88(4)	32(3)	27(3)	-8(2)	14(3)	-18(3)
F(6)	105(5)	23(3)	44(3)	-6(2)	21(3)	-20(3)
F(7)	84(4)	24(3)	40(3)	5(2)	15(3)	-10(2)
F(8)	53(3)	27(3)	24(3)	3(2)	7(2)	-2(2)
F(9)	39(3)	32(3)	32(3)	2(2)	0(2)	4(2)
F(19)	63(4)	41(3)	23(3)	4(2)	0(2)	9(3)
F(23)	198(8)	93(5)	24(3)	17(3)	41(4)	99(5)
F(30)	68(4)	31(3)	29(3)	-9(2)	-6(3)	14(2)
F(34)	39(3)	24(3)	28(2)	4(2)	11(2)	3(2)
F(52)	53(3)	37(3)	46(3)	18(2)	26(3)	17(2)
F(200)	49(3)	30(3)	35(3)	10(2)	18(2)	8(2)
F(201)	57(3)	20(3)	36(3)	3(2)	18(2)	7(2)
C(50)	47(6)	41(6)	41(6)	9(4)	21(5)	6(5)
C(51)	43(7)	64(7)	88(9)	22(7)	-4(6)	5(6)
C(52)	47(7)	102(10)	70(8)	27(7)	11(6)	18(7)
C(53)	109(12)	90(11)	71(9)	35(8)	30(8)	21(9)

C(54)	200(20)	45(8)	134(14)	51(9)	-45(14)	-21(10)
C(55)	139(13)	38(7)	85(9)	24(6)	-23(9)	-13(7)
C(56)	34(5)	34(5)	42(6)	-9(4)	9(4)	-7(4)
C(57)	53(6)	27(5)	58(6)	1(5)	22(5)	0(4)
C(58)	57(7)	23(5)	76(8)	-5(5)	20(6)	-4(5)
C(59)	49(6)	39(6)	62(7)	-19(5)	20(5)	-9(5)
C(60)	38(6)	48(6)	50(6)	-20(5)	2(5)	-10(5)
C(61)	33(5)	39(5)	41(6)	-6(4)	-1(4)	-1(4)
C(62)	44(6)	31(5)	42(6)	9(4)	16(5)	12(4)
C(63)	86(9)	48(6)	69(8)	-12(6)	44(7)	-19(6)
C(64)	74(9)	44(7)	126(12)	6(7)	62(9)	-6(6)
C(65)	75(10)	114(11)	74(9)	60(8)	44(8)	53(8)
C(66)	46(8)	230(20)	53(8)	69(10)	14(7)	17(10)
C(67)	44(7)	121(11)	49(7)	29(7)	4(6)	13(7)
C(68)	43(6)	33(6)	24(5)	5(4)	15(4)	10(4)

* The anisotropic displacement factor exponent takes the form: $-2\pi^2 [h^2 a^{*2} U^{11} + ... + 2 h k a^* b^* U^{12}]$.

Table U.5 Hydrogen Coordinates ($\times 10^4$) and Isotropic Displacement Parameters ($Å^2 \times 10^3$) for $F_{52}PcZn(OPPh_3)$•3Tol

	x	y	z	U(eq)
H(51)	9790	1288	1965	79
H(52)	10620	683	2593	87
H(53)	10342	-317	2606	106
H(54)	9235	-711	1992	159
H(55)	8405	-106	1364	108
H(57)	8024	2321	887	54
H(58)	7562	3098	1403	61
H(59)	7335	2962	2339	59
H(60)	7570	2048	2759	55
H(61)	8031	1271	2243	46
H(63)	9861	1860	1132	78
H(64)	10666	2202	444	93
H(65)	10302	1938	-494	102
H(66)	9134	1331	-743	132
H(67)	8328	989	-55	86
H(2P)	2057	9076	2767	25
H(3P)	2495	9876	3330	10
H(4P)	2620	10793	2925	93
H(5P)	2306	10911	1956	27
H(6P)	1868	10111	1392	0
H(7P1)	1000	9035	1595	51
H(7P2)	1817	8663	1833	51
H(7P3)	1851	9072	1297	51
H(2T)	2155	2580	1544	140
H(3T)	1864	1999	2298	124
H(4T)	539	2057	2633	105
H(5T)	-496	2697	2214	137
H(6T)	-205	3278	1460	150
H(7T1)	1352	3772	1182	250
H(7T2)	427	3579	906	250
H(7T3)	1254	3299	690	250
H(2S)	8089	9318	401	77
H(3S)	8092	8895	1287	86

H(4S)	7828	7898	1367	92
H(5S)	7560	7325	561	97
H(6S)	7557	7748	-325	105
H(7S1)	7398	9152	-633	144
H(7S2)	7836	8594	-876	144
H(7S3)	8410	9088	-549	144
H(2W)	9479	9509	892	69
H(3W)	8219	8971	757	80
H(4W)	7519	8841	-146	45
H(5W)	8080	9249	-916	60
H(6W)	9341	9787	-782	52
H(7W1)	10353	10367	454	86
H(7W2)	10452	10295	-198	86
H(7W3)	10879	9830	245	86
H(2Z)	2520	9480	3292	64
H(3Z)	2234	8639	2754	63
H(4Z)	1880	8712	1784	69
H(5Z)	1811	9626	1352	63
H(6Z)	2097	10467	1890	63
H(7Z1)	3033	10513	3120	139
H(7Z2)	2035	10593	3145	139
H(7Z3)	2464	10846	2625	139

APPENDIX V

UV-VIS MONITORED CATALYST STABILITY

Figures V.1 to V.4 present UV-vis spectra of the catalyst solutions prepared for the homogeneous aerobic coupling of thiols and photooxidation of (*S*)-(–)-citronellol. Spectra were taken at various times from the start of the reactions, as indicated in the graph legends. The catalyst analyzed in each case is noted at the top of each picture.

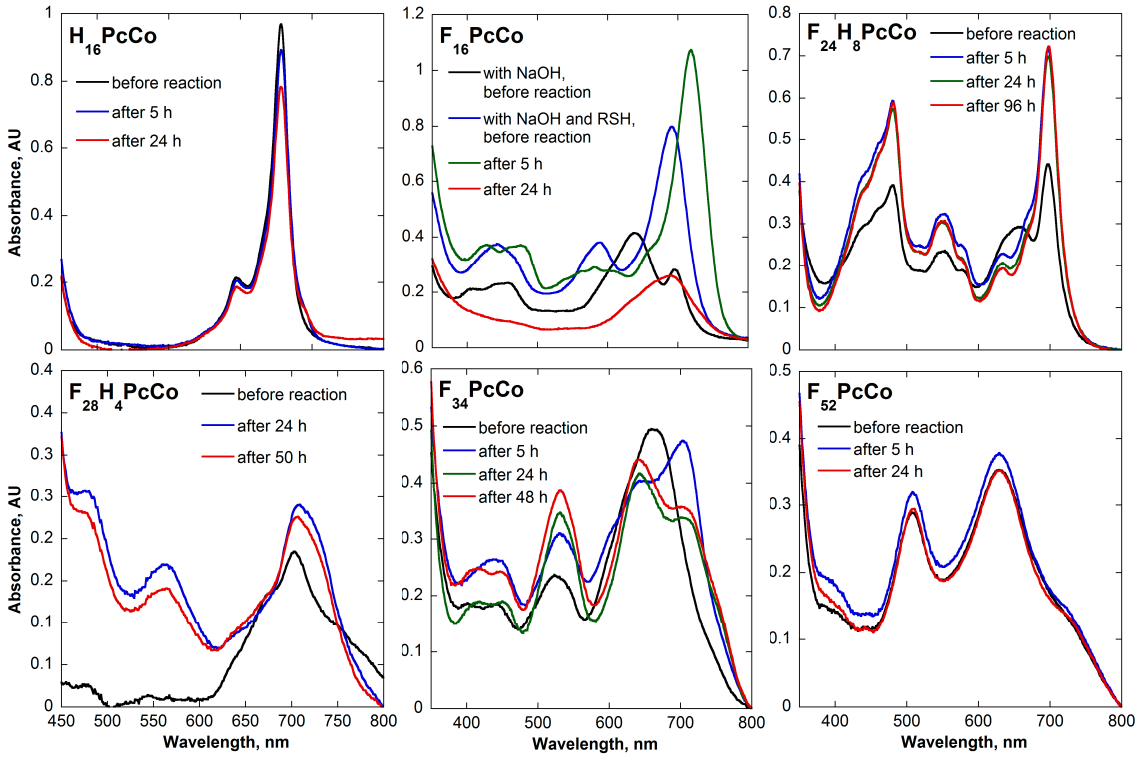

Figure V.1 UV-vis monitored time-dependent catalyst stability during the aerobic oxidation of 2-mercaptoethanol in THF. The spectrum for $F_{64}PcCo$ is similar to the one presented for the oxidation of 4-fluorobenzenethiol and has been omitted in order to avoid redundancy.

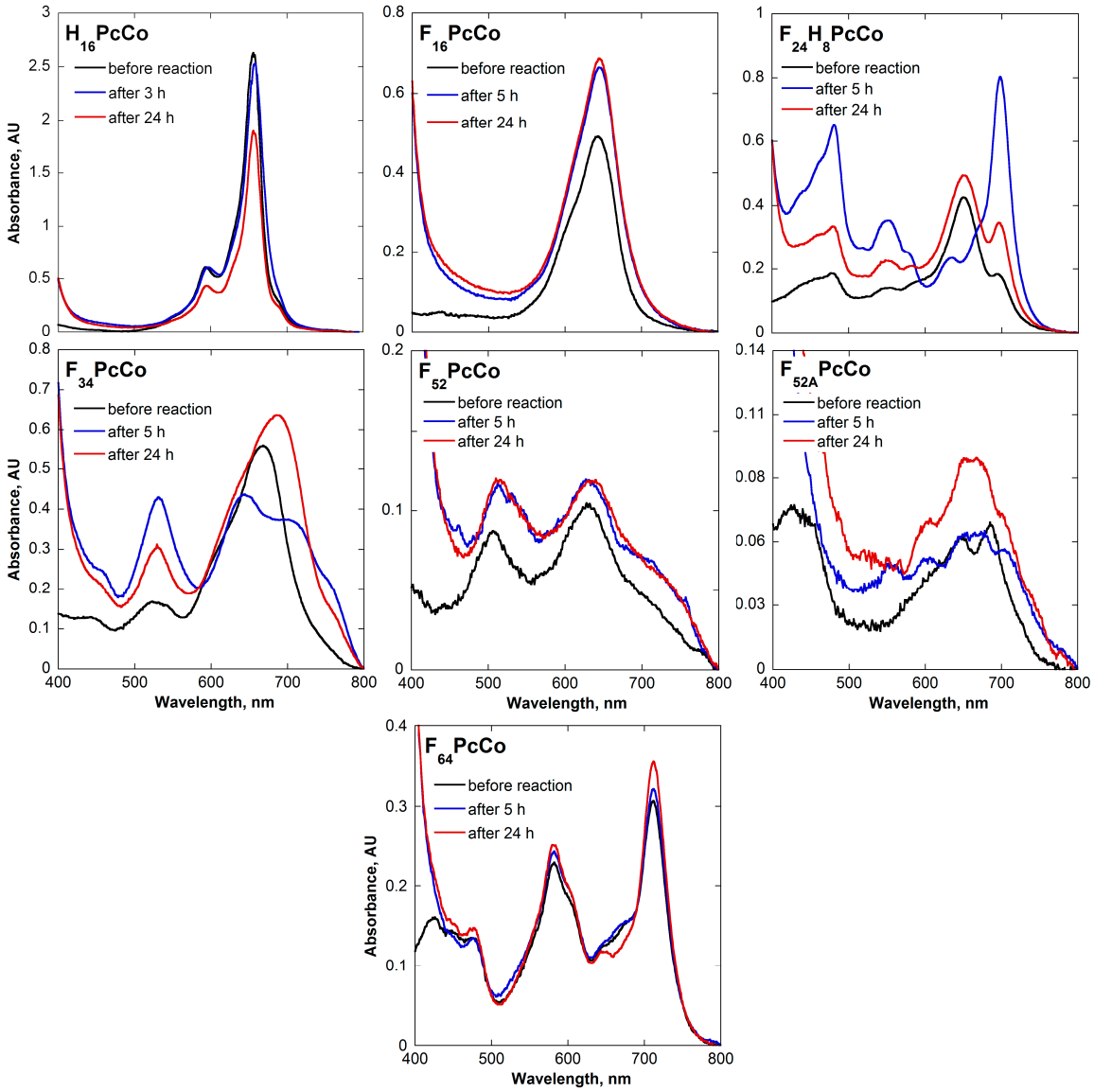

Figure V.2 UV-vis monitored time-dependent catalyst stability during the aerobic oxidation of 4-fluorobenzenethiol in THF.

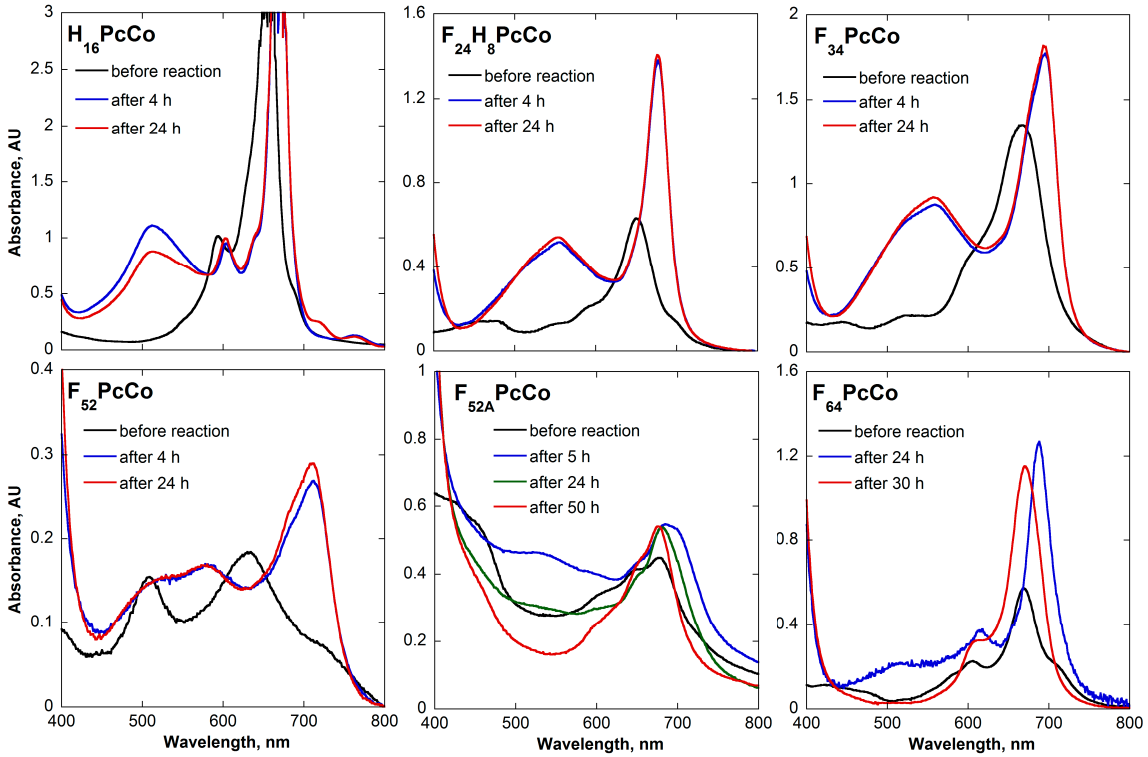

Figure V.3 UV-vis monitored time-dependent catalyst stability during the aerobic oxidation of perfluorobenzenethiol in THF.

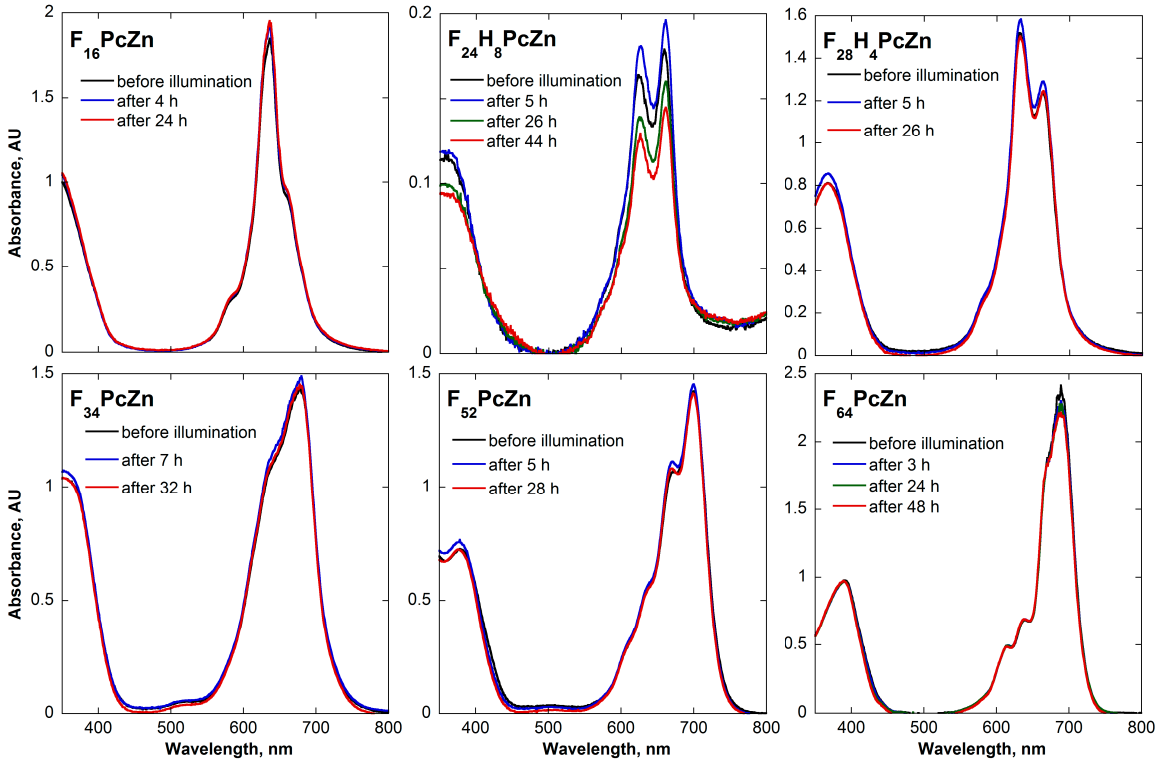

Figure V.4 UV-vis monitored time-dependent catalyst stability during the photooxidation of (*S*)-(–)-citronellol in ethanol. Stability analysis of H_{16}PcCo and its corresponding graph are detailed in Figure 7.8.

REFERENCES

1. (a) Trofimenko, S. *J. Am. Chem. Soc.* **1966**, *88*, 1842. (b) Trofimenko, S. *J. Am. Chem. Soc.* **1967**, *89*, 3148. (c) Trofimenko, S. *J. Am. Chem. Soc.* **1967**, *89*, 3165. (d) Trofimenko, S. *J. Am. Chem. Soc.* **1967**, *89*, 3170. (e) Trofimenko, S. *J. Am. Chem. Soc.* **1967**, *89*, 3904. (f) Trofimenko, S. *J. Am. Chem. Soc.* **1967**, *89*, 4948. (g) Trofimenko, S. *J. Am. Chem. Soc.* **1967**, *89*, 6288. (h) Trofimenko, S. *J. Am. Chem. Soc.* **1969**, *91*, 588.

2. Trofimenko, S. *Scorpionates: The Coordination Chemistry of Polypyrazolylborate Ligands*; Imperial College Press: London, 1999.

3. Pettinari, C. *Scorpionates II: Chelating Borate Ligands*; Imperial College Press: London, 2008.

4. Curtis, M. D.; Shiu, K.-B.; Butler, W. M. *Organometallics* **1983**, *2*, 1475.

5. Curtis, M. D.; Shiu, K.-B.; Butler, W. M. *J. Am. Chem. Soc.* **1986**, *108*, 1550.

6. Trofimenko, S. *Chem. Rev.* **1993**, *93*, 943.

7. Armstrong, W. H.; Spool, A.; Papaephthymiou, G. C.; Frankel, R. B.; Lippard, S. J. *J. Am. Chem. Soc*. **1984**, *106*, 3653.

8. Kitajima, N.; Moro-oka, Y. *Chem. Rev.* **1994**, *94*, 737 and references therein.

9. Schneider, J. L.; Carrier, S. M.; Ruggiero, C. E.; Young, V. G., Jr.; Tolman, W. B. *J. Am. Chem. Soc*. **1998**, *120*, 11408.

10. Berquist, C.; Parkin, G. *J. Am. Chem. Soc.* **1999**, *121*, 6322.

11. Han, R.; Looney, A.; McNeill, K.; Parkin, G.; Rheingold, A. L.; Haggerty, B. S. *J. Inorg. Biochem.* **1993**, *49*, 105.

12. Parkin, G. *Chem. Rev.* **2004**, *104*, 699.

13. Michiue, K.; Jordan, R. F. Jpn Kokai Tokkyo Koho JP 2005239910 A2 20050908, 2005.

14. (a) Karam, A.; Jimeno, M.; Lezam, J.; Catari, E.; Figueroa, A.; Rojas de Gasque, B. *J. Mol. Catal. A: Chem.* **2001**, *176*, 65. (b) Karam, A.; Casas, E.; Catari, E.; Pekerar, S.; Albornoz, A.; Méndez, B. *J. Mol. Catal. A: Chem.* **2005**, *238*, 233.

15. Nakazawa, H.; Ikai, S.; Imaoka, K.; Kai, Y.; Yano, T. *J. Mol. Catal. A: Chem.* **1998**, *132*, 33.

16. Janiak, C.; Lange, K. C. H.; Scharmann, T. G. *Appl. Organomet. Chem.* **2000**, *14*, 316.

17. Trzeciak, A. M.; Ziolkowski, J. J. *Appl. Organomet. Chem.* **2004**, *18*, 124.

18. Caballero, A.; Díaz-Requejo, M. M.; Trofimenko, S.; Belderrain, T. R.; Pérez, P. J. *J. Org. Chem.* **2005**, *70*, 6101.

19. Díaz-Requejo, M. M.; Belderrain, T. R.; Nicasio, M. C.; Trofimenko, S.; Pérez, P. J. *J. Am. Chem. Soc.* **2002**, *124*, 896.

20. Morilla, M. E.; Molina, M. J.; Díaz-Requejo, M. M.; Belderrain, T. R.; Nicasio, M. C.; Trofimenko, S.; Pérez, P. J. *Organometallics* **2003**, *22*, 2914.

21. (a) Handy, S. T.; Czopp, M. *Org. Lett.* **2001**, *3*, 1423. (b) Handy, S. T.; Ivanow, A.; Czopp, M. *Tetrahedron Lett.* **2006**, *47*, 1821. (c) Mairena, M. A.; Díaz-Requejo, M. M.; Belderrain, T. R.; Nicasio, M. C.; Trofimenko, S.; Pérez, P. J. *Organometallics* **2004**, *23*, 253.

22. Díaz-Requejo, M. M.; Caballero, A.; Belderrain, T. R.; Nicasio, M. C.; Trofimenko, S.; Pérez, P. J. *J. Am. Chem. Soc.* **2002**, *124*, 978.

23. Díaz-Requejo, M. M.; Mairena, M. A.; Belderrain, T. R.; Nicasio, M. C.; Trofimenko, S.; Pérez, P. J. *Chem. Commun.* **2001**, 1804.

24. Díaz-Requejo, M. M.; Belderrain, T. R.; Nicasio, M. C.; Pérez, P. J. *Organometallics* **2000**, *19*, 285.

25. Díaz-Requejo, M. M.; Belderrain, T. R.; Pérez, P. J. *Chem. Commun.* **2000**, 1853.

26. Chen, J.; Woo, L. K. *J. Organomet. Chem.* **2000**, *601*, 57.

27. Diaconu, D.; Hu, Z.; Gorun, S. M. *J. Am. Chem. Soc.* **2002**, *124*, 1564.

28. Gorun, S. M.; Hu, Z.; Stibrany, R. T.; Carpenter, G. *Inorg. Chim. Acta* **2000**, *297*, 383.

29. Takahashi, Y.; Hashimoto, M.; Hikichi, S.; Akita, M.; Moro-oka, Y. *Angew. Chem. Int. Ed.* **1999**, *38*, 3074.

30. Jones, W. D. *Inorg. Chem.* **2005**, *44*, 4475.

31. Northcutt, T. O.; Wick, D. D.; Vetter, A. J.; Jones, W. D. *J. Am. Chem. Soc.* **2001**, *123*, 7257.

32. Boutry, O.; Gutierrez, E.; Monge, A.; Nicasio, M. C.; Pérez, P. J.; Carmona, E. *J. Am. Chem. Soc.* **1992**, *114*, 7288.

33. Ghosh, C. K.; Hoyano, J. K.; Krentz, R.; Graham, W. A. G. *J. Am. Chem. Soc.* **1989**, *111*, 5480.

34. Braun, A.; Tscherniac, J. *Chem. Ber.* **1907**, *40*, 2709.

35. De Diesbach, H.; von der Weid, E. *Helv. Chem. Acta* **1927**, *10*, 886.

36. Danbridge, A. G.; Drescher, H. A.; Thomas, J. G.B. Patent 322169, 1928.

37. (a) Byrne, G. T.; Linstead, R. P.; Lowe, A. R. *J. Chem. Soc.* **1934**, 1017. (b) Linstead, R. P.; Lowe, A. R. *J. Chem. Soc.* **1934**, 1022. (c) Dent, C. E.; Linstead, R. P.; Lowe, A. R. *J. Chem. Soc.* **1934**, 1033. (d) Robertson, J. M.; Linstead, R. P.; Dent, C. E. *Nature* **1935**, *35*, 506.

38. Moser, F. H.; Thomas, A. L. *Phthalocyanine Compounds*; Reinhold Publishing Corporation: New York, 1963.

39. Berezin, B. D. *Coordination Compounds of Porphyrins and Phthalocyanines*; Wiley: Chichester, U.K., 1981.

40. Iodko, S. S.; Kaliya, O. L.; Kondratenko, N. V.; Lukyanets, E. A.; Popov, V. I.; Yagupol'skii, L. M. *Zh. Obshch. Khim.* **1983**, *53*, 901.

41. Linstead, R. P.; Weiss, F. T. *J. Chem. Soc.* **1950**, 2975.

42. Moser, F. H.; Thomas, A. L. *The Phthalocyanines*; CRC Press: Boca Raton, FL, 1983; Vols. 1,2.

43. Pawlowski, G.; Hanack, M. *Synthetic Communications* **1981**, *11*, 351.

44. (a) Oksengendler, I. G.; Kondratenko, N. V.; Lukyanets, E. A.; Yagupol'skii, L. M. *Zh. Org. Khim.* **1977**, *13*, 2234. (b) Oksengendler, I. G.; Kondratenko, N. V.; Lukyanets, E. A.; Yagupol'skii, L. M. *Zh. Org. Khim.* **1977**, *13*, 1554. (c) Oksengendler, I. G.; Kondratenko, N. V.; Lukyanets, E. A.; Yagupol'skii, L. M. *Zh. Org. Khim.* **1978**, *14*, 1046.

45. (a) Tomoda, H.; Saita, S.; Shiraishi, S. *Chemistry Lett.* **1983**, 313. (b) Takahashi, K.; Kawashima, M.; Tomita, Y.; Itoh, M. *Inorg. Chim. Acta* **1995**, *232*, 69. (c) Kobayashi, N.; Sasaki, N.; Higashi, Y.; Osa, T. *Inorg. Chem.* **1995**, *34*, 1636. (c) Kobayashi, N.; Ashida, T.; Osa, T. *Chemistry Lett.* **1992**, 2031.

46. (a) Yang, J.; Van DeMark, M. R. *J. Heterocyclic Chem.* **1995**, *32*, 1521. (b) Duro, J. A.; de la Torre, G.; Torres, T. *Tetrahedron Lett.* **1995**, *44*, 8079. (c) Kobayashi, N.; Sasaki, N.; Higashi, Y.; Osa, T. *Inorg. Chem.* **1995**, *34*, 1636.

47. *Phthalocyanines: Properties and Applications*; Leznoff, C. C., Lever, A. B. P., Eds.; VCH Publishers: New York, 1990–1996; Vols. 1–4.

48. Lukyanets, E. A.; Nemykin, V. N. *J. Porphyrins Phthalocyanines* **2010**, *14*, 1.

49. McKeown, N. B.; Budd, P. M. *Chem. Soc. Rev.* **2006**, *35*, 675.

50. Bonnett, R. *Chemical Aspects of Photodynamic Therapy*; Gordon and Breach Science Publishers: Amsterdam, 2000.

51. Bench, B. A. Ph.D. Dissertation, Brown University, Providence, RI, May 2001.

52. Minnes, R.; Weitman, H.; Lee, H.-J.; Gorun, S. M.; Ehrenberg, B. *Photochem. Photobiol.* **2006**, *82*, 593.

53. Elemans, J. A. A. W.; van Hameren, R.; Nolte, R. J. M.; Rowan, A. E. *Adv. Mater.* **2006**, *18*, 1251.

54. Chen, Y.; Hanack, M.; Blau, W. J.; Dini, D.; Liu, Y.; Lin, Y.; Bai, J. *J. Mat. Sci.* **2006**, *41*, 2169.

55. Gottlieb, H. E.; Kotlyar, V.; Nudelman, A. *J. Org. Chem.* **1997**, *62*, 7512.

56. Marat, K. SpinWorks, version 3.1.6.0. University of Manitoba, Winnipeg, 2009.

57. Sheldrick, G. M. SADABS, version 2.0; Multi-Scan Absorbtion Correction Program. University of Göttingen, Göttingen, Germany, 2001.

58. Sheldrick, G. M. SHELXTL, version 6.14; Program for Crystal Structure Determination. Bruker AXS Inc.: Madison, WI, 2004.

59. Mercury, version 2.4; The Cambridge Crystallographic Data Centre: Cambridge, U.K., 2001–2010.

60. (a) ConQuest, version 1.13; The Cambridge Crystallographic Data Centre: Cambridge, U.K., 2010. (b) Allen, F. H. *Acta Crystallogr. Sect. B* **2002**, *58*, 380.

61. (a) Łukasiewicz, M.; Ciunik, Z.; Wołowiec, S. *Polyhedron* **2000**, *19*, 2119. (b) Łukasiewicz, M.; Ciunik, Z.; Ruman, T.; Skora, M.; Wołowiec, S. *Polyhedron* **2001**, *20*, 237. (c) Ruman, T.; Łukasiewicz, M.; Ciunik, Z.; Wołowiec, S. *Polyhedron* **2001**, *20*, 2551. (d) Ruman, T.; Ciunik, Z.; Goclan, A.; Łukasiewicz, M.; Wołowiec, S. *Polyhedron* **2001**, *20*, 2965. (e) Ruman, T.; Ciunik, Z.; Szklanny, E.; Wołowiec, S. *Polyhedron* **2002**, *21*, 2743. (f) Ruman, T.; Ciunik, Z.; Wołowiec, S. *Polyhedron* **2003**, *22*, 581. (g) Ruman, T.; Ciunik, Z.; Wołowiec, S. *Polyhedron* **2004**, *23*, 219. (h) Kisała, J.; Białonska, A.; Ciunik, Z.; Kurek, S.; Wołowiec, S. *Polyhedron* **2006**, *25*, 3222.

62. Ruman, T.; Ciunik, Z.; Wołowiec, S. *Eur. J. Inorg. Chem.* **2003**, 2475.

63. Nishiwaki, T. *J. Chem. Soc. B* **1967**, 885.

64. Dias, H. V. R.; Jin, W.; Kim, H.-J.; Lu, H.-L. *Inorg. Chem.* **1996**, *35*, 2317.

65. Clarire, P. P. K.; Coe, P. L.; Jones, C. J.; McCleverty, J. A. *J. Fluorine Chem.* **1991**, *51*, 283.

66. Santini, C.; Pettinari, C.; Gioia Lobbia, G.; Leonesi, D.; Valle, G.; Calogero, S. *Polyhedron* **1998**, *17*, 3201.

67. Santini, C.; Gioia Lobbia, G.; Pettinari, C.; Pellei, M.; Valle, G.; Calogero, S. *Inorg. Chem.* **1998**, *37*, 890.

68. Santini, C.; Gioia Lobbia, G.; Pellei, M.; Pettinari, C.; Valle, G.; Calogero, S. *Inorg. Chim. Acta* **1998**, *282*, 1.

69. Ghosh, C. K.; Graham, W. A. G. *J. Am. Chem. Soc.* **1987**, *109*, 4726.

70. Ghosh, C. K.; Graham, W. A. G. *J. Am. Chem. Soc.* **1989**, *111*, 375.

71. Hu, Z.; George, G. N.; Gorun, S. M. *Inorg. Chem.* **2001**, *40*, 4812.

72. Hu, Z.; Williams, R. D.; Tran, D.; Spiro, T. G.; Gorun, S. M. *J. Am. Chem. Soc.* **2000**, *122*, 3556.

73. Fujisawa, K.; Yoshida, M.; Miyashita, Y.; Okamoto, K. *Polyhedron* **2009**, *28*, 1447.

74. Hu, Z. Ph.D. Dissertation, Brown University, Providence, RI, May 2001.

75. Albinati, A.; Bucher, U. E.; Gramlich, V.; Renn, O.; Ruegger, H.; Venanzi, L. M. *Inorg. Chim. Acta* **1999**, 284, 191.

76. Dias, H. V. R.; Kim, H.-J.; Lu, H.-L.; Rajeshwar, K.; de Tacconi, N. R.; Derecskei-Kovacs, A.; Marynick, D. S. *Organometallics* **1996**, *15*, 2994.

77. Effendy; Gioia Lobbia, G.; Marchetti, F.; Pellei, M.; Pettinari, C.; Pettinari, R.; Santini, C.; Skelton, B. W.; White, A. H. *Inorg. Chim. Acta* **2004**, *357*, 4247.

78. Dias, H. V. R.; Kim, H.-J. *Organometallics* **1996**, *15*, 5374.

79. Dias, H. V. R.; Wang, X.; Diyabalanage, H. V. K. *Inorg. Chem.* **2005**, *44*, 7322.

80. Dias, H. V. R.; Wu, J.; Wang, X.; Rangan, K. *Inorg. Chem*. **2007**, *46*, 1960.

81. Dias, H. V. R.; Wang, X. *Dalton Trans.* **2005**, 2985.

82. Bucher, U. E.; Currao, A.; Nesper, R.; Rüegger, H.; Venanzi, L. M.; Younger, E. *Inorg. Chem.* **1995**, *34*, 66.

83. Del Ministro, E.; Renn, O.; Rüegger, H.; Venanzi, L. M.; Burckhardt, U.; Gramlich, V. *Inorg. Chim. Acta* **1995**, *240*, 631.

84. Dias, H. V. R.; Goh, T. K. H. H. *Polyhedron* **2004**, *23*, 273.

85. Hu, Z.; Loas, A.; Gorun, S. M. *Inorg. Chim. Acta* **2009**, *362*, 4639.

86. Han, R.; Ghosh, P.; Desrosiers, P. J.; Trofimenko, S.; Parkin, G. *Dalton Trans*. **1997**, 3713.

87. (a) Dias, H. V. R.; Jin, W. *Inorg. Chem.* **1996**, *35*, 267. (b) Dias, H. V. R.; Wang, Z.; Jin, W. *Inorg. Chem.* **1997**, *36*, 6205. (c) Dias, H. V. R.; Lu, H.-L.; Gorden, J. D.; Jin, W. *Inorg. Chem.* **1996**, *35*, 2149. (d) Dias, H. V. R.; Jin, W. *Inorg. Chem.* **1996**, *35*, 3687. (e) Dias, H. V. R.; Jin, W. *J. Am. Chem. Soc*. **1995**, *117*, 11381. (f) Dias, H. V. R.; Jin, W. *Inorg. Chem.* **2000**, *39*, 815. (g) Dias, H. V. R.; Wang, Z. *Inorg. Chem.* **2000**, *39*, 3724. (h) Dias, H. V. R.; Wang, Z. *Inorg. Chem.* **2000**, *39*, 3890.

88. Dias, H. V. R.; Polach, S. A.; Goh, S.-K.; Archibong, E. F.; Marynick, D. S. *Inorg. Chem.* **2000**, *39*, 3894.

89. Dias, H. V. R.; Polach, S. A. *Inorg. Chem.* **2000**, *39*, 4676.

90. Ayers, A. E.; Dias, H. V. R. *Inorg. Chem.* **2002**, *41*, 3259.

91. Dias, H. V. R.; Jin, W. *Inorg. Chem.* **2003**, *42*, 5034.

92. Dias, H. V. R.; Browning, R. G.; Polach, S. A.; Diyabalanage, H. V. K.; Lovely, C. J. *J. Am. Chem. Soc*. **2003**, *125*, 9270.

93. Dias, H. V. R.; Batdorf, K. H.; Fianchini, M.; Diyabalanage, H. V. K.; Carnahan, S.; Mulcahy, R.; Rabiee, A.; Nelson, K.; van Waasbergen, J. G. *J. Inorg. Biochem.* **2006**, *100*, 158.

94. Van Waasbergen, L. G.; Fajdetic, I.; Fianchini, M.; Dias, H. V. R. *J. Inorg. Biochem.* **2007**, *101*, 1180.

95. Dias, H. V. R.; Ayers, A. E. *Polyhedron* **2002**, *21*, 611.

96. (a) Abu Salah, O. M.; Bruce, M. I. *J. Organomet. Chem.* **1974**, *87*, C15. (b) Abu Salah, O. M.; Ashby, G. S.; Bruce, M. I.; Pederzolli, E. A.; Walsh, J. D. *Aust. J. Chem.* **1979**, *32*, 1613. (c) Bruce, M. I.; Walsh, J. D. *Aust. J. Chem.* **1979**, *32*, 2753.

97. Gioia Lobbia, G.; Bonati, F.; Cecchi, P.; Pettinari, C. *Gazz. Chim. Ital.* **1991**, *121*, 355.

98. Gioia Lobbia, G.; Hanna, J. V.; Pellei, M.; Pettinari, C.; Santini, C.; Skelton, B. W.; White, A. H. *Dalton Trans.* **2004**, 951.

99. Youm, K.-T.; Huh, S.; Park, Y. J.; Park, S.; Choi, M.-G.; Jun, M.-J. *Chem. Commun.* **2004**, 2384.

100. Effendy; Gioia Lobbia, G.; Pettinari, C.; Santini, C.; Skelton, B. W.; White, A. H. *Dalton Trans.* **1998**, 2739.

101. Sadr, M. H.; Niaz, S. A.; Gorbani, S.; Gao, S.; Ng, S. W. *Acta Crystallogr., Sect. E: Struct. Rep. Online* **2008**, *64*, m158.

102. López, C.; Claramunt, R. M.; Trofimenko, S.; Elguero, J. *Can. J. Chem.* **1993**, *71*, 678.

103. Alkorta, I.; Elguero, J.; Donnadieu, B.; Etienne, M.; Jaffart, J.; Schagen, D.; Limbach, H.-H. *New J. Chem.* **1999**, *23*, 1231.

104. Gorun, S. M.; Bench, B. A.; Carpenter, G.; Beggs, M. W.; Mague, J. T.; Ensley, H. E. *J. Fluorine Chem.* **1998**, *91*, 37.

105. Bench, B. A.; Beveridge, A.; Sharman, W. M.; Diebold, G. J.; van Lier, J. E.; Gorun, S. M. *Angew. Chem. Int. Ed.* **2002**, *41*, 747.

106. Bench, B. A.; Brennessel, W. W.; Lee, H.-J.; Gorun, S. M. *Angew. Chem. Int. Ed.* **2002**, *41*, 750.

107. Beveridge, A.; Bench, B. A.; Gorun, S. M.; Diebold, G. J. *J. Phys. Chem. A* **2003**, *107*, 5138.

108. Keizer, S. P.; Mack, J.; Bench, B. A.; Gorun, S. M.; Stillman, M. J. *J. Am. Chem. Soc.* **2003**, *125*, 7067.

109. Lee, H.-J.; Brennessel, W. W.; Lessing, J. A.; Brucker, W. W.; Young, V. G., Jr.; Gorun, S. M. *Chem. Commun.* **2003**, 1576.

110. Liao, M.-S.; Kar, T.; Gorun, S. M.; Scheiner, S. *Inorg. Chem.* **2004**, *43*, 7151.

111. Liao, M.-S.; Watts, J. D.; Huang, M.-J.; Gorun, S. M.; Kar, T.; Scheiner, S. *J. Chem. Theory Comput.* **2005**, *1*, 1201.

112. Gerdes, R.; Łapok, Ł.; Tsaryova, O.; Wöhrle, D.; Gorun, S.M. *Dalton Trans.* **2009**, 1098.

113. Keil, C.; Tsaryova, O.; Himcinshi, C.; Wöhrle, D.; Hild, O. R.; Zahn, D. R. T.; Gorun, S. M.; Schlettwein, D. *Thin Solid Films* **2009**, *517*, 4379 and references therein.

114. Moons, H.; Łapok, Ł.; Loas, A.; van Doorslaer, S.; Gorun, S. M. *Inorg. Chem.* **2010**, *49*, 8779.

115. Kovalenko, S. V.; Peabody, S.; Manoharan, M; Clark, R. J.; Alabugin, I. V. *Org. Lett.* **2004**, *6(14)*, 2457.

116. Matsui, K.; Tobita, E.; Ando, M.; Kondo, K. *Chemistry Lett.* **1981**, 1719.

117. (a) Chang, Y.; Cai, C. *J. Fluorine Chem.* **2005**, *126*, 937. (b) Chang, Y.; Cai, C. *Tetrahedron Lett.* **2005**, *46*, 3161.

118. Chambers, R. D.; Edwards, A. R. *Tetrahedron* **1998**, *54*, 4949.

119. (a) Urata, H.; Fuchikami, T. *Tetrahedron Lett.* **1991**, *32*, 91. (b) Kitazume, T.; Nakajima, S. *J. Fluorine Chem.* **2004**, *125*, 1447.

120. Stillman, M. J.; Thomson, A. J. *J. Chem. Soc., Faraday Trans., II* **1974**, *70*, 790.

121. Lever, A. B. P. *Adv. Inorg. Radiochem.* **1965**, *7*, 27.

122. (a) Henriksson, A.; Roos, B.; Sundbom, M. *Theor. Chim. Acta* **1972**, *24*, 303. (b) Henriksson, A.; Sundbom, M. *Theor. Chim. Acta* **1972**, *24*, 213. (c) Lee, L. K.; Sabelli, N. H.; LeBreton, P. R. *J. Phys. Chem.* **1982**, *86*, 3926. (d) Sabelli, N. H.; Melendres, C. A. *J. Phys. Chem.* **1982**, *86*, 4342. (e) Hale, P. D.; Pietro, W. J.; Ratner, M. A.; Ellis, D. E.; Marks, T. J. *J. Am. Chem. Soc.* **1987**, *109*, 5943.

123. (a) Gouterman, M.; Wagniere, G. H.; Snyder, L. C. *J. Mol. Spectrosc.* **1963**, *11*, 108. (b) Zerner, M.; Gouterman, M. *Theor. Chim. Acta* **1966**, *4*, 44. (c) McHugh, A. J.; Gouterman, M.; Weiss, C. *Theor. Chim. Acta* **1972**, *24*, 346. (d) Schaffer, A. M.; Gouterman, M. *Theor. Chim. Acta* **1972**, *25*, 62. (e) Schaffer, A. M.; Gouterman, M.; Davidson, E. R. *Theor. Chim. Acta* **1973**, *30*, 9. (f) Gouterman, M. Optical Spectra and Electronic Structure of Porphyrins and Related Rings. In *The Porphyrins*, *Vol. III, Part A. Physical Chemistry*; Dolphin, D., Ed.; Academic Press: New York, 1978; pp 1–165.

124. Minor, P. C.; Gouterman, M.; Lever, A. B. P. *Inorg. Chem.* **1985**, *24*, 1894.

125. Nyokong, T.; Gasyna, Z.; Stillman, M. J. *Inorg. Chem.* **1985**, *26*, 1087.

126. Lever, A. B. P.; Pickens, S. R.; Minor, P. C.; Licoccia, S.; Ramaswamy, B. S.; Magnell, K. *J. Am. Chem. Soc.* **1981**, *103*, 6800.

127. (a) Leznoff, C. C; Marcuccio, S. M.; Greenberg, S.; Lever, A. B. P.; Tomer, K. B. *Can. J. Chem.* **1985**, *63*, 623. (b) Nevin, W. A.; Liu, W.; Greenberg, S.; Hempstead, M. R.; Marcuccio, S. M.; Melnik, M. M.; Leznoff, C. C.; Lever, A. B. P. *Inorg. Chem.* **1987**, *26*, 891. (c) Leznoff, C. C.; Lam, H.; Nevin, W. A.; Kobayashi, N.; Janda, P.; Lever, A. B. P. *Angew. Chem.* **1987**, *26*, 1021.

128. (a) Sielcken, O. E.; van Tilborg, M. M.; Roks, M. F. M.; Hendricks, R.; Drenth, W.; Nolte, R. J. M. *J. Am. Chem. Soc.* **1987**, *109*, 4261 and references therein. (b) Kobayashi, N.; Lever, A. B. P. *J. Am. Chem. Soc.* **1987**, *109*, 7433.

129. (a) Hush, N. S.; Woolsey, I. S. *Mol. Phys.* **1971**, *21*, 465. (b) Dodsworth, E. S.; Lever, A. B. P.; Seymour, P.; Leznoff, C. C. *J. Phys. Chem.* **1985**, *89*, 5698. (c) Gouterman, M.; Holten, D.; Lieberman, E. *Chem. Phys.* **1977**, *25*, 139.

130. Gasyna, Z.; Kobayashi, N.; Stillman, M. J. *J. Chem. Soc., Dalton Trans.* **1989**, 2397.

131. Hansch, C.; Leo, A.; Taft, R. W. *Chem. Rev.* **1991**, *91*, 165.

132. Charton, M. *Can. J. Chem.* **1960**, *38*, 2493.

133. Chen, Z.; Lohr, A.; Saha-Möller, C. R.; Würthner, F. *Chem. Soc. Rev.* **2009**, *38*, 564.

134. (a) West, W.; Pearce, S. *J. Phys. Chem.* **1965**, *69*, 1894. (b) Yang, Y.-C.; Ward, J. R.; Seiders, R. P. *Inorg. Chem.* **1985**, *24*, 1765.

135. Monahan, A. R.; Brado, J. A.; DeLuca, A. F. *J. Phys. Chem.* **1972**, *76*, 446.

136. Weitman, H.; Schatz, S.; Gottlieb, H. E.; Kobayashi, N.; Ehrenberg, B. *Photochem. Photobiol.* **2001**, *73*, 473.

137. Taft, R. W.; Kamlet, M. J. *J. Am. Chem. Soc.* **1976**, *98*, 2886.

138. Kamlet, M. J.; Abboud, J.-L. M.; Abraham, M. H.; Taft, R. W. *J. Org. Chem.* **1983**, *48*, 2877.

139. Pérez, A. C.; Mancini, P. M. *J. Phys. Org. Chem.* **2009**, *22*, 197.

140. Yoon, S. M.; Song, H. J.; Hwang, I.; Kim, K. S.; Choi, H. C. *Chem. Commun.* **2010**, *46*, 231.

141. (a) Brinkmann, H.; Kelting, C.; Makarov, S.; Tsaryova, O.; Schnurpfeil, G.; Wöhrle, D.; Schlettwein, D. *Phys. Stat. Sol. (a)* **2008**, *205*, 409. (b) Isoda, S.; Hashimoto, S.; Ogawa, T.; Kurata, H.; Moriguchi, S.; Kobayashi, T. *Mol. Cryst. Liq. Cryst.* **1994**, *247*, 191. (c) Schlettwein, D.; Tada, H.; Mashiko, S. *Langmuir* **2000**, *16*, 2872.

142. (a) Bobrovski, A. P.; Kholmogorov, V. E. *J. Phys. Chem. USSR* **1973**, *47*, 983. (b) Ferraudi, G. *Inorg. Chem.* **1979**, *18*, 1005. (c) Darwent, J. R.; McCubbin, I.; Porter, G. *J. Chem. Soc.* **1982**, *78*, 903. (d) Ohno, T.; Kato. S.; Yamada, A.; Tanno, T. *J. Phys. Chem.* **1983**, *87*, 773. (e) Ohtani, H.; Kobayashi, T.; Ohno, T.; Kato, S.; Tanno, T.; Yamada, A. *J. Phys. Chem.* **1984**, *88*, 4431. (f) Ough, E.; Gasyna, Z.; Stillman, M. J. *Inorg. Chem.* **1991**, *30*, 2301.

143. Spikes, J. D. *Photochem. Photobiol.* **1986**, *43*, 691.

144. (a) Ciliberto, E.; Doris, K. A.; Pietro, W. J.; Reisner, G. M.; Ellis, D. E.; Fragala, I.; Herbstein, F. H.; Ratner, M. A. *J. Am. Chem. Soc.* **1984**, *106*, 7748. (b) Schramm, C. J.; Scaringe, R. P.; Stojakovic, D. R.; Hoffman, B. M.; Ibers, J. A.; Marks, T. J. *J. Am. Chem. Soc.* **1980**, *102*, 6702. (c) DeWulf, D. W.; Leland, J. K.; Wheeler, B. L.; Bard, A. J.; Batzel, D. A.; Dininny, D. R.; Kenney, M. E. *Inorg. Chem.* **1987**, *26*, 266.

145. Turek, P.; Petit, P.; Andre, J.-J.; Simon, J.; Even, R.; Boudjema, B.; Guillaud, G.; Maitrot, M. *J. Am. Chem. Soc.* **1987**, *109*, 5119.

146. (a) Castaneda, F.; Plichon, V. *J. Electroanal. Chem.* **1987**, *236*, 163. (b) Besbes, S.; Plichon, V.; Simon, J.; Vaxiviere, J. *J. Electroanal. Chem.* **1987**, *237*, 61.

147. Ohno, O.; Ishikawa, N.; Matsuzawa, H.; Kaizu, Y.; Kobayashi, H. *J. Phys. Chem.* **1989**, *93*, 1713.

148. Orti, E.; Bredas, J. L.; Clarisse, C. *J. Chem. Phys.* **1990**, *92*, 1228.

149. Kaim, W.; Schwederski, B. *Bioinorganic Chemistry: Inorganic Elements in the Chemistry of Life*; Wiley: New York, 1994.

150. Dolphin, D.; Muljiani, Z.; Rousseau, K.; Borg, D. C.; Fajer, J.; Felton, R. H. *Ann. New York Acad. Sci.* **1973**, *206*, 177.

151. Basu, B.; Satapathy, S.; Bhatnagar, A. K. *Catal. Rev.* **1993**, *35*, 571.

152. Jocelyn, P. C. *Biochemistry of the SH Group*; Academic Press: London, 1972; p 94.

153. Zwart, J.; van der Weide, H. C.; Bröker, N.; Rummens, C.; Schuit, G. C. A. *J. Mol. Catal*. **1977**, *3*, 151.

154. (a) Surdhar, P. S.; Armstrong, D. A. *J. Phys. Chem.* **1986**, *90*, 5915. (b) Surdhar, P. S.; Armstrong, D. A. *J. Phys. Chem.* **1987**, *91*, 6532.

155. Buck, T.; Schulz-Ekloff, G.; Andreev, A.; Wöhrle, D. *J. Mol. Catal.* **1991**, *70*, 259.

156. Leung, P.-S. K.; Betterton, E. A.; Hoffmann, M. R. *J. Phys. Chem*. **1989**, *93*, 430.

157. Navid, A.; Tyapochkin, E. M.; Archer, C. J.; Kozliak, E. I. *J. Porphyrins Phthalocyanines* **1999**, *3*, 654.

158. Van Welzen, J.; van Herk, A. M.; German, A. L. *Makromol. Chem.* **1989**, *190*, 2477.

159. Schneider, G.; Spiller, W.; Stark, J.; Schulz-Ekloff, G.; Wöhrle, D. *Photochem. Photobiol.* **1994**, *60*, 333.

160. Tyapochkin, E. M.; Kozliak, E. I. *J. Porphyrins Phthalocyanines* **2001**, *5*, 405.

161. Shirai, H.; Tsuiki, H.; Masuda, E.; Koyama, T.; Hanabusa, K.; Kobayashi, N. *J. Phys. Chem*. **1991**, *95*, 417.

162. Fischer, H.; Buck, T.; Wöhrle, D.; Vassileva, M.; Andreev, A.; Schulz-Ekloff, G. *Langmuir* **1992**, *8*, 2720.

163. Leitão, A.; Rodrigues, A. *Chem. Eng. Sci.* **1989**, *44*, 1245.

164. Chatti, I.; Ghorbel, A.; Grange, P.; Colin, J. M. *Catal. Today* **2002**, *75*, 113.

165. (a) Van Welzen, J.; van Herk, A. M.; German, A. L. *Makromol. Chem.* **1987**, *188*, 1923. (b) Van Welzen, J.; van Herk, A. M.; German, A. L. *Makromol. Chem.* **1988**, *189*, 587.

166. (a) Leung, P.-S. K.; Hoffmann, M. R. *Environ. Sci. Technol.* **1988**, *22*, 275. (b) Wöhrle, D.; Buck, T.; Schneider, G.; Schulz-Ekloff, G.; Fischer, H. *J. Inorg. Organomet. Polym*. **1991**, *1*, 1. (c) Kotronarou, A.; Hoffmann, M. R. *Environ. Sci. Technol.* **1991**, *25*, 1153.

167. Schutten, J. H.; Piet, P.; German, A. L. *Makromol. Chem.* **1979**, *180*, 2341.

168. Tyapochkin, E. M.; Kozliak, E. I. *J. Mol. Catal. A: Chem.* **2005**, *242*, 1.

169. Schutten, J. H.; Beelen, T. P. M. *J. Mol. Catal.* **1981**, *10*, 85.

170. Martell, A. E.; Smith, R. M. *Critical Stability Constants*; Plenum Press: New York, 1977; Vol. 3.

171. Namuswe, F.; Kapser, G. D.; Sarjeant, A. A. N.; Krest, C.; Hayashi, T.; Green, M. T.; Moenne-Loccoz, P.; Goldberg, D. P. *J. Am. Chem. Soc.* **2008**, *130*, 14189.

172. (a) Zagal, J. H.; Griveau, S.; Silva, J. F.; Nyokong, T.; Bedioui, F. *Coord. Chem. Rev.* **2010**, *254*, 2755. (b) Bedioui, F.; Griveau, S.; Nyokong, T.; Appleby, A. J.; Caro, C. A.; Gulppi, M.; Ochoa, G.; Zagal, J. H. *Phys. Chem. Chem. Phys.* **2007**, *9*, 3383 and references therein.

173. Loas, A.; Gerdes, R.; Zhang, Y.; Gorun, S. M. *Dalton Trans.* **2011**, *40*, 5162.

174. Lever, A. B. P. *Inorg. Chim. Acta* **1993**, *203*, 171.

175. Huckstadt, H.; Homborg, H. *Z. Anorg. Allg. Chem.* **1998**, *624*, 715.

176. Lippard, S. J. *Nature* **2002**, *416*, 587.

177. Parmon, V.; Emeline, A. V.; Serpone, N. *Intern. J. Photoenergy* **2002**, *4*, 91.

178. Wöhrle, D.; Kaneko, M.; Nagai, K.; Suvorova, O.; Gerdes, R. Environmental Cleaning by Molecular Photocatalysts. In *Molecular Catalysts for Energy Conversion*; Springer Series in Materials Science, Vol. 111; Springer: Berlin, Germany, 2009; pp 263–297.

179. Wöhrle, D.; Tausch, M. W.; Stohrer, W.-D. *Photochemie*; Wiley-VCH: Weinheim, Germany, 1998.

180. Griesbeck, A. G.; Bartoschek, A. *Chem. Commun.* **2002**, 1594.

181. Juris, A.; Balzani, V.; Barigelletti, F.; Campagna, S.; Belser, P.; Vonzelewsky, A. *Coord. Chem. Rev.* **1988**, *84*, 85.

182. (a) Meyer, S.; Tietze, D.; Rau, S.; Schäfer, B.; Kreisel, G. *J. Photochem. Photobiol.* **2007**, *186*, 248. (b) Ribeiro, S. M.; Serra, A. C.; Rocha Gonsalves, A. M. d'A. *J. Catal.* **2008**, *256*, 331.

183. Monnerie, N.; Ortner, J. *J. Sol. Energy Eng.* **2001**, *123*, 171.

184. McKeown, N. B. *Phthalocyanine Materials: Synthesis, Structure and Function*; Cambridge University Press: Cambridge, U.K., 1998.

185. Barltrop, J. A.; Coyle, J. D. *Excited States in Organic Chemistry*; Wiley: New York, 1975.

186. Kopecky, J. *Organic Photochemistry: A Visual Approach*; VCH: Weinheim, Germany, 1992.

187. Kearns, D. R. *Chem. Rev.* **1971**, *71*, 395.

188. Sobbi, A. K.; Wöhrle, D.; Schlettwein, D. *J. Chem. Soc., Perkin Trans. 2* **1993**, *3*, 481.

189. Ohloff, G.; Klein, E.; Schenck, G. O. *Angew. Chem.* **1961**, *73*, 578.

190. Schnurpfeil, G.; Sobbi, A.; Spiller, W.; Kliesh, H.; Wöhrle, D. *J. Porphyrins Phthalocyanines* **1997**, *1*, 159.

191. Ozoemana, K.; Kuznetsova, N.; Nyokong, T. *J. Mol. Catal. A* **2001**, *176*, 29.